Dynamics of Atmospheric Flight

BERNARD ETKIN, C.M., D.Eng., FRSC, FAIAA, FCAE
University Professor Emeritus, Institute for Aerospace Studies (UTIAS)
and formerly Dean, Faculty of Applied Science and Engineering
University of Toronto

DOVER PUBLICATIONS, INC.
Mineola, New York

In my book, *Dynamics of Flight*, the dedication read "To the men of science and engineering whose contributions to aviation have made it a dominant force in shaping the destiny of mankind." I now add:

To those men of science and engineering, who with sensitivity and concern, develop and apply their technological arts towards a better future for man on Earth and in space.

Bibliographical Note

This Dover edition, first published in 2005, is an unabridged republication of the work originally published by John Wiley & Sons, Inc., New York, in 1972. The author has provided a new Errata list (pages 580–581) for the Dover edition.

Library of Congress Cataloging-in-Publication Data

Etkin, Bernard.
Dynamics of atmospheric flight / Bernard Etkin.
p. cm.
Originally published: New York : Wiley, 1972.
Includes bibliographical references and index.
ISBN 0-486-44522-4 (pbk.)
1. Aerodynamics. 2. Stability of airplanes. 3. Flight. I. Title.

TL570.E74 2005
629.132'.3—dc22

2005048479

Manufactured in the United States of America
Dover Publications, Inc., 31 East 2nd Street, Mineola, N.Y. 11501

Preface

This book originally was intended to be a modest revision of my earlier work, *Dynamics of Flight—Stability and Control*, published in 1959. As the task progressed, however, I found that the developments of the intervening decade, and the shift in my own approach to the subject, made a "modest revision" impossible. Thus this volume is virtually a new book, with organization and content substantially different from its predecessor. Two principal factors caused this change: (1) the proliferation of vehicle types and flight regimes, particularly hypersonic and space flight, and (2) the explosive growth of machine computation.

The first factor compelled me to abandon the long-standing simplifying assumption that the Earth's surface could be represented by a plane fixed in inertial space, and to include in the mathematical model all the complications that arise from the curvature and rotation of the Earth.

The second factor had two profound effects. One was that since we are no longer confined to primitive computation methods, it is commonplace nowadays in industry to construct highly sophisticated mathematical "simulations" of systems for the purpose of carrying out research and design studies. The emphasis on simple approximations is thereby reduced, and the need to set up accurate (even though complicated) mathematical models increased. The other effect of the computing revolution (on me at any rate) has been to produce a shift to modern algebra (vector/matrix analysis) as the basic tool for analysis. This is ideally suited to digital computation. A

tertiary effect has derived from the ready availability to me of sophisticated computing machinery, which I have used for the computation of many numerical examples, to illustrate both typical results and how to apply the theory.

I have continued as in the previous book, to emphasize fundamentals since, as I stated in the preface to *Dynamics of Flight—Stability and Control*, "The art of airplane and missile design is progressing so rapidly, and the configurations and flight regimes of interest are so varied that one is scarcely justified in speaking of typical configurations and typical results. Each new departure brings with it its own special problems. Engineers in this field must always be alert to discover these, and be adequately prepared to tackle them—they must be ready to discard long-accepted methods and assumptions, and to venture in new directions with confidence. The proper background for such ventures [and for such confidence] is a thorough understanding of the underlying principles and the essential techniques." To which T. Hacker (ref. 1.11) appropriately adds that some doubt should leaven the confidence and that "the effort for a thorough understanding of principles and techniques should be completed by the desire to further . . . the former and improve the latter."

Chapters 2 and 3 review the foundation in mathematics and system theory for the material that follows. Readers who are familiar with this material will find it useful for review and reference. For readers whose background has not included these topics, a study of these two chapters is essential to understanding the rest of the book. Chapters 4 and 5 continue with the building of a general mathematical model for flight vehicles and contain many explicit variations of such models. The aerodynamic side of the subject is explored next in Chapters 6 to 8, and specific applications, with many fully worked numerical illustrations, are given in Chapters 9 to 13. The example vehicles range from STOL to hypersonic. I have omitted the rather extensive appendices of data that were contained in the previous book, simply in the interests of economy. These data are now available in the USAF *Handbook of Stability and Control Methods* and the *Data Sheets* of The Royal Aeronautical Society. I also omitted, on the grounds of time and economy, a planned chapter on the dynamics of spacecraft entry into the atmosphere. However, the general equations of Chapter 5 embrace this application.

This book is written for both students and practicing engineers. Chapters 2 to 5 are not especially suited for an introductory course, but are appropriate for the more serious student who wishes to qualify as a practitioner in this field. The remaining chapters provide ample useful material for an introductory course when used in conjunction with a less rigorous development of the small-perturbation equations for the "flat-Earth" case.

I am grateful to my students, from whom I have learned so much, especially to those in my graduate course who used the manuscript as a text and who made useful suggestions. For helpful discussions, and constructive criticism, I thank P. C. Hughes, H. S. Ribner, G. F. D. Duff, and especially L. D. Reid, who wrote the first draft of Chapter 12. I received financial support from the U.S. Air Force, through AFOSR Grant No. 68-1490A, monitored by the Applied Mathematics branch.

For carrying out machine calculations I thank Terry Labrash, of the UTIAS staff, R. Lake and H. Gindl, undergraduate students and, above all, my son, David Alexander, who did the bulk of the computations in the summers while he was a high-school student.

I express my deepest gratitude to my wife, Maya, for giving up three summer vacations while I worked, and for her endless patience and constant encouragement. The encouragement and support of my daughter, Carol Elizabeth, also helped to sustain me throughout this task.

Toronto, 1971 BERNARD ETKIN

Contents

Introduction

CHAPTER 1

This book is about the *motion* of *vehicles* that *fly* in the atmosphere. As such it belongs to the branch of engineering science called applied mechanics. The three italicized words above warrant further discussion. To begin with *fly*—the dictionary definition is not very restrictive, although it implies motion through the air, the earliest application being of course to birds. However, we also say "a stone flies" or "an arrow flies," so the notion of sustention (lift) is not necessarily implied. Even the atmospheric medium is lost in "the flight of angels." We propose as a logical scientific definition that flying be defined as motion through a fluid medium or empty space. Thus a satellite "flies" through space and a submarine "flies" through the water. Note that a dirigible in the air and a submarine in the water are the same from a mechanical standpoint—the weight in each instance is balanced by buoyancy. They are simply separated by three orders of magnitude in density. By *vehicle* is meant any flying object that is made up of an arbitrary system of deformable bodies that are somehow joined together. To illustrate with some examples: (1) A rifle bullet is the simplest kind, which can be thought of as a single ideally-rigid body. (2) A jet transport is a more complicated vehicle, comprising a main elastic body (the airframe and all the parts attached to it), rotating subsystems (the jet engines), articulated subsystems (the aerodynamic controls) and fluid subsystems (fuel in tanks). (3) An astronaut attached to his orbiting spacecraft by a long flexible cable is a further complex example of the general kind of system we are concerned

with. Note that by the above definition a vehicle does not necessarily have to carry goods or passengers, although it usually does. The logic of the definitions is simply that the underlying engineering science is common to all these examples, and the methods of formulating and solving problems concerning the motion are fundamentally the same.

As is usual with definitions, we can find examples that don't fit very well. There are special cases of motion at an interface which we may or may not include in flying—for example, surface ships, hydrofoil craft and air-cushion vehicles. In this connection it is worth noting that developments of hydrofoils and ACV's are frequently associated with the Aerospace industry. The main difference between these cases, and those of "true" flight, is that the latter is essentially three-dimensional, whereas the interface vehicles mentioned (as well as cars, trains, etc.) move approximately in a two-dimensional field. The underlying principles and methods are still the same however, with certain modifications in detail being needed to treat these "surface" vehicles.

Now having defined *vehicles* and *flying*, we go on to look more carefully at what we mean by *motion*. It is convenient to subdivide it into several parts:

Gross Motion:
(i) Trajectory of the vehicle mass center.
(ii) "Attitude" motion, or rotations of the vehicle "as a whole."

Fine Motion:
(i) Relative motion of rotating or articulated sub-systems, such as engines, gyroscopes, or aerodynamic control surfaces.
(ii) Distortional motion of deformable structures, such as wing bending and twisting.
(iii) Liquid sloshing.

This subdivision is helpful both from the standpoint of the technical problems associated with the different motions, and of the formulation of their analysis. It is surely self-evident that studies of these motions must be central to the design and operation of aircraft, spacecraft, rockets, missiles, etc. To be able to formulate and solve the relevant problems, we must draw on several basic disciplines from engineering science. The relationships are shown on Fig. 1.1. It is quite evident from this figure that the practicing flight dynamicist requires intensive training in several branches of engineering science, and a broad outlook insofar as the practical ramifications of his work are concerned.

In the classes of vehicles, in the types of motions, and in the medium of flight, this book treats a restricted set of all possible cases. Its emphasis is on the flight of airplanes in the atmosphere. The general equations derived,

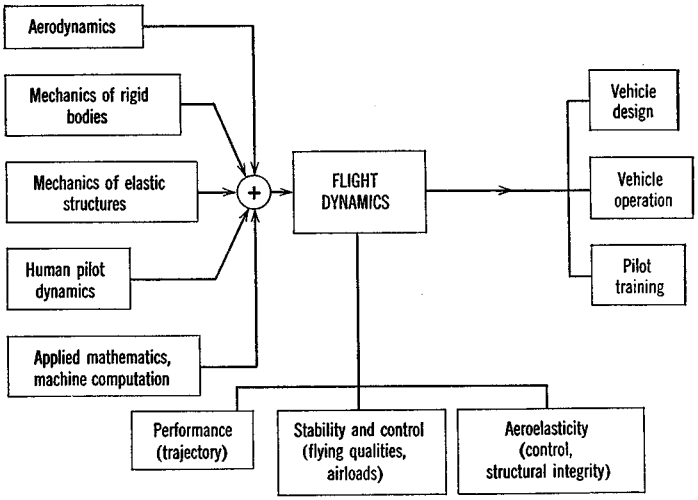

FIG. 1.1 Block diagram of disciplines.

and the methods of solution presented, are however readily modified and extended to treat the other situations that are embraced by the general problem.

All the *fundamental* science and mathematics needed to develop this subject existed in the literature by the time the Wright brothers flew. Newton, and other giants of the 18th and 19th centuries, such as Bernoulli, Euler, Lagrange, and Laplace, provided the building blocks in solid mechanics, fluid mechanics, and mathematics. The needed applications to aeronautics were made mostly after 1900 by workers in many countries, of whom special reference should be made to the Wright brothers, G. H. Bryan, F. W. Lanchester, J. C. Hunsaker, H. B. Glauert, B. M. Jones, and S. B. Gates. These pioneers introduced and extended the basis for analysis and experiment that underlies all modern practice.† This body of knowledge is well documented in several texts of that period, e.g. ref. 1.4. Concurrently, principally in the USA and Britain, a large body of aerodynamic data was accumulated, serving as a basis for practical design.

Newton's laws of motion provide the connection between environmental forces and resulting motion for all but relativistic and quantum-dynamical processes, including all of "ordinary" and much of celestial mechanics. What then distinguishes flight dynamics from other branches of applied mechanics?

† An excellent account of the early history is given in the 1970 von Kármán Lecture by C. D. Perkins (ref. 1.13).

Primarily it is the special nature of the force fields with which we have to be concerned, the absence of the kinematical constraints central to machines and mechanisms, and the nature of the control systems used in flight. The external force fields may be identified as follows:

"Strong" fields:
(i) Gravity
(ii) Aerodynamic
(iii) Buoyancy

"Weak" fields:
(iv) Magnetic
(v) Solar radiation

We should observe that two of these fields, aerodynamic and solar radiation, produce important heat transfer to the vehicle in addition to momentum transfer (force). Sometimes we cannot separate the thermal and mechanical problems (ref. 1.5). Of these fields only the strong ones are of interest for atmospheric and oceanic flight, the weak fields being important only in space. It should be remarked that even in atmospheric flight the gravity force can not always be approximated as a constant vector in an inertial frame. Rotations associated with Earth curvature, and the inverse square law, become important in certain cases of high-speed and high-altitude flight (Chapters 5 and 9).

The prediction and measurement of aerodynamic forces is the principal distinguishing feature of flight dynamics. The size of this task is illustrated by Fig. 1.2, which shows the enormous range of variables that need to be considered in connection with wings alone. To be added, of course, are the complications of propulsion systems (propellers, jets, rockets) and of compound geometries (wing + body + tail).

As remarked above, Newton's laws state the connection between force and motion. The commonest problem consists of finding the motion when the laws for the forces are given (all the numerical examples given in this book are of this kind). However we must be aware of certain important variations:

1. Inverse problems of first kind—the system and the motion are given and the forces have to be calculated.
2. Inverse problem of the second kind—the forces and the motion are given and the system constants have to be found.
3. Mixed problems—the unknowns are a mixture of variables from the force, system, and motion.

Examples of these inverse and mixed problems often turn up in research, when one is trying to deduce aerodynamic forces from the observed motion

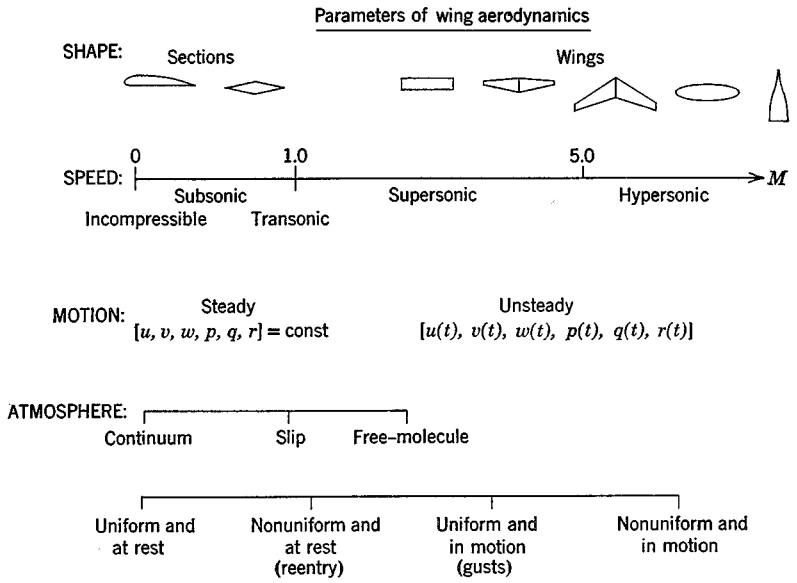

FIG. 1.2 Spectrum of aerodynamic problems for wings.

of a vehicle in flight or of a model in a wind tunnel. Another example is the deduction of harmonics of the Earth's gravity field from observed perturbations of satellite orbits. These problems are closely related to the "plant identification" or "parameter identification" problem that is of great current interest in system theory. (Inverse problems were treated in Chapter 11 of *Dynamics of Flight—Stability and Control*, but are omitted here.)

TYPES OF PROBLEMS

The main types of flight dynamics problem that occur in engineering practice are:

1. Calculation of "performance" quantities, such as speed, height, range, and fuel consumption.
2. Calculation of trajectories, such as launch, reentry, orbital and landing.
3. Stability of motion.
4. Response of vehicle to control actuation and to propulsive changes.
5. Response to atmospheric turbulence, and how to control it.
6. Aeroelastic oscillations (flutter).
7. Assessment of human-pilot/machine combination (handling qualities).

It takes little imagination to appreciate that, in view of the many vehicle types that have to be dealt with, a number of subspecialties exist within the ranks of flight dynamicists, related to some extent to the above problem categories. In the context of the modern aerospace industry these problems are seldom simple or routine. On the contrary they present great challenges in analysis, computation, and experiment.

THE TOOLS OF FLIGHT DYNAMICISTS

The tools used by flight dynamicists to solve the design and operational problems of vehicles may be grouped under three headings:

Analytical
Computational
Experimental

The analytical tools are essentially the same as those used in other branches of mechanics. Applied mathematics is the analyst's handmaiden (and sometimes proves to be such a charmer that she seduces him away from flight dynamics). One important branch of applied mathematics is what is now known as system theory, including stochastic processes and optimization. It has become a central tool for analysts. Another aspect of this subject that has received a great deal of attention in recent years is stability theory, sparked by the rediscovery in the English-speaking world of the 19th century work of Lyapunov. At least insofar as manned flight vehicles are concerned, vehicle stability per se is not as important as one might suppose. It is neither a necessary nor a sufficient condition for successful controlled flight. Good airplanes have had slightly unstable modes in some part of their flight regime, and on the other hand, a completely stable vehicle may have quite unacceptable handling qualities. It is *performance* criteria that really matter, so to expend a great deal of analytical and computational effort on finding stability boundaries of nonlinear and time-varying systems may not be really worthwhile. On the other hand, the computation of stability of small disturbances from a steady state, i.e. the linear eigenvalue problem that is normally part of the system study, is very useful indeed, and may well provide enough information about stability from a practical standpoint.

On the computation side, the most important fact is that the availability of machine computation has revolutionized practice in this subject over the past ten years. Problems of system performance, system design, and optimization that could not have been tackled at all a dozen years ago are now handled on a more or less routine basis.

The experimental tools of the flight dynamicist are generally unique to this field. First, there are those that are used to find the aerodynamic inputs.

Wind tunnels and shock tubes that cover most of the spectrum of atmospheric flight are now available in the major aerodynamic laboratories of the world. In addition to fixed laboratory equipment, there are aeroballistic ranges for dynamic investigations, as well as rocket-boosted and gun-launched free-flight model techniques. Hand in hand with the development of these general facilities has gone that of a myriad of sensors and instruments, mainly electronic, for measuring forces, pressures, temperatures, acceleration, angular velocity, etc.

Second, we must mention the flight simulator as an experimental tool used directly by the flight dynamicist. In it he studies mainly the matching of the man to the machine. This is an essential step for radically new flight situations, e.g. space capsule reentry, or transition of a tilt-wing VTOL airplane from hovering to forward speed. The ability of the pilot to control the vehicle must be assured long before the prototype stage. This cannot yet be done without test, although limited progress in this direction is being made through studies of mathematical models of human pilots. The prewar Link trainer, a rudimentary device, has evolved today into a highly complex, highly sophisticated apparatus. Special simulators, built for most new major aircraft types, provide both efficient means for pilot training, and a research tool for studying flying qualities of vehicles and dynamics of human pilots.

Analytical tools

CHAPTER 2

2.1 INTRODUCTION

This chapter contains a summary of the principal analytical tools that are used in the formulation and solution of problems of flight mechanics. Much of the content will be familiar to readers with a strong mathematical background, and they should make short work of it.

The topics treated are vector/matrix algebra, Laplace and Fourier transforms, random process theory, and machine computation. This selection is a reflection of current needs in research and industry. The vector/matrix formalism has been adopted as a principal mathematical tool because it provides a single powerful framework that serves for all of kinematics, dynamics, and system theory, and because it is at the same time a most suitable way of organizing analysis for digital computation.† The treatment is intended to be of an expository and summary nature, rather than rigorous, although some derivations are included. The student who wishes to pursue any of the topics in greater detail should consult the bibliography.

† Most computation centers have library programs for the manipulation of matrices. These are routine operations.

2.2 VECTOR/MATRIX ALGEBRA

As has already been remarked, this book is written largely in the language of matrix algebra. Since this subject is now so well covered in undergraduate mathematics courses and in numerous text books, (2.1, 2.11) we make only a few observations here.

In this treatment no formal distinction is made between vectors and matrices, the former being simply column matrices. In particular the familiar vectors of mechanics, such as force and velocity, are simply three-element column matrices. For the most part we use boldface capital letters for matrices, e.g. $\mathbf{A} = [a_{ij}]$, and boldface lower case for vectors, e.g. $\mathbf{v} = [v_j]$. The transpose and inverse are denoted by superscripts, e.g. $\mathbf{A}^T$, $\mathbf{A}^{-1}$. The scalar product then appears as

$$\mathbf{u} \cdot \mathbf{v} = \mathbf{u}^T\mathbf{v}$$

and the vector product as

$$\mathbf{u} \times \mathbf{v} = \tilde{\mathbf{u}}\mathbf{v}$$

where $\tilde{\mathbf{u}}$ is a skew-symmetric 3×3 matrix derived from the vector $\mathbf{u}$, i.e.

$$\tilde{\mathbf{u}} = \begin{bmatrix} 0 & -u_3 & u_2 \\ u_3 & 0 & -u_1 \\ -u_2 & u_1 & 0 \end{bmatrix}$$

As usual the identity matrix is denoted by

$$\mathbf{I} = [\delta_{ij}]$$

in which δ_{ij} is the Kronecker delta.

2.3 LAPLACE AND FOURIER TRANSFORMS

The quantities with which we have to deal in physical situations usually turn up naturally as functions of space and time. For example, the state or motion of a flight vehicle is a function of time, and the velocity of the atmosphere is a function of three space coordinates and time. It has been found to be very advantageous in many problems of analysis to abandon this "natural" form of the functions, and to work instead with certain "integral transforms" of them.

Table 2.1

	Fourier Series	Fourier Integral[a]	Fourier Transform[a]	One-Sided Laplace Transform
$x(t)$ defined in domain	$-T \leq t \leq T$	$-\infty \leq t \leq \infty$	$-\infty \leq t \leq \infty$	$0 \leq t \leq \infty$
Transform	$C_n = \frac{\omega_0}{2\pi} \int_{-T}^{T} x(t) e^{-in\omega_0 t}\, dt$ (2.3,1)	$C(\omega) = \frac{1}{2\pi} \int_{-\infty}^{\infty} x(t) e^{-i\omega t}\, dt$ (2.3,3)	$X(\omega) = \int_{-\infty}^{\infty} x(t) e^{-i\omega t}\, dt$ (2.3,5)	$\mathscr{L}[x(t)] = \bar{x}(s) = \int_{0}^{\infty} x(t) e^{-st}\, dt$ (2.3,7)
Inverse	$x(t) = \sum_{n=-\infty}^{\infty} C_n e^{in\omega_0 t}$ (2.3,2)	$x(t) = \int_{-\infty}^{\infty} C(\omega) e^{i\omega t}\, d\omega$ (2.3,4)	$x(t) = \frac{1}{2\pi} \int_{-\infty}^{\infty} X(\omega) e^{i\omega t}\, d\omega$ (2.3,6)	$x(t) = \frac{1}{2\pi i} \int_{c} \bar{x}(s) e^{st}\, ds$ (2.3,8)

[a] No real distinction is made in the literature between Fourier integrals and Fourier transforms. The convention adopted here makes the inverse of the former the limit of the Fourier series as $T \to \infty$, and the latter a special case of the one-sided Laplace transform in which the domain is altered and s is imaginary.

DEFINITIONS

Table 2.1 presents the common one-dimensional transforms of a function $x(t)$ and the companion "inversion formulae" or "reciprocal relations" that give the "natural" function in terms of its transform.

Multidimensional transforms are formed by successive application of these operations. (An example of this is given in Chapter 13.)

Before proceeding further with the discussion of Table 2.1, it is expedient to introduce here the step and impulse functions, which occur in the following tables of transforms.

The unit step function is (see Fig. 2.1)

$$x(t) = \mathbf{1}(t - T) \tag{2.3,9}$$

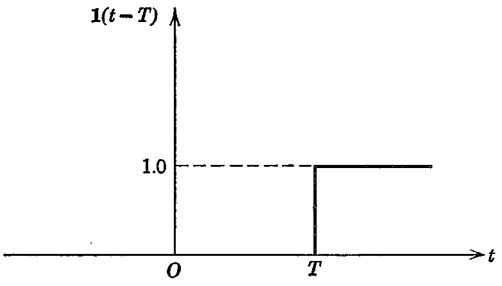

FIG. 2.1 Unit step function.

It has the values

$$x(t) = 0, \qquad t \leq T$$

$$x(t) = 1, \qquad t \geq T$$

The impulse function or delta function (more properly, the Dirac "distribution") (see Fig. 2.2) is defined to be†

$$\delta(t - T) = \lim_{\epsilon \to 0} f(\epsilon, t, T) \tag{2.3,10}$$

where $f(\epsilon, t, T)$ is for $\epsilon > 0$ a continuous function having the value zero except in the interval $T \leq t \leq T + \epsilon$ and such that its integral is unity, i.e.

$$\int_T^{T+\epsilon} f(\epsilon, t, T)\, dt = 1$$

† The limit in (2.3,10) has a rigorous meaning in the sense of distributions, despite the fact that it does not exist in the classical sense.

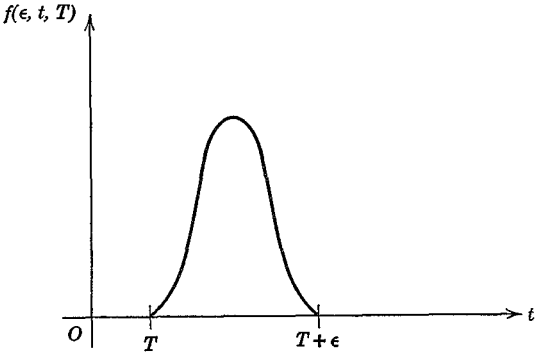

FIG. 2.2 The impulse function.

It follows that

$$\int_0^t \delta(t - T)\, dt = \mathbf{1}(t - T) \tag{2.3,11}$$

and hence that

$$\delta(t - T) = \frac{d}{dt}\,\mathbf{1}(t - T)$$

When the T is omitted from (2.3,9) and (2.3,10) it is assumed to be zero (as in Table 2.2, item 2).

Table 2.2

Some Fourier Transform Pairs

	$x(t)$	$X(\omega)$
1	$\delta(t - T)$	$e^{-i\omega T}$
2	$\delta(t)$	1
3	$e^{i\Omega t}$	$2\pi\,\delta(\omega - \Omega)$
4	1	$2\pi\,\delta(\omega)$
5	$\cos \Omega t$	$\pi[\delta(\omega + \Omega) + \delta(\omega - \Omega)]$
6	$\sin \Omega t$	$i\pi[\delta(\omega + \Omega) - \delta(\omega - \Omega)]$
7	$\frac{1}{2}\,\mathrm{sgn}\, t$	$\dfrac{1}{i\omega}$
8	$\mathbf{1}(t)$	$\dfrac{1}{i\omega} + \pi\,\delta(\omega)$

In the first column of Table 2.1 is given the complex form of the Fourier series for describing a function in the finite range $-T$ to T, in terms of fundamental circular frequency $\omega_0 = \pi/T$. The coefficients C_n are related to those of the real Fourier series

$$x(t) = \sum_{n=0}^{\infty} (A_n \cos n\omega_0 t + B_n \sin n\omega_0 t) \qquad (a) \quad (2.3,12)$$

by

$$\begin{aligned} C_n &= \tfrac{1}{2}(A_n - iB_n) \qquad n \geq 0 \\ C_n &= \tfrac{1}{2}(A_n + iB_n) \qquad n \leq 0 \end{aligned} \qquad (b)$$

and the coefficients A_n and B_n are given by

$$A_n = \frac{1}{T}\int_{-T}^{T} x(t) \cos n\omega_0 t \, dt \qquad (c)$$

$$B_n = \frac{1}{T}\int_{-T}^{T} x(t) \sin n\omega_0 t \, dt \qquad (d)$$

The amplitude of the spectral component of frequency $n\omega_0$ is

$$(A_n{}^2 + B_n{}^2)^{1/2} = 2\,|C_n| \qquad (e)$$

When $T \to \infty$, the Fourier series representation of a function $x(t)$ passes over formally to the Fourier integral representation, as given in the second column. In this limiting process

$$n\omega_0 \to \omega, \qquad \text{and} \qquad C(\omega) = \lim_{\omega_0 \to 0} \frac{C_n}{\omega_0} \qquad (2.3,13)$$

The Fourier transform that follows in the third column is essentially the same as the Fourier integral, with trivial differences in notation and the factor $1/2\pi$. In some definitions, both the transform and its inverse have the factor $1/\sqrt{2\pi}$. Some useful Fourier transforms are presented in Table 2.2.

From one mathematical viewpoint, $C(\omega)$ and $X(\omega)$ do not exist as point functions of ω for functions $x(t)$ that do not vanish at ∞. This is evidently the case for items 3 to 8 of Table 2.2. However, from the theory of distributions, these transform pairs, some of which contain the singular δ function, are valid ones (see ref. 2.3). Items 1 and 2 are easily verified by substituting $x(t)$ into (2.3,5) and items 3 to 6 by substituting $X(\omega)$ into (2.3,6). Formal integration of $x(t)$ in item 7 produces the $X(\omega)$ shown plus a periodic term of infinite frequency. The latter has no effect on the integral of $X(\omega)$, which over any range $d\omega > 0$ is $(1/i\omega)\, d\omega$. Item 8 is obtained by adding item 7 to $\frac{1}{2}$ of item 4. The one-sided Laplace transform, in the fourth column of Table 2.1, is seen to differ from the Fourier transform in the domain of t and in the fact that the complex number s replaces the imaginary number $i\omega$.

The two notations shown in (2.3,7) are used interchangeably. The curve c on which the line integral is taken in the inverse Laplace transform (2.3,8) is an infinite line parallel to the imaginary axis and lying to the right of all the poles of $\bar{x}(s)$. If its poles all lie in the left half-plane then c may be the imaginary axis and (2.3,8) reduces exactly to (2.3,6).

ONE-SIDED LAPLACE TRANSFORM†

The Laplace transform is a major conceptual and analytical tool of system theory, and hence we explore its properties in more detail below. Table 2.3 lists the Laplace transforms of a number of commonly occurring functions. It should be noted that (i) the value of the function for $t < 0$ is not relevant to $\bar{x}(s)$ and (ii) that the integral (2.3,7) may diverge for some $x(t)$ in combination with some values of s, in which case $\bar{x}(s)$ does not exist. This restriction is weak, and excludes few cases of interest to engineers. (iii) When the function is zero for $t < 0$, the Fourier transform is obtained from the Laplace transform by replacing s by $i\omega$.

TRANSFORMS OF DERIVATIVES

Given the function $x(t)$, the transforms of its derivatives can be found from (2.3,7).

$$\mathscr{L}\left[\frac{dx}{dt}\right] = \int_0^\infty e^{-st}\frac{dx}{dt}\,dt$$

$$= \int_{t=0}^{\infty} e^{-st}\,dx = xe^{-st}\Big|_{t=0}^{\infty} + s\int_0^\infty xe^{-st}\,dt$$

When $xe^{-st} \to 0$ as $t \to \infty$ (only this case is considered), then

$$\mathscr{L}\left[\frac{dx}{dt}\right] = -x(0) + s\bar{x}(s) \qquad (2.3,14)$$

where $x(0)$ is the value of $x(t)$ when $t = 0$.‡ The process may be repeated to find the higher derivatives by replacing $x(t)$ in (2.3,14) by $\dot{x}(t)$, and so on. The result is

$$\mathscr{L}\left[\frac{d^n x}{dt^n}\right] = -\frac{d^{n-1}x}{dt^{n-1}}(0) - s\frac{d^{n-2}x}{dt^{n-2}}(0) - \cdots + s^n\bar{x} \qquad (2.3,15)$$

† In the two-sided Laplace transform, the lower limit of the integral is $-\infty$ instead of zero.

‡ To avoid ambiguity when dealing with step functions, $t = 0$ should always be interpreted as $t = 0^+$.

Table 2.3
Laplace Transforms

	$x(t)$	$\bar{x}(s)$
1	$\delta(t)$	1
2	$\delta(t - T)$	e^{-sT}
3	1 or $\mathbf{1}(t)$	$\frac{1}{s}$
4	$\mathbf{1}(t - T)$	$\frac{e^{-sT}}{s}$
5	$f(t - T)\mathbf{1}(t - T)$	$e^{-sT}\mathscr{L}[f(t)]$
6	t	$\frac{1}{s^2}$
7	$\frac{t^{n-1}}{(n-1)!}$	$\frac{1}{s^n}$
8	e^{at}	$\frac{1}{s - a}$
9	$\sin at$	$\frac{a}{s^2 + a^2}$
10	$\cos at$	$\frac{s}{s^2 + a^2}$
11	te^{at}	$\frac{1}{(s - a)^2}$
12	$\frac{t^{n-1}}{(n-1)!}e^{at}$	$\frac{1}{(s - a)^n}$
13	$e^{at}\sin bt$	$\frac{b}{(s - a)^2 + b^2}$
14	$e^{at}\cos bt$	$\frac{s - a}{(s - a)^2 + b^2}$
15	$\sinh at$	$\frac{a}{s^2 - a^2}$
16	$\cosh at$	$\frac{s}{s^2 - a^2}$
17	$e^{at}\sinh bt$	$\frac{b}{(s - a)^2 - b^2}$
18	$e^{at}\cosh bt$	$\frac{s - a}{(s - a)^2 - b^2}$
19	$\dot{x}(t)$	$s\bar{x}(s) - x(0)$
20	$e^{at}x(t)$	$\bar{x}(s - a)$

TRANSFORM OF AN INTEGRAL

The transform of an integral can readily be found from that derived above for a derivative. Let the integral be

$$y = \int x(t)\, dt$$

and let it be required to find $\bar{y}(s)$. By differentiating with respect to t, we get

$$\frac{dy}{dt} = x(t)$$

whence
$$\bar{x}(s) = \mathscr{L}\left[\frac{dy}{dt}\right] = s\bar{y}(s) - y(0)$$

and
$$\bar{y}(s) = \frac{1}{s}\bar{x}(s) + \frac{1}{s}y(0) \tag{2.3,16}$$

EXTREME VALUE THEOREMS

Equation (2.3,14) may be rewritten as

$$-x(0) + s\bar{x}(s) = \int_0^\infty e^{-st}\dot{x}(t)\, dt$$
$$= \lim_{T\to\infty} \int_0^T e^{-st}\dot{x}(t)\, dt$$

We now take the limit $s \to 0$ while T is held constant, i.e.

$$-x(0) + \lim_{s\to 0} s\bar{x}(s) = \lim_{T\to\infty} \int_0^T \lim_{s\to 0} e^{-st}\dot{x}(t)\, dt$$
$$= \lim_{T\to\infty} \int_0^T \dot{x}(t)\, dt = \lim_{T\to\infty} [x(T) - x(0)]$$

Hence
$$\lim_{s\to 0} s\bar{x}(s) = \lim_{T\to\infty} x(T) \tag{2.3,17}$$

This result, known as the *final value theorem*, provides a ready means for determining the asymptotic value of $x(t)$ for large times from the value of its Laplace transform.

In a similar way, by taking the limit $s \to \infty$ at constant T, the integral vanishes for all finite $\dot{x}(t)$ and we get the *initial value theorem*.

$$\lim_{s\to\infty} s\bar{x}(s) = x(0) \tag{2.3,18}$$

2.4 APPLICATION TO DIFFERENTIAL EQUATIONS

The Laplace transform finds one of its most important uses in the theory of linear differential equations. The commonest application in airplane dynamics is to ordinary equations with constant coefficients. The technique for the general case is given in Sec. 3.2. Here we illustrate it with the simple but important example of a spring-mass-damper system acted on by an external force (Fig. 2.3). The differential equation of the system is

$$\ddot{x} + 2\zeta\omega_n\dot{x} + \omega_n{}^2x = f(t) \tag{2.4,1}$$

$2\zeta\omega_n$ is the viscous resistance per unit mass, c/m, $\omega_n{}^2$ is the spring rate per unit mass, k/m, and $f(t)$ is the external force per unit mass. The Laplace

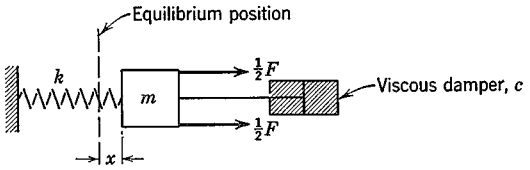

FIG. 2.3 Linear second-order system: $m\ddot{x} = F - kx - c\dot{x}$.

transform of (2.4,1) is formed by multiplying through by e^{-st} and integrating term by term from zero to infinity. This gives

$$\mathscr{L}[\ddot{x}] + 2\zeta\omega_n\mathscr{L}[\dot{x}] + \omega_n{}^2\mathscr{L}[x] = \mathscr{L}[f(t)] \tag{2.4,2}$$

Upon using the results of Sec. 2.3, this equation may be written

$$s^2\bar{x} + 2\zeta\omega_n s\bar{x} + \omega_n{}^2\bar{x} = \bar{f} + \dot{x}(0) + sx(0) + 2\zeta\omega_n x(0) \tag{2.4,3}$$

or

$$\bar{x}(s) = \frac{\bar{f} + \dot{x}(0) + (s + 2\zeta\omega_n)x(0)}{s^2 + 2\zeta\omega_n s + \omega_n{}^2} \tag{2.4,4}$$

The original differential equation (2.4,1) has been converted by the transformation into the algebraic equation (2.4,3) which is easily solved (2.4,4) to find the transform of the unknown function. In the numerator of the right-hand side of (2.4,4) we find a term dependent on the excitation ($\bar{f}$), and terms dependent on the initial conditions [$\dot{x}(0)$ and $x(0)$]. The denominator is the *characteristic polynominal* of the system. As exemplified here, finding the Laplace transform of the desired solution $x(t)$ is usually a very simple process. The heart of the problem is the passage from the transform $\bar{x}(s)$ to the function $x(t)$. Methods for carrying out the inverse transformation

are described in Sec. 2.5. Before proceeding to these, however, some general comments on the method are in order.

One of the advantages of solving differential equations by the Laplace transform is that the initial conditions are automatically taken into account. When the inverse transformation of (2.4,4) is carried out, the solution applies for the given forcing function $f(t)$ *and* the given initial conditions. By contrast, when other methods are used, a general solution is usually obtained which has in it a number of arbitrary constants. These must subsequently be fitted to the initial conditions. This process, although simple in principle, becomes extremely tedious for systems of order higher than the third. A second convenience made possible by the transform method is that in systems of many degrees of freedom, represented by simultaneous differential equations, the solution for any one variable may be found independently of the others.

2.5 METHODS FOR THE INVERSE TRANSFORMATION

THE USE OF TABLES OF TRANSFORMS

Extensive tables of transforms (like Table 2.3) have been published (see Bibliography) which are useful in carrying out the inverse process. When the transform involved can be found in the tables, the function $x(t)$ is obtained directly.

THE METHOD OF PARTIAL FRACTIONS

In some cases it is convenient to expand the transform $\bar{x}(s)$ in partial fractions, so that the elements are all simple ones like those in Table 2.3. The function $x(t)$ can then be obtained simply from the table. We shall demonstrate this procedure with an example. Let the second-order system of Sec. 2.4 be initially quiescent, i.e. $x(0) = 0$, and $\dot{x}(0) = 0$, and let it be acted upon by a constant unit force applied at time $t = 0$. Then $f(t) = \mathbf{1}(t)$, and $\bar{f}(s) = 1/s$ (see Table 2.3). From (2.4,4), we find that

$$\bar{x}(s) = \frac{1}{s(s^2 + 2\zeta\omega_n s + \omega_n 2)} \tag{2.5,1}$$

Let us assume that the system is aperiodic: i.e. that $\zeta > 1$. Then the roots of the characteristic equation are real and equal to

$$\lambda_{1,2} = n \pm \omega' \tag{2.5,2}$$

where
$$n = -\zeta\omega_n$$
$$\omega' = \omega_n(\zeta^2 - 1)^{1/2}$$

The denominator of (2.5,1) can be written in factored form so that

$$\bar{x}(s) = \frac{1}{s(s - \lambda_1)(s - \lambda_2)} \tag{2.5,3}$$

Now let (2.5,3) be expanded in partial fractions,

$$\bar{x}(s) = \frac{A}{s} + \frac{B}{(s - \lambda_1)} + \frac{C}{(s - \lambda_2)} \tag{2.5,4}$$

By the usual method of equating (2.5,3) and (2.5,4), we find

$$A = \frac{1}{\lambda_1\lambda_2}$$
$$B = \frac{1}{\lambda_1(\lambda_1 - \lambda_2)}$$
$$C = \frac{1}{\lambda_2(\lambda_2 - \lambda_1)}$$

Therefore

$$\bar{x}(s) = \frac{1/\lambda_1\lambda_2}{s} + \frac{1/\lambda_1(\lambda_1 - \lambda_2)}{s - \lambda_1} + \frac{1/\lambda_2(\lambda_2 - \lambda_1)}{s - \lambda_2}$$

By comparing these three terms with items 3 and 8 of Table 2.3, we may write down the solution immediately as

$$x(t) = \frac{1}{\lambda_1\lambda_2} + \frac{1}{\lambda_1(\lambda_1 - \lambda_2)} e^{\lambda_1 t} - \frac{1}{\lambda_2(\lambda_1 - \lambda_2)} e^{\lambda_2 t}$$
$$= \frac{1}{\omega_n{}^2}\left[1 + \frac{n - \omega'}{2\omega'} e^{(n+\omega')t} - \frac{n + \omega'}{2\omega'} e^{(n-\omega')t}\right] \tag{2.5,5}$$

HEAVISIDE EXPANSION THEOREM

When the transform is a ratio of two polynomials in s, the method of partial fractions can be generalized. Let

$$\bar{x}(s) = \frac{N(s)}{D(s)}$$

where $N(s)$ and $D(s)$ are polynomials, and the degree of $D(s)$ is higher than that of $N(s)$. Let the roots of the *characteristic equation* $D(s) = 0$ be a_r, so that

$$D(s) = (s - a_1)(s - a_2) \cdots (s - a_n)$$

Then the inverse of the transform is

$$x(t) = \sum_{r=1}^{n} \left\{ \frac{(s - a_r)N(s)}{D(s)} \right\}_{s=a_r} e^{a_r t} \tag{2.5,6}$$

The effect of the factor $(s - a_r)$ in the numerator is to cancel out the same factor of the denominator. The substitution $s = a_r$ is then made in the reduced expression.

In applying this theorem to (2.5,3), we have the three roots $a_1 = 0$, $a_2 = \lambda_1$, $a_3 = \lambda_2$, and $N(s) = 1$. With these roots, (2.5,5) follows immediately from (2.5,6).

REPEATED ROOTS

When two or more of the roots are the same, then the expansion theorem given above fails. For then, after canceling one of the repeated factors from $D(s)$ by the factor $(s - a_r)$ of the numerator, still another remains and becomes zero when s is set equal to a_r. Some particular cases of equal roots are shown in Table 2.3, items 6, 7, 11, and 12. The method of partial fractions, coupled with these entries in the table, suffices to deal conveniently with most cases encountered in stability and control work. However, for cases not conveniently handled in this way, a general formula is available for dealing with repeated roots. Equation (2.5,6) is used to find that part of the solution which corresponds to single roots. To this is added the solution corresponding to each multiple factor $(s - a_r)^m$ of $D(s)$. This is given by

$$\left[\frac{(s - a_r)^2 N(s)}{D(s)} \right]_{s=a_r} t e^{a_r t} + \left\{ \frac{d}{ds} \left[\frac{(s - a_r)^2 N(s)}{D(s)} \right] \right\}_{s=a_r} e^{a_r t} \qquad \text{for} \qquad m = 2 \tag{2.5,7}$$

and by

$$\sum_{n=0}^{m-1} \left\{ \frac{d^n}{ds^n} \left[\frac{(s - a_r)^m N(s)}{D(s)} \right] \right\}_{s=a_r} \frac{t^{m-n-1}}{n!(m - n - 1)!} e^{a_r t} \qquad \text{for} \qquad m > 2$$

2.6 RANDOM PROCESS THEORY

There are important problems in flight dynamics that involve the response of systems to random inputs. Examples are the motion of an airplane in

atmospheric turbulence, aeroelastic buffeting of the tail when it is in the wing wake, and the response of an automatically controlled vehicle to random noise in the command signal. The method of describing these random functions is the heart of the engineering problem, and determines which features of the input and the response are singled out for attention. The treatment of such functions is the subject matter of *generalized harmonic analysis*. It is not our intention to present a rigorous treatment of this involved subject here. However, a few of the more important aspects are discussed, with emphasis on the physical interpretation.

STATIONARY RANDOM VARIABLE

Consider a random variable $u(t)$, as shown in Fig. 2.4. The average value of $u(t)$ over the interval $(t_1 - T)$ to $(t_1 + T)$ depends on the mid-time t_1, and

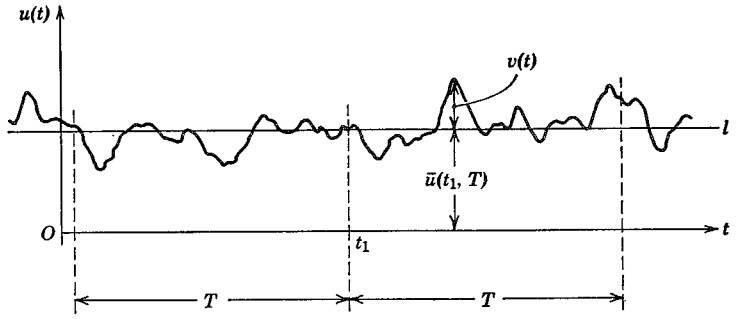

FIG. 2.4 Random variable.

the interval width,

$$\bar{u}(t_1, T) = \frac{1}{2T} \int_{t_1-T}^{t_1+T} u(t)\, dt \tag{2.6,1}$$

The function is said to have a *stationary* mean value $\bar{u}$ if the limit of $\bar{u}(t_1, T)$ as $T \to \infty$ is independent of t_1: i.e.

$$\bar{u} = \lim_{T \to \infty} \frac{1}{2T} \int_{t_1-T}^{t_1+T} u(t)\, dt \tag{2.6,2}$$

If, in addition, all other statistical properties of $u(t)$ are independent of t_1, then it is a stationary random variable. We shall be concerned here only with such functions, and, moreover, only with the deviation $v(t)$ from the mean (see Fig. 2.4). The average value of $v(t)$ is zero.

ENSEMBLE AVERAGE

In the above discussion, the *time* average of a single function was used. Another important kind of average is the *ensemble* average. Imagine that the physical situation that produced the random variable of Fig. 2.4 has been repeated many times, so that a large number of records are available as in Fig. 2.5.

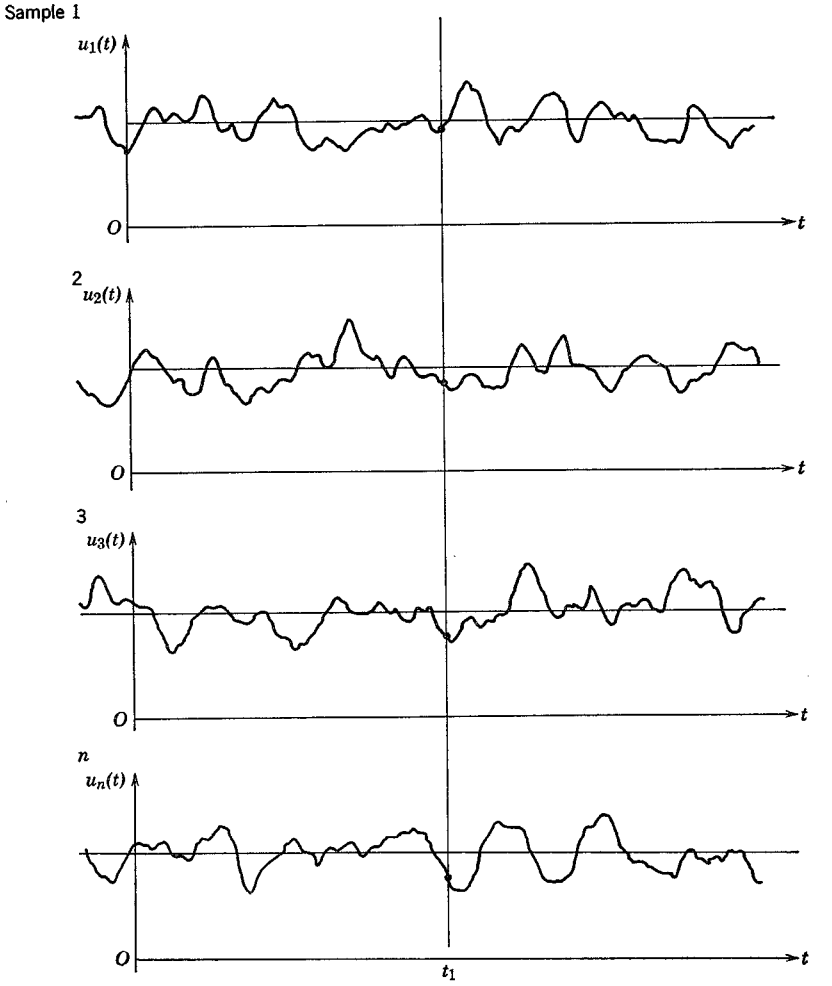

FIG. 2.5 Ensemble of random variables.

The ensemble average corresponding to the particular time t_1 is expressed in terms of the samples $u_i(t_1)$ as

$$\langle u(t_1)\rangle = \lim_{n\to\infty} \langle u(t_1, n)\rangle = \lim_{n\to\infty} \frac{1}{n} [u_1(t_1) + u_2(t_1) \cdots u_n(t_1)] \qquad (2.6,3)$$

If the process is stationary, $\langle u(t_1)\rangle = \langle u\rangle$, independent of t_1. The process is said to be *ergodic* if the ensemble and time averages are the same, i.e. $\langle u\rangle = \bar{u}$. This will be the case, for example, if the records are obtained from a single physical system with random starting conditions. In this book we are concerned only with stationary ergodic processes.

HARMONIC ANALYSIS OF $v(t)$

The deviation $v(t)$ may be represented over the interval $-T$ to T (t_1 having been set equal to zero) by the real Fourier series (2.3,12), or by its complex counterpart (2.3,2). Since $v(t)$ has a zero mean, then from (2.3,12*c*) $A_0 = 0$. Since (2.3,12*d*) shows that B_0 also is zero, it follows from (2.3,12*b*) that $C_0 = 0$ too. The Fourier series representation consists of replacing the actual function over the specified interval by the sum of an infinite set of sine and cosine waves—i.e. we have a *spectral representation* of $x(t)$. The amplitudes and frequencies of the individual components can be portrayed by a *line spectrum*, as in Fig. 2.6. The lines are uniformly spaced at the interval $\omega_0 = \pi/T$, the fundamental frequency corresponding to the interval $2T$.

The function described by the Fourier series is periodic, with period $2T$, while the random function we wish to represent is not periodic. Nevertheless, a good approximation to it is obtained by taking a very large interval $2T$. This makes the interval ω_0 very small, and the spectrum lines become more densely packed.

If this procedure is carried to the limit $T \to \infty$, the coefficients A_n, B_n, C_n all tend to zero, and this method of spectral representation of $x(t)$ fails. This limiting process is just that which leads to the Fourier integral (see 2.3,4 to 2.3,6) with the limiting value of C_n leading to $C(\omega)$ as shown by (2.3,13). A random variable over the range $-\infty < t < \infty$ does not satisfy the condition for $C(\omega)$ to exist as a point function of ω. Nevertheless, over any infinitesimal $d\omega$ there is a well-defined average value, which allows a proper representation in the form of the Fourier-Stieltjes integral

$$v(t) = \int_{\omega=-\infty}^{\infty} e^{i\omega t}\, dc \qquad (2.6,4)$$

It may be regarded simply as the limit of the sum (2.3,2) with $n\omega_0 \to \omega$ and $C_n \to dc$. Equation (2.6,4) states that we may conceive of the function

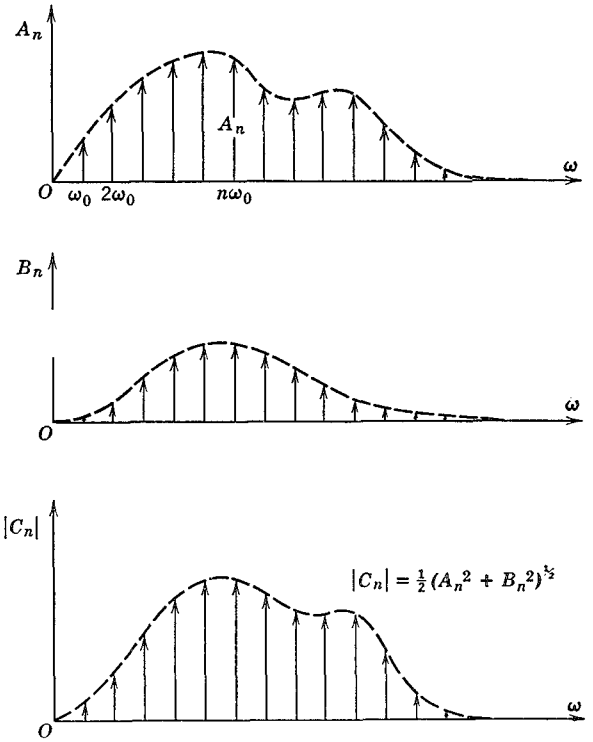

FIG. 2.6 Line spectra of a function.

$v(t)$ as being made up of an infinite sum of elementary spectral components, each of bandwidth $d\omega$, of the form e^{iwt}, i.e. sinusoidal and of amplitude dc. If the derivative $dc/d\omega$ existed, it would be the $C(\omega)$ of (2.3,4).

CORRELATION FUNCTION

The *correlation function* (or covariance) of two functions $v_1(t)$ and $v_2(t)$ is defined as

$$R_{12}(\tau) = \langle v_1(t)v_2(t + \tau)\rangle \qquad (2.6,5)$$

i.e. as the average (ensemble or time) of the product of the two variables with time separation τ. If $v_1(t) = v_2(t)$ it is called the *autocorrelation*, otherwise it is the *cross-correlation*. If $\tau = 0$ (2.6,5) reduces to

$$R_{12}(0) = \langle v_1 v_2\rangle \qquad (2.6,6)$$

and the autocorrelation to

$$R_{11}(0) = \langle v_1^2 \rangle = \overline{v_1^2} \tag{2.6,7}$$

A nondimensional form of $R(\tau)$ is the correlation coefficient

$$\hat{R}_{12}(\tau) = \frac{R_{12}(\tau)}{\bar{v}_1 \bar{v}_2} \tag{2.6,8}$$

where $\bar{v}$ indicates the root-mean-square (rms) value, $\sqrt{\overline{v^2}}$. It is obviously true from symmetry considerations that, for stationary processes, $R_{11}(\tau) = R_{11}(-\tau)$, i.e. the autocorrelation is an even function of τ. It is also generally true that for *random* variables, $R_{12}(\tau) \to 0$ as $\tau \to \infty$.

It is clear from the definition (2.6,5) that interchanging the order of v_1 and v_2 is equivalent to changing the sign of τ. That is

$$R_{12}(\tau) = R_{21}(-\tau) \tag{2.6,8a}$$

If R_{12} is an *even* function of τ, then $R_{12}(\tau) = R_{12}(-\tau)$ and $R_{12}(\tau) = R_{21}(\tau)$. If it is an *odd* function of τ, then $R_{12}(\tau) = -R_{12}(-\tau)$.

The most general case is a sum of the form

$$R_{12}(\tau) = R_{12}(\tau)_{\text{even}} + R_{12}(\tau)_{\text{odd}} \tag{2.6,8b}$$

whence $$R_{21}(\tau) = R_{12}(\tau)_{\text{even}} - R_{12}(\tau)_{\text{odd}}$$

SPECTRUM FUNCTION

The *spectrum function* is by definition the Fourier integral of $R_{12}(\tau)$, i.e.

$$\Phi_{12}(\omega) = \frac{1}{2\pi} \int_{-\infty}^{\infty} R_{12}(\tau) e^{-i\omega\tau} d\tau \tag{2.6,9}$$

and exists for all random variables in view of the vanishing of R as $\tau \to \infty$. It follows from the inversion formula (2.3,4) that

$$R_{12}(\tau) = \int_{-\infty}^{\infty} \Phi_{12}(\omega) e^{i\omega\tau} d\omega \tag{2.6,10}$$

To obtain the physical interpretation of the spectrum function, consider a special case of (2.6,10), i.e.

$$R_{11}(0) = \int_{-\infty}^{\infty} \Phi_{11}(\omega)\, d\omega$$

or by virtue of (2.6,7)

$$\overline{v_1^2} = \int_{-\infty}^{\infty} \Phi_{11}(\omega)\, d\omega \tag{2.6,11}$$

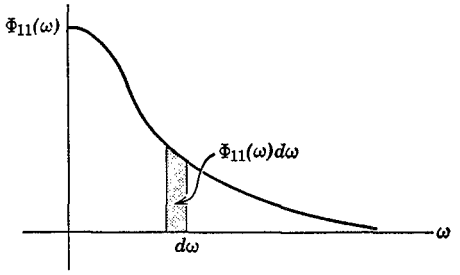

FIG. 2.7 Spectrum function.

Thus the area under the curve of the spectrum function gives the mean-square value of the random variable, and the area $\Phi(\omega)\,d\omega$ gives the contribution of the elemental bandwidth $d\omega$ (see Fig. 2.7).

In order to see the connection between the spectrum function and the harmonic analysis, consider the mean square of a function represented by a Fourier series, i.e.

$$\begin{aligned}\overline{v^2}(T) &= \frac{1}{2T}\int_{-T}^{T} v^2(t)\,dt \\ &= \frac{1}{2T}\int_{-T}^{T}\left(\sum_{n=0}^{\infty} A_n \cos n\omega_0 t + B_n \sin n\omega_0 t\right) \\ &\quad \times \left(\sum_{m=0}^{\infty} A_m \cos m\omega_0 t + B_m \sin m\omega_0 t\right) dt\end{aligned}$$

Because of the orthogonality property of the trigonometric functions, all the integrals vanish except those containing $A_n{}^2$ and $B_n{}^2$, so that

$$\overline{v^2} = \sum_{n=0}^{\infty} \tfrac{1}{2}(A_n{}^2 + B_n{}^2) \tag{2.6,12}$$

From (2.3,12*b*), $A_n{}^2 + B_n{}^2 = 4\,|C_n|^2$, whence

$$\overline{v^2} = 2\sum_{n=0}^{\infty} |C_n|^2 = \sum_{n=-\infty}^{\infty} |C_n|^2 = \sum_{n=-\infty}^{\infty} C_n^* C_n \tag{2.6,13}$$

where the * denotes, as usual, the conjugate complex number.

The physical significance of $|C_n|^2$ is clear. It is the contribution to $\overline{v^2}$ that comes from the spectral component having the frequency $n\omega_0$. We may rewrite this contribution as

$$\delta_n \overline{v^2} = \frac{C_n^* C_n}{\omega_0}\,\omega_0 \tag{2.6,14}$$

Now writing $\omega_0 = \delta\omega$ and interpreting $\delta\overline{v^2}$ as the contribution from the band width $(n - \frac{1}{2})\omega_0 \leq \omega \leq (n + \frac{1}{2})\omega_0$, we have

$$\delta_n\overline{v^2} = \frac{C_n^* C_n}{\omega_0}\,\delta\omega \tag{2.6,15}$$

The summation of these contributions for all n is $\overline{v^2}$, and by comparison with (2.6,11) we may identify the spectral density as

$$\Phi_{11}(\omega) = \lim_{\omega_0 \to 0} \frac{C_n^* C_n}{\omega_0} \tag{2.6,16}$$

More generally, for the cross spectrum of v_i and v_j;

$$\Phi_{ij}(\omega) = \lim_{\omega_0 \to 0} \frac{C_{i_n}^* C_{j_n}}{\omega_0} \tag{2.6,17}$$

Now in many physical processes v^2 can be identified with instantaneous power, as when v is the current in a resistive wire or the pressure in a plane acoustic wave. Generalizing from such examples, $v^2(t)$ is often called the instantaneous power, $\overline{v^2}$ the average power, and $\Phi_{11}(\omega)$ the *power spectral density*. By analogy $\Phi_{12}(\omega)$ is often termed the *cross-power spectral density*.

From (2.6,9), and the symmetry properties of R_{12} given by (2.6,8*b*), and by noting that the real and imaginary parts of $e^{-i\omega\tau}$ are also respectively even and odd in τ it follows easily that

$$\Phi_{12}(\omega) = \Phi_{21}^*(\omega) \tag{2.6,17a}$$

The result given in (2.6,17) is sometimes expressed in terms of Fourier transforms of truncated functions as follows. Let $v_i(t; T)$ denote the truncated function

$$\begin{aligned} v_i(t;T) &= v_i(t) \quad \text{for } |t| \leq T \\ v_i(t;T) &= 0 \qquad \text{for } |t| > T \end{aligned} \tag{2.6,18}$$

and let $$V_i(\omega; T) = \int_{-\infty}^{\infty} v_i(t; T) e^{-i\omega t}\,dt = \int_{-T}^{T} v_i(t) e^{-i\omega t}\,dt \tag{2.6,19}$$

be the associated Fourier transform. Comparing (2.6,19) with (2.3,1) in Table 2.1 ($\omega = n\omega_0$) we see that

$$C_{i_n} = \frac{\omega_0}{2\pi} V_i(n\omega_0; T) \tag{2.6,20}$$

Hence from (2.6,17) we get

$$\Phi_{ij}(\omega) = \lim_{\omega_0 \to 0} \frac{\omega_0}{4\pi^2} V_i^*(n\omega_0; T) \cdot V_j(n\omega_0; T) \tag{2.6,21}$$

On substitution of $\omega_0 = \pi/T$ and $\omega = n\omega_0$, this becomes finally,

$$\Phi_{ij}(\omega) = \lim_{T\to\infty} \frac{1}{4\pi T} V_i^*(\omega; T) V_j(\omega; T) \tag{2.6,22}$$

The special case of power spectral density is given by

$$\Phi_{ii}(\omega) = \lim_{T\to\infty} \frac{1}{4\pi T} |V_i(\omega; T)|^2 \tag{2.6,22a}$$

CORRELATION AND SPECTRUM OF A SINUSOID

The autocorrelation of a sine wave of amplitude a and frequency Ω is given by

$$R(\tau) = \lim_{T\to\infty} \frac{a^2}{2T} \int_{-T}^{T} \sin \Omega t \sin (\Omega t + \Omega\tau)\, dt$$

After integrating and taking the limit, the result is the cosine wave

$$R(\tau) = \frac{a^2}{2} \cos \Omega\tau \tag{2.6,23}$$

It follows that the spectrum function is $1/2\pi$ times the Fourier transform of (2.6,23), which from Table 2.2 is

$$\Phi(\omega) = \frac{a^2}{4} [\delta(\omega + \Omega) + \delta(\omega - \Omega)] \tag{2.6,23a}$$

i.e. a pair of spikes at frequencies $\pm\Omega$.

PROBABILITY PROPERTIES OF RANDOM VARIABLES

An important goal in the study of random processes is to predict the probability of a given event—for example, in flight through turbulence, the occurrence of a given bank angle, or vertical acceleration. In order to achieve this aim, more information is needed than has been provided above in the spectral representation of the process and we must go to a probabilistic description.

Consider an infinite set of values of $v(t_1)$ sampled over an infinite ensemble of the function. The *amplitude* distribution or *probability density* of this set is then expressed by the function $f(v)$, Fig. 2.8*a*, defined such that the $\lim_{\Delta v\to 0} f(v)\, \Delta v$ is the fraction of all the samples that fall in the range Δv. This fraction is then given by the area of the strip shown. It follows that

$$\int_{-\infty}^{\infty} f(v)\, dv = 1 \tag{2.6,24}$$

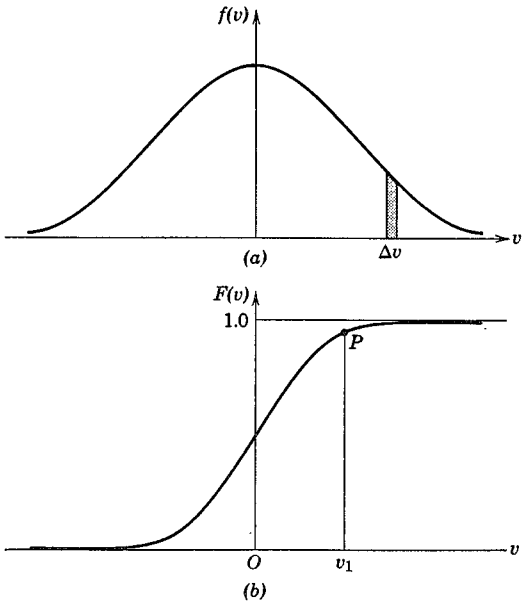

FIG. 2.8 Distribution functions. (*a*) Probability density function. (*b*) Cumulative distribution.

The cumulative distribution is given by

$$F(v) = \int_{-\infty}^{v} f(v)\, dv \tag{2.6,24a}$$

and is illustrated in Fig. 2.8*b*. The ordinate at P gives the fraction of all the samples that have values $v < v_1$. The distribution that we usually have to deal with in turbulence and noise is the *normal* or *Gaussian* distribution, given by

$$f(v) = \frac{1}{\sigma\sqrt{2\pi}} \exp\left(-\frac{v^2}{2\sigma^2}\right) \tag{2.6,25}$$

where σ is the standard deviation or variance of v, and is exactly the rms value used in (2.6,8)

$$\sigma = \bar{\bar{v}} \tag{2.6,26}$$

Note that σ can be computed from either the autocorrelation (2.6,7) or the spectrum function (2.6,11).

MEAN VALUE OF A FUNCTION OF *v*

Let $g(v)$ be any function of v. Then if we calculate all the values g_n associated with all the samples $v_n(t_1)$ referred to above we can obtain the ensemble

mean $\langle g \rangle$. Now it is clear that of all the samples the fraction that falls in the infinitesimal range $g_i \leq g \leq g_i + \Delta g$ corresponding to the range of v $v_i \leq v \leq v_i + \Delta v$ is $f(v_i)\,\Delta v$. If now we divide the whole range of g into such equal intervals Δg the mean of g is clearly

$$\langle g \rangle = \lim_{\Delta v \to 0} \sum_{i=1}^{\infty} g_i f(v_i)\,\Delta v$$

or

$$\langle g \rangle = \int_{-\infty}^{\infty} g(v) f(v)\,dv \tag{2.6,27}$$

Equation (2.6,27) is of fundamental importance in the theory of probability. From it there follow at once the formulae for the *moments* of the distributions:

$$\langle v \rangle = \int_{-\infty}^{\infty} v f(v)\,dv = \text{1st moment of } f \tag{2.6,28a}$$

or

$$\langle v^2 \rangle = \int_{-\infty}^{\infty} v^2 f(v)\,dv = \text{2nd moment of } f \tag{2.6,28b}$$

$$\langle v^n \rangle = \int_{-\infty}^{\infty} v^n f(v)\,dv = n\text{th moment of } f \tag{2.6,28c}$$

For the particular case we have been discussing, $\langle v \rangle = 0$ and $\langle v^2 \rangle = \sigma^2$.

JOINT PROBABILITY

Let $v_1(t)$ and $v_2(t)$ be two random variables, with probability distributions $f_1(v_1)$ and $f_2(v_2)$. The *joint probability* distribution is denoted $f(v_1, v_2)$, and is defined like $f(v)$. Thus $f(v_1, v_2)\,\Delta S$ is the fraction of an infinite ensemble of pairs (v_1, v_2) that fall in the area ΔS of the v_1, v_2 plane (see Fig. 2.9). If v_1 and v_2 are independent variables, i.e. if the probability $f(v_1)$ is not dependent in any way on v_2, and vice versa, the joint probability is simply the product of the separate probabilities

$$f(v_1, v_2) = f_1(v_1) f_2(v_2) \tag{2.6,29}$$

From the theorem for the mean, (2.6,27) the correlation of two variables can be related to the joint probability. Thus

$$R_{12} = \langle v_1 v_2 \rangle = \iint_{-\infty}^{\infty} v_1 v_2 f(v_1, v_2)\,dv_1\,dv_2 \tag{2.6,30}$$

For independent variables, we may use (2.6,29) in (2.6,30) to get

$$R_{12} = \int_{-\infty}^{\infty} v_1 f(v_1)\,dv_1 \times \int_{-\infty}^{\infty} v_2 f(v_2)\,dv_2$$
$$= \langle v_1 \rangle \langle v_2 \rangle$$

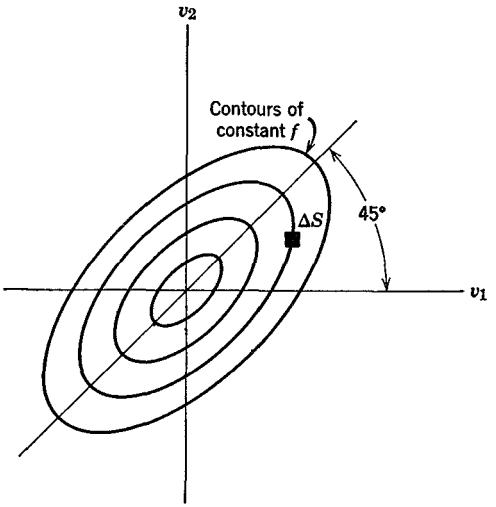

FIG. 2.9 Bivariate distribution.

and is zero if either variable has a zero mean. Thus statistical independence implies zero correlation, although the reverse in not generally true.

The general form for the joint probability of variables that are separately normally distributed, and that are not necessarily independent is

$$f(v_1, v_2 \cdots v_n) = \frac{1}{(2\pi)^{n/2} |\mathbf{M}|^{1/2}} \exp\left(-\tfrac{1}{2} n_{ij} v_i v_j\right) \qquad (2.6,31)$$

where $|\mathbf{M}|$ is the determinant of the matrix of second moments:

$$\mathbf{M} = [m_{ij}]$$
$$m_{ij} = \langle v_i v_j \rangle$$
$$\mathbf{N} = [n_{ij}] = \mathbf{M}^{-1}$$

For two variables this yields the *bivariate normal distribution* for which

$$\mathbf{M} = \begin{bmatrix} \sigma_1^2 & R_{12} \\ R_{12} & \sigma_2^2 \end{bmatrix}$$
$$|\mathbf{M}| = \sigma_1^2 \sigma_2^2 - R_{12}^2$$
$$\mathbf{M}^{-1} = \frac{1}{|\mathbf{M}|} \begin{bmatrix} \sigma_2^2 & -R_{12} \\ -R_{12} & \sigma_1^2 \end{bmatrix} \qquad (2.6,32)$$

and $$f(v_1, v_2) = \frac{1}{2\pi(\sigma_1^2\sigma_2^2 - R_{12}^2)^{1/2}} \exp\left(-\frac{1}{2}\frac{\sigma_2^2 v_1^2 - 2R_{12}v_1v_2 + \sigma_1^2 v_2^2}{\sigma_1^2\sigma_2^2 - R_{12}^2}\right)$$

If v_1 and v_2 are the values of $v(t)$ at two times, e.g.

$$v_1 = v(t)$$
$$v_2 = v(t + \tau)$$

Then $\sigma_1^2 = \sigma_2^2 = \sigma^2$, $R_{12} = R(\tau)$ [see (2.6,5)] and the joint probability is a function of the parameter τ, viz.

$$f(v_1, v_2; \tau) = \frac{1}{2\pi(\sigma^4 - R^2(\tau))^{1/2}} \exp\left(-\frac{1}{2}\frac{\sigma^2(v_1^2 + v_2^2) - 2v_1v_2R(\tau)}{\sigma^4 - R(\tau)^2}\right) \tag{2.6,33}$$

The inverse relation, from the theorem for the mean value is

$$R(\tau) = \int_{-\infty}^{\infty}\int v_1v_2 f(v_1, v_2; \tau)\, dv_1\, dv_2 \tag{2.6,34}$$

As shown in Fig. 2.9, the principal axes of the figure formed by the contours of constant f for given $R(\tau)$ are inclined at 45°. The contours themselves are ellipses.

JOINT DISTRIBUTION OF A FUNCTION AND ITS SLOPE

We shall require the joint distribution function $f(v, \dot{v}; 0)$ for a function $v(t)$ that has a normal distribution. The correlation of v and $\dot{v}$ is

$$R_{v\dot{v}}(\tau) = \lim_{T\to\infty} \frac{1}{2T}\int_{-T}^{T} v(t)\dot{v}(t + \tau)\, dt$$

In particular, when $\tau = 0$

$$R_{v\dot{v}}(0) = \lim_{T\to\infty} \frac{1}{2T}\int_{-T}^{T} v\frac{dv}{dt}\, dt$$
$$= \lim_{T\to\infty} \frac{1}{2T}\int_{-T}^{T} \tfrac{1}{2}dv^2 = \lim_{T\to\infty} \frac{1}{4T}[v^2(T) - v^2(-T)] \tag{2.6,35}$$

which is zero for a finite stationary variable. It follows therefore from (2.6,33) that $f(v, \dot{v}; 0)$ reduces to the product form of two statistically independent functions, i.e.

$$f(v, \dot{v}; 0) = f_1(v) \cdot f_2(\dot{v})$$
$$= \frac{1}{2\pi\sigma_1\sigma_2} \exp\left(-\frac{v^2}{2\sigma_1^2} - \frac{\dot{v}^2}{2\sigma_2^2}\right) \tag{2.6,36}$$

To evaluate f we need only the two variances. $\sigma_1 = \bar{v}$ we have pointed out previously can be found from either $R_{11}(\tau)$ or $\Phi_{11}(\omega)$. To find $\sigma_2 = \bar{\dot{v}}$ we have recourse to the spectral representation (2.6,4), from which it follows that

$$\dot{v}(t) = \int_{\omega=-\infty}^{\infty} i\omega e^{i\omega t}\, dc \tag{2.6,37}$$

From this we deduce that the complex amplitude of a spectral component of $\dot{v}$ is $i\omega$ times the amplitude of the same component of v. From (2.6,15) it then follows that the spectrum function for $\dot{v}$ is related to that for v by

$$\Phi_{\dot{v}\dot{v}}(\omega) = \omega^2 \Phi_{vv}(\omega) \tag{2.6,38}$$

and finally that

$$\sigma_2{}^2 = \langle \dot{v}^2 \rangle = \int_{-\infty}^{\infty} \Phi_{\dot{v}\dot{v}}(\omega)\, d\omega = \int_{-\infty}^{\infty} \omega^2 \Phi_{vv}(\omega)\, d\omega \tag{2.6,39}$$

Thus it appears that the basic information required in order to calculate $f(v, \dot{v})$ is the power spectral density of v, $\Phi_{vv}(\omega)$. From it we can get both $\langle v^2 \rangle$ and $\langle \dot{v}^2 \rangle$ and hence $f(v, \dot{v}; 0)$.

The autocorrelation of $\dot{v}$ can be related simply to that of v as follows. Consider the derivative of $R(\tau)$

$$\frac{d}{d\tau} R_{vv}(\tau) = \frac{d}{d\tau} \langle v(t) v(t + \tau) \rangle$$

Since the differential and averaging operations are commutative their order may be interchanged to give

$$\begin{aligned} \frac{d}{d\tau} R_{vv}(\tau) &= \left\langle v(t) \frac{\partial}{\partial \tau} v(t + \tau) \right\rangle \\ &= \langle v(t) \dot{v}(t + \tau) \rangle \end{aligned}$$

Now let $(t + \tau) = u$, so that

$$\frac{d}{d\tau} R_{vv}(\tau) = \langle v(u - \tau) \dot{v}(u) \rangle$$

We now differentiate again at constant u, to get

$$\begin{aligned} \frac{d^2}{d\tau^2} R_{vv}(\tau) &= \left\langle \frac{\partial}{\partial \tau} v(u - \tau) \dot{v}(u) \right\rangle \\ &= -\langle \dot{v}(u - \tau) \dot{v}(u) \rangle \\ &= -R_{\dot{v}\dot{v}}(\tau) \end{aligned}$$

i.e.

$$R_{\dot{v}\dot{v}}(\tau) = -\frac{d^2}{d\tau^2} R_{vv}(\tau) \tag{2.6,40}$$

ORDINATE-CROSSING RETURN PERIOD

With reference to Fig. 2.10, let us define an "event" as a crossing of the random curve through the strip Δv at v. The time Δt associated with a single event that has a slope in the range $\Delta \dot{v}$ is

$$\Delta t = \frac{\Delta v}{|\dot{v}|}$$

During a total time $T \to \infty$, the portion spent in the domain Δv, $\Delta \dot{v}$ of the $(v, \dot{v})$ space is

$$\Delta T = Tf(v, \dot{v})\, \Delta v\, \Delta \dot{v}$$

Hence, the total number of events with slopes in the range $\Delta \dot{v}$ in the time T

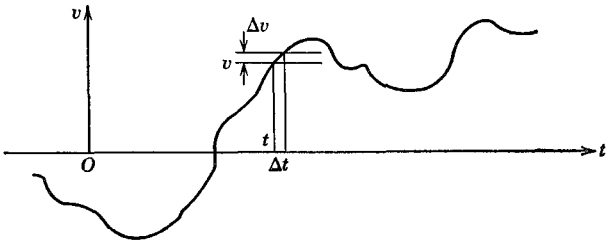

FIG. 2.10 Upward crossing at level v.

must be $\Delta T/\Delta t$, and the average number per unit time is

$$dN(v, \dot{v}) = \frac{1}{T}\frac{\Delta T}{\Delta t} = |\dot{v}|\, f(v, \dot{v})\, \Delta \dot{v}$$

On passing to the limit $\Delta v \to 0$ and integrating we get

$$N(v) = \int_{-\infty}^{\infty} f(v, \dot{v})\, |\dot{v}|\, d\dot{v} \tag{2.6,41}$$

When (2.6,36) is substituted into (2.6,41) the result of integration is:

$$N(v) = \frac{1}{\pi}\frac{\sigma_2}{\sigma_1} e^{-v^2/2{\sigma_1}^2}$$

and

$$N(0) = \frac{1}{\pi}\frac{\sigma_2}{\sigma_1} \tag{2.6,42}$$

whence

$$N(v) = N(0)e^{-v^2/2{\sigma_1}^2}$$

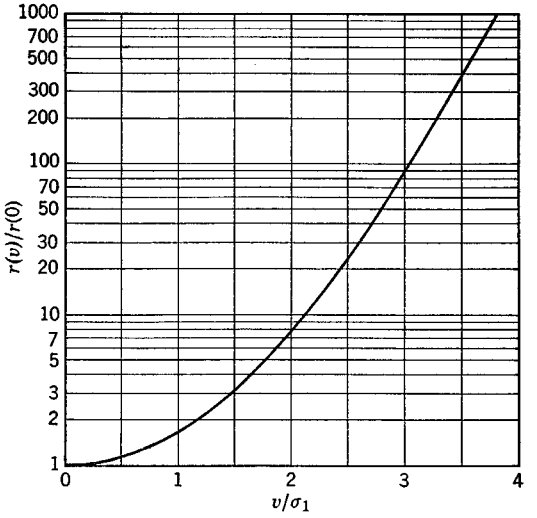

FIG. 2.11 Return period.

Since $N(v)$ includes both upward and downward crossings, the average number of upward crossings, or "positive events" is

$$N_+(v) = \tfrac{1}{2}N(v) = \frac{1}{2\pi}\frac{\sigma_2}{\sigma_1}e^{-v^2/2{\sigma_1}^2} \tag{2.6,43}$$

The average interval between positive events is called the *return period.*

$$r(v) = \frac{1}{N_+(v)} = 2\pi\frac{\sigma_1}{\sigma_2}e^{v^2/2{\sigma_1}^2} \tag{2.6,44}$$

which is plotted in Fig. 2.11.

DISTRIBUTION OF PEAKS

It is observed that for the larger values of v most, but not all, local maxima are immediately preceded by a positive event as defined above. This is illustrated in Fig. 2.4 where the events are defined by the line l. Thus (2.6,43) can also be interpreted as a good approximation to the number of peaks per unit time that are greater than v. It follows that the distribution of peaks per unit time is given approximately by

$$f_p(v) \doteq -\frac{dN_+(v)}{dv} = \frac{1}{2\pi}\frac{\sigma_2}{{\sigma_1}^3}ve^{-v^2/2{\sigma_1}^2} \tag{2.6,45}$$

and has the form shown on Fig. 2.12.

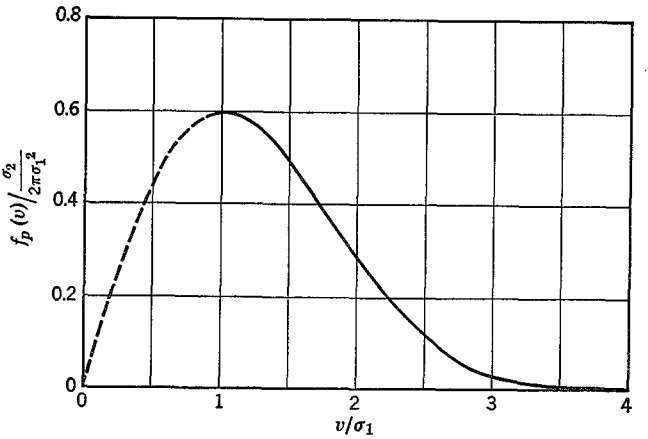

FIG. 2.12 Distribution of peaks per unit time.

PROBABILITY OF A POSITIVE EVENT DURING TIME t_1

We now wish to find the probability that a positive event, as defined above, will occur in a given time t_1. Let t_1 be divided into a sequence of equal intervals Δt such that the following two conditions are met

(i) $\Delta t \ll r(v)$

(ii) The probability of an event during any particular interval Δt is independent of whether an event has occurred in any previous interval. (See below for discussion of this condition.)

Since $N_+(v)$ gives the average time density of events, then the probability of an event in Δt is (for $\Delta t \to 0$)

$$p(v, \Delta t) = \Delta t N_+(v) = \frac{\Delta t}{r(v)} \tag{2.6,46}$$

and the probability that there will be *no* event in Δt is

$$q(v, \Delta t) = 1 - p = 1 - \frac{\Delta t}{r(v)} \tag{2.6,47}$$

Hence the probability that there is no event in n successive intervals is, by virtue of condition (ii) above,

$$q(v, n\Delta t) = \left(1 - \frac{\Delta t}{r(v)}\right)^n$$

If a positive event is identified with "failure" of a system, then clearly $q(v, n\,\Delta t)$ is the probability of "survival"† for a time $t_1 = n\,\Delta t$, i.e.

$$q(v, t_1) = \left(1 - \frac{t_1}{nr(v)}\right)^n \tag{2.6,48}$$

Hence the probability of failure is

$$p(v, t_1) = 1 - q(v, t_1) = 1 - \left(1 - \frac{t_1}{nr(v)}\right)^n \tag{2.6,49}$$

For large times t_1 (the usual practical case) n may be very large and the term in parentheses may be represented by its limit

$$\lim_{n\to\infty}\left(1 - \frac{a}{n}\right)^n = e^{-a} \tag{2.6,50}$$

so that the survival probability is

$$q(v, t_1) = e^{-t_1/r(v)} \tag{2.6,51a}$$

and the failure probability is

$$p(v, t_1) = 1 - e^{-t_1/r(v)} \tag{2.6,51b}$$

This result is general, and can be applied for any stationary random process. If the process is the Gaussian one previously discussed, then $r(v)$ is given by (2.6,44), and (2.6,51*b*) becomes

$$p(v, t_1) = 1 - \exp\left[-\frac{t_1}{r(0)}\, e^{-v^2/2\sigma_1^2}\right] \tag{2.6,52}$$

Equations (2.6,51*b*) and (2.6,52) are plotted in Fig. 2.13. It should be noted that the probability of failure associated with $t_1 = r$ is $(1 - 1/e)$ or 0.63, and that the curves in (*b*) fall rather steeply over a fairly narrow range of v. Equation (2.6,51*a*) is a particular case of the Poisson distribution, for zero events in a time t_1.

† A more rigorous treatment of survival probability covering nonstationary and non-Gaussian processes is given by Rice and Beer (ref. 2.8) and is applied to launch vehicles by Beer and Lennox (ref. 2.9).

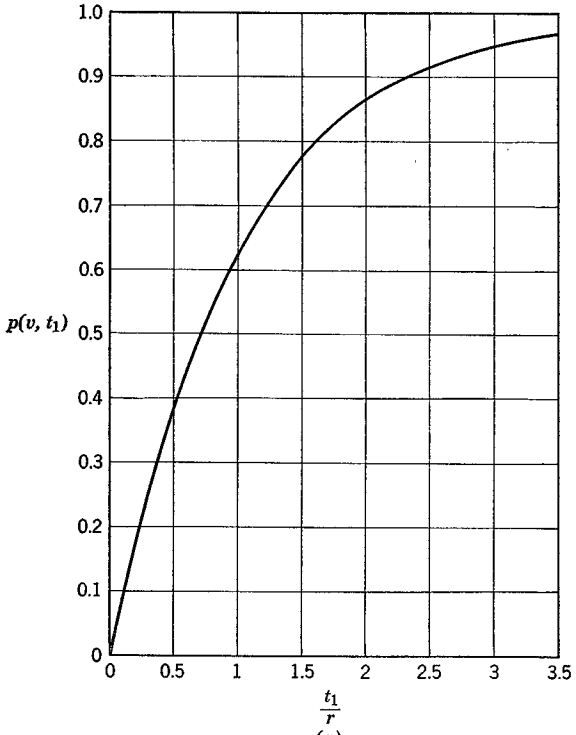
1.0
0.9
0.8
0.7
0.6
0.5
0.4
0.3
0.2
0.1
0
$p(v, t_1)$
0
0.5
1
1.5
2
2.5
3
3.5
$\frac{t_1}{r}$

(a)

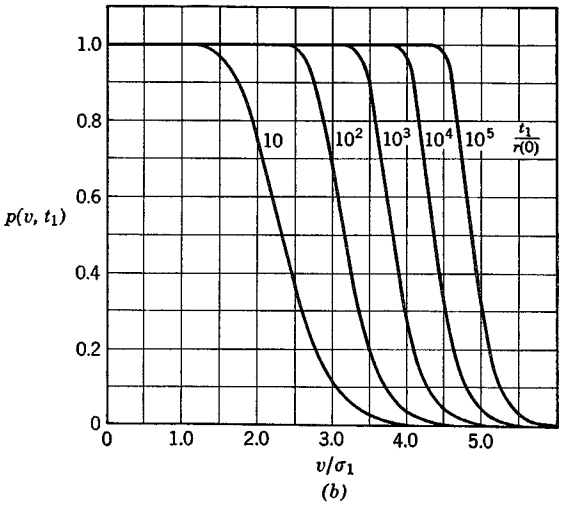
1.0
0.8
0.6
0.4
0.2
0
$p(v, t_1)$
10
10^2
10^3
10^4
10^5
$\frac{t_1}{r(0)}$
0
1.0
2.0
3.0
4.0
5.0
v/σ_1

(b)

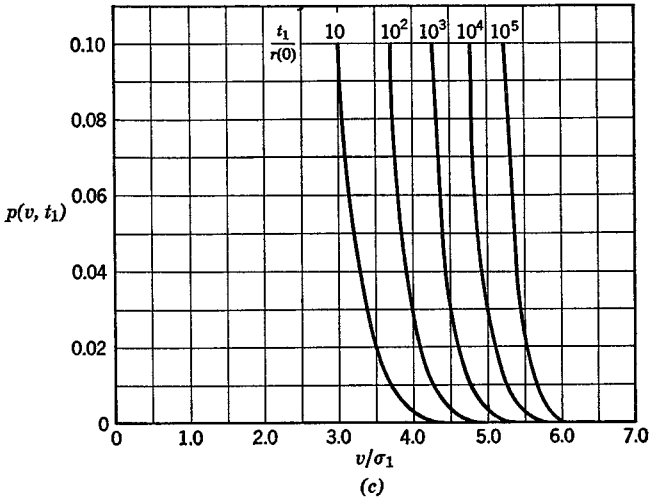

FIG. 2.13 Failure probability.

DISCUSSION OF CONDITION (ii)

We return now to the condition of statistical independence of adjacent intervals. This implies that the joint probability $f(v_1, v_2) = f(v_1)f(v_2)$ where v_1 and v_2 are values of the variable during two adjacent intervals $\Delta_1 t$ and $\Delta_2 t$, as illustrated in Fig. 2.14. We saw [following (2.6,30)] that statistical independence implies zero correlation. In the present context we may *infer* statistical independence from zero correlation. Thus we require that

$$R_{v_1 v_2} = \overline{v_1 v_2} = 0 \tag{2.6,53}$$

the average being taken over the range $0 \leq t' \leq \Delta t$. Now if we define a *characteristic correlation time by*

$$\tau^* = \frac{1}{\langle v^2 \rangle} \int_0^\infty R(\tau)\, d\tau \tag{2.6,54}$$

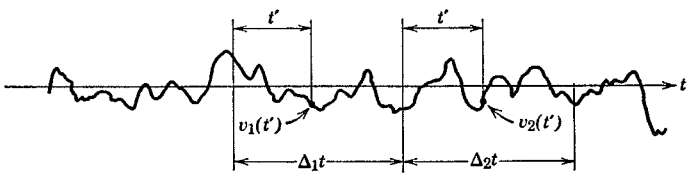

FIG. 2.14

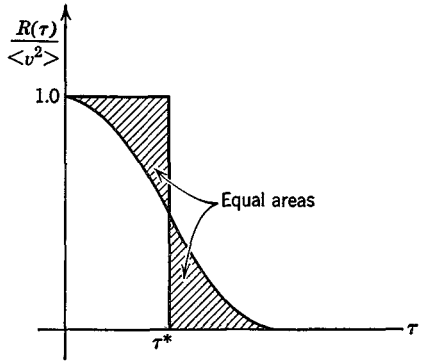

FIG. 2.15 Characteristic correlation time.

as illustrated in Fig. 2.15, and require that $\Delta t \gg \tau^*$, then it is evident that condition (2.6,53) will be satisfied. Since the present results will normally be of interest only for large r and large t_1, this condition can be met while still keeping n very large.†

2.7 MACHINE COMPUTATION

This section deals with a topic that does not belong to the *theory* of flight dynamics, but is of transcendent importance, overshadowing all else, when it comes to *application* of the theory. That topic is the use of computing machines for the solution of equations and the simulation of systems. Without them modern aerospace vehicles and missions could probably not be designed and analyzed at all within practical limitations; with them there is virtually no practical problem in flight dynamics that cannot be solved.

Except when the most extreme simplifications are employed, the equations of flight dynamics are quite complicated, and considerable labor must be expended in their solution. The labor is especially heavy during the design and development of a new vehicle, for then the solutions must be repeated many times, with different values of the parameters that define the vehicle and the flight condition. The process is more or less continuous, in that, as the design progresses, changes are constantly made, improved estimates of the aerodynamic parameters become available from wind-tunnel testing, aeroelastic calculations are refined, and testing of control-system and guidance components provides accurate data on their performance. Recalculation is required at many stages to include these improvements in the data. The number of computing man-hours involved in this procedure for a modern

† For example, when applied to flight through turbulence, t_1 corresponds to the total distance flown, and τ^* corresponds to the "scale" of the turbulence.

aerospace vehicle would be astronomical if all the computations had to be performed by hand (i.e. with slide rule or desk computer).

In addition to merely making it *possible* to carry out the minimum amount of analysis that is essential to the achievement of a successful design, the great speed and flexibility of computing machines have led to other important advantages. With them it is feasible to conduct elaborate design studies in which many parameters are varied in order to optimize the design, i.e. to find the best compromise between various conflicting requirements. Another advantage is that the analysis can be much more accurate, in that fewer simplifications and approximations need be made (e.g. more degrees of freedom can be retained).

Among the most important points in this connection is the possibility of retaining nonlinearities in the equations. Adequate analytical methods of dealing with nonlinear systems either do not exist or are too cumbersome for routine application. By contrast, computing machines permit the introduction of squares and products of variables, transcendental functions, backlash (dead space), dry friction (stick-slip), experimental curves, and other nonlinear features with comparative ease. They go even further, in making possible the introduction into the computer setup of actual physical components, such as hydraulic or electric servos, control surfaces, human pilots, and autopilots. This technique is, of course, superior in accuracy to any analytical representation of the dynamic characteristics of these elements. The ultimate in this type of "computing" involves the use of the whole airplane in a ground test, with only the airframe aerodynamics simulated by the computer. A human pilot can be incorporated in such tests for maximum realism. A related development is the flight simulator as used for pilot training and research on handling qualities (see Chapter 12). It is basically a computer simulation of a given airplane, incorporating a replica of the cockpit and all the controls and instruments. The pilot "flying" the simulator experiences in a more or less realistic fashion the characteristic responses of the simulated vehicle. Such simulators or trainers have been used to great advantage in reducing the flight time required for pilot training on new vehicle types.

Digital machine computation is, of course, part of the training of all engineering students, and we assume the necessary background in that subject. Analog computation however is not so universally taught, and many students who come to the study of flight dynamics have had no prior experience with it. These we refer to refs. 2.6, 2.7, and 2.12. As a further aid, one example of analog computation is presented rather fully in Sec. 10.2.

System Theory

CHAPTER 3

3.1 CONCEPTS AND TERMINOLOGY

The branch of modern engineering analysis known as *system theory* is highly relevant to the study of the flight of vehicles in the atmosphere and in space. The word *system* has long been current in such applications as "control system," "navigation system," and "hydraulic system." In our present context we identify the vehicle itself as a system, of which the above examples are subsidiary systems, or associated systems.

We do not attempt to offer here a precise definition† of a system—suffice it to say that it is an element, or an interconnected set of elements that is clearly identifiable and that has a *state* defined by the values of a set of variables that characterize its instantaneous condition. The elements may be physical objects or devices, or they may be purely mathematical, i.e. equations expressing relationships among the variables. In the case of a physical system, the governing equations may or may not be known. A set of equations that constitutes a *mathematical model* of a physical system, is a *mathematical system* that is a more or less faithful image of the physical system, depending on the assumptions and approximation contained therein. The set of n variables that defines the state of the system is the *state vector*,

† See for example ref. 3.1, Sec. 1.10.

and the corresponding n-dimensional space is the state space. Some or all of the state variables, or quantities derived from them, are arbitrarily termed, according to the circumstances of the experiment or analysis, as *outputs*. The exact specification of a system is usually arbitrary, as will be seen in the following example; the "boundary" of the system under consideration in any given circumstance is chosen by the analyst or experimenter to suit his purpose.

In addition to the state variables, there is usually associated with a system a second set of variables called *inputs*. These are actions upon the system the physical origins of which are outside the system. Some of these are independent of the state of the system, being determined by processes entirely external to it; these are the nonautonomous inputs. Others, the *autonomous* inputs, have values fixed by those of the state variables themselves, owing to internal interconnections or feedbacks, or a as result of environmental fields (e.g. gravity, aerodynamic, or electromagnetic) that produce reactions that are functions of the state variables. An output of one system may be an input to another, or to itself if there is a simple feedback. The state variables are unique functions of the nonautonomous inputs and of the initial conditions of the system. A system with only autonomous inputs is an autonomous system.

Every system has, as well as its state variables and inputs, a set of *system parameters* that characterize the properties of its elements—e.g. areas masses, and inductances. When these are constant, or nearly so, it is convenient to consider them as a separate set. On the other hand, if some of them vary substantially in a manner that depends on the state variables, they may usefully be transferred to the latter set. The problem of system *design*, after the general configuration has been established, is primarily one of optimization in the system parameter space. Still another set of parameters is that associated with the environment—e.g. atmospheric density, gravitational field, and radiation field. In *adaptive* systems, some system parameters are made to be functions of the state variables and/or environmental parameters in order to achieve acceptable performance over a wider range of operating conditions than would otherwise be possible.

The following example will serve to illustrate some of the above concepts.

EXAMPLE

Figure 3.1 shows a system S comprising a planar arrangement of rigid bodies m_i, massless springs k_i, viscous damper c, and an inductive displacement transducer T. (Its voltage is $e(t) = \text{const.}\, x_3$.) The midpoint g of m_1, and mass m_3, are constrained to move vertically. The system, bounded by the dashed line, is made up of all these separate elements. The nonautonomous

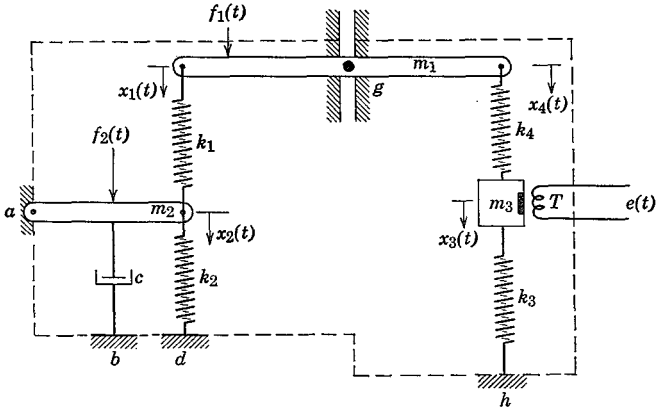

FIG. 3.1 An example of a system.

inputs are the arbitrary external forces f_1 and f_2 acting on the masses and the *state variables* are the coordinates of the joints, $x_i(t)$, their velocities $v_i(t) = \dot{x}_i$, and the voltage $e(t)$ of the transducer. Any of this set might be taken as outputs. Here, however, the output happens to be $e(t)$. If f_1 and f_2 were zero, the system would be autonomous and capable only of free vibration associated with nonequilibrium initial conditions. The external reactions at the points of connection to the fixed base, a, b, d, h, and g are functions of the state variables x_i and v_i, and hence are autonomous inputs. The *parameters* of the system are the masses of m_i, the stiffnesses of k_i, the damping constant of c, the transducer constant, and the geometrical dimensions. It should be pointed out that although there is a minimum number of coordinates (state variables x_i and v_i) required to specify the state of the system, eight in this example, this number may be arbitrarily increased by redundant variables if it is convenient to do so. For example, we might add the transducer output, the four accelerations $a_i = \dot{v}_i$, and the forces in the springs, even though they are, by virtue of the physical laws governing the system, not independent of the x_i and v_i. (Indeed the mathematical statement of this dependence is the main ingredient in the formulation of the system equations.) The minimum number of state variables required is the *order* of the system.

The arbitrariness of the choice of system, and its dependence on the aim of the investigation is illustrated by the fact that we might choose as a system for study any of the individual elements of S, or any of the subsystems obtained by combinations of them. Furthermore, the set of state variables

might be still further augmented by adding such items as the stresses and strains in m_1 and m_2.

Finally, the release of simplifying approximations such as rigidity of the bodies, and masslessness of the springs, would require further elaborate additions to the state variables.

BLOCK DIAGRAM

The input/output system relations are conveniently illustrated by the use of block diagrams, as in Fig. 3.2. Figure 3.2*a* is the overall system diagram showing inputs f_1 and f_2 and output e and Fig. 3.2*b* is the combined block diagram of the subsystems, showing the sort of interconnections and feedbacks that are typically encountered in real systems.

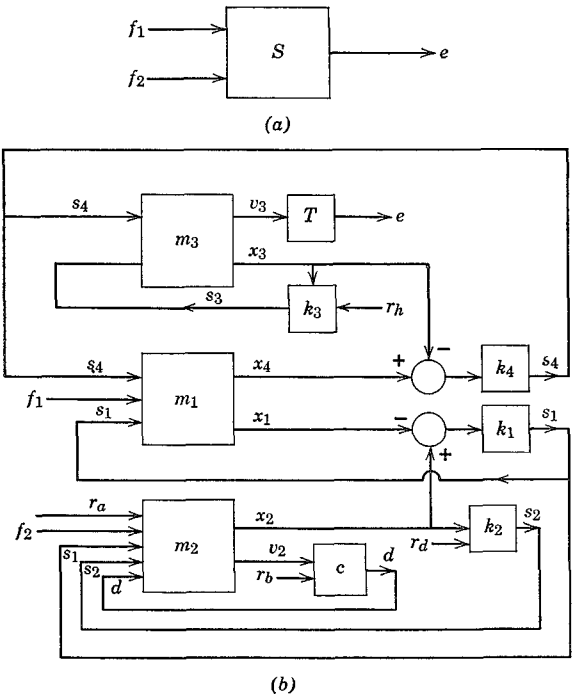

FIG. 3.2 Block diagram. (*a*) Complete system. (*b*) Detailed block diagram. s_i = spring forces. d = damper force. r_i = reaction forces.

LINEARITY AND TIME INVARIANCE

A system is *linear* if its governing equations are linear in the state variables. In that case the time functions giving the state variables are simply proportional to the magnitude of nonautonomous input functions of given shape when the initial conditions are zero, and to the initial conditions if there are no nonautonomous inputs. If the parameters of the system and of the environment are constants, then the system is *time invariant.* The simplest class of systems is that which has both these properties—linearity and time invariance—and these can be completely analyzed by the available methods of linear mathematics. We shall denote these as *linear/invariant* systems. Departure from either of these conditions leads to mathematical problems for which there may be no general methods of solution apart from numerical computation.

EQUILIBRIUM, CONTROL, AND STABILITY

Equilibrium denotes a steady state of the system, one in which all the state variables are constant in time. The "motion" corresponding to equilibrium is represented by a point in the state space. The nonautonomous inputs associated with equilibrium must be zero or constant, the zero case preferably corresponding to the equilibrium point at the origin. The usual way of changing the equilibrium state, i.e. of exercising *control* over the system is by means of the nonautonomous inputs, the appropriate subset of which can hence be termed the *control vector*, and the associated space the *control space.* The result of applying control is to cause the equilibrium point to move away from the origin in state space, and the locus of all its possible positions defines a region that is a map of the domain of the control vector in control space. The control is adequate only if this region contains all the desired operating states of the system (e.g. orientation angles and speeds of a flight vehicle).

Stability embraces a class of concepts that, while readily appreciated intuitively, are not easily defined in a universal way. In the past, a common view of system stability has been that it is a property of the equilibrium state, as follows. Let a system be in equilibrium, and for convenience let the equilibrium point be chosen as the origin of state space. Now let the initial state for the autonomous system be at a point P (see Fig. 3.3*a*) in the immediate neighborhood of O. Three possibilities exist for the subsequent motion, illustrated by the three trajectories a, b, and c in the figure.

(*a*) The state point moves back to the origin.
(*b*) It remains finite but >0 for all subsequent time
(*c*) It goes off to infinity.

The trajectory will of course, for a given system, depend on the direction of OP in state space. For example, Fig. 3.3*b* shows the equilibrium of a ball on a saddle surface. It is evident that displacement in the x direction leads to a type (*c*) trajectory and displacement in the y direction (in the presence of damping) to one of type (*a*). In this view of stability, the equilibrium point would be said to be stable if only type (*a*) trajectories could occur regardless of the direction of OP, and unstable if type (*c*) trajectories could occur. The saddle point is therefore an unstable equilibrium. The question of the magnitude of OP must be considered as well. If the system is linear, the conclusion about stability is independent of the magnitude of OP, but if it is not the size of the initial disturbance (i.e. of OP) does matter. It may well be that the system is stable for small disturbances, but unstable for large ones, as illustrated in Fig. 3.3*c*. The initial states for which the origin is stable in such a case lie within some region $\mathscr{R}$ of the state space as illustrated in Fig. 3.3*a*, and this is the "region of stability of O."

More recently, the rediscovery of the work on stability by Lyapunov (ref. 3.2) (see also Sec. 3.5) has had a great influence on this subject. In the Lyapunov viewpoint, we speak not of the stability of a system, but of the stability of a particular solution of a system of equations. The solution may be quite general, for example the forced motion of a nonlinear time-varying system with particular initial conditions. Equilibrium is a special case of such a solution. In this special case the Lyapunov definition is as follows. Let δ and ϵ be the radii of two hyperspheres in state space with centers at the equilibrium point, symbolically represented in two dimensions in Fig. 3.3*d*. These surfaces are such that for all initial states lying inside S_1 the subsequent solution lies for all time inside S_2. Then the origin is a stable point if there exists a $\delta > 0$ for all $\epsilon > 0$, no matter how small ϵ becomes. That is, the solution can be made arbitrarily small by choosing the initial conditions small enough. If the solutions tends ultimately to zero, then the origin is *asymptotically stable*. If, when 0 is asymptotically stable, there exists a region $\mathscr{R}$ such that all trajectories that originate within it decay to the origin, then $\mathscr{R}$ is a finite region of stability. This notion is identical with that previously described. If $\mathscr{R}$ is an infinite sphere then the origin is *globally stable*. Note that if a linear system is asymptotically stable it is also globally stable. This fact is somewhat academic since in nature "linear" systems always become nonlinear for "very large" state vectors.

The Lyapunov condition for a region of stability $\mathscr{R}$ will be met whenever the solution is a "well-behaved" function of the initial conditions—that is, if $\partial x_i(T)/\partial x_j(0)$ is finite in $\mathscr{R}$ for all i, j and T where $\mathbf{x}$ is the state vector. In particular this must hold in the limit as $T \to \infty$.

A striking illustration of this point of view is afforded by the unstable

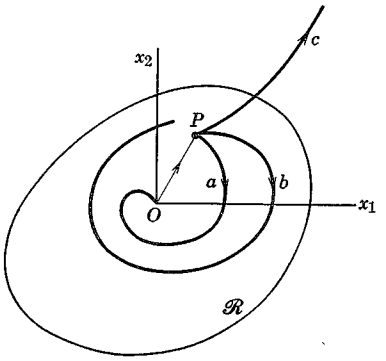

(a)

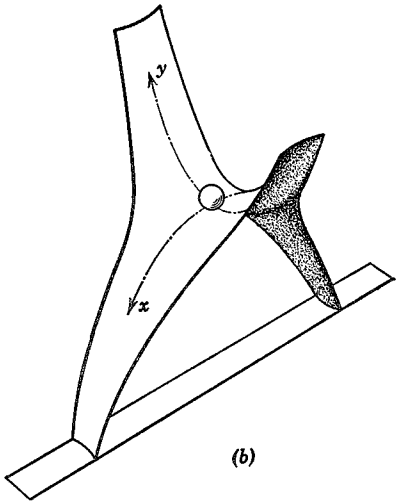

(b)

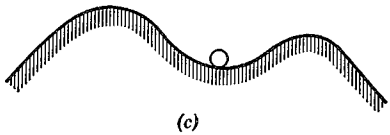

(c)

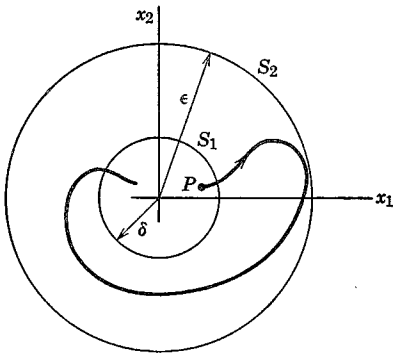

(d)

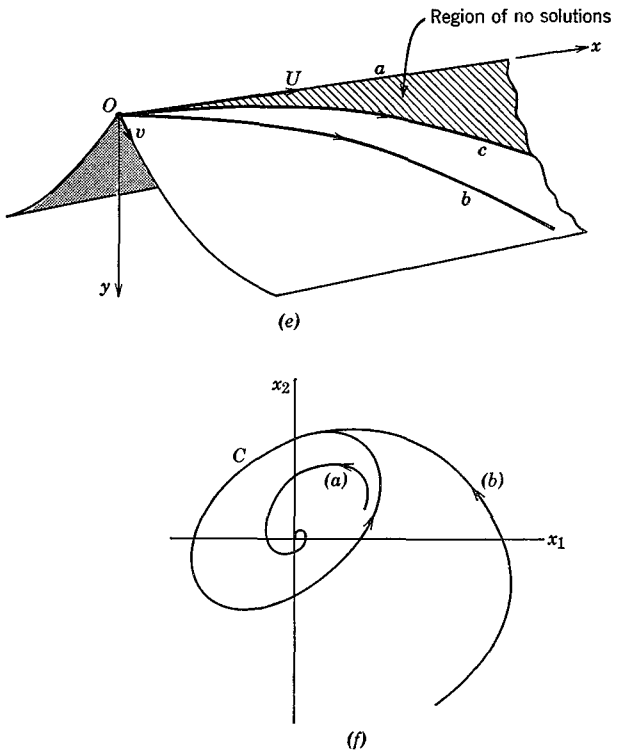

FIG. 3.3 Stability of equilibrium. (*a*) Trajectories in state space. (*b*) Saddle point. (*c*) Finite region of stability. (*d*) Lyapunov definition of stability. (*e*) Illustrating discontinuity in solutions. (*f*) Limit cycle.

system of Fig. 3.3*e*, in which a particle is free to slide without friction along a horizontal pointed ridge. The sides are infinite in the x and y directions. One solution, of course, is uniform rectilinear motion at speed U on the ridge (trajectory a). If a small initial tangential velocity v in the downhill direction be added, the motion is a trajectory such as b. In the limit as $v \to 0$, the limiting trajectory is one like c, tangent to $0x$ at the origin. Thus there is a gap between a and c that contains no solutions at all for the given U even for finite times. If the top of the ridge were rounded off instead of pointed the solutions for all finite t would be continuous in v. However even in that case, as $t \to \infty$ the $\lim_{v \to 0} y/v \to \infty$, so that $y(\infty)$ is not a continuous function of v, and hence the basic solution a is unstable.

When the solution to be investigated is not the simple one discussed above, i.e. equilibrium, the stability criterion is still that of continuity, as above.

Alternatively, the general case can be reduced to the particular case as follows. Let the system equation be

$$\dot{\mathbf{x}} = \mathbf{f}(\mathbf{x}, t) \tag{3.1,1}$$

and let the particular solution be $\mathbf{x}_0(t)$. Now let the variation from $\mathbf{x}_0$ associated with a change in the initial condition only be

$$\mathbf{y} = \mathbf{x}(t) - \mathbf{x}_0(t) \tag{3.1,2}$$

Hence

$$\begin{aligned} \dot{\mathbf{y}} &= \dot{\mathbf{x}}(t) - \dot{\mathbf{x}}_0(t) \\ &= \mathbf{f}(\mathbf{x}, t) - \mathbf{f}(\mathbf{x}_0, t) \end{aligned}$$

or

$$\dot{\mathbf{y}} = \mathbf{f}(\mathbf{y} + \mathbf{x}_0(t), t) - \mathbf{f}(\mathbf{x}_0(t), t) \tag{3.1,3}$$

Since $\mathbf{x}_0(t)$ is presumed known, then (3.1,3) is an equation of the form

$$\dot{\mathbf{y}} = \mathbf{g}(\mathbf{y}, t) \tag{3.1,4}$$

for which $\mathbf{y} = 0$ is the solution corresponding to $\mathbf{x}(t) = \mathbf{x}_0(t)$. Thus (3.1,4) defines a system that has an equilibrium point at the origin, and the discussion of its stability has already been given. In this way the stability of any transient solution is reduced to that of stability of equilibrium.

A particular kind of solution that is of interest is the limit cycle, illustrated again in two dimensions, in Fig. 3.3*f* by the closed curve C. It may be orbitally stable, in which case neighboring trajectories such as (b) are asymptotic to it, or unstable, in which case neighboring trajectories such as (a) starting arbitrarily close to C, never come back to it.

Finally, we should remark that Lyapunov's definition is concerned only with variations in the initial conditions of a solution. Clearly there are two other important practical cases: (1) stability with respect to perturbations in the input, and (2) stability with respect to system or environmental parameters. Stability with respect to perturbations in the input or the system parameters can be defined in a manner quite analogous to that with respect to the initial conditions.

3.2 TRANSFER FUNCTIONS

System analysis frequently reduces to the calculation of system outputs for given inputs. A convenient and powerful tool in such analysis is the *transfer function*, a function $G(s)$ of the Laplace transform variable s that relates a particular input $x(t)$ and output $y(t)$ as follows,

$$G(s) = \frac{\bar{y}(s)}{\bar{x}(s)} \tag{3.2,1}$$

where $(^-)$ denotes the Laplace transform (see Sec. 2.3). So long as $x(t)$ and $y(t)$ are Laplace transformable the transfer function defined by (3.2,1) exists. However, it will in general be a function of the initial values of y and its derivatives, and moreover, for nonlinear and time-varying systems, of the particular input $x(t)$ as well. Such a transfer function is of relatively little use. We can however obtain a unique function $G(s)$ if (i) the system is linear and time invariant, and (ii) it is initially quiescent, i.e. at rest at the origin in state space with no inputs. We shall therefore restrict ourselves in the following to this special situation. (A companion concept, the describing function, useful for nonlinear systems is described in Sec. 3.5.) With a unique transfer function, the output $y(t)$ for *any* input $x(t)$ is found by taking the inverse Laplace transform of

$$\bar{y}(s) = G(s)\bar{x}(s) \tag{3.2,2}$$

The transfer function is thus seen to be the mathematical embodiment of all the system characteristics relevant to the particular input/output pair. For linear/invariant systems, we shall see below that the computation of $G(s)$ is always possible in principle, and usually in practice.

When, as required above, $x(t)$ and $y(t)$ are zero for $t < 0$, the Laplace and Fourier transforms are simply related, i.e. $\bar{x}(i\omega) = X(\omega)$. It follows that

$$G(i\omega) = \frac{Y(\omega)}{X(\omega)} \tag{3.2,2a}$$

Sometimes it is $G(i\omega)$ that is called the transfer function.

With a multivariable system, there is more than one input/output pair. In that case, let $G_{ij}(s)$ be the transfer function that relates the output $y_i(t)$ to the input $x_j(t)$. All the input/output relations are then given by

$$\bar{y}_i(s) = \sum_{j=1}^{m} G_{ij}(s)\,\bar{x}_j(s) \tag{3.2,3a}$$

or

$$\bar{\mathbf{y}}(s) = \mathbf{G}\bar{\mathbf{x}}(s) \tag{3.2,3b}$$

where

$$\mathbf{G} = [G_{ij}(s)] \tag{3.2,3c}$$

is an $n \times m$ matrix associated with n outputs and m inputs. It need not be square since one output can be influenced by any number of inputs and vice versa. Note from (3.2,3a) that

$$G_{ij} = \frac{\partial \bar{y}_i}{\partial \bar{x}_j} \tag{3.2,3d}$$

STATIC GAIN

Consider the output $y(t)$ that results from the unit-step input $x(t) = \mathbf{1}(t)$. From Table 2.3, item 3, the transform of the input is

$$\bar{x}(s) = \frac{1}{s}$$

and hence

$$\bar{y}(s) = \frac{G(s)}{s}$$

The final value theorem (2.3,17) therefore gives

$$\lim_{t\to\infty} y(t) = \lim_{s\to 0} s\bar{y}(s) = \lim_{s\to 0} G(s)$$

This limit is the *static gain*, K, so that

$$K = \lim_{s\to 0} G(s) \tag{3.2,4}$$

EXAMPLE

Let us find the transfer function of the second-order system of Fig. 2.3. The governing differential equation is (2.4,1), in which $f(t)$ is the input and $x(t)$ is the output. The Laplace transform is (2.4,3). Since the initial conditions $x(0)$ and $\dot{x}(0)$ are specified to be zero, then

$$\bar{x}(s)(s^2 + 2\zeta\omega_n s + \omega_n{}^2) = \bar{f}(s)$$

or from (3.2,1)

$$G(s) = \frac{\bar{x}(s)}{\bar{f}(s)} = \frac{1}{s^2 + 2\zeta\omega_n s + \omega_n{}^2} \tag{3.2,5}$$

The static gain K is found to be

$$K = \lim_{s\to 0} G(s) = \frac{1}{\omega_n{}^2} \tag{3.2,6}$$

SYSTEMS IN SERIES

When two subsystems are in series, as in Fig. 3.4, the overall transfer function is

$$G(s) = \frac{\bar{z}(s)}{\bar{x}(s)} = \frac{\bar{z}(s)}{\bar{y}(s)} \cdot \frac{\bar{y}(s)}{\bar{x}(s)}$$

whence

$$G(s) = G_1(s) \cdot G_2(s)$$

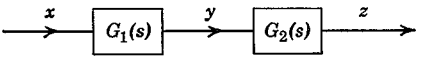

FIG. 3.4 Systems in series.

Similarly, for n subsystems in series, the result is

$$G(s) = G_1(s) \cdot G_2(s) \cdots G_n(s) \tag{3.2,7}$$

SYSTEM WITH FEEDBACK

Figure 3.5 shows a general *feedback* arrangement, containing two subsystems. When used as a feedback controller, ϵ is called the *actuating signal*,† $G(s)$ the forward-path transfer function and $H(s)$ the feedback transfer function. As indicated ϵ is the difference between x and z, so

$$\bar{\epsilon} = \bar{x} - \bar{z}$$

$$\bar{y} = G(\bar{x} - \bar{z})$$

$$\bar{z} = H\bar{y}$$

whence it follows easily that the overall transfer function is

$$\frac{\bar{y}}{\bar{x}} = \frac{G}{1 + GH} \tag{3.2,8}$$

and the actuating-signal transfer function is

$$\frac{\bar{\epsilon}}{\bar{x}} = \frac{1}{1 + GH} \tag{3.2,9}$$

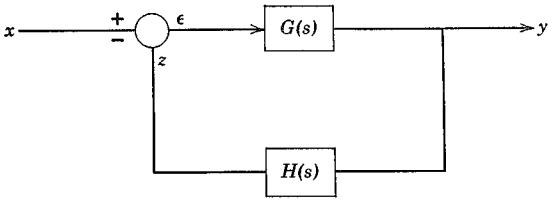

FIG. 3.5 General feedback system.

† The designation *error* is reserved for the difference $x - y$, the aim of such a control system being to force y to be equal to x.

TRANSFER FUNCTIONS OF GENERAL LINEAR/INVARIANT SYSTEM

The transfer functions of a physical system that exists and is available for testing can be found from experiment, by making suitable measurements of its inputs and outputs. Here we are concerned with obtaining the transfer function by analysis. The experimental method is based in any case on the analytical formalism that we develop in the following. The procedure begins, of course, with the application of the appropriate physical laws that govern the behavior of the system. When the complete set of equations that express these laws has been formulated, it will, for linear/invariant systems, usually appear as a set of coupled differential equations of mixed order. A particularly simple example (the second-order system) was given above, and it demonstrates what may be called the direct method of finding transfer functions. That is, form the Laplace transform of the system equations, just as they naturally occur, and solve for the appropriate ratios. We give a further illustration below for a pair of coupled second-order equations (a fourth-order system), such as might arise in the analysis of a double pendulum, or two massive particles on a stretched string, or two coupled L-R-C circuits, etc. The example equations are

$$\begin{aligned} \dddot{x} + a_1\ddot{y} + a_2\dot{x} + a_3x + a_4y &= f_1 \\ \ddot{x} + b_1\ddot{y} + b_2\dot{y} + b_3x + b_4y &= f_2 \end{aligned} \tag{3.2,10}$$

On forming the Laplace transforms, with

$$x(0) \equiv y(0) \equiv \dot{x}(0) \equiv \dot{y}(0) = 0 \tag{3.2,11}$$

the result is

$$\begin{aligned} \bar{x}(s^2 + a_2s + a_3) + \bar{y}(a_1s^2 + a_4) &= \bar{f}_1 \\ \bar{x}(s^2 + b_3) + \bar{y}(b_1s^2 + b_2s + b_4) &= \bar{f}_2 \end{aligned} \tag{3.2,12}$$

which can readily be solved for the four required transfer functions. We rewrite (3.2,12) as

$$\mathbf{B}\begin{bmatrix} \bar{x} \\ \bar{y} \end{bmatrix} = \begin{bmatrix} \bar{f}_1 \\ \bar{f}_2 \end{bmatrix} \tag{3.2,13}$$

where

$$\mathbf{B} = \begin{bmatrix} (s^2 + a_2s + a_3) & (a_1s^2 + a_4) \\ (s^2 + b_3) & (b_1s^2 + b_2s + b_4) \end{bmatrix}$$

and the solution is

$$\begin{bmatrix} \bar{x} \\ \bar{y} \end{bmatrix} = \mathbf{G}\begin{bmatrix} \bar{f}_1 \\ \bar{f}_2 \end{bmatrix} \tag{3.2,14}$$

where
$$\mathbf{G} = \mathbf{B}^{-1} = \begin{bmatrix} G_{xf_1} & G_{xf_2} \\ G_{yf_1} & G_{yf_2} \end{bmatrix} \tag{3.2,15}$$

is the matrix of the four transfer functions that relate x and y outputs to f_1 and f_2 inputs. There are however two other state variables, making the required total of four, and consequently there are four more transfer functions to be found. The additional variables are the two rates

$$\begin{aligned} \dot{x} &= u \\ \dot{y} &= v \end{aligned} \tag{3.2,16}$$

The transforms of (3.2,16) with zero initial values are

$$\begin{aligned} s\bar{x} &= \bar{u} \\ s\bar{y} &= \bar{v} \end{aligned}$$

whence the four additional transfer functions are [see (3.2,3*d*)]

$$G_{uf_1} = \frac{\partial \bar{u}}{\partial \bar{f}_1} = s\frac{\partial \bar{x}}{\partial \bar{f}_1} = sG_{xf_1} \tag{3.2,17}$$

and similarly

$$G_{vf_1} = sG_{yf_1}; \qquad G_{uf_2} = sG_{xf_2}; \qquad G_{vf_2} = sG_{yf_2}$$

An alternative procedure for finding the matrix of system transfer functions consists of putting the equations in the standard first-order form. Any nth-order system of linear equations can be expressed as a set of n first-order equations. Consider (3.2,10) for example. By using (3.2,16) they become

$$\begin{aligned} \dot{u} + a_1\dot{v} &= -a_2u - a_3x - a_4y + f_1 \\ \dot{u} + b_1\dot{v} &= -b_2v - b_3x - b_4y + f_2 \end{aligned} \tag{3.2,18}$$

which together with (3.2,16) are the required four first-order equations. They are not yet in the standard form, however. For that, one first solves (3.2,18) for $\dot{u}$ and $\dot{v}$, which are linear functions of u, v, x, y, f_1, and f_2. Combining the result with (3.2,16) yields a matrix equation of the form

$$\begin{bmatrix} \dot{x} \\ \dot{y} \\ \dot{u} \\ \dot{v} \end{bmatrix} = \mathbf{A}\begin{bmatrix} x \\ y \\ u \\ v \end{bmatrix} + \mathbf{C}\begin{bmatrix} f_1 \\ f_2 \end{bmatrix} \tag{3.2,19}$$

where $\mathbf{A}$ is a 4×4 matrix, and $\mathbf{C}$ is a 4×2 matrix. (The determination of $\mathbf{A}$ and $\mathbf{C}$ is left as an exercise for the reader.)

Equation (3.2,19) is an example of the canonical form, which for the general linear system is

$$\dot{\mathbf{y}} = \mathbf{A}\mathbf{y} + \mathbf{C}\mathbf{x} \tag{3.2,20}$$

where $\mathbf{y}$ is the state n-vector and $\mathbf{x}$ the nonautonomous input r-vector. $\mathbf{A}$ (an $n \times n$ matrix) and $\mathbf{C}$ (an $n \times r$ matrix) may in general be time dependent. Here however, we are confining the discussion to invariant systems, and hence the Laplace transform of (3.2,20) is simply, for $\mathbf{y}(0) = 0$

$$s\bar{\mathbf{y}} = \mathbf{A}\bar{\mathbf{y}} + \mathbf{C}\bar{\mathbf{x}} \tag{3.2,21}$$

or

$$(s\mathbf{I} - \mathbf{A})\bar{\mathbf{y}} = \mathbf{C}\bar{\mathbf{x}}$$

where $\mathbf{I}$ is the identity matrix. It follows that

$$\bar{\mathbf{y}} = (s\mathbf{I} - \mathbf{A})^{-1}\mathbf{C}\bar{\mathbf{x}} \tag{3.2,22}$$

From (3.2,3*b*) we can therefore identify $\mathbf{G}$ as

$$\mathbf{G} = (s\mathbf{I} - \mathbf{A})^{-1}\mathbf{C} \tag{3.2,23}$$

It can in principle be evaluated whenever $\mathbf{A}$ and $\mathbf{C}$ are known.

3.3 AUTONOMOUS LINEAR/INVARIANT SYSTEMS

The general equation for linear/invariant systems is (3.2,20). When the system is autonomous and hence has zero input it reduces to

$$\dot{\mathbf{y}} = \mathbf{A}\mathbf{y} \tag{3.3,1}$$

When the initial state vector is $\mathbf{y}(0)$, the Laplace transform of (3.3,1) is

$$s\bar{\mathbf{y}} = \mathbf{A}\bar{\mathbf{y}} + \mathbf{y}(0)$$

or

$$(s\mathbf{I} - \mathbf{A})\bar{\mathbf{y}} = \mathbf{y}(0) \tag{3.3,2}$$

Define

$$\mathbf{B}(s) = s\mathbf{I} - \mathbf{A}$$

$$= \begin{bmatrix} s - a_{11} & -a_{12} & \cdots & -a_{1n} \\ -a_{21} & s - a_{22} & & \cdot \\ \cdot & & & \cdot \\ \cdot & & & \cdot \\ \cdot & & & \\ -a_{n1} & & & (s - a_{nn}) \end{bmatrix} \tag{3.3,3}$$

in which a_{ij} are the elements of **A**. **B** is called the *characteristic matrix* of the system. Equation (3.3,2) then becomes

$$\mathbf{B}(s)\bar{\mathbf{y}} = \mathbf{y}(0)$$

whence

$$\bar{\mathbf{y}} = \mathbf{B}^{-1}(s)\mathbf{y}(0) \tag{3.3,4}$$

where

$$\mathbf{B}^{-1} = \frac{\text{adj } \mathbf{B}}{|\mathbf{B}|} \tag{3.3,5}$$

By virtue of the definition of the adjoint matrix (ref. 2.1) it is evident that the elements of adj **B** and of $|\mathbf{B}|$ are polynomials in s. $|\mathbf{B}|$ is called the *characteristic determinant*, and its expansion

$$|\mathbf{B}| = f(s) \tag{3.3,6}$$

is the *characteristic polynomial*. It is evident from (3.3,3) that $f(s)$ is of the nth degree. Hence

$$\begin{aligned} f(s) &= s^n + c_{n-1}s^{n-1} + \cdots c_0 \\ &= (s - \lambda_1)(s - \lambda_2) \cdots (s - \lambda_n) \end{aligned} \tag{3.3,7}$$

where $\lambda_1 \cdots \lambda_n$ are the roots of $f(s) = 0$, the *characteristic equation*. We now rewrite (3.3,4) as

$$\bar{\mathbf{y}}(s) = \frac{\text{adj } \mathbf{B}(s)}{f(s)} \cdot \mathbf{y}(0) \tag{3.3,8}$$

The inversion theorem (2.5,6) can be applied to (3.3,8) for each element of $\bar{\mathbf{y}}$, and the column of these inverses is the inverse of $\bar{\mathbf{y}}(s)$, i.e.

$$\mathbf{y}(t) = \sum_{r=1}^{n} \left\{ \frac{(s - \lambda_r) \text{ adj } \mathbf{B}(s)}{f(s)} \right\}_{s=\lambda_r} \mathbf{y}(0)e^{\lambda_r t} \tag{3.3,9}$$

We now define the vector

$$\mathbf{y}_r = \left\{ \frac{(s - \lambda_r) \text{ adj } \mathbf{B}(s)}{f(s)} \right\}_{s=\lambda_r} \mathbf{y}(0) \tag{3.3,9a}$$

and hence can write the general solution of (3.3,1) that satisfies the initial conditions as

$$\mathbf{y}(t) = \sum_{r=1}^{n} \mathbf{y}_r e^{\lambda_r t} \tag{3.3,10}$$

It follows that $\mathbf{y}(0) = \sum_{r=1}^{n} \mathbf{y}_r$. Note also that by setting $t = 0$ in (3.3,9) the summation therein is shown to be equal to the identity matrix **I**.

COMPACT FORM OF SOLUTION

A more compact form of the solution is available. Define the exponential function of a matrix $\mathbf{M}$ by an infinite series (like the ordinary exponential of a scalar), i.e.†

$$e^{\mathbf{M}} = \mathbf{I} + \mathbf{M} + \frac{1}{2!}\mathbf{M}^2 + \cdots \tag{3.3,11}$$

It is evident then that

$$\begin{aligned}\frac{d}{dt}e^{\mathbf{A}t} &= \frac{d}{dt}\left(\mathbf{I} + \mathbf{A}t + \frac{1}{2!}\mathbf{A}^2t^2 + \cdots\right)\\ &= \mathbf{A} + \mathbf{A}^2t + \frac{1}{2!}\mathbf{A}^3t^2 + \cdots\\ &= \mathbf{A}e^{\mathbf{A}t}\end{aligned} \tag{3.3,12}$$

Thus it can be verified by substitution that

$$\mathbf{y}(t) = e^{\mathbf{A}t}\mathbf{y}(0) \tag{3.3,13}$$

is a solution of (3.3,1) that has the initial value $\mathbf{y}(0)$.

EIGENVALUES AND EIGENVECTORS

The roots λ_r of the characteristic equations are known as eigenvalues, or characteristic values. Corresponding to each of them is a special set of initial conditions that lead to a specially simple solution in which only one term of (3.3,10) remains, i.e.

$$\begin{aligned}\mathbf{y}(t) &= \mathbf{u}_r e^{\lambda_r t} \quad (a)\\ \text{where}\qquad \mathbf{y}(0) &= \mathbf{u}_r \quad (b)\end{aligned} \tag{3.3,14}$$

Since the solution of the autonomous system corresponding to a given set of initial conditions is unique, then if (3.3,14*a*) is a possible solution (and we shall show that it is), then (3.3,14*b*) gives the unique set of initial conditions that produce it. The general solution (3.3,10) is seen to be a superposition of these special solutions. $\mathbf{u}_r$ is the *eigenvector* corresponding to λ_r, and (3.3,14*a*) is the associated *eigenfunction*. Substitution of (3.3,14) into (3.3,1) gives

$$\begin{aligned}(\lambda_r\mathbf{I} - \mathbf{A})\mathbf{u}_r &= 0 \quad (a)\\ \text{or}\qquad \mathbf{B}(\lambda_r)\mathbf{u}_r &= 0 \quad (b)\end{aligned} \tag{3.3,15}$$

† For a discussion of the practical computation of $e^{\mathbf{M}}$ see Appendix D-8 of ref. 3.1.

Since the expansion of (3.3,15) is a set of homogeneous algebraic equations in the unknowns u_{ir} a nontrivial solution exists only if the determinant equals zero, i.e. if

$$|\mathbf{B}(\lambda_r)| = 0 \tag{3.3,16}$$

However, the λ_r are the roots of the characteristic equation $|\mathbf{B}(s)| = 0$, and hence the condition (3.3,16) is automatically met. The vectors $\mathbf{u}_r$ are then any that satisfy (3.3,15). It should be noted that since the r.h.s. of (3.3,15) is zero, the multiplication of any eigenvector by a scalar produces another eigenvector that has the same "direction" but different magnitude. To find $\mathbf{u}_r$ we observe that, from the definition of an inverse (3.3,5),

$$\text{adj}\,\mathbf{B} = \mathbf{B}^{-1}|\mathbf{B}| \tag{3.3,17}$$

Premultiplying by $\mathbf{B}$ yields

$$\mathbf{B}\,\text{adj}\,\mathbf{B} = |\mathbf{B}|\mathbf{I} = f(s)\mathbf{I} \tag{3.3,18}$$

For any eigenvalue λ_r, we have $f(\lambda_r) = 0$, and hence

$$\mathbf{B}(\lambda_r)\,\text{adj}\,\mathbf{B}(\lambda_r) = \mathbf{0} \tag{3.3,19}$$

Since the null matrix has all its columns zero, then it follows that *each column* of adj $\mathbf{B}(\lambda_r)$ is a vector that satisfies (3.3,15*b*). Hence any nonzero column of adj $\mathbf{B}(\lambda_r)$ (if there are more than one, they differ only by constant factors) is an eigenvector corresponding to λ_r. The eigenvalues and eigenvectors are the most important properties of autonomous systems. From them one can deduce everything required about its performance and stability. This is illustrated in detail for flight vehicles in Chapter 9.

The n eigenvectors form the *eigenmatrix*

$$\mathbf{U} = [\mathbf{u}_1\mathbf{u}_2 \cdots \mathbf{u}_n] = [u_{ij}]$$

in which u_{ij} is the ith component of the jth vector.

ORTHOGONAL EIGENVECTORS

When the matrix $\mathbf{A}$ is symmetric (not, unfortunately, a common occurrence in the equations of flight vehicles) the system is called self-adjoint, and the eigenvectors have the convenient special property of being orthogonal, or normal. That is, the scalar product of any vector with any other is zero, i.e.,

$$\mathbf{u}_j{}^T\mathbf{u}_i = \mathbf{u}_j \cdot \mathbf{u}_i = 0 \qquad i \neq j \tag{3.3,20}$$

In more general cases, when the system is not self-adjoint, and $\mathbf{A}$ is an arbitrary $n \times n$ matrix, the eigenvectors are neither real nor orthogonal. However, there still exists a reciprocal basis of the eigenvectors, i.e. a

set of n vectors $\mathbf{v}_i$ orthonormal to the set $\mathbf{u}_i$, i.e. such that

$$\mathbf{v}_i^T \mathbf{u}_j = [\delta_{ij}]$$

Thus the matrix $\mathbf{V}$ of the vectors $\mathbf{v}_i$ evidently satisfies the condition

$$\mathbf{V}^T \mathbf{U} = \mathbf{I}$$

and clearly

$$\mathbf{V}^T = \mathbf{U}^{-1}$$

i.e. the columns of $\mathbf{V}$ are the rows of $\mathbf{U}^{-1}$. The question now naturally arises as to what system (the adjoint system) has $\mathbf{v}_i$ as its eigenvectors, and whether its matrix, $\mathbf{B}$ say, has any relation to $\mathbf{A}$. It can be shown that (ref. 3.1) $\mathbf{B} = \mathbf{A}^T$, i.e. that the matrix of the system adjoint to $\mathbf{A}$ is $\mathbf{A}^T$ and its eigenvectors are orthogonal to those of $\mathbf{A}$.

COMPUTATION OF EIGENVALUES AND EIGENVECTORS

For low-order systems, the characteristic determinant can be directly expanded and the characteristic equation (3.3,7) written out. If $n \leq 4$, analytical solutions exist for the roots. For large-order systems the eigenvalues and eigenvectors are computed from the system matrix $\mathbf{A}$ by digital machine methods (refs. 3.3, 3.4). A discussion of these methods and of their recommended spheres of application is beyond the scope of this volume. Suffice it to say that practical methods and computing routines are available in most computation centers for extracting the eigenvalues and eigenvectors for systems of very large order, even for $n > 100$.

It is worthwhile describing one fairly direct approach to computation of eigenvectors. Consider (3.3,15*b*) as a homogeneous set of scalar equations with λ_r known and the n components of $\mathbf{u}_r$ as the unknowns. Now divide through all the equations by any one of the unknowns, say u_{mr}, so that there results n equations for $(n - 1)$ ratios u_{ir}/u_{mr}. By dropping any one of the equations and transposing the coefficients of u_{mr} to the r.h.s., a complete set of $(n - 1)$ equations is obtained for the $(n - 1)$ ratios. These can be solved by any conventional method to yield the ratios of all the components of $\mathbf{u}_r$ to u_{mr}. The equations will of course have complex coefficients for complex eigenvalues, and real coefficients for real eigenvalues. This process for a third-order system would go as follows:

$$b_{11}(\lambda_r)u_{1r} + b_{12}(\lambda_r)u_{2r} + b_{13}(\lambda_r)u_{3r} = 0$$

$$b_{21}(\lambda_r)u_{1r} + b_{22}(\lambda_r)u_{2r} + b_{23}(\lambda_r)u_{3r} = 0$$

$$b_{31}(\lambda_r)u_{1r} + b_{32}(\lambda_r)u_{2r} + b_{33}(\lambda_r)u_{3r} = 0$$

After dividing by u_{3r} and dropping the third equation we get

$$b_{11}\frac{u_{1r}}{u_{3r}} + b_{12}\frac{u_{2r}}{u_{3r}} = -b_{13}$$

$$b_{21}\frac{u_{1r}}{u_{3r}} + b_{22}\frac{u_{2r}}{u_{3r}} = -b_{23}$$

The solution of this set of equations gives the two required ratios in terms of which the eigenvector is $[u_{1r}/u_{3r}, u_{2r}/u_{3r}, 1]$. There are two difficulties associated with this method. The first is that if u_{3r} turns out to be very small relative to u_{1r} and u_{2r} the equations will be ill-conditioned, and a different choice for the component to divide by has to be made. The second is that when λ is complex, there are really two sets of equations to be solved for the real and imaginary parts of the ratios.

Clearly the eigenvector corresponding to the conjugate eigenvalue λ_r^* will be itself the conjugate of u_r, so only one of the pair need be calculated.

REPEATED ROOTS

When the procedure given in the foregoing is applied to calculate eigenvectors for cases of multiple roots of the characteristic equation, additional possibilities occur. (See refs. 3.3 and 2.2.) Let the multiple root occur at $s = \lambda_p$

(i) If adj $\mathbf{B}(\lambda_p)$ is not a null matrix, then its nonzero columns give a single eigenvector, just as for distinct eigenvalues. In that case there is only one eigenvector for the multiple root.

(ii) If adj $\mathbf{B}(\lambda_p)$ is null, and its first derivative d/ds adj $\mathbf{B}(s)\big|_{s=\lambda_p}$ is not, then there are two linearly independent columns of the latter that give two independent eigenvectors.

(iii) If the first derivative is also null, then higher derivatives will yield successively larger numbers of eigenvectors.

EQUATIONS IN NONSTANDARD FORM

It is not necessary, nor always more convenient, to work with the system equations in standard first-order form, as was done above. The characteristic equation can be found directly from the equations as they are initially formulated, the "natural" form. Consider (3.2,10) for example. The autonomous equations are

$$\begin{aligned} \ddot{x} + a_1\ddot{y} + a_2\dot{x} + a_3x + a_4y &= 0 \\ \ddot{x} + b_1\ddot{y} + b_2\dot{y} + b_3x + b_4y &= 0 \end{aligned} \qquad (3.3,21)$$

Assume there is an eigenfunction solution like (3.3,14), i.e.

$$\begin{bmatrix} x \\ y \end{bmatrix} = \begin{bmatrix} x(0) \\ y(0) \end{bmatrix} e^{\lambda t} \tag{3.3,22}$$

When (3.3,22) is substituted into (3.3,21) the result is

$$\begin{bmatrix} (\lambda^2 + a_2\lambda + a_3) & (a_1\lambda^2 + a_4) \\ (\lambda^2 + b_3) & (b_1\lambda^2 + b_2\lambda + b_4) \end{bmatrix} \begin{bmatrix} x(0) \\ y(0) \end{bmatrix} = 0 \tag{3.3,23}$$

The square matrix of (3.3,23) is exactly the same as **B** in (3.2,13), λ replacing s. Since (3.3,23) are homogeneous equations the determinant of **B** must be zero. Expanding it leads exactly to the correct characteristic equation, just as would be obtained from the standard first-order form. Equation (3.3,23) is of the same form as (3.3,15*b*) and the same argument for finding an eigenvector applies—i.e. a column $(x(0), y(0))$ that satisfies (3.3,23) is any nonvanishing column of adj **B**. To complete the eigenvector we need $\dot{x}(0)$ and $\dot{y}(0)$. These are simply, from (3.3,22),

$$\begin{bmatrix} \dot{x}(0) \\ \dot{y}(0) \end{bmatrix} = \lambda \begin{bmatrix} x(0) \\ y(0) \end{bmatrix} \tag{3.3,24}$$

where λ is the appropriate eigenvalue.

CHARACTERISTIC OR NATURAL MODES

Solutions of the kind given by (3.3,14) describe special simple motions called *natural modes* or simply *modes* of the system. If the eigenvectors are orthogonal, the modes are normal or orthogonal modes. When λ is real, the modes are exponential in form, as in Fig. 3.6*a* and *b*—increasing in magnitude for λ positive, and diminishing for λ negative. Thus $\lambda < 0$ corresponds to stability, usually termed static stability in the aerospace vehicle context, and $\lambda > 0$ corresponds to static instability, or *divergence*. The times to double or half of the starting value illustrated in the figure are given by

$$\begin{aligned} t_{\text{double}} &= \frac{.693}{\lambda}, \qquad \lambda > 0 \\ t_{\text{half}} &= -\frac{.693}{\lambda}, \qquad \lambda < 0 \end{aligned} \tag{3.3,25}$$

When one λ_r is complex, for real matrices **A**, there is always a second that is its conjugate, and the conjugate pair, denoted (letting $r = 1, 2$)

$$\lambda_{1,2} = n \pm i\omega$$

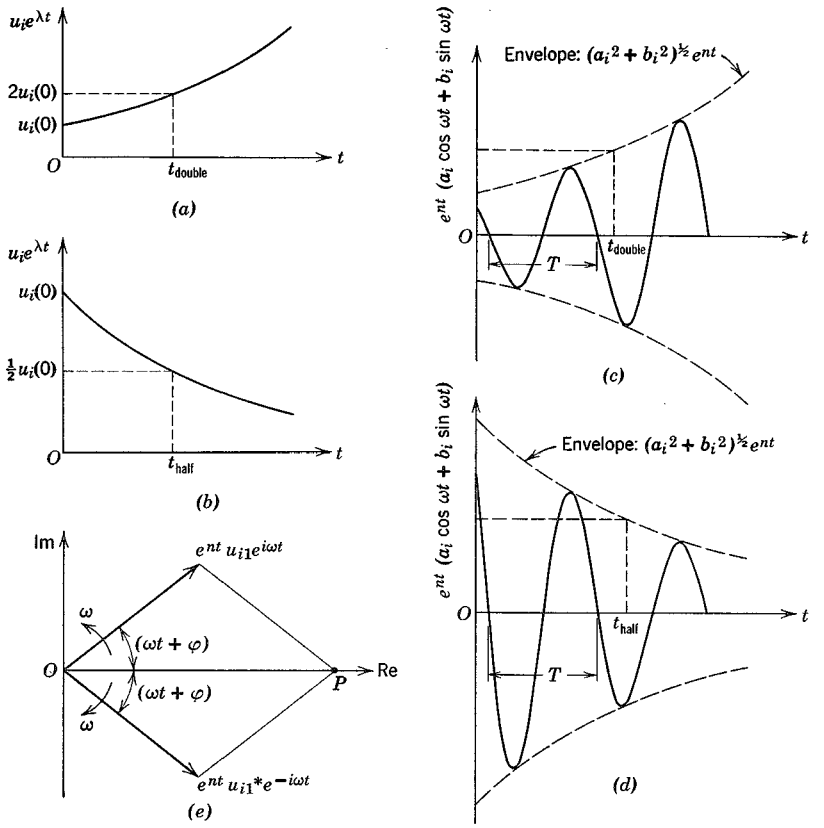

FIG. 3.6 Types of natural mode.

define an oscillatory mode of period $T = 2\pi/\omega$ as we shall now show. The sum of the two particular solutions (3.3,14) corresponding to the complex pair of roots is

$$\mathbf{y} = \mathbf{u}_1 e^{(n+i\omega)t} + \mathbf{u}_2 e^{(n-i\omega)t}$$

where $\mathbf{u}_1$ and $\mathbf{u}_2$ are the eigenvectors for the two λ's. On factoring out e^{nt} we get

$$\mathbf{y} = e^{nt}(\mathbf{u}_1 e^{i\omega t} + \mathbf{u}_2 e^{-i\omega t}) \qquad (3.3,26)$$

If the elements of the system matrix **A** are real, then the corresponding elements of $\mathbf{u}_1$ and $\mathbf{u}_2$ always turn out to be conjugate complex pairs, i.e.

$$\mathbf{u}_2 = \mathbf{u}_1^*$$

and (3.3,26) becomes

$$\mathbf{y} = e^{nt}(\mathbf{a} \cos \omega t + \mathbf{b} \sin \omega t) \tag{3.3,27}$$

where $\mathbf{a} = \mathbf{u}_1 + \mathbf{u}_1^*$ and $\mathbf{b} = i(\mathbf{u}_1 - \mathbf{u}_1^*)$ are real vectors. Equation (3.3,27) describes, for any particular state variable y_i, an oscillatory variation that increases if $n > 0$ (*dynamic instability*, or *divergent oscillation*) and decreases (*damped oscillation*) if $n < 0$—see Fig. 3.6*c* and *d*. The initial condition corresponding to (3.3,27) is

$$\mathbf{y}(0) = \mathbf{a} = \mathbf{u}_1 + \mathbf{u}_1^* \tag{3.3,28}$$

With reference to Fig. 3.6*c* and *d*, some useful measures of the rate of growth or decay of the oscillation are:

Time to double or half:

$$t_{\text{double}} \text{ or } t_{\text{half}} = \frac{.693}{|n|} = \frac{.693}{|\zeta|\omega_n} \qquad (a) \qquad (3.3,29)$$

Cycles to double or half:

$$N_{\text{double}} \text{ or } N_{\text{half}} = .110\,\frac{\omega}{|n|} = .110\,\frac{\sqrt{1-\zeta^2}}{|\zeta|} \qquad (b)$$

Logarithmic decrement (log of ratio of successive peaks):

$$\delta = \log_e \frac{e^{nt}}{e^{n(t+T)}} = -nT = 2\pi\,\frac{\zeta}{\sqrt{1-\zeta^2}}$$
$$= -.693/N_{\text{double}} \quad \text{or} \quad .693/N_{\text{half}} \qquad (c)$$

In the above equations,

$\omega_n = (\omega^2 + n^2)^{1/2}$, the "undamped" circular frequency

$\zeta = -n/\omega_n$, the damping ratio

One significance of the eigenvectors is seen to be that they determine the relative values of the state variables (the "direction" of the state vector in state space) in a characteristic mode. If the mode is nonperiodic, the eigenvector defines a fixed line through the origin in state space, and the motion in the mode is given by that of a point moving exponentially along this line. If the mode is oscillatory, the state vector is given by (3.3,27), and the locus of $\mathbf{y}$ is clearly a plane figure in the ($\mathbf{a}$, $\mathbf{b}$) plane through the origin. If $n = 0$, it is an ellipse, otherwise it is an increasing or decreasing elliptic spiral. The vectors $\mathbf{a}$ and $\mathbf{b}$ are twice the real and imaginary parts respectively of the complex eigenvector associated with the mode. It should be emphasized that these modes are special simple motions of the system that can occur if

the initial conditions are correctly chosen. In them all the variables change together in the same manner, i.e. have the same frequency and rate of growth or decay. It is instructive to consider the Argand diagram corresponding to (3.3,26). For any component y_i we have

$$y_i = e^{nt}(u_{i1}e^{i\omega t} + u_{i1}^* e^{-i\omega t}) \tag{3.3,30}$$

which is depicted graphically in Fig. 3.6*e*, where $u_{i1} = |u_{i1}|\, e^{i\varphi}$. The two vectors are conjugate, i.e. symmetric w.r.t. the real axis, and rotate in opposite directions with angular speed ω. The real value $y_i(t)$ is given by their sum, the vector **OP**. As they rotate, the two vectors shrink or grow in length, according to the sign of n.

Once again it is necessary to consider separately the case of repeated roots. Let us treat specifically the double root, i.e. $m = 2$ in (2.5,7). Then (3.3,14) is no longer the appropriate particular solution. Instead, we get from (2.5,7) a particular solution of the form

$$\mathbf{y}(t) = \mathbf{u}_r e^{\lambda_r t} + \mathbf{v}_r t e^{\lambda_r t} \tag{3.3,31}$$

where $\mathbf{u}_r$ and $\mathbf{v}_r$ are constant vectors, $\mathbf{u}_r$ being the initial state $\mathbf{u}_r = \mathbf{y}(0)$. On substituting (3.3,31) into (3.3,1), and dividing out $e^{\lambda t}$, we find

$$(\lambda_r \mathbf{u}_r + \mathbf{v}_r) + \lambda_r \mathbf{v}_r t = \mathbf{A}\mathbf{u}_r + \mathbf{A}\mathbf{v}_r t \tag{3.3,32}$$

Since this must hold for all t, we may set $t = 0$, obtaining

$$(\lambda_r \mathbf{u}_r + \mathbf{v}_r) = \mathbf{A}\mathbf{u}_r \qquad (a)$$

or

$$\begin{aligned} \mathbf{v}_r &= (\mathbf{A} - \lambda_r \mathbf{I})\mathbf{u}_r \\ &= -\mathbf{B}(\lambda_r)\mathbf{u}_r \qquad (b) \end{aligned} \tag{3.3,33}$$

where $\mathbf{B}$ is given by (3.3,3), and (3.3,31) becomes

$$\mathbf{y}(t) = (\mathbf{I} - \mathbf{B}(\lambda_r)t)\mathbf{u}_r e^{\lambda_r t} \tag{3.3,34}$$

After substituting (3.3,33*a*) in (3.3,32) a second relation is obtained, i.e.

$$\lambda_r \mathbf{v}_r t = \mathbf{A}\mathbf{v}_r t$$

valid for all t, and hence

$$(\lambda_r \mathbf{I} - \mathbf{A})\mathbf{v}_r = 0 \tag{3.3,35}$$

Equation (3.3,31) will be a solution of (3.3,1) as assumed, if there exist a λ_r and a $\mathbf{v}_r$ that satisfy (3.3,35), and if $\mathbf{u}_r$ given by (3.3,33*b*) is not infinite. The first of these conditions requires that the original characteristic equation be satisfied, i.e.

$$|\lambda_r \mathbf{I} - \mathbf{A}| = 0$$

It will now, because of the double root, be of the form

$$f(\lambda) = (\lambda - \lambda_r)^2 g(\lambda) = 0 \qquad g(\lambda_r) \neq 0 \tag{3.3,36}$$

and this condition is of course satisfied. The second condition is met by any eigenvalues found as described previously for repeated roots. Finally, the value of $\mathbf{u}_r$ can be shown to be given by

$$\mathbf{u}_r = \left(\frac{d}{d\lambda}\,\mathbf{v}(\lambda)\right)_{\lambda=\lambda_r} \tag{3.3,37}$$

where $\mathbf{v}(\lambda)$ is the column of adj $\mathbf{B}$ that gives the eigenvector $\mathbf{v}_r$.

CHARACTERISTIC COORDINATES

In this section we show how the given system of simultaneous, or coupled, real differential equations can be transformed into a new set of separate or uncoupled equations, one for each of the new variables. This decoupling is produced by in effect selecting the eigenvectors as the coordinate system for the state space instead of the original coordinates, the y_i.

Let the $n \times n$ matrix formed of the n eigenvectors be

$$\mathbf{U} = [\mathbf{u}_1 \mathbf{u}_2 \cdots \mathbf{u}_n] \tag{3.3,38}$$

Now let us define a new set of system variables (state space coordinates) q_i by the transformation

$$\mathbf{y} = \mathbf{U}\mathbf{q}; \qquad \mathbf{q} = \mathbf{U}^{-1}\mathbf{y} \tag{3.3,39}$$

(Recall that for self-adjoint systems, $\mathbf{U}$ is an orthogonal matrix and $\mathbf{U}^T = \mathbf{U}^{-1}$; the above transformation is then orthogonal. In general, however, this is not the case.) It follows from (3.3,39) that

$$\mathbf{y}(t) = \sum_{i=1}^{n} \mathbf{u}_i q_i(t) \tag{3.3,40}$$

i.e. that the state vector is a superposition of n vectors parallel to the eigenvectors. The $q_i(t)$ are the *characteristic coordinates*. Comparison with (3.3,10) shows that they must be of the form $\alpha_i e^{\lambda_i t}$ where α_i are arbitrary constants. Substitution of (3.3,39) into the differential equation of the system, (3.3,1) then yields

$$\mathbf{U}\dot{\mathbf{q}} = \mathbf{A}\mathbf{U}\mathbf{q}$$

or, premultiplying by $\mathbf{U}^{-1}$,

$$\dot{\mathbf{q}} = \mathbf{U}^{-1}\mathbf{A}\mathbf{U}\mathbf{q} \tag{3.3,41}$$

We must now examine the matrix $\mathbf{U}^{-1}\mathbf{A}\mathbf{U}$. Using (3.3,38) we have

$$\begin{aligned} \mathbf{A}\mathbf{U} &= \mathbf{A}[\mathbf{u}_1 \mathbf{u}_2 \cdots \mathbf{u}_n] \\ &= [\mathbf{A}\mathbf{u}_1 \mathbf{A}\mathbf{u}_2 \cdots \mathbf{A}\mathbf{u}_n] \end{aligned} \tag{3.3,42}$$

But the defining condition on the eigenvectors is

$$\mathbf{A}\mathbf{u}_i = \lambda_i \mathbf{u}_i$$

whence

$$\begin{aligned}\mathbf{AU} &= [\mathbf{u}_1\lambda_1\mathbf{u}_2\lambda_2 \cdots \mathbf{u}_n\lambda_n] \\ &= \mathbf{U}\Lambda\end{aligned} \tag{3.3,43}$$

where

$$\Lambda = \begin{bmatrix} \lambda_1 & 0 & 0 & \cdots & 0 \\ 0 & \lambda_2 & & & \cdot \\ 0 & & & & \cdot \\ \cdot & & & & \cdot \\ \cdot & & & & \\ \cdot & & & & \\ 0 & \cdot & \cdot & \cdot & \lambda_n \end{bmatrix} \tag{3.3,44}$$

is a diagonal matrix of the eigenvalues. It follows from (3.3,43) that

$$\mathbf{U}^{-1}\mathbf{A}\mathbf{U} = \Lambda \tag{3.3,45}$$

and that (3.3,41) becomes

$$\dot{\mathbf{q}} = \Lambda\mathbf{q} \tag{3.3,46}$$

This is the desired transformed system of differential equations, and since Λ is diagonal, each contains only one of the q's. The ith member is

$$\dot{q}_i = \lambda_i q_i \tag{3.3,47}$$

from which we get at once that

$$q_i = q_i(0)e^{\lambda_i t}$$

and hence (3.3,40) becomes

$$\mathbf{y}(t) = \sum_{i=1}^{n} \mathbf{u}_i q_i(0) e^{\lambda_i t} \tag{3.3,48}$$

Since $\mathbf{q}(0) = \mathbf{U}^{-1}\mathbf{y}(0)$ from (3.3,39), then (3.3,48) is seen to be a practical form for the solution of autonomous linear/invariant systems. An alternative form for (3.3,48) is

$$\begin{aligned}\mathbf{y}(t) &= \mathbf{U}\begin{bmatrix} e^{\lambda_1 t} & 0 & 0 & \cdots \\ 0 & e^{\lambda_2 t} & & \\ 0 & \cdot & & \\ \cdot & & \cdot & \\ \cdot & & & \cdot \\ \cdot & & & e^{\lambda_n t} \end{bmatrix}\mathbf{q}(0) \\ &= \mathbf{U}e^{\Lambda t}\mathbf{U}^{-1}\mathbf{y}(0)\end{aligned} \tag{3.3,49}$$

where, as can be verified by direct expansion, $\exp \Lambda t$ gives the diagonal matrix of the exponential coefficients. Comparison of (3.3,49) with (3.3,13) shows that

$$e^{\Lambda t} = \mathbf{U} e^{\Lambda t} \mathbf{U}^{-1} \tag{3.3,50}$$

The usual situation in vehicle dynamics is that some of the eigenvalues and eigenvectors occur in conjugate complex pairs. Thus some members of (3.3,46) will correspondingly be complex pairs. These may be transformed into a set of second-order equations, one for each complex pair of q_i. Thus let q_j and $q_{j+1} = q_j^*$ be such a pair. The corresponding equations are

$$\begin{aligned} \dot{q}_j &= \lambda_j q_j \\ \dot{q}_j^* &= \lambda_j^* q_j^* \end{aligned} \tag{3.3,51}$$

Let

$$q_j = \alpha_j + i\beta_j$$

and

$$\lambda_j = n_j + i\omega_j \tag{3.3,52}$$

The α_j and β_j are now real linear combinations of the original variables y_i that can be calculated by expanding (3.3,39). The pair of conjugate equations are now expanded by means of (3.3,52) to give

$$\begin{aligned} \dot{\alpha}_j + i\dot{\beta}_j &= (n_j + i\omega_j)(\alpha_j + i\beta_j) \\ \dot{\alpha}_j - i\dot{\beta}_j &= (n_j - i\omega_j)(\alpha_j - i\beta_j) \end{aligned}$$

Taking real and imaginary parts of either of the above leads to the alternative pair of first-order coupled equations

$$\begin{aligned} \dot{\alpha}_j &= n_j \alpha_j - \omega_j \beta_j \\ \dot{\beta}_j &= \omega_j \alpha_j + n_j \beta_j \end{aligned} \tag{3.3,53}$$

Finally, by eliminating α_j or β_j we get a pair of uncoupled real second-order equations

$$\begin{aligned} \ddot{\alpha}_j - 2n\dot{\alpha}_j + (n^2 + \omega^2)\alpha_j &= 0 \\ \ddot{\beta}_j - 2n\dot{\beta}_j + (n^2 + \omega^2)\beta_j &= 0 \end{aligned} \tag{3.3,54}$$

These equations for the α, β replace the original pair of complex first-order equations (3.3,51). However, the number of arbitrary constants in the solutions of (3.3,54) is still only two, i.e. $\alpha_j(0)$ and $\beta_j(0)$, since (3.3,53) fix the inital values of $\dot{\alpha}_j$ and $\dot{\beta}_j$.

STABILITY CRITERIA

As noted in the foregoing, the stability of a linear/invariant system is determined by the roots of the characteristic equation. A characteristic mode

will be divergent if its real part is positive, and convergent if the real part is negative, the latter denoting asymptotic stability. It is not necessary, however, actually to solve the characteristic equation in order to find whether the roots have positive real parts. This can be determined from its coefficients alone. The conditions on the coefficients that must be satisfied were first stated by Routh (ref. 3.5), who derived them from a theorem of Cauchy. Let the characteristic equation be

$$c_n s^n + c_{n-1} s^{n-1} + \cdots + c_0 = 0 \qquad (c_n > 0) \tag{3.3,55}$$

The coefficient c_n can always be made positive by changing signs throughout, so the requirement $c_n > 0$ is not restrictive. The necessary and sufficient condition for asymptotic stability (*i.e. that no root of the equation shall be* zero or have a positive real part) is that each of a series of test functions shall be positive. The test functions are constructed by the simple scheme shown below. Write the coefficients of (3.3,55) in two rows as follows:

$$c_n \; c_{n-2} \; c_{n-4} \cdots$$
$$c_{n-1} \; c_{n-3} \; c_{n-5} \cdots$$

Now construct additional rows by cross-multiplication:

$$P_{31} \; P_{32} \; P_{33} \cdots$$
$$P_{41} \; P_{42} \; P_{43} \cdots$$
$$P_{51} \cdots$$
$$\text{etc.}$$

where

$$P_{31} = c_{n-1}c_{n-2} - c_n c_{n-3}, \qquad P_{32} = c_{n-1}c_{n-4} - c_n c_{n-5}, \text{ etc.}$$

and

$$P_{41} = P_{31}c_{n-3} - P_{32}c_{n-1}, \qquad P_{42} = P_{31}c_{n-5} - c_{n-1}P_{33}, \text{ etc.}$$
$$P_{51} = P_{41}P_{32} - P_{31}P_{42}, \text{ etc.}$$

The required test functions $F_0 \cdots F_n$ are then the elements of the first column, $c_n, c_{n-1}, P_{31} \cdots P_{n+1,1}$. If they are all positive, then there are no unstable roots. The number of test functions is $n + 1$, and the last one, F_n, always contains the product $c_0 F_{n-1}$. Duncan (ref. 3.6, Sec. 4.10) has shown that the vanishing of c_0 and of F_{n-1} represent significant critical cases. If the system is stable, and some design parameter is then varied in such a way as to lead to instability, then the following conditions hold:

(a) If only c_0 changes from + to −, then one real root changes from negative to positive; i.e. one divergence appears in the solution (Fig. 3.6).

(b) If only F_{n-1} changes from + to −, then the real part of one complex pair of roots changes from negative to positive; i.e. one divergent oscillation appears in the solution (Fig. 3.6).

Thus the conditions $c_0 = 0$ and $F_{n-1} = 0$ define boundaries between stability and instability. The former is the boundary between stability and static instability, and the latter is the boundary between stability and a divergent oscillation.

TEST FUNCTIONS FOR A CUBIC

Let the cubic equation be

$$As^3 + Bs^2 + Cs + D = 0 \qquad (A > 0)$$

Then

$$F_0 = A, \qquad F_1 = B, \qquad F_2 = BC - AD, \qquad F_3 = D(BC - AD)$$

The necessary and sufficient conditions for all the test functions to be positive are that A, B, D, and $(BC - AD)$ be positive. It follows that C also must be positive.

TEST FUNCTIONS FOR A QUARTIC

Let the quartic equation be

$$As^4 + Bs^3 + Cs^2 + Ds + E = 0 \qquad (A > 0)$$

Then the test functions are $F_0 = A$, $F_1 = B$, $F_2 = BC - AD$, $F_3 = F_2D - B^2E$, $F_4 = F_3BE$. The necessary and sufficient conditions for these test functions to be positive are

$$A, B, D, E > 0$$

and

$$D(BC - AD) - B^2E > 0 \qquad (3.3,50)$$

It follows that C also must be positive. The quantity on the left-hand side of (3.3,50) is commonly known as *Routh's discriminant.*

TEST FUNCTIONS FOR A QUINTIC

Let the quintic equation be

$$As^5 + Bs^4 + Cs^3 + Ds^2 + Es + F = 0 \qquad (A > 0)$$

Then the test functions are $F_0 = A$, $F_1 = B$, $F_2 = BC - AD$, $F_3 = F_2D - B(BE - AF)$, $F_4 = F_3(BE - AF) - F_2^2F$, $F_5 = F_4F_2F$. These test functions will all be positive provided that

$$A, B, D, F, F_2, F_4 > 0$$

It follows that C and E also are necessarily positive.

COMPLEX CHARACTERISTIC EQUATION

There may arise certain situations in which some of the coefficients of the differential equations of the system are complex instead of real, and consequently some of the coefficients of the characteristic equation are complex too. The criteria for stability in that case are discussed by Morris (ref. 3.7).

3.4 RESPONSE OF LINEAR/INVARIANT SYSTEMS

As remarked in Sec. 3.2, one of the basic problems of system analysis is that of calculating the system output for a given input, i.e. its *response*. This is the problem of nonautonomous performance, in contrast with the

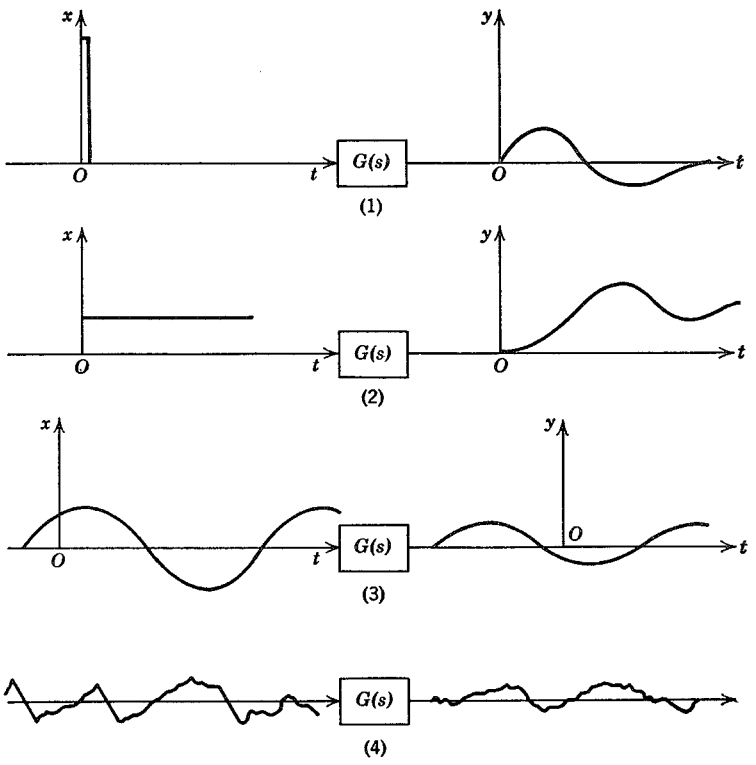

FIG. 3.7 The four basic response problems. (1) Impulse response. (2) Step response. (3) Frequency response. (4) Response to random input.

autonomous behavior treated in the preceding section. The former is associated with nonzero inputs and zero initial conditions, whereas the reverse holds for the latter.

It is evident that the transfer function defined in Sec. 3.2 supplies all that is required for such response calculations—and provided that the input and transfer function are not too complicated, the whole procedure can be carried out analytically, leading to closed-form results. The method, of course, is to calculate the Laplace transform of the input, and then carry out the inverse transformation of $\bar{y}(s) = G(s)\bar{x}(s)$. When this is not practical, it is necessary to resort to machine computation to get answers.

The major response properties of linear/invariant systems can be displayed by considering four basic kinds of input, as illustrated in Fig. 3.7. These are treated individually in the sections that follow. Before proceeding to them, however, we shall first digress to consider a useful interpretation of the transfer functions of high-order systems.

INTERPRETATION OF HIGH-ORDER SYSTEM AS A CHAIN

The transfer function for any selected input/output pair can be found as an element of $\mathbf{G}$ given by (3.2,23), i.e.

$$\mathbf{G} = \mathbf{B}^{-1}\mathbf{C}$$

where $\mathbf{B} = s\mathbf{I} - \mathbf{A}$, as in Sec. 3.3 and $\mathbf{A}$ and $\mathbf{C}$ are the constant matrices that define the system. In view of the definition of the inverse matrix we see that $\mathbf{G}$ is given by

$$\mathbf{G} = \frac{\text{adj } \mathbf{B}}{f(s)}\,\mathbf{C} \tag{3.4,1}$$

where $f(s)$ is the characteristic polynomial (3.3,7). As already pointed out in Sec. 3.3 the elements of adj $\mathbf{B}$ are also polynomials in s. It follows from (3.4,1) and (3.3,7) that each element of $\mathbf{G}$ is of the form

$$G_{ij} = \frac{N(s)}{(s - \lambda_1)(s - \lambda_2)\cdots(s - \lambda_n)} \tag{3.4,2}$$

where $N(s)$ is some polynomial. Now some of the eigenvalues λ_r are real, but others occur in complex pairs, so to obtain a product of factors containing only real numbers we rewrite the denominator thus

$$f(s) = \prod_{r=1}^{m} (s - \lambda_r) \prod_{r=m+1}^{\frac{1}{2}(n+m)} (s^2 + a_r s + b_r) \tag{3.4,3}$$

Here λ_r are the m real roots of $f(s)$ and the quadratic factors with real coefficients a_r and b_r produce the $(n - m)$ complex roots. It is then clearly

evident that the transfer function (3.4,2) is also the overall transfer function of the fictitious system made up of the series of elements shown in Fig. 3.8. The leading component $N(s)$ is of course particular to the system, but all the remaining ones are of one or other of two simple kinds. These two, first-order components and second-order components, may therefore be regarded as the basic building blocks of linear/invariant systems. It is for this reason that it is important to understand their characteristics well—the

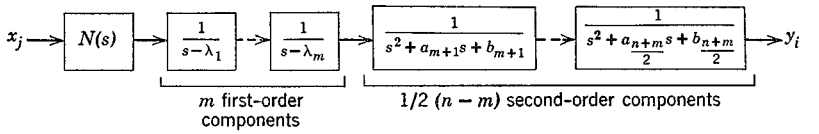

FIG. 3.8 High-order system as a "chain."

properties of all higher-order systems can be inferred directly from those of these two basic elements.

IMPULSE RESPONSE

The system is specified to be initially quiescent and at time zero is subjected to a single impulsive input

$$x_j(t) = \delta(t) \tag{3.4,4}$$

The Laplace transform of the ith component of the output is then

$$\bar{y}_i(s) = G_{ij}(s)\ \bar{\delta}(s)$$

which, from Table 2.3, item 1, becomes

$$\bar{y}_i(s) = G_{ij}(s)$$

This response to the unit impulse is called the *impulsive admittance* and is denoted $h_{ij}(t)$. It follows that

$$\bar{h}_{ij}(s) = G_{ij}(s) \qquad (a)$$

i.e. $G(s)$ is the Laplace transform of $h(t)$

$$G_{ij}(s) = \int_0^\infty h_{ij}(t)e^{-st}\,dt \qquad (b) \tag{3.4,5}$$

From the inversion theorem, (2.3,8) $h_{ij}(t)$ is then given by

$$h_{ij}(t) = \frac{1}{2\pi i}\int_c G_{ij}(s)e^{st}\,ds \tag{3.4,6}$$

Now if the system is stable, all the poles of $G_{ij}(s)$ lie in the left half of the s plane, and this is the usual case of interest. The line integral of (3.4,6) can then be taken on the imaginary axis, $s = i\omega$, so that (3.4,6) leads to

$$h_{ij}(t) = \frac{1}{2\pi} \int_{-\infty}^{\infty} e^{i\omega t} G_{ij}(i\omega)\, d\omega \tag{3.4,7}$$

i.e. it is the inverse Fourier transform of $G_{ij}(i\omega)$. The significance of $G_{ij}(i\omega)$ will be seen later.

For a first-order component with eigenvalue λ the differential equation is

$$\dot{y} - \lambda y = x \tag{3.4,8}$$

for which we easily get

$$G(s) = \bar{h}(s) = \frac{1}{s - \lambda} \tag{3.4,9}$$

The inverse is found directly from item 8 of Table 2.3 as

$$h(t) = e^{\lambda t}$$

For convenience in interpretation, λ is frequently written as $\lambda = -1/T$, where T is termed the *time constant* of the system. Then

$$h(t) = e^{-t/T} \tag{3.4,10}$$

A graph of $h(t)$ is presented in Fig. 3.9*a*, and shows clearly the significance of the time constant T.

For a second-order system the differential equation is (2.4,1) from which it easily follows that

$$G(s) = \bar{h}(s) = \frac{1}{s^2 + 2\zeta\omega_n s + {\omega_n}^2} \tag{3.4,11}$$

Let the eigenvalues be $\lambda = n \pm i\omega$, (cf. 2.5,2) where

$$n = -\zeta\omega_n$$

$$\omega = \omega_n(1 - \zeta^2)^{1/2}$$

then $\bar{h}(s)$ becomes

$$\begin{aligned} \bar{h}(s) &= \frac{1}{(s - n - i\omega)(s - n + i\omega)} \\ &= \frac{1}{(s^2 - n^2) + \omega^2} \end{aligned} \tag{3.4,11a}$$

and the inverse is found from item 13, Table 3.3 to be

$$h(t) = \frac{1}{\omega} e^{nt} \sin \omega t \tag{3.4,12}$$

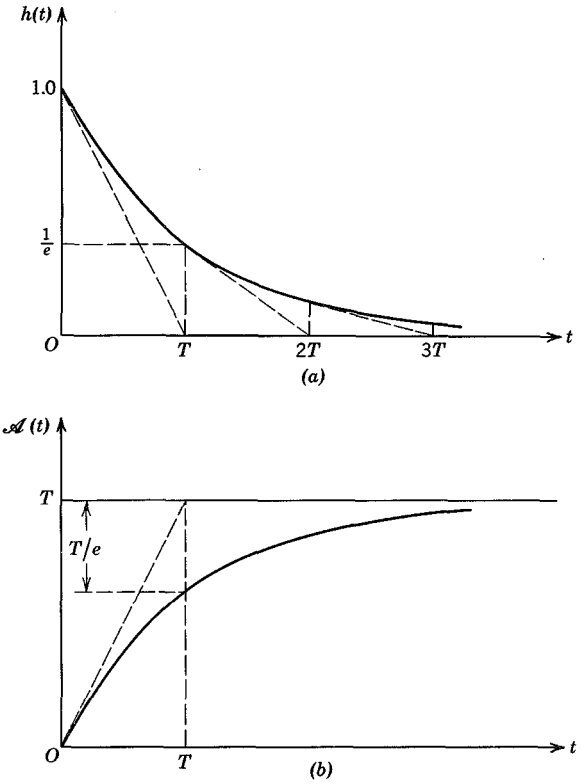

FIG. 3.9 Admittances of a first-order system.

For a stable system n is negative and (3.4,12) describes a damped sinusoid of frequency ω. This is plotted for various ζ in Fig. 3.10. Note that the coordinates are so chosen as to lead to a one-parameter family of curves. Actually the above result only applies for $\zeta \leq 1$. The corresponding expression for $\zeta \geq 1$ is easily found by the same method and is

$$h(t) = \frac{1}{\omega'} e^{nt} \sinh \omega' t \qquad (3.4,13)$$

where

$$\omega' = \omega_n(\zeta^2 - 1)^{1/2}$$

Graphs of (3.4,13) are also included in Fig. 3.10, although in this case the second-order representation could be replaced by two first-order elements in series.

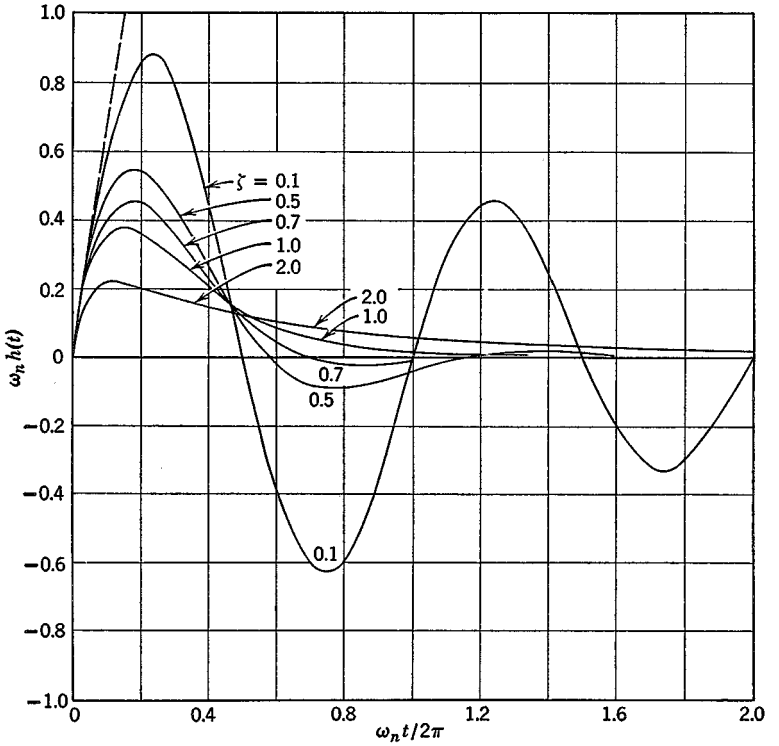

FIG. 3.10 Impulsive admittance of second-order systems.

RELATION BETWEEN IMPULSE RESPONSE AND AUTONOMOUS SOLUTION

It follows from (3.4,5*a*) that the matrix of impulse response functions $\mathbf{H} = [h_{ij}]$ is related to that of the transfer functions by

$$\bar{\mathbf{H}}(s) = \mathbf{G}(s) \tag{3.4,14}$$

Furthermore, from (3.2,23) we have that $\mathbf{G}(s) = \mathbf{B}^{-1}(s)\mathbf{C}$, so that

$$\bar{\mathbf{H}}(s) = \mathbf{B}^{-1}(s)\mathbf{C} \tag{3.4,15}$$

or

$$\mathbf{B}^{-1}(s) = \bar{\mathbf{H}}(s)\mathbf{C}^{-1} \tag{3.4,16}$$

Now in the autonomous case we have (3.3,4)

$$\bar{\mathbf{y}}(s) = \mathbf{B}^{-1}(s)\mathbf{y}(0) \tag{3.3,4}$$

Substitution of (3.4,16) into (3.3,4) yields the result for the autonomous solution with initial condition $y(0)$, i.e.

$$\bar{\mathbf{y}}(s) = \bar{\mathbf{H}}(s)\mathbf{C}^{-1}\mathbf{y}(0)$$

or

$$\mathbf{y}(t) = \mathbf{H}(t)\mathbf{C}^{-1}\mathbf{y}(0) \tag{3.4,17}$$

STEP-FUNCTION RESPONSE

This is like the impulse response treated above except that the input is the unit step function $\mathbf{1}(t)$, with transform $1/s$. The response in this case is called the *indicial admittance*, and is denoted $\mathscr{A}_{ij}(t)$. It follows then that

$$\bar{\mathscr{A}}_{ij}(s) = G_{ij}(s)\bar{\mathbf{1}}(s) = \frac{G_{ij}(s)}{s} \qquad (a) \tag{3.4,18}$$

or

$$\bar{\mathscr{A}}_{ij}(s) = \frac{\bar{h}_{ij}(s)}{s} \qquad (b)$$

Since the initial values (at $t = 0^-$) of $h_{ij}(t)$ and $\mathscr{A}_{ij}(t)$ are both zero, the theorem (2.3,16) shows that

$$\mathscr{A}_{ij}(t) = \int_0^t h_{ij}(\tau)\, d\tau \qquad (a)$$

or

$$h_{ij}(t) = \frac{d\mathscr{A}_{ij}(t)}{dt} \qquad (b) \tag{3.4,19}$$

Thus $\mathscr{A}_{ij}(t)$ can be found either by direct inversion of (3.4,18*b*) (see examples in Sec. 2.5) or by integration of $h_{ij}(t)$. By either method the results for first- and second-order systems are readily obtained, and are as follows (for a single input/output pair the indicial subscript is dropped):

First-order system:

$$\mathscr{A}(t) = T(1 - e^{-t/T}) \tag{3.4,20}$$

Second-order system:

$$\mathscr{A}(t) = \frac{1}{\omega_n^2}\left[1 - e^{nt}(\cos \omega t - \frac{n}{\omega}\sin \omega t)\right], \qquad \zeta < 1 \tag{3.4,21}$$

and for $\zeta > 1$, $\mathscr{A}(t)$ is given by the r.h.s. of (2.5,5).

Graphs of the indicial responses are given in Figs. 3.9*b* and 3.11.

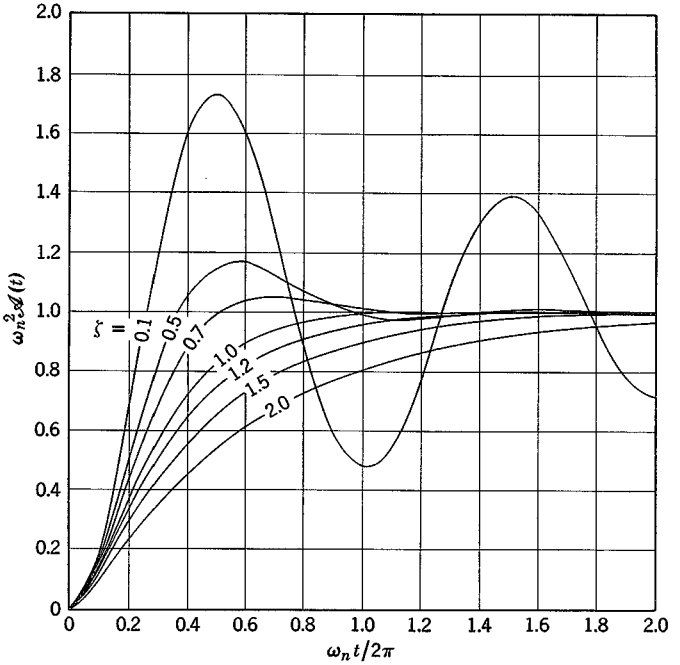

FIG. 3.11 Indicial admittance of second-order systems.

FREQUENCY RESPONSE

When a stable linear/invariant system has a sinusoidal input, then after some time the transients associated with the starting conditions die out, and there remains only a steady-state sinusoidal response at the same frequency as that of the input. Its amplitude and phase are generally different from those of the input, however, and the expression of these differences is embodied in the frequency-response function.

Consider a single input/output pair, and let the input be the sinusoid $a_1 \cos \omega t$. We find it convenient to replace this by the complex expression $x = A_1 e^{i\omega t}$, of which $a_1 \cos \omega t$ is the real part. A_1 is known as the *complex amplitude* of the wave. The output sinusoid can be respresented by a similar expression, $y = A_2 e^{i\omega t}$, the real part of which is the physical output. As usual, x and y are interpreted as rotating vectors whose projections on the real axis give the relevant physical variables (see Fig. 3.12*a*).

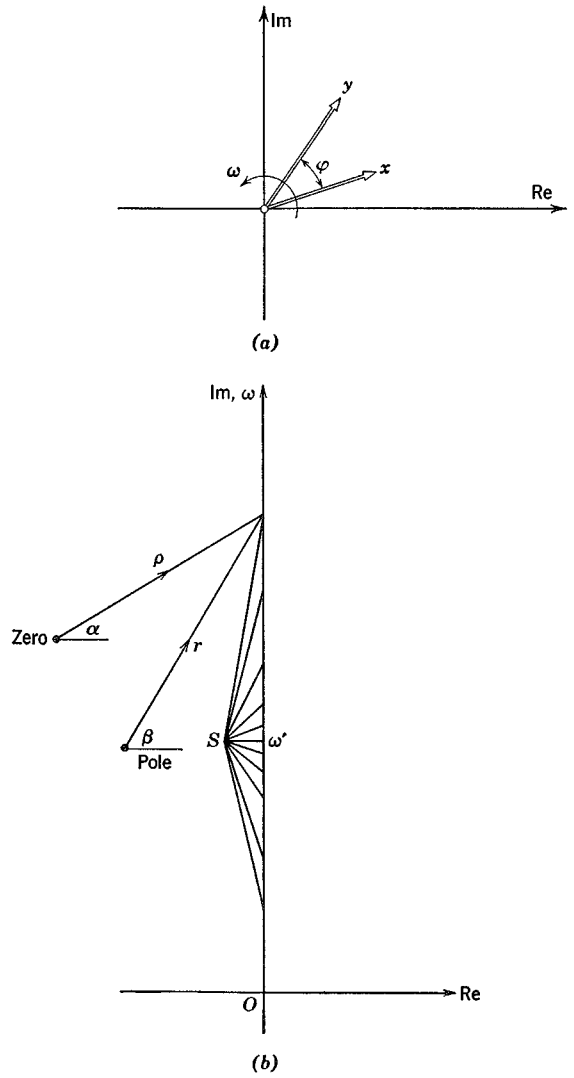

FIG. 3.12 (*a*) Complex input and output. (*b*) Effect of singularity close to axis.

From Table 2.3, item 8, the transform of x is

$$\bar{x} = \frac{A_1}{s - i\omega}$$

Therefore

$$\bar{y} = A_1 \frac{G(s)}{s - i\omega}$$

The function $G(s)$ is given by (3.4,2) so that

$$\bar{y} = A_1 \frac{N(s)}{(s - i\omega)f(s)} \tag{3.4,22}$$

The roots of the denominator of the r.h.s. are

$$\lambda_1 \cdots \lambda_n,\ i\omega$$

so that the application of the expansion theorem (2.5,6) yields the complex output

$$\begin{aligned} y(t) &= A_1 \sum_{r=1}^{n+1} \left[\frac{(s - \lambda_r)N(s)}{(s - i\omega)f(s)} \right]_{s=\lambda_r} e^{\lambda_r t} \\ &= A_1 \left[\frac{N(i\omega)}{f(i\omega)} e^{i\omega t} + c_1 e^{\lambda_1 t} + c_2 e^{\lambda_2 t} + \cdots + c_n e^{\lambda_n t} \right] \end{aligned} \tag{3.4.23}$$

Since we have stipulated that the system is stable, all the roots $\lambda_1 \cdots \lambda_n$ of the characteristic equation have negative real parts. Therefore $e^{\lambda_r t} \to 0$ as $t \to \infty$, and the steady-state periodic solution is

$$y(t) = A_1 \frac{N(i\omega)}{f(i\omega)} e^{i\omega t}, \qquad t \to \infty$$

or

$$\begin{aligned} y(t) &= A_1 G(i\omega) e^{i\omega t} \\ &= A_2 e^{i\omega t} \end{aligned}$$

Thus

$$A_2 = A_1 G(i\omega) \tag{3.4,24}$$

is the complex amplitude of the output, or

$$G(i\omega) = \frac{A_2}{A_1} \tag{3.4,25}$$

the *frequency response function*, is the ratio of the complex amplitudes. In general, $G(i\omega)$ is a complex number, varying with the circular frequency ω. Let it be given in polar form by

$$G(i\omega) = KMe^{i\varphi} \tag{3.4,26}$$

where K is the static gain (3.2,4). Then

$$\frac{A_2}{A_1} = KMe^{i\varphi} \tag{3.4,27}$$

From (3.4,27) we see that the amplitude ratio of the steady-state output to the input is $|A_2/A_1| = KM$: i.e. that the output amplitude is $a_2 = KMa_1$, and that the phase relation is as shown on Fig. 3.12. The output leads the input by the angle φ. The quantity M, which is the modulus of $G(i\omega)$ divided by K, we call the magnification factor, or *dynamic gain*, and the product KM we call the *total gain*. It is important to note that M and φ are frequency-dependent.

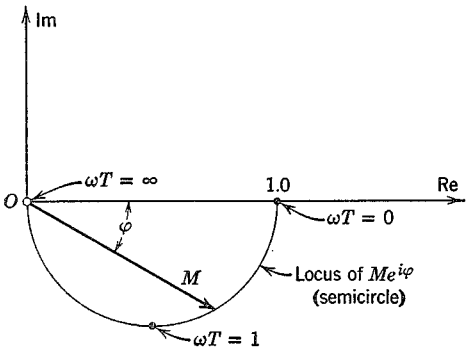

FIG. 3.13 Vector plot of $Me^{i\varphi}$ for first-order systems.

Graphical representations of the frequency response commonly take the form of either vector plots of $Me^{i\varphi}$ (Nyquist diagram) or plots of M and φ as functions of frequency (Bode diagram). Examples of these are shown in Figs. 3.13 to 3.17.

EFFECT OF POLES AND ZEROS ON FREQUENCY RESPONSE

We have seen (3.4,2) that the transfer function of a linear/invariant system is a ratio of two polynomials in s, the denominator being the characteristic polynomial. The roots of the characteristic equation are the *poles* of the transfer function, and the roots of the numerator polynomial are its *zeros*. Whenever a pair of complex poles or zeros lies close to the imaginary axis, a characteristic peak or valley occurs in the amplitude of the frequency-response curve together with a rapid change of phase angle at the corresponding value of ω. Several examples of this phenomenon are to be seen in the frequency response curves in Figs. 10.3, 10.11, and 10.12. The reason for

this behavior is readily appreciated by putting (3.4,2) in the following form:

$$G(s) = \frac{(s - z_1) \cdot (s - z_2) \cdots (s - z_m)}{(s - \lambda_1) \cdot (s - \lambda_2) \cdots (s - \lambda_n)}$$

where the λ_i are the characteristic roots (poles) and the z_i are the zeros of $G(s)$. Let

$$(s - z_k) = \rho_k e^{i\alpha_k}$$
$$(s - \lambda_k) = r_k e^{i\beta_k}$$

where ρ, r, α, β are the distances and angles shown in Fig. 3.12*b* for a point $s = i\omega$ on the imaginary axis. Then

$$|G| = \prod_{k=1}^{m} \rho_k \Big/ \prod_{k=1}^{n} r_k$$
$$\varphi = \sum_{1}^{m} \alpha_k - \sum_{1}^{n} \beta_k$$

When the singularity is close to the axis, with imaginary coordinate ω' as illustrated for point S on Fig. 3.12*b*, we see that as ω passes through ω', a sharp minimum occurs in ρ or r, as the case may be, and the angle α or β increases rapidly through approximately 180°. Thus we have the following cases:

1. For a pole, in the left half-plane, there results a peak in $|G|$ and a reduction in φ of about 180°.
2. For a zero in the left half-plane, there is a valley in $|G|$ and an increase in φ of about 180°.
3. For a zero in the right half-plane, there is a valley in $|G|$ and a decrease in φ of about 180°.

FREQUENCY RESPONSE OF FIRST-ORDER SYSTEM

The first-order transfer function, written in terms of the time constant T is

$$G(s) = \frac{1}{s + 1/T} \tag{3.4,28}$$

whence

$$K = \lim_{s \to 0} G(s) = T$$

The frequency response is determined by the vector $G(i\omega)$

$$G(i\omega) = KMe^{i\varphi} = \frac{T}{1 + i\omega T}$$

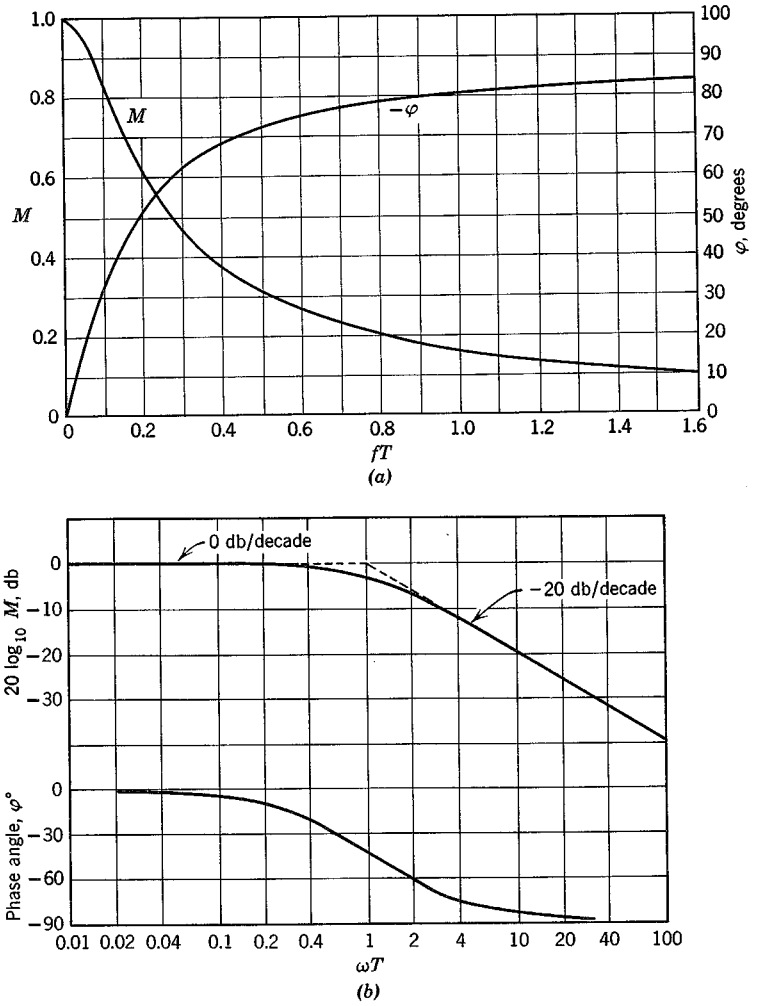

FIG. 3.14 Frequency-response curves—first-order system.

whence

$$Me^{i\varphi} = \frac{1 - i\omega T}{1 + \omega^2 T^2} \tag{3.4,29}$$

From (3.4,29), M and φ are found to be

$$M = \frac{1}{(1 + \omega^2 T^2)^{\frac{1}{2}}} \tag{3.4,30}$$
$$-\varphi = \tan^{-1} \omega T$$

A vector plot of $Me^{i\varphi}$ is shown in Fig. 3.13. This kind of diagram is sometimes called the transfer-function locus. Plots of M and φ are given in Figs. 3.14*a* and *b*. The abscissa is fT or $\log \omega T$ where $f = \omega/2\pi$, the input frequency. This is the only parameter of the equations, and so the curves are applicable to all first-order systems. It should be noted that at $\omega = 0$, $M = 1$ and $\varphi = 0$. This is always true because of the definitions of K and $G(s)$—it can be seen from (3.2,4) that $G(0) = K$.

FREQUENCY RESPONSE OF A SECOND-ORDER SYSTEM

The transfer function of a second-order system is given in (3.4,11). The frequency-response vector is therefore

$$Me^{i\varphi} = \frac{{\omega_n}^2}{({\omega_n}^2 - \omega^2) + 2i\zeta\omega_n\omega} \tag{3.4,31}$$

From the modulus and argument of (3.4,31), we find that

$$M = \frac{1}{\{[1 - (\omega/\omega_n)^2]^2 + 4\zeta^2(\omega/\omega_n)^2\}^{\frac{1}{2}}}$$
$$\varphi = -\tan^{-1} \frac{2\zeta\omega/\omega_n}{1 - (\omega/\omega_n)^2} \tag{3.4,32}$$

A representative vector plot of $Me^{i\varphi}$, for damping ratio $\zeta = 0.4$, is shown in Fig. 3.15, and families of M and φ are shown in Figs. 3.16 and 3.17. Whereas a single pair of curves serves to define the frequency response of all first-order systems (Fig. 3.14), it takes two families of curves, with the damping ratio as parameter, to display the characteristics of all second-order systems. The importance of the damping as a parameter should be noted. It is especially powerful in controlling the magnitude of the resonance peak which occurs near unity frequency ratio. At this frequency the phase lag is by contrast independent of ζ, as all the curves pass through $\varphi = -90°$ there. For all values of ζ, $M \to 1$ and $\varphi \to 0$ as $\omega/\omega_n \to 0$. This shows that, whenever a system is driven by an oscillatory input whose frequency is low compared to

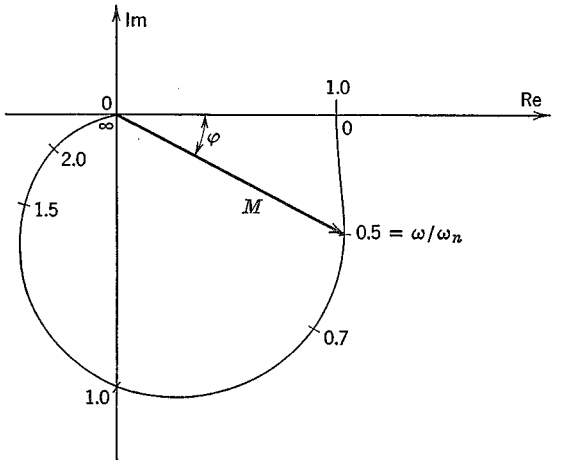

FIG. 3.15 Vector plot of $Me^{i\varphi}$ for second-order system. Damping ratio $\zeta = 0.4$.

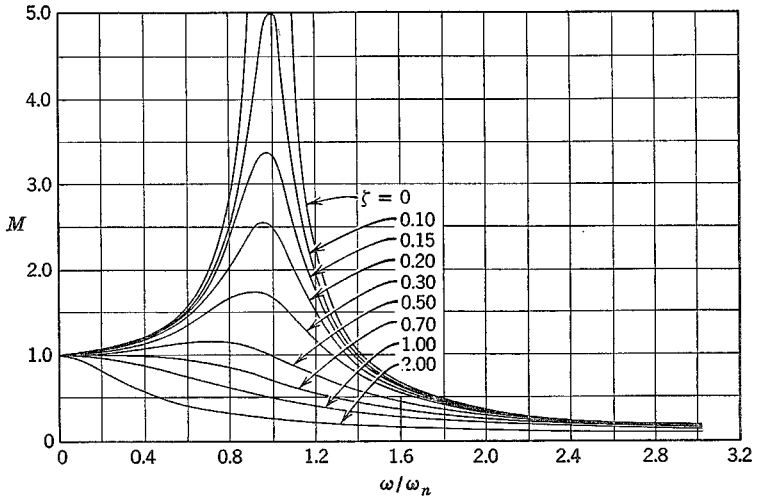

FIG. 3.16 Frequency-response curves—second-order system.

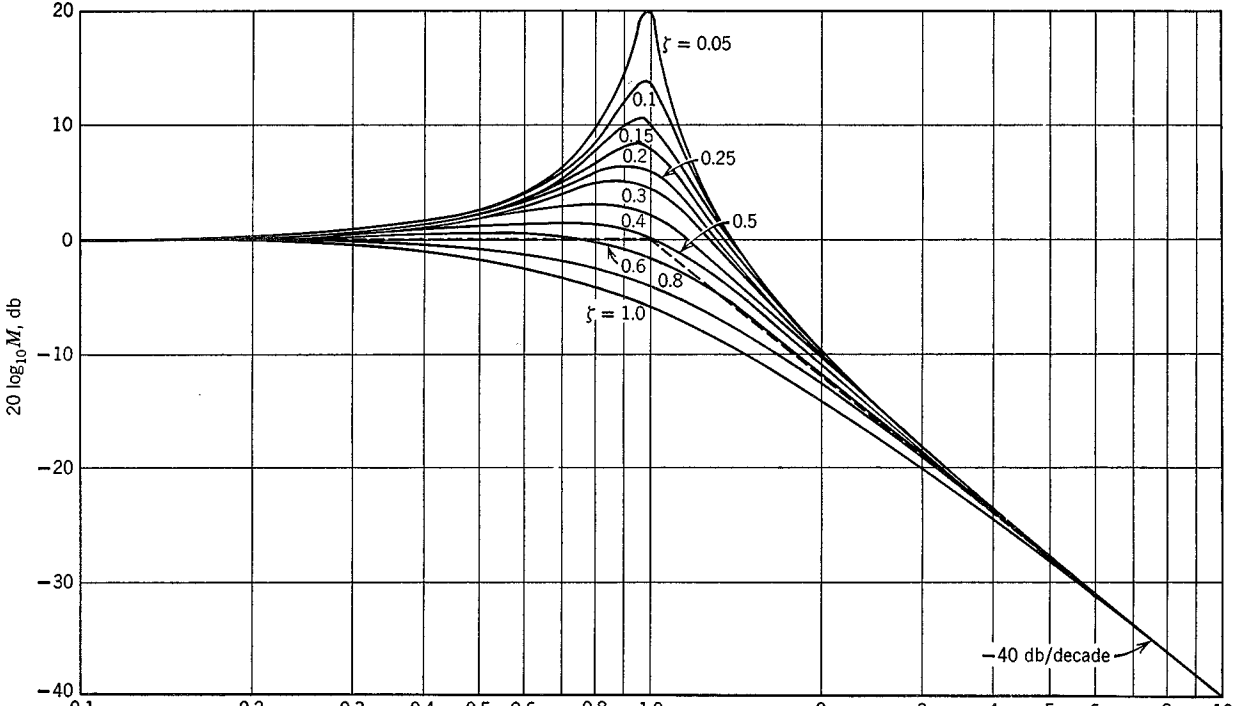
20
10
0
−10
−20
−30
−40
20 log10M, db
ζ = 0.05
0.1
0.15
0.2
0.25
0.3
0.4
0.5
0.6
0.8
ζ = 1.0
−40 db/decade
0.1
0.2
0.3
0.4
0.5
0.6
0.8
1.0
2
3
4
5
6
8
10
ω/ωn

(a)

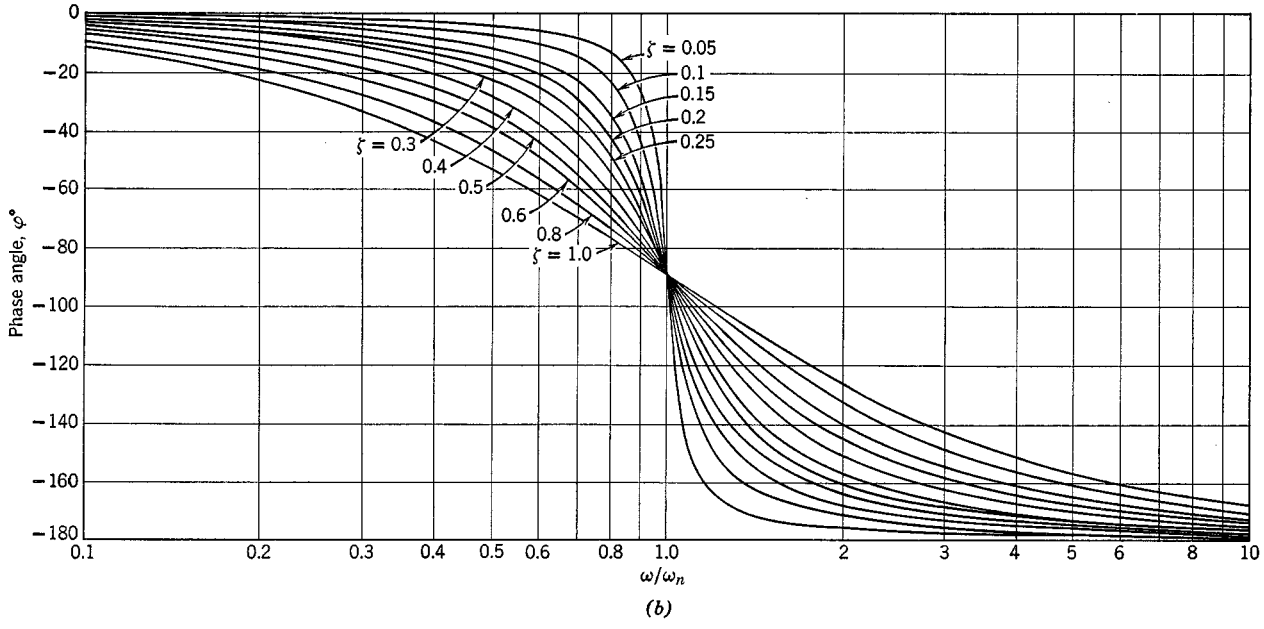

FIG. 3.17 Frequency-response curves—second-order system.

the undamped natural frequency, the response will be *quasistatic*. That is, at each instant, the output will be the same as though the instantaneous value of the input were applied statically.

The behavior of the output when ζ is near 0.7 is interesting. For this value of ζ, it is seen that φ is very nearly linear with ω/ω_n up to 1.0. Now the phase lag can be interpreted as a time lag, $\tau = (\varphi/2\pi)T = \varphi/\omega$ where T is the period. The output wave form will have its peaks retarded by τ sec relative to the input. For the value of ζ under consideration, $\varphi/(\omega/\omega_n) \doteq \pi/2$ or $\varphi/\omega = \pi/2\omega_n = \frac{1}{4}T_n$, where $T_n = 2\pi/\omega_n$, the undamped natural period. Hence we find that, for $\zeta \doteq 7$, there is a nearly constant time lag $\tau \doteq \frac{1}{4}T_n$, independent of the input frequency, for frequencies below resonance.

The "chain" concept of higher-order systems is especially helpful in relation to frequency response. It is evident that the phase changes through the individual elements are simply additive, so that higher-order systems tend to be characterized by greater phase lags than low-order ones. Also the individual amplitude ratios of the elements are multiplied to form the overall ratio. More explicitly, let

$$G(s) = G_1(s) \cdot G_2(s) \cdots G_n(s)$$

be the overall transfer function of n elements. Then

$$\begin{aligned} G(i\omega) &= G_1(i\omega) \cdot G_2(i\omega) \cdots G_n(i\omega) \\ &= (K_1M_1 \cdot K_2M_2 \cdots K_nM_n)e^{i(\varphi_1+\varphi_2+\cdots\varphi_n)} \\ &= KMe^{i\varphi} \end{aligned}$$

so that

$$KM = \prod_{r=1}^{n} K_rM_r \qquad (a)$$

$$\varphi = \sum_{r=1}^{n} \varphi_r \qquad (b) \qquad (3.4,33)$$

On logarithmic plots (Bode diagrams) we note that

$$\log KM = \sum_{r=1}^{n} \log K_rM_r \qquad (3.4,34)$$

Thus the log of the overall gain is obtained as a sum of the logs of the component gains, and this fact, together with the companion result for phase angle (3.4,33) greatly facilitates graphical methods of analysis and system design.

RELATION BETWEEN IMPULSE RESPONSE AND FREQUENCY RESPONSE

We saw earlier (3.4,7), that $h(t)$ is the inverse Fourier transform of $G(i\omega)$, which we can now identify as the frequency response vector. The reciprocal

Fourier transform relation then gives

$$G(i\omega) = \int_{-\infty}^{\infty} h(t)e^{-i\omega t}dt \tag{3.4,35}$$

i.e. *the frequency response and impulsive admittance are a Fourier transform pair.*

An alternative to (3.4,7) that involves the integration of a real variable over only positive ω can be derived from the properties of $h(t)$ and $G(i\omega)$. Since ω is always preceded by the factor i in $G(i\omega)$, it follows that $G^*(i\omega) = G(-i\omega)$ where $(\ )^*$ denotes the complex conjugate. Hence

$$\begin{aligned} h(t) &= \frac{1}{2\pi}\int_{-\infty}^{\infty} e^{i\omega t}G(i\omega)\,d\omega = \frac{1}{2\pi}\int_{0}^{\infty}[e^{i\omega t}G(i\omega) + e^{-i\omega t}G^*(i\omega)]\,d\omega \\ &= \frac{K}{2\pi}\int_{0}^{\infty}\left\{e^{i\omega t}M(\omega)e^{i\varphi(\omega)} + e^{-i\omega t}M(\omega)e^{-i\varphi(\omega)}\right\}d\omega \\ &= \frac{K}{2\pi}\int_{0}^{\infty} M\{e^{i(\omega t+\varphi)} + e^{-i(\omega t+\varphi)}\}\,d\omega \\ &= \frac{K}{\pi}\int_{0}^{\infty} M\cos(\omega t + \varphi)\,d\omega \\ &= \frac{K}{\pi}\int_{0}^{\infty} M\cos\omega t\cos\varphi\,d\omega - \frac{K}{\pi}\int_{0}^{\infty} M\sin\omega t\sin\varphi\,d\omega \end{aligned} \tag{3.4,36}$$

Since $h(t) = 0$ for $t < 0$, then the second term on the r.h.s. of (3.4,36) is equal to the first term for $t < 0$. But the second term is an odd function of t whereas the first is even. Hence the two terms are equal and opposite for $t < 0$ and equal for $t > 0$. Thus

$$h(t) = \frac{2}{\pi}K\int_{0}^{\infty} M(\omega)\cos\varphi(\omega)\cdot\cos\omega t\,d\omega \tag{3.4,37}$$

which is the desired result.

SUPERPOSITION THEOREM (CONVOLUTION INTEGRAL, DUHAMEL'S INTEGRAL)

The theorem of this section facilitates the calculation of transient responses of linear systems to complicated forcing functions. The general response appears as the superposition of responses to a sequence of steps or impulses which simulate the actual forcing function.

Let $\bar{x}_1(s)$ be the transform of $x_1(t)$

and $\bar{x}_2(s)$ be the transform of $x_2(t)$

Then the function $x_3(t)$ whose transform is the product $\bar{x}_3 = \bar{x}_1\bar{x}_2$ is

$$x_3(t) = \int_{\tau=0}^{t} x_1(\tau)x_2(t-\tau)\,d\tau \tag{3.4,38}$$

Proof:

$$\bar{x}_3 = \int_0^\infty e^{-su}x_1(u)\,du \times \int_0^\infty e^{-sv}x_2(v)\,dv$$

where u and v are dummy variables of integration. This is equivalent to the double integral

$$\bar{x}_3(s) = \iint_S e^{-s(u+v)}x_1(u)x_2(v)\,du\,dv$$

where S is the area of integration shown in Fig. 3.18*a*. Now let the region of

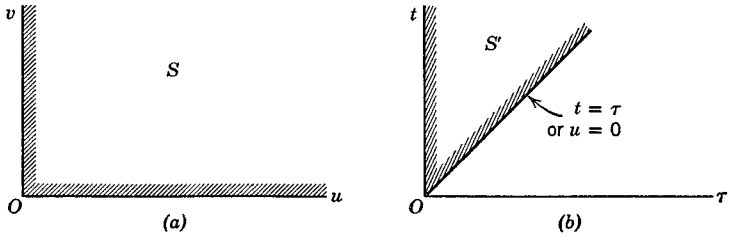

FIG. 3.18 (*a*) The (u, v) plane. (*b*) The (t, τ) plane.

integration be transformed into the t, τ plane by the substitution

$$u + v = t$$

$$v = \tau$$

Then

$$\bar{x}_3(s) = \iint_{S'} e^{-st}x_1(t-\tau)x_2(\tau)\,dS'$$

where S' is the region shown in Fig. 3.18*b*. Integration first with respect to τ gives

$$\bar{x}_3(s) = \int_{t=0}^{\infty} e^{-st}\,dt \int_{\tau=0}^{t} x_1(t-\tau)x_2(\tau)\,d\tau$$

Therefore, by definition (2.3,7)

$$x_3(t) = \int_{\tau=0}^{t} x_1(t-\tau)x_2(\tau)\,d\tau \qquad \text{Q.E.D.}$$

We now apply this result when the system $G(s)$ is subjected to an arbitrary input $x(t)$. The response is given by

$$\bar{y}(s) = G(s)\bar{x}(s)$$

Now we saw earlier that $G(s) = \bar{h}(s)$ (3.4,5*a*), so

$$\bar{y}(s) = \bar{h}(s)\bar{x}(s) \tag{3.4,39}$$

whence (3.4,38) yields

$$\begin{aligned} y(t) &= \int_{\tau=0}^{t} h(t-\tau)x(\tau)\,d\tau \qquad (a) \\ \text{or} \qquad y(t) &= \int_{\tau=0}^{t} h(\tau)x(t-\tau)\,d\tau \qquad (b) \end{aligned} \tag{3.4,40}$$

The preceding equation applies to a single input/output pair. For a multivariable system we would obviously have as the extension of (3.4,40*a*) (and similarly for 3.4,40*b*)

$$\begin{aligned} y_i(t) &= \int_{\tau=0}^{t} \sum_j h_{ij}(t-\tau)x_j(\tau)\,d\tau \qquad (a) \\ \text{or} \qquad \mathbf{y}(t) &= \int_{\tau=0}^{t} \mathbf{H}(t-\tau)\mathbf{x}(\tau)\,d\tau \qquad (b) \end{aligned} \tag{3.4,41}$$

where **H** is the rectangular matrix of impulse response functions.

By considering a slightly modified form of (3.4,39) we can obtain a companion result involving $\mathscr{A}(t)$ instead of $h(t)$. We may write (see 3.4,18*b*)

$$\begin{aligned} \bar{y}(s) &= \frac{\bar{h}(s)}{s} \cdot s\bar{x}(s) \\ &= \bar{\mathscr{A}}(s)\{\mathscr{L}[\dot{x}] + x(0)\} \\ &= \bar{\mathscr{A}}(s)\mathscr{L}[\dot{x}] + \bar{\mathscr{A}}(s)x(0) \end{aligned}$$

Again applying (3.4,38) we get

$$\begin{aligned} y(t) &= \mathscr{A}(t)x(0) + \int_{\tau=0}^{t} \mathscr{A}(t-\tau)\dot{x}(\tau)\,d\tau \qquad (a) \\ \text{or} \qquad y(t) &= \mathscr{A}(t)x(0) + \int_{\tau=0}^{t} \mathscr{A}(\tau)\dot{x}(t-\tau)\,d\tau \qquad (b) \end{aligned} \tag{3.4,42}$$

As with the impulse response, the matrix form of (3.4,42*a*) for example, for a multivariable system, is

$$\mathbf{y}(t) = \mathscr{A}(t)\mathbf{x}(0) + \int_{\tau=0}^{t} \mathscr{A}(t-\tau)\dot{\mathbf{x}}(\tau)\, d\tau \tag{3.4,43}$$

SOLUTION INCLUDING INITIAL CONDITIONS

The general solution of (3.2,21) for arbitrary $\mathbf{y}(0)$ and arbitrary $\mathbf{x}(t)$ is obtained by superposition of the complementary function (3.4,17) and the "particular integral" (3.4,41 or 43). Thus in general

$$\mathbf{y}(t) = \mathbf{H}(t)\mathbf{C}^{-1}\mathbf{y}(0) + \int_{\tau=0}^{t} \mathbf{H}(t-\tau)\mathbf{x}(\tau)\, d\tau \tag{3.4,44}$$

The physical significance of (3.4,40*a*) and (3.4,42*a*) for example is brought out by considering them in the one-dimensional case as the limits of the following sums

$$y(t) = \sum h(t-\tau)x(\tau)\,\Delta\tau \qquad (a)$$

$$y(t) = \mathscr{A}(t)x(0) + \sum \mathscr{A}(t-\tau)\dot{x}(\tau)\,\Delta\tau \qquad (b) \tag{3.4,45}$$

Typical terms of the summations are illustrated on Figs. 3.19 and 3.20. The summation forms are quite convenient for computation, especially when the interval $\Delta\tau$ is kept constant.

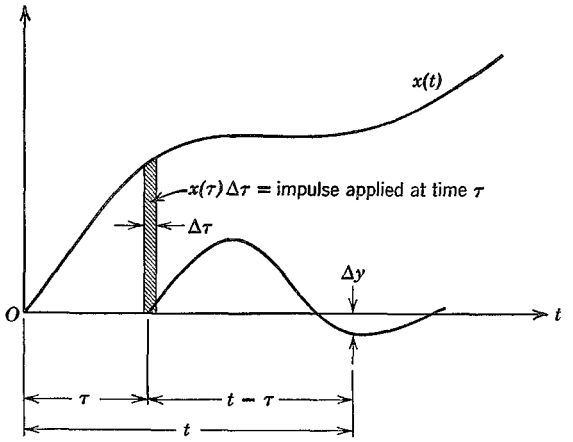

FIG. 3.19 Duhamel's integral—impulse form.

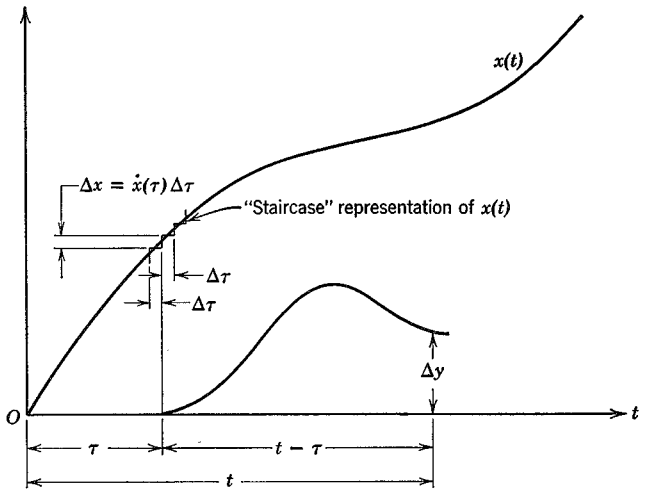

FIG. 3.20 Duhamel's integral—indicial form.

RESPONSE TO A SET OF STATIONARY RANDOM INPUTS

We now consider the case when the system response is a sum of responses to a set of random inputs. An example of this situation is the roll response of an airplane flying through a turbulent atmosphere, when there is a multiple input associated with the three components of the atmospheric motion, each contributing to the output via a different transfer function. Figure 3.21 shows an example in which a number of inputs combine to form a single output. More generally, for n inputs and m outputs related by an $(m \times n)$

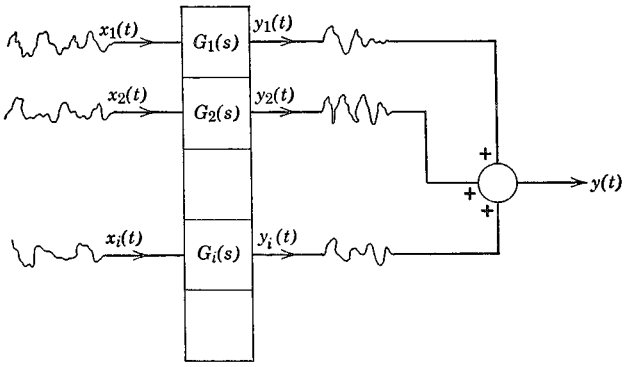

FIG. 3.21 Response to a set of random inputs.

transfer function matrix $\mathbf{G}(s)$

$$\bar{\mathbf{y}}(s) = \mathbf{G}(s)\bar{\mathbf{x}}(s)$$

By virtue of (3.2,2*a*) the transfer function matrix likewise connects the Fourier transforms of the inputs and outputs,

$$\mathbf{Y}(\omega) = \mathbf{G}(i\omega)\mathbf{X}(\omega) \qquad (a) \tag{3.4,46}$$

or with reference to truncated functions, see (2.6,19),

$$\mathbf{Y}(\omega; T) = \mathbf{G}(i\omega)\mathbf{X}(\omega; T) \qquad (b)$$

Now the cross-spectral density of two components (y_i and y_j) of $\mathbf{y}$ is given by (2.6,22)

$$\Phi_{y_i y_j} = \lim_{T\to\infty} \frac{1}{4T}\, Y_i^*(\omega; T) Y_j(\omega; T) \tag{3.4,47}$$

The matrix of $\Phi_{y_i y_j}$ is therefore

$$\begin{aligned}
\mathbf{\Phi}_y &= \lim_{T\to\infty} \frac{1}{4T}\, \mathbf{Y}^*(\omega; T)\mathbf{Y}^T(\omega; T) \\
&= \lim_{T\to\infty} \frac{1}{4T}\, [\mathbf{G}(i\omega)\mathbf{X}(\omega; T)]^*[\mathbf{G}(i\omega)\mathbf{X}(\omega; T)]^T \\
&= \lim_{T\to\infty} \frac{1}{4T}\, \mathbf{G}^*(i\omega)\mathbf{X}^*(\omega; T)\mathbf{X}^T(\omega; T)\mathbf{G}^T(i\omega) \\
&= \mathbf{G}^*(i\omega)\left[\lim_{T\to\infty} \frac{1}{4T}\, \mathbf{X}^*(\omega; T)\mathbf{X}^T(\omega; T)\right]\mathbf{G}^T(i\omega)
\end{aligned}$$

or

$$\mathbf{\Phi}_y = \mathbf{G}^*\mathbf{\Phi}_x\mathbf{G}^T \tag{3.4,48}$$

From (3.4,48) it follows that the power spectral density of y_i (a diagonal element of $\mathbf{\Phi}_y$) is

$$\Phi_{y_i y_i}(\omega) = \sum_{k=1}^{n}\sum_{l=1}^{n} G_{ik}^*(i\omega)\Phi_{x_k x_l}(\omega)G_{il}(i\omega) \tag{3.4,49}$$

and that if the input cross spectra are zero

$$\Phi_{y_i y_i}(\omega) = \sum_{k=1}^{n} |G_{ik}(i\omega)|^2\, \Phi_{x_k x_k}(\omega) \tag{3.4,50}$$

This is a very important result for application to flight dynamics since it provides a way of calculating the output power spectral density from a knowledge of all the input cross spectra and the relevant transfer functions. An important special case is that in which there is only one input, $x(t)$ and one output, $y(t)$. Then (3.4,50) reduces to

$$\Phi_{yy}(\omega) = |G(i\omega)|^2\, \Phi_{xx}(\omega) \tag{3.4,51}$$

This is the most commonly used input/output relation for random processes. It will be recalled (see Sec. 2.6) that most of the interesting probability properties of $y(t)$ can be deduced from $\Phi_{yy}(\omega)$.

A USEFUL THEOREM CONCERNING MEAN-SQUARE RESPONSE

In some calculations, it is not required to have the spectrum of the output, its mean-square value being all the information wanted. In such cases the desired result may be obtained more simply than by first calculating Φ_{yy} and then integrating it. The method is given in ref. 3.12 for single and dual inputs. We present below only the theorem for a single input.

Let the system, with transfer function $G(s)$, be subjected to a transient input $x(t)$, with corresponding transient output $y(t)$. The integral square of the output is given by Parseval's theorem (see ref. 2.4, Sec. 120).

$$E = \int_0^\infty y^2(t)\,dt = \frac{1}{2\pi}\int_{-\infty}^{\infty} Y^*(\omega)\,Y(\omega)\,d\omega \tag{3.4,52}$$

where $Y(\omega)$ is the Fourier transform of $y(t)$. Now the Fourier transform of the output is given by (3.2,2*a*) as

$$Y(\omega) = G(i\omega)X(\omega)$$

and hence

$$\begin{aligned} E &= \frac{1}{2\pi}\int_{-\infty}^{\infty} G(i\omega)G^*(i\omega)X(\omega)X^*(\omega)\,d\omega \\ &= \frac{1}{2\pi}\int_{-\infty}^{\infty} |G(i\omega)|^2\,|X(\omega)|^2\,d\omega \end{aligned} \tag{3.4,53}$$

Now we also have from (3.4,51) that if the input is a random function, the mean-square output is

$$\begin{aligned} \overline{y^2} &= \int_{-\infty}^{\infty} \Phi_{yy}(\omega)\,d\omega \\ &= \int_{-\infty}^{\infty} |G(i\omega)|^2\,\Phi_{xx}(\omega)\,d\omega \end{aligned} \tag{3.4,54}$$

By comparing (3.4,53) and (3.4,54), we see that $\overline{y^2} = E$ if

$$2\pi\Phi_{xx}(\omega) = |X(\omega)|^2 \tag{3.4,55}$$

That is, if one can find a transient $x(t)$ whose Fourier transform is related by (3.4,55) to the power spectrum of the given random function, then $\overline{y^2}$ can be calculated from the output of the transient. This may prove to be a much easier and more economical computation, whether an analog or digital computer is used. In particular, for spectrum functions like those of atmospheric

turbulence (the "Dryden" spectra) the following are suitable transients:

Spectrum Function $\Phi_{xx}(\omega)$	Equivalent transient $x(t)$	
$\frac{1}{2\pi}\frac{A^2}{\gamma^2+\omega^2}$	$Ae^{-\gamma t}$	(3.4,56)
$\frac{A^2}{2\pi}\frac{b^2+\omega^2}{(a^2+\omega^2)^2}$	$A[1-(a-b)t]e^{-at}$	(3.4,57)

The advantages for analog computation are that no random function generator is needed, and that the computation using a single transient input takes much less time.

3.5 TIME-VARYING AND NONLINEAR SYSTEMS

In the preceding sections we have presented the methods for analysis of linear/invariant systems. These systems are the simplest kind and the methods of analysis are in effect omnipotent, in that in principle they provide complete exact solutions for all such systems. Only sheer size provides limits to practical computation.

On the other hand, linear time-varying systems (linear systems with non-constant coefficients) and nonlinear systems present no such comfortable picture. Their characteristics are not simply classified and there are no general methods comparable in power to those of linear analysis. In the aerospace field, nonlinearities and time variation occur in several ways. The fundamental dynamical equations (see Chapter 5) are nonlinear in the inertia terms and in the kinematical variables. The external forces, especially the aerodynamic ones, may contain inherent nonlinearities. When the flight path is a transient, as in reentry, rocket launch, or a landing flare, the aerodynamic coefficients are time-varying as well. In the automatic and powered control systems so widely used in aerospace vehicles, there commonly occur nonlinear control elements such as limiters, switches, dead-bands, and others. Finally, the human pilot, actively present in most flight-control situations, is the ultimate in time-varying nonlinear systems (see Chapter 12).

Although completely general methods, apart from machine computation of course, are not available for analyzing the performance and stability of time-varying and nonlinear systems, there are nevertheless many important particular methods suitable for particular classes of problems. This subject is much too large for a comprehensive treatment here. The reader is referred to refs. 3.8–3.10 for treatises devoted to the subject.

It should be pointed out that even when a flight vehicle system is essentially nonlinear, much may be learned about it by first carrying out a linear analysis of small disturbances from a reference steady state or reference transient. This normally provides a good base from which to extend the analysis to

include nonlinear effects, as well as a limiting check "point" for subsequent computation and analysis. Of the particular methods available for studying nonlinear systems, we consider two sufficiently relevant to flight dynamics to present brief introductions to them below.

DESCRIBING FUNCTION

In the simplest terms, a *describing function* of a system is a transfer function that linearly connects an input/output pair approximately—i.e. it provides a linear approximation to the actual system that is best in a certain sense.

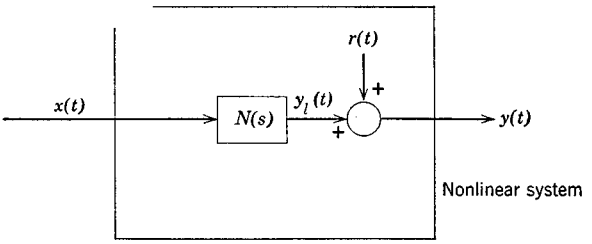

FIG. 3.22 Model of nonlinear system.

Figure 3.22 shows a nonlinear system with a particular input $x(t)$ and output $y(t)$. The output is presumed to be made up of the sum of a part $y_l(t)$ lineary related to the input

$$\bar{y}_l(s) = N(s)\bar{x}(s) \tag{3.5,1}$$

and a *remnant* $r(t)$ that makes up the difference. Clearly, if $r(t)$ is "small" enough compared to $y(t)$, then $y_l(t)$ provides a useful evaluation of the system performance. When an appropriate measure of $r(t)$ is minimized, $N(s)$ becomes the corresponding describing function. For transient inputs, a suitable measure would be $\int r^2\,dt$; for steady-state inputs, periodic or stochastic (the usual case treated), $\overline{r^2}$ is the quantity minimized. It is seen that a different describing function is obtained for every input to a given system—i.e. the describing function, unlike the transfer function of a linear system, is a function of the input.

STEADY-STATE DESCRIBING FUNCTION

The relations implied by Fig. 3.22 can be reinterpreted as in Fig. 3.23. Now applying (3.4,50) we get the spectral density of $r(t)$

$$\Phi_{rr}(\omega) = \Phi_{yy}(\omega) - N(i\omega)\Phi_{yx}(\omega) - N^*(i\omega)\Phi_{xy}(\omega) + N^*(i\omega)N(i\omega)\Phi_{xx}(\omega) \tag{3.5,2}$$

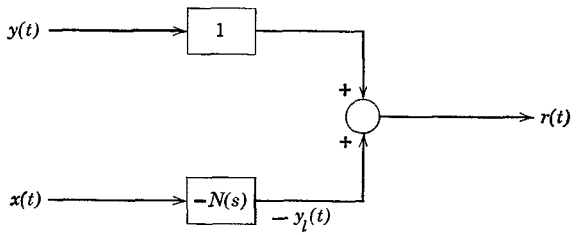

FIG. 3.23 Alternative model of nonlinear system.

Since $\Phi_{yx} = \Phi_{xy}^*$ by (2.6,15*b*), then

$$\Phi_{rr}(\omega) = \Phi_{yy}(\omega) - [\Phi_{yx}(\omega)N(i\omega) + (\Phi_{yx}(\omega)N(i\omega))^*] + N^*(i\omega)N(i\omega)\Phi_{xx}(\omega) \tag{3.5,3}$$

We now wish to find the particular function $N(i\omega)$ that minimizes $\overline{r^2} = \int_{-\infty}^{\infty} \Phi_{rr}(\omega)\, d\omega$. This can be done by the classical method of variational calculus, as follows.

Let us assume that $N(i\omega)$ is not exactly that which minimizes $\overline{r^2}$ but differs from it slightly, i.e.

$$N(i\omega) = \bar{N}(i\omega) + \epsilon f(i\omega) \tag{3.5,4}$$

where $\bar{N}(i\omega)$ is the optimal function sought, $f(i\omega)$ is an arbitrary continuous function, and ϵ is a small parameter. Then $\bar{N}(i\omega)$ is given by the solution of

$$\frac{\partial}{\partial \epsilon} \int_{-\infty}^{\infty} \Phi_{rr}(\omega)\, d\omega \bigg|_{\epsilon=0} = 0 \tag{3.5,5}$$

When (3.5,4) is substituted into (3.5,3) and the l.h.s. of (3.5,5) is evaluated, the result is

$$\int_{-\infty}^{\infty} \{-[\Phi_{yx}(\omega)f(i\omega) + \Phi_{yx}^*(\omega)f^*(i\omega)] + \Phi_{xx}(\omega)[\bar{N}^*(i\omega)f(i\omega) + f^*(i\omega)\bar{N}(i\omega)]\}\, d\omega = 0$$

or

$$\int_{-\infty}^{\infty} \{f(i\omega)[\Phi_{xx}(\omega)\bar{N}^*(i\omega) - \Phi_{yx}(\omega)] + f^*(i\omega)[\Phi_{xx}(\omega)\bar{N}(i\omega) - \Phi_{yx}^*(\omega)]\}\, d\omega = 0 \tag{3.5,6}$$

Since $f(i\omega)$ is an arbitrary function, the integral can only be zero if the two expressions in square brackets are both zero. Since one is simply the conjugate of the other they are simultaneously zero, and the required condition is

$$N(i\omega) = \bar{N}(i\omega) = \frac{\Phi_{xy}(\omega)}{\Phi_{xx}(\omega)} \tag{3.5,7}$$

SINUSOIDAL DESCRIBING FUNCTION

When a stable linear system has a sinusoidal input $x = A_1 e^{i\Omega t}$ the steady-state output $y(t)$ after the initial transients have decayed is a sinusoid of the same frequency, and the input/output relation is given by (3.4,20). A "well-behaved" nonlinear system with such an input will have a steady-state output that is also periodic, but not sinusoidal, other harmonics being present. Whereas the input spectrum is a "spike," the output spectrum is a "comb." Other behavior is conceivable, but the above describes the usual situation; we assume it to be the case here. Since the mean product of sinusoids of different frequency is zero, the only Fourier component of the output that has a nonvanishing correlation R_{xy} with the input is the fundamental, i.e. the component that has the same frequency Ω as the input.

Since Φ_{xy} is the Fourier integral of R_{xy}, it follows that only the fundamental component y_f of y contributes to Φ_{xy}. From (2.6,22) we have

$$\begin{aligned} \Phi_{xy_f} &= \lim_{T\to\infty} \frac{1}{4T} X^*(i\omega; T) Y_f(i\omega; T) \\ \Phi_{xx} &= \lim_{T\to\infty} \frac{1}{4T} X^*(i\omega; T) X(i\omega; T) \end{aligned} \tag{3.5,8}$$

The ratio (3.5,7) then leads simply to

$$N(i\omega) = \frac{Y_f(i\omega)}{X(i\omega)} \tag{3.5,9}$$

where $Y_f(i\omega)$ and $X(i\omega)$ are the Fourier transforms of the sinusoids, given in Table 2.2. Now if these sinusoids are described by

$$x = A_1 e^{i\Omega t}; \qquad y_f = A_2 e^{i\Omega t}$$

where A_1 and A_2 are the complex amplitudes of the input and output fundamental, respectively, we get, using item 3, Table 2.2,

$$N(i\omega) = \frac{A_2}{A_1} \tag{3.5,10}$$

which is identical with the frequency-response function given by (3.5,20) provided that we regard the fundamental as the total output.

Evidently the sinusoidal describing function leads to a remnant made up of all the lower and higher harmonics of the output.

TWO-INPUT DESCRIBING FUNCTIONS

If two inputs to a nonlinear system contribute to the output y, as in Fig. 3.24 we may define two describing functions by the same principle as used

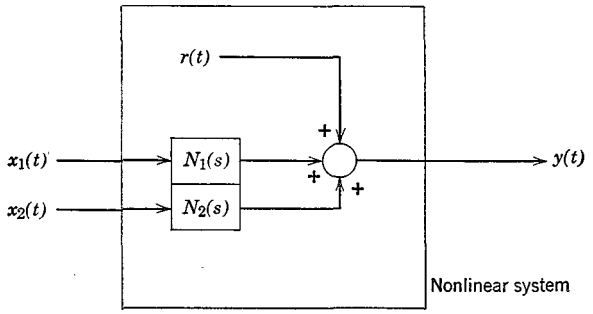

FIG. 3.24 Nonlinear system with two inputs.

above for one input. The method is basically the same, but the details are a little more involved. The result for N_1 is

$$N_1(i\omega) = \frac{\Phi x_1 y \Phi x_2 x_2 - \Phi x_2 y \Phi x_1 x_2}{\Phi x_1 x_1 \Phi x_2 x_2 - |\Phi x_1 x_2|^2} \tag{3.5,11}$$

and that for $N_2(i\omega)$ is obtained by permuting the subscripts 1 and 2. Note that if x_1 and x_2 are uncorrelated, so that the cross-spectral density $\Phi_{x_1 x_2} = 0$, then (3.5,11) reduces to (3.5,7), the formula for a single input.

LYAPUNOV STABILITY THEORY

The second general method for treating nonlinear systems is Lyapunov's theory.

The stability of linear/invariant systems was shown in Sec. 3.3 to be completely determined by the eigenvalues, and certain criteria were presented that could be applied to the characteristic equation to predict the stability properties of the roots. In that case we may say that we have investigated the stability by studying the properties of the solutions. This is possible of course only because we have an adequate theory for the solutions. For more general systems, this approach may not be possible since the solutions are not in general known. A method of treating the stability of equilibrium for any system, which does not require a knowledge of the solutions, has been given by Lyapunov (refs. 3.2, 3.8). We present below a brief outline of the main concepts but refer the reader to refs. 3.2 and 3.8 for a fuller treatment and for the methods of finding the appropriate Lyapunov functions.

We begin with a simple analogy by considering a ball at the bottom of a cup of arbitrary shape. The bottom is a position of stable equilibrium with respect to all disturbances small enough that the ball is not projected over the rim. This stable condition can be viewed from the standpoint of the

total energy E of the ball. If E is less than the potential energy E_{crit} associated with the height of the lowest point on the rim, then escape is impossible, and the system is stable. Note that the lowest point in the cup is a point of minimum potential energy, and that the minimum of E corresponds to equilibrium there. In any real case, there will be frictional dissipation, so that $\dot{E}$ *is negative* whenever there is motion, and if the ball is started anywhere in the cup with $E < E_{\text{crit}}$, it will eventually come to rest at the bottom.

The Lyapunov theory is basically nothing more than a generalization of the above concept, and indeed for some physical systems, the energy itself is a suitable *Lyapunov function*. More generally, a Lyapunov function $V(x_1 \cdots x_n)$ is any positive definite function of all the state variables x_i that is zero at the origin (an equilibrium state) and that increases monotonically within a region $\mathscr{R}$ of state space as one proceeds along the vector **grad** $V = \nabla V$, i.e. it is a "cup-shaped" function with its "bottom" at the equilibrium point the stability of which is to be investigated. The critical question is whether $\dot{V}$ is positive, negative or zero in $\mathscr{R}$. If positive, the state point "climbs up the V hill" proceeding ever farther from the origin, indicating instability. If negative, the state point descends continuously until it comes to rest at the origin, and the system is asymptotically stable. If $\dot{V} = 0$, then the only motion possible is an orbital trajectory in which the state point remains on the surface $V = \text{const}$. These cases are illustrated in Fig. 3.25 for a two-dimensional state space. The essence of the problem is of course to find a suitable V function. Ideally one wants that function that gives the exact stability boundary in state space. This ideal is not usually achieved

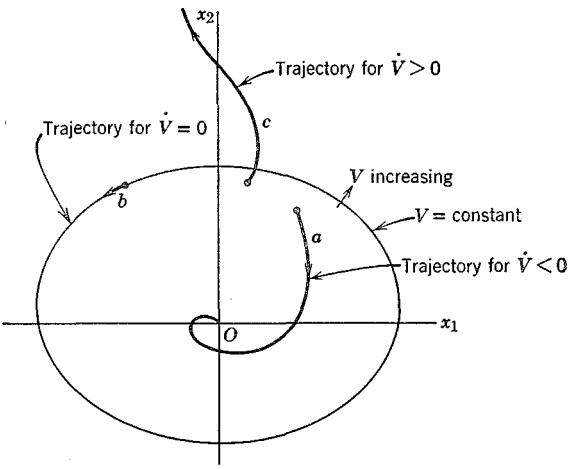

FIG. 3.25 Trajectories in state space.

for other than linear/invariant systems, or simple mechanical ones such as the ball in the cup.

The great advantage of this approach is that $\dot{V}$ can be calculated directly from the differential equations, no solutions of them being needed. Let the equations be given by

$$\dot{\mathbf{x}} = \mathbf{f}(\mathbf{x}, t)$$

or in component form

$$\begin{aligned} \dot{x}_1 &= f_1(x_i, t) \\ &\cdot \\ &\cdot \\ &\cdot \\ \dot{x}_n &= f_n(x_i, t) \end{aligned}$$

Then

$$\begin{aligned} \dot{V} &= \frac{\partial V}{\partial x_1}\dot{x}_1 + \cdots \frac{\partial V}{\partial x_n}\dot{x}_n \\ &= \frac{\partial V}{\partial x_1}f_1 + \cdots \frac{\partial V}{\partial x_n}f_n \\ &= \mathbf{grad}\, V \cdot \mathbf{f} \end{aligned}$$

Since both V and f are known $\dot{V}$ can be calculated directly, and the stability properties inferred from how its sign varies with position in state space.

The main disadvantage of the Lyapunov approach is that the functions V are to a certain extent arbitrary, and hence can in most cases only provide a conservative estimate of stability. For example, if it is found that the limit of the monotonically increasing V for negative $\dot{V}$ is a certain surface S in state space, then it can be said that the system is stable for disturbances sufficiently small that the initial state point lies within S, but it is not known whether it may be stable beyond S, since a different V function might have produced a larger domain of stability. It should be pointed out that for some problems in mechanics, as distinct from control systems (which have been the principal object of applications of Lyapunov theory) the Hamiltonian of the system can be a useful Lyapunov function (see Pringle, ref. 3.11).

The previous discussion has related to the stability of an equilibrium point (the origin in state space). However there are many important situations in the flight of aircraft and spacecraft when there is no steady state, as in the take-off and landing of aircraft, and the launch and reentry of spacecraft. If the state vector in such transient situations changes "slowly" with time (what constitutes "slowness" must be determined in each case), then a point-by-point stability analysis may be useful. In that case, each point on the trajectory is treated as a constant reference state (equilibrium) and the stability of disturbances from it is investigated in the manner discussed

above. When the transient is "rapid," i.e. when the characteristic times (e.g. periods and damping times) of the disturbance motions are long enough that large changes can occur in the reference transient during these time intervals, then the "quasi-steady" analysis may be meaningless. In this case the stability analysis of the transient can be transformed into that of an equilibrium point as explained on p. 50, and the Lyapunov analysis for equilibrium again applied.

A general comment about the usefulness of stability analysis in aerospace systems is in order. It is a fact that stability is neither a necessary nor a sufficient condition for the successful performance of aerospace missions. A stable airplane may have unsatisfactory handling qualities, and vice versa; and an unstable flight path for a lifting entry vehicle may be perfectly acceptable within the tolerances on initial conditions that are practically available. Thus the determination of stability boundaries of nonlinear and time-varying systems does not appear to be an objective to which a great deal of effort should be applied. Of more direct import are appropriate performance criteria. These may take many forms depending on the vehicle and mission—for example, pilot rating in aircraft and terminal errors for reentry vehicles.

Reference frames and transformations

CHAPTER 4

When formulating and solving problems in flight dynamics, a number of frames of reference (coordinate axes) must be used for specifying relative positions and velocities, components of vectors (forces, velocities, accelerations etc.) and elements of matrices (aerodynamic derivatives, moments and products of inertia, etc.). The equations of motion may be written from the standpoint of an observer fixed in any of the reference frames, the choice being a matter of convenience and preference, and formulae must be available for transforming quantities of interest from one frame to another. For example, in an interplanetary space flight mission, one might need Earth-fixed axes, target-fixed axes, vehicle-fixed axes, and axes fixed to the distant stars. In atmospheric flight, we commonly use Earth-fixed axes, vehicle-fixed axes, trajectory-fixed axes, and atmosphere-fixed axes. The references frames needed for subsequent analytical developments are defined in the following, and a suitable system of notation is introduced.

4.1 NOTATION

Let F_a and F_b be two right-handed reference frames, with coordinate axes denoted as in Fig. 4.1. Note that two alternative systems are used: (x, y, z) or (x_1, x_2, x_3), the choice at any time being governed by custom and

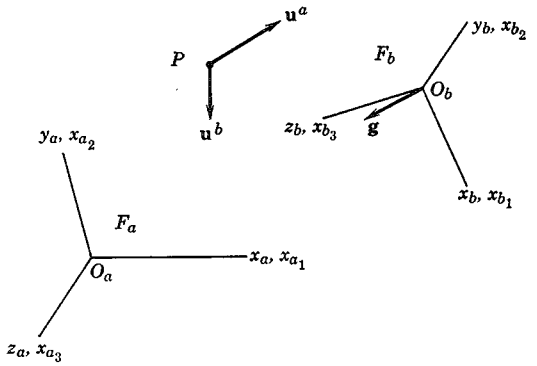

FIG. 4.1 Notations for coordinate axes.

convenience. In general the two frames have relative motion, both linear and angular.

Consider now the description of a typical vector which does not depend on the motion of the frame of reference. For example let F_a be the Earth, F_b a moving rigid vehicle, and the vector in question be the gravitational force exerted by the former on the latter, represented by $\mathbf{g}$ in Fig. 4.1. The vector $\mathbf{g}$ is the same for observers in both F_a and F_b in the sense that they would both find it to be of the same magnitude, and of the same orientation relative to any third frame. The components of $\mathbf{g}$ along the axes of F_a and F_b are of course in general different, and we denote them by

$$\mathbf{g}_a = \begin{bmatrix} g_{x_a} \\ g_{y_a} \\ g_{z_a} \end{bmatrix} = \begin{bmatrix} g_{a_1} \\ g_{a_2} \\ g_{a_3} \end{bmatrix}$$

$$\mathbf{g}_b = \begin{bmatrix} g_{x_b} \\ g_{y_b} \\ g_{z_b} \end{bmatrix} = \begin{bmatrix} g_{b_1} \\ g_{b_2} \\ g_{b_3} \end{bmatrix} \tag{4.1,1}$$

(How to calculate one set of components from the other is treated in Sec. 4.4.)

A more complicated situation arises when we consider vectors that do depend on the motion of the reference frame, i.e. that are not the same for two observers, one in F_a and the other in F_b. For example, consider the velocities of a point P relative to F_a and F_b. These are two different vectors, each of which may have its components given in the directions of *either* set of axes, leading to four sets of components.

The practice followed in this text is to use different symbols for physically different vectors, or appropriate subscripts or superscripts. Thus $\boldsymbol{\omega}$ usually represents the angular velocity of a reference frame relative to inertial space, and a superscript identifies the rotating frame. For example $\boldsymbol{\omega}^E$ is the angular velocity of an Earth-fixed frame F_E. Again, $\mathbf{v}_0$ and $\mathbf{v}_c$ give the inertial velocities of points 0 and C, the frame of reference for components being identified with a further subscript, so that $\mathbf{v}_{0_W}$ is the column matrix of the components of $\mathbf{v}_0$ along the axes of F_W (wind axes).

In the example of Fig. 4.1, we may let $\mathbf{u}^a$ be the velocity of P relative to F_a and $\mathbf{u}^b$ its velocity relative to F_b. The four sets of components are then

$$\mathbf{u}_a{}^a, \mathbf{u}_b{}^a \qquad \text{and} \qquad \mathbf{u}_a{}^b, \mathbf{u}_b{}^b$$

each being a column matrix as in (4.1,1).

It should be emphasized that the transformation that transforms $\mathbf{u}^a$ into $\mathbf{u}^b$ is quite different from that which transforms $\mathbf{u}_a{}^a$ into $\mathbf{u}_b{}^a$, and the two should not be confused (see Sec. 4.6).

Notwithstanding the above general rules, certain exceptions to this form of notation are made in the subsequent treatments. These are in conformity with a long tradition of usage in flight dynamics, and bring the main equations derived into harmony with most past and current North American literature on the subject.

4.2 DEFINITIONS OF REFERENCE FRAMES USED IN VEHICLE DYNAMICS

The principal reference frames used in vehicle dynamics are defined below, and illustrated in Figs. 4.2 to 4.7.

4.2.1 INERTIAL REFERENCE FRAME F_I (INERTIAL AXES, $O_I x_I y_I z_I$)

In every dynamics problem there must be an inertial reference frame, either explicitly defined, or lurking implicitly in the background. This frame is fixed, or in uniform rectilinear translation, relative to the distant stars; in it Newton's second law is valid for the motion of a particle, in the sense that if $\mathbf{f}$ be the sum of all *external* forces acting on the particle, and $\mathbf{a}$ its acceleration relative to F_I, then $\mathbf{f} = m\mathbf{a}$. If $\mathbf{a}$ is acceleration relative to a reference frame that has rotation, or acceleration of its origin, this equation does not hold, and additional terms that depend on the motion of the reference

frame must be added to the equation (see Sec. 5.1). The velocity of the vehicle mass center relative to F_I is denoted $\mathbf{V}^I$.

4.2.2 EARTH-FIXED REFERENCE FRAME, F_E (EARTH AXES $O_E x_E y_E z_E$)

In many problems of airplane dynamics, the rotation $\boldsymbol{\omega}^E$ of the Earth relative to F_I can be neglected, and any reference frame fixed to the Earth can be used as an inertial frame. In hypervelocity and space flight this is generally not the case, however, and the angular velocity of the Earth must usually be included in the analysis. Two Earth-fixed frames are of interest, as illustrated in Fig. 4.2. F_{EC} is the "Earth-center" frame with origin at the center of the Earth and axis directions fixed by a reference point on the equator and the Earth's axis. This frame is useful when the Earth's rotation must be considered. F_E is an Earth-surface frame, with origin near the vehicle if possible, and with $O_E z_E$ directed vertically down. $O_E x_E y_E$ is the local horizontal plane, $O_E x_E$ points north, and $O_E y_E$ east.

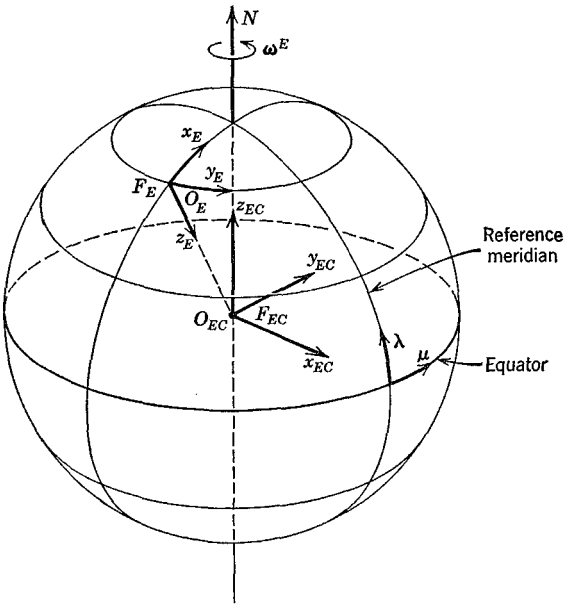

FIG. 4.2 Earth axes. (λ, μ) = latitude, longitude.

4.2.3 VEHICLE-CARRIED VERTICAL FRAME, F_V (AXES $O_V y_V z_V$)

This is a reference frame in which the origin O_V is attached to the vehicle, usually at the mass center C, and in which $O_V z_V$ is directed vertically downward, i.e. along the local **g** vector. The directions of the remaining axes can be specified in any convenient way. We choose $O_V x_V$ to point to the north, and $O_V y_V$ east. In many applications the origin of F_E is near enough to the vehicle that Earth curvature is negligible, and then F_V has axes parallel to F_E, as illustrated in Fig. 4.3.

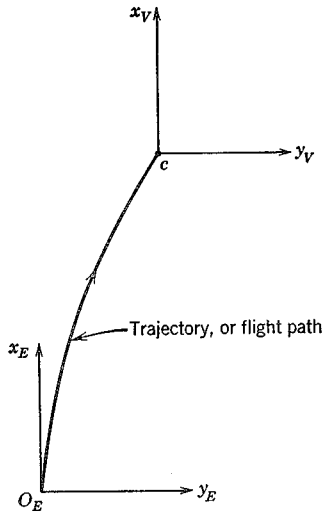

FIG. 4.3 The local (F_E) and vehicle-carried (F_V) vertical reference frames.

Since F_E and F_V are both chosen so that their respective x axes point north, then F_E can be made parallel to F_V by the two consecutive rotations

(i) $-\Delta\lambda$ around $O_E y_E$
(ii) $\Delta\mu$ around $O_{EC} z_{EC}$

where
$$\Delta\lambda = \lambda - \lambda_E$$
$$\Delta\mu = \mu - \mu_E$$

and
(λ, μ) are latitude and longitude of O_V
(λ_E, μ_E) are latitude and longitude of O_E.

The angular velocity of F_V relative to F_I is $\boldsymbol{\omega}^V$.

4.2.4 ATMOSPHERE-FIXED REFERENCE FRAME, F_A (AXES $O_A x_A y_A z_A$)

Since the relevant velocity for aerodynamic forces in atmospheric flight is that of the vehicle relative to the local atmosphere, it is essential to be concerned with the motion of the latter. When the atmosphere is, or is assumed to be, at rest relative to the Earth, then F_A and F_E are the same. If the atmosphere is in uniform motion relative to F_E, with velocity $\mathbf{W}$, then F_A is convected relative to F_E with that velocity.

If the motion of the atmosphere is nonuniform in time or space (as is in reality always the case) then F_A is so chosen that the space and time averages of the motion of the atmosphere relative to F_A taken over the space-time domain of concern in the problem, are zero. The motion of F_A relative to F_E is in this case also a constant velocity $\mathbf{W}$. (A treatment of flight in a turbulent atmosphere is given in Chapter 13.)

The velocity of the vehicle mass center relative to F_A is denoted by $\mathbf{V}$ so that its velocity relative to F_E is

$$\mathbf{V}^E = \mathbf{V} + \mathbf{W} \tag{4.2,1}$$

4.2.5 AIR-TRAJECTORY REFERENCE FRAME F_W (WIND AXES, $O_W x_W y_W z_W$)

This reference frame has origin fixed to the vehicle, usually at the mass center C, and the $O_W x_W$ axis is directed along the velocity vector $\mathbf{V}$ of the vehicle relative to the atmosphere. The axis $O_W z_W$ lies in the plane of symmetry of the vehicle if it has one, otherwise is arbitrary. If the atmosphere were at rest, then O_W would trace out the trajectory of the vehicle relative to the Earth, and $O_W x_W$ would be always tangent to it. The frame F_W has angular velocity $\boldsymbol{\omega}^W$ relative to F_I. Although by doing so we depart from the general scheme, in the interest of simplicity we shall denote the components of $\boldsymbol{\omega}^W$ in F_W by $[p_W, q_W, r_W]$.

4.2.6 BODY-FIXED REFERENCE FRAME F_B (BODY AXES, $Oxyz$)

Any set of axes fixed in a rigid body is a body-fixed reference frame. If the body is not rigid, i.e. if it has articulated parts such as control surfaces, or elastic motions, then the body axes are chosen to be those for which the resultant linear and angular momenta of the relative motions of articulation and elastic distortion vanish. This choice is always possible (see Sec. 5.1). The origin of the body axes is usually the mass center C. A particular set

of body axes with special properties are principal axes of inertia, denoted F_P.

Flight vehicles almost invariably have a plane of symmetry (to a good approximation); this plane is chosen to be Cxz, with z directed "downward."

Body axes play an especially important role in flight dynamics, and there is a tradition of notation associated with them. This is given in Fig. 4.8. Note that the subscript B is dropped when there is no possibility of confusion. The angular velocity of F_B relative to F_I is $\boldsymbol{\omega}$ (p, q, r), and the components of $\mathbf{V}_B$ are (u, v, w).

4.2.7 STABILITY AXES F_S $(O_S x_S y_S z_S)$

Stability axes are a special set of body axes used primarily in the study of small disturbances from a steady reference flight condition. If the reference flight condition is symmetric, i.e., if $\mathbf{V}$ lies in the plane of symmetry, then F_S coincides with the wind axes F_W in the reference condition, but departs from it, moving with the body, during the disturbance. If the reference flight condition is not symmetric, i.e. with sideslip, then $O_S x_S$ is chosen to lie on the projection of $\mathbf{V}$ in the plane of symmetry, with $O_S z_S$ also in the plane of symmetry.

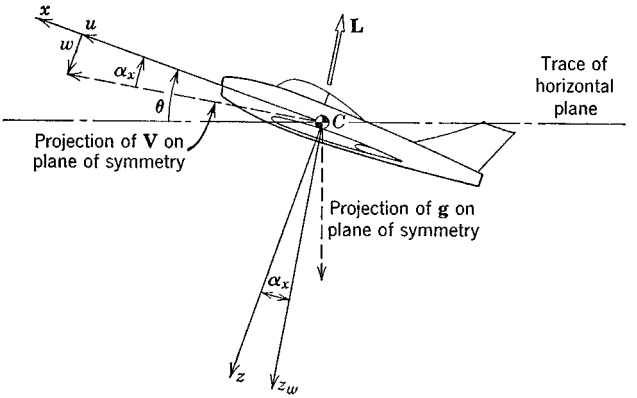

FIG. 4.4 Plane of symmetry—Cxz; $\mathbf{L}$ = lift vector.

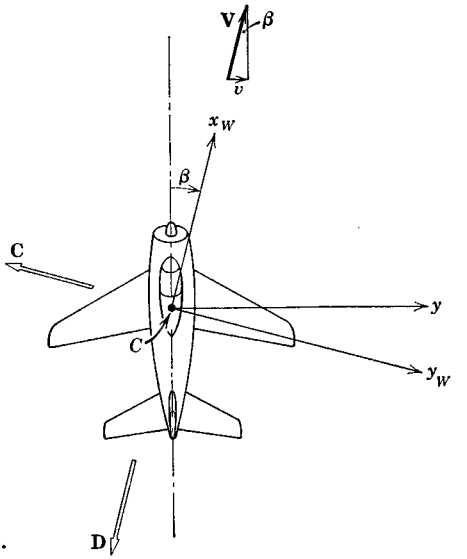

FIG. 4.5 Plane Cx_Wy_W: **D**, **C** = drag and cross-wind force vectors.

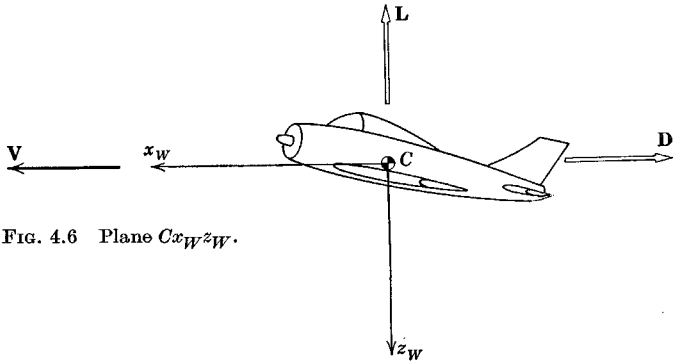

FIG. 4.6 Plane Cx_Wz_W.

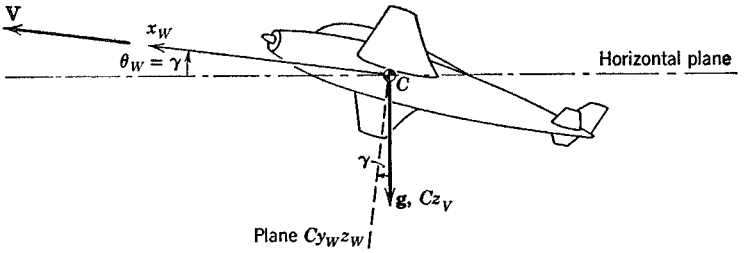

FIG. 4.7 **V**, **g** plane.

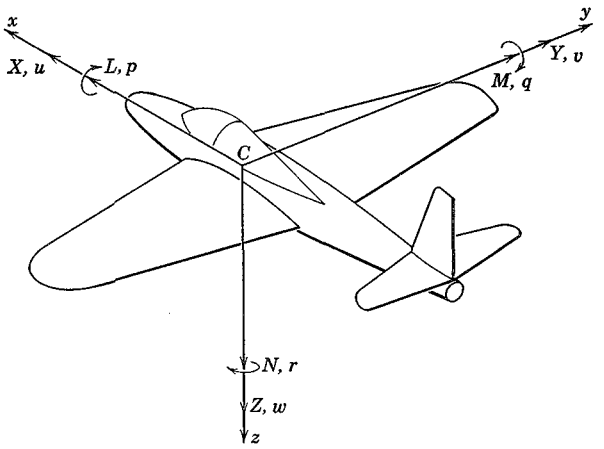

FIG. 4.8 Notation for body axes.

L = rolling moment p = rate of roll
M = pitching moment q = rate of pitch
N = yawing moment r = rate of yaw
$[X, Y, Z]$ = components of resultant aerodynamic force
$[u, v, w]$ = components of velocity of C relative to atmosphere

4.3 DEFINITION OF THE ANGLES

THE VEHICLE EULER ANGLES

The orientation of any reference frame relative to another can be given by three angles, which are the consecutive rotations about the axes z, y, x in that order that carry one frame into coincidence with the other. This is a particular case of *Euler angles*. In flight dynamics, the Euler angles used are those which rotate the vehicle-carried vertical frame F_V into coincidence with the relevant axis system. Only two sets are commonly used, those for the body axes F_B, and for the wind axes F_W. The angles are denoted (ψ, θ, ϕ) for body axes, including the special case F_S, and $(\psi_W, \theta_W, \phi_W)$ for wind axes. Figure 4.9 shows the sequence of rotations.

(i) A rotation ψ about $O_V z_V$, carrying the axes to $O_V x_2 y_2 z_2$. ψ is the *azimuth* angle
(ii) A rotation θ about $O_V y_2$, carrying the axes to $O_V x_3 y_3 z_3$. θ is the *elevation* angle

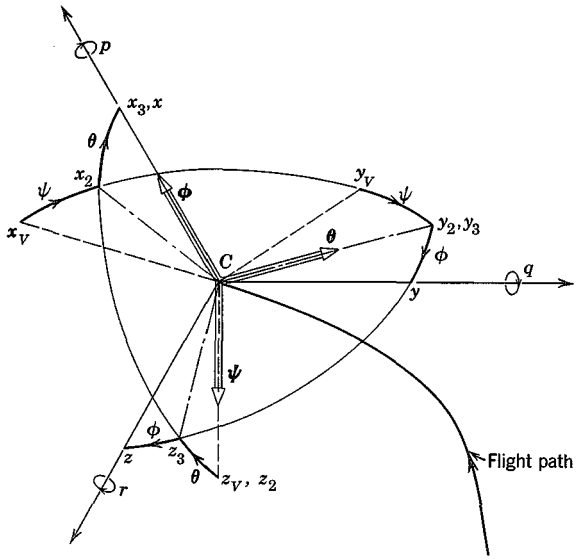

FIG. 4.9 The Euler angles.

(iii) A rotation $\boldsymbol{\phi}$ about $O_V x_3$, carrying the axes to their final position $O_V xyz$. ϕ is the *bank* angle.

In order to avoid ambiguities which can otherwise result in the set of angles (ψ, θ, ϕ) the ranges are limited to

$$-\pi \leq \psi < \pi \quad \text{or} \quad 0 \leq \psi < 2\pi$$

$$-\frac{\pi}{2} \leq \theta \leq \frac{\pi}{2}$$

$$-\pi \leq \phi < \pi \quad \text{or} \quad 0 \leq \phi < 2\pi$$

The Euler angles are then unique for most orientations of the vehicle,† although it should be noted that in a continuous steady rotation, such as rolling, the time variation of ϕ for example is a discontinuous sawtooth function.

As shown in Fig. 4.7, the angle θ_W is also commonly denoted by γ, called the *angle of climb* for an obvious reason.

† There is an ambiguity for the angles defining a vertical dive, since $(\psi, \theta, \phi) = (a + b, -\pi/2, -a)$ gives the same final orientation regardless of a. $a = 0$ would be the natural choice, and this special case does not seem to cause any difficulties.

THE AERODYNAMIC ANGLES

The linear motion **V** of the vehicle relative to the atmosphere can be given either by its three orthogonal components (u, v, w) in a body-axis system (see examples in Figs. 4.4 to 4.7), or alternatively by the magnitude V and two suitably defined angles. These angles, which are of fundamental importance in determining the aerodynamic forces that act on the vehicle, are defined thus:

Angle of attack (see Fig. 4.4):

$$\alpha_x = \tan^{-1}\frac{w}{u} \qquad -\pi \leq \alpha_x \leq \pi \tag{4.3,2}$$

Sideslip angle (see Fig. 4.5):

$$\beta = \sin^{-1}\frac{v}{V} \qquad -\pi \leq \beta \leq \pi \tag{4.3,3}$$

It is most important to note that α_x as here defined will be the same as that commonly used in aerodynamic theory and in wind-tunnel testing only if the body axis Cx is parallel to the basic aerodynamic reference direction, i.e. the mean aerodynamic chord or the zero-lift line.† Otherwise it differs by a constant. When the body axes used are stability axes F_S, the latter will normally be the case. It follows that the velocity components in the body axes are

$$\begin{aligned} u &= V\cos\beta\cos\alpha_x \\ v &= V\sin\beta \\ w &= V\cos\beta\sin\alpha_x \end{aligned} \tag{4.3,4}$$

It will be observed that, in the sense of Euler angles, the aerodynamic angles relate the two frames F_W and F_B by the rotation sequence $(-\beta, \alpha_x, 0)$ which carry the former into the latter.

4.4 TRANSFORMATION OF A VECTOR

Let **v** be a vector with the components

$$\mathbf{v}_a = \begin{bmatrix} v_{a_1} \\ v_{a_2} \\ v_{a_3} \end{bmatrix} \text{ in } F_a \qquad \text{and} \qquad \mathbf{v}_b = \begin{bmatrix} v_{b_1} \\ v_{b_2} \\ v_{b_3} \end{bmatrix} \text{ in } F_b$$

† The symbol α is reserved for the angle of attack of the zero-lift line of the vehicle when its controls are in neutral position.

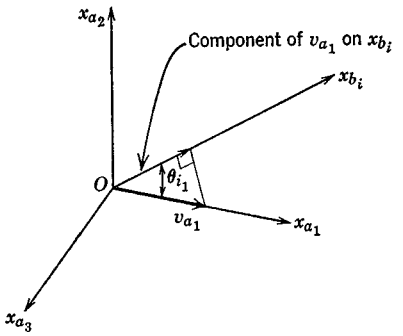

FIG. 4.10 Component of vector.

The component of v_{a_1} in the direction of x_{b_i} is $v_{a_1} \cos(\theta_{i1})$ where θ_{i1} denotes the angle between $O_b x_{b_i}$ and $O_a x_{a_1}$ (see Fig. 4.10). Thus by adding the three components of v_{a_j} in the direction of x_{b_i} we get

$$v_{b_i} = \sum_{j=1}^{3} l_{ij} v_{a_j} \qquad i = 1 \cdots 3 \tag{4.4,1}$$

where

$$l_{ij} = \cos(\theta_{ij}) \tag{4.4,2}$$

are the nine direction cosines. Equation (4.4,1) is evidently the matrix product

$$\begin{aligned} &\mathbf{v}_b = \mathbf{L}_{ba}\mathbf{v}_a \qquad (a) \\ &\text{where} \\ &\mathbf{L}_{ba} = [l_{ij}] \qquad (b) \end{aligned} \tag{4.4,3}$$

and constitutes the required transformation formula. Its inverse readily reverses the transformation to give

$$\mathbf{v}_a = \mathbf{L}_{ba}^{-1}\mathbf{v}_b = \mathbf{L}_{ab}\mathbf{v}_b \tag{4.4,4}$$

where

$$\mathbf{L}_{ab} \equiv \mathbf{L}_{ba}^{-1}$$

PROPERTIES OF THE L MATRIX

Since $\mathbf{v}_a$ and $\mathbf{v}_b$ are physically the same vector $\mathbf{v}$, the magnitude of $\mathbf{v}_a$ must be the same as that of $\mathbf{v}_b$, i.e. v^2 is an invariant of the transformation. From (4.4,3) this requires

$$v^2 = \mathbf{v}_b{}^T\mathbf{v}_b = \mathbf{v}_a{}^T\mathbf{L}_{ba}{}^T\mathbf{L}_{ba}\mathbf{v}_a = \mathbf{v}_a{}^T\mathbf{v}_a \tag{4.4,5}$$

It follows from the last equality of (4.4,5) that

$$\mathbf{L}_{ba}{}^T\mathbf{L}_{ba} = \mathbf{I} \tag{4.4,6}$$

Equation (4.4,6) is known as the *orthogonality condition* on $\mathbf{L}_{ba}$. From (4.4,6) it follows that

$$|\mathbf{L}_{ba}|^2 = 1$$

and hence that $|\mathbf{L}_{ba}|$ is never zero and the inverse of $\mathbf{L}_{ba}$ always exists. In view of (4.4,6) we have, of course, that

$$\mathbf{L}_{ba}{}^T = \mathbf{L}_{ba}{}^{-1} = \mathbf{L}_{ab} \tag{4.4,7}$$

i.e. that the inverse and the transpose are the same. Equation (4.4,6) together with (4.4,3*b*) yields a set of conditions on the direction cosines, i.e.

$$\sum_{k=1}^{3} l_{ki} l_{kj} = \delta_{ij} \tag{4.4,8}$$

It follows from (4.4,8) that the columns of $\mathbf{L}_{ba}$ are vectors that form an orthogonal set (hence the name "orthogonal matrix") and that they are of unit length.

Since (4.4,8) are a set of six relations among the nine l_{ij}, then only three of them are independent. These three are an alternative to the three independent Euler angles for specifying the orientation of one frame relative to another.

4.5 THE L MATRIX IN TERMS OF ROTATION ANGLES

The transformations associated with single rotations about the three coordinate axes are now given. In each case F_a represents the initial frame, F_b the frame after rotation, and the notation for $\mathbf{L}$ identifies the axis and

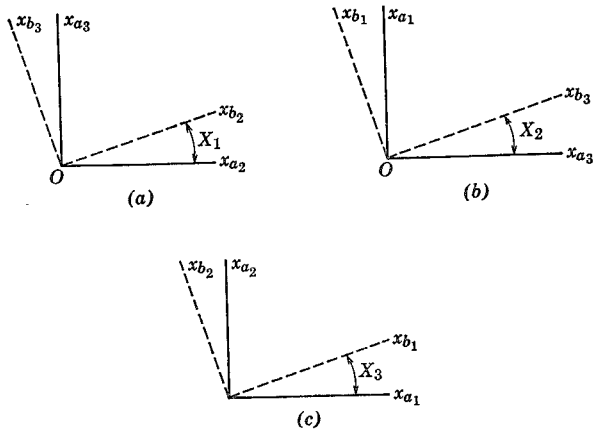

FIG. 4.11 The three basic rotations. (*a*) About x_{a_1}. (*b*) About x_{a_2}. (*c*) About x_{a_3}.

the angle of the rotation (see Fig. 4.11). Thus in each case

$$\mathbf{v}_b = \mathbf{L}_i(X_i)\mathbf{v}_a \tag{4.5,1}$$

By inspection of the angles in Fig. 4.11, the following matrices are readily verified.

$$\begin{aligned}
\mathbf{L}_1(X_1) &= \begin{bmatrix} 1 & 0 & 0 \\ 0 & \cos X_1 & \sin X_1 \\ 0 & -\sin X_1 & \cos X_1 \end{bmatrix} \\
\mathbf{L}_2(X_2) &= \begin{bmatrix} \cos X_2 & 0 & -\sin X_2 \\ 0 & 1 & 0 \\ \sin X_2 & 0 & \cos X_2 \end{bmatrix} \\
\mathbf{L}_3(X_3) &= \begin{bmatrix} \cos X_3 & \sin X_3 & 0 \\ -\sin X_3 & \cos X_3 & 0 \\ 0 & 0 & 1 \end{bmatrix}
\end{aligned} \tag{4.5,2}$$

The transformation matrix for any sequence of rotations can be constructed readily from the above basic formulas. For the case of Euler angles, which rotate frame F_V into F_B as defined in Sec. 4.3, the matrix corresponds to the sequence $(X_3, X_2, X_1) = (\psi, \theta, \phi)$, giving

$$\mathbf{L}_{BV} = \mathbf{L}_1(\phi) \cdot \mathbf{L}_2(\theta) \cdot \mathbf{L}_3(\psi) \tag{4.5,3}$$

[The sequence of angles in (4.5,3) is opposite to that of the rotations, since each transformation matrix *pre*multiplies the vector arrived at in the previous step.] The result of multiplying the three matrices is

$$\mathbf{L}_{BV} = \begin{bmatrix} \cos\theta\cos\psi & \cos\theta\sin\psi & -\sin\theta \\ \sin\phi\sin\theta\cos\psi - \cos\phi\sin\psi & \sin\phi\sin\theta\sin\psi + \cos\phi\cos\psi & \sin\phi\cos\theta \\ \cos\phi\sin\theta\cos\psi + \sin\phi\sin\psi & \cos\phi\sin\theta\sin\psi - \sin\phi\cos\psi & \cos\phi\cos\theta \end{bmatrix} \tag{4.5,4}$$

We shall also wish to make use of the matrix for transforming vectors from the frame F_W to F_B, and this corresponds to the sequence of rotations $(X_3, X_2, X_1) = (-\beta, \alpha_x, 0)$ whence

$$\mathbf{L}_{BW} = \mathbf{L}_2(\alpha_x) \cdot \mathbf{L}_3(-\beta)$$

or

$$\mathbf{L}_{BW} = \begin{bmatrix} \cos\alpha_x\cos\beta & -\cos\alpha_x\sin\beta & -\sin\alpha_x \\ \sin\beta & \cos\beta & 0 \\ \sin\alpha_x\cos\beta & -\sin\alpha_x\sin\beta & \cos\alpha_x \end{bmatrix} \tag{4.5,5}$$

4.6 TRANSFORMATION OF THE DERIVATIVE OF A VECTOR

Consider a vector $\mathbf{v}$ that is being observed simultaneously from two frames F_a and F_b that have relative rotation—say F_b rotates with angular velocity $\boldsymbol{\omega}$ relative to F_a, which we may regard as fixed. The rotation does not invalidate the argument of Sec. 4.4, so that

$$\mathbf{v}_b = \mathbf{L}_{ba}\mathbf{v}_a \tag{4.4,3}$$

The derivatives of $\mathbf{v}_a$ and $\mathbf{v}_b$ are of course

$$\dot{\mathbf{v}}_a = \begin{bmatrix} \dot{v}_{x_a} \\ \dot{v}_{y_a} \\ \dot{v}_{z_a} \end{bmatrix} \quad \text{and} \quad \dot{\mathbf{v}}_b = \begin{bmatrix} \dot{v}_{x_b} \\ \dot{v}_{y_b} \\ \dot{v}_{z_b} \end{bmatrix} \tag{4.6,1}$$

where $\dot{v}_{x_a} = (d/dt)(v_{x_a})$, etc. It is important to note that $\dot{\mathbf{v}}_a$ and $\dot{\mathbf{v}}_b$ are not simply two sets of components of the *same* vector, but are actually two *different* vectors.

Now because F_b rotates relative to F_a, the direction cosines l_{ij} are changing with time, and the derivative of (4.4,3) is

$$\dot{\mathbf{v}}_b = \mathbf{L}_{ba}\dot{\mathbf{v}}_a + \dot{\mathbf{L}}_{ba}\mathbf{v}_a \tag{4.6,2}$$

or alternatively

$$\dot{\mathbf{v}}_a = \mathbf{L}_{ab}\dot{\mathbf{v}}_b + \dot{\mathbf{L}}_{ab}\mathbf{v}_b$$

the second terms representing the effect of the rotation.

Since $\dot{\mathbf{L}}$ must be independent of $\mathbf{v}$, the matrix $\mathbf{L}_{ab}$ can readily be identified by considering the case when $\mathbf{v}_b$ is constant, see Fig. 4.12. For then, from the fundamental definitions of derivative and cross product, the derivative of $\mathbf{v}$ as seen from F_a is readily shown to be

$$\frac{d\mathbf{v}}{dt} = \boldsymbol{\omega} \times \mathbf{v} \tag{4.6,3}$$

The matrix equivalent of (4.6,3) is

$$\dot{\mathbf{v}}_a = \tilde{\boldsymbol{\omega}}_a \mathbf{v}_a \tag{4.6,4}$$

where

$$\tilde{\boldsymbol{\omega}}_a = \begin{bmatrix} 0 & -\omega_{z_a} & \omega_{y_a} \\ \omega_{z_a} & 0 & -\omega_{x_a} \\ -\omega_{y_a} & \omega_{x_a} & 0 \end{bmatrix}$$

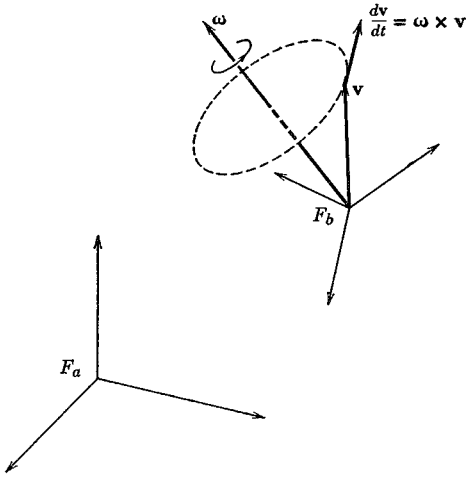

FIG. 4.12 Rotating vector of constant magnitude.

The corresponding result from (4.6,2) is

$$\dot{\mathbf{v}}_a = \dot{\mathbf{L}}_{ab}\mathbf{v}_b \tag{4.6,5}$$

It follows from equating (4.6,4) and (4.6,5) that

$$\dot{\mathbf{L}}_{ab}\mathbf{v}_b = \tilde{\boldsymbol{\omega}}_a\mathbf{v}_a$$

or

$$\dot{\mathbf{L}}_{ab}\mathbf{v}_b = \tilde{\boldsymbol{\omega}}_a\mathbf{L}_{ab}\mathbf{v}_b \tag{4.6,6}$$

for all $\mathbf{v}_b$. Whence

$$\dot{\mathbf{L}}_{ab} = \tilde{\boldsymbol{\omega}}_a\mathbf{L}_{ab}$$

and

$$\tilde{\boldsymbol{\omega}}_a = \dot{\mathbf{L}}_{ab}\mathbf{L}_{ba}$$

Finally if the above argument be repeated with F_b considered fixed, and F_a having angular velocity $-\boldsymbol{\omega}$, we clearly arrive at the reciprocal result

$$\dot{\mathbf{L}}_{ba} = -\tilde{\boldsymbol{\omega}}_b\mathbf{L}_{ba} \tag{4.6,7}$$

From (4.6,6) and (4.6,7), recalling that $\tilde{\boldsymbol{\omega}}$ is skew-symmetric so that $\tilde{\boldsymbol{\omega}}^T = -\tilde{\boldsymbol{\omega}}$, the reader can readily derive the result

$$\tilde{\boldsymbol{\omega}}_a = \mathbf{L}_{ab}\tilde{\boldsymbol{\omega}}_b\mathbf{L}_{ba} \tag{4.6,8}$$

From (4.6,2), (4.6,6), and (4.6,7) we have the alternative relations

$$\begin{aligned}\dot{\mathbf{v}}_b &= \mathbf{L}_{ba}\dot{\mathbf{v}}_a - \tilde{\boldsymbol{\omega}}_b\mathbf{v}_b \\ \dot{\mathbf{v}}_a &= \mathbf{L}_{ab}\dot{\mathbf{v}}_b + \tilde{\boldsymbol{\omega}}_a\mathbf{v}_a\end{aligned} \tag{4.6,9}$$

with two additional permutations made possible by (4.6,8). A particular form we shall finally want for application is that which uses the components of $\dot{\mathbf{v}}_a$ transformed into F_b, viz.

$$\mathbf{L}_{ba}\dot{\mathbf{v}}_a = \dot{\mathbf{v}}_b + \tilde{\boldsymbol{\omega}}_b\mathbf{v}_b \tag{4.6,10}$$

4.7 TRANSFORMATION OF A MATRIX

Equation (4.6,8) is an example of the transformation of a matrix the elements of which are dependent on the frame of reference. Generally the matrix of interest **A** occurs in an equation of the form

$$\mathbf{v} = \mathbf{A}\mathbf{u} \tag{4.7,1}$$

where the elements of the (physical) vectors **u** and **v** and of the matrix **A** are all dependent on the reference frame. We write (4.7,1) for each of the two frames F_a and F_b, i.e.

$$\begin{aligned}\mathbf{v}_a &= \mathbf{A}_a\mathbf{u}_a \qquad (a) \\ \mathbf{v}_b &= \mathbf{A}_b\mathbf{u}_b \qquad (b)\end{aligned} \tag{4.7,2}$$

and transform the second to

$$\mathbf{L}_{ba}\mathbf{v}_a = \mathbf{A}_b\mathbf{L}_{ba}\mathbf{u}_a$$

Premultiplying by $\mathbf{L}_{ab}$ we get

$$\mathbf{v}_a = \mathbf{L}_{ab}\mathbf{A}_b\mathbf{L}_{ba}\mathbf{u}_a \tag{4.7,3}$$

By comparison with (4.7,2a) we get the general result

$$\mathbf{A}_a = \mathbf{L}_{ab}\mathbf{A}_b\mathbf{L}_{ba} \tag{4.7,4}$$

General equations of unsteady motion

CHAPTER 5

The basis for analysis, computation, or simulation of the unsteady motions of flight vehicles is the mathematical model of the vehicle and of its subsidiary systems, i.e. their general equations of motion. Although a useful first step is to treat the vehicle as a single rigid body, and many important results can be derived from this model, we cannot in general avoid facing up to the reality of the situation, which is that vehicles are deformable and contain articulated or rotating subsystems such as control surfaces and engines. Furthermore the external forces and couples that act on aircraft and spacecraft are in general complicated functions of shape and of motion. This is especially true of the aerodynamic forces in atmospheric flight which are known only approximately. The attention that must be devoted to their representation dominates the formulation of the mathematical model. The forces and couples provided by the space environment (gravitational, magnetic, radiation pressure) are generally not so uncertain, and the problem of deriving an adequate mathematical model is consequently less difficult for spacecraft during extra-atmospheric operation.

In the following sections, we first treat the general motion of a particle over the rotating Earth, then derive the dynamical and kinematical equations for an arbitrary deformable vehicle in flight. Finally the equations for small disturbance from steady flight are presented in both dimensional and nondimensional form.

5.1 VELOCITY AND ACCELERATION IN AN ARBITRARILY MOVING FRAME

All of the reference frames with which we are concerned, except F_I of course, are in motion relative to inertial space. F_W and F_B in particular have quite arbitrary motion, including acceleration of the origin, and rotation. Since in many applications, we want to express the position, inertial velocity,

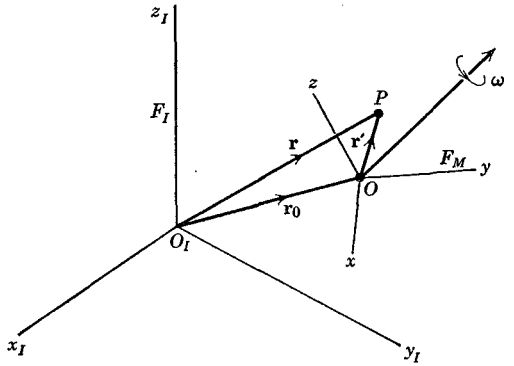

FIG. 5.1 Moving coordinate system.

and inertial acceleration of a particle in components parallel to the axes of these moving frames, we need general theorems that allow for arbitrary motion of the origin, and arbitrary angular velocity of the frame. These theorems are presented below.

Let $F_M(Oxyz)$ be any moving frame with origin at O and with angular velocity $\boldsymbol{\omega}$ relative to F_I. Let $\mathbf{r} = \mathbf{r}_0 + \mathbf{r}'$ be the position vector of a point P of F_M (see Fig. 5.1). Then the velocity and acceleration of P relative to F_I are

$$\begin{aligned} \mathbf{v}_I &= \dot{\mathbf{r}}_I \\ \mathbf{a}_I &= \ddot{\mathbf{r}}_I \end{aligned} \tag{5.1,1}$$

We want expressions for the velocity and acceleration of P in terms of the components of $\mathbf{r}'$ in F_M. Expanding the first of (5.1,1)

$$\begin{aligned} \mathbf{v}_I &= \dot{\mathbf{r}}_{o_I} + \dot{\mathbf{r}}'_I \\ &= \mathbf{v}_{o_I} + \dot{\mathbf{r}}'_I \end{aligned} \tag{5.1,2}$$

where $\mathbf{v}_o = \dot{\mathbf{r}}_o$ is the velocity of O relative to F_I. The velocity components in

F_M are given by

$$\mathbf{v}_M = \mathbf{L}_{MI}\mathbf{v}_I = \mathbf{L}_{MI}(\mathbf{v}_{o_I} + \dot{\mathbf{r}}'_I) = \mathbf{v}_{o_M} + \mathbf{L}_{MI}\dot{\mathbf{r}}'_I$$

From the rule for transforming derivatives (4.6,10)

$$\mathbf{L}_{MI}\dot{\mathbf{r}}'_I = \dot{\mathbf{r}}'_M + \tilde{\boldsymbol{\omega}}_M\mathbf{r}'_M \tag{5.1,3}$$

whence

$$\mathbf{v}_M = \mathbf{v}_{o_M} + \dot{\mathbf{r}}'_M + \tilde{\boldsymbol{\omega}}_M\mathbf{r}'_M \tag{5.1,4}$$

The first term of (5.1,4) is the velocity of O relative to F_I, the second is the velocity of P relative to F_M, and the last is the "transport velocity," i.e. the velocity relative to F_I of the point of F_M that is momentarily coincident with P. The total velocity of P relative to F_I is the sum of these three components. Following traditional practice in flight dynamics, we denote

$$\boldsymbol{\omega}_M = \begin{bmatrix} p \\ q \\ r \end{bmatrix}, \qquad \mathbf{r}'_M = \begin{bmatrix} x \\ y \\ z \end{bmatrix} \tag{5.1,5}$$

(When necessary, subscripts are added to the components to identify particular moving frames.)

The scalar expansion of (5.1,4) is then

$$\begin{aligned} v_x &= v_{o_x} + \dot{x} + qz - ry \\ v_y &= v_{o_y} + \dot{y} + rx - pz \\ v_z &= v_{o_z} + \dot{z} + py - qx \end{aligned} \tag{5.1,6}$$

These expressions then give the components, parallel to the moving coordinate axes, of the velocity of P relative to the *inertial* frame.

On differentiating $\mathbf{v}_I$ and using (5.1,4) we find the components of inertial acceleration parallel to the F_M axes to be

$$\begin{aligned} \mathbf{a}_M &= \mathbf{L}_{MI}\dot{\mathbf{v}}_I = \dot{\mathbf{v}}_M + \tilde{\boldsymbol{\omega}}_M\mathbf{v}_M \\ &= \dot{\mathbf{v}}_{o_M} + \ddot{\mathbf{r}}'_M + \dot{\tilde{\boldsymbol{\omega}}}_M\mathbf{r}'_M + \tilde{\boldsymbol{\omega}}_M\dot{\mathbf{r}}'_M + \tilde{\boldsymbol{\omega}}_M\mathbf{v}_{o_M} + \tilde{\boldsymbol{\omega}}_M\dot{\mathbf{r}}'_M + \tilde{\boldsymbol{\omega}}_M\tilde{\boldsymbol{\omega}}_M\mathbf{r}'_M \\ &= \mathbf{a}_{o_M} + \ddot{\mathbf{r}}'_M + \dot{\tilde{\boldsymbol{\omega}}}_M\mathbf{r}'_M + 2\tilde{\boldsymbol{\omega}}_M\dot{\mathbf{r}}'_M + \tilde{\boldsymbol{\omega}}_M\tilde{\boldsymbol{\omega}}_M\mathbf{r}'_M \end{aligned} \tag{5.1,7}$$

where $\mathbf{a}_{o_M} = \dot{\mathbf{v}}_{o_M} + \tilde{\boldsymbol{\omega}}_M\mathbf{v}_{o_M} = \mathbf{L}_{MI}\dot{\mathbf{v}}_{o_I}$ is the acceleration of O relative to F_I.

The total inertial acceleration of P is seen to be composed of the following parts:

$\mathbf{a}_o$: the acceleration of the origin of the moving frame

$\ddot{\mathbf{r}}'$: the acceleration of P relative to the moving frame

$\dot{\tilde{\boldsymbol{\omega}}}\mathbf{r}'$: the "tangential" acceleration owing to rotational acceleration of the frame F_M

$2\tilde{\boldsymbol{\omega}}\dot{\mathbf{r}}'$: the Coriolis acceleration

$\tilde{\boldsymbol{\omega}}\tilde{\boldsymbol{\omega}}\mathbf{r}'$: the centripetal acceleration

Three of the five terms vanish when the frame F_M has no rotation, and only $\ddot{\mathbf{r}}'$ remains if it is inertial. Note that the Coriolis acceleration is perpendicular to $\boldsymbol{\omega}$ and $\dot{\mathbf{r}}'$, and the centripetal acceleration is directed along the perpendicular from P to $\boldsymbol{\omega}$. The scalar expansion of (5.1,7) gives the required inertial acceleration components of P as

$$\begin{aligned} a_x &= a_{o_x} + \ddot{x} + 2q\dot{z} - 2r\dot{y} - x(q^2 + r^2) + y(pq - \dot{r}) + z(pr + \dot{q}) \\ a_y &= a_{o_y} + \ddot{y} + 2r\dot{x} - 2p\dot{z} + x(pq + \dot{r}) - y(p^2 + r^2) + z(qr - \dot{p}) \\ a_z &= a_{o_z} + \ddot{z} + 2p\dot{y} - 2q\dot{x} + x(pr - \dot{q}) + y(qr + \dot{p}) - z(p^2 + q^2) \end{aligned} \quad (5.1,8)$$

5.2 ANGULAR VELOCITIES OF THE SEVERAL REFERENCE FRAMES

Since the formulae for velocity and acceleration given above involve the angular velocity of the moving frame, we need convenient expressions for the angular velocities of the frames we shall be using. These expressions are developed below.

ANGULAR VELOCITY $\boldsymbol{\omega}^E$ OF F_E AND F_{EC}

The motion of the Earth consists of a superposition of rotation on its axis, precession and nutation of its axis, rotation in its orbit around the sun, and additional motions of the solar system and the galaxy. Although any of these may be significant for problems of space flight, only the first-mentioned is likely to be of any importance for atmospheric flight, and even that one is often negligible We shall assume therefore that the Earth's axis is fixed in inertial space, and that its motion is one of constant rotation at speed ω^E on this axis. Its angular velocity vector is (see Figs. 4.2 and 5.2)

$$\boldsymbol{\omega}^E{}_{EC} = \begin{bmatrix} 0 \\ 0 \\ \omega^E \end{bmatrix}; \quad \boldsymbol{\omega}^E{}_E = \begin{bmatrix} \cos\lambda_E \\ 0 \\ -\sin\lambda_E \end{bmatrix} \omega^E; \quad \boldsymbol{\omega}^E{}_V = \begin{bmatrix} \cos\lambda \\ 0 \\ -\sin\lambda \end{bmatrix} \omega^E \quad (5.2,1)$$

where ω^E is the rate of rotation, one revolution per day, or 7.27×10^{-5} rad/sec, λ_E is the latitude of O_E, and λ is the latitude of O_V.

ANGULAR VELOCITY ω^V OF F_V

Let the origin of F_V be at (λ, μ) at time t, and let it, in time δt, undergo infinitesimal displacement to $(\lambda + \delta\lambda, \mu + \delta\mu)$. It can be carried from its initial to its final positions by the two rotations (i)—$\delta\lambda$ around an axis

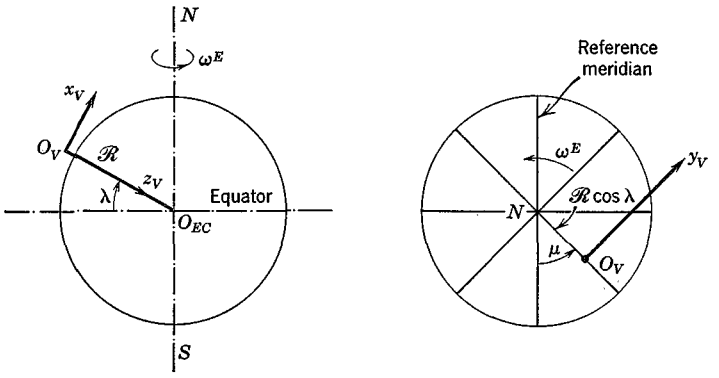

FIG. 5.2 Geocentric polar coordinates.

through the Earth center parallel to $O_V y_V$ and (ii) $\delta\mu$ around $O_{EC}z_{EC}$. Hence the angular displacement relative to Earth is given approximately by the vector

$$\delta\mathbf{n} \doteq -\mathbf{j}_V\,\delta\lambda + \mathbf{k}_{EC}\,\delta\mu \tag{5.2,2}$$

where $\mathbf{j}_V$ and $\mathbf{k}_{EC}$ are unit vectors on $O_V y_V$ and $O_{EC}z_{EC}$, respectively. The angular velocity of F_V relative to F_E is then exactly

$$\boldsymbol{\omega}^V - \boldsymbol{\omega}^E = \lim_{\delta t\to 0}\frac{\delta\mathbf{n}}{\delta t} = -\mathbf{j}_V\dot{\lambda} + \mathbf{k}_{EC}\dot{\mu} \tag{5.2,3}$$

On taking components of (5.2,3) in F_V, and using (5.2,1) we get

$$\boldsymbol{\omega}^V{}_V = \begin{bmatrix} (\omega^E + \dot{\mu})\cos\lambda \\ -\dot{\lambda} \\ -(\omega^E + \dot{\mu})\sin\lambda \end{bmatrix} \tag{5.2,4}$$

The components of $\boldsymbol{\omega}^V$ in F_W or F_B are, of course, obtained by premultiplying (5.2,4) by $\mathbf{L}_{WV}$ or $\mathbf{L}_{BV}$, respectively.

ANGULAR VELOCITIES $\boldsymbol{\omega}^W$, $\boldsymbol{\omega}$ OF F_W, F_B

The orientation of the moving frames F_W and F_B are given relative to F_V by the Euler angles ψ, θ, ϕ (Sec. 4.3). Subscript W denotes F_W and no subscript denotes F_B. The result is derived below for F_B, that for F_W being similar.

With reference to Fig. 4.9, let $\mathbf{i}$, $\mathbf{j}$, $\mathbf{k}$ be unit vectors of F_B, the subscripts

V, 2, 3 denoting the directions of the axes shown in the figure. By an argument identical with that for (5.2,2) and (5.2,3) we have the relative velocity

$$\boldsymbol{\omega} - \boldsymbol{\omega}^V = \mathbf{i}\dot{\phi} + \mathbf{j}_3\dot{\theta} + \mathbf{k}_2\,\dot{\psi} \tag{5.2,5}$$

By applying (4.5,2) (an exercise for the reader), the components of $\mathbf{i}$, $\mathbf{j}_3$, and $\mathbf{k}_2$ in F_B are found to be

$$\mathbf{i} = \begin{bmatrix} 1 \\ 0 \\ 0 \end{bmatrix} \qquad \mathbf{j}_3 = \begin{bmatrix} 0 \\ \cos\phi \\ -\sin\phi \end{bmatrix} \qquad \mathbf{k}_2 = \begin{bmatrix} -\sin\theta \\ \cos\theta\sin\phi \\ \cos\theta\cos\phi \end{bmatrix} \tag{5.2,6}$$

It follows that $\boldsymbol{\omega} - \boldsymbol{\omega}^V$ is given by

$$(\boldsymbol{\omega} - \boldsymbol{\omega}^V) = \begin{bmatrix} P \\ Q \\ R \end{bmatrix} = \begin{bmatrix} \dot{\phi} - \dot{\psi}\sin\theta \\ \dot{\theta}\cos\phi + \dot{\psi}\cos\theta\sin\phi \\ \dot{\psi}\cos\theta\cos\phi - \dot{\theta}\sin\phi \end{bmatrix} \tag{5.2,7}$$

where capital letters denote the components of the relative angular velocity. When $\boldsymbol{\omega}^V$ and $\boldsymbol{\omega}^E$ are both negligible, then $[P, Q, R] = [p, q, r]$, the angular velocity of F_B relative to F_I. Equation (5.2,7) can be written as the matrix product

$$\begin{bmatrix} P \\ Q \\ R \end{bmatrix} = \mathbf{R}\begin{bmatrix} \dot{\phi} \\ \dot{\theta} \\ \dot{\psi} \end{bmatrix} \qquad (a) \tag{5.2,8}$$

where

$$\mathbf{R} = \begin{bmatrix} 1 & 0 & -\sin\theta \\ 0 & \cos\phi & \sin\phi\cos\theta \\ 0 & -\sin\phi & \cos\phi\cos\theta \end{bmatrix} \qquad (b)$$

Inverting (5.2,8a) we get the Euler angle rates as

$$\begin{bmatrix} \dot{\phi} \\ \dot{\theta} \\ \dot{\psi} \end{bmatrix} = \begin{bmatrix} 1 & \sin\phi\tan\theta & \cos\phi\tan\theta \\ 0 & \cos\phi & -\sin\phi \\ 0 & \sin\phi\sec\theta & \cos\phi\sec\theta \end{bmatrix}\begin{bmatrix} P \\ Q \\ R \end{bmatrix} \tag{5.2,9}$$

Adding the subscript W in (5.2,8) and (5.2,9) to $[P, Q, R]$, $[\phi, \theta, \psi]$ gives the corresponding wind-axes equations. Note that these are transcendental differential equations for the Euler angles, and as such have exact analytical solutions only in special simple cases. Note also that the transformation matrix $\mathbf{R}$, unlike $\mathbf{L}$, is not orthogonal.

Equations (5.2,9) can be used to calculate the Euler angle rates from the relative angular velocities (P, Q, R). The latter can in turn be found from the "absolute" rates (p, q, r) by the first equality of (5.2,7), and (5.2,4), i.e.

$$\begin{bmatrix} P \\ Q \\ R \end{bmatrix} = \begin{bmatrix} p \\ q \\ r \end{bmatrix} - \mathbf{L}_{BV} \begin{bmatrix} (\omega^E + \dot{\mu}) \cos \lambda \\ -\dot{\lambda} \\ -(\omega^E + \dot{\mu}) \sin \lambda \end{bmatrix} \tag{5.2,10}$$

with a similar equation for wind axes obtained by adding the subscript W and substituting $\mathbf{L}_{WV}$ for $\mathbf{L}_{BV}$.

THE DIRECTION COSINE RATES

When the direction cosines of the moving frame are used instead of the Euler angles to define its orientation relative to F_V, then the differential equations needed follow directly from (4.6,7). Let $\mathbf{L}_{BV} = [l_{ij}]$ (the same treatment holds for $\mathbf{L}_{WV}$). Then from (4.6,7)

$$\begin{bmatrix} \dot{l}_{11} & \dot{l}_{12} & \dot{l}_{13} \\ \dot{l}_{21} & \dot{l}_{22} & \dot{l}_{23} \\ \dot{l}_{31} & \dot{l}_{32} & \dot{l}_{33} \end{bmatrix} = - \begin{bmatrix} 0 & -R & Q \\ R & 0 & -P \\ -Q & P & 0 \end{bmatrix} \begin{bmatrix} l_{11} & l_{12} & l_{13} \\ l_{21} & l_{22} & l_{23} \\ l_{31} & l_{32} & l_{33} \end{bmatrix} \tag{5.2,11}$$

These constitute nine differential equations for the nine l_{ij}. Actually only three of the nine are independent (a rigid body has only three rotational degrees of freedom), and the additional six equations provided by (4.4,8) reduce the number of independent l_{ij} to three. In the force equations given later, the direction cosines that would replace the Euler angle terms are those for the angles between the moving axes of F_W and z_V, i.e. (with l_{ij} now denoting components of $\mathbf{L}_{WV}$) l_{13}, l_{23}, and l_{33}. The differential equations for these are, from (5.2,11),

$$\begin{aligned} \dot{l}_{13} &= Rl_{23} - Ql_{33} \\ \dot{l}_{23} &= -Rl_{13} + Pl_{33} \\ \dot{l}_{33} &= Ql_{13} - Pl_{23} \end{aligned} \tag{5.2,11a}$$

and for some problems only these three direction cosines are needed. Whether direction cosines or Euler angles are preferable in any particular application depends on the situation, and on the kind of computing machinery to be used.

THE AERODYNAMIC ANGLE RATES

We shall find it convenient later to have the angular velocity of F_B relative to F_W expressed in terms of the derivatives of the aerodynamic angles.

Let $\mathbf{j}_B$ and $\mathbf{k}_W$ be unit vectors in the directions of Cy_B and Cz_W, respectively. Then it follows from the definitions of α_x and β (Sec. 4.3) [and an argument like that for (5.2,3)] that the angular velocity of F_B relative to F_W is

$$\begin{aligned}\boldsymbol{\omega}_{\text{rel}} &= \boldsymbol{\omega} - \boldsymbol{\omega}^W \\ &= -\mathbf{k}_W\dot{\beta} + \mathbf{j}_B\dot{\alpha}_x\end{aligned} \tag{5.2,12}$$

Taking the components of (5.2,12) in F_W we have (see also Sec. 4.2,5)

$$\mathbf{L}_{WB}\begin{bmatrix}p\\q\\r\end{bmatrix} - \begin{bmatrix}p_W\\q_W\\r_W\end{bmatrix} = -\begin{bmatrix}0\\0\\1\end{bmatrix}\dot{\beta} + \mathbf{L}_{WB}\begin{bmatrix}0\\1\\0\end{bmatrix}\dot{\alpha}_x$$

or

$$\begin{bmatrix}p_W\\q_W\\r_W\end{bmatrix} = \mathbf{L}_{WB}\begin{bmatrix}p\\q-\dot{\alpha}_x\\r\end{bmatrix} + \begin{bmatrix}0\\0\\1\end{bmatrix}\dot{\beta} \tag{5.2,13}$$

After expansion, this gives the scalar equations

$$\begin{aligned}
p_W &= p\cos\alpha_x\cos\beta + (q-\dot{\alpha}_x)\sin\beta + r\sin\alpha_x\cos\beta && (a)\\
q_W &= -p\cos\alpha_x\sin\beta + (q-\dot{\alpha}_x)\cos\beta - r\sin\alpha_x\sin\beta && (b)\\
r_W &= -p\sin\alpha_x + r\cos\alpha_x + \dot{\beta} && (c)
\end{aligned} \tag{5.2,14}$$

From the last two of (5.2,14) the values of $\dot{\alpha}_x$ and $\dot{\beta}$ are conveniently expressed in terms of the angular velocities of F_B and F_W as

$$\begin{aligned}
\dot{\alpha}_x &= q - q_W\sec\beta - p\cos\alpha_x\tan\beta - r\sin\alpha_x\tan\beta && (a)\\
\dot{\beta} &= r_W + p\sin\alpha_x - r\cos\alpha_x && (b)
\end{aligned} \tag{5.2,15}$$

The group of three equations actually wanted subsequently is (5.2,14*a*) and (5.2,15).

Since (5.2,12) may alternatively be written

$$\boldsymbol{\omega}_{\text{rel}} = (\boldsymbol{\omega} - \boldsymbol{\omega}^V) - (\boldsymbol{\omega}^W - \boldsymbol{\omega}^V)$$

it follows that (5.2,13) through (5.2,15) apply equally when the angular velocities of F_B and F_W are relative to F_V instead of F_I. Then the lower-case (p, q, r) are replaced in them by (P, Q, R).

5.3 POSITION, VELOCITY, AND ACCELERATION OF THE VEHICLE MASS CENTER

POSITION AND VELOCITY RELATIVE TO THE EARTH

The location of the vehicle mass center relative to Earth is given by the spherical polar coordinates $\mathscr{R}$ (geocentric radius), μ (longitude), and λ (latitude). Their rates of change are related to the F_V components of velocity relative to Earth by (see Fig. 5.2)

$$\begin{aligned} \dot{\mathscr{R}} &= -V^E{}_{z_V} \\ \dot{\mu} &= \frac{1}{\mathscr{R}\cos\lambda} V^E{}_{y_V} \\ \dot{\lambda} &= \frac{1}{\mathscr{R}} V^E{}_{x_V} \end{aligned} \tag{5.3,1}$$

The components of $\mathbf{V}^E$ are in turn given by [see (4.2,1)]

$$\mathbf{V}^E{}_V = \mathbb{L}_{VW}(\mathbf{V}_W + \mathbf{W}_W) = \mathbb{L}_{VB}(\mathbf{V}_B + \mathbf{W}_B) \tag{5.3,2}$$

where

$$\mathbf{V}_W = \begin{bmatrix} V \\ 0 \\ 0 \end{bmatrix}; \qquad \mathbf{W}_W = \begin{bmatrix} W_{x_W} \\ W_{y_W} \\ W_{z_W} \end{bmatrix} \tag{5.3,3}$$

$$\mathbf{V}_B = \begin{bmatrix} u \\ v \\ w \end{bmatrix}; \qquad \mathbf{W}_B = \begin{bmatrix} W_x \\ W_y \\ W_z \end{bmatrix}$$

and V is the airspeed of the vehicle, i.e. its speed relative to the atmosphere. When the atmosphere is at rest relative to Earth, $\mathbf{W} = 0$ and (5.3,2), (5.3,3), and (4.5,4) yield

$$\begin{aligned} V^E{}_{x_V} &= V\cos\theta_W\cos\psi_W \\ V^E{}_{y_V} &= V\cos\theta_W\sin\psi_W \\ V^E{}_{z_V} &= -V\sin\theta_W \end{aligned} \tag{5.3,4}$$

Substitution of (5.3,4) into (5.3,1) provides the polar coordinates in the

more convenient forms

$$\begin{aligned} \dot{\mathscr{R}} &= V \sin \theta_W \\ \dot{\mu} &= \frac{V}{\mathscr{R}} \cos \theta_W \sin \psi_W \sec \lambda \\ \dot{\lambda} &= \frac{V}{\mathscr{R}} \cos \theta_W \cos \psi_W \end{aligned} \tag{5.3,5}$$

Using the body-axis velocity components an alternative system of equations is

$$\begin{bmatrix} \dot{\lambda}\mathscr{R} \\ \dot{\mu}\mathscr{R} \cos \lambda \\ -\dot{\mathscr{R}} \end{bmatrix} = \mathbf{L}_{VB} \begin{bmatrix} u \\ v \\ w \end{bmatrix} \tag{5.3,6}$$

When the motion considered takes place over only a small portion of the Earth's surface, the latter may be regarded as locally flat, and the vehicle position is then more conveniently referenced to a frame F_E located in its immediate vicinity—for example, at the initial point of the trajectory. In this case F_V may be assumed parallel to F_E, and the position coordinates of the mass center (x_E, y_E, z_E) are governed by the differential equations

$$\begin{aligned} \dot{x}_E &= V \cos \theta_W \cos \psi_W \\ \dot{y}_E &= V \cos \theta_W \sin \psi_W \\ \dot{z}_E &= -V \sin \theta_W \end{aligned} \tag{5.3,7}$$

INERTIAL ACCELERATION

We have two particular requirements for the inertial acceleration of a particle in a moving reference frame: one is for the F_W or F_B components of the acceleration of C or O_V, the vehicle mass center, and the other is for the F_B components of the acceleration of a particle in arbitrary motion relative to the vehicle. Other reference frames may be of interest for application to special dynamics problems, or for the analysis of navigation and guidance systems in which expressions are needed for the outputs of accelerometers mounted on inertial platforms that are oriented in accordance to some particular navigation scheme. The two applications first mentioned above are developed here; and as a matter of interest, we give also the formulation needed for a particular navigation application.

Acceleration of C. The basic equation for the inertial acceleration of the mass center is (5.1,7), in which the moving point is O_V, in the rotating frame F_E. $\dot{\mathbf{r}}'$ is then the velocity of the mass center relative to Earth, which we have denoted $\mathbf{V}^E$. We assume here, as in Sec. 5.2, that the Earth's axis is

fixed in inertial space, and that $\dot{\boldsymbol{\omega}} = 0$. Thus the acceleration $\mathbf{a}_0$ of the origin of F_E is the centripetal acceleration associated with Earth rotation. A numerical comparison shows that this acceleration is usually negligible when compared with g. It is zero at the poles, and of order $1/1000\, g$ at the equator (sea level). The same holds true for the centripetal acceleration $\tilde{\boldsymbol{\omega}}\tilde{\boldsymbol{\omega}}\mathbf{r}'$ of (5.1,7)—i.e. it is usually negligible. Of the two terms that remain in (5.1,7) $\ddot{\mathbf{r}}' = \dot{\mathbf{V}}^E$ and the Coriolis acceleration is $2\tilde{\boldsymbol{\omega}}^E\mathbf{V}^E$. The latter depends on the magnitude and direction of the vehicle velocity, and is at most $10\%\, g$ at orbital speed. It can of course be larger at higher speeds. This term must therefore be kept in the mathematical model, even though it is at times negligible. Finally then, the approximation we use for the acceleration of C is

$$\mathbf{a}_{C_E} = \dot{\mathbf{V}}^E{}_E + 2\tilde{\boldsymbol{\omega}}^E{}_E\mathbf{V}^E{}_E \tag{5.3,8}$$

To transform (5.3,8) into the moving frame F_W we use (4.6,10) noting that the angular velocity of F_W relative to F_E is $(\boldsymbol{\omega}^W - \boldsymbol{\omega}^E)$ to obtain

$$\begin{aligned}\mathbf{a}_{C_W} &= \mathbf{L}_{WE}\mathbf{a}_{C_E} = \mathbf{L}_{WE}(\dot{\mathbf{V}}^E{}_E + 2\tilde{\boldsymbol{\omega}}^E{}_E\mathbf{V}^E{}_E)\\ &= \dot{\mathbf{V}}^E{}_W + (\tilde{\boldsymbol{\omega}}^W - \tilde{\boldsymbol{\omega}}^E)_W\mathbf{V}^E{}_W + 2\mathbf{L}_{WE}\tilde{\boldsymbol{\omega}}^E{}_E\mathbf{V}^E{}_E\end{aligned} \tag{5.3,9}$$

The last term is treated as follows:

$$\mathbf{L}_{WE}\tilde{\boldsymbol{\omega}}^E{}_E\mathbf{V}^E{}_E = (\mathbf{L}_{WE}\tilde{\boldsymbol{\omega}}^E{}_E\mathbf{L}_{EW})(\mathbf{L}_{WE}\mathbf{V}^E{}_E) = \tilde{\boldsymbol{\omega}}^E{}_W\mathbf{V}^E{}_W \tag{5.3,10}$$

whence

$$\begin{aligned}\mathbf{a}_{C_W} &= \dot{\mathbf{V}}^E{}_W + (\tilde{\boldsymbol{\omega}}^W - \tilde{\boldsymbol{\omega}}^E)_W\mathbf{V}^E{}_W + 2\tilde{\boldsymbol{\omega}}^E{}_W\mathbf{V}^E{}_W\\ &= \dot{\mathbf{V}}^E{}_W + (\tilde{\boldsymbol{\omega}}^W + \tilde{\boldsymbol{\omega}}^E)_W\mathbf{V}^E{}_W\end{aligned} \tag{5.3,11}$$

To obtain the scalar expansion of (5.3,11) we note that $\mathbf{V}^E{}_W$ is given by [see (5.3,3)]

$$\mathbf{V}^E{}_W = \begin{bmatrix} V \\ 0 \\ 0 \end{bmatrix} + \begin{bmatrix} W_{x_W} \\ W_{y_W} \\ W_{z_W} \end{bmatrix} \tag{5.3,12}$$

$\boldsymbol{\omega}^W{}_W$ is given by

$$\boldsymbol{\omega}^W{}_W = \begin{bmatrix} p_W \\ q_W \\ r_W \end{bmatrix} \tag{5.3,13}$$

and [see (5.2,1)]

$$\boldsymbol{\omega}^E{}_W = \begin{bmatrix} p^E{}_W \\ q^E{}_W \\ r^E{}_W \end{bmatrix} = \mathbf{L}_{WV}\begin{bmatrix} \cos\lambda \\ 0 \\ -\sin\lambda \end{bmatrix}\omega^E \tag{5.3,14}$$

where the notation $p^E{}_W$ etc. identifies the components of $\boldsymbol{\omega}^E$ in the frame F_W.

When the atmosphere is at rest, $\mathbf{W} = 0$ and the components of (5.3,11) are

$$\begin{aligned} a_{C_{x_W}} &= \dot{V} \\ a_{C_{y_W}} &= V(r^E{}_W + r_W) \\ a_{C_{z_W}} &= -V(q^E{}_W + q_W) \end{aligned} \tag{5.3,15}$$

[Note that $\boldsymbol{\omega}^E$ and $\boldsymbol{\omega}^W$ are *both* angular velocities relative to inertial space, and that the sum $(r^E{}_W + r_W)$ for example, is *not* the resultant yaw rate of F_W relative to F_I, as one might be tempted to infer from (5.3,15).]

For the frame F_B, the same procedure yields instead of (5.3,11)

$$\mathbf{a}_{C_B} = \dot{\mathbf{V}}^E{}_B + (\tilde{\boldsymbol{\omega}} + \tilde{\boldsymbol{\omega}}^E)_B \mathbf{V}^E{}_B \tag{5.3,16}$$

The scalar components of the vectors of (5.3,16) are

$$\mathbf{V}^E{}_B = \begin{bmatrix} u \\ v \\ w \end{bmatrix} + \begin{bmatrix} W_x \\ W_y \\ W_z \end{bmatrix} \tag{5.3,17}$$

$$\boldsymbol{\omega}_B = \begin{bmatrix} p \\ q \\ r \end{bmatrix}, \qquad \boldsymbol{\omega}^E{}_B = \begin{bmatrix} p^E{}_B \\ q^E{}_B \\ r^E{}_B \end{bmatrix} = \mathbb{L}_{BV} \begin{bmatrix} \cos\lambda \\ 0 \\ -\sin\lambda \end{bmatrix} \omega^E$$

Again for a stationary atmosphere, (5.3,16) is expanded with the aid of (5.3,17) to give

$$\begin{aligned} a_{C_x} &= \dot{u} + (q + q^E{}_B)w - (r + r^E{}_B)v \\ a_{C_y} &= \dot{v} + (r + r^E{}_B)u - (p + p^E{}_B)w \\ a_{C_z} &= \dot{w} + (p + p^E{}_B)v - (q + q^E{}_B)u \end{aligned} \tag{5.3,18}$$

Acceleration of a Particle in F_B. A particle having coordinates (x, y, z) in F_B has inertial acceleration components in the directions of the axes of F_B given by (5.1,8), in which $\mathbf{a}_0$ is the inertial acceleration of the origin of F_B and (p, q, r) are the components of $\boldsymbol{\omega}$. Since the origin of F_B is the vehicle mass center then $\mathbf{a}_0 = \mathbf{a}_C$ and its components are those given above in (5.3,18). The required equations are then obtained by substituting (5.3,18) for $\mathbf{a}_0$ in (5.1,8).

The Navigation Case. From the general relations already given, it is a straightforward, although tedious, calculation to derive the equations for the acceleration components $\mathbf{a}_V$ of a moving particle. This particular set of components is that measured by an inertial navigation system in which accelerometers are mounted on a stabilized platform that is "Schuler tuned" to maintain one axis vertical, and is "torqued" to maintain one horizontal

axis directed north. In the navigation application, the accelerations of interest are very small, and are in effect integrated twice over long periods of time to give position. Thus the small centripetal acceleration [the last term of (5.1,7)] is not negligible, and the complete equation must be used. The acceleration of the origin of F_V (which may be taken to be the location of the inertial platform in this application) is then [cf. (5.3,8)]

$$\mathbf{a}_{o_E} = \dot{\mathbf{V}}^E{}_E - (\tilde{\boldsymbol{\omega}}^E \tilde{\boldsymbol{\omega}}^E \mathbf{k}_V \mathscr{R})_E + 2\tilde{\boldsymbol{\omega}}^E{}_E \mathbf{V}^E{}_E \tag{5.3,19}$$

where $\mathbf{k}_V$ is a unit vector on Cz_V, and the second term is the centripetal acceleration previously neglected. After transforming to F_V, i.e. $\mathbf{a}_{oV} = \mathbf{L}_{VE}\mathbf{a}_{o_E}$, (5.3,19) gives

$$\mathbf{a}_{oV} = \dot{\mathbf{V}}^E{}_V + (\tilde{\boldsymbol{\omega}}^V - \tilde{\boldsymbol{\omega}}^E)_V \mathbf{V}^E{}_V - (\tilde{\boldsymbol{\omega}}^E \tilde{\boldsymbol{\omega}}^E \mathbf{k}_V \mathscr{R})_V + 2\tilde{\boldsymbol{\omega}}^E{}_V \mathbf{V}^E{}_V \tag{5.3,20}$$

$\boldsymbol{\omega}^V{}_V$ and $\boldsymbol{\omega}^E{}_V$ are given respectively by (5.2,4) and (5.2,1), and from (5.3,1)

$$\mathbf{V}^E{}_V = \begin{bmatrix} \mathscr{R}\dot{\lambda} \\ \mathscr{R}\dot{\mu}\cos\lambda \\ -\dot{\mathscr{R}} \end{bmatrix} \tag{5.3,21}$$

The components of the unit vector $\mathbf{k}_V$ in F_V are of course [0, 0, 1]. After substituting the above expressions into (5.3,20) and expanding the matrices, the following system of equations in $(\mathscr{R}, \lambda, \mu)$ are obtained:

$$\begin{aligned} a_{o_{x_V}} &= \mathscr{R}\ddot{\lambda} + 2\dot{\mathscr{R}}\dot{\lambda} + \mathscr{R}\sin\lambda\cos\lambda(\omega^E + \dot{\mu})^2 \\ a_{o_{y_V}} &= \mathscr{R}\cos\lambda\ddot{\mu} + 2(\omega^E + \dot{\mu})(\dot{\mathscr{R}}\cos\lambda - \mathscr{R}\dot{\lambda}\sin\lambda) \\ a_{o_{z_V}} &= -\ddot{\mathscr{R}} + \mathscr{R}\dot{\lambda}^2 + \mathscr{R}\cos^2\lambda(\omega^E + \dot{\mu})^2 \end{aligned} \tag{5.3,22}$$

When accelerometers provide measurements of the l.h.s. of (5.3,22), a navigation computer can in principle solve the three equations for the geocentric position $(\mathscr{R}, \lambda, \mu)$. For horizontal flight or when $\dot{\mathscr{R}}$ can be neglected, the result is simpler, i.e.

$$\begin{aligned} a_{o_{x_V}} &= \mathscr{R}\ddot{\lambda} + \mathscr{R}\sin\lambda\cos\lambda(\omega^E + \dot{\mu})^2 \\ a_{o_{y_V}} &= -\mathscr{R}\cos\lambda\ddot{\mu} - 2(\omega^E + \dot{\mu})\mathscr{R}\dot{\lambda}\sin\lambda \end{aligned} \tag{5.3,23}$$

This is a pair of equations for the latitude and longitude of the vehicle. To mechanize them for analog or digital computation, they would be more conveniently rearranged as

$$\begin{aligned} \ddot{\lambda} &= \frac{1}{\mathscr{R}} a_{o_{x_V}} - \sin\lambda\cos\lambda(\omega^E + \dot{\mu})^2 \\ \ddot{\mu} &= \frac{1}{\mathscr{R}}\sec\lambda a_{o_{y_V}} + 2(\omega^E + \dot{\mu})\dot{\lambda}\tan\lambda \end{aligned} \tag{5.3,24}$$

5.4 EQUATIONS OF MOTION OF AN ARBITRARY SYSTEM

The equations of motion result from the application of Newton's laws of motion to the material system that constitutes the flight vehicle. Consider

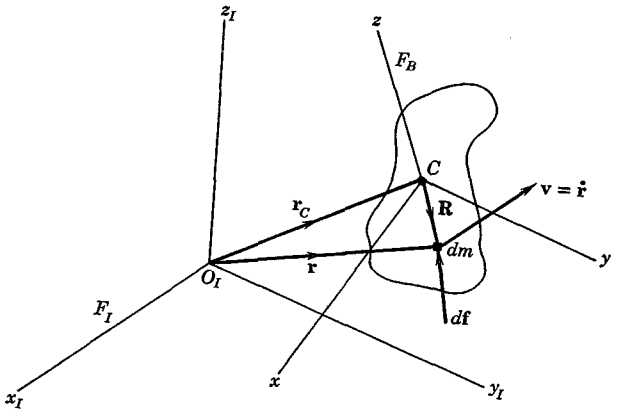

FIG. 5.3 Application of Newton's Law to an element of a body.

an element of mass dm, and an inertial frame of reference F_I (see Fig. 5.3). (Since only one reference frame is used in the following argument, no identifying subscript is appended to the vector symbols. The subscript I should be understood.) Newton's second law provides the equation of motion of dm, i.e.

$$d\mathbf{f} = \ddot{\mathbf{r}}\, dm = \dot{\mathbf{v}}\, dm \tag{5.4,1}$$

Here $d\mathbf{f}$ is the resultant of all the forces acting on dm, $\mathbf{r}$ is its position vector, and $\mathbf{v}$ its velocity. In this form, the equation is valid *only* in an inertial frame of reference.

Taking the cross product of (5.4,1) with $\mathbf{r}$ yields the moment equation

$$\mathbf{r} \times d\mathbf{f} = \mathbf{r} \times \dot{\mathbf{v}}\, dm \tag{5.4,2}$$

Now let the angular momentum of dm w.r.t. O be defined as

$$d\mathbf{h}' = \mathbf{r} \times \mathbf{v}\, dm \tag{5.4,3}$$

It follows that

$$\frac{d}{dt}(d\mathbf{h}') = (\dot{\mathbf{r}} \times \mathbf{v} + \mathbf{r} \times \dot{\mathbf{v}})\, dm$$

$$= (\mathbf{v} \times \mathbf{v} + \mathbf{r} \times \dot{\mathbf{v}})\, dm$$

Since $\mathbf{v} \times \mathbf{v} = 0$,

$$\frac{d}{dt}(d\mathbf{h}') = \mathbf{r} \times \dot{\mathbf{v}}\, dm$$

which is the r.h.s. of (5.4,2). We therefore have

$$d\mathbf{G}' = \frac{d}{dt}\, d\mathbf{h}' \tag{5.4,4}$$

where

$$d\mathbf{G}' = \mathbf{r} \times d\mathbf{f} \tag{5.4,5}$$

is the moment of $d\mathbf{f}$ about O.

We now integrate (5.4,1) and (5.4,4) for a system of particles comprising a general deformable body of mass m. First we note that the mass center C of the body is located at $\mathbf{r}_C$, given by

$$m\mathbf{r}_C = \int \mathbf{r}\, dm \tag{5.4,6}$$

Differentiating once yields

$$m\mathbf{v}_C = \int \dot{\mathbf{r}}\, dm \tag{5.4,7}$$

and a second time

$$m\mathbf{a}_C = \int \dot{\mathbf{v}}\, dm \tag{5.4,8}$$

where $\mathbf{v}_C$ and $\mathbf{a}_C$ are respectively the velocity and acceleration of the mass center relative to F_I. The integral of (5.4,1) is obtained from (5.4,8) as

$$\boxed{\mathbf{f} = m\mathbf{a}_C} \tag{5.4,9}$$

where $\mathbf{f} = \int d\mathbf{f}$ is the vector sum of all the forces acting on all the elements. Since the internal forces, those which one element of the system exerts upon another, occur in equal and opposite pairs by Newton's third law of motion, they vanish from $\int d\mathbf{f}$: $\mathbf{f}$ is then the resultant *external* force acting on the system m. Similarly, the integral over m of (5.4,4) is simply,

$$\mathbf{G}' = \frac{d}{dt}\, \mathbf{h}' \tag{5.4,9b}$$

where $\mathbf{G}' = \int \mathbf{r} \times d\mathbf{f}$ is the resultant external moment about O, and

$$\mathbf{h}' = \int \mathbf{r} \times \mathbf{v}\, dm \tag{5.4,10}$$

is the resultant angular momentum about O. Let

$$\mathbf{r} = \mathbf{r}_C + \mathbf{R} \tag{5.4,11a}$$

as shown on Fig. 5.3. Note that from (5.4,6)

$$\int \mathbf{R}\, dm = 0 \tag{5.4,11b}$$

Then we may expand (5.4,9*b*) as follows:

$$\int (\mathbf{r}_C + \mathbf{R}) \times d\mathbf{f} = \frac{d}{dt} \int (\mathbf{r}_C + \mathbf{R}) \times \mathbf{v}\, dm$$

Since $\mathbf{r}_C$ is constant, it can come outside the integrals, to give

$$\mathbf{r}_C \times \mathbf{f} + \int \mathbf{R} \times d\mathbf{f} = \mathbf{r}_C \times \int \dot{\mathbf{v}}\, dm + \frac{d}{dt} \int \mathbf{R} \times \mathbf{v}\, dm$$

From (5.4,8) and (5.4,9) the leading terms on the l.h.s. and r.h.s. are seen to be equal, so the equation reduces to

$$\boxed{\mathbf{G} = \dot{\mathbf{h}}} \qquad (a) \tag{5.4,12}$$

where

$$\mathbf{G} = \int \mathbf{R} \times d\mathbf{f} \qquad (b)$$

and

$$\mathbf{h} = \int \mathbf{R} \times \mathbf{v}\, dm \quad (c)$$

are, respectively, the moment and angular momentum about C. Note that (5.4,9*b*) has the same simple form as (5.4,12) even though the former is referenced to a fixed point in inertial space, and the latter to a moving point, the mass center. This simple form does not hold, for arbitrary motion of the systems, for any moving reference point except the mass center.

Equations (5.4,9) and (5.4,12) are the two fundamental vector equations, equivalent to six scalar equations, that relate the "gross" motion of the body to the external forces that act on it. The description of the "fine" motion (distortion and articulation) requires additional equations that are given subsequently.

THE ANGULAR MOMENTUM

With components in F_I, the angular momentum of the general deformable body is from (5.4,12*c*), on converting to matrix notation,

$$\begin{aligned} \mathbf{h}_I &= \int \tilde{\mathbf{R}}_I \mathbf{v}_I\, dm \\ &= \int \tilde{\mathbf{R}}_I \dot{\mathbf{R}}_I\, dm \end{aligned} \tag{5.4,13}$$

It is not convenient, as will be seen later, to have the angular momentum components referred to fixed axes. In fact we want its components along the axes F_B, attached to the moving vehicle. From (4.6,10)

$$\dot{\mathbf{R}}_I = \mathbf{L}_{IB}(\dot{\mathbf{R}}_B + \tilde{\boldsymbol{\omega}}_B \mathbf{R}_B) \tag{5.4,14}$$

whence (5.4,13) gives the components of $\mathbf{h}$ in F_B as

$$\mathbf{h}_B = \mathbf{L}_{BI}\mathbf{h}_I = \int \mathbf{L}_{BI}\tilde{\mathbf{R}}_I \mathbf{L}_{IB}\dot{\mathbf{R}}_B \, dm + \int \mathbf{L}_{BI}\tilde{\mathbf{R}}_I \mathbf{L}_{IB}\tilde{\boldsymbol{\omega}}_B \mathbf{R}_B \, dm$$

Now the matrix $\tilde{\mathbf{R}}$ transforms according to the rule (4.7,4), so that $\mathbf{L}_{BI}\tilde{\mathbf{R}}_I\mathbf{L}_{IB} = \tilde{\mathbf{R}}_B$ and we get for $\mathbf{h}_B$

$$\mathbf{h}_B = \int \tilde{\mathbf{R}}_B \dot{\mathbf{R}}_B dm + \int \tilde{\mathbf{R}}_B \tilde{\boldsymbol{\omega}}_B \mathbf{R}_B \, dm \tag{5.4,15}$$

When the body is rigid, $\dot{\mathbf{R}}_B = 0$, and the first term vanishes. [Note that $\int \dot{\mathbf{R}}_B \, dm$ vanishes in any case because the origin is the mass center, see (5.4,11*b*).] The second term of (5.4,15) is therefore identified as the "rigid-body component" of $\mathbf{h}$, and the first term as the "deformation component." To evaluate the second term, we note that $\tilde{\boldsymbol{\omega}}\mathbf{R} = -\tilde{\mathbf{R}}\boldsymbol{\omega}$ (Since $\boldsymbol{\omega} \times \mathbf{R} = -\mathbf{R} \times \boldsymbol{\omega}$) and hence

$$\int \tilde{\mathbf{R}}_B \tilde{\boldsymbol{\omega}}_B \mathbf{R}_B \, dm = -\int \tilde{\mathbf{R}}_B \tilde{\mathbf{R}}_B \boldsymbol{\omega}_B \, dm \tag{5.4,16}$$

Since $\tilde{\boldsymbol{\omega}}_B$ is constant with respect to the integration, we may write

$$-\int \tilde{\mathbf{R}}_B \tilde{\mathbf{R}}_B \boldsymbol{\omega}_B \, dm = \mathscr{I}_B \boldsymbol{\omega}_B \tag{5.4,17}$$

where

$$\mathscr{I}_B = -\int \tilde{\mathbf{R}}_B \tilde{\mathbf{R}}_B \, dm \tag{5.4,18*a*}$$

(note the identity $\tilde{\mathbf{R}}\tilde{\mathbf{R}} = \mathbf{R}^T\mathbf{R}\mathbf{I} - \mathbf{R}\mathbf{R}^T$). After expansion of (5.4,18*a*) and integration we get

$$\mathscr{I}_B = \begin{bmatrix} I_x & -I_{xy} & -I_{zx} \\ -I_{xy} & I_y & -I_{yz} \\ -I_{zx} & -I_{yz} & I_z \end{bmatrix} = \begin{bmatrix} A & -F & -E \\ -F & B & -D \\ -E & -D & C \end{bmatrix} \tag{5.4,18*b*}$$

The two notations for the elements of $\mathscr{I}$ given in (5.4,18*b*) are both traditional and in current use in flight dynamics literature. These elements are the

moments and products of inertia, i.e.

$$I_x = A = \int (y^2 + z^2)\, dm, \quad \text{etc.}$$

$$I_{xy} = F = \int xy\, dm, \qquad \text{etc.} \tag{5.4,19}$$

Note that the inertia matrix transforms according to (4.7,4), so that for two reference frames F_{B_1} and F_{B_2} we have

$$\mathscr{I}_{B_2} = \mathbf{L}_{B_2B_1} \mathscr{I}_{B_1} L_{B_1B_2} \tag{5.4,20a}$$

For any $\mathscr{I}_{B_1}$, there always exists a transformation $\mathbf{L}_{B_1B_2}$ that produces a diagonal matrix $\mathscr{I}_{B_2}$ (see ref. 5.1). F_{B_2} is then a set of *principal axes,* for which the products of inertia all vanish. When the vehicle has a plane of symmetry, then the x and z principal axes lie in it. If the body axes F_B are obtained from the principal axes by a rotation ϵ about Cy, the elements of $\mathscr{I}_B$ are found from (5.4,20a) to be

$$\begin{aligned} I_x &= I_{x_p} \cos^2 \epsilon + I_{z_p} \sin^2 \epsilon \\ I_y &= I_{y_p} \\ I_z &= I_{x_p} \sin^2 \epsilon + I_{z_p} \cos^2 \epsilon \\ I_{zx} &= \tfrac{1}{2}(I_{z_p} - I_{x_p}) \sin 2\epsilon \\ I_{xy} &= I_{yz} = 0 \end{aligned} \tag{5.4,20b}$$

where the subscript p denotes principal axes.

Let us denote the deformation component of $\mathbf{h}$ by

$$\mathbf{h}_B^* = \int \tilde{\mathbf{R}}_B \dot{\mathbf{R}}_B\, dm \tag{5.4,21}$$

so that (5.4,15) gives the total angular momentum

$$\mathbf{h}_B = \mathbf{h}_B^* + \mathscr{I}_B \boldsymbol{\omega}_B \tag{5.4,22}$$

From (5.4,21) we can evaluate $\mathbf{h}_B^*$ as

$$\mathbf{h}_B^* = \begin{bmatrix} \int (y\dot{z} - \dot{y}z)\, dm \\ \int (z\dot{x} - \dot{z}x)\, dm \\ \int (x\dot{y} - \dot{x}y)\, dm \end{bmatrix} \tag{5.4,23}$$

ROTATING SUBSYSTEM

When the relative motion in question (i.e. of the system w.r.t. F_B) is that of a rigid rotating subsystem (such as an engine rotor or propeller in an aircraft or an inertia wheel in a spacecraft) with angular velocity $\boldsymbol{\omega}^r$ relative to the main body, then we have, over the spinning component,

$$\dot{\mathbf{R}}_B = \tilde{\boldsymbol{\omega}}^r{}_B \mathbf{R}^r{}_B$$

where $\mathbf{R}^r{}_B$ is the position vector of a mass element relative to an origin anywhere on the axis of rotation. Ordinarily the mass center of the spinning body lies on its axis, and this is the natural choice of origin for $\mathbf{R}^r{}_B$. In that case it is easily shown (an exercise for the reader) that the contribution of the rotor to $\mathbf{h}^*$, denoted $\mathbf{h}^r$, is

$$\mathbf{h}^r{}_B = \mathscr{I}^r{}_B \boldsymbol{\omega}^r{}_B \tag{5.4,24}$$

where $\mathscr{I}^r{}_B$ is the inertia matrix of the rotor with respect to centroidal axes parallel to those of F_B. If moreover the spin axis is a principal axis of inertia of the rotor the vector $\mathbf{h}^r$ is collinear with $\boldsymbol{\omega}^r$, and has magnitude $I^r\omega^r$ where I^r is the moment of inertia of the rotor about the spin axis. Naturally, there is one term like (5.4,24) for each rotor.

THE REMAINDER OF h*

The remainder of $\mathbf{h}^*$ ordinarily comes from the motion of hinged parts and from elastic deformation, although there are other kinds of possible relative motion, such as fuel sloshing which is important in liquid-fueled rockets (ref. 5.14). This total remainder is denoted by $\mathbf{h}^e$. We now show that it is possible always to choose a set of body-axes F_B for which $\mathbf{h}^e$ vanishes. These are termed "mean axes" by Milne (ref. 5.2).

Consider two centroidal reference frames F_{B_1} and F_{B_2} for which the angular momenta are

$$\begin{aligned} \mathbf{h}_{B_1} &= \int \tilde{\mathbf{R}}_{B_1} \dot{\mathbf{R}}_{B_1}\, dm + \mathscr{I}_{B_1} \boldsymbol{\omega}_{B_1} + \sum_i \mathbf{h}^{r_i}{}_{B_1} \qquad (a) \\ \mathbf{h}_{B_2} &= \int \tilde{\mathbf{R}}_{B_2} \dot{\mathbf{R}}_{B_2}\, dm + \mathscr{I}_{B_2} (\boldsymbol{\omega} + \Delta\boldsymbol{\omega})_{B_2} + \sum_i \mathbf{h}^{r_i}{}_{B_2} \qquad (b) \end{aligned} \tag{5.4,25}$$

Here the summations are the contributions of spinning rotors, $\dot{\mathbf{R}}$ in the integrals represents the residual relative motion, and $\Delta\boldsymbol{\omega}$ is the angular velocity of F_{B_2} relative to F_{B_1}. The first term of (5.4,25*b*) can be transformed as

follows:

$$\mathbf{h}^e{}_{B_2} = \int \tilde{\mathbf{R}}_{B_2}\dot{\mathbf{R}}_{B_2}\,dm = \int (\mathbf{L}_{B_2B_1}\tilde{\mathbf{R}}_{B_1}\mathbf{L}_{B_1B_2})\{\mathbf{L}_{B_2B_1}(\dot{\mathbf{R}}_{B_1} + \Delta\tilde{\boldsymbol{\omega}}_{B_1}\mathbf{R}_{B_1})\}\,dm$$

$$= \mathbf{L}_{B_2B_1}\left\{\int \tilde{\mathbf{R}}_{B_1}\dot{\mathbf{R}}_{B_1}\,dm + \int \tilde{\mathbf{R}}_{B_1}\Delta\tilde{\boldsymbol{\omega}}_{B_1}\mathbf{R}_{B_1}\,dm\right\}$$

Applying (5.4,17) to the last term, we get

$$\mathbf{h}^e{}_{B_2} = \mathbf{L}_{B_2B_1}\left\{\int \tilde{\mathbf{R}}_{B_1}\dot{\mathbf{R}}_{B_1}\,dm + \mathscr{I}_{B_1}\Delta\boldsymbol{\omega}_{B_1}\right\} \tag{5.4,26}$$

It follows that the angular momentum $\mathbf{h}^e{}_{B_2}$ of the distortional relative motion vanishes in F_{B_2} if

$$\int \tilde{\mathbf{R}}_{B_1}\dot{\mathbf{R}}_{B_1}\,dm + \mathscr{I}_{B_1}\Delta\boldsymbol{\omega}_{B_1} = 0$$

or if

$$\Delta\boldsymbol{\omega}_{B_1} = -\mathscr{I}_{B_1}^{-1}\int \tilde{\mathbf{R}}_{B_1}\dot{\mathbf{R}}_{B_1}\,dm \tag{5.4,27}$$

Equation (5.4,27) provides the condition that the axis system F_{B_2} must satisfy if the angular momentum $\mathbf{h}_{B_2}$ referred to it is to have the form

$$\mathbf{h}_B = \mathscr{I}_B\boldsymbol{\omega}_B + \sum_i \mathbf{h}^{r_i}{}_B \tag{5.4,28}$$

This condition will be met when F_{B_2} has the orientation required by $\mathbf{L}_{B_1B_2}(t)$ that satisfies the differential equation [see (4.6,6)]

$$\dot{\mathbf{L}}_{B_1B_2} = \Delta\tilde{\boldsymbol{\omega}}_{B_1}\mathbf{L}_{B_1B_2} \tag{5.4,29}$$

It is not necessary actually to solve (5.4,27 and 29) for $\mathbf{L}_{B_1B_2}$ in order to make use of mean axes. Our concern here is simply to establish their existence. We note that when the body axes are mean axes, the following relations must hold for the distortional motion. Since the origin is the mass center,

$$\int \dot{x}'\,dm = \int \dot{y}'\,dm = \int \dot{z}'\,dm = 0 \qquad (a)$$

and from (5.4,23) (5.4,30)

$$\int (y\dot{z}' - \dot{y}'z)\,dm = \int (z\dot{x}' - \dot{z}'x)\,dm = \int (x\dot{y}' - \dot{x}'y)\,dm = 0 \qquad (b)$$

in which the prime denotes the distortional component of the velocity relative to F_B. The use of mean axes, and the consequent elimination of distortional contributions to $\mathbf{h}^*$ has the effect of eliminating the main inertial

coupling between the distortional degrees of freedom and those of the rigid body. Some coupling still remains through $\mathscr{J}$ however, see (5.6,7).

5.5 FORCE EQUATIONS IN WIND AXES

The force equation of motion is (5.4,9). In wind axes it becomes

$$\mathbf{f}_W = m\mathbf{a}_{C_W}$$

with $\mathbf{a}_{C_W}$ given by (5.3,11). For the particular case of a stationary atmosphere (5.3,15) gives the acceleration components, so that the scalar equations of motion are

$$\begin{aligned} f_{x_W} &= m\dot{V} \\ f_{y_W} &= mV(r^E{}_W + r_W) \\ f_{z_W} &= -mV(q^E{}_W + q_W) \end{aligned} \tag{5.5,1}$$

Although all the terms of (5.5,1) may be needed for applications to hypervelocity flight, there are numerous exceptions in which the Earth rotation can be neglected. The result is then much simpler, viz.

$$\begin{aligned} f_{x_W} &= m\dot{V} \\ f_{y_W} &= mVr_W \\ f_{z_W} &= -mVq_W \end{aligned} \tag{5.5,2}$$

Not only is (5.5,2) simpler in form than (5.5,1), but the angular velocities r_W and q_W that appear in it are those of F_W relative to Earth and not to inertial space, and are themselves correspondingly simpler.

THE FORCE VECTOR

The force vector for atmospheric flight consists of two parts, the aerodynamic reaction (including propulsive force) $\mathbf{A}$, and the weight $m\mathbf{g}$, i.e.

$$\mathbf{f} = \mathbf{A} + m\mathbf{g} \tag{5.5,3}$$

In the wind-axis system F_W, the components of $\mathbf{A}$ are given by

$$\mathbf{A}_W = \begin{bmatrix} X_W \\ Y_W \\ Z_W \end{bmatrix} \tag{5.5,4}$$

It is convenient further to subdivide **A** into the "configuration aerodynamics" and the propulsive force thus

$$\mathbf{A}_W = -\begin{bmatrix} D \\ C \\ L \end{bmatrix} + \begin{bmatrix} T_{x_W} \\ T_{y_W} \\ T_{z_W} \end{bmatrix} \tag{5.5,5}$$

Where D is drag, C is side force, and L is lift. The directions of D, C, L relative to the vehicle are illustrated in Figs. 4.4 to 4.6. The separation of the thrust from the other forces is to some extent always arbitrary, but is nevertheless useful. Any of the components of **T** may be large when we consider the flight of rockets or of V/STOL aircraft, although in the cruising flight of airplanes only T_{x_W} is usually significant. Finally the gravity force is given by

$$\mathbf{g}_V = \begin{bmatrix} 0 \\ 0 \\ g \end{bmatrix}$$

and

$$m\mathbf{g}_W = m\mathbf{L}_{WV}\mathbf{g}_V \tag{5.5,6}$$

In terms of the wind-axes Euler angles† this becomes, from (4.5,4)

$$m\mathbf{g}_W = mg\begin{bmatrix} -\sin\theta_W \\ \cos\theta_W \sin\phi_W \\ \cos\theta_W \cos\phi_W \end{bmatrix} \tag{5.5,7}$$

so that the expanded set of scalar equations is

$$\begin{aligned} T_{x_W} - D - mg\sin\theta_W &= m\dot{V} && (a) \\ T_{y_W} - C + mg\cos\theta_W \sin\phi_W &= mV({r^E}_W + r_W) && (b) \\ T_{z_W} - L + mg\cos\theta_W \cos\phi_W &= -mV({q^E}_W + q_W) && (c) \end{aligned} \tag{5.5,8}$$

The terms ${r^E}_W$ and ${q^E}_W$ will vanish when Earth rotation is negligible.

The above equations are most conveniently regarded as having the primary dependent variables V, r_W, q_W. However they are not complete in the sense that the aerodynamic and thrust forces contained in them are functions not only of the above three variables, but also of p_W, and of the aerodynamic angles α and β (see Sec. 4.3). The moment equations and some additional kinematic relations must be used to complete the mathematical system; these are presented in the following sections. Little use has been found for

† The elements of $\mathbf{L}_{WV}$, i.e. the direction cosines of F_W, can be used as the orientation unknowns instead of the Euler angles, see Sec. 5.2.

the moment equations in the F_W frame, and these are given below only for F_B.

5.6 FORCE AND MOMENT EQUATIONS IN BODY AXES (EULER'S EQUATIONS)

The force equation of motion in F_B is [see (5.4,9)]

$$\mathbf{f}_B = m\mathbf{a}_{C_B}$$

with $\mathbf{a}_{C_B}$ given by (5.3,16). Again particularizing, as in Sec. 5.5, to the case of a stationary atmosphere, (5.3,18) give the required components of acceleration. With the aerodynamic force in body axes denoted by

$$\mathbf{A}_B = \begin{bmatrix} X \\ Y \\ Z \end{bmatrix} \tag{5.6,1}$$

in accordance with traditional usage, and treating gravity as in Sec. 5.5, the scalar equations become

$$\begin{aligned} X - mg\sin\theta &= m[\dot{u} + (q^E{}_B + q)w - (r^E{}_B + r)v] \\ Y + mg\cos\theta\sin\phi &= m[\dot{v} + (r^E{}_B + r)u - (p^E{}_B + p)w] \\ Z + mg\cos\theta\cos\phi &= m[\dot{w} + (p^E{}_B + p)v - (q^E{}_B + q)u] \end{aligned} \tag{5.6,2}$$

Again, when the Earth rotation can be neglected entirely, $(p^E{}_B, q^E{}_B, r^E{}_B)$ vanish.

The moment equation in frame F_I is (5.4,12), i.e.

$$\mathbf{G}_I = \dot{\mathbf{h}}_I \tag{5.6,3}$$

or in body axes,

$$\mathbf{G}_B = \mathbf{L}_{BI}\mathbf{G}_I = \dot{\mathbf{h}}_B + \tilde{\boldsymbol{\omega}}_B\mathbf{h}_B \tag{5.6,4}$$

The conventional notation for $\mathbf{G}_B$ and $\mathbf{h}_B$ is

$$\mathbf{G}_B = \begin{bmatrix} L \\ M \\ N \end{bmatrix}, \qquad \mathbf{h}_B = \begin{bmatrix} h_x \\ h_y \\ h_z \end{bmatrix} \tag{5.6,5}$$

[despite the fact that L is also used for lift (5.5,5)]. In atmospheric flight $\mathbf{G}$ normally comes from aerodynamic, propulsive, and control forces; in space flight however, magnetic forces, solar radiation pressure, and gravitational

torques may all contribute importantly to it. The scalar expansion of (5.6,4) is

$$\begin{aligned} L &= \dot{h}_x + qh_z - rh_y \\ M &= \dot{h}_y + rh_x - ph_z \\ N &= \dot{h}_z + ph_y - qh_x \end{aligned} \tag{5.6,6}$$

When mean axes are used, (5.4,28) gives $\mathbf{h}_B$, and in that case (5.6,4) can be expressed as

$$\mathbb{G}_B = \dot{\mathscr{I}}_B\boldsymbol{\omega}_B + \mathscr{I}_B\dot{\boldsymbol{\omega}}_B + \tilde{\boldsymbol{\omega}}_B\mathscr{I}_B\boldsymbol{\omega}_B + \sum_i \dot{\mathbf{h}}^{r_i}{}_B + \sum_i \tilde{\boldsymbol{\omega}}_B\mathbf{h}^{r_i}{}_B \tag{5.6,7}$$

Note that in (5.6,7) the rotation of the Earth does not appear explicitly, even though no assumption has been made concerning it. It does however occur implicitly in $\boldsymbol{\omega}$, which is the angular velocity of F_B relative to inertial space. The matrix expansion of (5.6,7) is

$$\begin{aligned} \begin{bmatrix} L \\ M \\ N \end{bmatrix} &= \begin{bmatrix} \dot{I}_x & -\dot{I}_{xy} & -\dot{I}_{zx} \\ -\dot{I}_{xy} & \dot{I}_y & -\dot{I}_{yz} \\ -\dot{I}_{zx} & -\dot{I}_{yz} & \dot{I}_z \end{bmatrix} \begin{bmatrix} p \\ q \\ r \end{bmatrix} + \begin{bmatrix} I_x & -I_{xy} & -I_{zx} \\ -I_{xy} & I_y & -I_{yz} \\ -I_{zx} & -I_{yz} & I_z \end{bmatrix} \begin{bmatrix} \dot{p} \\ \dot{q} \\ \dot{r} \end{bmatrix} \\ &+ \begin{bmatrix} 0 & -r & q \\ r & 0 & -p \\ -q & p & 0 \end{bmatrix} \begin{bmatrix} I_x & -I_{xy} & -I_{zx} \\ -I_{xy} & I_y & -I_{yz} \\ -I_{zx} & -I_{yz} & I_z \end{bmatrix} \begin{bmatrix} p \\ q \\ r \end{bmatrix} + \begin{bmatrix} \sum_i \dot{h}_x{}^{r_i} \\ \sum_i \dot{h}_y{}^{r_i} \\ \sum_i \dot{h}_z{}^{r_i} \end{bmatrix} \\ &+ \begin{bmatrix} 0 & -r & q \\ r & 0 & -p \\ -q & p & 0 \end{bmatrix} \begin{bmatrix} \sum_i h_x{}^{r_i} \\ \sum_i h_y{}^{r_i} \\ \sum_i h_z{}^{r_i} \end{bmatrix} \end{aligned} \tag{5.6,8}$$

Owing to its length, there is little advantage in presenting the full scalar expansion of the complete equation (5.6,8). For the restricted case in which $\dot{\mathscr{I}}$ is negligible, and there are no rotor terms, that is, for a rigid body, it is

$$\begin{aligned} L &= I_x\dot{p} - I_{yz}(q^2 - r^2) - I_{zx}(\dot{r} + pq) - I_{xy}(\dot{q} - rp) - (I_y - I_z)qr \\ M &= I_y\dot{q} - I_{zx}(r^2 - p^2) - I_{xy}(\dot{p} + qr) - I_{yz}(\dot{r} - pq) - (I_z - I_x)rp \\ N &= I_z\dot{r} - I_{xy}(p^2 - q^2) - I_{yz}(\dot{q} + rp) - I_{zx}(\dot{p} - qr) - (I_x - I_y)pq \end{aligned} \tag{5.6,9}$$

It is usually the case for flight vehicles that Cxz is a plane of symmetry.

In that case $I_{xy} = I_{yz} = 0$, and (5.6,9) simplify to

$$\begin{aligned} L &= I_x\dot{p} - I_{zx}(\dot{r} + pq) - (I_y - I_z)qr \\ M &= I_y\dot{q} - I_{zx}(r^2 - p^2) - (I_z - I_x)rp \\ N &= I_z\dot{r} - I_{zx}(\dot{p} - qr) - (I_x - I_y)pq \end{aligned} \tag{5.6,10}$$

Finally, when the axes are principal, I_{zx} as well vanishes, and we obtain the simplest form of the moment equations

$$\begin{aligned} L &= I_x\dot{p} - (I_y - I_z)qr \\ M &= I_y\dot{q} - (I_z - I_x)rp \\ N &= I_z\dot{r} - (I_x - I_y)pq \end{aligned} \tag{5.6,11}$$

5.7 DISCUSSION OF THE SYSTEM OF EQUATIONS

We have presented in the preceding sections a large number of complicated coupled equations that describe the kinematics and dynamics of a vehicle in flight over a spherical rotating Earth. (The student may be forgiven if he is slightly bewildered by them at this point!) Our purpose here is to evaluate these equations, show the relationships between them, and present the essential structure of the system.

Much of the complexity has resulted from the inclusion of the rotation of the earth (the $\boldsymbol{\omega}^E$ terms) and its curvature (the $\boldsymbol{\omega}^V$ terms) in the mathematical model. We have already shown (Sec. 5.3) that the centripetal acceleration associated with $\boldsymbol{\omega}^E$ is usually negligible, and that the Coriolis acceleration is small but not quite negligible. To gain further insight into the $\boldsymbol{\omega}^E$ and $\boldsymbol{\omega}^V$ terms we look at the z component of the force equation for horizontal flight on the equator. Thus with $\theta_W = \phi_W = 0$, (5.5,8c) gives

$$-L + T_{z_W} + mg = -mV(q^E{}_W + q_W) \tag{5.7,1}$$

With $\psi_W = 90°$ for eastward flight and $\lambda = 0$, (5.3,14) and (4.5,4) yield

$$q^E{}_W = -\omega^E \tag{5.7,2}$$

Since the Euler angles are constants, then from (5.2,8) $P_W = Q_W = R_W = 0$, and from (5.2,10)

$$q_W = -(\omega^E + \dot{\mu}) \tag{5.7,3}$$

From (5.3,5), $\dot{\mu} = V/\mathscr{R}$, so that finally (5.7,1) becomes

$$\begin{aligned} -L + T_{z_W} + mg &= mV\left(2\omega^E + \frac{V}{\mathscr{R}}\right) \\ &= 2mV\omega^E + \frac{mV^2}{\mathscr{R}} \end{aligned} \tag{5.7,4}$$

The first term on the r.h.s. is the Coriolis force due to Earth rotation, and when V equals orbital speed (about 26,000 fps) amounts to about $\frac{1}{10}$ mg. The second term is due to Earth curvature (in the "flat" Earth approximation $\mathscr{R} = \infty$ and this term vanishes), and at orbital speed makes up the balance, about 90%, of mg. [Note that V is speed relative to F_E, not relative to F_I, and that the exact form of (5.7,4) would have the additional small term $+m\mathscr{R}\omega^{E^2}$ on the r.h.s.] Both terms on the r.h.s. of (5.7,4) increase with speed, the first linearly, the second quadratically, and each amounts to 1% of the weight when the speed is about $\frac{1}{10}$ of orbital speed, i.e. about 2600 fps for atmospheric flight. This speed therefore seems a useful boundary below which both $\boldsymbol{\omega}^E$ and $\boldsymbol{\omega}^V$ can be neglected, and above which they should be included for accurate results. It corresponds to a Mach number of about $2\frac{1}{2}$ to 3, depending on altitude, so that at low supersonic speeds, as for first generation supersonic transports, these terms are just marginally small—perhaps not quite negligible for range calculations. For all high supersonic speeds and hypersonic speeds they would be of increasing importance.

The preceding argument, being based on the force equation of motion, has validity only for trajectory calculations, i.e. for calculations of the flight path. When the problem of interest concerns attitude dynamics, i.e. the relatively rapid rotational motions of the vehicle relative to F_V, the situation is quite different. For then $\boldsymbol{\omega}^E$ and $\boldsymbol{\omega}^V$ can be important only if they are appreciable compared to $\boldsymbol{\omega}$ (greater than 1% say). Now $\omega^E \approx 7 \times 10^{-5}$ rad/sec is extremely small compared to most technically important vehicle rotations, and ω^V has a maximum value at orbital speed of about 10^{-3} rad/sec which is also negligible in this context. Hence both $\boldsymbol{\omega}^E$ and $\boldsymbol{\omega}^V$ terms are normally negligible insofar as the moment equations are concerned.

Two alternatives have been presented for the dynamical force equations: in wind axes and body axes. Both are used in current practice, and there are no overriding advantages for either system. The wind-axes form is generally more convenient for trajectory analysis, in which the attitude of the vehicle is prescribed a priori, and the moment equations are not used at all. For combined trajectory and attitude motions, either a "mixed" form of the equations, or the body-axes form, is normally employed. In hovering flight, when $V = 0$, and the angles α and β are not defined, the body-axes form is virtually mandatory. It is convenient to use a particular mixed form of the force equations for the analysis of small perturbations from a steady reference state (see Sec. 5.10).

On the other hand, there is only one reasonable choice for the moment equations. Only in F_B is $\mathscr{I}$ constant for a rigid body. To use any other reference frame adds unnecessary complication.

Little has been said in the foregoing sections about the aerodynamic forces and moments that appear in the equations: (D, C, L, and T) in (5.5,8), (X, Y, Z) in (5.6,2), and (L, M, N) in (5.6,8). These depend on the local ambient density, the motion of the vehicle relative to the atmosphere, and on nonautonomous control inputs. Thus for a rigid vehicle, they are functions (more exactly, functionals, see Sec. 5.10) of $\rho(\mathscr{R})$ the density, of (V, α_x, β), or (u, v, w), of (p, q, r),† and of a set of control variables. There are other ways, besides its appearance in ρ, in which the altitude (i.e. $\mathscr{R}$), can occur as a nontrivial independent variable in the equations. One is when there is a wind gradient with height, e.g. $W_x(\mathscr{R})$, and another is when the vehicle flies close to the ground, so that there is a "ground effect" on the aerodynamic field of the vehicle. In the latter case the aerodynamic forces can be very strong functions of height. A third case is when the gravitational inverse square law is included, i.e. $g = g(\mathscr{R})$. For near-orbital velocities at very high altitudes, it has been shown (ref. 5.4) that this refinement is necessary.

The structure of the mathematical system for a rigid vehicle ($\dot{\mathscr{I}} = 0$) in the more general high-speed case, and the interrelations among the variables, is displayed in Figs. 5.4 and 5.5. Each set of scalar equations is regarded as a subsystem that produces three dependent variables as outputs. The inputs are the quantities needed to calculate the outputs from the given equations. All the quantities shown immediately to the right of the square blocks can be found by algebraic solution of the equations. The aerodynamic terms in the force and moment equations have all been replaced by the state variables of which they are functions, and control forces and moments. On checking, the reader will find that all the autonomous variables needed as inputs on the left-hand side are available as outputs on the right-hand side.

To recapitulate, the mathematical models described by Figs. 5.4 and 5.5 are subject only to the following assumptions

(i) The Earth is a sphere rotating on an axis fixed in inertial space, and $\mathbf{g}$ is a radial vector.
(ii) The centripetal acceleration associated with Earth rotation is neglected.
(iii) The atmosphere is at rest relative to the Earth.
(iv) The vehicle is a rigid body.

None of these restrictions is made from any fundamental necessity, and any of them may be removed when the application requires it, at the cost of additional complexity.

† Actually the angular velocity of the vehicle relative to the atmosphere is $\boldsymbol{\omega} - \boldsymbol{\omega}^E$, and it is the components of this vector, not (p, q, r), that strictly speaking should be used in the calculation of aerodynamic forces and moments. However $\boldsymbol{\omega}^E$ is so small that in the majority of applications no significant error is incurred by neglecting it.

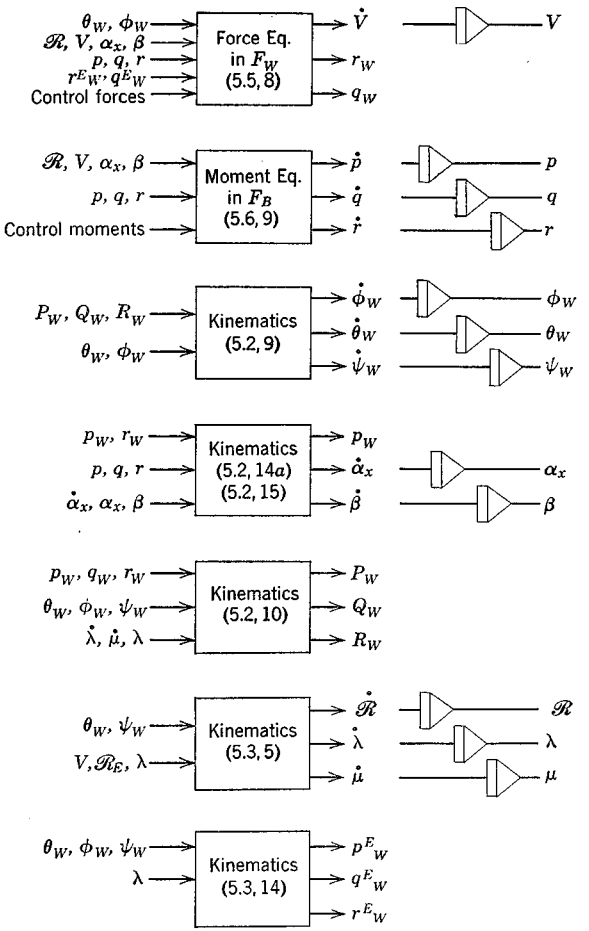

FIG. 5.4 Block diagram of equations for rigid vehicle. Spherical rotating earth. Combined wind and body axes.

5.8 THE FLAT-EARTH APPROXIMATION

We have shown above that a wide and important range of flight dynamics problems, corresponding roughly to $M < 3$, can be treated adequately with a significantly simpler mathematical model than that given in Figs. 5.4 and 5.5—that is, by neglecting $\boldsymbol{\omega}^E$ and $\boldsymbol{\omega}^V$ or alternatively by treating the Earth as a stationary plane in inertial space. The reduced equations obtained by

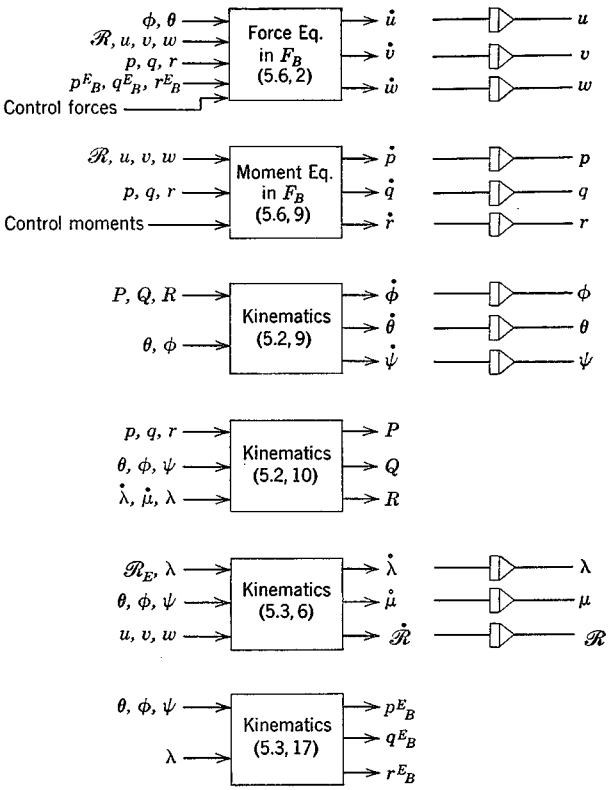

FIG. 5.5 Block diagram of equations for rigid vehicle. Spherical rotating earth. Body axis system.

neglecting all $\boldsymbol{\omega}^E$ and $\boldsymbol{\omega}^V$ terms in the more general ones are collected below for a rigid vehicle having a plane of symmetry.

$$
\begin{aligned}
T_{x_W} - D - mg\sin\theta_W &= m\dot{V} && (a)\\
T_{y_W} - C + mg\cos\theta_W\sin\phi_W &= mVr_W && (b)\\
T_{z_W} - L + mg\cos\theta_W\cos\phi_W &= -mVq_W && (c)
\end{aligned}
\qquad (5.8,1)
$$

$$
\begin{aligned}
X - mg\sin\theta &= m(\dot{u} + qw - rv) && (a)\\
Y + mg\cos\theta\sin\phi &= m(\dot{v} + ru - pw) && (b)\\
Z + mg\cos\theta\cos\phi &= m(\dot{w} + pv - qu) && (c)
\end{aligned}
\qquad (5.8,2)
$$

$$
\begin{aligned}
L &= I_x\dot{p} - I_{zx}(\dot{r} + pq) - (I_y - I_z)qr && (a)\\
M &= I_y\dot{q} - I_{zx}(r^2 - p^2) - (I_z - I_x)rp && (b)\\
N &= I_z\dot{r} - I_{zx}(\dot{p} - qr) - (I_x - I_y)pq && (c)
\end{aligned}
\qquad (5.8,3)
$$

$$\dot{\phi}_W = p_W + q_W \sin\phi_W \tan\theta_W + r_W \cos\phi_W \tan\theta_W \qquad (a)$$
$$\dot{\theta}_W = q_W \cos\phi_W - r_W \sin\phi_W \qquad (b) \qquad (5.8,4)$$
$$\dot{\psi}_W = (q_W \sin\phi_W + r_W \cos\phi_W) \sec\theta_W \qquad (c)$$

(Without subscript W, (5.8,4) apply to body axes.)

$$\dot{\alpha}_x = q - q_W \sec\beta - p\cos\alpha_x \tan\beta - r\sin\alpha_x \tan\beta \qquad (a)$$
$$\dot{\beta} = r_W + p\sin\alpha_x - r\cos\alpha_x \qquad (b) \qquad (5.8,5)$$
$$p_W = p\cos\alpha_x\cos\beta + (q - \dot{\alpha}_x)\sin\beta + r\sin\alpha_x\cos\beta \qquad (c)$$

$$\dot{x}_E = V\cos\theta_W\cos\psi_W \qquad (a)$$
$$\dot{y}_E = V\cos\theta_W\sin\psi_W \qquad (b) \qquad (5.8,6)$$
$$\dot{z}_E = -V\sin\theta_W \qquad (c)$$

$$\begin{bmatrix}\dot{x}_E\\ \dot{y}_E\\ \dot{z}_E\end{bmatrix} = \mathbf{L}_{VB}\begin{bmatrix}u\\ v\\ w\end{bmatrix} \qquad (5.8,7)$$

Following traditional usage, L is used above as a symbol for both lift force and rolling moment. The context usually makes it quite clear which

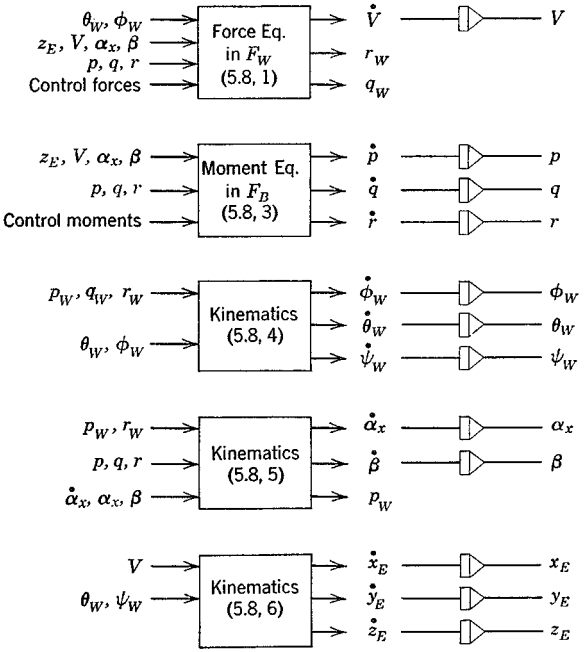

FIG. 5.6 Block diagram of equations for rigid vehicle with plane of symmetry. Combined wind and body axes. Flat-Earth approximation.

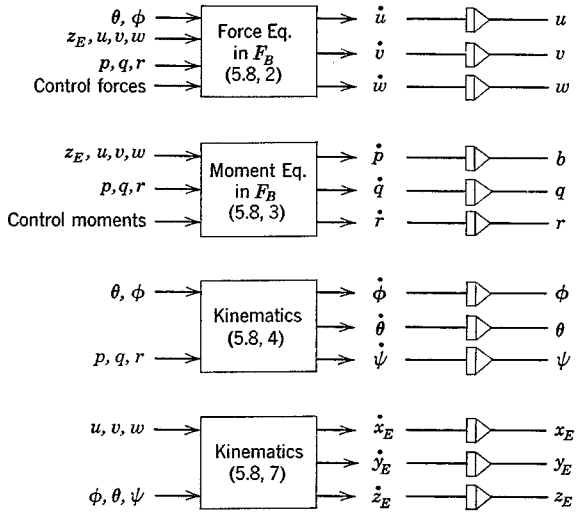

FIG. 5.7 Block diagram of equations for vehicle with plane of symmetry. Body axes. Flat-Earth approximation.

is meant, and even the novice seldom has difficulty with this ambiguity. In the nondimensional form of the equations, the ambiguity disappears, different symbols being used for the two quantities.

The block diagrams for the above equations are given in Figs. 5.6 and 5.7 for the combined and body-axes systems, respectively. Since in the case of body axes there are no kinematical relations needed to connect the two axis systems, the number of equations is twelve instead of 15. However the force equations (5.8,2) and the position equations (5.8,7) are then more complex than (5.8,1) and (5.8,6) which they replace, so the advantage resulting from the reduction of size is offset by greater complexity in the remaining members. The state variables of Figs. 5.6 and 5.7 are conveniently grouped for identification as follows:

(u, v, w) or (V, α_x, β)	give translation of vehicle relative to Earth.
(p, q, r)	give rotation of vehicle relative to Earth.
(x_E, y_E, z_E)	give position of vehicle relative to Earth axes.
(ϕ, θ, ψ)	give angular orientation of vehicle relative to F_V.
$(\phi_W, \theta_W, \psi_W)$	give orientation of wind axes. $\theta_W = \gamma$ is the angle of climb, and ψ_W is the heading of flight path.
(p_W, q_W, r_W)	give angular velocity of the wind axes.

5.9 STEADY STATES

It is of interest to deduce from the preceding general equations what "equilibrium points" exist for a flight vehicle. Neglecting motion of the Earth center, a true state of rest in inertial space occurs only when the vehicle travels due west at a rate exactly equal to that of the local eastward motion of the Earth. This is too restricted a case to be useful. Equilibrium in a more general dynamical sense corresponds to equilibrium of all the external forces, i.e. a state of zero acceleration, or rectilinear motion. On a round Earth, this kind of equilibrium is also not useful, since the flight path would then either intersect the Earth, or go off into space. The useful definition is that of an "aerodynamic steady state," in which the motion, the aerodynamic field, and gravity are all constant in the frame F_B. Thus the aerodynamic pressure distribution and the gravity components are constant with time. Such a state requires, first, that (u, v, w) or (V, α_x, β) and the rates of rotation $(\omega - \omega^E)_B$ of F_B relative to the atmosphere or to F_E be constants. Second, the Euler angles θ, ϕ that affect the gravity components must be constant. Constancy of aerodynamic forces at constant (V, α_x, β) also requires constant air density, i.e. constant altitude flight. Thus $\theta_W = 0$. Now consider the force equation (5.6,2). By postulate, the derivative terms are zero, and the left-hand side is constant. It follows that these equations can be solved for the constant values of

$$(\boldsymbol{\omega}^E + \boldsymbol{\omega})_B = \begin{bmatrix} p^E{}_B + p \\ q^E{}_B + q \\ r^E{}_B + r \end{bmatrix}$$

Since the sum and difference (line 14 above) of $\boldsymbol{\omega}^E{}_B$ and $\boldsymbol{\omega}_B$ are constants, then they must be separately constant. Since (α, β) and (p, q, r) are constants, then from (5.2,13), (p_W, q_W, r_W) are also constant, and transforming the constant $\boldsymbol{\omega}^E{}_B$ into F_W leads to a constant $\boldsymbol{\omega}^E{}_W$. Now the components of $\boldsymbol{\omega}^E$ can be constant in F_W and/or F_B, with the constraint of constant altitude, only if the motion of the frame is a rigid-body rotation around the Earth's axis. *Thus the path of the vehicle mass center must be a circle around the axis, i.e. it must be a minor circle of the Earth, lying on a parallel of latitude.* Analytically this means that $\lambda = \text{const}$, and $\psi = \pm\pi/2$. The conditions for this most general steady state may then be summarized as follows, taking the

option $\psi_W = \pi/2$ (eastward flight):

$$\begin{aligned} \psi_W &= \pi/2 & \mathscr{R} &= \text{const} \\ \theta_W &= 0 & \lambda &= \text{const} \\ \phi_W &= \text{const} & \dot{\mu} &= V/\mathscr{R} \sec \lambda \end{aligned} \tag{5.9,1}$$

$$\begin{bmatrix} V \\ \alpha_x \\ \beta \end{bmatrix} = \text{const}, \qquad \begin{bmatrix} u \\ v \\ w \end{bmatrix} = \text{const}, \qquad \begin{bmatrix} p \\ q \\ r \end{bmatrix} = \text{const} \tag{5.9,2}$$

From (5.2,8)

$$\begin{bmatrix} P_W \\ Q_W \\ R_W \end{bmatrix} = 0 \tag{5.9,3}$$

From (5.2,10)

$$\begin{bmatrix} p_W \\ q_W \\ r_W \end{bmatrix} = -\begin{bmatrix} 0 \\ \cos(\lambda - \phi_W) \\ \sin(\lambda - \phi_W) \end{bmatrix} (\omega^E + \dot{\mu}) \tag{5.9,4}$$

From (5.3,14)

$$\begin{bmatrix} {p^E}_W \\ {q^E}_W \\ {r^E}_W \end{bmatrix} = -\begin{bmatrix} 0 \\ \cos(\lambda - \phi_W) \\ \sin(\lambda - \phi_W) \end{bmatrix} \omega^E \tag{5.9,5}$$

The wind-axis force equations (5.5,8) then reduce to

$$\begin{aligned} T_{x_W} - D &= 0 \\ T_{y_W} - C + mg \sin \phi_W &= -mV \sin(\lambda - \phi_W)(2\omega^E + \dot{\mu}) \\ T_{z_W} - L + mg \cos \phi_W &= mV \cos(\lambda - \phi_W)(2\omega^E + \dot{\mu}) \end{aligned} \tag{5.9,6}$$

The reduced moment equations for this case are of little interest, since they contain only second-degree terms in (p, q, r), and the latter are clearly of order $(\omega^E + \dot{\mu})$, which is at most about 10^{-3} rad/sec for suborbital flight. They therefore reduce to $L \doteq M \doteq N \doteq 0$.

To be exact, even this restricted steady state cannot exist, for the following reasons:

(i) All real vehicles in horizontal flight have propulsion systems that utilize fuel, so m is never strictly constant.

(ii) The Earth is not a perfect sphere, so that flight at constant altitude (i.e. air density) is not strictly flight on a circle.

(iii) The atmospheric density is never exactly constant and the wind never exactly zero at a given height.

These deviations from the idealized steady state are, of course, not important enough to invalidate its usefulness.

If the Earth rotation $\boldsymbol{\omega}^E$ can be neglected, then clearly no one minor circle is preferable to any other, and the steady state can be on any minor circle over the Earth. In the flat-Earth approximation, the minor circle becomes any circle parallel to the ground surface. If in addition the variation of ρ with height can be neglected, as for a shallow climb or glide, the most general steady state becomes a vertical helix, i.e. a climbing or gliding turn.

5.10 THE SMALL-DISTURBANCE THEORY

A particular form of the system equations that has been used with enormous success ever since the beginnings of this subject is the linearized model for small disturbances about a reference condition of steady rectilinear flight over a flat Earth. This theory yields much valuable information and many important insights with relatively little effort. It gives correct enough results for engineering purposes over a surprisingly wide range of applications, including stability and control response. There are, of course, limitations. It is not suitable for spinning, post-stall gyrations, nor any other application in which large variations occur in the state variables.

The reasons for the relative success of this approach are twofold: (i) in many cases the major aerodynamic effects are truly nearly linear functions of the state variables, and (ii) disturbed flight of considerable violence can correspond to relatively small values of the linear- and angular-velocity disturbances.

CHOICE OF AXES

A convenient choice for the axes in the small-disturbance model is to use wind axes for the lift-force and drag-force equations (5.8,1*a* and *c*), and body axes for the remaining force and moment equations (5.8,2*b* and 5.8,3). For vehicles having a plane of symmetry two sets of uncoupled equations are found, the *longitudinal* and the *lateral*. Since the pitching moment equation turns out to be the same in both axis systems, the longitudinal equations are then in wind axes, and the lateral in body axes.

NOTATION FOR SMALL DISTURBANCES

The reference steady state is taken to be symmetric rectilinear flight, although the more general case can readily be handled by the same approach

(ref. 5.3). The steady-state values are denoted by subscript e (for equilibrium) and changes from them by the prefix Δ. Thus for example

$$\begin{aligned} V &= V_e + \Delta V \\ \phi &= \phi_e + \Delta\phi \\ p &= p_e + \Delta p \\ L &= L_e + \Delta L \\ &\text{etc.} \end{aligned} \tag{5.10,1}$$

Since the steady state selected is wings-level translation, we can have at most the following nonzero reference values of the state variables:

$$V_e,\ \alpha_{x_e},\ \theta_{W_e},\ \psi_{W_e} \tag{5.10,2}$$

All other motion and angle variables are zero in the reference state and for these the prefix Δ is not needed. θ_{W_e} as well will be zero if the reference state is horizontal flight, as it must be when we include the variation of air density with height. However, we keep θ_{W_e} as nonzero in order to include the case of constant density within the analysis. θ_W, the angle of climb, is replaced with the more common symbol γ.

FURTHER ASSUMPTIONS

In the classical linear equations, m and g are constants, the vehicle is assumed to have a plane of symmetry, and the momenta of spinning rotors is excluded. The latter assumption is easily relaxed when rotor terms are important. As a particular choice for body axes we select F_S, *the stability axes*, for which $\alpha_{x_e} = w_e = 0$ (see Sec. 4.2.7). Since the initial heading has no special significance in the flat-Earth approximation, we also set $\psi_{W_e} = 0$.

Instead of α_x, the angle of attack of the x_S axis, we choose for the angle of attack variable that of the *zero lift line* (see Sec. 6.1). It is denoted simply α, and of course is not zero in the reference state. α and α_x differ only by a constant in any particular case.

In treating the thrust terms of (5.8,1) we wish to make allowance for rather general conditions, such as can occur in VTOL and STOL flight, when the thrust vector may be at large angles to the direction of motion. We therefore assume conditions as illustrated in Fig. 5.8. We further assume that the thrust vector rotates rigidly with the vehicle when it is perturbed. This implies that any rotation of the thrust relative to the vehicle is to be accounted for by adding suitable increments to L, D, and Y.

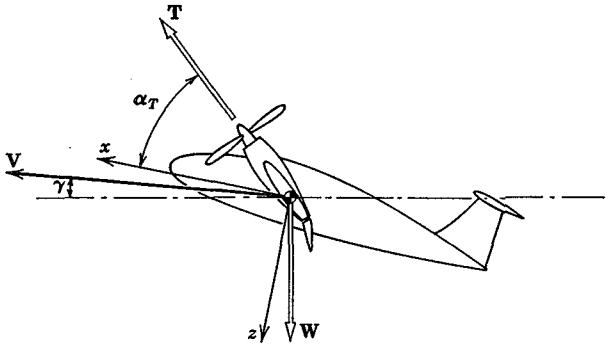

FIG. 5.8 Thrust vector at large angle to **V**.

In the perturbed state, the thrust vector in body axes is

$$\mathbf{T}_B = (T_e + \Delta T)\begin{bmatrix} \cos \alpha_T \\ 0 \\ -\sin \alpha_T \end{bmatrix}$$

and in the wind axes is

$$\mathbf{T}_W = \mathbf{L}_{WB}\mathbf{T}_B$$

On making use of (4.5,5) (with $\alpha_x = \Delta\alpha$ therein) and linearizing, the result is

$$T_{x_W} = (T_e + \Delta T)\cos \alpha_T - \Delta\alpha T_e \sin \alpha_T \qquad (a)$$

$$T_{y_W} = -\beta T_e \cos \alpha_T \qquad (b) \qquad (5.10,3)$$

$$T_{z_W} = -(T_e + \Delta T)\sin \alpha_T - \Delta\alpha T_e \cos \alpha_T \qquad (c)$$

THE LINEAR EQUATIONS

In linearizing the appropriate members of (5.8,1) to (5.8,7), we assume that all the perturbation quantities ΔV, $\Delta\alpha$, p, etc., are small, and that squares and products of them may be neglected. It follows that $\cos \Delta\gamma \doteq 1$, and $\sin \Delta\gamma \doteq \Delta\gamma$. Thus (5.8,1$a$) for example becomes

$$(T_e + \Delta T)\cos \alpha_T - \Delta\alpha T_e \sin \alpha_T - (D_e + \Delta D) - mg \sin (\gamma_e + \Delta\gamma) = m\dot{V}$$

or, on expanding the trigonometric term,

$$(T_e \cos \alpha_T - D_e - mg \sin \gamma_e) + \Delta T \cos \alpha_T - \Delta\alpha T_e \sin \alpha_T - \Delta D - mg \cos \gamma_e \Delta\gamma = m\dot{V}$$

The part in brackets vanishes, since the reference state must satisfy the equations, and hence the final perturbation equation is

$$\Delta T \cos \alpha_T - \Delta\alpha T_e \sin \alpha_T - \Delta D - mg \cos \gamma_e \Delta\gamma = m\dot{V} \quad (5.10,4)$$

Note that no approximation has been made here concerning γ_e. The equation applies to flight at any angle of climb or descent up to vertical flight. Proceeding in a similar manner for all the other equations, the result is

$$\begin{aligned} \Delta T \cos \alpha_T - \Delta\alpha T_e \sin \alpha_T - \Delta D - mg \cos \gamma_e \Delta\gamma &= m\dot{V} && (a) \\ \Delta Y + mg \cos \gamma_e \phi &= m(\dot{v} + V_e r) && (b) \end{aligned} \quad (5.10,5)$$

$$\Delta T \sin \alpha_T + \Delta\alpha T_e \cos \alpha_T + \Delta L + mg \sin \gamma_e \Delta\gamma = mV_e q_W \quad (c)$$

$$\begin{aligned} \Delta L &= I_x \dot{p} - I_{zx} \dot{r} && (a) \\ \Delta M &= I_y \dot{q} && (b) \\ \Delta N &= I_z \dot{r} - I_{zx} \dot{p} && (c) \end{aligned} \quad (5.10,6)$$

$$\begin{aligned} \dot{\phi} &= p + r \tan \gamma_e && (a)\dagger \\ \dot{\gamma} &= q_W && (b) \\ \dot{\psi} &= r \sec \gamma_e && (c)\dagger \end{aligned} \quad (5.10,7)$$

$$q_W = q - \dot{\alpha} \quad (5.10,8)$$

$$\begin{aligned} \dot{x}_E &= V_e \cos \gamma_e + \cos \gamma_e \Delta V - V_e \sin \gamma_e \Delta\gamma && (a) \\ \dot{y}_E &= V_e \cos \gamma_e \cdot \psi + v && (b) \\ \dot{z}_E &= -V_e \sin \gamma_e - \sin \gamma_e \Delta V - V_e \cos \gamma_e \Delta\gamma && (c) \end{aligned} \quad (5.10,9)\ddagger$$

Note that the order of the terms in (5.10,8) has been rearranged slightly as compared with (5.8,5) and that two of the latter are not needed. Of (5.10,9) the first and third come from (5.8,6), and the second from (5.8,7).

Although the moment equations (5.10,6) were obtained by a linearization of (5.8,3), which are the equations for a rigid body, they are in fact valid for a deformable body. This is because the first term on the r.h.s. of (5.6,8) contains only the products of first-order rotations and rates of change of inertia coefficients. The latter are also first order in the linear model, and hence the distortional coupling terms are second order and negligible.

Because of the simplicity of the linear kinematical relations, it is convenient to eliminate q_W and to regroup the equations as follows.

† Equations (5.10,7*a* and *c*) cannot be regarded as a small-perturbation equation when $\gamma_e \to \pm 90°$ for then $\dot{\phi}$ and $\dot{\psi} \to \infty$ for any finite r.

‡ Equations (5.10,9) are not strictly *perturbation* equations, albeit linear, because of the presence of the constant terms $V_e \cos \gamma_e$ and $-V_e \sin \gamma_e$. The perturbations are strictly $(\dot{x}_E - V_e \cos \gamma_e)$, $\dot{y}_E$, and $(\dot{z}_E + V_e \sin \gamma_e)$.

Longitudinal aerodynamic characteristics—part 1

CHAPTER 6

In the preceding chapters we have presented the general analytical foundations for solving problems concerning the motion of flight vehicles in the atmosphere. As was emphasized, however, the details of the problems and the character of the results obtained are dominated by the aerodynamic characteristics of the vehicle. It is essential therefore to explore the aerodynamic aspect of the subject in some depth before proceeding to particular studies of vehicle dynamics. To this end, this and the following two chapters are devoted to a discussion of the main aerodynamic features of flight vehicles that are of concern for vehicle motion. Included is a body of material, traditionally referred to as "static stability and control" that relates to the control displacements and forces required to maintain steady rectilinear flight, or to maintain a steady "pull-up." These are important items, both in relation to handling qualities and to their use as stability criteria. Clearly the spectrum of vehicle types and operating conditions of interest is extremely broad—from air-cushion vehicles and helicopters on the one hand to hypersonic aircraft and entry vehicles on the other. It is obviously not practical to present a comprehensive coverage of the aerodynamics of all these types within the scope of this text. The items selected for treatment are those considered to be particularly instructive and of rather broad application. With this basis it is hoped that the reader should be able to extrapolate the methods and approaches presented to other situations with which he may be

concerned. One topic completely excluded, because it requires an extensive treatment to be meaningful at all, is the aerodynamic characteristics of rotorcraft. References 6.1 to 6.4 give considerable information on this and other relevant topics in aerodynamics.

6.1 THE BASIC LONGITUDINAL FORCES

The basic flight condition for most vehicles is symmetric steady flight. In this condition the velocity and force vectors are as illustrated in Fig. 6.1.

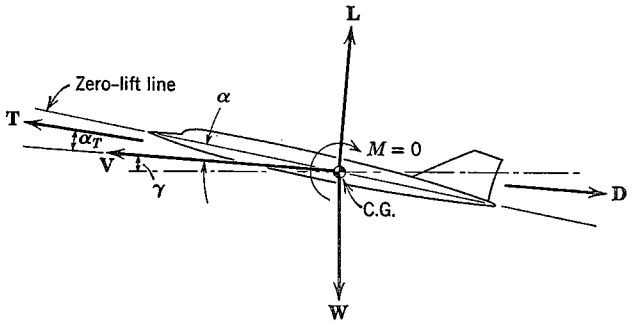

FIG. 6.1 Steady symmetric flight.

The steady-state condition was fully described in Sec. 5.9. All the nonzero forces and motion variables are members of the set defined as "longitudinal" in Chapter 5, and hence we see the central importance of longitudinal aerodynamics. The two main aerodynamic parameters of this condition are V and α.

Nothing can be said in general about the way the thrust vector varies with V and α, since it is so dependent on the type of propulsion unit—rockets, jet, propeller, or prop-jet. Two particular idealizations are of interest, however,

(i) T independent of V, i.e. constant thrust; an approximation for rockets and pure jets.
(ii) TV independent of V, i.e. constant power; an approximation for reciprocating engines with constant-speed propellers.

The variation of steady-state lift and drag with α for subsonic and supersonic Mach numbers ($\mathbf{M} <$ about 5) are characteristically as shown in Fig. 6.2 for the range of attached flow over the surfaces of the vehicle (refs. 6.5, 6.6). Over a useful range of α (below the stall) the coefficients are given accurately

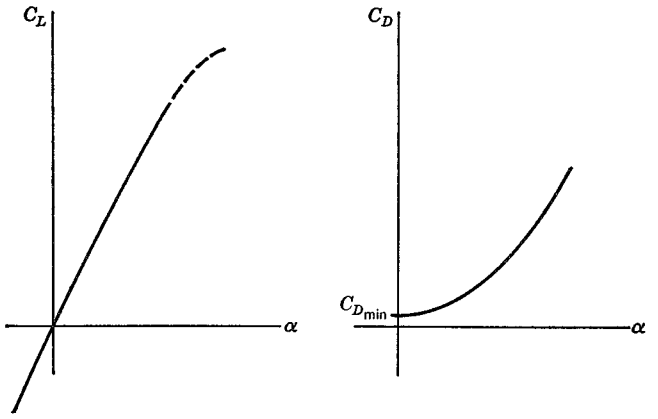

FIG. 6.2 Lift and drag for subsonic and supersonic speeds.

enough by

$$C_L = C_{L_\alpha}\alpha \tag{6.1,1}$$

$$C_D = C_{D_{min}} + KC_L^2 \tag{6.1,2}$$

The three constants C_{L_α}, $C_{D_{min}}$, K are principally functions of the configuration shape, thrust coefficient, and Mach number.

Significant departure from the above idealizations may, of course, be anticipated in some cases. The minimum of C_D may occur at a value of $\alpha > 0$, and the curvature of the C_L vs. α relation may be an important consideration for flight at high C_L. When the vehicle is a "slender body," e.g. a slender delta, or a slim wingless body, the C_L curve may have a characteristic upward curvature even at small α (ref. 6.7). The upward curvature of C_L at small α is inherently present at hypersonic Mach numbers (ref. 6.8). For the nonlinear cases, a suitable formulation for C_L is (ref. 6.9)

$$C_L = (\tfrac{1}{2}C_{N_\alpha} \sin 2\alpha + C_{N_{\alpha\alpha}} \sin \alpha \,|\sin \alpha|) \cos \alpha \tag{6.1,3}$$

where C_{N_α} and $C_{N_{\alpha\alpha}}$ are coefficients (independent of α) that depend on the Mach number and configuration. [Actually C_N here is the coefficient of the aerodynamic force component normal to the wing chord, and C_{N_α} is the value of C_{L_α} at $\alpha = 0$, as can easily be seen by linearizing (6.1,3) with respect to α.] Equation (6.1,2) for the drag coefficient can serve quite well for flight dynamics applications up to hypersonic speeds ($\mathbf{M} > 5$) at which theory indicates that the exponent of C_L decreases from 2 to $\frac{3}{2}$. Miele (ref. 6.10) presents in Chapter 6 a very useful and instructive set of typical lift and drag data for a wide range of vehicle types, from subsonic to hypersonic.

6.2 PITCH STIFFNESS AND POSSIBLE CONFIGURATIONS FOR FLIGHT

In Fig. 6.1 we have shown that the pitching moment M is zero, which is, of course, one of the conditions for equilibrium. It is intuitively evident, without recourse to any formal stability theory, that there might be something wrong with a flight vehicle that at constant speed and with fixed controls, experienced a positive (nose-up) pitching moment ΔC_m following an increase $\Delta\alpha$ in the angle of attack from its equilibrium value. This is illustrated in curve a of Fig. 6.3 (i.e. $C_{m_\alpha} > 0$). For then the moment ΔC_m

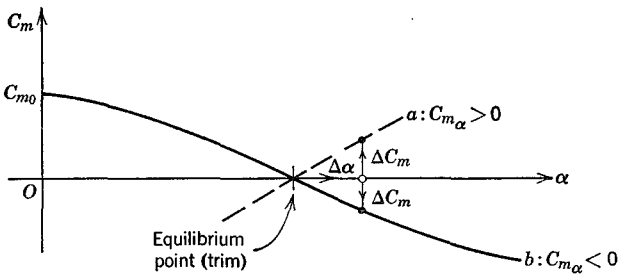

FIG. 6.3 Pitch stiffness.

would be such as to increase further the perturbation in α. On the other hand, if the C_m vs α relation is as in curve b, ($C_{m_\alpha} < 0$) the moment following the disturbance is negative, and tends to restore α to its equilibrium value. The latter case is exactly parallel to that of a mass on a spring, which when disturbed from equilibrium, experiences a restoring force. The vehicle possesses as it were an "aerodynamic torsion spring" that tries to hold α constant at its equilibrium value. This property has traditionally been called "*static stability*" in pitch. In view of the more formal, more precise meaning now usually attached to the word *stability* (see Chapter 3), a more appropriate designation is *positive pitch stiffness*. The complete stability theory of the longitudinal motion (see Chapter 9) shows that positive pitch stiffness ($C_{m_\alpha} < 0$) is in general neither necessary nor sufficient for stability. However, it is nevertheless a very important practical design criterion, the violation of which leads to consequences that can rarely be tolerated. The great importance of pitch stiffness makes calculation or measurement of $C_m(\alpha)$ one of the central features of the aerodynamic design of all flight vehicles. This curve is typically monotonic in α over the usable flight range, as in Fig. 6.3, curve b.

We may conclude then, that a satisfactory flight configuration must not only have $C_m = 0$ at some $\alpha > 0$ in order to *trim* (i.e. be in pitch equilibrium) at positive lift, but at the same time must usually have $C_{m_\alpha} < 0$. Alternatively, as can be seen from Fig. 6.3, it must have $C_{m_0} > 0$ and $C_{m_\alpha} < 0$. It is somewhat simpler to use the latter form of the criterion to assess the possibilities for flight.

We state here without proof (this is given in Sec. 6.3) that $\partial C_m/\partial\alpha$ can be made negative for virtually any combination of lifting surfaces and bodies by placing the center of gravity far enough forward. Thus it is not the stiffness requirement, taken by itself, that restricts the possible configurations, but rather that it must coexist with zero moment. Since a proper choice of the C.G. location can ensure a negative $\partial C_m/\partial\alpha$, *then any configuration with a positive* C_{m_0} *can satisfy the conditions for flight at* $L > 0$.

Figure 6.4 shows the C_{m_0} of conventional airfoil sections. If an airplane were

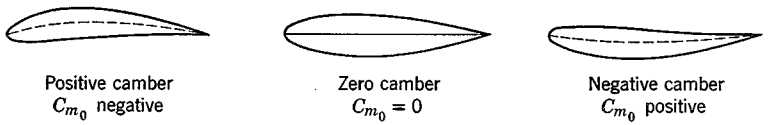

FIG. 6.4 C_{m_0} of airfoil sections.

to consist of a straight wing alone (flying wing), then the wing camber would determine the airplane characteristics as follows:

Negative camber—flight possible at $\alpha > 0$; i.e. $C_L > 0$.

Zero camber—flight possible only at $\alpha = 0$, or $C_L = 0$.

Positive camber—flight not possible at any positive α or C_L.

For straight-winged tailless airplanes, only the negative camber satisfies the conditions for flight. Effectively the same result is attained if a flap, deflected upward, is incorporated at the trailing edge of a symmetrical airfoil. A conventional low-speed airplane, with essentially straight wings and positive camber, could fly upside down without a tail, provided the C.G. were far enough forward. The positively cambered straight wing can be used only in conjunction with an auxiliary device which provides the positive C_{m_0}. The solution adopted by experimenters as far back as Samuel Henson (1842) and John Stringfellow (1848) was to add a tail behind the wing. The Wright brothers (1903) used a tail ahead of the wing (Canard configuration). Either of these alternatives can supply a positive C_{m_0} as illustrated in Fig. 6.5. When the wing is at zero lift, the auxiliary surface must provide a nose-up

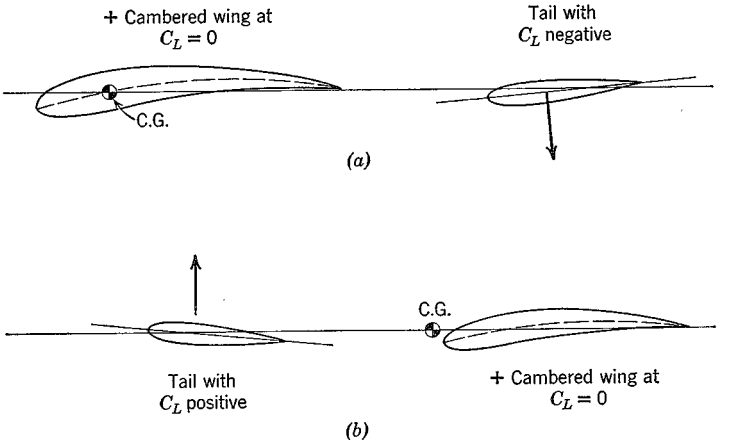

FIG. 6.5 Wing-tail arrangements with positive C_{m_0}. (*a*) Conventional arrangement. (*b*) Tail-first or Canard arrangement.

moment. The conventional tail must therefore be at a negative angle of attack, and the Canard tail at a positive angle.

An alternative to the wing-tail combination is the swept-back wing with twisted tips (Fig. 6.6). When the net lift is zero, the forward part of the wing has positive lift, and the rear part negative. The result is a positive couple, as desired.

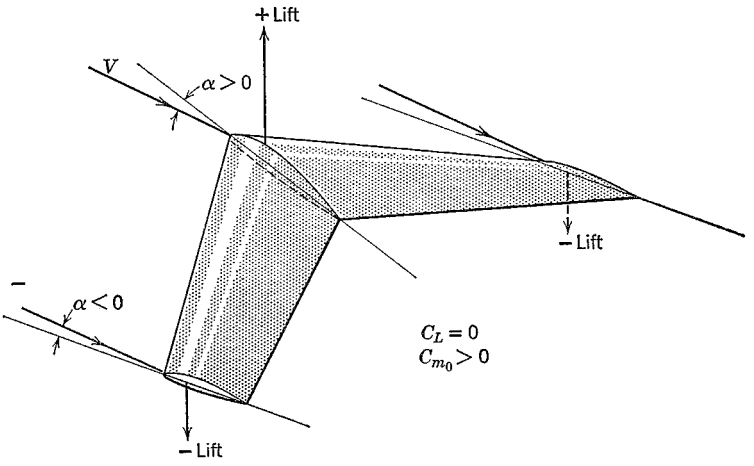

FIG. 6.6 Swept-back wing with twisted tips.

A variant of the swept-back wing is the delta wing. The positive C_{m_0} can be achieved with such planforms by twisting the tips, by employing negative camber, or by incorporating an upturned tailing edge flap.

6.3 PITCH STIFFNESS OF A GENERAL CONFIGURATION

Having established above the central importance of the derivative C_{m_α} for satisfactory flight, we turn now to a detailed discussion of it for a general vehicle configuration. We consider the vehicle to be composed of a body, a wing, a tail and propulsive units. If any of these are absent (as for a tailless airplane, a wingless missile, or a glider) the appropriate deletions from the analysis are readily made.

The pressure distribution over the surfaces of a vehicle in steady rectilinear motion, and the consequent integrated forces and moments, are functions of angle of attack α, control surface angles, Mach number **M**, Reynolds number R_e, thrust coefficient C_T, and dynamic pressure $\frac{1}{2}\rho V^2$. The last-mentioned parameter enters because of aeroelastic effects. If the vehicle is flexible, then a change in dynamic pressure, with all other variables constant, produces a change in shape, and hence of the forces and moments.

In the following discussion the only restriction in relation to the above parameters is that of steady rectilinear flight. Specifically, power effects, flexibility, and compressibility effects are not excluded.

PITCHING MOMENT OF A WING

The force system acting on an isolated wing, in symmetric flight, can be represented as a lift L_w and drag D_w acting at a reference point, the mean aerodynamic center, together with a pitching moment $M_{\text{a.c.}_w}$ (Fig. 6.7).

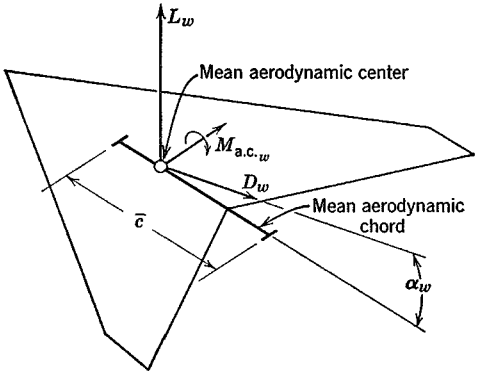

FIG. 6.7 Aerodynamic forces on the wing.

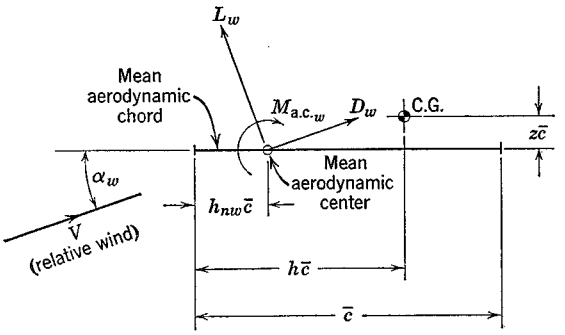

FIG. 6.8 Moment about the C.G. in the plane of symmetry.

The inviscid theory of thin wings at small α_w predicts that the moment about the aerodynamic center is invariant with α_w, and this is indeed very often the case in reality. However, it is possible that $M_{a.c._w}$ may vary with α_w, and this case is included in the following. The moment of the force system of Fig. 6.7 about the vehicle center of gravity (see Fig. 6.8) is given by

$$M_w = M_{a.c._w} + (L_w \cos \alpha_w + D_w \sin \alpha_w)(h - h_{n_w})\bar{c} + (L_w \sin \alpha_w - D_w \cos \alpha_w)z\bar{c} \quad (6.3,1)$$

For many flight situations, including the cruising flight of all classes of fixed-wing aircraft, the angle of attack is small enough to justify the approximations $\sin \alpha_w \doteq \alpha_w$, $\cos \alpha_w \doteq 1$. We take this to be the case here, bearing in mind the consequent restriction on the validity of the resulting equations.

Equation (6.3,1) is made nondimensional by dividing through by $\frac{1}{2}\rho V^2 S\bar{c}$. It then becomes

$$C_{m_w} = C_{m_{a.c._w}} + (C_{L_w} + C_{D_w}\alpha_w)(h - h_{n_w}) + (C_{L_w}\alpha_w - C_{D_w})z \quad (6.3,2)$$

Although it may occasionally be necessary to retain all the terms in (6.3,2), experience has shown that the last one is frequently negligible, and that $C_{D_w}\alpha_w$ may often be neglected in comparison with C_{L_w}. With these simplifications, we obtain

$$C_{m_w} = C_{m_{a.c._w}} + C_{L_w}(h - h_{n_w}) \quad (6.3,3)$$

Equation (6.3,3) will be used to represent the wing pitching moment in the discussions that follow.

PITCHING MOMENT OF A BODY AND NACELLES

The influence of the body and nacelles are complex. A body alone in an airstream is subjected to aerodynamic forces. These, like those on the wing, may be represented over moderate ranges of angle of attack by lift and drag forces at an aerodynamic center, and a pitching couple. When the wing and body are put together, however, a simple superposition of the aerodynamic forces which act upon them separately does not give a correct result. Strong interference effects are usually present, the flow field of the wing affecting the forces on the body, and vice versa.

These interference flow fields are illustrated for subsonic flow in Fig. 6.9. Part (*a*) shows the pattern of induced velocity along the body that is caused by the wing vortex system. This induced flow produces a positive moment that increases with wing lift or α. Hence a positive (destabilizing) contribution to C_{m_α} results. Part (*b*) shows an effect of the body on the wing. When the body axis is at angle α to the stream, there is a cross-flow component $V \sin \alpha$. The body distorts this flow locally, leading to cross-flow

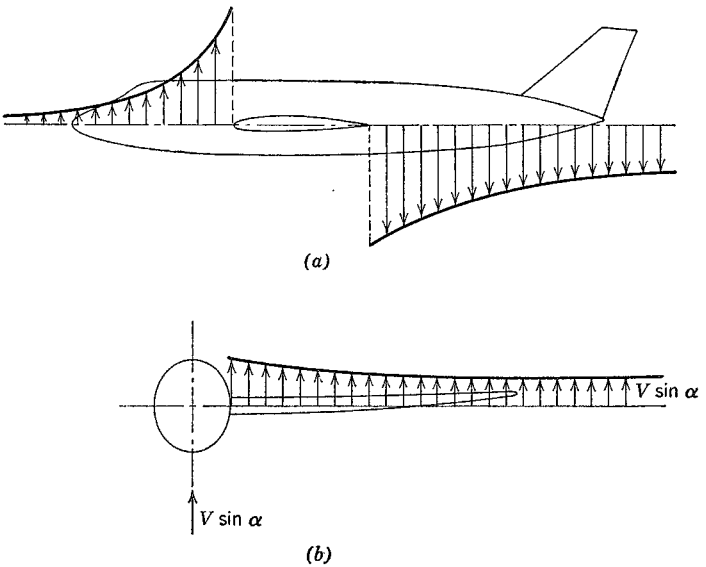

FIG. 6.9 Example of mutual interference flow fields of wing and body—subsonic flow. (*a*) Qualitative pattern of upwash and downwash induced along the body axis by the wing vorticity. (*b*) Qualitative pattern of upwash induced along wing by the cross-flow past the body.

components that can be of order $2V \sin \alpha$ at the body-wing intersection. There is a resulting change in the wing lift distribution.

The result of adding a body and nacelles to a wing may usually be interpreted as a shift (forward) of the mean aerodynamic center, an increase in the lift-curve slope, and a negative increment in $C_{m_{a.c.}}$. The equation that corresponds to (6.3,3) for a wing-body-nacelle combination is then of the same form, but with different values of the parameters. The subscript wb is used to denote these values.

$$C_{m_{wb}} = C_{m_{a.c._{wb}}} + C_{L_{wb}}(h - h_{n_{wb}}) \tag{6.3,4}$$

PITCHING MOMENT OF A TAIL

The forces on an isolated tail are represented just like those on an isolated wing. When the tail is mounted on an airplane, however, important interferences occur. The most significant of these, and one that is usually predictable by aerodynamic theory, is a downward deflection of the flow at the tail caused by the wing. This is characterized by the mean downwash angle ϵ. Blanking of part of the tail by the body is a second effect, and a reduction of the relative wind when the tail lies in the wing wake is the third.

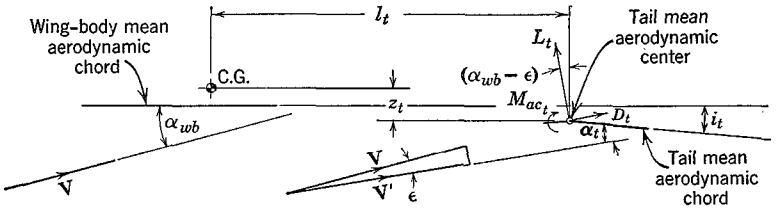

FIG. 6.10 Forces acting on the tail.

Figure 6.10 depicts the forces acting on the tail. **V** is the relative wind vector of the airplane, and **V**′ is the average or effective relative wind at the tail. The tail lift and drag forces are by definition respectively perpendicular and parallel to **V**′. The reader should note the tail angle i_t, which in keeping with Fig. 6.5 must be negative. The moment $M_{a.c._t}$ is the pitching moment of the tail about its own aerodynamic center. This is zero for a symmetrical tail section, and in any case would come mainly from the deflection of the elevator.

The contribution of the tail to the airplane lift, which by definition is perpendicular to **V**, is

$$L_t \cos \epsilon - D_t \sin \epsilon$$

ϵ is usually a small angle, and $D_t\epsilon$ may be neglected compared with L_t. The contribution of the tail to the airplane lift then becomes simply L_t. We introduce the symbol C_{L_t} to represent the lift coefficient of the tail, based on the airplane dynamic pressure $\frac{1}{2}\rho V^2$ and the tail area S_t.

$$C_{L_t} = \frac{L_t}{\frac{1}{2}\rho V^2 S_t} \tag{6.3,5}$$

The reader should note that the lift coefficient of the tail is often based on the local dynamic pressure at the tail, which differs from $\frac{1}{2}\rho V^2$ when the tail lies in the wing wake. This practice entails carrying the ratio V'/V in many subsequent equations. The definition employed here amounts to incorporating V'/V into the tail lift-curve slope $a_t = \partial C_{L_t}/\partial \alpha_t$. This quantity is in any event different from that for the isolated tail, owing to the interference effects previously noted. This circumstance is handled in various ways in the literature. Sometimes a tail efficiency factor η_t is introduced, the isolated tail lift slope being multiplied by η_t. In other treatments, η_t is used to represent $(V'/V)^2$. In the convention adopted here, a_t is the lift-curve slope of the tail, as measured in situ on the airplane, and based on the dynamic pressure $\frac{1}{2}\rho V^2$. This is the quantity that is directly obtained in a wind-tunnel test.

From Fig. 6.10 we find the pitching moment of the tail about the C.G. to be

$$\begin{aligned} M_t = &-l_t[L_t \cos(\alpha_{wb} - \epsilon) + D_t \sin(\alpha_{wb} - \epsilon)] \\ &- z_t[D_t \cos(\alpha_{wb} - \epsilon) - L_t \sin(\alpha_{wb} - \epsilon)] + M_{ac_t} \end{aligned} \tag{6.3,6}$$

Experience has shown that in the majority of instances the dominant term in this equation is the first one, and that all others are negligible by comparison. Only this case will be dealt with here. The reader is left to extend the analysis to situations where this approximation is not valid. With the above approximation, and that of small angles,

$$M_t = -l_t L_t = -l_t C_{L_t} \tfrac{1}{2}\rho V^2 S_t$$

Upon conversion to coefficient form, we obtain

$$C_{m_t} = \frac{M_t}{\frac{1}{2}\rho V^2 S\bar{c}} = -\frac{l_t}{\bar{c}}\frac{S_t}{S} C_{L_t} \tag{6.3,7}$$

The combination $l_t S_t/S\bar{c}$ is the ratio of two volumes characteristic of the airplane's geometry. It is commonly called the "horizontal-tail volume ratio," or more simply, the "tail volume." It is denoted here by V_H. Thus

$$C_{m_t} = -V_H C_{L_t} \tag{6.3,8}$$

Since the center of gravity is not a fixed point, but varies with the loading condition and fuel consumption of the vehicle, V_H in (6.3,8) is not a constant

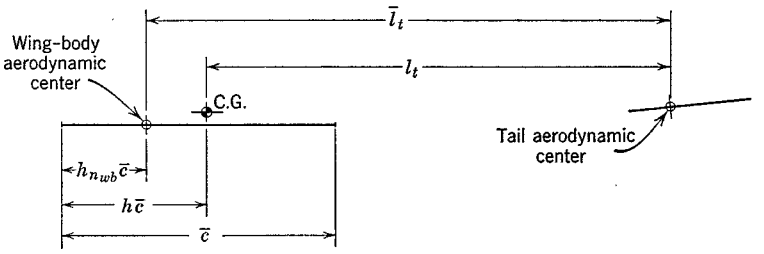

FIG. 6.11 Wing-body and tail aerodynamic centers.

(although it does not vary much). It is a little more convenient to calculate the moment of the tail about a fixed point, the mean aerodynamic center of the wing-body combination, and to use this moment in the subsequent algebraic manipulations. Figure 6.11 shows the relevant relationships, and we define

$$\bar{V}_H = \frac{\bar{l}_t S_t}{\bar{c} S} \tag{6.3,9}$$

which leads to

$$V_H = \bar{V}_H - \frac{S_t}{S}(h - h_{n_{wb}}) \tag{6.3,10}$$

The moment of the tail about the wing-body aerodynamic center is then [cf. (6.3,8)]

$$\bar{C}_{m_t} = -\bar{V}_H C_{L_t} \tag{6.3,11}$$

and its moment about the C.G, is, from substitution of (6.3,10) into (6.3,8)

$$C_{m_t} = -\bar{V}_H C_{L_t} + C_{L_t}\frac{S_t}{S}(h - h_{n_{wb}}) \tag{6.3,12}$$

PITCHING MOMENT OF A PROPULSIVE SYSTEM

The moment provided by a propulsive system is in two parts: (1) that coming from the forces acting on the unit itself, e.g. the thrust and in-plane force acting on a propeller, and (2) that coming from the interaction of the propulsive slipstream with the other parts of the airplane. These are discussed in more detail in Sec. 7.3. We assume that the interference part is included in the moments already given for the wing, body, and tail, and denote by C_{m_p} the remaining moment from the propulsion units.

TOTAL PITCHING MOMENT

On summing (6.3,4) and (6.3,12) and adding the contribution C_{m_p} for the propulsive system, we obtain the total pitching moment about the C.G.,

$$C_m = C_{m_{\text{a.c.}_{wb}}} + \left(C_{L_{wb}} + C_{L_t}\frac{S_t}{S}\right)(h - h_{n_{wb}}) - \overline{V}_H C_{L_t} + C_{m_p} \tag{6.3,13}$$

Since C_{L_t} is a coefficient based on S_t, then $C_{L_t}S_t/S$ is the tail contribution to C_L, and the total lift coefficient of the vehicle is

$$C_L = C_{L_{wb}} + C_{L_t}\frac{S_t}{S} \tag{6.3,14}$$

Equation (6.3,13) therefore becomes

$$C_m = C_{m_{\text{a.c.}_{wb}}} + C_L(h - h_{n_{wb}}) - \overline{V}_H C_{L_t} + C_{m_p} \tag{6.3,15}$$

It is worthwhile repeating that no assumptions about thrust, compressibility, or aeroelastic effects have been made in respect of (6.3,15). The pitch stiffness $(-C_{m_\alpha})$ is now obtained from (6.3,15). Recall that the aerodynamic centers of the wing-body combination and of the tail are fixed points, so that

$$C_{m_\alpha} = \frac{\partial C_{m_{\text{a.c.}_{wb}}}}{\partial \alpha} + C_{L_\alpha}(h - h_{n_{wb}}) - \overline{V}_H \frac{\partial C_{L_t}}{\partial \alpha} + \frac{\partial C_{m_p}}{\partial \alpha} \tag{6.3,16}$$

If a true aerodynamic center in the classical sense exists, then $\partial C_{m_{\text{a.c.}_{wb}}}/\partial\alpha$ is zero and

$$C_{m_\alpha} = C_{L_\alpha}(h - h_{n_{wb}}) - \overline{V}_H \frac{\partial C_{L_t}}{\partial \alpha} + \frac{\partial C_{m_p}}{\partial \alpha} \tag{6.3,17}$$

C_{m_α} as given by (6.3,16) or (6.3,17) is a constant that depends linearly on the C.G. position, h. Since C_{L_α} is usually large, the magnitude and sign of C_{m_α} depend strongly on h. This is the basis of the statement in Sec. 6.2 that C_{m_α} can always be made negative by a suitable choice of h. The C.G. position h_n for which C_{m_α} is zero is of particular significance, since this represents a boundary between positive and negative pitch stiffness. In this book we define h_n as the *neutral point*, N.P. It has the same significance for the vehicle as a whole as does the aerodynamic center for a wing alone, and indeed the term *vehicle aerodynamic center* is an acceptable alternative to "neutral point."

The location of the N.P. is readily calculated from (6.3,16), i.e.

$$0 = \frac{\partial C_{m_{\text{a.c.}_{wb}}}}{\partial \alpha} + C_{L_\alpha}(h_n - h_{n_{wb}}) - \overline{V}_H \frac{\partial C_{L_t}}{\partial \alpha} + \frac{\partial C_{m_p}}{\partial \alpha}$$

or

$$h_n = h_{n_{wb}} - \frac{1}{C_{L_\alpha}} \left(\frac{\partial C_{m_{\text{a.c.}_{wb}}}}{\partial \alpha} - \overline{V}_H \frac{\partial C_{L_t}}{\partial \alpha} + \frac{\partial C_{m_p}}{\partial \alpha} \right) \tag{6.3,18}$$

Substitution of (6.3,18) back into (6.3,16) simplifies the latter to

$$C_{m_\alpha} = C_{L_\alpha}(h - h_n) \tag{6.3,19}$$

which is valid whether $C_{m_{\text{a.c.}_{wb}}}$ and C_{m_p} vary with α or not. Equation (6.3,19) clearly provides an excellent way of finding h_n from test results, i.e. from measurements of C_{m_α} and C_{L_α}. The difference between the C.G. position and the N.P. is sometimes called the *static margin*,

$$K_n = (h_n - h) \tag{6.3,20}$$

Since the criterion to be satisfied is $C_{m_\alpha} < 0$, i.e. positive pitch stiffness, then we see that we must have $h < h_n$, or $K_n > 0$. In other words the C.G. must be forward of the N.P. The farther forward the C.G. the greater is K_n, and in the sense of "static stability" the more stable the vehicle.

It must be emphasized that C_{m_α} and C_{L_α} are partial derivatives. This means that all other significant arguments, normally $\mathbf{M}$, C_T, and $\frac{1}{2}\rho V^2$ are kept constant. This is especially important to keep in mind when experimental results are being used. If these parameters are unimportant or absent, as in the gliding flight of a rigid vehicle at low $\mathbf{M}$, then C_m and C_L are functions of α only, C_m is a unique function of C_L, and (6.3,19) yields

$$h - h_n = \frac{dC_m}{dC_L} \tag{6.3,21}$$

Equation (6.3,21) is sometimes used in practice as a definition of the neutral point, but as is clear from the foregoing, it contains some dangers. Since C_m and C_L are in the general case each functions of several independent variables, then the derivative dC_m/dC_L is not mathematically defined, and indeed different values for it can be calculated depending on what constraints are imposed on the independent variables. With particular constraints it indeed turns out to be a useful index of stability, and this point is treated further in Sec. 9.3.

LINEAR LIFT AND MOMENT

When the forces and moments on the wing, body, tail, and propulsive system are linear in α, as may be near enough the case in reality, some

additional useful relations can be obtained. We then have

$$C_{L_{wb}} = a_{wb}\alpha_{wb} \tag{6.3,22}$$

$$C_{L_t} = a_t\alpha_t \tag{6.3,23}$$

and

$$C_{m_p} = C_{m_{0_p}} + \frac{\partial C_{m_p}}{\partial \alpha} \cdot \alpha \tag{6.3,24}$$

Furthermore, if $C_{m_{wb}}$ is linear in $C_{L_{wb}}$, it follows from (6.3,4) that $C_{m_{a.c.wb}}$ does not vary with $C_{L_{wb}}$, i.e. that a true aerodynamic center exists. Figure 6.10 shows that the tail angle of attack is

$$\alpha_t = \alpha_{wb} + i_t - \epsilon \tag{6.3,25}$$

and hence

$$C_{L_t} = a_t(\alpha_{wb} + i_t - \epsilon) \tag{6.3,26}$$

The downwash ϵ can usually be adequately approximated by

$$\epsilon = \epsilon_0 + \frac{\partial \epsilon}{\partial \alpha}\alpha_{wb} \tag{6.3,27}$$

The downwash ϵ_0 at $C_{L_{wb}} = 0$ results from the induced velocity field of the body and from wing twist; the latter produces a vortex wake and downwash field even at zero total lift. The constant derivative $\partial\epsilon/\partial\alpha$ occurs because the main contribution to the downwash at the tail comes from the wing trailing vortex wake, the strength of which is, in the linear case, proportional to C_L.

The tail lift coefficient then is

$$C_{L_t} = a_t\left[\alpha_{wb}\left(1 - \frac{\partial \epsilon}{\partial \alpha}\right) + i_t - \epsilon_0\right] \tag{6.3,28}$$

and the total lift, from (6.3,14) is

$$C_L = a_{wb}\alpha_{wb}\left[1 + \frac{a_t}{a_{wb}}\frac{S_t}{S}\left(1 - \frac{\partial \epsilon}{\partial \alpha}\right)\right] + a_t\frac{S_t}{S}(i_t - \epsilon_0) \qquad (a)$$

or

$$C_L = (C_L)_0 + a\alpha_{wb} \qquad (b) \tag{6.3,29}$$

or

$$C_L = a\alpha \qquad (c)$$

where

$$(C_L)_0 = a_t\frac{S_t}{S}(i_t - \epsilon_0) \tag{6.3,30}$$

is the lift of the tail when $\alpha_{wb} = 0$;

$$a = \frac{\partial C_L}{\partial \alpha} = a_{wb}\left[1 + \frac{a_t}{a_{wb}}\frac{S_t}{S}\left(1 - \frac{\partial \epsilon}{\partial \alpha}\right)\right] \tag{6.3,31}$$

is the lift-curve slope of the whole configuration; and α is the angle of attack

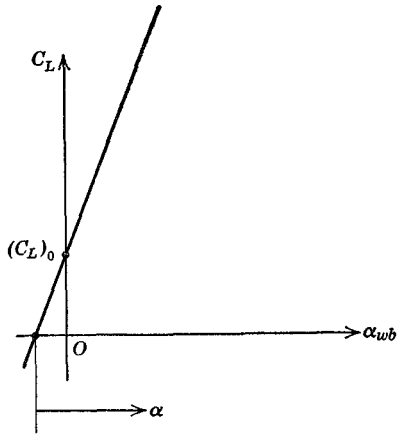

FIG. 6.12 Graph of total lift.

of the zero-lift line of the whole configuration (see Fig. 6.12). Note that, since i_t is negative, then $(C_L)_0$ is negative. The difference between α and α_{wb} is found by equating (6.3,29*b* and *c*) to be

$$\alpha - \alpha_{wb} = \frac{a_t}{a}\frac{S_t}{S}(i_t - \epsilon_0) \tag{6.3,32}$$

When the linear relations for C_L, C_{L_t} and C_{m_p} are substituted into (6.3,15) the following results can be obtained after some algebraic reduction:

$$C_m = C_{m_0} + C_{m_\alpha}\alpha \qquad (a)$$
$$C_m = \bar{C}_{m_0} + C_{m_\alpha}\alpha_{wb} \qquad (b) \tag{6.3,33}$$

where
$$C_{m_\alpha} = a(h - h_{n_{wb}}) - a_t\bar{V}_H\left(1 - \frac{\partial\epsilon}{\partial\alpha}\right) + \frac{\partial C_{m_p}}{\partial\alpha} \qquad (a)$$

or
$$C_{m_\alpha} = a_{wb}(h - h_{n_{wb}}) - a_t V_H\left(1 - \frac{\partial\epsilon}{\partial\alpha}\right) + \frac{\partial C_{m_p}}{\partial\alpha} \qquad (b) \tag{6.3,34}$$

and
$$C_{m_0} = C_{m_{\text{a.c.}_{wb}}} + C_{m_{0_p}} + a_t\bar{V}_H(\epsilon_0 - i_t) \times \left[1 - \frac{a_t}{a}\frac{S_t}{S}\left(1 - \frac{\partial\epsilon}{\partial\alpha}\right)\right] \qquad (a)$$
$$\bar{C}_{m_0} = C_{m_{\text{a.c.}_{wb}}} + \bar{C}_{m_{0_p}} + a_t V_H(\epsilon_0 - i_t) \qquad (b) \tag{6.3,35}$$

where
$$\bar{C}_{m_{0_p}} = C_{m_{0_p}} + (\alpha - \alpha_{wb})\frac{\partial C_{m_p}}{\partial\alpha} \qquad (c)$$

$$h_n = h_{n_{wb}} + \frac{a_t}{a}\bar{V}_H\left(1 - \frac{\partial\epsilon}{\partial\alpha}\right) - \frac{1}{a}\frac{\partial C_{m_p}}{\partial\alpha} \tag{6.3,36}$$

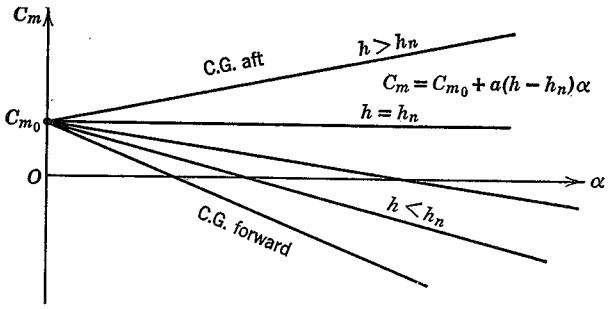

FIG. 6.13 Effect of C.G. location on C_m curve.

Note that since $\bar{C}_{m_0}$ is the pitching moment at zero α_{wb}, not at zero total lift, its value depends on h (via V_H), whereas C_{m_0}, being the moment at zero total lift, represents a couple and is hence independent of C.G. position. All the above relations apply to tailless aircraft by putting $\bar{V}_H = 0$. Another useful relation comes from integrating (6.3,19), i.e.

$$C_m = C_{m_0} + C_L(h - h_n) \qquad (a)$$

or

$$C_m = C_{m_0} + a\alpha(h - h_n) \qquad (b) \qquad (6.3,37)$$

Figure 6.13 shows the linear C_m vs. α relation, and Fig. 6.14 shows the resultant system of lift and moment that corresponds to (6.3,37), i.e. a force C_L and a couple C_{m_0} at the N.P.

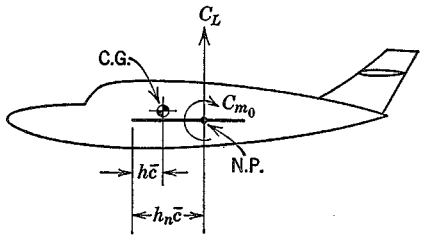

FIG. 6.14 Total lift and moment acting on vehicle.

6.4 LONGITUDINAL CONTROL

In this section we discuss the longitudinal control of the vehicle from a *static* point of view. That is, we concern ourselves with how the equilibrium state of steady rectilinear flight is governed by the available controls. Basically there are two kinds of changes that can be made by the pilot or

automatic control system—a change of propulsive thrust, or a change of configuration. Included in the latter are the operation of aerodynamic controls—elevators, wing flaps, spoilers, and horizontal tail rotation. Since the equilibrium state is dominated by the requirement $C_m = 0$, the most powerful controls are those that have the greatest effect on C_m.

Figure 6.13 shows that another theoretically possible way of changing the trim condition is to move the C.G., which changes the value of α at which $C_m = 0$. Moving it forward reduces the trim α or C_L, and hence produces an increase in the trim speed. This method was actually used by Lilienthal, a pioneer of aviation, in gliding flights during 1891–1896, in which he shifted his body to move the C.G. It has the inherent disadvantage, apart from practical difficulties, of changing C_{m_α} at the same time, reducing the pitch stiffness and hence stability, when the trim speed is reduced.

The longitudinal control now generally used is aerodynamic. A variable pitching moment is provided by moving the elevator, which may be all or part of the tail, or a trailing-edge flap in a tailless design. Deflection of the elevator through an angle δ_e produces increments in both the C_m and C_L of the airplane. The ΔC_L caused by the elevator of aircraft with tails is small enough to be neglected for many purposes. This is not so for tailless aircraft, where the ΔC_L due to elevators is usually significant. We shall assume that the lift and moment increments for both kinds of airplane are linear in δ_e, which is a fair representation of the characteristics of typical controls at high Reynolds number. Therefore,

$$\Delta C_L = C_{L_\delta}\delta_e \qquad (a)$$

$$C_L = C_L(\alpha) + C_{L_\delta}\delta_e \qquad (b) \qquad (6.4{,}1)$$

$$\Delta C_m = C_{m_\delta}\delta_e \qquad (c)$$

and

$$C_m = C_m(\alpha) + C_{m_\delta}\delta_e \qquad (d)$$

where $C_{L_\delta} = \partial C_L/\partial\delta_e$, $C_{m_\delta} = \partial C_m/\partial\delta_e$, and $C_L(\alpha)$, $C_m(\alpha)$ are the "basic" lift and moment when $\delta_e = 0$. The usual convention is to take down elevator as positive (Fig. 6.15*a*). This leads to positive C_{L_δ} and negative C_{m_δ}. The deflection of the elevator through a constant positive angle then shifts the C_m–α curve downward, without change of slope (Fig. 6.15*b*). At the same time the zero-lift angle of the airplane is slightly changed (Fig. 6.15*c*).

In the case of linear lift and moment, we have

$$C_L = C_{L_\alpha}\alpha + C_{L_\delta}\delta_e \qquad (a)$$

$$C_m = C_{m_0} + C_{m_\alpha}\alpha + C_{m_\delta}\delta_e \qquad (b) \qquad (6.4{,}2)$$

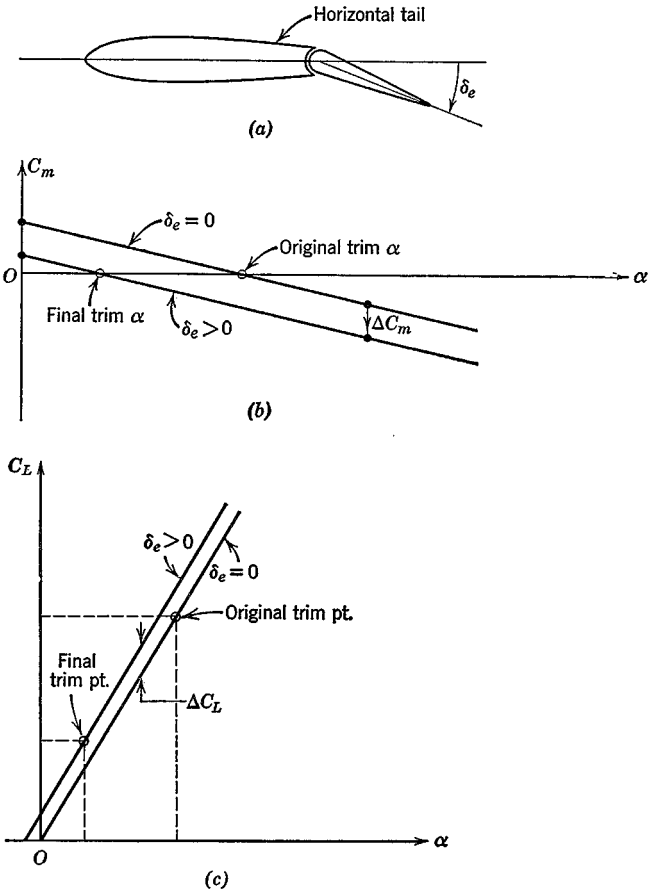

FIG. 6.15 Effect of elevator angle on C_m curve. (*a*) Elevator angle. (*b*) $C_m - \alpha$ curve. (*c*) $C_L - \alpha$ curve.

THE DERIVATIVES C_{L_δ} AND C_{m_δ}

Equation (6.3,14) gives the vehicle lift, with $S_t = 0$ for tailless types, of course. Hence

$$C_{L_\delta} = \frac{\partial C_L}{\partial \delta_e} = \frac{\partial C_{L_{wb}}}{\partial \delta_e} + \frac{S_t}{S}\frac{\partial C_{L_t}}{\partial \delta_e} \tag{6.4,3}$$

in which only the first term applies for tailless aircraft and the second for conventional tail elevators or all moving tails (when i_t is used instead of δ_e).

We define the elevator lift effectiveness as

$$a_e = \frac{\partial C_{L_t}}{\partial \delta_e} \tag{6.4,4}$$

so that (6.4,3) becomes

$$C_{L_\delta} = \frac{\partial C_{L_{wb}}}{\partial \delta_e} + a_e \frac{S_t}{S} \tag{6.4,5}$$

The total vehicle C_m is given for both tailed and tailless types by (6.3,15). For the latter, of course, $\bar{V}_H = 0$. Taking the derivative w.r.t. δ_e gives

$$C_{m_\delta} = \frac{\partial C_{m_{\text{a.c.}_{wb}}}}{\partial \delta_e} + C_{L_\delta}(h - h_{n_{wb}}) - \bar{V}_H \frac{\partial C_{L_t}}{\partial \delta_e} + \frac{\partial C_{m_p}}{\partial \delta_e} \tag{6.4,6}$$

We may usually neglect the last term, since there is unlikely to be any propulsive-elevator interaction that cannot be included in a_e. Then (6.4,6) becomes

$$C_{m_\delta} = \frac{\partial C_{m_{\text{a.c.}_{wb}}}}{\partial \delta_e} + C_{L_\delta}(h - h_{n_{wb}}) - a_e \bar{V}_H \tag{6.4,7}$$

Summarizing for both types of vehicle, we have

With tails:

$$\begin{aligned} C_{L_\delta} &= a_e \frac{S_t}{S} && (a) \\ C_{m_\delta} &= -a_e \bar{V}_H + C_{L_\delta}(h - h_{n_{wb}}) && (b) \end{aligned} \tag{6.4,8}$$

Tailless:

$$\begin{aligned} C_{L_\delta} &= \frac{\partial C_L}{\partial \delta_e} && (a) \\ C_{m_\delta} &= \frac{\partial C_{m_{\text{a.c.}}}}{\partial \delta_e} + C_{L_\delta}(h - h_n) && (b) \end{aligned} \tag{6.4,9}$$

In the last case, the subscript wb is, of course, redundant and has been dropped. The primary parameters to be predicted or measured are a_e for tailed aircraft, and $\partial C_L/\partial \delta_e$, $\partial C_{m_{\text{a.c.}}}/\partial \delta_e$ for tailless.

ELEVATOR ANGLE TO TRIM

The trim condition is $C_m = 0$, whence from (6.4,1*d*)

$$\delta_{e_{\text{trim}}} = -\frac{C_m(\alpha)}{C_{m_\delta}} \tag{6.4,10}$$

and the corresponding lift coefficient is

$$\begin{aligned} C_{L_{\text{trim}}} &= C_L(\alpha) + C_{L_\delta}\,\delta_{e_{\text{trim}}} \\ &= C_L(\alpha) - \frac{C_{L_\delta}}{C_{m_\delta}} C_m(\alpha) \end{aligned} \tag{6.4,11}$$

When the linear lift and moment relations (6.4,2) apply the equations for trim are

$$\begin{aligned} C_{L_\alpha}\alpha_{\text{trim}} + C_{L_\delta}\delta_{e_{\text{trim}}} &= C_{L_{\text{trim}}} \\ C_{m_\alpha}\alpha_{\text{trim}} + C_{m_\delta}\delta_{e_{\text{trim}}} &= -C_{m_0} \end{aligned} \tag{6.4,12}$$

These equations are solved for α and δ_e to give

$$\alpha_{\text{trim}} = \frac{C_{m_0}C_{L_\delta} + C_{m_\delta}C_{L\text{trim}}}{\Delta} \qquad (a)$$

$$\delta_{e\text{trim}} = -\frac{C_{m_0}C_{L_\alpha} + C_{m_\alpha}C_{L\text{trim}}}{\Delta} \qquad (b) \tag{6.4,13}$$

$$\frac{d\delta_{e\text{trim}}}{dC_{L\text{trim}}} = -\frac{C_{m_\alpha}}{\Delta} = -\frac{C_{L_\alpha}}{\Delta}(h - h_n) \qquad (c)$$

where

$$\Delta = C_{L_\alpha}C_{m_\delta} - C_{L_\delta}C_{m_\alpha} \qquad (d)$$

and is normally negative. The values of Δ for the two types of airplane are readily calculated from (6.4,8 and 9) together with (6.3,19) to give

Tailed:

$$\Delta = C_{L_\alpha}[C_{L_\delta}(h_n - h_{n_{wb}}) - a_e\,\overline{V}_H] \qquad (a)$$

Tailless:

$$\Delta = C_{L_\alpha}\frac{\partial C_{m_{\text{a.c.}}}}{\partial \delta_e} \qquad (b) \tag{6.4,14}$$

and both are independent of h. From (6.4,13a) we get the *trimmed lift curve:*

$$C_{L\text{trim}} = -\frac{C_{m_0}C_{L_\delta}}{C_{m_\delta}} + \frac{\Delta}{C_{m_\delta}}\alpha_{\text{trim}} \tag{6.4,15}$$

and the slope is given by

$$\left(\frac{dC_L}{d\alpha}\right)_{\text{trim}} = C_{L_\alpha} - \frac{C_{L_\delta}}{C_{m_\delta}} C_{m_\alpha} \tag{6.4,16}$$

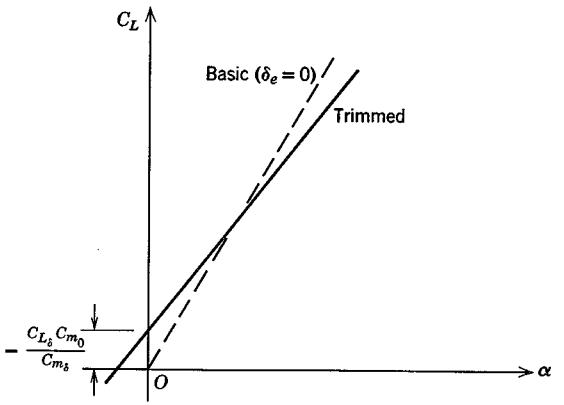

FIG. 6.16 Trimmed lift curve.

The trimmed lift-curve slope is seen to be less than C_{L_α} by an amount that depends on C_{m_α}, i.e. on the static margin, and that vanishes when $h = h_n$. The difference is only a few percent for tailed airplanes at normal C.G. position, but may be appreciable for tailless vehicles because of their larger C_{L_δ}. The relation between the basic and trimmed lift curves is shown in Fig. 6.16.

Equation (6.4,13*b*) is plotted on Fig. 6.17, showing how $\delta_{e_{\text{trim}}}$ varies with $C_{L_{\text{trim}}}$ and C.G. position when the aerodynamic coefficients are constant.

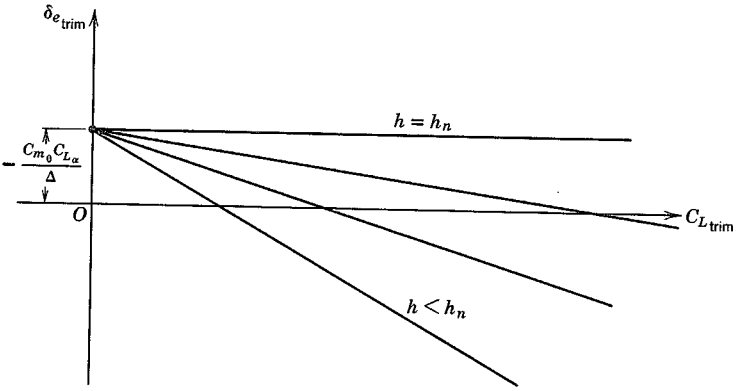

FIG. 6.17 Elevator angle to trim at various C.G. positions.

VARIATION OF $\delta_{e_{\text{trim}}}$ WITH SPEED

When, in the absence of compressibility, aeroelastic effects, and propulsive system effects, the aerodynamic coefficients of (6.4,13) are constant, the variation of $\delta_{e_{\text{trim}}}$ with speed is simple. Then $\delta_{e_{\text{trim}}}$ is a unique function of $C_{L_{\text{trim}}}$ for each C.G. position. Since $C_{L_{\text{trim}}}$ is in turn fixed by the equivalent airspeed,† for horizontal flight

$$C_{L_{\text{trim}}} = \frac{W}{\frac{1}{2}\rho_0 V_E{}^2 S} \tag{6.4,17}$$

then $\delta_{e_{\text{trim}}}$ becomes a unique function of V_E. The form of the curves is shown in Fig. 6.18 for representative values of the coefficients.

The variation of $\delta_{e_{\text{trim}}}$ with $C_{L_{\text{trim}}}$ or speed shown on Figs. 6.17 and 6.18 is the normal and desirable one. For any C.G. position, an increase in trim speed from any initial value to a larger one requires a downward deflection of the elevator (a forward movement of the pilot's control). The "gradient" of the movement $\partial\delta_{e_{\text{trim}}}/\partial V_E$ is seen to decrease with rearward movement of the C.G. until it vanishes altogether at the N.P. In this condition the pilot in effect has no control over trim speed, and control of the vehicle becomes very difficult. For even more rearward positions of the C.G. the gradient reverses, and the controllability deteriorates still further.

When the aerodynamic coefficients vary with speed, the above simple analysis must be extended. In order to be still more general, we shall in the

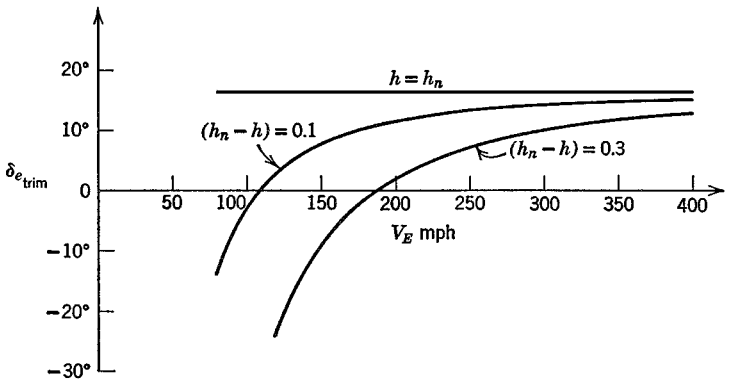

FIG. 6.18 Example of variation of elevator angle to trim with speed and C.G. position.

† Equivalent airspeed (EAS) is $V_E = V\sqrt{\rho/\rho_0}$ where ρ_0 is standard sea-level density.

following explicitly include propulsive effects as well, by means of the parameter π, which stands for the state of the pilot's propulsion control (e.g. throttle position). π = constant therefore denotes fixed-throttle and, of course, for horizontal flight at varying speed, π must be a function of V that is compatible with $T = D$. For angles of climb or descent in the normal range of conventional airplanes $L \doteq W$ is a reasonable approximation, and we adopt it in the following. When nonhorizontal flight is thus included, π becomes an independent variable, with the angle of climb γ then becoming a function of π, V, and altitude.

The two basic conditions then, for trimmed steady flight on a straight line are

$$\begin{aligned} C_m &= 0 \\ L &= C_L \tfrac{1}{2}\rho V^2 S = W \end{aligned} \tag{6.4,18}$$

and in accordance with the postulates made above, we write

$$\begin{aligned} C_m &= C_m(\alpha, V, \delta_e, \pi) \\ C_L &= C_L(\alpha, V, \delta_e, \pi) \end{aligned} \tag{6.4,19}$$

Now let $(\ )_e$ denote one state that satisfies (6.4,18) and consider a small change from it, denoted by differentials, to another such state. From (6.4,18) we get, for ρ = const,

$$dC_m = 0 \tag{6.4,20}$$

and

$$C_L V^2 = \text{const}$$

or

$$2V_e C_{L_e} dV + V_e^2 dC_L = 0$$

so that

$$dC_L = -2C_{L_e}\frac{dV}{V_e} = -2C_{L_e} d\hat{V} \tag{6.4,21}$$

where $\hat{V}$ is defined in Table 5.1. Taking the differentials of (6.4,19) and equating to (6.4,20 and 21) we get

$$\begin{aligned} C_{L_\alpha} d\alpha + C_{L_\delta} d\delta_e &= -C_{L_\pi} d\pi - (C_{L_V} + 2C_{L_e})\, d\hat{V} \\ C_{m_\alpha} d\alpha + C_{m_\delta} d\delta_e &= -C_{m_\pi} d\pi - C_{m_V} d\hat{V} \end{aligned} \tag{6.4,22}$$

where $C_{L_V} = \partial C_L/\partial \hat{V}$ and $C_{m_V} = \partial C_m/\partial \hat{V}$. From (6.4,22) we get the solution for $d\delta_e$ as

$$d\delta_e = \frac{1}{\Delta}\left\{[(C_{L_V} + 2C_{L_e})C_{m_\alpha} - C_{L_\alpha} C_{m_V}]\, d\hat{V} + (C_{L_\pi} C_{m_\alpha} - C_{L_\alpha} C_{m_\pi})\, d\pi\right\} \tag{6.4,23}$$

There are two possibilities, π constant and π variable. In the first case

(fixed throttle), $d\pi = 0$ and

$$\left(\frac{d\delta_{e_{\text{trim}}}}{d\hat{V}}\right)_{\pi} = \frac{(C_{L_V} + 2C_{L_e})C_{m_\alpha} - C_{L_\alpha}C_{m_V}}{\Delta} \tag{6.4,24}$$

It will be shown in Chapter 9 that the vanishing of this quantity is a true criterion of stability, i.e. it must be >0 for a stable airplane. In the second case, for example exactly horizontal flight, $\pi = \pi(V)$ and the π term on the r.h.s. of (6.4,23) remains. For such cases the gradient $(d\delta_{e_{\text{trim}}}/d\hat{V})$ is not necessarily related to stability. For purposes of calculating the propulsion contributions, the terms $C_{L_\pi}\, d\pi$ and $C_{m_\pi}\, d\pi$ in (6.4,23) would be evaluated as dC_{L_p} and dC_{m_p} [see the notation of (6.3,13)]. These contributions to the lift and moment are discussed in Sec. 7.3.

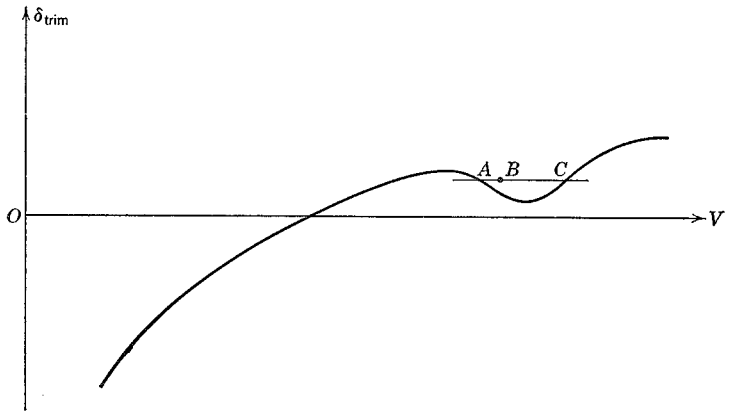

FIG. 6.19 Reversal of δ_{trim} slope at transonic speeds, π = const.

The derivatives C_{L_V} and C_{m_V} (see Sec. 7.8) may be quite large owing to slipstream effects on STOL airplanes, or Mach number effects near transonic speeds. These variations with M can result in reversal of the slope of $\delta_{e_{\text{trim}}}$ as illustrated on Fig. 6.19. The negative slope at A, according to the stability criterion referred to above, indicates that the airplane is unstable at A. This can be seen as follows. Let the airplane be in equilibrium flight at the point A, and be subsequently perturbed so that its speed increases to that of B with no change in α or δ_e. Now at B the elevator angle is too positive for trim: i.e. there is an unbalanced nose-down moment on the airplane. This puts the airplane into a dive and increases its speed still further. The speed will continue to increase until point C is reached, when the δ_e is again the

correct value for trim, but here the slope is positive and there is no tendency for the speed to change any further.

STATIC STABILITY LIMIT, h_s

The critical C.G. position for zero elevator trim slope (i.e. for stability) can be found by setting (6.4,24) equal to zero. Recalling that $C_{m_\alpha} = C_{L_\alpha}(h - h_n)$, this yields

$$h - h_n - \frac{C_{m_V}}{C_{L_V} + 2C_{L_e}} = 0 \tag{6.4,25}$$

or $$h = h_s$$

where $$h_s = h_n + \frac{C_{m_V}}{C_{L_V} + 2C_{L_e}} \tag{6.4,26}$$

Depending on the sign of C_{m_V}, h_s may be greater or less than h_n. In terms of h_s, (6.4,24) can be rewritten as

$$\left(\frac{d\delta_{e_{\text{trim}}}}{d\hat{V}}\right)_\pi = \frac{C_{L_\alpha}}{\Delta}(C_{L_V} + 2C_{L_e})(h - h_s) \tag{6.4,27}$$

$(h - h_s)$ is the "stability margin," which may be greater or less than the static margin.

FLIGHT DETERMINATION OF h_n AND h_s

For the general case, (6.3,19) suggests that the measurement of h_n requires the measurement of C_{m_α} and C_{L_α}. Flight measurements of aerodynamic derivatives such as these can be made by dynamic techniques. However, in the simpler case when the complications presented by propulsive, compressibility, or aeroelastic effects are absent, then the relations implicit in Figs. 6.17 and 6.18 lead to a means of finding h_n from the elevator trim curves. In that case all the coefficients of (6.4,13) are constants, and

$$\frac{d\delta_{e_{\text{trim}}}}{dC_{L_{\text{trim}}}} = -\frac{C_{m_\alpha}}{\Delta} \tag{6.4,28}$$

or $$\frac{d\delta_{e_{\text{trim}}}}{dC_{L_{\text{trim}}}} = -\frac{C_{L_\alpha}}{\Delta}(h - h_n) \tag{6.4,29}$$

Thus measurements of the slope of $\delta_{e_{\text{trim}}}$ vs. $C_{L_{\text{trim}}}$ at various C.G. positions produce a curve like that of Fig. 6.20, in which the intercept on the h axis is the required N.P.

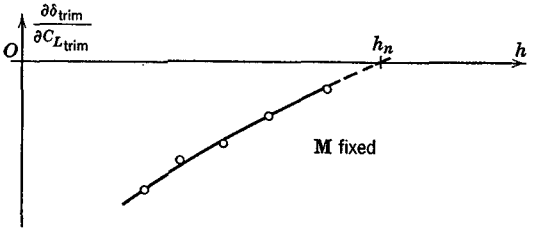

FIG. 6.20 Determination of stick-fixed neutral point from flight test.

When speed effects are present, it is clear from (6.4,27) that a plot of $(d\delta_{e_{trim}}/d\hat{V})_x$ against h will determine h_s as the point where the curve crosses the h axis.

6.5 CONTROL HINGE MOMENT

The aerodynamic forces on any control surface produce a moment about the hinge. Figure 6.21 shows a typical tail surface incorporating an elevator with a tab. The tab usually exerts a negligible effect on the lift of the aerodynamic surface to which it is attached, although its influence on the hinge moment is large.

The coefficient of elevator hinge moment is defined by

$$C_{he} = \frac{H_e}{\frac{1}{2}\rho V^2 S_e \bar{c}_e}$$

Here H_e is the moment, about the elevator hinge line, of the aerodynamic forces on the elevator and tab, S_e is the area of that portion of the elevator and tab that lies *aft of the elevator hinge line*, and $\bar{c}_e$ is a mean chord of the same portion of the elevator and tab. Sometimes $\bar{c}_e$ is taken to be the geometric mean value, i.e. $\bar{c}_e = S_e/2s_e$, and other times it is the root-mean square of c_e. The taper of elevators is usually slight, and the difference between the two values is generally small. The reader is cautioned to note which definition is employed when using reports on experimental measurements of C_{he}.

Of all the aerodynamic parameters required in stability and control analysis, the hinge-moment coefficients are most difficult to determine with precision. A large number of geometrical parameters influence these coefficients, and the range of design configurations is wide. Scale effects tend to be larger than for many other parameters, owing to the sensitivity of the hinge moment to the state of the boundary layer at the trailing edge. Two-dimensional airfoil theory shows that the hinge moment of simple flap controls

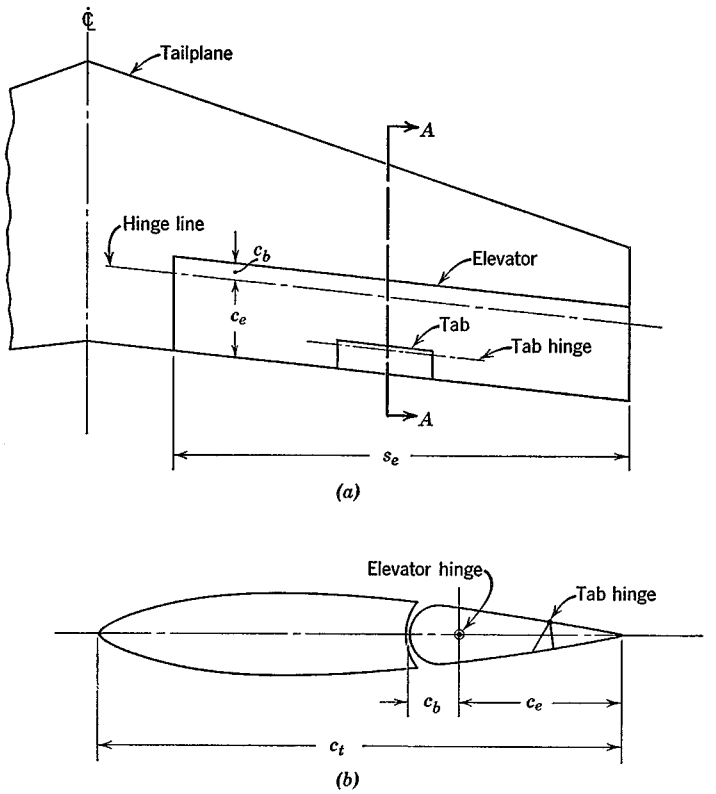

FIG. 6.21 Elevator and tab geometry. (a) Plan view. (b) Section A–A.

is linear with angle of attack and control angle in both subsonic and supersonic flow.

The normal-force distributions typical of subsonic flow associated with changes in α and δ are shown qualitatively in Fig. 6.22. The force acting on the movable flap has a moment about the hinge that is quite sensitive to its location. Ordinarily the hinge moments in both cases (a) and (b) shown are negative.

In many practical cases it is a satisfactory engineering approximation to assume that for finite surfaces C_{he} is a linear function of α_s, δ_e, and δ_t. The reader should note however that there are important exceptions in which strong nonlinearities are present. An example is the Frise aileron, shown with a typical C_h curve, in Fig. 6.23.

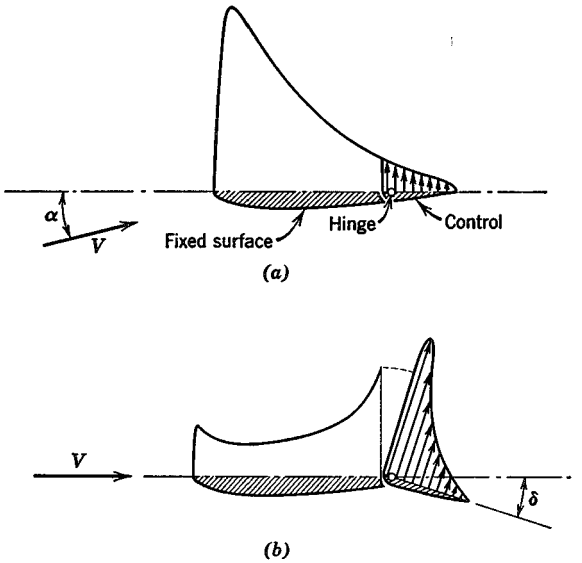

FIG. 6.22 Normal-force distribution over control surface at subsonic speed. (*a*) Force distribution over control associated with α at $\delta = 0$. (*b*) Force distribution over control associated with δ at zero α.

We assume that C_{he} is linear, as follows,

$$C_{he} = b_0 + b_1\alpha_s + b_2\delta_e + b_3\delta_t \tag{6.5.1}$$

where

$$b_1 = \frac{\partial C_{he}}{\partial \alpha_s} = C_{he_{\alpha_s}}$$

$$b_2 = \frac{\partial C_{he}}{\partial \delta_e} = C_{he_{\delta}}$$

$$b_3 = \frac{\partial C_{he}}{\partial \delta_t} = C_{he_{\delta_t}}$$

α_s is the angle of attack of the surface to which the control is attached (wing or tail), and δ_t is the angle of deflection of the tab (positive down). The determination of the hinge moment then resolves itself into the determination of b_0, b_1, b_2, and b_3. The geometrical variables that enter are elevator chord ratio c_e/c_t, balance ratio c_b/c_e, nose shape, hinge location, gap, trailing-edge angle, and planform. When a set-back hinge is used, some of the pressure acts ahead of the hinge, and the hinge moment is less than that of a simple flap with a hinge at its leading edge. The force that the control system must

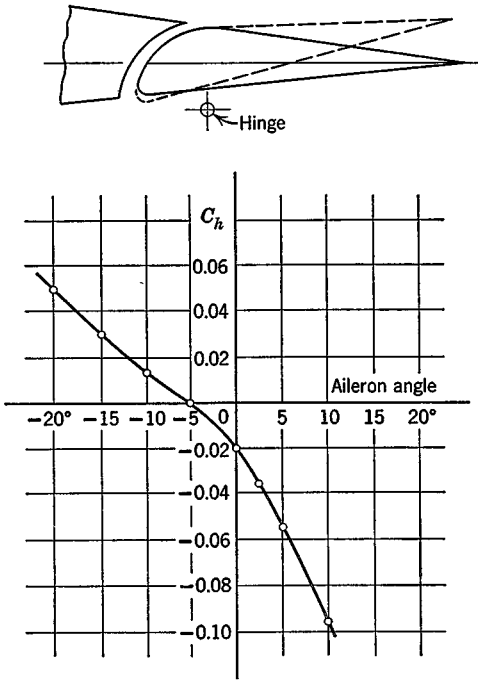

FIG. 6.23 Typical hinge moment of Frise aileron. Wing $\alpha = 2°$. R.N. $= 3.3 \times 10^6$.

exert to hold the elevator at the desired angle is in direct proportion to the hinge moment.

We shall find it convenient subsequently to have an equation like (6.5,1) with α instead of α_s. For tailless aircraft, α_s is equal to α, but for aircraft with tails, $\alpha_s = \alpha_t$. Let us write for both types

$$C_{he} = C_{he_0} + C_{he_\alpha}\alpha + b_2\delta_e + b_3\delta_t \tag{6.5,2}$$

where for tailless aircraft $C_{he_0} = b_0$, $C_{he_\alpha} = b_1$. For aircraft with tails, the relation between α and α_t is derived from (6.3,25) and (6.3,32), i.e.

$$\alpha_t = \alpha\left(1 - \frac{\partial\epsilon}{\partial\alpha}\right) - (\epsilon_0 - i_t)\left[1 - \frac{a_t}{a}\frac{S_t}{S}\left(1 - \frac{\partial\epsilon}{\partial\alpha}\right)\right] \tag{6.5,3}$$

whence it follows that for tailed aircraft, with symmetrical airfoil sections in the tail, for which $b_0 = 0$,

$$\begin{aligned} C_{he_0} &= b_1(i_t - \epsilon_0)\left[1 - \frac{a_t}{a}\frac{S_t}{S}\left(1 - \frac{\partial\epsilon}{\partial\alpha}\right)\right] \qquad (a) \\ C_{he_\alpha} &= b_1\left(1 - \frac{\partial\epsilon}{\partial\alpha}\right) \qquad (b) \end{aligned} \tag{6.5,4}$$

6.6 INFLUENCE OF A FREE ELEVATOR ON LIFT AND MOMENT

In Sec. 6.3 we have dealt with the pitch stiffness of an airplane the controls of which are fixed in position. Even with a completely rigid structure, which never exists, a manually operated control cannot be regarded as fixed. A human pilot is incapable of supplying an ideal rigid constraint. When irreversible power controls are fitted, however, the stick-fixed condition is closely approximated. A characteristic of interest from the point of view of flying qualities is the stability of the airplane when the elevator is completely free to rotate about its hinge under the influence of the aerodynamic pressures that act upon it. Normally, the stability in the control-free condition is less than with fixed controls. It is desirable that this difference

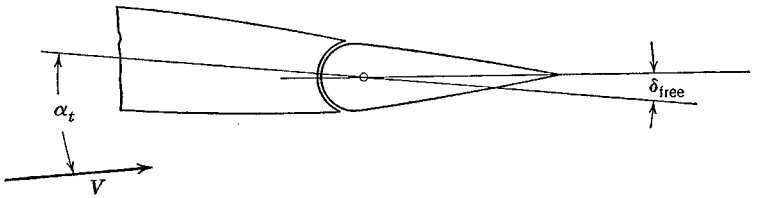

FIG. 6.24 Elevator floating angle.

should be small. Since friction is always present in the control system, the free control is never realized in practice either. However, the two ideal conditions, free control and fixed control, represent the possible extremes.

When the control is free, then $C_{he} = 0$, so that from (6.5,2)

$$\delta_{e_{\text{free}}} = -\frac{1}{b_2}(C_{he_0} + C_{he_\alpha}\alpha + b_3\delta_t) \tag{6.6,1}$$

The typical upward deflection of a free-elevator on a tail is shown in Fig. 6.24. The corresponding lift and moment are

$$\begin{aligned} C_{L_{\text{free}}} &= C_{L_\alpha}\alpha + C_{L_\delta}\delta_{e_{\text{free}}} \\ C_{m_{\text{free}}} &= C_{m_0} + C_{m_\alpha}\alpha + C_{m_\delta}\delta_{e_{\text{free}}} \end{aligned} \tag{6.6,2}$$

After substituting(6.6,1) into (6.6,2), we get

$$\begin{aligned} C_{L_{\text{free}}} &= C'_{L_0} + C'_{L_\alpha}\alpha \qquad (a) \\ C_{m_{\text{free}}} &= C'_{m_0} + C'_{m_\alpha}\alpha \qquad (b) \end{aligned} \tag{6.6,3}$$

where

$$C'_{L_0} = -\frac{C_{L_\delta}}{b_2}(C_{he_0} + b_3\delta_t) \qquad (a)$$

$$a' = C'_{L_\alpha} = C_{L_\alpha} - \frac{C_{L_\delta}C_{he_\alpha}}{b_2} \qquad (b) \qquad (6.6,4)$$

$$C'_{m_0} = C_{m_0} - \frac{C_{m_\delta}}{b_2}(C_{he_0} + b_3\delta_t) \qquad (a)$$

$$C'_{m_\alpha} = C_{m_\alpha} - \frac{C_{m_\delta}C_{he_\alpha}}{b_2} \qquad (b) \qquad (6.5,6)$$

When due consideration is given to the usual signs of the coefficients in these equations, we see that the two important gradients C_{L_α} and C_{m_α} are reduced in absolute magnitude when the control is released. This leads, broadly speaking, to a reduction of stability.

FREE-ELEVATOR FACTOR

When the elevator is part of the wing, as on a tailless aircraft, and the elevator is free, the lift-curve slope is given by (6.6,4*b*), i.e.

$$a' = a\left(1 - \frac{C_{L_\delta}b_1}{ab_2}\right) \qquad (6.6,6)$$

The factor in parentheses is the *free elevator factor* F, and normally has a value less than unity. Likewise, when the elevator is part of the tail, the floating angle can be related to α_t, viz.

$$C_{he} = b_1\alpha_t + b_2\delta_{\text{free}} + b_3\delta_t = 0$$

or

$$\delta_{e_{\text{free}}} = -\frac{1}{b_2}(b_1\alpha_t + b_3\delta_t) \qquad (6.6,7)$$

and the tail lift coefficient is

$$C'_{L_t} = a_t\alpha_t + a_e\delta_{e_{\text{free}}}$$

$$= a_t\left(1 - \frac{a_e}{a_t}\frac{b_1}{b_2}\right)\alpha_t - \frac{a_e b_3}{b_2}\delta_t \qquad (6.6,8)$$

The effective lift-curve slope is

$$\frac{\partial C'_{L_t}}{\partial \alpha_t} = Fa_t \qquad (6.6,9)$$

where $F = \left(1 - \frac{a_e}{a_t}\frac{b_1}{b_2}\right)$ is the *free-elevator factor* for a tail. If Fa_t be used in

place of a_t and a' in place of a, then all the equations given in Sec. 6.3 hold for tailed aircraft with a free elevator.

CONTROL-FREE NEUTRAL POINT

It is evident from the preceding comment that the N.P. of a tailed aircraft when the control is free is given by (6.3,36) as

$$h'_n = h_{n_{wb}} + \frac{Fa_t}{a'}\bar{V}_H\left(1 - \frac{\partial\epsilon}{\partial\alpha}\right) - \frac{1}{a'}\frac{\partial C_{m_p}}{\partial\alpha} \tag{6.6,10}$$

Alternatively, we can derive the N.P. location from (6.6,5*b*), for we know from (6.3,19) that

$$C'_{m_\alpha} = C'_{L_\alpha}(h - h'_n) \qquad (a)$$

or

$$(h - h'_n) = \frac{C'_{m_\alpha}}{C'_{L_\alpha}} = \frac{1}{a'}\left(C_{m_\alpha} - \frac{C_{m_\delta}C_{h_{e_\alpha}}}{b_2}\right) \tag{6.6,11}$$

$$= \frac{1}{a'}\left[a(h - h_n) - \frac{C_{m_\delta}C_{h_{e_\alpha}}}{b_2}\right] \qquad (b)$$

Since C_{m_δ} is of different form for the two main types of aircraft, we proceed separately below.

Tailless Aircraft. C_{m_δ} is given by (6.4,9) and $C_{h_{e_\alpha}} = b_1$. When these are substituted into (6.6,11) the result is

$$h - h'_n = \frac{a}{a'}(h - h_n) - \frac{b_1}{a'b_2}C_{L_\delta}(h - h_n) - \frac{b_1}{a'b_2}\frac{\partial C_{m_{a.c.}}}{\partial\delta_e}$$

$$= \frac{(h - h_n)}{a'}\left(a - \frac{b_1}{b_2}C_{L_\delta}\right) - \frac{b_1}{a'b_2}\frac{\partial C_{m_{a.c.}}}{\partial\delta_e}$$

By virtue of (6.6,6) this becomes

$$h - h'_n = h - h_n - \frac{b_1}{a'b_2}\frac{\partial C_{m_{a.c.}}}{\partial\delta_e}$$

or

$$h'_n = h_n + \frac{b_1}{a'b_2}\frac{\partial C_{m_{a.c.}}}{\partial\delta_e} \tag{6.6,12}$$

Tailed Aircraft. C_{m_δ} is given by (6.4,8), so (6.6,11) becomes for this case

$$(h - h'_n) = \frac{a}{a'}(h - h_n) - \frac{C_{h_{e_\alpha}}}{a'b_2}C_{L_\delta}(h - h_{n_{wb}}) + \frac{C_{h_{e_\alpha}}}{a'b_2}a_e\bar{V}_H$$

Using (6.6,4*b*) this becomes

$$h - h'_n = h - \frac{1}{a'}\left(ah_n - \frac{C_{he_\alpha}C_{L_\delta}}{b_2}h_{n_{wb}}\right) + \frac{C_{he_\alpha}}{a'b_2}a_e\bar{V}_H$$

We replace $h_{n_{wb}}$ by $(h_{n_{wb}} - h_n) + h_n$ to get

$$h'_n = h_n + \frac{C_{he_\alpha}C_{L_\delta}}{b_2a'}(h_n - h_{n_{wb}}) - \frac{a_eC_{he_\alpha}}{a'b_2}\bar{V}_H$$

Finally, using (6.4,8) for C_{L_δ}, and (6.5,4) for C_{he_α}, we get

$$h'_n = h_n - \frac{a_e}{a'}\frac{b_1}{b_2}\left(1 - \frac{\partial\epsilon}{\partial\alpha}\right)\left(-(h_n - h_{n_{wb}})\frac{S_t}{S} + \bar{V}_H\right) \qquad (6.6,13)$$

The difference $(h'_n - h)$ is called the *control-free static margin*, K'_n. When representative numerical values are used in (6.6,13) one finds that $h_n - h'_n$ may be typically about 0.08. This represents a substantial forward movement of the N.P., with consequent reduction of static margin, pitch stiffness, and stability.

6.7 THE USE OF TABS

TRIM TABS

In order to fly at a given speed, or C_L, it has been shown in Sec. 6.4 that a certain elevator angle $\delta_{e_{\text{trim}}}$ is required. When this differs from the free-floating angle $\delta_{e_{\text{free}}}$, a force is required to hold the elevator. When flying for long periods at a constant speed, it is very fatiguing for the pilot to maintain such a force. The trim tabs are used to relieve the pilot of this load by causing $\delta_{e_{\text{trim}}}$ and $\delta_{e_{\text{free}}}$ to coincide. The trim-tab angle required is calculated below.

When C_{he} and C_m are both zero, the tab angle is obtained from (6.5,2) as

$$\delta_{t_{\text{trim}}} = -\frac{1}{b_3}(C_{he_0} + C_{he_\alpha}\alpha_{\text{trim}} + b_2\delta_{e_{\text{trim}}}) \qquad (6.7,1)$$

On substituting from (6.4,13), (which implies neglecting $\partial C_m/\partial\delta_t$) we get

$$\delta_{t_{\text{trim}}} = -\frac{1}{b_3}\left[C_{he_0} + \frac{C_{m_0}}{\Delta}(C_{he_\alpha}C_{L_\delta} - b_2C_{L_\alpha}) + \frac{C_{L_{\text{trim}}}}{\Delta}(C_{he_\alpha}C_{m_\delta} - b_2C_{m_\alpha})\right]$$

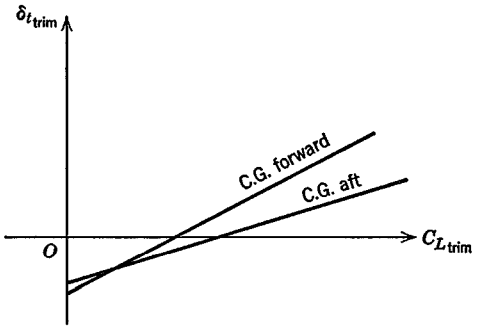

FIG. 6.25 Tab angle to trim.

which is linear in $C_{L_{trim}}$ for constant h, as shown in Fig. 6.25. The dependence on h is simple, since from (6.6,11) we find that

$$(C_{he_\alpha}C_{m_\delta} - b_2C_{m_\alpha}) = -a'b_2(h - h'_n)$$

and hence

$$\delta_{t_{trim}} = -\frac{1}{b_3}\left[C_{he_0} + \frac{C_{m_0}}{\Delta}(C_{he_\alpha}C_{L_\delta} - b_2C_{L_\alpha}) - \frac{a'b_2}{\Delta}(h - h'_n)C_{L_{trim}}\right] \quad (6.7,2)$$

This result applies to both tailed and tailless aircraft, provided only that the appropriate values of the coefficients are used. It should be realized, of course, in reference to Fig. 6.25, that each different $C_{L_{trim}}$ in a real flight situation corresponds to a different set of values of $\mathbf{M}$, $\frac{1}{2}\rho V^2$, and C_T, so that in general the coefficients of (6.7,2) vary with C_L, and the graphs will depart from straight lines.

Equation (6.7,2) shows that the slope of the δ_t vs $C_{L_{trim}}$ curve is proportional to the control-free static margin. When the coefficients are constants, we have

$$\frac{d\delta_{t_{trim}}}{dC_{L_{trim}}} = \frac{b_2}{b_3}\frac{a'}{\Delta}(h - h'_n) \quad (6.7,3)$$

The similarity between (6.7,3) and (6.4,13c) is noteworthy, i.e. the trim-tab slope bears the same relation to the control-free N.P. as the elevator angle slope does to the control-fixed N.P. It follows that flight determination of h'_n from measurements of $d\delta_{t_{trim}}/dC_{L_{trim}}$ is possible subject to the same restrictions as discussed in relation to the measurement of h_n on p. 221.

GEARED TABS

The coefficient b_2 dominates the hinge moment of a control, and hence the control force. It gives the rate at which the hinge moment increases with

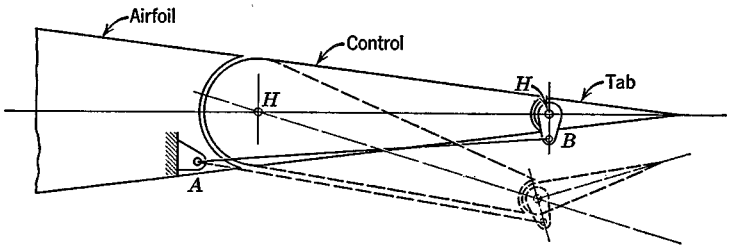

FIG. 6.26 Geometry of geared tab.

control angle. The need for reduction of b_2 by aerodynamic means was referred to in Sec. 6.5. One such means, which is very effective, is the geared or servo tab. The geometry of such a tab is illustrated in Fig. 6.26. The angle of the tab relative to the control surface is determined by the rigid link AB. When arranged as shown, downward movement of the control is accompanied by an automatic upward movement of the tab. The hinge moment caused by the tab is then of the sense which assists the control movement. If B were moved to the upper surface of the tab, so that AB crossed HH, then the opposite effect would be obtained. This arrangement, known as an antiservo, or antibalance tab can be used when a control is otherwise overbalanced, or too closely balanced. It provides a means of achieving a zero or positive b_1 without any detrimental effect on b_2, as follows. The balance, c_b (Fig. 6.21), is chosen large enough so that b_1 becomes zero or positive. The control will then have b_2 either too small or even positive. This is then corrected by introducing an antiservo geared tab.

Suppose that, when the elevator moves through an angle δ_e, the tab displacement is $-\gamma\delta_e$. γ, called the "tab gearing," is positive for a servo tab and negative for an antiservo tab. The hinge-moment coefficient will then be

$$\begin{aligned} C_{he} &= b_0 + b_1\alpha_t + b_2\delta_e + b_3\delta_t \\ &= b_0 + b_1\alpha_t + b_2\left(1 - \frac{b_3}{b_2}\gamma\right)\delta_e \end{aligned} \tag{6.7,6}$$

The servo tab thus in effect reduces the value of b_2 by the factor

$$\left(1 - \frac{b_3}{b_2}\gamma\right).$$

SPRING TABS

The effect of the "speed-squared law" on control forces at high speeds has led to the development of the "spring tab." The effect of this device is to

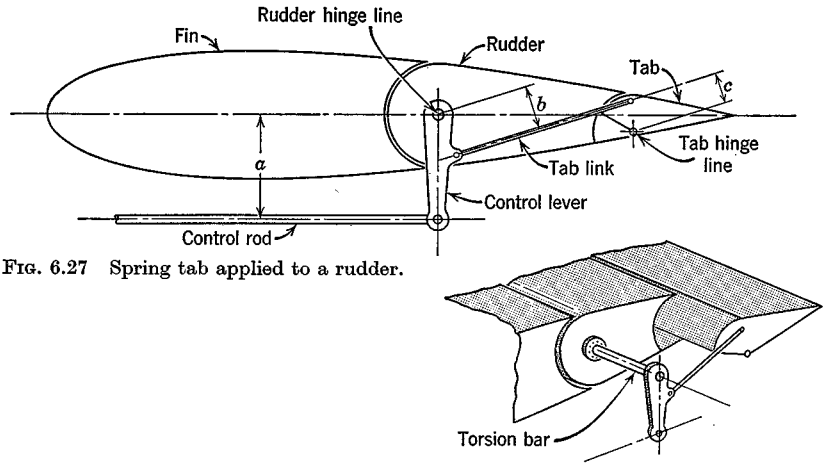

FIG. 6.27 Spring tab applied to a rudder.

mitigate the influence of speed. Figure 6.27 shows the principle. The system functions as follows. When a force is applied through the control rod to the control lever, the latter rotates through some angle θ. The control surface would rotate through the same angle, and the tab not move at all, if the control lever were *rigidly* connected to the surface. However, this is not so, and the torsion bar twists through some angle ϕ. The surface displacement is then $\delta = \theta - \phi$. The movement of the control lever *relative* to the surface (angle ϕ), causes the tab link to move and deflect the tab, just as though it were a geared tab. Now with all other factors equal, an increase in speed will require an increase in the control-rod load to hold the same surface angle. But an increase in this force introduces extra twist into the torsion bar, and hence increases the tab deflection. Thus, as the speed increases, an increasing *proportion* of the hinge moment is balanced by the tab, and a decreasing proportion by the pilot or control system. In effect, the system behaves like a geared servo tab, the gearing of which increases with speed.

SERVO TABS

When the pilot's control force acts only to deflect the tab, and not the main surface, it is designated a *servo* tab. This result is attained if the torsion spring of Fig. 6.27 is replaced by a free hinge. The control lever then becomes an idler and the force in the control rod is simply the reaction to the tab hinge moment, which is of course relatively small. The angle through which the control surface deflects is then governed by the kinematics of the linkage,

and the equilibrium of aerodynamic and control rod moments about the main surface hinge.

Both spring tabs and servo tabs are effective devices for reducing control forces on large high-speed airplanes. However, both add an additional degree of freedom to the control system dynamics, and this is a potential source of trouble due to vibration or flutter.

6.8 CONTROL FORCE TO TRIM

One of the important handling characteristics of an airplane is the force required of the pilot to hold the elevator at the angle required for trim, and the manner in which this force varies with speed. If friction in the control system be neglected, the stick force is simply related to the elevator hinge moment. The hinge moment itself, as can be deduced from the definition of C_{he} is roughly proportional to the square of the speed, and the cube of the airplane size. Large high-speed airplanes therefore have serious control problems, since the forces required may be too large for a human pilot to supply. Much development has gone into attempts to arrive at purely aerodynamic solutions to this difficulty. The devices employed include various forms of nose balance, and the use of geared and spring tabs. Closely balanced controls have experienced difficulties because of the sensitivity of the hinge moment to such factors as nose shape and gap, which are inevitably subject to variations in manufacture.

Another approach is to relieve the pilot of some or all of the aerodynamic load through the use of power controls. These may be designed so that the pilot supplies a fixed proportion of the control force, the power system supplying the remainder. A system of this kind is illustrated in Fig. 11.4. With such "ratio"-type controls, the *feel* has the same character as when power is absent, i.e. the stick forces vary with speed, and in maneuvers, in the same way. Alternatively, the power controls may be irreversible, in that none of the aerodynamic load is carried directly to the pilot. Such systems are fitted with devices that produce a synthetic feel at the stick. The stick-force characteristics can then be made virtually whatever the designer wishes. Other classes of control system provide the pilot with power amplification rather than force amplification, i.e. the power system acts so as to increase the control deflection above that which would follow from the unpowered kinematics. This has the same net effect as the ratio-type control, however, since a greater mechanical advantage can then be supplied to the pilot than would be possible without the power boost. A detailed discussion of a variety of control concepts and mechanisms is given by Kolk (ref. 6.11), to which the student is recommended.

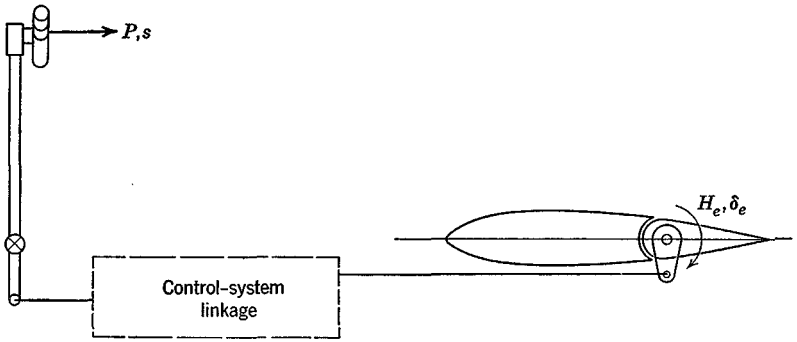

FIG. 6.28 Schematic diagram of an elevator control system.

Figure 6.28 is a schematic representation of a reversible control system. The box denoted "control system linkage" represents any assemblage of levers, rods, pulleys, cables, and power-boost elements that comprise a general control system. We assume that the elements of the linkage and the structure to which it is attached are ideally rigid, so that no strain energy is stored in them. We also neglect friction, and assume that the movement of the control is slow enough that the automatic power elements have nearly zero error (e.g. the link AB in Fig. 11.4 does not rotate appreciably). The system then has one degree of freedom. P is the force applied by the pilot, (positive to the rear) s is the displacement of the hand grip, and the work done by the power boost system is W_b. Considering a small quasistatic displacement from equilibrium (i.e. no kinetic energy appears in the control system), conservation of energy gives

$$P\,ds + dW_b + H_e\,d\delta_e = 0 \tag{6.8,1}$$

or

$$P = -\frac{dW_b}{ds} - \frac{d\delta_e}{ds}H_e$$

Now the nature of ratio or power boost controls is such that dW_b/ds is proportional to P or H_e. Hence we can write

$$P = (G_1 - G_2)H_e \tag{6.8,2}$$

where $G_1 = -\dfrac{d\delta_e}{ds} > 0$, the *elevator gearing* (rad/ft)

and $G_2 = \dfrac{dW_b/ds}{H_e}$, the *boost gearing* ($\text{ft}^{-1}$)

In the example of Fig. 11.4, θ_J is zero in a steady state, and clearly the work done by the hydraulic system is $dW_b = \text{const} \times J\, ds$, where the constant derives from the various lever ratios; and $J = \text{const} \times H_e$. Hence $dW_b/ds = \text{const} \times H_e$. The latter constant, easily found from the geometry, is G_2. Finally, we write

$$P = GH_e \tag{6.8,3}$$

where $G = G_1 - G_2$. For fixed G_1, i.e. *for a given movement of the control surface to result from a given displacement of the pilot's control*, then the introduction of power boost is seen to reduce G and hence P. G may be designed to be constant over the whole range of δ_e, or it may, by the use of special linkages and power systems, be made variable in almost any desired manner.

Introduction of the hinge-moment coefficient gives the expression for P as

$$P = GC_{he}S_e\bar{c}_e\tfrac{1}{2}\rho V^2 \tag{6.8,4}$$

and the variation of P with flight speed depends on both V^2 and on how C_{he} varies with speed.

The value of C_{he} at trim for arbitrary tab angle is given by

$$C_{he} = C_{he_0} + C_{he_\alpha}\alpha_{\text{trim}} + b_2\delta_{e_{\text{trim}}} + b_3\delta_t \tag{6.8,5}$$

From (6.7,1) we see that

$$C_{he} = b_3(\delta_t - \delta_{t_{\text{trim}}}) \tag{6.8,6}$$

i.e. the hinge moment is zero when $\delta_t = \delta_{t_{\text{trim}}}$ as expected, and linearly proportional to the difference. From (6.7,2) then the hinge moment is

$$C_{he} = b_3\delta_t + C_{he_0} + \frac{C_{m_0}}{\Delta}(C_{he_\alpha}C_{L_\delta} - b_2C_{L_\alpha}) - \frac{a'b_2}{\Delta}(h - h'_n)C_{L_{\text{trim}}} \tag{6.8,7}$$

Except at hypervelocities, the lift equals the weight in horizontal flight, so that

$$C_{L_{\text{trim}}} = \frac{w}{\tfrac{1}{2}\rho V^2} \tag{6.8,8}$$

where $w = W/S$, the "wing loading." When (6.8,7 and 8) are substituted into (6.8,4) the result obtained is

$$P = A + B\tfrac{1}{2}\rho V^2 \tag{6.8,9}$$

where

$$A = -GS_e\bar{c}_e w\frac{a'b_2}{\Delta}(h - h'_n)$$

$$B = GS_e\bar{c}_e\left[b_3\delta_t + C_{he_0} + \frac{C_{m_0}}{\Delta}(C_{he_\alpha}C_{L_\delta} - b_2C_{L_\alpha})\right]$$

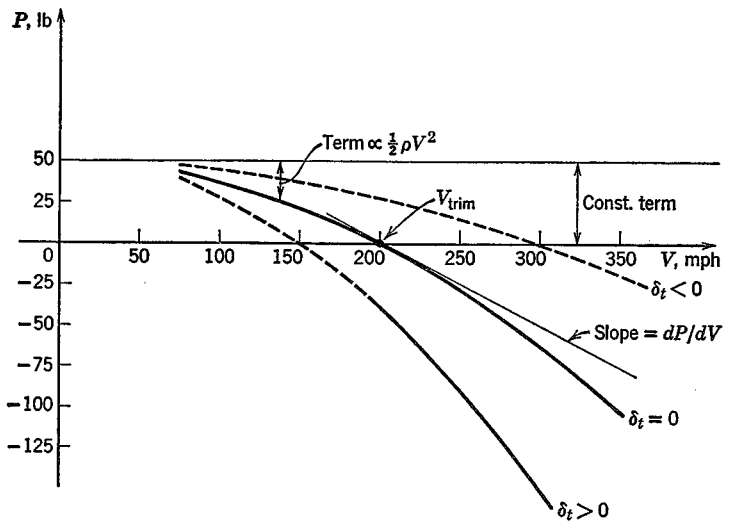

FIG. 6.29 Example of low-speed control force.

The typical parabolic variation of P with V when the aerodynamic coefficients are all constant, is shown in Fig. 6.29. The following conclusions may be drawn.

1. Other things remaining equal, $P \propto S_e \bar{c}_e$, i.e. to the cube of the airplane size. This indicates a very rapid increase in stick forces with size.
2. P is directly proportional to the gearing G.
3. The C.G. position only affects the constant term (apart from a second-order influence on C_{m_δ}). A forward movement of the C.G. produces an upward translation of the curve.
4. The weight of the airplane enters only through the wing loading, a quantity that tends to be constant for airplanes serving a given function, regardless of weight. An increase in wing loading has the same effect as a forward shift of the C.G.
5. The part of P that varies with $\frac{1}{2}\rho V^2$ decreases with height, and increases as the speed squared.
6. Of the terms contained in B, none can be said in general to be negligible. All of them are "built-in" constants except for δ_t.
7. The effect of the trim tab is to change the coefficient of $\frac{1}{2}\rho V^2$, and hence the curvature of the parabola in Fig. 6.29. Thus it controls the intercept of the curve with the V axis. This intercept is denoted V_{trim}; it is the speed for zero stick force.

6.9 CONTROL FORCE GRADIENT

It was pointed out in Sec. 6.7 how the trim tabs can be used to reduce the stick force to zero. A significant handling characteristic is the gradient of P with V at $P = 0$. The manner in which this changes as the C.G. is moved aft is illustrated in Fig. 6.30. The trim tab is assumed to be set so as to keep V_{trim} the same. The gradient dP/dV is seen to decrease in magnitude as the C.G.

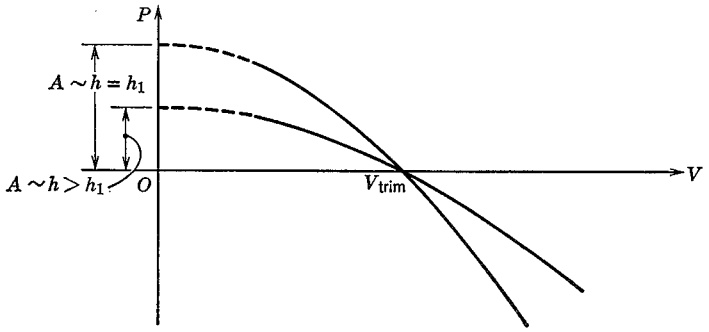

FIG. 6.30 Effect of C.G. location on control-force gradient at fixed trim speed.

moves backward. When it is at the control-free neutral point, $A = 0$ for aircraft with or without tails, and, under the stated conditions, the P–V graph becomes a straight line lying on the V axis. This is an important characteristic of the control-free N.P.; i.e. when the C.G. is at that point, no force is required to change the trim speed.

A quantitative analysis of the control-force gradient follows.

The force is given by (6.8,9). From it we obtain the derivative

$$\frac{\partial P}{\partial V} = B\rho V$$

At the speed V_{trim}, $P = 0$, and $B = -A/\frac{1}{2}\rho V^2_{\text{trim}}$, whence

$$\frac{\partial P}{\partial V} = -\frac{2A}{V_{\text{trim}}} \tag{6.9,1}$$

A is given following (6.8,9). Substituting the value into (6.9,1) we get

$$\frac{\partial P}{\partial V} = 2GS_e\bar{c}_e \frac{a'b_2}{\Delta} \frac{w}{V_{\text{trim}}} (h - h'_n) \tag{6.9,2}$$

From (6.9,2) we deduce the following:

1. The control-force gradient is proportional to $S_e\bar{c}_e$; i.e. to the cube of airplane size.
2. It is inversely proportional to the trim speed; i.e. it increases with decreasing speed. This effect is also evident in Fig. 6.29.
3. It is directly proportional to wing loading.
4. It is *independent* of height for a given true speed, but *decreases* with height for a fixed V_E.
5. It is directly proportional to the control-free static margin.

Thus, in the absence of compressibility, the elevator control will be "heaviest" at sea-level, low-speed, forward C.G. and maximum weight.

6.10 MANEUVERABILITY—ELEVATOR ANGLE AND CONTROL FORCE PER g

In this section we investigate the elevator angle and control force required to hold a vehicle in a steady pull-up with load factor† n (Fig. 6.31). The concepts discussed here were introduced by S. B. Gates, ref. 6.12. The flight-path tangent is horizontal at the point under analysis, and hence the net normal force is $L - W = (n - 1)W$ vertically upward. The normal acceleration is therefore $(n - 1)g$.

When the vehicle is in straight horizontal flight at the same speed and altitude, the elevator angle and control force to trim are δ_e and P, respectively. When in the pull-up, these are changed to $\delta_e + \Delta\delta_e$ and $P + \Delta P$. The ratios $\Delta\delta_e/(n - 1)$ and $\Delta P/(n - 1)$ are known, respectively, as the *elevator angle per g*, and the *control force per g*. These two quantities provide a measure of the maneuverability of the vehicle; the smaller they are, the more maneuverable it is.

The angular velocity of the airplane is fixed by the speed and normal acceleration (Fig. 6.31).

$$q = \frac{(n - 1)g}{V} \tag{6.10,1}$$

As a consequence of this angular velocity, the field of the relative air flow past the airplane is curved. It is as though the machine were attached to the end of a whirling arm pivoted at O. This curvature of the flow field alters the pressure distribution and the aerodynamic forces from their values in translational flight. The change is large enough that it must be taken into account in the equations describing the motion.

† The load factor is the ratio of lift to weight, $n = L/W$. It is unity in straight horizontal flight.

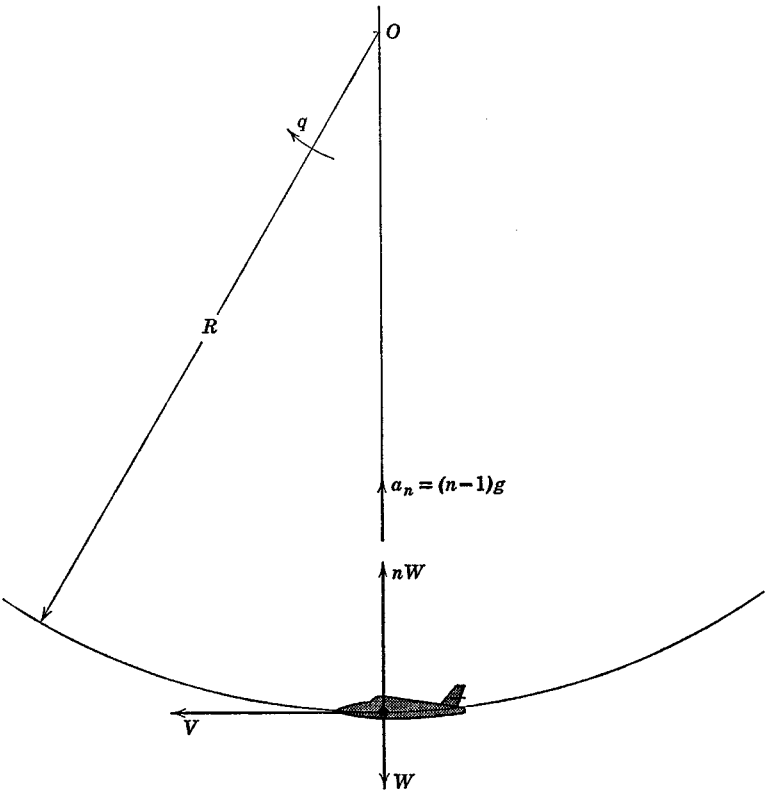

FIG. 6.31 Airplane in a pull-up.

We assume that q and the increments $\Delta\alpha$, $\Delta\delta_e$ etc. between the rectilinear and curved flight conditions are small, so that the increments in lift and moment may be written

$$\Delta C_L = C_{L_\alpha}\Delta\alpha + C_{L_q}\hat{q} + C_{L_\delta}\Delta\delta_e \tag{6.10,2}$$

$$\Delta C_m = C_{m_\alpha}\Delta\alpha + C_{m_q}\hat{q} + C_{m_\delta}\Delta\delta_e \tag{6.10,3}$$

where $\hat{q} = q\bar{c}/2V$, $C_{L_q} = \partial C_L/\partial\hat{q}$, $C_{m_q} = \partial C_m/\partial\hat{q}$ (see Sec. 5.13). The q derivatives are discussed in Sec. 7.9. In this form, these equations apply to any configuration. From (6.10,1) we get

$$\hat{q} = (n-1)\frac{g\bar{c}}{2V^2}$$

which is more conveniently expressed in terms of C_W and μ (see Table 5.1), i.e.

$$\hat{q} = (n-1)\frac{C_W}{2\mu} \tag{6.10,4}$$

Since the curved flight condition is also assumed to be steady, i.e. without angular acceleration, then $\Delta C_m = 0$. Finally, we can relate ΔC_L to n thus:

$$\Delta C_L = \frac{nW - W}{\frac{1}{2}\rho V^2 S} = (n-1)C_W \tag{6.10,5}$$

Equations (6.10,2 and 3) therefore become

$$(n-1)C_W = C_{L_\alpha}\Delta\alpha + (n-1)C_{L_q}\frac{C_W}{2\mu} + C_{L_\delta}\Delta\delta_e$$

$$0 = C_{m_\alpha}\Delta\alpha + (n-1)C_{m_q}\frac{C_W}{2\mu} + C_{m_\delta}\Delta\delta_e$$

which are readily solved for $\Delta\alpha$ and $\Delta\delta_e$ to yield the elevator angle per g

$$\frac{\Delta\delta_e}{n-1} = -\frac{C_W}{\Delta}\left[C_{m_\alpha} - \frac{1}{2\mu}(C_{L_q}C_{m_\alpha} - C_{L_\alpha}C_{m_q})\right] \quad (a)$$

and

$$\frac{\Delta\alpha}{n-1} = \frac{1}{C_{L_\alpha}}\left(C_W - C_{L_q}\frac{C_W}{2\mu} - C_{L_\delta}\frac{\Delta\delta_e}{n-1}\right) \quad (b) \tag{6.10,6}$$

where Δ is given by (6.4,13). As has been shown in Sec. 6.4 Δ does not depend on C.G. position, hence the variation of $\Delta\delta_e/(n-1)$ with h is provided by the terms in the numerator. Writing $C_{m_\alpha} = C_{L_\alpha}(h - h_n)$ (6.10,6*a*) becomes

$$\frac{\Delta\delta_e}{n-1} = -\frac{C_W C_{L_\alpha}(2\mu - C_{L_q})}{2\mu\Delta}\left(h - h_n + \frac{C_{m_q}}{2\mu - C_{L_q}}\right) \tag{6.10,7}$$

The derivatives C_{L_q} and C_{m_q} both in general vary with h, the former linearly, the latter quadratically, (see Sec. 7.9). Thus (6.10,7), although it appears to be linear in h, is not exactly so. For airplanes with tails, C_{L_q} can usually be neglected altogether when compared with 2μ, and the variation of C_{m_q} with h is slight. The equation is then very nearly linear with h, as illustrated in Fig. 6.32. For tailless airplanes, the variation may show more curvature. The point where $\Delta\delta_e/(n-1)$ is zero is called the *control-fixed maneuver point*, and is denoted by h_m, as shown. From (6.10,7) we see that

$$h_m = h_n - \frac{C_{m_q}(h_m)}{2\mu - C_{L_q}(h_m)} \tag{6.10,8}$$

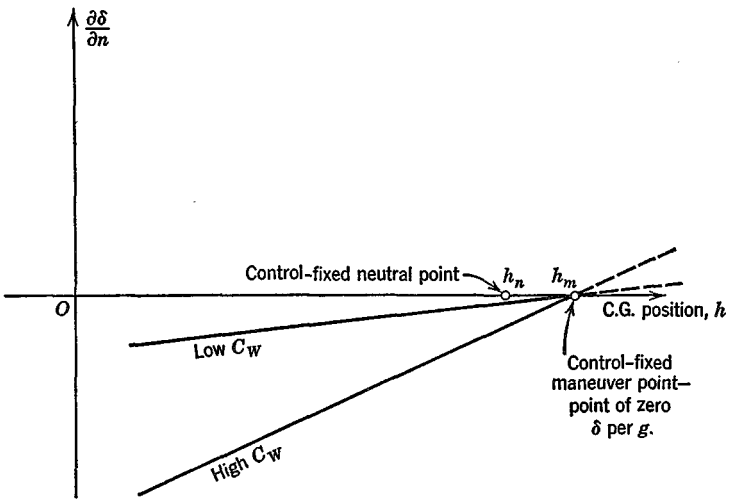

FIG. 6.32 Elevator angle per g.

where $C_{m_q}(h_m)$ and $C_{L_q}(h_m)$ are the values of these two derivatives evaluated for $h = h_m$. When C_{m_q} and C_{L_q} can be assumed to be independent of h, (6.10,7) reduces to

$$\frac{\Delta\delta_e}{n-1} = -\frac{C_W C_{L_\alpha}(2\mu - C_{L_q})}{2\mu\Delta}(h - h_m) \tag{6.10,9}$$

The difference $(h_m - h)$ is known as the *control-fixed maneuver margin.*

CONTROL FORCE PER g

From (6.8,4) we get the incremental control force

$$\Delta P = GS_e\bar{c}_e \tfrac{1}{2}\rho V^2 \Delta C_{he} \tag{6.10,10}$$

C_{he} is given for rectilinear flight by (6.5,2). Since it too will in general be influenced by q, we write for the incremental value ($\Delta\delta_t = 0$)

$$\Delta C_{he} = C_{he_\alpha}\Delta\alpha + C_{h_{\hat{q}}}\hat{q} + b_2\Delta\delta_e \tag{6.10,11}$$

The derivative $C_{h_{\hat{q}}}$ is discussed in Sec. 7.9. Using (6.10,4) and (6.10,6*b*), (6.10,11) is readily expanded to give

$$\frac{\Delta C_{he}}{n-1} = \frac{C_W}{2\mu C_{L_\alpha}}[(2\mu - C_{L_q})C_{he_\alpha} + C_{h_{\hat{q}}} C_{L_\alpha}] + \frac{\Delta\delta_e}{n-1}\left(b_2 - \frac{C_{L_\delta}C_{he_\alpha}}{C_{L_\alpha}}\right) \tag{6.10,12}$$

From (6.6,4) we note that the last parenthetical factor is $b_2 C'_{L_\alpha}/C_{L_\alpha}$ or $b_2 a'/a$. For $\Delta\delta_e$ we use the approximation (6.10,9) in the interest of simplicity and the result for ΔC_{he} after some algebraic reduction is

$$\frac{\Delta C_{he}}{n-1} = -\frac{C_W}{2\mu}\frac{a'b_2}{\Delta}(2\mu - C_{L_q})(h - h'_m) \qquad (6.10,13)$$

where

$$h'_m = h_m + \frac{\Delta}{a'b_2}\left(\frac{C_{he_\alpha}}{C_{L_\alpha}} + \frac{C_{h_q}}{2\mu - C_{L_q}}\right) \qquad (6.10,14)$$

In keeping with earlier nomenclature, h'_m is the *control-free maneuver point* and $(h'_m - h)$ is the corresponding *margin*. On noting that $C_W \frac{1}{2}\rho V^2$ is the wing loading w, we find the control force per g is given by

$$Q = \frac{\Delta P}{n-1} = -GS_e\bar{c}_e w \frac{a'b_2}{2\mu\Delta}(2\mu - C_{L_q})(h - h'_m) \qquad (6.10,15)$$

Note that this result applies to both tailed and tailless aircraft provided that the appropriate derivatives are used. The following conclusions may be drawn from (6.10,15).

1. The control force per g increases linearly from zero as the C.G. is moved forward from the control-free maneuver point, and reverses sign for $h > h'_m$.

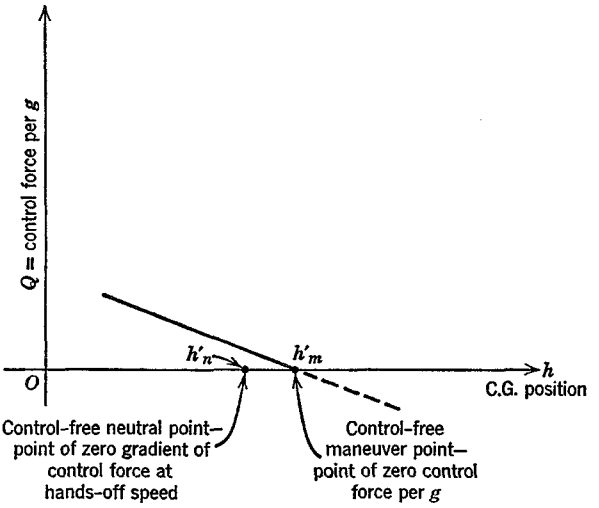

FIG. 6.33 Control force per g.

2. It is directly proportional to the wing loading. High wing loading produces "heavier" controls.
3. For similar aircraft of different size but equal wing loading, $Q \propto S_e \bar{c}_e$; i.e. to the cube of the linear size.
4. Neither C_L nor V enters the expression for Q explicitly. Thus, apart from **M** and Reynolds number effects, Q is independent of speed.
5. The factor μ which appears in (6.10,14) causes the separation of the control-free neutral and maneuver points to vary with altitude, size, and wing loading, in the same manner as the interval $(h_m - h_n)$.

Figure 6.33 shows a typical variation of Q with C.G. position. The statement made above that the control force per g is "reversed" when $h > h'_m$ must be interpreted correctly. In the first place this does not necessarily mean a reversal of control movement per g, for this is governed by the elevator angle per g. If $h'_m < h < h_m$, then there would be reversal of Q without reversal of control movement. In the second place, the analysis given applies only to the *steady state* at load factor n, and throws no light whatsoever on the transition between unaccelerated flight and the pull-up condition. No matter what the value of h, the *initial* control force and movement required to start the maneuver will be in the normal direction (backward for a pull-up), although one or both of them may have to be reversed before the final steady state is reached.

Longitudinal aerodynamic characteristics—part 2

CHAPTER 7

7.1 BOB WEIGHTS AND SPRINGS

The control-force characteristics of manual-control systems can be modified by the introduction of weights and springs, as illustrated schematically in Fig. 7.1. When a spring, or bungee, is used as in Fig. 7.1*b*, it is

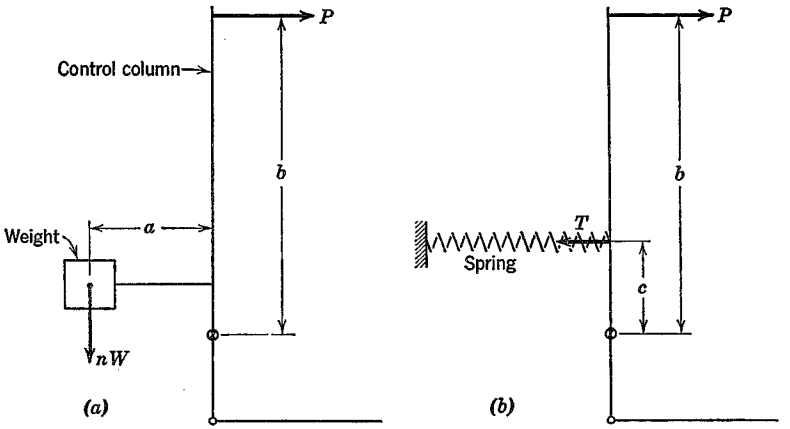

FIG. 7.1 Bob weight and spring. (*a*) Bob weight. (*b*) Spring.

usually so designed that it exerts a nearly constant force on the control column. Thus both weight and spring require an additive stick force ΔP to maintain equilibrium. These forces are

$$\Delta P = nW\frac{a}{b} \quad \text{for the weight}$$

$$\Delta P = T\frac{c}{b} \quad \text{for the spring}$$

where $n = 1$ for rectilinear flight, and is given by (6.10,4) for a pull-up.

EFFECT UPON CONTROL FORCE TO TRIM AND h'_n

The added constant term in the control force will produce a change in the characteristic as shown in Fig. 7.2. The figure illustrates the case where the

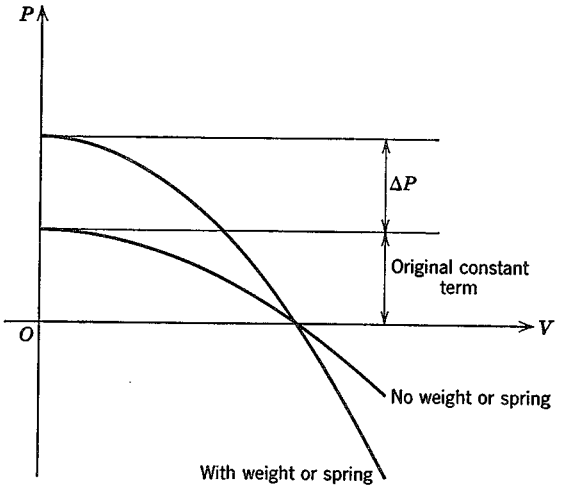

FIG. 7.2 Effect of bob weight and spring on the control-force characteristic. The trim tab is set to trim at the same speed in both cases.

trim tab is set to produce the same trim speed as when the ΔP is absent. The parabolic part of the variation is different for the two cases (see 6.8,9) because of the altered trim-tab setting. It is clear from the figure that the net result of adding the ΔP and moving the tab is to produce a steeper gradient at the given trim speed. Now the gradient has been shown in Sec. 6.9 to depend on the control-free static margin $(h'_n - h)$. Thus the *increased gradient corresponds to an apparent backward shift of the control-free neutral*

point. The same conclusion is reached by consideration of the constant term of (6.8,9), which is proportional to $(h'_n - h)$. The apparent shift of the neutral point may be calculated directly from it, i.e.

$$\Delta P = GS_e\bar{c}_e w \frac{a'b_2}{\Delta} \Delta h'_n$$

or

$$\Delta h'_n = \frac{\Delta}{a'b_2} \frac{\Delta P}{GS_e\bar{c}_e w} \tag{7.1,1}$$

The term "apparent shift" of the N.P. is used above because the N.P. location depends on C'_{L_α} and C'_{m_α}, and the latter are not influenced at all by ΔP. This is readily demonstrated. When the pilot exerts no additional force on the control, the hinge moment is given by

$$\frac{\Delta P}{G\frac{1}{2}\rho V^2 S_e\bar{c}_e} = C_{he_0} + C_{h_\alpha}\alpha + b_2\delta_e + b_3\delta_t \tag{7.1,2}$$

and hence the free elevator angle becomes

$$\delta_{e_{\text{free}}} = \frac{1}{b_2}\left(\frac{\Delta P}{G\frac{1}{2}\rho V^2 S_e\bar{c}_e} - C_{he_0} - C_{h_\alpha}\alpha - b_3\delta_t\right) \tag{7.1,3}$$

Equation (7.1,3) shows that the presence of ΔP at constant speed simply changes $\delta_{e_{\text{free}}}$ by a constant. Consequently, substitution of (7.1,3) into (6.6,2) leads to the same values of C'_{L_α} and C'_{m_α} as given previously by (6.6,5). Hence from (6.6,11*a*) h'_n is unchanged.

EFFECT UPON STICK FORCE PER g AND h'_m

When ΔP is provided by a spring, then it is not dependent in any way on acceleration of the airplane. Hence the addition of a spring does not alter the stick force per g or the maneuver point. The bob weight, on the other hand, is affected by airplane acceleration. At load factor n, the effective weight of the bob is increased from W to nW, and hence induces an additional stick force of $(n - 1)\,\Delta P$. The stick force per g is thereby increased by the amount

$$\Delta Q = \frac{(n-1)\,\Delta P}{n-1} = \Delta P$$

Since Q is proportional to $h'_m - h$, this increase moves the maneuver point aft. Consideration of (6.10,15) shows this shift to be

$$\Delta h'_m = \frac{\Delta P}{GS_e\bar{c}_e w} \frac{2\mu\,\Delta}{a'b_2(2\mu - C_{L_q})} \tag{7.1,4}$$

This movement of the maneuver point however, unlike that of the N.P., is real, since the maneuver point is *defined* by the control force per g.

7.2 INFLUENCE OF HIGH-LIFT DEVICES ON TRIM AND PITCH STIFFNESS

Conventional airplanes utilize a wide range of aerodynamic devices for increasing $C_{L_{max}}$. These include various forms of trailing edge elements (plain flaps, split flaps, slotted flaps, etc.), leading edge elements (drooped nose, slats, slots, etc.) and purely fluid mechanical solutions such as boundary layer control by blowing. Each of these has its own characteristic effects on the lift and pitching moment curves, and it is not feasible to go into them in depth here. The specific changes that result from the "configuration-type" devices, i.e. flaps, slots, etc., can always be incorporated by making the appropriate changes to $C_{m_{a.c._{wb}}}$ and $C_{L_{wb}}$ in (6.3,4) and following through the consequences. Consider for example the common case of part-span trailing edge flaps on a conventional tailed airplane. The main aerodynamic effects of such flaps are illustrated in Fig. 7.3.†

1. Their deflection distorts the shape of the spanwise distribution of lift on the wing, increasing the vorticity behind the flap tips, as in (*a*).
2. They have the same effect locally as an increase in the wing-section camber, i.e. a negative increment in $C_{m_{a.c.}}$ and a positive increment in $C_{L_{wb}}$.
3. The downwash at the tail is increased; both ϵ_0 and $\partial\epsilon/\partial\alpha$ will in general change.

The change in wing-body C_m is obtained from (6.3,4) as

$$\Delta C_{m_{wb}} = \Delta C_{m_{a.c._{wb}}} + \Delta C_{L_{wb}}(h - h_{n_{wb}}) \tag{7.2,1}$$

The change in airplane C_L is

$$\Delta C_L = \Delta C_{L_{wb}} - a_t \frac{S_t}{S} \Delta\epsilon \tag{7.2,2}$$

and the change in tail pitching moment is

$$\Delta C_{m_t} = a_t V_H \Delta\epsilon \tag{7.2,3}$$

When the increments $\Delta C_{m_{a.c._{wb}}}$ and $\Delta C_{L_{wb}}$ are constant with α, then the only

† Note that α is still the angle of attack of the zero-lift line of the basic configuration, and that the lift with flap deflected is not zero at zero α.

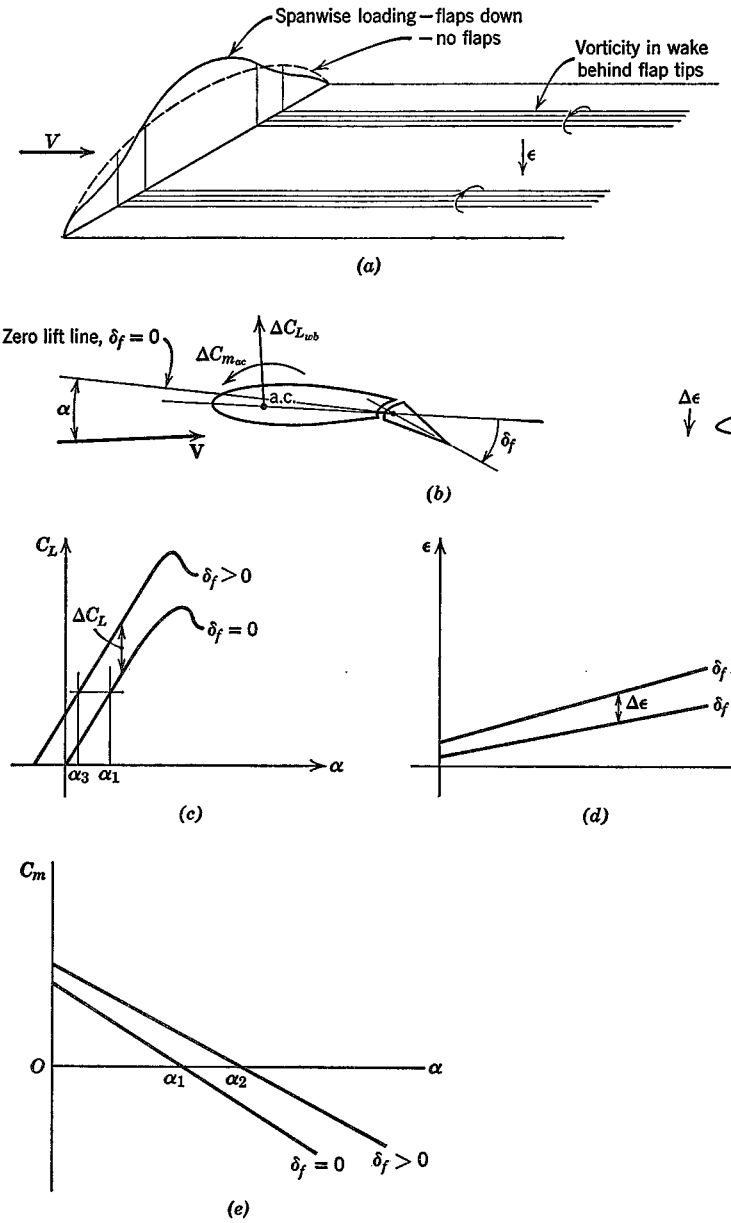

FIG. 7.3 Effect of part-span flaps. (*a*) Change of lift distribution and vorticity. (*b*) Changes in forces and moments. (*c*) Change in C_L. (*d*) Change in downwash. (*e*) Change in C_m.

effect on C_{L_α} and C_{m_α} is that of $\partial\epsilon/\partial\alpha$, and from (6.3,31) and (6.3,34*a*) these are

$$\Delta a = \Delta C_{L_\alpha} = -a_t \frac{S_t}{S} \Delta \frac{\partial \epsilon}{\partial \alpha} \tag{7.2,4}$$

$$\Delta C_{m_\alpha} = (h - h_{n_{wb}}) \Delta a + a_t \overline{V}_H \Delta \frac{\partial \epsilon}{\partial \alpha} \tag{7.2,5}$$

The net result on the C_L and C_m curves is obviously very much configuration dependent. If the $C_m - \alpha$ relation were as in Fig. 7.3*e*, then the trim change would be very large, from α_1 at $\delta_f = 0$ to α_2 after flap deflection. The C_L at α_2 is much larger than at α_1 and hence if the flap operation is to take place without change of trim speed, a down-elevator deflection would be needed to reduce α_{trim} to α_3 (Fig. 7.3*c*). This would result in a nose-down rotation of the aircraft.

7.3 INFLUENCE OF THE PROPULSIVE SYSTEM ON TRIM AND PITCH STIFFNESS

The influence of the propulsive system upon trim and stability may be both important and complex. The range of conditions to be considered in this connection is extremely wide. In the first place, there are several types of propulsive units in common use—reciprocating-engine-driven propellers, turbojets, propeller-jets, and rockets. In the second place, the operating condition may be anything from hovering to reentry. Finally, the variations in engine-plus-vehicle geometry are very great. The analyst may have to deal with such widely divergent cases as a high-aspect-ratio straight-winged airplane with six wing-mounted counterrotating propellers or a low-aspect-ratio delta with buried jet engines. Owing to its complexity, a definite and comprehensive treatment of propulsive system influences on stability is not possible. There does not exist sufficient theoretical or empirical information to enable reliable predictions to be made under all the above-mentioned conditions. However, certain of the major effects of propellers and propulsive jets are sufficiently well understood to make it worth while to discuss them, and this is done in the following.

In a purely formal sense, of course, it is only necessary to add the appropriate direct effects, $C_{m_{\delta_p}}$ and $\partial C_{m_p}/\partial\alpha$ in (6.3,34 and 35), together with the indirect effects on the various wing-body and tail coefficients in order to calculate all the results with power on.

When calculating the trim curves (i.e. elevator angle, tab angle, and control force to trim) the thrust must be that required to maintain equilibrium at the condition of speed and angle of climb being investigated (see

Sec. 6.4). For example (see Fig. 6.1), for flight at speeds below about $M = 3$ (see Sec. 5.9) and assuming that $\alpha_T \ll 1$

$$\begin{aligned} C_T &= C_D + C_W \sin\gamma \qquad (a) \\ C_W \cos\gamma &= C_L + C_T\alpha_T \qquad (b) \end{aligned} \tag{7.3,1}$$

Solving for C_T, we get

$$C_T = \frac{C_D + C_L \tan\gamma}{1 - \alpha_T \tan\gamma} \tag{7.3,2}$$

Except for very steep climb angles, $\alpha_T \tan\gamma \ll 1$, and we may write approximately,

$$C_T = C_D + C_L \tan\gamma \tag{7.3,3}$$

Let the thrust line be offset by a distance z_P from the C.G. (as in Fig. 7.5) and neglecting for the moment all other thrust contributions to the pitching

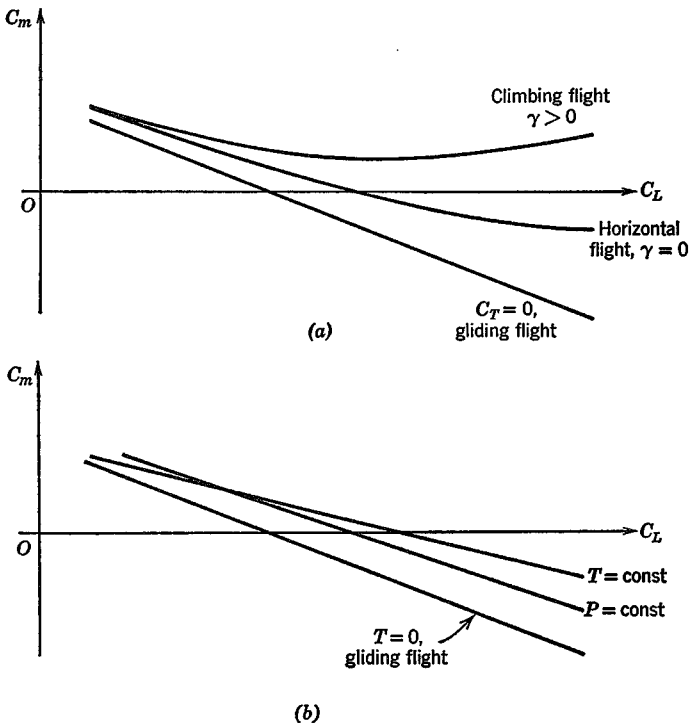

FIG. 7.4 Effect of direct thrust moment on C_m curves. (*a*) Constant γ. (*b*) Constant thrust and power.

moment but Tz_p, we have

$$C_{m_p} = C_T \frac{z_p}{\bar{c}}$$

$$= (C_D + C_L \tan \gamma) \frac{z_p}{\bar{c}} \tag{7.3,4}$$

Now let C_D be given by the parabolic polar (6.1,2), so that

$$C_{m_p} = (C_{D_{\min}} + KC_L^2 + C_L \tan \gamma) \frac{z_p}{\bar{c}} \tag{7.3,5}$$

Strictly speaking, the values of C_D and C_L in (7.3,4 and 5) are those for trimmed flight, i.e. with $\delta_e = \delta_{e_{trim}}$. For the purposes of this discussion of propulsion effects we shall neglect the effects of δ_e on C_D and C_L, and assume that the values in (7.3,5) are those corresponding to $\delta_e = 0$. The addition of this propulsive effect to the C_m curve for rectilinear gliding flight in the absence of aeroelastic and compressibility effects might then appear as in Fig. 7.4*a*. We note that the gradient $-dC_m/dC_L$ for any value of $\gamma > 0$ is less than for unpowered flight. If dC_m/dC_L is used uncritically as a criterion for stability [as in (6.3,21)] an *entirely erroneous conclusion* may be drawn from such curves.

(i) Within the assumptions made above, the thrust moment Tz_p is *independent of* α, hence $\partial C_{m_p}/\partial \alpha = 0$ and there is *no change* in the N.P. from that for unpowered flight.

(ii) A true analysis of stability when *both* speed and α are changing requires that the propulsive system controls (e.g. the throttle) be kept *fixed*, whereas each point on the curves of Fig. 7.4*a* corresponds to a *different* throttle setting. This parallels exactly the argument of Sec. 6.4 concerning the elevator trim slope. For in fact, under the stated conditions, the $C_m - C_L$ curve is transformed into a curve of $\delta_{e_{trim}}$ vs. V by using the relations $\delta_{e_{trim}} = -C_m(\alpha)/C_{m_\delta}$ and $C_L = W/\frac{1}{2}\rho V^2 S$. The slopes of C_m vs. C_L and $\delta_{e_{trim}}$ vs. V will vanish together.

If a graph of C_m vs. C_L be prepared for fixed throttle, then γ will be a variable along it, and its gradient dC_m/dC_L *is* an index of stability, as shown in Chapter 9. The two idealized cases of constant thrust and constant power are of interest. If the thrust at fixed throttle does not change with speed, then we easily find

$$C_{m_p} = \frac{T}{W} C_L \frac{z_p}{\bar{c}} \qquad (a)$$

and

$$\frac{dC_{m_p}}{dC_L} = \frac{T}{W} \frac{z_p}{\bar{c}} \qquad (b) \tag{7.3,6}$$

If the power P is invariant, instead of the thrust, then $T = P/V$ and we find

$$C_{m_p} = \frac{P}{W}\sqrt{\frac{\rho}{2w}}\,\frac{z_p}{\bar{c}}\,C_L^{3/2} \qquad (c) \tag{7.3,6}$$

whence

$$\frac{dC_{m_p}}{dC_L} = \frac{3}{2}\,\frac{P}{W}\sqrt{\frac{\rho}{2w}}\,\frac{z_p}{\bar{c}}\,C_L^{1/2} \qquad (d)$$

Thus in the constant thrust case, the power-off $C_m - C_L$ graph simply has its slope changed by the addition of thrust, and in the constant power case the shape is changed as well. The form of these changes is illustrated in Fig. 7.4*b* and it is evident by comparison with 7.4*a* that the behavior of dC_m/dC_L is quite different in these two situations.

THE INFLUENCE OF RUNNING PROPELLERS

The forces on a single propeller are illustrated in Fig. 7.5, where α_p is the angle of attack of the local flow at the propeller. It is most convenient to resolve the resultant into the two components T along the axis, and N_p in

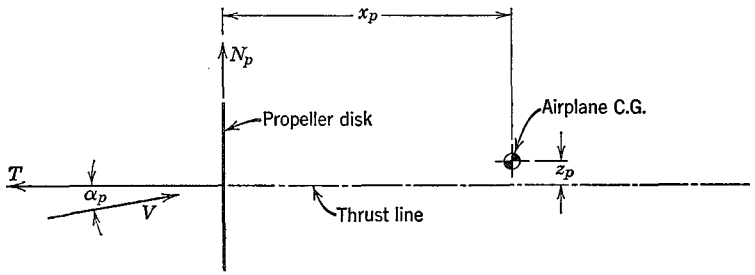

FIG. 7.5 Forces on a propeller.

the plane of the propeller. The moment asociated with T has already been treated above, and does not affect C_{m_α}. That due to N_p is

$$\Delta C_m = C_{N_p}\,\frac{x_p}{\bar{c}}\,\frac{S_p}{S} \tag{7.3,7}$$

where $C_{N_p} = N_p/\frac{1}{2}\rho V^2 S_p$ and S_p is the propeller disk area. To get the total ΔC_m for several propellers, increments such as (7.3,7) must be calculated for each and summed. Theory shows (ref. 7.4) that for small angles C_{N_p} is proportional to α_p. Hence N_p contributes to both $C_{m_{0_p}}$ and $\partial C_{m_p}/\partial\alpha$. The latter is

$$\frac{\partial C_{m_p}}{\partial \alpha} = \frac{S_p}{S}\,\frac{x_p}{\bar{c}}\,\frac{\partial C_{N_p}}{\partial \alpha_p}\,\frac{\partial \alpha_p}{\partial \alpha} \tag{7.3,8}$$

If the propeller were situated far from the flow field of the wing, then $\partial\alpha_p/\partial\alpha$ would be unity. However, for the common case of wing-mounted tractor propellers with the propeller plane close to the wing, there is a strong upwash ϵ_p at the propeller. Thus

$$\alpha_p = \alpha + \epsilon_p + \text{const} \qquad (a)$$

and

$$\frac{\partial\alpha_p}{\partial\alpha} = 1 + \frac{\partial\epsilon_p}{\partial\alpha} \qquad (b) \qquad (7.3,9)$$

where the constant in (7.3,9*a*) is the angle of attack of the propeller axis relative to the airplane zero-lift line. Finally,

$$\frac{\partial C_{m_p}}{\partial\alpha} = \frac{S_p}{S}\frac{x_p}{\bar{c}}\left(1 + \frac{\partial\epsilon_p}{\partial\alpha}\right)\frac{\partial C_{N_p}}{\partial\alpha_p} \qquad (7.3,10)$$

INCREASE OF WING LIFT

When a propeller is located ahead of a wing, the high-velocity slipstream causes a distortion of the lift distribution, and an increase in the total lift. This is a principal mechanism in obtaining high lift on so-called deflected slipstream STOL airplanes. For accurate results that allow for the details of wing and flap geometry powered-model testing is needed. However, for some cases there are available theoretical results (refs. 7.5 to 7.7) suitable for estimates. Both theory and experiment show that the lift increment tends to be linear in α for constant C_T, and hence has the effect of increasing a_{wb}, the lift-curve slope for the wing-body combination. From (6.3,36) this is seen to reduce the effect of the tail on the N.P. location, and can result in a decrease of pitch stiffness.

EFFECTS ON THE TAIL

The propeller slipstream can affect the tail principally in two ways. (1) Depending on how much if any of the tail lies in it, the effective values of a_t and a_e will experience some increase. (2) The downwash values ϵ_0 and $\partial\epsilon/\partial\alpha$ may be appreciably altered in any case. Methods of estimating these effects are at best uncertain, and powered-model testing is needed to get results with engineering precision for most new configurations. However, some empirical methods (refs. 7.8 to 7.10) are available that are suitable for some cases.

EXAMPLE OF PROPELLER EFFECT

Figure 7.6 shows the large effects of thrust on a deflected-slipstream STOL configuration. The data presented are from wind-tunnel tests reported in

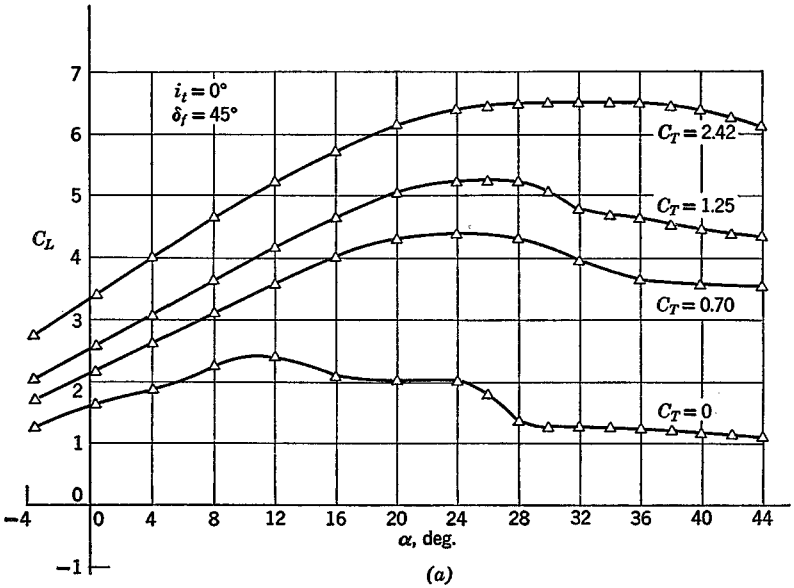
$i_t = 0°$
$\delta_f = 45°$
$C_T = 2.42$
$C_T = 1.25$
$C_T = 0.70$
$C_T = 0$
C_L
α, deg.

(a)

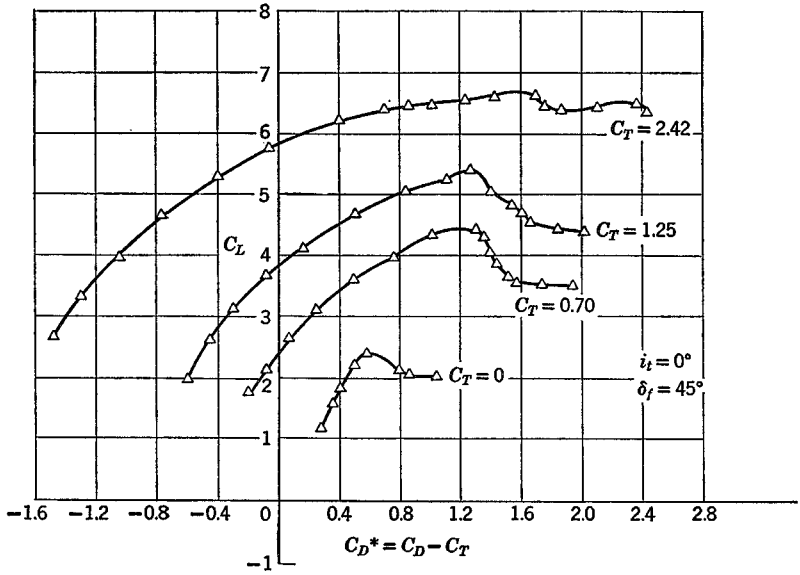
$C_T = 2.42$
$C_T = 1.25$
$C_T = 0.70$
$C_T = 0$
$i_t = 0°$
$\delta_f = 45°$
C_L
$C_D^* = C_D - C_T$

(b)

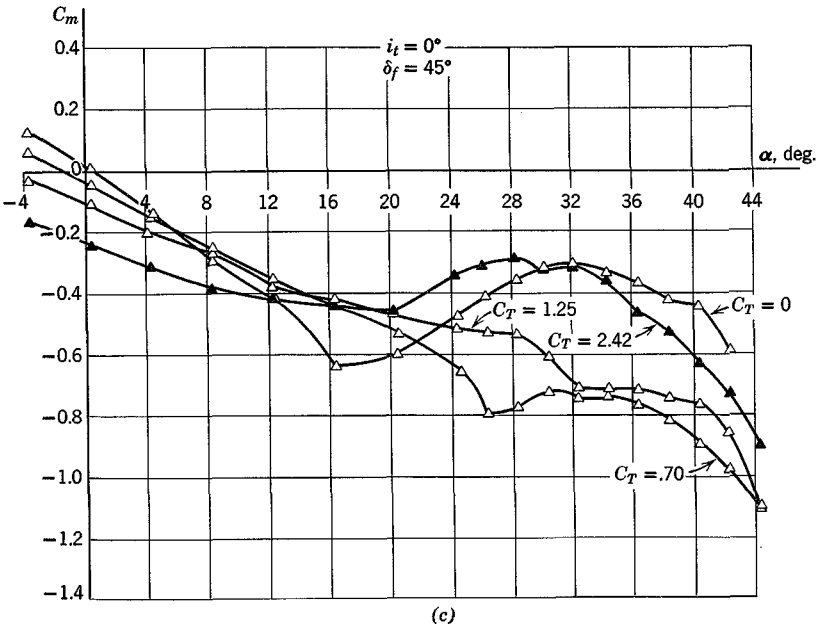

FIG. 7.6 Longitudinal characteristics of a deflected-slipstream STOL configuration (from ref. 7.11). (*a*) C_L vs. α. (*b*) C_L vs. C_D. (*c*) C_m vs. α.

ref. 7.11. The configuration has two tractor propellers, full-span double slotted flaps deflected 45°, and a high tail. The drag coefficient C_D^* plotted on Fig. 7.6*b* is the net streamwise force, and includes the thrust as a negative drag. The effect of the slipstreams on the downwash was large. For the case shown, $\partial\epsilon/\partial\alpha$ increased by 100% between $C_T = 0$ and 1.25. At the same time C_{L_α} increased from .068 to .130. A large decrease in static margin at $\alpha = 0$ due to adding thrust is found from the data:

$$C_T = 0 \quad : \quad K_n = -\frac{C_{m_\alpha}}{C_{L_\alpha}} = \frac{.025}{.068} = .37$$

$$C_T = 1.25: \quad K_n = -\frac{C_{m_\alpha}}{C_{L_\alpha}} = \frac{.0120}{.130} = .09$$

This represents a forward movement of the N.P. of 28% $\bar{c}$.

THE INFLUENCE OF JET ENGINES

The direct thrust moment of jet engines is treated as shown at the beginning of this section, the constant-thrust idealization given in (7.3,6)

often being adequate. In addition, however, there is a normal force on jet engines as well as on propellers.

Jet Normal Force. The air which passes through a propulsive duct experiences, in general, changes in both the direction and magnitude of its velocity. The change in magnitude is the principal source of the thrust, and the direction change entails a force normal to the thrust line. The magnitude and line of action of this force can be found from momentum considerations. Let the mass flow through the duct be m' slugs per second, and the velocity

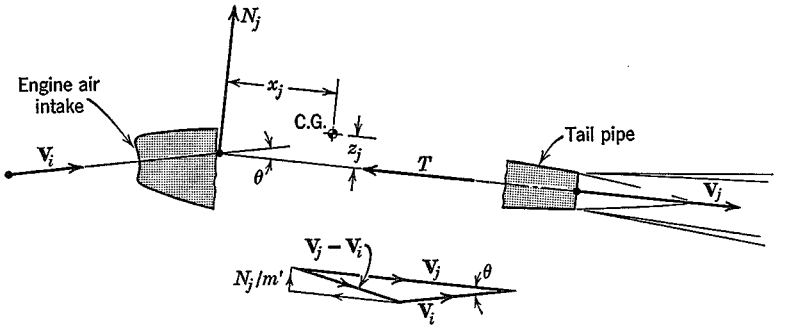

FIG. 7.7 Momentum change of engine air.

vectors at the inlet and outlet be $\mathbf{V}_i$ and $\mathbf{V}_j$. Application of the momentum principle then shows that the reaction on the airplane of the air flowing through the duct is

$$\mathbf{F} = -m'(\mathbf{V}_j - \mathbf{V}_i) + \mathbf{F}'$$

where $\mathbf{F}'$ is the resultant of the pressure forces acting across the inlet and outlet areas. For the present purpose, $\mathbf{F}'$ may be neglected, since it is approximately in the direction of the thrust T. The component of $\mathbf{F}$ normal to the thrust line is then found as in Fig. 7.7. It acts through the intersection of $\mathbf{V}_i$ and $\mathbf{V}_j$. The magnitude is given by

$$N_j = m' V_i \sin \theta$$

or, for small angles,

$$N_j = m' V_i \theta \tag{7.3,11}$$

In order to use this relation, both V_i and θ are required. It is assumed that V_i has that direction which the flow would take in the absence of the engine; i.e. θ equals the angle of attack of the thrust line α_j plus the upwash angle due to wing induction ϵ_j.

$$\theta = \alpha_j + \epsilon_j \tag{7.3,12}$$

It is further assumed that the magnitude V_i is determined by the mass flow and inlet area; thus

$$V_i = \frac{m'}{A_i \rho_i} \tag{7.3,13}$$

where A_i is the inlet area, and ρ_i the density in the inlet. We then get for N_j the expression

$$N_j = \frac{m'^2}{A_i \rho_i} (\alpha_j + \epsilon_j)$$

The corresponding pitching-moment coefficient is

$$\Delta C_m = \frac{m'^2}{A_i \rho_i} \frac{x_j}{\frac{1}{2}\rho V^2 S \bar{c}} (\alpha_j + \epsilon_j) \tag{7.3,14}$$

Since the pitching moment given by (7.3,14) varies with α at constant thrust, then there is a change in C_{m_α} given by

$$\Delta C_{m_\alpha} = \frac{m'^2}{A_i \rho_i} \frac{1}{\frac{1}{2}\rho V^2 S \bar{c}} \left[x_j \left(1 + \frac{\partial \epsilon_j}{\partial \alpha} \right) + \theta \frac{\partial x_j}{\partial \alpha} \right] \tag{7.3,15}$$

The quantities m' and ρ_i can be determined from the engine performance data, and for subsonic flow, $\partial \epsilon_j / \partial \alpha$ is the same as the value $\partial \epsilon_p / \partial \alpha$ used for propellers. $\partial x_j / \partial \alpha$ can be calculated from the geometry.

Jet Induced Inflow. A spreading jet entrains the air that surrounds it, as illustrated in Fig. 7.8, thereby inducing a flow toward the jet axis. If a tailplane is placed in the induced flow field, the angle of attack will be modified by this inflow. A theory of this phenomenon which allows for the curvature of the jet due to angle of attack has been formulated by Ribner

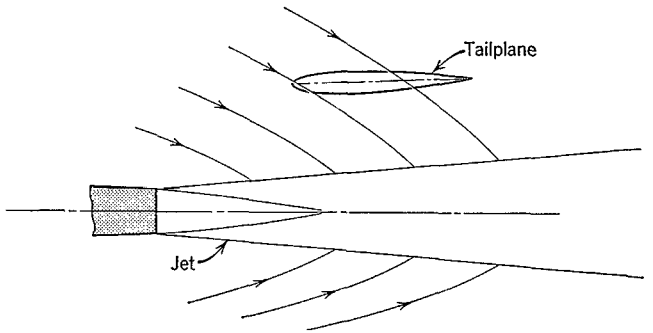

FIG. 7.8 Jet-induced inflow.

(ref. 7.2). This inflow at the tail may vary with α sufficiently to reduce the stability by a significant amount.

7.4 EFFECT OF STRUCTURAL FLEXIBILITY

Many vehicles when flying near their maximum speed are subject to important aeroelastic phenomena. Broadly speaking, we may define these as the feedback effects upon the aerodynamic forces of changes in the shape of the airframe caused by the aerodynamic forces. No real structure is ideally rigid, and aircraft are no exception. Indeed the structures of flight vehicles are very flexible when compared with bridges, buildings, and earthbound machines. This flexibility is an inevitable characteristic of structures designed to be as light as possible. The aeroelastic phenomena which result may be subdivided under the headings static and dynamic. The static cases are those in which we have steady-state distortions associated with steady loads. Examples are aileron reversal, wing divergence, and the reduction of longitudinal stability. Dynamic cases include buffeting and flutter. In these the time dependence is an essential element. From the practical design point of view, the elastic behavior of the airplane affects all three of its basic characteristics: namely performance, stability, and structural integrity. This subject occupies a well-established position as a separate branch of aeronautical engineering. For further information the reader is referred to one of the books devoted to it (refs. 5.11 and 5.12).

In this section we take up by way of example a relatively simple aeroelastic effect; namely, the influence of fuselage flexibility on longitudinal stiffness and control. Assume that the tail load L_t bends the fuselage so that the tail rotates through the angle $\Delta\alpha_t = -kL_t$ (Fig. 7.9) while the wing angle of attack remains unaltered. The net angle of attack of the tail will then be

$$\alpha_t = \alpha_{wb} - \epsilon + i_t - kL_t$$

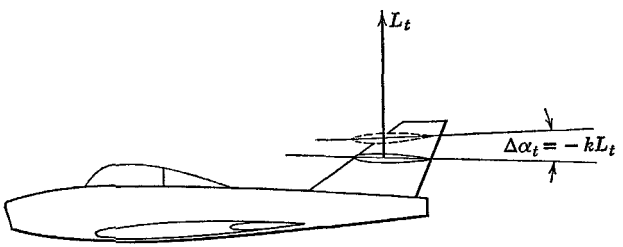

FIG. 7.9 Tail rotation due to fuselage bending.

and the tail lift coefficient at $S_e = 0$ will be

$$C_{L_t} = a_t\alpha_t = a_t(\alpha_{wb} - \epsilon + i_t - kL_t)$$

But $L_t = C_{L_t}\tfrac{1}{2}\rho V^2 S_t$, whence

$$C_{L_t} = a_t(\alpha_{wb} - \epsilon + i_t - kC_{L_t}\tfrac{1}{2}\rho V^2 S_t) \tag{7.4,1}$$

Solving for C_{L_t}, we get

$$C_{L_t} = \frac{a_t}{1 + ka_t S_t \tfrac{1}{2}\rho V^2}(\alpha_{wb} - \epsilon + i_t) \tag{7.4,2}$$

Comparison of (7.4,2) with (6.3,26) shows that the tail effectiveness has been reduced by the factor $1/[1 + ka_t(\rho/2)V^2 S_t]$. The main variable in this expression is V, and it is seen that the reduction is greatest at high speeds. From (6.3,36), we find that the reduction in tail effectiveness causes the neutral point to move forward. The shift is given by

$$\Delta h_n = \frac{\Delta a_t}{a}\,\bar{V}_H\left(1 - \frac{\partial\epsilon}{\partial\alpha}\right) \tag{7.4,3}$$

where

$$\Delta a_t = a_t\left(\frac{1}{1 + ka_t\tfrac{1}{2}\rho V^2 S_t} - 1\right) \tag{7.4,4}$$

The elevator effectiveness is also reduced by the bending of the fuselage. For, if we consider the case when δ_e is different from zero, then (7.4,1) becomes

$$C_{L_t} = a_t(\alpha_{wb} - \epsilon + i_t - kC_{L_t}\tfrac{1}{2}\rho V^2 S_t) + a_e\delta_e$$

and (7.4,2) becomes

$$C_L = \frac{a_t(\alpha_{wb} - \epsilon + i_t) + a_e\delta_e}{1 + ka_t\tfrac{1}{2}\rho V^2 S_t}$$

Thus the same factor $1/(1 + ka_t\tfrac{1}{2}\rho V^2 S_t)$ which operates on the tail lift slope a_t also multiplies the elevator effectiveness a_e.

7.5 GROUND EFFECT

At landing and take-off airplanes fly for very brief (but none the less extremely important) time intervals close to the ground. The presence of the ground modifies the flow past the airplane significantly, so that large changes may take place in the trim and stability. For conventional airplanes, the take-off and landing cases provide some of the governing design criteria.

The presence of the ground imposes a boundary condition which inhibits the downward flow of air normally associated with the lifting action of the

wing and tail. The reduced downwash has three main effects, being in the usual order of importance:

(i) A reduction in ϵ, the downwash angle at the tail.
(ii) An increase in the wing-body lift slope a_{wb}.
(iii) An increase in the tail lift slope a_t.

The problem of calculating the stability and control near the ground then resolves itself into estimating these three effects. When appropriate values of $\partial\epsilon/\partial\alpha$, a_{wb}, and a_t have been found, their use in the equations of the foregoing sections will readily yield the required information. The most important items to be determined are the elevator angle and stick force required to maintain $C_{L_{\max}}$ in level flight close to the ground. It will usually be found that the ratio a_t/a_{wb} is decreased by the presence of the ground. Equation (6.3,36) shows that this would tend to move the neutral point forward. However, the reduction in $\partial\epsilon/\partial\alpha$ is usually so great that the net effect is a large rearward shift of the neutral point. Since the value of $C_{m_{\text{a.c.}}}$ is only slightly affected, it turns out that the elevator angle required to trim at $C_{L_{\max}}$ is much larger than in flight remote from the ground. It commonly happens that this is a critical design condition on the elevator, and may govern the ratio S_e/S_t, or the forward C.G. limit (see Sec. 7.6).

7.6 C.G. LIMITS

One of the dominant parameters of longitudinal stability and control has been shown in Chapter 6 to be the fore-and-aft location of the C.G. The question now arises as to what range of C.G. position is consistent with satisfactory flying qualities. This is a critical design problem, and one of the most important aims of stability and control analysis is to provide the answer to it. Since aircraft always carry some disposable load (e.g. fuel, armaments), and since they are not always loaded identically to begin with (variations in passenger and cargo load), it is always necessary to cater for a variation in the C.G. position. The range to be provided for is kept to a minimum by proper location of the items of variable load, but still it often becomes a difficult matter to keep the flying qualities acceptable over the whole C.G. range. Sometimes the problem is not solved, and the airplane is subjected to restrictions on the fore-and-aft distribution of its variable load when operating at part load.

THE AFT LIMIT

The most rearward allowable location of the C.G. is determined by considerations of longitudinal stability and control sensitivity. The behavior of

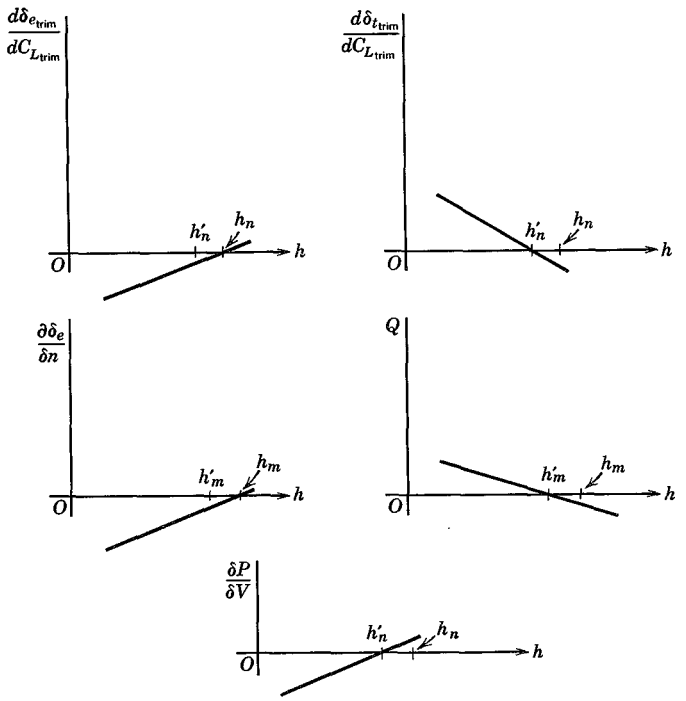

FIG. 7.10 The five control gradients.

the five principal gradients discussed in Chapter 6 are summarized in Fig. 7.10 for the case when the aerodynamic coefficients are independent of speed. From the handling qualities point of view, none of the gradients should be "reversed," i.e. they should have the signs associated with low values of h. When the controls are reversible, this requires that $h < h'_n$. If the controls are irreversible, and if the artificial feel system is suitably designed, then the control force gradient $\partial P/\partial V$ can be kept negative to values of $h > h'_n$, and the rear limit can be somewhat farther back than with reversible controls. The magnitudes of the gradients are also important. If they are allowed to fall to very small values the vehicle will be too sensitive to the controls. When the coefficients do not depend on speed, as assumed for Fig. 7.10, the N.P. also gives the stability boundary (this is proved in Chapter 9), the vehicle becoming unstable for $h > h'_n$ with free controls or $h > h_n$ with fixed controls. If the coefficients are not independent of speed, e.g. $C_m = C_m(\mathbf{M})$, then the C.G. boundary for stability will be different and may be forward of the N.P. However (this is also shown in Chapter 9) the

nature of the instability is very much dependent on whether C_{m_α} is greater or less than zero, i.e. on whether the C.G. is forward or aft of the relevant N.P. In the former case the instability is less severe than in the latter, and hence the N.P. still provides a good practical criterion for stability.

By the use of automatic control systems (see Chapter 11) it is possible to increase the natural stability of a flight vehicle. *Stability augmentation systems* (SAS) are in widespread use on a variety of airplanes and rotorcraft. If such a system is added to the longitudinal controls of an airplane, it permits the use of more rearward C.G. positions than otherwise, but the risk of failure must be reckoned with, for then the airplane is reduced to its "natural" stability, and would still need to be manageable by a human pilot.

THE FORWARD LIMIT

As the C.G. moves forward, the stability of the airplane increases, and larger control movements and forces are required to maneuver or change the trim. The forward C.G. limit is therefore based on control considerations and may be determined by any one of the following requirements:

(i) The stick force per g shall not exceed a specified value.
(ii) The stick-force gradient at trim, $\partial P/\partial V$, shall not exceed a specified value.
(iii) The stick force required to land, from trim at the approach speed, shall not exceed a specified value.
(iv) The elevator angle required to land shall not exceed maximum up elevator.
(v) The elevator angle required to raise the nose-wheel off the ground at take-off speed shall not exceed the maximum up elevator.

7.7 LONGITUDINAL AERODYNAMIC DERIVATIVES

The small-disturbance equations of motion given in Chapter 5 used the technique of expressing aerodynamic forces and moments in terms of the aerodynamic derivatives. The remainder of this chapter is devoted to a discussion of these derivatives. Some of the main aerodynamic derivatives have already been discussed in some detail in Chapter 6, i.e. C_{L_α}, C_{m_α}, C_{he_α}, C_{L_δ}, C_{m_δ}, and $C_{h_{e\delta}}$. Of the remaining α derivatives, C_{D_α} is immediately obtained from (6.1,2) as

$$C_{D_\alpha} = 2KC_{L_e}C_{L_\alpha} \tag{7.7,1}$$

where C_{L_e} is the value of C_L in the reference equilibrium flight condition.

The thrust derivative C_{T_α} is not readily predicted by theory, and would usually be small enough to neglect.

7.8 THE V DERIVATIVES (C_{T_V}, C_{D_V}, C_{L_V}, C_{m_V}, C_{he_V})

This group of derivatives gives the changes that occur in the coefficient when the flight speed V changes, while the other variables, i.e. α, q, z_E, δ_e, remain constant. It is important to remember that the propulsion controls (e.g. the throttle) are also kept fixed.

THE DERIVATIVE C_{T_V}

The derivative C_{T_V} depends on the type of propulsion system, specifically on how T varies with V at fixed throttle. In general it is given by

$$C_{T_V} = \frac{\partial C_T}{\partial \hat{V}}\bigg|_e = V_e \frac{\partial C_T}{\partial V}\bigg|_e = V_e \frac{\partial}{\partial V}\frac{T}{\frac{1}{2}\rho V^2 S}\bigg|_e$$

$$= \frac{(\partial T/\partial V)_e}{\frac{1}{2}\rho V_e S} - \frac{2T_e}{\frac{1}{2}\rho V_e{}^2 S}$$

$$= \frac{(\partial T/\partial V)_e}{\frac{1}{2}\rho V_e S} - 2C_{T_e} \tag{7.8,1}$$

For constant-thrust propulsion, as for jet and rocket engines, $\partial T/\partial V = 0$

and $$C_{T_V} = -2C_{T_e}$$

For constant-power propulsion, $TV = \text{const}$, whence

$$T\,dV + V\,dT = 0$$

so that $$\left(\frac{\partial T}{\partial V}\right)_e = -\frac{T_e}{V_e}$$

and $$C_{T_V} = -3C_{T_e} \tag{7.8,2}$$

Note that, from (7.3,2)

$$C_{T_e} = \left(\frac{C_D + C_L \tan\gamma}{1 - \alpha_T \tan\gamma}\right)_e$$

For piston-engine-propeller systems, the usual fixed-control case implies fixed throttle and constant RPM. In that case the brake horsepower is constant, and the thrust is given by

$$TV = \eta P_B \tag{7.8,3}$$

where η = propulsive efficiency and P_B is the engine shaft power. We then have

$$T\,dV + V\,dT = P_B\,d\eta$$

or
$$\left(\frac{\partial T}{\partial V}\right)_e = -\frac{T_e}{V_e} + \frac{P_B}{V_e}\left(\frac{\partial \eta}{\partial V}\right)_e \tag{7.8,4}$$

and
$$C_{T_V} = -3C_{T_e} + \frac{P_B}{\frac{1}{2}\rho V_e^2 S}\left(\frac{\partial \eta}{\partial V}\right)_e$$

After substituting for P_B from (7.8,3) we get

$$C_{T_V} = -3C_{T_e} + C_{T_e}\frac{V_e}{\eta_e}\left(\frac{\partial \eta}{\partial V}\right)_e \tag{7.8,5}$$

This relation is useful, since the variation of η with V would normally be known for a propeller-driven airplane.

THE DERIVATIVE C_{D_V}

In order to include all the main effects of speed changes formally, we shall assume that the drag coefficient is a function of Mach number $\mathbf{M}$, the dynamic pressure

$$p_d = \tfrac{1}{2}\rho V^2 \tag{7.8,6}$$

and the thrust coefficient, i.e.

$$C_D = C_D(\mathbf{M}, p_d, C_T)$$

Then

$$C_{D_V} = V_e\frac{\partial C_D}{\partial V}\bigg|_e = V_e\frac{\partial C_D}{\partial \mathbf{M}}\frac{\partial \mathbf{M}}{\partial V}\bigg|_e + V_e\frac{\partial C_D}{\partial p_d}\frac{\partial p_d}{\partial V}\bigg|_e + V_e\frac{\partial C_D}{\partial C_T}\frac{\partial C_T}{\partial V}\bigg|_e$$

Since $\mathbf{M} = V/a$, where a is the speed of sound, then

$$\frac{\partial \mathbf{M}}{\partial V} = \frac{1}{a}\,; \quad \frac{\partial p_d}{\partial V} = \rho V \quad \text{and} \quad V_e\frac{\partial C_T}{\partial V}\bigg|_e = C_{T_V}$$

Thus
$$C_{D_V} = \mathbf{M}\frac{\partial C_D}{\partial \mathbf{M}} + \rho_e V_e^2\frac{\partial C_D}{\partial p_d} + C_{T_V}\frac{\partial C_D}{\partial C_T} \tag{7.8,7}$$

The aeroelastic effect on C_{D_V} (the p_d term) is not likely to be large enough to need to be included in other than exceptional cases.

THE DERIVATIVES C_{L_v}, C_{m_v}, C_{he_v}

The derivations for these three derivatives are exactly the same as for C_{D_v} above, and the results are exactly the same as (7.8,7) except that C_D is replaced by the appropriate coefficient.

The Mach number effect on these three derivatives can be calculated from aerodynamic theory for both subsonic and supersonic flow. It is quite sensitive to the shape of the wing, high-aspect ratio straight wings being most affected by $\mathbf{M}$, and highly-swept and delta wings being least affected. An upper limit is obtained by considering two-dimensional flow. For subsonic edges, the Prandtl-Glauert theory† and simple sweep theory combine to give for an infinite wing of sweepback angle Λ

$$C_L = \frac{a_i \alpha}{(1 - \mathbf{M}^2 \cos^2 \Lambda)^{\frac{1}{2}}}, \qquad \mathbf{M} \cos \Lambda < 1$$

where a_i is the lift-curve slope in incompressible flow. Whence

$$\mathbf{M} \frac{\partial C_L}{\partial \mathbf{M}} = \frac{\mathbf{M}^2 \cos^2 \Lambda}{1 - \mathbf{M}^2 \cos^2 \Lambda} C_L \tag{7.8,8}$$

In level flight, with $L = W$, $\mathbf{M}^2 C_L$ is a constant, so that $\mathbf{M}\, \partial C_L / \partial \mathbf{M}$ varies as $1/(1 - \mathbf{M}^2 \cos^2 \Lambda)$. The theory of course breaks down at $\mathbf{M} \simeq \sec \Lambda$ where an infinite value would be predicted, but nevertheless large values of $\mathbf{M}\, \partial C_L / \partial \mathbf{M}$ may be expected near that Mach number. At supersonic speeds, two-dimensional theory for swept wings gives the result

$$C_L = \frac{4\alpha \cos \Lambda}{(\mathbf{M}^2 \cos^2 \Lambda - 1)^{\frac{1}{2}}}, \qquad \mathbf{M} \cos \Lambda > 1$$

After differentiating with respect to $\mathbf{M}$, the result obtained is again (7.8,8), which therefore applies for infinite yawed wings at both subsonic and supersonic speeds. The results given above derive from a linear theory that predicts proportional changes in the pressure distribution when $\mathbf{M}$ is changed—i.e. the pressure distributions remain unaltered in form, but changed in magnitude. Hence the results for C_m and C_{he} would be of the same form, i.e.

$$\mathbf{M} \frac{\partial C_m}{\partial \mathbf{M}} = \frac{\mathbf{M}^2 \cos^2 \Lambda}{1 - \mathbf{M}^2 \cos^2 \Lambda} C_{m_e} = 0 \tag{7.8,9}$$

and

$$\mathbf{M} \frac{\partial C_h}{\partial \mathbf{M}} = \frac{\mathbf{M}^2 \cos^2 \Lambda}{1 - \mathbf{M}^2 \cos^2 \Lambda} C_{he_e} \tag{7.8,10}$$

† A. M. Kuethe and J. D. Schetzer, *Foundations of Aerodynamics*, Secs. 11.6, 11.14.

The vanishing of $\partial C_m/\partial \mathbf{M}$ will hold only for truly subsonic and truly supersonic flows. In the transition region between them there is a very important redistribution of pressure, such that the center of pressure on two-dimensional wings moves from .25c in subsonic flow to .50c in supersonic flow. This would lead to a negative $\partial C_m/\partial \mathbf{M}$, possibly of large magnitude, in the transonic range. The vagaries of transonic flow are such that test results are the only way to get reasonably reliable results in this speed range.

No general rules can be given for the derivatives with respect to p_d or C_T. Aeroelastic analysis or wind-tunnel testing must be used to find these. By way of example, we can calculate the contribution to $\partial C_m/\partial p_d$ associated with the fuselage bending treated in Sec. 7.4. We found there that the lift coefficient of the tail is given by

$$C_{L_t} = \frac{a_t}{1 + ka_t p_d S_t} (\alpha_{wb} - \epsilon + i_t) \tag{7.8,11}$$

The pitching moment contributed by the tail is (6.3,8)

$$C_{m_t} = -V_H C_{L_t}$$

Hence

$$\left(\frac{\partial C_m}{\partial p_d}\right)_{\text{tail}} = -V_H \frac{\partial C_{L_t}}{\partial p_d} \tag{7.8,12}$$

When (7.8,11) is differentiated with respect to p_d and simplified, and the resulting expression is substituted into (7.8,12), we obtain the result

$$\left(\frac{\partial C_m}{\partial p_d}\right)_{\text{tail}} = -C_{m_t} \frac{ka_t S_t}{1 + ka_t p_d S_t} \tag{7.8,13}$$

The corresponding contribution to C_{m_V} is

$$(C_{m_V})_{\text{tail}} = -C_{m_t} \frac{2p_d ka_t S_t}{1 + ka_t p_d S_t} \tag{7.8,14}$$

All the factors in this expression are positive, except for C_{m_t}, which may be of either sign. The contribution of the tail to C_{m_V} may therefore be either positive or negative. The tail pitching moment is usually positive at high speeds and negative at low speeds. Therefore its contribution to C_{m_V} is usually negative at high speeds and positive at low speeds. Since the dynamic pressure occurs as a multiplying factor in (7.8,14), then the aerolastic effect on C_{m_V} goes up with speed and down with altitude.

Figure 7.6 shows the large effects of thrust coefficient on C_L, C_D, C_m and values of the associated derivatives $\partial C_L/\partial C_T$ etc. can be found from data in this form.

7.9 THE q DERIVATIVES (C_{L_q}, C_{m_q}, C_{he_q})

These derivatives represent the aerodynamic effects that accompany rotation of the airplane about a spanwise axis through the C.G. while α remains zero. An example of this kind of motion was treated in Sec. 6.10 (i.e. the steady pull-up). Figure 7.11*b* shows the general case in which the flight path is arbitrary. This should be contrasted with the situation illustrated in Fig. 7.11*a*, where $q = 0$ while α is changing.

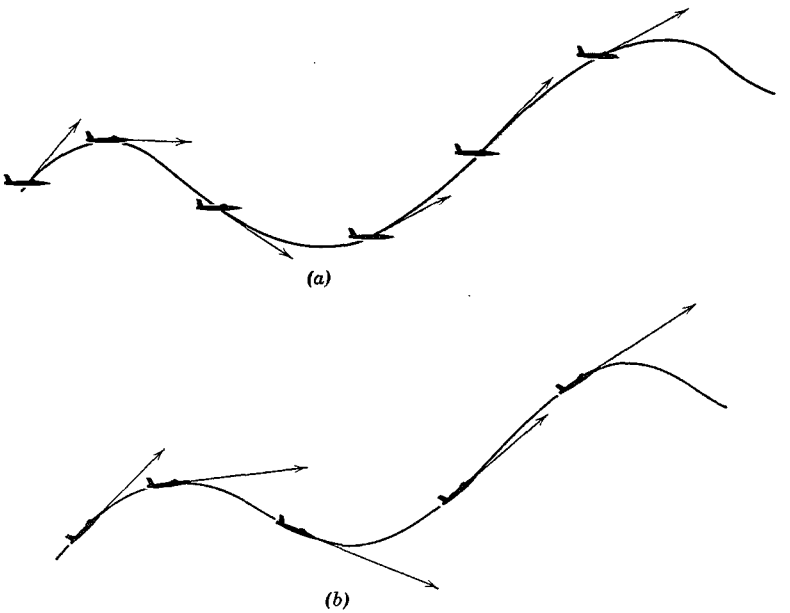

FIG. 7.11 (*a*) Motion with zero q, but varying α. (*b*) Motion with zero α, but varying q.

Both the wing and the tail are affected by the rotation, although, when the airplane has a tail, the wing contribution to C_{L_q} and C_{m_q} is often negligible in comparison with that of the tail. In such cases it is common practice to increase the tail effect by an arbitrary amount, of the order of 10%, to allow for the wing and body.

CONTRIBUTIONS OF A TAIL

As illustrated in Fig. 7.12, the main effect of q on the tail is to increase its angle of attack by (ql_t/V) radians. It is this change in α_t that accounts for

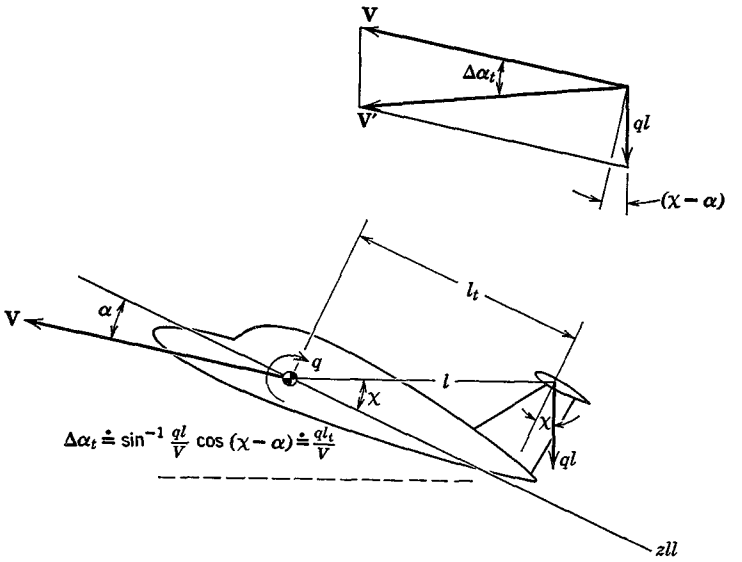

FIG. 7.12 Effect of pitch velocity on tail angle of attack.

the changed forces on the tail. The assumption is implicit in the following derivations that the instantaneous forces on the tail correspond to its instantaneous angle of attack; i.e. no account is taken of the fact that it takes a finite time for the tail lift to build up to its steady-state value following a sudden change in q. [A method of including this refinement has been given by Tobak (ref. 7.12).] The derivatives obtained are therefore *quasistatic*.

C_{L_q} OF A TAIL

The change in tail lift associated with q is

$$\Delta C_{L_t} = a_t \Delta\alpha_t = a_t \frac{ql_t}{V}$$

and the corresponding change in total lift coefficient is

$$\Delta C_L = \frac{S_t}{S}\Delta C_{L_t} = a_t \frac{S_t}{S}\frac{ql_t}{V}$$

It follows that the tail contribution to C_{L_q} is

$$(C_{L_q})_{\text{tail}} = \frac{\Delta C_L}{\hat{q}} = \frac{\Delta C_L}{q}\frac{2V}{\bar{c}}$$

$$= 2a_t V_H \tag{7.9,1}$$

C_{m_q} OF A TAIL

The increment in C_m corresponding to ΔC_{L_t} is

$$\Delta C_m = -V_H \, \Delta C_{L_t}$$

and it follows easily that

$$(C_{m_q})_{\text{tail}} = \frac{\Delta C_m}{\hat{q}} = -2a_t \frac{l_t}{\bar{c}} V_H \tag{7.9,2}$$

THE DERIVATIVE C_{he_q}

For a tail elevator, the change in α_t produces a change in hinge moment given by [see (6.5,1)]

$$\Delta C_{he} = b_1 \frac{q l_t}{V}$$

whence it follows that $$C_{he_q} = \frac{\Delta C_{he}}{\hat{q}} = 2b_1 \frac{l_t}{\bar{c}}$$

CONTRIBUTIONS OF A WING

As previously remarked, on airplanes with tails the wing contributions to the q derivatives are frequently negligible. However, if the wing is highly swept or of low aspect ratio, it may have significant values of C_{L_q} and C_{m_q}; and of course, on tailless airplanes, the wing supplies the major contribution. The q derivatives of wings alone are therefore of great engineering importance.

Unfortunately, no simple formulas can be given, because of the complicated dependence on the wing planform and the Mach number. However, the following discussion of the physical aspects of the flow indicates how linearized wing theory can be applied to the problem. Consider a plane lifting surface, at zero α, with forward speed V and angular velocity q about a spanwise axis (Fig. 7.13). Each point in the wing has a velocity component, relative to the resting atmosphere, of qx normal to the surface. This velocity distribution is shown in the figure for the central and tip chords. Now there is an equivalent cambered wing which would have the identical distribution of velocities normal to its surface when in rectilinear translation at speed V. This is illustrated in Fig. 7.14*a*. The cross section of the curved surface S is

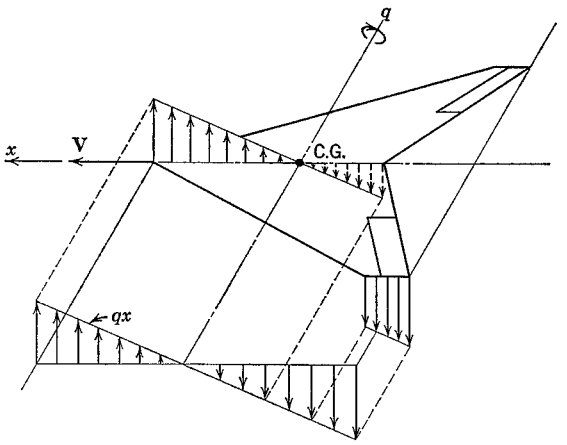

FIG. 7.13 Wing velocity distribution due to pitching.

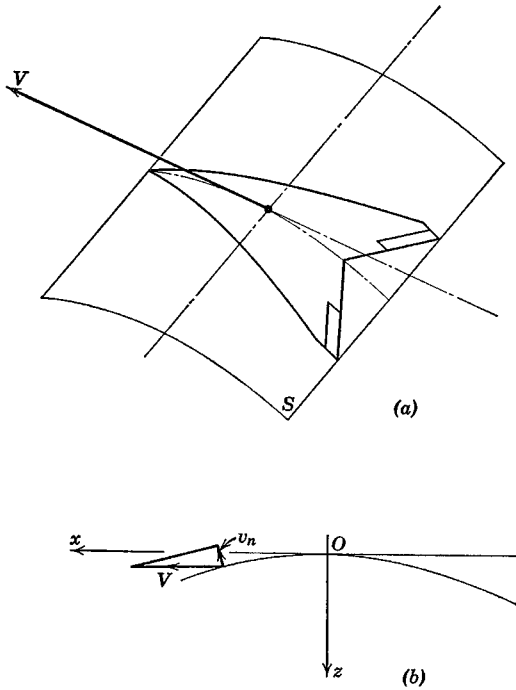

FIG. 7.14 The equivalent cambered wing.

shown in (*b*). The normal velocity distribution will be the same as in Fig. 7.13 if

$$V\frac{\partial z}{\partial x} = qx \quad \text{or} \quad \frac{\partial z}{\partial x} = \frac{q}{V}x$$

Hence

$$z = \frac{1}{2}\frac{q}{V}x^2 \tag{7.9,4}$$

and the cross section of S is a parabolic arc. In linearized wing theory, both subsonic and supersonic, the boundary condition is the same for the original plane wing with rotation q and the equivalent curved wing in rectilinear flight. The problem of finding the q derivatives then is reduced to that of finding the pressure distribution over the equivalent cambered wing. Because of the form of (7.9,4), the pressures are proportional to q/V. From the pressure distribution, C_{L_q}, C_{m_q}, and $C_{h_{e_q}}$ can all be calculated. The derivatives can in principle also be found by experiment, by testing a model of the equivalent wing.

The values obtained by this approach are quasistatic; i.e. they are steady-state values corresponding to $\alpha = 0$ and a small constant value of q. This implies that the flight path is a circle (as in Fig. 6.32), and hence that the vortex wake is not rectilinear. Now both the linearized theory and the wind-tunnel measurement apply to a straight wake, and to this extent are approximate. Since the values of the derivatives obtained are in the end applied to arbitrary flight paths, as in Fig. 7.11*b*, there is little point in correcting them for the curvature of the wake.

The error involved in the application of the quasistatic derivatives to unsteady flight is not so great as might be expected. It has been shown that, when the flight path is a sine wave, the quasistatic derivatives apply so long as the reduced frequency is small, i.e.

$$k = \frac{\omega\bar{c}}{2V} \ll 1$$

where ω is the circular frequency of the pitching oscillation. If l is the wavelength of the flight path, then

$$k = \pi\frac{\bar{c}}{l}$$

so that the condition $k \ll 1$ implies that the wavelength must be long compared to the chord, e.g. $l > 60\bar{c}$ for $k < .05$.

DEPENDENCE ON h

Because the axis of rotation, Fig. 7.13, passes through the C.G., the results obtained are dependent on h. The nature of this variation is found as

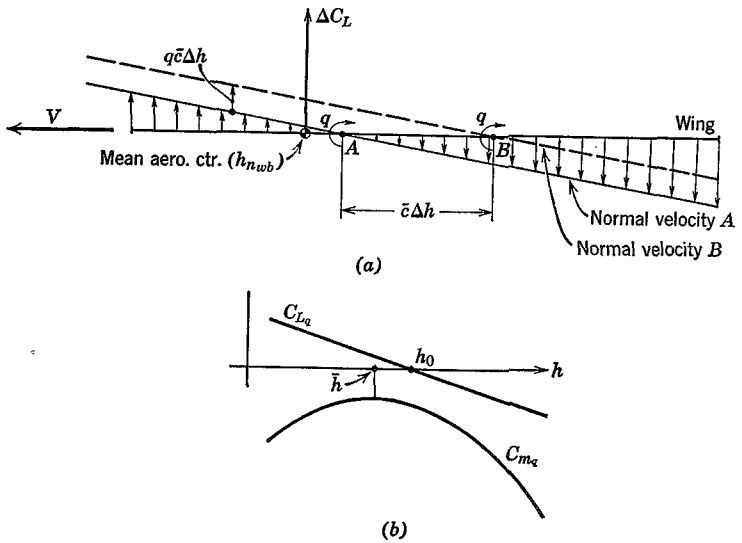

FIG. 7.15 Effect of C.G. location on C_{L_α}, C_{m_α}.

follows. Let the axis of rotation be at A, Fig. 7.15, and let the associated lift and moment be

$$C_{L_A} = C_{L_{q_A}}\hat{q}; \qquad C_{m_A} = C_{m_{q_A}}\hat{q} \tag{7.9,5}$$

Now let the axis of rotation be moved to B, with the change in normal velocity distribution shown on the figure. Since the two normal velocity distributions differ by a constant, (the upward translation $q\bar{c}\,\Delta h$) the difference between the two pressure distributions is that associated with a flat plate at angle of attack

$$\alpha = -\frac{q\bar{c}}{V}\Delta h \tag{7.9,6}$$

This angle of attack introduces a lift increment acting at the wing aerodynamic center of amount

$$\Delta C_L = C_{L_\alpha}\alpha = -\frac{q\bar{c}}{V}\Delta h C_{L_\alpha} \tag{7.9,7}$$

so that for axis of rotation B,

$$C_{L_B} = C_{L_{q_A}}\hat{q} - 2C_{L_\alpha}\Delta h\hat{q}$$

or

$$\Delta C_{L_q} = -2C_{L_\alpha}\Delta h \tag{7.9,8}$$

i.e. C_{L_q} is linear in h. The incremental moment about B is

$$\begin{aligned}\Delta C_m &= C_{L_{q_A}} \hat{q}\,\Delta h + \Delta C_L(h_B - h_{n_{wb}}) \\ &= [C_{L_{q_A}}\,\Delta h - 2C_{L_\alpha}\,\Delta h(h_B - h_{n_{wb}})]\hat{q}\end{aligned}$$

and

$$\Delta C_{m_q} = [C_{L_{q_A}} - 2C_{L_\alpha}(h_B - h_{n_{wb}})]\,\Delta h \tag{7.9,9}$$

whence C_{m_q} is quadratic in h. From (7.9,8) and (7.9,9) by taking the limit as $\Delta h \to 0$ we get

$$\begin{aligned}\frac{\partial C_{L_q}}{\partial h} &= -2C_{L_\alpha} \qquad (a) \\ \frac{\partial C_{m_q}}{\partial h} &= C_{L_q} - 2C_{L_\alpha}(h - h_{n_{wb}}) \qquad (b)\end{aligned} \tag{7.9,10}$$

By integrating (7.9,10)

$$\begin{aligned}C_{L_q} &= -2C_{L_\alpha}(h - h_0) \qquad (a) \\ C_{m_q} &= \bar{C}_{m_q} - 2C_{L_\alpha}(h - \bar{h})^2 \qquad (b)\end{aligned} \tag{7.9,11}$$

The forms of C_{L_q} and C_{m_q} are sketched on Fig. 7.15*b*. h_0 is the C.G. position for zero C_{L_q}, $\bar{h}$ that for maximum C_{m_q}, and $\bar{C}_{m_q}$ is the maximum (least negative) value of C_{m_q}. From (7.9,10*b*) and (7.9,11*a*), we find

$$\bar{h} = \tfrac{1}{2}(h_0 + h_{n_{wb}}) \tag{7.9,12}$$

The linear theory of two-dimensional thin wings gives for supersonic flow:

$$\begin{aligned}h_0 &= \bar{h} = \tfrac{1}{2} \\ \bar{C}_{m_q} &= -\frac{2}{3\sqrt{\mathbf{M}^2 - 1}}\end{aligned} \tag{7.9,13}$$

and for subsonic flow:

$$\begin{aligned}h_0 &= \tfrac{3}{4} \\ \bar{h} &= \tfrac{1}{2} \\ \bar{C}_{m_q} &= 0\end{aligned} \tag{7.9,14}$$

PITCH DAMPING OF PROPULSIVE JETS

When gases flow at high velocity inside jet or rocket engines, there is a consequent rate of change of moment of inertia which leads to an inertia term in the moment equation [$\dot{\mathscr{I}}_B\boldsymbol{\omega}_B$ in (5.6,7)]. Instead of retaining it as a term on the r.h.s., it is convenient to transpose it to the l.h.s. and treat it as an external moment $\Delta\mathbf{G}_B = -\dot{\mathscr{I}}_B\boldsymbol{\omega}_B$. Considering only pitching motion,

$$\boldsymbol{\omega}_B = \begin{bmatrix} 0 \\ q \\ 0 \end{bmatrix} \tag{7.9,15}$$

the corresponding terms in the scalar moment equations (5.6,8) are

$$\begin{aligned} \Delta L &= \dot{I}_{xy} q \\ \Delta M &= -\dot{I}_y q \\ \Delta N &= \dot{I}_{yz} q \end{aligned} \tag{7.9,16}$$

The corresponding q derivatives are therefore

$$\begin{aligned} \Delta L_q &= \dot{I}_{xy} \\ \Delta M_q &= -\dot{I}_y \\ \Delta N_q &= \dot{I}_{yz} \end{aligned} \tag{7.9,17}$$

We restrict ourselves to consideration only of propulsion systems that have inertial symmetry with respect to the xz plane, so $I_{xy} = I_{yz} = 0$, and only ΔM_q remains. Figure 7.16 shows three types of propulsion system, for each

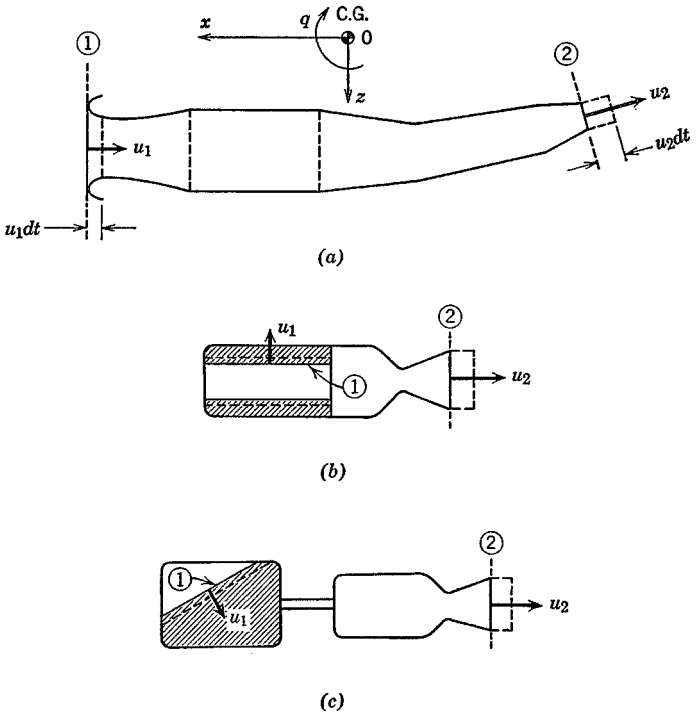

FIG. 7.16 Mechanism of jet damping. (*a*) Jet engine and duct. (*b*) Solid fuel rocket. (*c*) Liquid fuel rocket.

of which we assume that the velocities are uniform across surfaces 1 and 2. For the jet engine 1 is the air inlet and for the rockets it is the moving boundary of the fuel. u_2 is the jet exit velocity, u_1 is the inlet velocity for the jet, and the rate of movement of the relevant interface for the rockets.

The Oxz coordiate system of Fig. 7.16 is taken fixed to the solid part of the vehicle, and we focus our attention on the material system comprising the solid, liquid, and gaseous constituents of the vehicle at time zero. The boundaries of this system move in a time dt as illustrated; as a result its mass center moves away from the origin O, and its moment of inertia changes. Let I_y be the moment of inertia around O, and I'_y be that around the displaced mass center, at coordinates $(\bar{x}, \bar{z})$. By the parallel axis theorem for moment of inertia we have

$$I'_y = I_y - m(\bar{x}^2 + \bar{z}^2)$$

where m is, of course, the *total* vehicle mass. It follows that

$$\dot{I}'_y = \dot{I}_y - 2m\left(\bar{x}\frac{d\bar{x}}{dt} + \bar{z}\frac{d\bar{z}}{dt}\right)$$

and at $t = 0$, when $\bar{x} = \bar{z} = 0$, $\dot{I}'_y = \dot{I}_y$. Thus the movement of the mass center associated with the jet flow does not contribute to the jet damping effect explicitly. The change in I_y in time dt is given by

$$dI_y = dt\int_{A_2} \rho_2 u_2(x_2^2 + z_2^2)\, dA_2 - dt\int_{A_1} \rho_1 u_1(x_1^2 + z_1^2)\, dA_1 \quad (7.9,18)$$

In the second term, for a jet engine, ρ_1 is, of course, the density of the inlet air. For a rocket it is, strictly speaking, the difference in density between the fuel and the adjacent gas. For all practical purposes the latter can clearly be neglected. If $\bar{x}^2$ and $\bar{z}^2$ are the component mean-square distances to the surfaces A_1 and A_2, (7.9,18) can be expressed as

$$\dot{I}_y = \rho_2 u_2 A_2(\bar{x}_2^2 + \bar{z}_2^2) - \rho_1 u_1 A_1(\bar{x}_1^2 + \bar{z}_1^2) \quad (7.9,19)$$

Now $\rho_i u_i A_i$ is the mass flux across A_i, and may be taken constant for all three types of system (the fuel mass flow in jet engines is much smaller than the air mass flow). Thus

$$\dot{I}_y = m'[(\bar{x}_2^2 - \bar{x}_1^2) + (\bar{z}_2^2 - \bar{z}_1^2)] \quad (7.9,20)$$

where $m' = A_i \rho_i u_i$ is the mass flow rate out of the jet. In many practical cases, for elongated slender vehicles, the z^2 terms may be negligibly small. The result for the pitch damping in that case is

$$\Delta M_q = -m'(\bar{x}_2^2 - \bar{x}_1^2) \quad (7.9,21)$$

It will be negative, corresponding to positive damping, whenever the C.G. is closer to the inlet or the fuel surface than to the nozzle exit. For compactness we may write ξ^2 for $(\bar{x}_2^2 - \bar{x}_1^2) + (\bar{z}_2^2 - \bar{z}_1^2)$ so that

$$\Delta M_q = -m'\xi^2 \tag{7.9,22}$$

The nondimensional coefficient follows as

$$\Delta C_{m_q} = -4\frac{m'}{\rho V S}\frac{\xi^2}{\bar{c}^2} \tag{7.9,23}$$

It varies inversely as speed for constant propulsive mass flow m'. The thrust of the engine is given by

$$T = m'V_j$$

where V_j is the final velocity of the jet relative to the vehicle, so that (7.9,23) can be rewritten in terms of T instead of m'. The result is

$$\Delta C_{m_q} = -2C_T\frac{V}{V_j}\frac{\xi^2}{\bar{c}^2} \tag{7.9,24}$$

For jet airplanes in cruising flight this contribution to C_{m_q} is usually negligible. Only at high values of C_T, and when the C_{m_q} of the rest of the airplane is small, would it be significant. On the other hand, a rocket booster at lift-off, when the speed is low, has practically zero external aerodynamic damping and the jet damping becomes very important.

7.10 THE $\dot{\alpha}$ DERIVATIVES ($C_{L_{\dot{\alpha}}}$, $C_{m_{\dot{\alpha}}}$, $C_{h_{e\dot{\alpha}}}$)

The $\dot{\alpha}$ derivatives owe their existence to the fact that the pressure distribution on a wing or tail does not adjust itself instantaneously to its equilibrium value when the angle of attack is suddenly changed. The calculation of this effect, or its measurement, involves unsteady flow. In this respect, the $\dot{\alpha}$ derivatives are very different from those discussed previously, which can all be determined on the basis of steady-state aerodynamics.

CONTRIBUTIONS OF A WING

Consider a wing in horizontal flight at zero α. Let it be subjected to a downward impulse, so that it suddenly acquires a constant downward velocity component. Then, as shown in Fig. 7.17, its angle of attack undergoes a step increase. The lift then responds in a transient manner (the indicial response) the form of which depends on whether **M** is greater or less than 1.

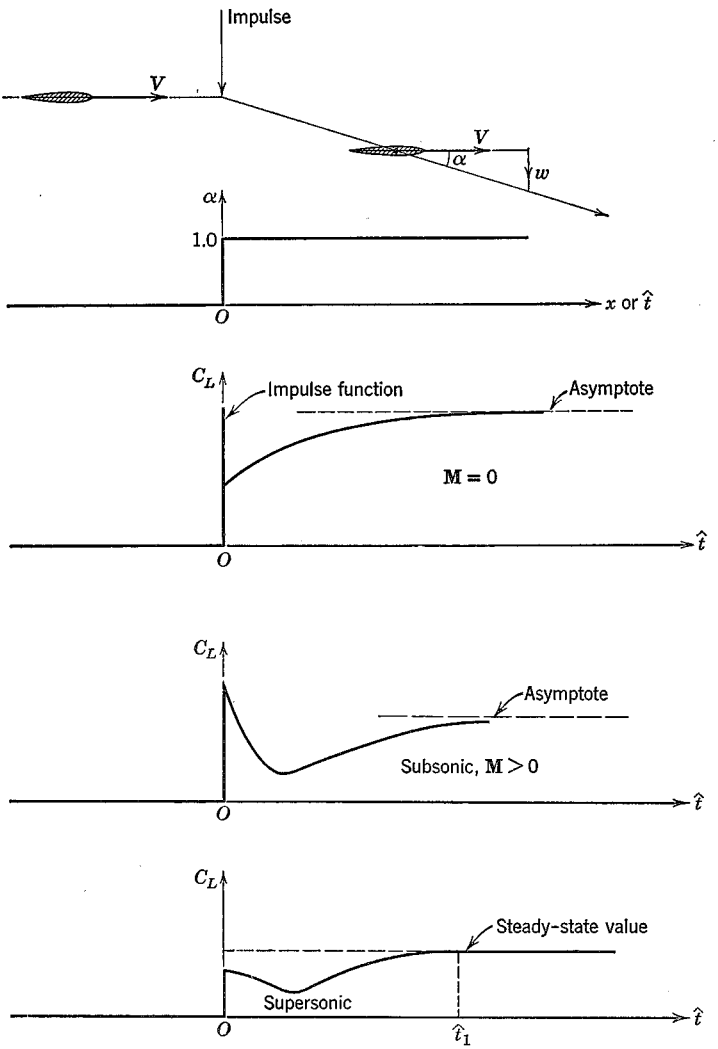

FIG. 7.17 Lift response to step change in α. (After Tobak, *NACA Rept. 1188.*)

In subsonic flight, the vortices which the wing leaves behind it can influence it at all future times, so that the steady state is approached only asymptotically. In supersonic flight, the upstream traveling disturbances move more slowly than the wing, so that it outstrips the disturbance field of the initial impulse in a finite time t_1. From that time on the lift remains constant.

In order to find the lift associated with $\dot{\alpha}$, let us consider the motion of an airfoil with a small constant $\dot{\alpha}$, but with $q = 0$. The motion, and the angle of attack, are shown in Fig. 7.18. The method used follows that introduced by Tobak (ref. 7.12). We assume that the differential equation which relates $C_L(\hat{t})$ with $\alpha(\hat{t})$ is linear. Hence the method of superposition may be used to derive the response to a linear $\alpha(\hat{t})$. Let the admittance be $A(\hat{t})$. Then, [cf. (5.11,2)], the lift coefficient at time $\hat{t}$ is

$$C_L(\hat{t}) = \int_{\tau=0}^{\hat{t}} A(\hat{t} - \tau)\alpha'(\tau)\, d\tau$$

Since $\alpha'(\tau) = D\alpha = \text{constant}$, then

$$C_L(\hat{t}) = D\alpha \int_{\tau=0}^{\hat{t}} A(\hat{t} - \tau)\, d\tau \tag{7.10,1}$$

The ultimate C_L response to a unit-step α input is C_{L_α}. Let the lift defect be $f(\hat{t})$: i.e.

$$A(\hat{t}) = C_{L_\alpha} - f(\hat{t})$$

Then (7.10,1) becomes

$$\begin{aligned} C_L(\hat{t}) &= D\alpha C_{L_\alpha}\hat{t} - D\alpha \int_{\tau=0}^{\hat{t}} f(\hat{t} - \tau)\, d\tau \\ &= C_{L_\alpha}\alpha - S\, D\alpha \end{aligned} \tag{7.10,2}$$

where $S(\hat{t}) = \int_{\tau=0}^{\hat{t}} f(\hat{t} - \tau)\, d\tau$. The term $S\ D\alpha$ is shown on Fig. 7.18. Now, if the idea of representing the lift by means of aerodynamic derivatives is to be valid, we must be able to write, for the motion in question,

$$C_L(\hat{t}) = C_{L_\alpha}\alpha(\hat{t}) + C_{L_{\dot{\alpha}}} D\alpha \tag{7.10,3}$$

where C_{L_α} and $C_{L_{\dot{\alpha}}}$ are constants. Comparing (7.10,2 and 3), we find that $C_{L_{\dot{\alpha}}} = -S(\hat{t})$, a function of time. Hence, during the initial part of the motion, as already pointed out in Sec. 5.11 the *derivative concept is invalid.* However, for all finite wings,† the area $S(\hat{t})$ converges to a finite value as $\hat{t}$ increases indefinitely. In fact, for supersonic wings, S reaches its limiting value in a finite time, as is evident from Fig. 7.17. Thus (7.10,3) is valid,‡ with constant

† For two-dimensional incompressible flow, the area $S(\hat{t})$ diverges as $t \to \infty$. That is, the derivative concept is definitely *not* applicable to that case.

‡ Exactly for supersonic wings, and approximately for subsonic wings.

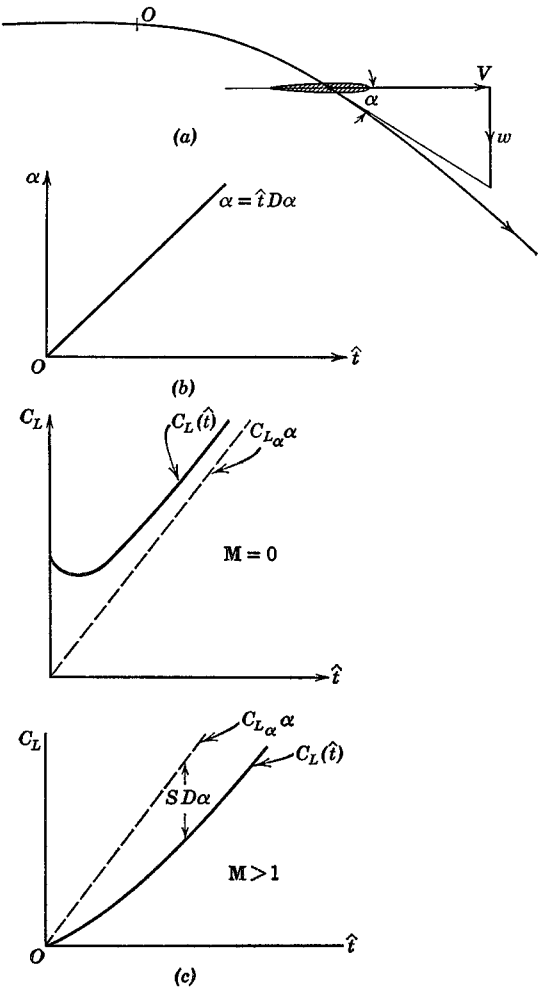

FIG. 7.18 Lift associated with $\dot{\alpha}$.

$C_{L_{\dot{\alpha}}}$, for values of $\hat{t}$ greater than a certain minimum. This minimum is not large, being the time required for the wing to travel a few chord lengths. In the time range where S is constant, or differs only infinitesimally from its asymptotic value, the $C_L(\hat{t})$ curve of Fig. 7.18*c* is parallel to $C_{L_\alpha}\alpha$. A similar situation exists with respect to C_m and C_{he}.

We see from Fig. 7.18 that $C_{L_{\dot{\alpha}}}$, which is the $\lim_{\hat{t}\to\infty} -S(\hat{t})$ can be positive for $\mathbf{M} = 0$ and negative for larger values of $\mathbf{M}$.

There is a second useful approach to the $\dot{\alpha}$ derivatives, and that is via consideration of oscillating wings. This method has been widely used experimentally, and extensive treatments of wings in oscillatory motion are available in the literature,† primarily in relation to flutter problems. Because of the time lag previously noted, the amplitude and phase of the oscillatory lift will be different from the quasisteady values. Let us represent the periodic angle of attack and lift coefficient by the complex numbers

$$\alpha = \alpha_0 e^{i\omega t} \qquad \text{and} \qquad C_L = C_{L_0} e^{i\omega t} \tag{7.10,4}$$

where α_0 is the amplitude (real) of α, and C_{L_0} is a complex number such that $|C_{L_0}|$ is the amplitude of the C_L response, and arg C_{L_0} is its phase angle. The relation between C_{L_0} and α_0 appropriate to the low frequencies characteristic

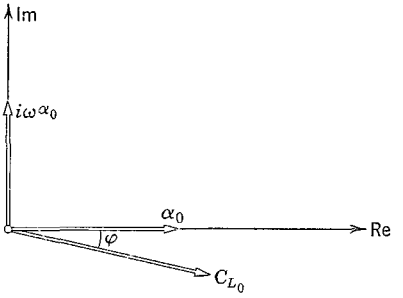

FIG. 7.19 Vector diagram of lift response to oscillatory α.

of dynamic stability is illustrated in Fig. 7.19. In terms of these vectors, we may derive the value of $C_{L_{\dot{\alpha}}}$ as follows. The $\dot{\alpha}$ vector is

$$\dot{\alpha} = i\omega\alpha_0 e^{i\omega t}$$

Thus C_L may be expressed as

$$C_L = R[C_{L_0}]e^{i\omega t} + iI[C_{L_0}]e^{i\omega t}$$

$$= R[C_{L_0}]\frac{\alpha}{\alpha_0} + I[C_{L_0}]\frac{\dot{\alpha}}{\omega\alpha_0}$$

Hence

$$C_{L_{\dot{\alpha}}} = \frac{\partial C_L}{\partial(\dot{\alpha}\bar{c}/2V)} = \frac{I[C_{L_0}]}{k\alpha_0} \tag{7.10,5}$$

or, if the amplitude α_0 is unity, $C_{L_{\dot{\alpha}}} = I[C_{L_0}]/k$, where k is the reduced frequency $\omega\bar{c}/2V$.

To assist in forming a physical picture of the behavior of a wing under these conditions, we give here the results for a two-dimensional‡ airfoil in

† See bibliography.

‡ Rodden and Giesing (ref. 7.15) have extended and generalized this method. In particular they give results for finite wings.

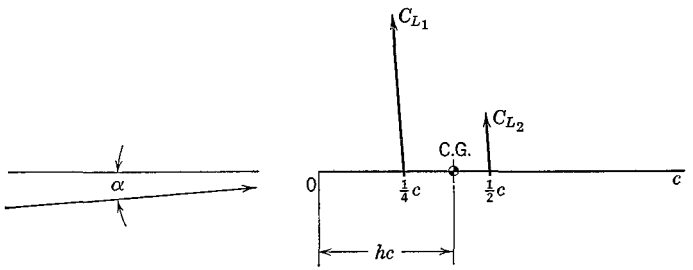

FIG. 7.20 Lift on oscillating two-dimensional airfoil.

incompressible flow. The motion of the airfoil is a plunging oscillation; i.e. it is like that shown in Fig. 7.11*a*, except that the flight path is a sine wave. The instantaneous lift on the airfoil is given in two parts (see Fig. 7.20):

$$C_L = C_{L_1} + C_{L_2}$$

where

$$C_{L_1} = 2\pi\left[\alpha F(k) + \left(\frac{\dot{\alpha}c}{2V}\right)\frac{G(k)}{k}\right] \tag{7.10,6}$$

$$C_{L_2} = \pi\left(\frac{\dot{\alpha}c}{2V}\right)$$

and $F(k)$ and $G(k)$ are the real and imaginary parts of the Theodorsen function $C(k)$, plotted in Fig. 7.21. The lift that acts at the midchord is proportional to $\dot{\alpha} = \ddot{z}/V$, where z is the translation (vertically downward) of the airfoil. That is, it represents a force opposing the downward acceleration of the airfoil. This force is exactly that which is required to impart an acceleration $\ddot{z}$ to a mass of air contained in a cylinder, the diameter of which equals the chord c. This is known as the "apparent additional mass." It is as though the mass of the airfoil were increased by this amount. Except in cases of very low relative density $\mu = 2m/\rho S\bar{c}$, this added mass is small compared to that of the airplane itself, and hence the force C_{L_2} is relatively unimportant. Physically, the origin of this force is in the reaction of the air which is associated with its downward acceleration. The other component, C_{L_1}, which acts at the $\frac{1}{4}$ chord point, is associated with the circulation around the airfoil, and is a consequence of the imposition of the Kutta–Joukowski condition at the trailing edge. It is seen that it contains one term proportional to α and another proportional to $\dot{\alpha}$. From Fig. 7.19, the pitching-moment coefficient about the C.G. is obtained as

$$C_m = C_{L_1}(h - \tfrac{1}{4}) + C_{L_2}(h - \tfrac{1}{2}) \tag{7.10,7}$$

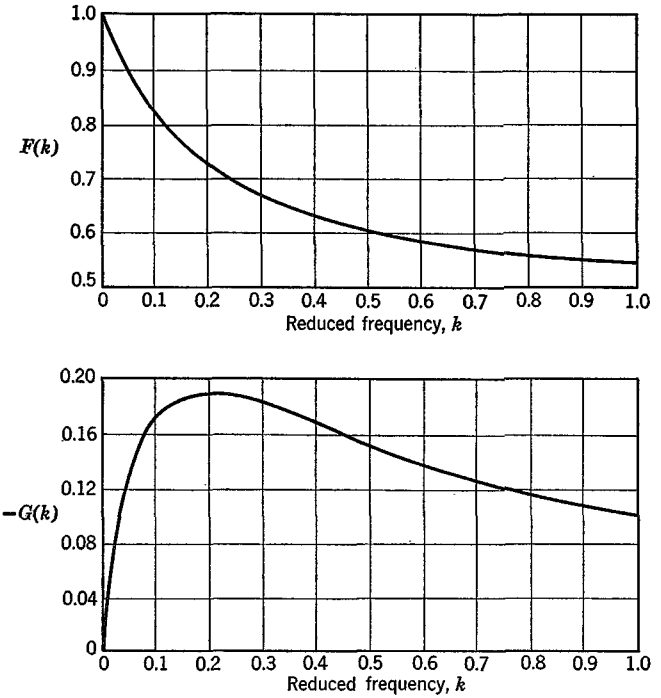

FIG. 7.21 The Theodorsen function.

From (7.10,6 and 7), the following derivatives are found for frequency k.

$$\begin{aligned} C_{L_\alpha} &= 2\pi F(k) \\ C_{L_{\dot\alpha}} &= \pi + 2\pi \frac{G(k)}{k} \\ C_{m_\alpha} &= 2\pi F(k)(h - \tfrac{1}{4}) \\ C_{m_{\dot\alpha}} &= \pi(h - \tfrac{1}{2}) + 2\pi \frac{G(k)}{k}(h - \tfrac{1}{4}) \end{aligned} \tag{7.10,8}$$

The awkward situation is evident, from (7.10,8), that the derivatives are frequency-dependent. That is, in free oscillations one does not know the value of the derivative until the solution to the motion (i.e. the frequency) is known. In cases of forced oscillations at a given frequency, this difficulty is not present.

When dealing with the rigid-body motions of flight vehicles, the characteristic nondimensional frequencies k are usually small, $k << 1$. Hence it is

reasonable to use the $F(k)$ and $G(k)$ corresponding to $k \to 0$. For the two-dimensional incompressible case described above, $\lim_{k\to 0} F(k) = 1$, so that $C_{L_\alpha} = 2\pi$ and $C_{m_\alpha} = 2\pi(h - \frac{1}{4})$, the theoretical steady-flow values. This conclusion, that C_{L_α} and C_{m_α} are the quasistatic values, also holds for finite wings at all Mach numbers. The results for $C_{L_{\dot\alpha}}$ and $C_{m_{\dot\alpha}}$ are not so clear, however, since $\lim G(k)/k$ given above is infinite. This singularity is marked for the example of two-dimensional flow given above, but is not evident for finite wings at moderate aspect ratio. Miles (refs. 7.13, 7.14) indicates that the $k \log k$ term responsible for the singularity is not significant for aspect ratios less than 10, and the numerical calculations of Rodden and Giesing (ref. 7.15) show no difficulty at values of k as low as .001. Filotas' (ref. 7.16) more recent solutions for finite wings bear out Miles' contention. Thus for finite wings definite values of $C_{L_{\dot\alpha}}$ and $C_{m_{\dot\alpha}}$ can be associated with small but nonvanishing values of k. If the airfoil has a control flap, the hinge moment associated with $\dot\alpha$, $C_{he_{\dot\alpha}}$, behaves like $C_{L_{\dot\alpha}}$ and $C_{m_{\dot\alpha}}$. The limiting values described above can be obtained from a first-order-in-frequency analysis of an oscillating wing. To summarize, *the $\dot\alpha$ derivatives of a wing alone may be computed from the indicial responses of lift, pitching moment, and hinge moment, or from first-order-in-frequency analysis of harmonically plunging wings.*

CONTRIBUTIONS OF A TAIL

There is an approximate method for evaluating the contributions of a tail surface, which is satisfactory in many cases. This is based on the concept of the *lag of the downwash*. It neglects entirely the nonstationary character of the lift response of the tail to changes in tail angle of attack, and attributes the result entirely to the fact that the downwash at the tail does not respond instantaneously to changes in wing angle of attack. The downwash is assumed to be dependent primarily on the strength of the wing's trailing vortices in the neighborhood of the tail. Since the vorticity is convected with the stream, then a change in the circulation at the wing will not be felt as a change in downwash at the tail until a time $\Delta t = l_t/V$ has elapsed, where l_t is the tail length (Fig. 6.10). It is therefore assumed that the instantaneous downwash at the tail, $\epsilon(t)$, corresponds to the wing α at time $(t - \Delta t)$. The corrections to the quasistatic downwash and tail angle of attack are therefore

$$\Delta\epsilon = -\frac{\partial\epsilon}{\partial\alpha}\dot\alpha\,\Delta t = -\frac{\partial\epsilon}{\partial\alpha}\dot\alpha\,\frac{l_t}{V}$$

$$= -\Delta\alpha_t \qquad (7.10{,}9)$$

$C_{L_{\dot{\alpha}}}$ OF A TAIL

The correction to the tail lift coefficient for the downwash lag is

$$\Delta C_{L_t} = a_t \Delta\alpha_t = a_t \dot{\alpha} \frac{l_t}{V} \frac{\partial \epsilon}{\partial \alpha} \tag{7.10,10}$$

The correction to the airplane lift is therefore

$$\Delta C_L = a_t \dot{\alpha} \frac{l_t}{V} \frac{\partial \epsilon}{\partial \alpha} \frac{S_t}{S}$$

and

$$(C_{L_{\dot{\alpha}}})_{\text{tail}} = \frac{\partial C_L}{\partial\left(\frac{\dot{\alpha}\bar{c}}{2V}\right)} = -2a_t V_H \frac{\partial \epsilon}{\partial \alpha} \tag{7.10,11}$$

$C_{m_{\dot{\alpha}}}$ OF A TAIL

The correction to the pitching moment is obtained from ΔC_{L_t} as

$$\Delta C_m = -V_H \Delta C_{L_t} = -a_t \dot{\alpha} \frac{\partial \epsilon}{\partial \alpha} \frac{l_t}{V} V_H$$

Therefore

$$\frac{\partial C_m}{\partial \dot{\alpha}} = -a_t V_H \frac{l_t}{V} \frac{\partial \epsilon}{\partial \alpha}$$

and

$$(C_{m_{\dot{\alpha}}})_{\text{tail}} = \frac{\partial C_m}{\partial\left(\frac{\dot{\alpha}\bar{c}}{2V}\right)} = -2a_t V_H \frac{l_t}{\bar{c}} \frac{\partial \epsilon}{\partial \alpha} \tag{7.10,12}$$

$C_{he_{\dot{\alpha}}}$ OF A TAIL

The correction to α_t produces a change in the elevator hinge moment

$$\Delta C_{he} = C_{he_{\alpha_t}} \Delta\alpha_t = C_{he_{\alpha_t}} \frac{\partial \epsilon}{\partial \alpha} \dot{\alpha} \frac{l_t}{V}$$

Therefore

$$\frac{\partial C_{he}}{\partial \dot{\alpha}} = C_{he_{\alpha_t}} \frac{\partial \epsilon}{\partial \alpha} \frac{l_t}{V}$$

and

$$C_{he_{\dot{\alpha}}} = \frac{\partial C_{he}}{\partial\left(\frac{\dot{\alpha}\bar{c}}{2V}\right)} = 2C_{he_{\alpha_t}} \frac{l_t}{\bar{c}} \frac{\partial \epsilon}{\partial \alpha} \tag{7.10,13}$$

7.11 AERODYNAMIC TRANSFER FUNCTIONS

Finally, it should be remarked that there is no need to accept the small inaccuracy associated with the use of unsteady derivatives such as $C_{L_{\dot{\alpha}}}$, etc. In Sec. 5.11 it was shown how the use of aerodynamic transfer functions could avoid this difficulty entirely, and equations (5.14,1 to 3) were presented for this purpose. To obtain a transfer function from the indicial response, (5.11,6) can be applied. Thus if the step-function response of Fig. 7.17 is designated $A_{L\alpha}(\hat{t})$, then

$$\hat{G}_{L\alpha}(s) = s\bar{A}_{L\alpha}(s)$$

and similarly for all other transfer functions that appear in (5.14,1 to 3).

When the information available is in the form of a frequency-response analysis or measurement, then the transfer function can be obtained from it directly. From (3.4,25) we have the general relation for frequency response of a linear system in terms of the transfer function. Thus, let $G_{av}(s)$ be the transfer function relating any aerodynamic coefficient C_a to any state variable v and $G_{av}(ik)$ be the frequency-response vector giving C_a for periodic v. $G(s)$ is obtained from $G(ik)$ by replacing ik by s, or k by $-is$.

7.12 THE z DERIVATIVES (C_{T_z}, C_{D_z}, C_{L_z}, C_{m_z})

There are two main classes of z derivatives; those that are associated with ground proximity, and those that are associated with vertical gradients in the properties of the atmosphere. Of the latter the density gradient is the most important, and others can probably be ignored most of the time.

We have described some of the effects of ground proximity in Sec. 7.5. To calculate the associated z derivatives one needs the data, either theoretical or experimental, on the variation of the various coefficients with height above ground. For configurations with large power effects, i.e. strong slipstreams or jets impinging on the ground, testing is generally required to get good results. The ground effects can be very large, and the z derivatives can exert a very important influence on the vehicle dynamics at landing and take-off.

As to the effects of atmospheric gradients, the gradient $\partial\rho/\partial z$ has already been explicity included in the equations of motion (5.13,16), so that if T, D, L, M all vary exactly as ρ when the speed is constant then C_{T_z} etc. will all be zero. This assumption is probably good enough for D, L, and M, but not always for T. If the vehicle uses air-breathing engines, then $T \propto \rho$ is reasonable, and $C_{T_z} = 0$; but if a constant-thrust rocket is used, then we have

$\partial T/\partial z = 0$, and from the analysis on p. 183,

$$C_{T_z} = -C_{T_e}\frac{\partial \hat{\rho}}{\partial \hat{z}} \tag{7.12,1}$$

The only other atmospheric gradients that might need to be included are those associated with Reynolds number R_e and Mach number $\mathbf{M}$. Sometimes, for very high altitudes the particulate nature of air becomes a factor. The Knudson number

$$K_n = \frac{\lambda}{l}$$

where λ is the mean free path and l is a characteristic length of the vehicle, may then be used as an aerodynamic parameter. It is not a new independent variable, being related to $\mathbf{M}$ and R_e:

$$K_n = 1.26\sqrt{\gamma}\,\frac{\mathbf{M}}{R_e}$$

where γ is the ratio of specific heats. For air a rough approximation is $K_n \simeq \mathbf{M}/R_e$. The circumstances when these gradients might be important are those involving very rapid changes of the flow field with the parameter in question—for example, near $\mathbf{M} = 1$, the variations of $\mathbf{M}$ with height due to sound-speed gradient; and near the R_e for boundary layer transition. A typical derivative would be calculated thus. Let C_x stand for any of $C_T \cdots C_m$; then

$$C_{x_z} = \frac{\partial C_x}{\partial \hat{z}} = \frac{\partial C_x}{\partial \mathbf{M}}\frac{\partial \mathbf{M}}{\partial \hat{z}} + \frac{\partial C_x}{\partial R_e}\frac{\partial R_e}{\partial \hat{z}} \tag{7.12,2}$$

where

$$\frac{\partial \mathbf{M}}{\partial \hat{z}} = \frac{\bar{c}}{2}\frac{\partial}{\partial z}\left(\frac{V}{a}\right) = -\frac{V\bar{c}}{2a^2}\frac{\partial a}{\partial z} = -\mathbf{M}\frac{\bar{c}}{2a}\frac{\partial a}{\partial z}$$

and

$$\frac{\partial R_e}{\partial \hat{z}} = \frac{\bar{c}}{2}\frac{\partial}{\partial z}\left(\frac{Vl}{\nu}\right) = -\frac{\bar{c}Vl}{2\nu^2}\frac{\partial \nu}{\partial z} = -R_e\frac{\bar{c}}{2\nu}\frac{\partial \nu}{\partial z}$$

Finally,

$$C_{x_z} = -\mathbf{M}\frac{\bar{c}}{2a}\frac{\partial a}{\partial z}\frac{\partial C_x}{\partial \mathbf{M}} - R_e\frac{\bar{c}}{2\nu}\frac{\partial \nu}{\partial z}\frac{\partial C_x}{\partial R_e} \tag{7.12,3}$$

7.13 AEROELASTIC DERIVATIVES

In Sec. 5.12 there were introduced certain aerodynamic derivatives associated with the deformations of the airplane. These are of two kinds: those that appear in the rigid-body equations, and those that appear in the added equations of the elastic degrees of freedom. These are illustrated in

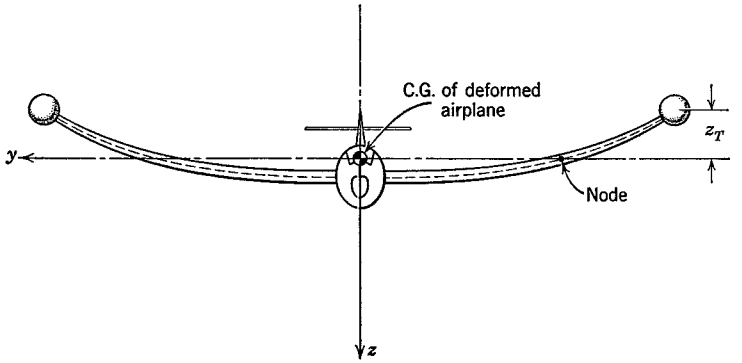

FIG. 7.22 Symmetrical wing bending.

this section by consideration of the hypothetical vibration mode shown in Fig. 7.22. In this mode it is assumed that the fuselage and tail are rigid, and have a motion of vertical translation only. The flexibility is all in the wing, and it bends without twisting. The functions describing the mode (5.12,1) are therefore:

$$\begin{aligned} x' &= x - x_0 = 0 \\ y' &= y - y_0 = 0 \\ z' &= z - z_0 = h(y)z_T \end{aligned} \tag{7.13,1}$$

For the generalized coordinate, we have used the wing-tip deflection z_T. $h(y)$ is then a normalized function describing the wing bending mode.

In view of the fact that the elastic degrees of freedom are only important in relation to stability and control when their frequencies are relatively low, approaching those of the rigid-body modes, then it is reasonable to use the same approximation for the aerodynamic forces as is used in calculating stability derivatives. That is, if quasisteady flow theory is adequate for the aerodynamic forces associated with the rigid-body motions, then we may use the same theory for the elastic motions.

In the example chosen, we assume that the only significant forces are those on the wing and tail, and that these are to be computed from quasisteady flow theory. In the light of these assumptions, some of the representative derivatives of both types are discussed below. As a preliminary, the forces induced on the wing and tail by the elastic motion are treated first.

FORCES ON THE WING

The vertical velocity of the wing section distant y from the center line is

$$\dot{z} = h(y)\dot{z}_T \tag{7.13,2}$$

and the corresponding change in wing angle of attack is

$$\Delta\alpha(y) = h(y)\dot{z}_T/V \tag{7.13,3}$$

This angle-of-attack distribution can be used with any applicable steady-flow wing theory to calculate the incremental local section lift. (It will of course be proportional to $\dot{z}_T/V$.) Let it be denoted in coefficient form by $C'_l(y)\dot{z}_T/V$, and the corresponding increment in wing total lift coefficient by $C'_{Lw}\dot{z}_T/V$. $C'_l(y)$ and C'_{Lw} are thus the values corresponding to unit value of the non-dimensional quantity $\dot{z}_T/V$.

FORCE ON THE TAIL

The tail experiences a downward velocity $h(0)\dot{z}_T$, and also, because of the altered wing lift distribution, a downwash change $(\partial\epsilon/\partial\dot{z}_T)\dot{z}_T$. Hence the net change in tail angle of attack is

$$\begin{aligned}\Delta\alpha_t &= h(0)\dot{z}_T/V - \frac{\partial\epsilon}{\partial\dot{z}_T}\dot{z}_T \\ &= \left[h(0) - \frac{\partial\epsilon}{\partial(\dot{z}_T/V)}\right]\frac{\dot{z}_T}{V}\end{aligned} \tag{7.13,4}$$

This produces an increment in the tail lift coefficient of amount

$$\Delta C_{L_t} = a_t\left[h(0) - \frac{\partial\epsilon}{\partial(\dot{z}_T/V)}\right]\frac{\dot{z}_T}{V} \tag{7.13,5}$$

THE DERIVATIVE $L_{\dot{z}_T}$

This derivative describes the contribution of wing bending velocity to the lift acting on the airplane. A suitable nondimensional form is $\partial C_L/\partial(\dot{z}_T/V)$:

$$\Delta C_L = C'_{Lw}\frac{\dot{z}_T}{V} + a_t\left[h(0) - \frac{\partial\epsilon}{\partial(\dot{z}_T/V)}\right]\frac{\dot{z}_T}{V}\frac{S_t}{S}$$

and hence

$$\frac{\partial C_L}{\partial(\dot{z}_T/V)} = C'_{Lw} + a_t\left[h(0) - \frac{\partial\epsilon}{\partial(\dot{z}_T/V)}\right]\frac{S_t}{S} \tag{7.13,6}$$

THE DERIVATIVE A_{n_α}

This derivative (see 5.12,12) represents the contribution to the generalized force in the bending degree of freedom, associated with a change in the angle of attack of the airplane. A suitable nondimensional form is obtained by defining

$$C_{\mathscr{F}} = \frac{\mathscr{F}}{\frac{1}{2}\rho V^2 S}$$

Then the appropriate nondimensional derivative is $C_{\mathscr{F}_\alpha}$.

Let the wing lift distribution due to a perturbation α in the angle of attack (constant across the span) be given by $C_{l_\alpha}(y)\alpha$. Then in a virtual displacement in the wing bending mode δz_T, the work done by this wing loading is

$$\delta W = -\int_{-b/2}^{b/2} \alpha C_{l_\alpha}(y) h(y)\, \delta z_T \tfrac{1}{2}\rho V^2 c(y)\, dy$$

where $c(y)$ is the local wing chord. The corresponding contribution to $\mathscr{F}$ is

$$\frac{\partial W}{\partial z_T} = -\alpha \tfrac{1}{2}\rho V^2 \int_{-b/2}^{b/2} C_{l_\alpha}(y) h(y) c(y)\, dy$$

and to $C_{\mathscr{F}_\alpha}$ is

$$\frac{1}{\frac{1}{2}\rho V^2 S}\frac{\partial^2 W}{\partial z_T\, \partial \alpha} = -\frac{1}{S}\int_{-b/2}^{b/2} C_{l_\alpha}(y) h(y) c(y)\, dy \qquad (7.13,7)$$

The tail also contributes to this derivative. For the tail lift associated with α is

$$a_t \alpha \left(1 - \frac{\partial \epsilon}{\partial \alpha}\right) \tfrac{1}{2}\rho V^2 S_t$$

and the work done by this force during the virtual displacement is

$$-a_t \alpha \left(1 - \frac{\partial \epsilon}{\partial \alpha}\right) \tfrac{1}{2}\rho V^2 S_t h(0)\, \delta z_T$$

Therefore the contribution to $C_{\mathscr{F}}$ is

$$-a_t \alpha \left(1 - \frac{\partial \epsilon}{\partial \alpha}\right) \frac{S_t}{S} h(0)$$

and to $C_{\mathscr{F}_\alpha}$ is

$$-a_t \frac{S_t}{S} h(0) \left(1 - \frac{\partial \epsilon}{\partial \alpha}\right) \qquad (7.13,8)$$

The total value of $C_{\mathscr{F}_\alpha}$ is then the sum of (7.13,7 and 8.)

THE DERIVATIVE b_{11} (SEE 5.12,12)

This derivative identifies the contribution of $\dot{z}_T$ to the generalized aerodynamic force in the distortion degree of freedom. We have defined the associated wing load distribution above by the local lift coefficient $C_l'(y)\dot{z}_T/V$. As in the case of the derivative A_{n_α} above, the work done by this loading is calculated, with the result that the wing contributes

$$\frac{\partial C_{\mathscr{F}}}{\partial(\dot{z}_T/V)} = \frac{1}{\frac{1}{2}\rho V^2 S}\frac{\partial^2 W}{\partial z_T\, \partial(\dot{z}_T/V)} = -\frac{1}{S}\int_{-b/2}^{b/2} C_l'(y) h(y) c(y)\, dy \qquad (7.13,9)$$

Table 7.1

Summary—Longitudinal Derivatives

	C_T	C_D	C_L	C_m	C_{he}
V	$\frac{(\partial T/\partial V)_e}{\frac{1}{2}\rho V_e S} - 2C_{T_e}$	$\mathbf{M}\frac{\partial C_D}{\partial \mathbf{M}} + \rho_e V_e^2 \frac{\partial C_D}{\partial p_d} + C_{T_V}\left(\frac{\partial C_D}{\partial C_T}\right)_e$	$\mathbf{M}\frac{\partial C_L}{\partial \mathbf{M}} + \rho_e V_e^2 \frac{\partial C_L}{\partial p_d} + C_{T_V}\left(\frac{\partial C_L}{\partial C_T}\right)_e$	$\mathbf{M}\frac{\partial C_m}{\partial \mathbf{M}} + \rho_e V_e^2 \frac{\partial C_m}{\partial p_d} + C_{T_V}\left(\frac{\partial C_m}{\partial C_T}\right)_e$	$\mathbf{M}\frac{\partial C_{he}}{\partial \mathbf{M}} + \rho_e V_e^2 \frac{\partial C_{he}}{\partial p_d} + C_{T_V}\left(\frac{\partial C_{he}}{\partial C_T}\right)_e$
α	N.A.[a]	$2KC_{L_e}C_{L_\alpha}$	C_{L_α}	$C_{L_\alpha}(h - h_n)$	$b_1\left(1 - \frac{\partial \epsilon}{\partial \alpha}\right)$
$\dot{\alpha}$	Neg.[b]	Neg.	*[c] $2a_t V_H \frac{\partial \epsilon}{\partial \alpha}$	* $-2a_t V_H \frac{l_t}{\bar{c}} \frac{\partial \epsilon}{\partial \alpha}$	* $2b_1 \frac{l_t}{\bar{c}} \frac{\partial \epsilon}{\partial \alpha}$
q	Neg.	Neg.	$-2C_{L_\alpha}(h - h_0) + 2a_t V_H$	$\overline{C}_{m_q} - 2C_{L_\alpha}(h - \bar{h})^2 - 2a_t V_H \frac{l_t}{\bar{c}} - 2C_T \frac{V}{V_j}\frac{\xi^2}{\bar{c}^2}$	$2b_1 \frac{l_t}{\bar{c}}$
δ_e	Neg.	Neg.	$a_e \frac{S_t}{S}$	$-a_e V_H$	b_2

[a] N. A. means no convenient formula available.
[b] "Neg." means usually negligible.
[c] The asterisk means contribution of the tail only.

Likewise, the contribution of the tail is calculated here as for $A_{n\alpha}$, and is found to be

$$-a_t \frac{S_t}{S} h(0)\left[h(0) - \frac{\partial \epsilon}{\partial(\dot{z}_T/V)}\right] \qquad (7.13,10)$$

The total value of $\partial C_{\mathscr{Z}}/\partial(\dot{z}_T/V)$ is then the sum of (7.13,9 and 10.).

7.14 SUMMARY OF THE FORMULAE

The formulae that are frequently wanted for reference are collected in Table 7.1. Where an entry in the table shows only a tail contribution, it is not implied that wing and body effects are not important, but only that no convenient formula is available.

Lateral aerodynamic characteristics

CHAPTER 8

In the preceding two chapters we have discussed the aerodynamic characteristics of symmetrical configurations flying with the velocity vector in the plane of symmetry. As a result the only nonzero motion variables were V, α, and q, and the only nonzero forces and moments were T, D, L, and M. We now turn to the cases in which the velocity vector is not in the plane of symmetry, and in which rolling and yawing motions (β, p, r) are present. The associated force and moment coefficients are C_C or C_y, C_l, and C_n (see Table 5.1).

One of the simplifying aspects of the longitudinal motion is that the rotation is about one axis only (the y axis), and hence the rotational stiffness about that axis is a very important criterion for the dynamic behavior. This simplicity is lost when we go to the lateral motions, for then the rotation takes place about two axes (x and z). The moments associated with these rotations are cross-coupled, i.e. roll rotation p produces yawing moments C_n as well as rolling moment C_l, and yaw displacements β and rate r both produce rolling *and* yawing moments. Furthermore, the roll and yaw controls are also often cross-coupled—deflection of the ailerons can produce significant yawing moments, and deflection of the rudder can produce significant rolling moments.

Another important difference between the two cases is that in "normal" flight—i.e. steady rectilinear symmetric motion, all the lateral motion and

force variables are zero. Hence there is no *fundamental* trimming problem—the ailerons and rudder would be nominally undeflected. In actuality of course, these controls do have a secondary trimming function whenever the vehicle has either geometric or inertial asymmetries—e.g. one engine off, or multiple propellers all rotating the same way. Because the gravity vector in normal flight also lies in the plane of symmetry, the C.G. position is not a dominant parameter for the lateral characteristics as it is for the longitudinal. Thus the C.G. limits, as discussed in Sec. 7.6 are governed by considerations deriving from the longitudinal characteristics.

8.1 YAW STIFFNESS (WEATHERCOCK STABILITY)

By exactly the same argument as used for pitch stiffness (Sec. 6.2), we conclude that flight vehicles should have positive yaw stiffness, i.e. (see Fig. 8.1) $\partial C_n/\partial\beta > 0$. For then a perturbation in β will produce a restoring moment N that tends to keep the velocity vector in the plane of symmetry.

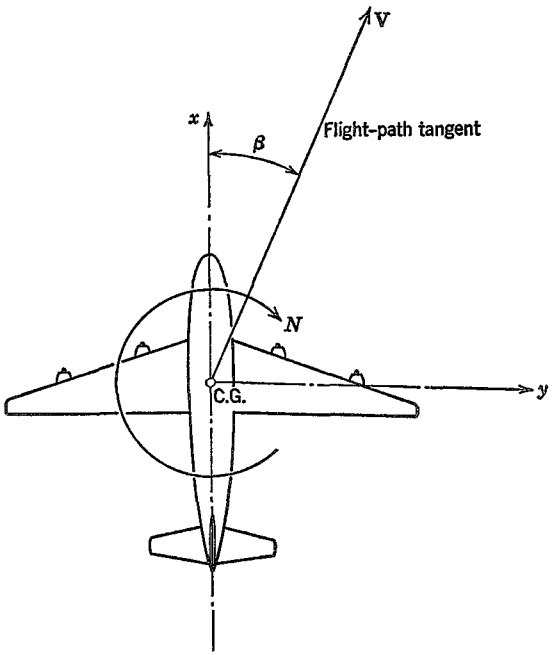

FIG. 8.1 Sideslip angle and yawing moment.

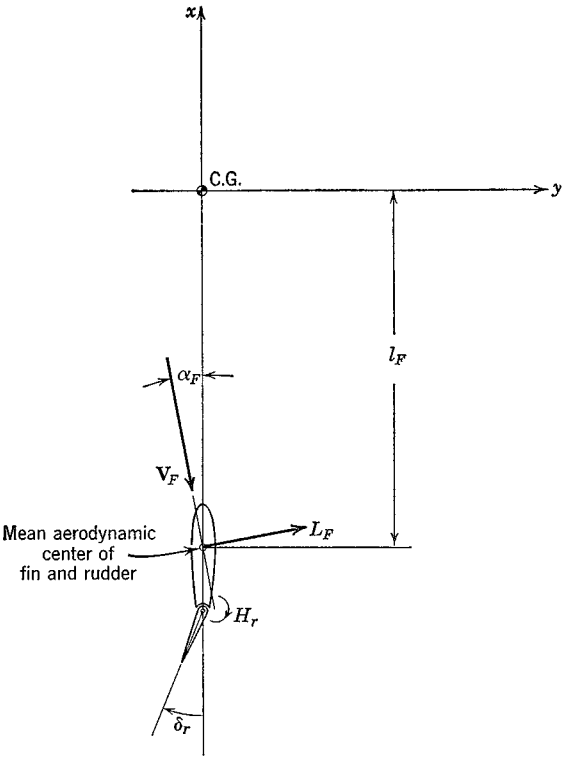

FIG. 8.2 Vertical-tail sign conventions.

C_{n_β} is found from wind-tunnel measurements of the yawing moment, or when these are not available, can be estimated by synthesising the contributions of the various components of the vehicle. The principal contributions are those of the body and the tail. By contrast with C_{m_α}, the wing makes a relatively small contribution to C_{n_β}.

In Fig. 8.2 are shown the relevant geometry and the lift force L_F acting on the vertical tail surface. If the surface were alone in an airstream, the velocity vector $\mathbf{V}_F$ would be that of the free stream, so that (cf. Fig. 8.1) α_F would be equal to $-\beta$. When installed on an airplane, however, changes in both magnitude and direction of the local flow at the tail take place. These changes may be caused by the propellor slipstream, and by the wing and fuselage when the airplane is yawed. The angular deflection is allowed for by introducing the sidewash angle σ, analogous to the downwash angle ϵ. σ is positive when it corresponds to a flow in the y direction: i.e. when it tends to

increase α_F. Thus the angle of attack is

$$\alpha_F = -\beta + \sigma \tag{8.1,1}$$

and in the linear case the lift coefficient of the vertical-tail surface is

$$C_{L_F} = a_F(-\beta + \sigma) + a_r\delta_r \tag{8.1,2}$$

The lift is then

$$L_F = C_{L_F}\frac{\rho}{2}V^2S_F \tag{8.1,3}$$

Just as with the horizontal tail, any difference between V_F and V is absorbed into the coefficients a_F and a_r. The yawing moment is

$$N_F = -C_{L_F}\frac{\rho}{2}V^2S_Fl_F$$

whence

$$C_{n_F} = -C_{L_F}\frac{S_Fl_F}{Sb} \tag{8.1,4}$$

The ratio S_Fl_F/Sb is analogous to the horizontal-tail volume ratio, and is therefore called the *vertical-tail volume ratio*, denoted here by V_V. Equation (8.1,4) then reads

$$C_{n_F} = -V_VC_{L_F} \tag{8.1,5}$$

and the corresponding contribution to the weathercock stability is

$$C_{n_\beta}|_{\text{fin}} = \frac{\partial C_{n_F}}{\partial\beta} = -V_V\frac{\partial C_{L_F}}{\partial\beta} = V_Va_F\left(1 - \frac{\partial\sigma}{\partial\beta}\right) \tag{8.1,6}$$

The Sidewash Factor $\partial\sigma/\partial\beta$. Generally speaking the sidewash is difficult to estimate with engineering precision. Suitable wind-tunnel tests are required for this purpose. The contribution from the fuselage arises through its behavior as a lifting body when yawed. Associated with the side force that develops is a vortex wake which induces a lateral-flow field at the tail. The sidewash from the propeller is associated with the side force which acts upon it when yawed, and may be estimated by the method of ref. 7.3, previously cited in Sec. 7.3. The contribution from the wing is associated with the asymmetric structure of the flow that develops when the airplane is yawed. This phenomenon is especially pronounced with low-aspect-ratio swept wings. It is illustrated in Fig. 8.3.

The Velocity Ratio V_F/V. When the vertical tail is not in a propeller slipstream, V_F/V is unity. When it is in a slipstream, the effective velocity increment may be dealt with as for a horizontal tail (see Sec. 7.3).

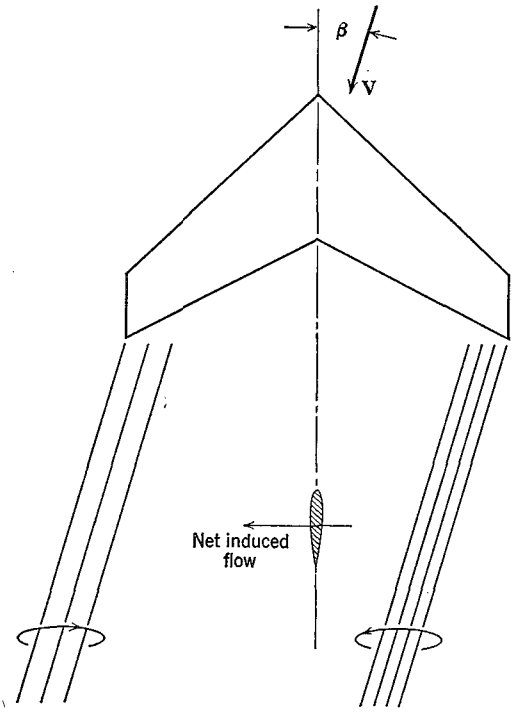

FIG. 8.3 Vortex wake of yawed wing.

Contribution of Propeller Normal Force. The yawing moment produced by the normal force which acts on the yawed propeller is calculated in the same way as the pitching-moment increment dealt with in Sec. 7.3. The result is similar to (7.3,10)

$$\frac{\partial C_{np}}{\partial \beta} = -\frac{x_p}{b}\frac{S_p}{S}\frac{\partial C_{Np}}{\partial \alpha_p} \tag{8.1,7}$$

This is known as the propeller fin effect, and is negative, i.e. destabilizing, when the propeller is forward of the C.G., but is usually positive for pusher propellers.

8.2 YAW CONTROL

In most flight conditions it is desired to maintain the sideslip angle equal to zero. If the airplane has positive weathercock stability, and is truly

symmetrical, then it will tend to fly in this condition. However, yawing moments may act upon the airplane as a result of unsymmetrical thrust (e.g. one engine inoperative). slipstream rotation, or the unsymmetrical flow field associated with turning flight. Under these circumstances, β can be kept zero only by the application of a control moment. The control that provides this is the rudder. Another condition requiring the use of the rudder is the steady side-slip, a maneuver sometimes used, particularly with light aircraft, to increase the drag and hence the glide path angle. From (8.1,2 and 5), the rate of change of yawing moment with rudder deflection is given by

$$C_{n_\delta} = \frac{\partial C_n}{\partial \delta_r} = -V_V \frac{\partial C_{L_F}}{\partial \delta_r} = -a_r V_V \tag{8.2,1}$$

This derivative is sometimes called the "rudder power." It must be large enough to make it possible to maintain zero sideslip under the most extreme conditions of asymmetric thrust and turning flight.

A second useful index of the rudder control is the steady sideslip angle which could be maintained by a given rudder angle if the aileron angle, roll rate, and yaw rate were all zero. The total yawing moment would then be

$$C_n = C_{n_\beta}\beta + C_{n_\delta}\delta_r \tag{8.2,2}$$

For steady motion, $C_n = 0$, and hence the desired ratio is

$$\frac{\beta}{\delta_r} = -\frac{C_{n_\delta}}{C_{n_\beta}} \tag{8.2,3}$$

The rudder hinge moment and control force are treated in a manner similar to that employed for the elevator. Let the rudder hinge-moment coefficient be given by

$$C_{hr} = b_1\alpha_F + b_2\delta_r \tag{8.2,4}$$

The rudder pedal force will then be given by

$$\begin{aligned} P &= G\frac{\rho}{2}V^2 S_r c_r(b_1\alpha_F + b_2\delta_r) \\ &= G\frac{\rho}{2}V^2 S_r c_r[b_1(-\beta + \sigma) + b_2\delta_r)] \end{aligned} \tag{8.2,5}$$

where G is the rudder system gearing.

The effect of a free rudder on the yaw stiffness is found by setting $C_{hr} = 0$ in (8.2,4). Then the rudder floating angle is

$$\delta_{\text{free}} = -\frac{b_1}{b_2}\alpha_F \tag{8.2,6}$$

The vertical-tail lift coefficient with rudder free is found from (8.1,2) to be

$$C'_{L_F} = a_F\alpha_F - a_r\frac{b_1}{b_2}\alpha_F$$

$$= a_F\alpha_F\left(1 - \frac{a_r}{a_F}\frac{b_1}{b_2}\right) \qquad (8.2,7)$$

The free control factor for the rudder is thus seen to be of the same form as that for the elevator (see Sec. 6.6) and to have a similar effect.

8.3 ROLL STIFFNESS

Consider a vehicle constrained, as on bearings in a wind tunnel, to one degree of freedom-rolling about the x axis. The forces and moments resulting from a fixed displacement ϕ are fundamentally different in character from those associated with the rotations α and β about the other two axes. In the first place if the x axis coincides with the velocity vector **V**, *no aerodynamic change whatsoever* follows from the fixed rotation ϕ (see Fig. 8.4). The aerodynamic field remains symmetrical with respect to the plane of symmetry, the resultant aerodynamic force remains in that plane, and no changes occur in any of the aerodynamic coefficients. Thus the roll stiffness C_{l_ϕ} is zero in that case.

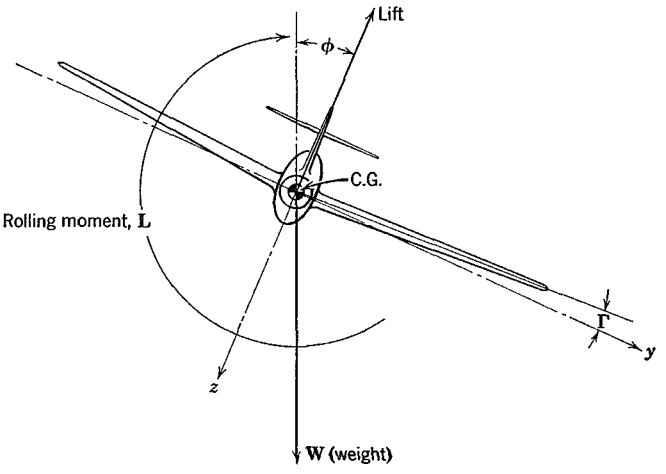

FIG. 8.4 Rolled airplane.

If the x axis does not coincide with $\mathbf{V}$, then a second-order roll stiffness results through the medium of the derivative C_{l_β}. Let the angle of attack of the x axis be α_x (Fig. 4.4), then the velocity vector when $\phi = 0$ is

$$\mathbf{V}_1 = \begin{bmatrix} V \cos \alpha_x \\ 0 \\ V \sin \alpha_x \end{bmatrix} \tag{8.3,1}$$

After rolling through angle ϕ about Ox, the velocity vector is (cf. Sec. 4.5)

$$\mathbf{V}_2 = \mathbf{L}_1(\phi)\mathbf{V}_1 = \begin{bmatrix} V \cos \alpha_x \\ V \sin \alpha_x \sin \phi \\ V \sin \alpha_x \cos \phi \end{bmatrix} \tag{8.3,2}$$

Thus the sideslip component is $v = V \sin \alpha_x \sin \phi$, and the sideslip angle is (4.3.3)

$$\beta = \sin^{-1} \frac{v}{V} = \sin^{-1} (\sin \alpha_x \sin \phi) \tag{8.3,3}$$

As a result of this positive β, and the usually negative C_{l_β} there is a restoring rolling moment $C_{l_\beta}\beta$ i.e.

$$\Delta C_l = C_{l_\beta} \sin^{-1} (\sin \alpha_x \sin \phi) \tag{8.3,4a}$$

For small α_x, we get the approximate result

$$\Delta C_l \doteq C_{l_\beta} \sin^{-1} (\alpha_x \sin \phi) \doteq C_{l_\beta} \alpha_x \sin \phi \tag{8.3,4b}$$

and if ϕ also is small,

$$\Delta C_l \doteq C_{l_\beta} \alpha_x \phi \tag{8.3,4c}$$

The stiffness derivative for rolling about Ox is then from (8.3,4a)

$$\frac{\partial C_l}{\partial \phi} = C_{l_\beta} \frac{\sin \alpha_x \cos \phi}{(1 - \sin^2 \alpha_x \sin^2 \phi)^{1/2}} \tag{8.3,5a}$$

or for $\alpha_x << 1$,

$$\frac{\partial C_l}{\partial \phi} \doteq C_{l_\beta} \alpha_x \cos \phi \tag{8.3,5b}$$

or for α_x, $\phi << 1$

$$\frac{\partial C_l}{\partial \phi} \doteq C_{l_\beta} \alpha_x \tag{8.3,5c}$$

Thus there is a roll stiffness that resists rolling if α_x is >0, and would tend to keep the wings level. If rolling occurs about a wind axis, the stiffness is zero and the vehicle has no preferred roll angle. If $\alpha_x < 0$, then the stiffness

is negative and the vehicle would roll to the position $\phi = 180°$, at which point $C_l = 0$ and $C_{l_\phi} < 0$.

The above discussion applies to a vehicle constrained, as stated, to one degree of freedom. *It should not be thought that the derivative* C_{l_ϕ} *so deduced should be introduced into the rolling moment equation* (5.13,17*b*)! The rolling moment we have discussed above arises solely from the aerodynamic effect of β, and as such is *already included* in the term $C_{l_\beta}\beta$ of the equation. The usefulness of the above point of view is that it helps one to understand the behavior of free motions that consist principally of rolling about an axis in the plane of symmetry.

Having shown above that airplanes have no first-order aerodynamic roll stiffness, it is worthwhile to digress at this point to show why they nevertheless have an inherent tendency to fly with wings level. They do so because of a secondary effect, involving gravity and C_{l_β}. When rolled to an angle ϕ, there is a weight component $mg \sin \phi$ in the y direction (Fig. 8.4). This induces a sideslip velocity to the right, with consequent $\beta > 0$, and a rolling moment $C_{l_\beta}\beta$ that tends to bring the wings level. The rolling and yawing motions that result from such an initial condition are however strongly coupled, so no significant conclusions can be drawn about the behavior except by a dynamic analysis (see Chapter 9).

8.4 ROLLING CONTROL

The angle of bank of the airplane is controlled by the ailerons. The primary function of these controls is to produce a rolling moment, although they frequently introduce a yawing moment as well. The effectiveness of the ailerons in producing rolling and yawing moments is described by the two control derivatives $\partial C_l/\partial \delta_a$ and $\partial C_n/\partial \delta_a$. The aileron angle δ_a is defined as the mean value of the angular displacements of the two ailerons. It is positive when the right aileron movement is downward (see Fig. 8.5). The derivative $\partial C_l/\partial \delta_a$ is normally negative, right aileron down producing a roll to the left.

For simple flap-type ailerons, the increase in lift on the right side and the decrease on the left side produce a drag differential which gives a positive (nose-right) yawing moment. Since the normal reason for moving the right aileron down is to initiate a turn to the left, then the yawing moment is seen to be in just the wrong direction. It is therefore called *aileron adverse yaw*. On high-aspect-ratio airplanes this tendency may introduce decided difficulties in lateral control. Means for avoiding this particular difficulty include the use of spoilers and Frise ailerons. Spoilers are illustrated in Fig. 8.6. They achieve the desired result by reducing the lift and increasing the drag on the side where the spoiler is raised. Thus the rolling and yawing moments

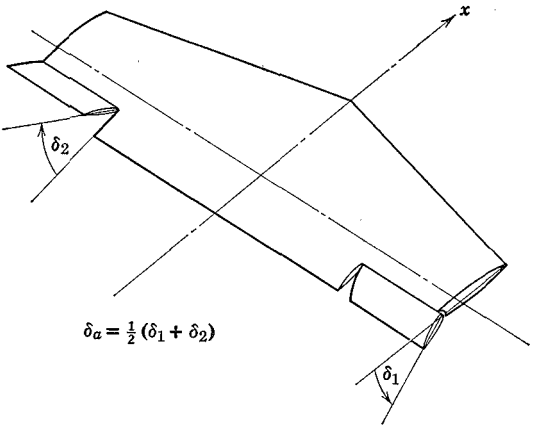

FIG. 8.5 Aileron angle.

developed are mutually complementary with respect to turning. Frise ailerons (Fig. 6.23) diminish the adverse yaw or eliminate it entirely by increasing the drag on the side of the upgoing aileron. This is achieved by the shaping of the aileron nose and the choice of hinge location. When deflected upward, the gap between the control surface and the wing is increased, and the relatively sharp nose protrudes into the stream. Both these geometrical factors produce a drag increase.

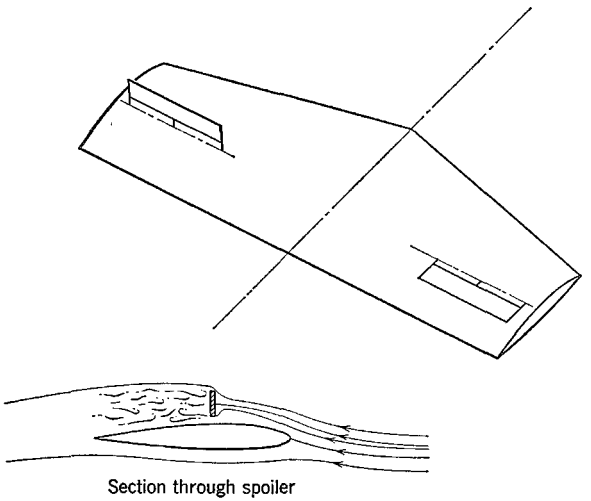

FIG. 8.6 Spoilers.

The deflection of the ailerons leads to still additional yawing moments once the airplane acquires a roll rate. These are caused by the altered flow about the wing and tail. These effects are discussed in Sec. 8.6 (C_{n_p}), and are illustrated in Figs. 8.12 and 8.15.

A final remark about aileron controls is in order. They are functionally distinct from the other two controls in that they are *rate* controls. If the airplane is restricted only to rotation about the wind axis, then the application of a constant aileron angle results in a steady *rate* of roll. The elevator and rudder, on the other hand, are *displacement* controls. When the airplane is constrained to the relevant single-axis degree of freedom, a constant deflection of these controls produces a constant angular *displacement* of the airplane. It appears that both rate and displacement controls are acceptable to pilots.

AILERON REVERSAL

There is an important aeroelastic effect on roll control by ailerons that is significant on most conventional airplanes at both subsonic and supersonic speeds. This results from the elastic distortion of the wing structure associated with the aerodynamic load increment produced by the control. As illustrated in Fig. 6.22, the incremental load caused by deflecting a control flap at subsonic speeds has a centroid somewhere near the middle of the wing chord. At supersonic speeds the control load acts mainly on the deflected surface itself, and hence has its centroid even farther to the rear. If this load centroid is behind the elastic axis of the wing structure, then a nose-down twist of the main wing surface results. The reduction of angle of attack corresponding to $\delta > 0$ causes a reduction in lift on the surface as compared with the rigid case, and a consequent reduction in the control effectiveness. The form of the variation of $C_{l_{\delta_a}}$ with $\frac{1}{2}\rho V^2$ for example can be seen by considering an idealized model of the phenomenon. Let the aerodynamic torsional moment resulting from equal deflection of the two ailerons be $T(y) \propto \frac{1}{2}\rho V^2 \delta_a$ and let $T(y)$ be antisymmetric, $T(y) = -T(-y)$. The twist distribution corresponding to $T(y)$ is $\theta(y)$, also antisymmetric, such that $\theta(y)$ is proportional to T at any reference station, and hence proportional to $\frac{1}{2}\rho V^2 \delta_a$. Finally, the antisymmetric twist causes an antisymmetric increment in the lift distribution, giving a proportional rolling moment increment $\Delta C_l = k\frac{1}{2}\rho V^2 \delta_a$. The total rolling moment due to aileron deflection is then

$$\Delta C_l = (C_{l_{\delta_a}})_{\text{rigid}} \delta_a + k\tfrac{1}{2}\rho V^2 \delta_a \tag{8.4,1}$$

and the control effectiveness is

$$C_{l_{\delta_a}} = (C_{l_{\delta_a}})_{\text{rigid}} + k\tfrac{1}{2}\rho V^2 \tag{8.4,2}$$

As noted above, $(C_{l_{\delta_a}})_{\text{rigid}}$ is negative, and k is positive if the centroid of the aileron-induced lift is aft of the wing elastic axis, the common case. Hence $|C_{l_{\delta_a}}|$ diminishes with increasing speed, and vanishes at some speed V_R, the *aileron reversal speed.* Hence

$$0 = (C_{l_{\delta_a}})_{\text{rigid}} + k\tfrac{1}{2}\rho V_R^2$$

or

$$k = -(C_{l_{\delta_a}})_{\text{rigid}} / \tfrac{1}{2}\rho V_R^2 \tag{8.4,3}$$

Substitution of (8.4,3) into (8.4,2) yields

$$C_{l_{\delta_a}} = (C_{l_{\delta_a}})_{\text{rigid}}\left(1 - \frac{V^2}{V_R^2}\right) \tag{8.4,4}$$

This result, of course, applies strictly only if the basic aerodynamics are not Mach-number dependent, i.e. so long as V_R is at a value of $\mathbf{M}$ appreciably below 1.0. Otherwise k and $(C_{l_{\delta_a}})_{\text{rigid}}$ are both functions of $\mathbf{M}$, and the equation corresponding to (8.4,4) is

$$C_{l_{\delta_a}}(\mathbf{M}) = (C_{l_{\delta_a}})_{\text{rigid}}(\mathbf{M}) - \frac{k(\mathbf{M})}{k(\mathbf{M}_R)}(C_{l_{\delta_a}})_{\text{rigid}}(\mathbf{M}_R)\frac{V^2}{V_R^2} \tag{8.4,5}$$

where $\mathbf{M}_R$ is the reversal Mach number.

It is evident from (8.4,4) that the torsional stiffness of the wing has to be great enough to keep V_R appreciably higher than the maximum flight speed if unacceptable loss of aileron control is to be avoided.

8.5 THE β DERIVATIVES (C_{y_β}, C_{l_β}, C_{n_β}, C_{hr_β})

The sideslip derivatives are all obtainable from static wind-tunnel tests on yawed models. Generally speaking, estimation methods are not very reliable, and testing is needed for accurate results.

THE DERIVATIVE C_{y_β}

We shall assume that the thrust vector remains in the xz plane, so that it does not contribute to the Y force. Then in terms of C_C and C_D (see Fig. 4.5) we have

$$C_y = -C_C \cos\beta - C_D \sin\beta$$

and

$$C_{y_\beta} = \left(C_C \sin\beta - \frac{\partial C_C}{\partial\beta}\cos\beta - C_D\cos\beta - \frac{\partial C_D}{\partial\beta}\sin\beta\right)_{\beta=\beta_e}$$

where β_e, the equilibrium value, is zero. Hence

$$C_{y_\beta} = -C_D - \frac{\partial C_C}{\partial \beta} \tag{8.5,1}$$

The main contributions to C_C usually come from the body and the tail, the wing contribution being minor. That from the tail is readily estimated. From (8.1,3) we have

$$(\Delta C)_{\text{tail}} = -C_{L_F} \frac{\rho}{2} V^2 S_F$$

and

$$(\Delta C_C)_{\text{tail}} = -C_{L_F} \frac{S_F}{S}$$

whence

$$(C_{y_\beta})_{\text{tail}} = \frac{S_F}{S} \frac{\partial C_{L_F}}{\partial \beta} = -\frac{S_F}{S} a_F \left(1 - \frac{\partial \sigma}{\partial \beta}\right) \tag{8.5,2}$$

The C_D term of (8.5,1) would often be small compared to the tail contribution (8.5,2), and the whole derivative C_{y_β} often has negligible effect on the vehicle dynamics.

THE DERIVATIVE C_{l_β}

By contrast with C_{y_β}, the derivative C_{l_β}, known as the *dihedral effect*, is of paramount importance. We have already noted its relation to roll stiffness and to the tendency of airplanes to fly with wings level. The primary contribution to C_{l_β} is from the wing—its dihedral angle, aspect ratio, and sweep all being important parameters.

The effect of wing dihedral is illustrated in Fig. 8.7. With the coordinate system shown, the normal velocity component V_n on the right wing panel (R) is, for small dihedral angle Γ,

$$\begin{aligned} V_n &= w \cos \Gamma + v \sin \Gamma \\ &\doteq w + v\Gamma \end{aligned}$$

and that on the other panel is $w - v\Gamma$. The terms $\pm v\Gamma/V = \pm\beta\Gamma$ represent opposite changes in the angle of attack of the two panels resulting from sideslip. The "upwind" panel has its angle of attack and therefore its lift increased, and vice versa. The result is a rolling moment approximately linear in both β and Γ, and hence a fixed value of C_{l_β} for a given Γ. This part of C_{l_β} is essentially independent of wing angle of attack so long as the flow remains attached.

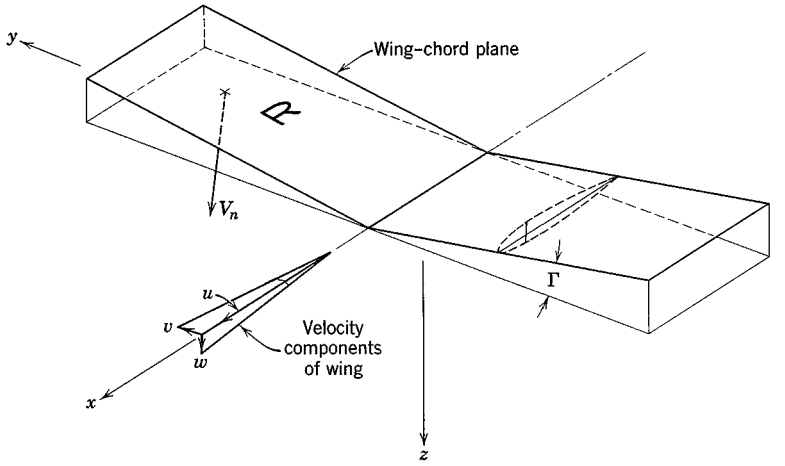

FIG. 8.7 Dihedral effect.

$$V_n = \text{normal velocity of panel } R$$
$$= w \cos \Gamma + v \sin \Gamma \doteqdot w + v\Gamma$$

$$\therefore \ \Delta\alpha \text{ of } R \text{ due to dihedral} \doteqdot \frac{v\Gamma}{V} = \frac{V\beta\Gamma}{V} = \beta\Gamma$$

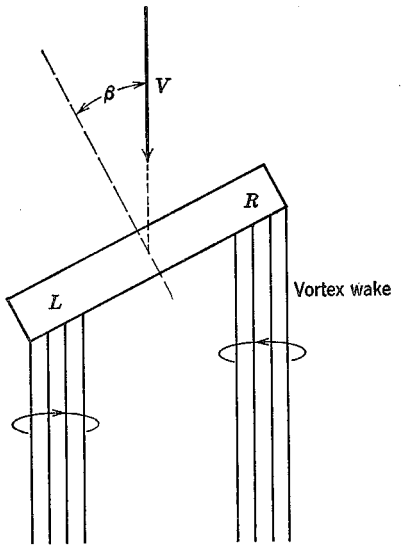

FIG. 8.8 Yawed lifting wing.

Even in the absence of dihedral, a flat lifting wing panel has a C_{l_β} proportional to C_L. Consider the case of Fig. 8.8. The vertical induced velocity (downwash) of the vortex wake is greater at L than at R simply by virtue of the geometry of the wake. Hence the local wing angle of attack and lift are less at L than at R, and a negative C_l results. Since this effect depends, essentially linearly, on the strength of the vortex wake, which is itself proportional to the wing C_L, then the result is $\Delta C_{l_\beta} \propto C_L$.

INFLUENCE OF FUSELAGE ON C_{l_β}

The flow field of the body interacts with the wing in such a way as to modify its dihedral effect. To illustrate this, consider a long cylindrical body, of circular cross section, yawed with respect to the main stream. Consider only the cross-flow component of the stream, of magnitude $V\beta$, and the flow pattern which it produces about the body. This is illustrated in Fig. 8.9. It

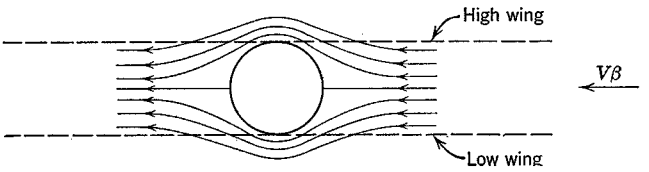

FIG. 8.9 Influence of body on C_{l_β}.

is clearly seen that the body induces vertical velocities which, when combined with the mainstream velocity, alter the local angle of attack of the wing. When the wing is at the top of the body (high-wing), then the angle-of-attack distribution is such as to produce a negative rolling moment: i.e. the dehedral effect is enhanced. Conversely, when the airplane has a low wing, the dihedral effect is diminished by the fuselage interference. The magnitude of the effect is dependent upon the fuselage length ahead of the wing, its cross-section shape, and the planform and location of the wing. Generally, this explains why high-wing airplanes usually have less wing dihedral than low-wing airplanes.

INFLUENCE OF SWEEP ON C_{l_β}

Wing sweep is a major parameter affecting C_{l_β}. Consider the swept yawed wing illustrated in Fig. 8.10. According to simple sweep theory it is the velocity V_n normal to a wing reference line ($\frac{1}{4}$ chord line for subsonic, i.e. for supersonic) that determines the lift. It follows obviously that the lift is greater

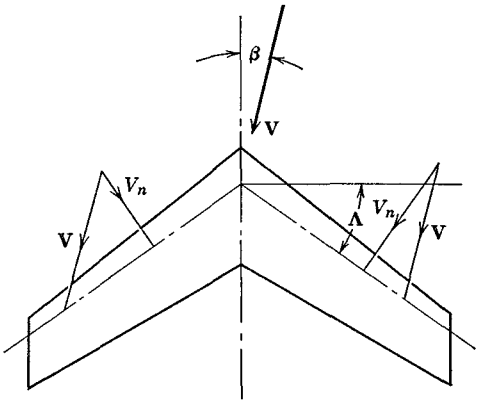

FIG. 8.10 Dihedral effect of a swept wing.

on the right half of the wing shown than on the left half, and hence that there is a negative rolling moment. The rolling moment would be expected for small β to be proportional to

$$C_L[(V_n{}^2)_{\text{right}} - (V_n{}^2)_{\text{left}}] = C_L V^2[\cos^2(\Lambda - \beta) - \cos^2(\Lambda + \beta)]$$
$$\doteq 2C_L\beta V^2 \sin 2\Lambda$$

The proportionality with C_L and β is correct, but the sin 2Λ factor is not a good approximation to the variation with Λ. The result is a $C_{l_\beta} \propto C_L$, that can be calculated by the methods of linear wing theory.

INFLUENCE OF FIN ON C_{l_β}

The sideslipping airplane gives rise to a side force on the vertical tail as explained in Sec. 8.1. When the aerodynamic center of the vertical surface is appreciably offset from the rolling axis (Fig. 8.11) then this force may produce a significant rolling moment. From (8.1,2 and 3) with $\delta_r = 0$ this

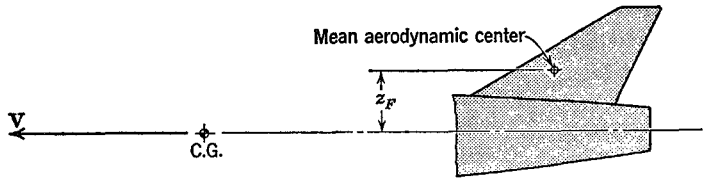

FIG. 8.11 Dihedral effect of the vertical tail.

moment is found to be

$$a_F(-\beta + \sigma)\frac{\rho}{2}V^2 S_F z_F$$

whence

$$\Delta C_l = a_F(-\beta + \sigma)\frac{S_F z_F}{Sb}$$

and

$$\Delta C_{l_\beta} = -a_F\left(1 - \frac{\partial\sigma}{\partial\beta}\right)\frac{S_F z_F}{Sb} \tag{8.5,3}$$

THE DERIVATIVE C_{n_β}

This is the yaw stiffness derivative, already treated in detail in Sec. 8.1.

THE DERIVATIVE C_{hr_β}

This derivative gives the rudder hinge moment due to sideslip. It is analogous to the elevator hinge moment due to angle of attack. It is given by

$$\frac{\partial C_{hr}}{\partial\beta} = C_{hr_{\alpha_F}}\frac{\partial\alpha_F}{\partial\beta}$$

where $C_{hr_{\alpha_F}}$ is the appropriate coefficient—see (6.5,1). By using (8.1,1) we get

$$C_{hr_\beta} = -C_{hr_{\alpha_F}}\left(1 - \frac{\partial\sigma}{\partial\beta}\right) \tag{8.5,4}$$

8.6 THE p DERIVATIVES (C_{y_p}, C_{l_p}, C_{n_p}, C_{ha_p}, C_{hr_p})

When an airplane rolls with angular velocity p about its x axis in the reference state (the flight direction for wind axes), its motion is instantaneously like that of a screw. This motion affects the airflow (local angle of attack) at all stations of the wing and tail surfaces. This is illustrated in Fig. 8.12 for two points: a wing tip and the fin tip. It should be noted that the non-dimensional rate of roll, $\hat{p} = pb/2V$ is, for small p, the angle (in radians) of the helix traced by the wing tip. These angle-of-attack changes bring about alterations in the aerodynamic load distribution over the surfaces, and thereby introduce perturbations in the forces and moments. The change in the wing load distribution also causes a modification to the trailing vortex sheet. The vorticity distribution in it is no longer symmetrical about the x axis, and a sidewash (positive, i.e. to the right) is induced at a vertical tail conventionally placed. This further modifies the angle-of-attack distribution on the vertical-tail surface. This sidewash due to rolling is characterized by the derivative

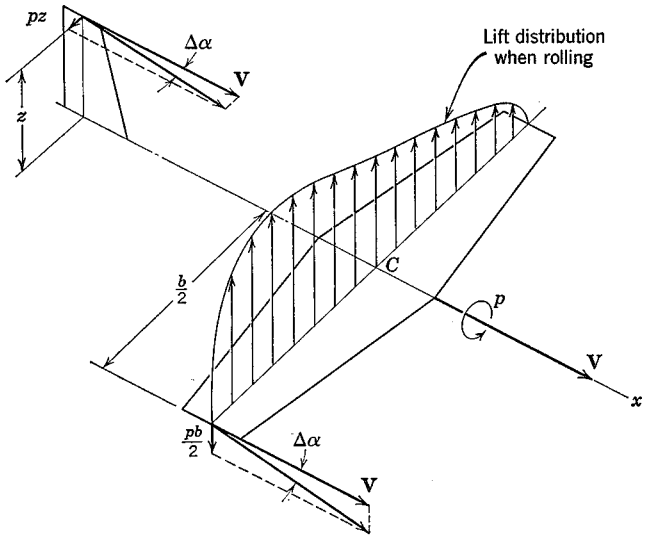

FIG. 8.12 Angle of attack changes due to p.

$\partial\sigma/\partial\hat{p}$. It has been studied theoretically and experimentally by Michael (ref. 8.1), who has shown its importance in relation to correct estimation of the tail contributions to the rolling derivatives. Finally, the helical motion of the wing produces a trailing vortex sheet which is not flat, but helical. For the small rates of roll admissible in a linear theory, this effect may be neglected with respect to both wing and tail forces.

THE DERIVATIVE C_{y_p}

The side force due to rolling is often negligible. When it is not, the contributions that need to be considered are those from the wing† and from the vertical tail. The vertical-tail effect may be estimated in the light of its angle-of-attack change (Fig. 8.12) as follows. Let the mean change in α_F (Fig. 8.2) due to the rolling velocity be

$$\Delta\alpha_F = -\frac{pz_F}{V} + p\frac{\partial\sigma}{\partial p}$$

where z_F is an appropriate mean height of the fin. Introducing the

† For the effect of the wing at low speeds, see ref. (8.4).

nondimensional rate of roll, we may rewrite this as

$$\Delta\alpha_F = -\hat{p}\left(2\frac{z_F}{b} - \frac{\partial\sigma}{\partial\hat{p}}\right) \tag{8.6,1}$$

The incremental side-force coefficient on the fin is obtained from $\Delta\alpha_F$,

$$\Delta C_{y_F} = a_F\,\Delta\alpha_F = -a_F\hat{p}\left(2\frac{z_F}{b} - \frac{\partial\sigma}{\partial\hat{p}}\right) \tag{8.6,2}$$

where a_F is the lift-curve slope of the vertical tail. The incremental side force on the airplane is then given by

$$\Delta C_y = \frac{S_F}{S}\Delta C_{y_F} = -a_F\hat{p}\frac{S_F}{S}\left(2\frac{z_F}{b} - \frac{\partial\sigma}{\partial\hat{p}}\right)$$

whence

$$(C_{y_p})_{\text{tail}} = -a_F\frac{S_F}{S}\left(2\frac{z_F}{b} - \frac{\partial\sigma}{\partial\hat{p}}\right) \tag{8.6,3}$$

THE DERIVATIVE C_{l_p}

C_{l_p} is known as the *damping-in-roll* derivative. It expresses the resistance of the airplane to rolling. Except in unusual circumstances, only the wing contributes significantly to this derivative. As can be seen from Fig. 8.12, the angle of attack due to p varies linearly across the span, from the value $pb/2V$ at the right wing tip to $-pb/2V$ at the left tip. This antisymmetric α distribution produces an antisymmetric increment in the lift distribution as shown in Fig. 8.13. In the linear range this is superimposed on the symmetric

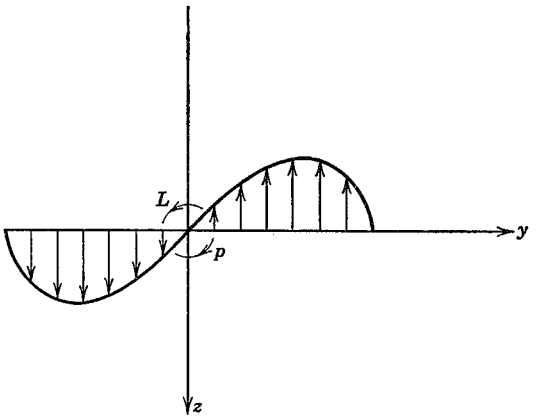

FIG. 8.13 Spanwise lift distribution due to rolling.

lift distribution associated with the wing angle of attack in undisturbed flight. The large rolling moment L produced by this lift distribution is proportional to the tip angle of attack $\hat{p}$, and C_{l_p} is a negative constant, so long as the local angle of attack remains below the local stalling angle.

If the wing angle of attack at the center line, $\alpha_w(0)$, is large, then the incremental value due to p may take some sections of the wing beyond the stalling angle, as shown in Fig. 8.14. [Actually, for finite span wings, there is

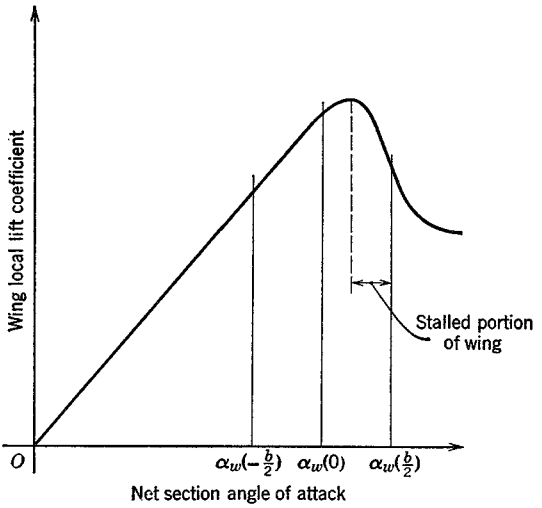

FIG. 8.14 Reduction of C_{l_p} due to wing stall.

an additional induced angle of attack distribution $\alpha_i(y)$ due to the vortex wake that modifies the net sectional value still further. We neglect this correction here in the interest of making the main point.] When this happens $|C_{l_p}\hat{p}|$ is reduced in magnitude from the linear value and if $\alpha_w(0)$ is large enough, will even change sign. When this happens, the wing will autorotate, the main characteristic of spinning flight.

THE DERIVATIVE C_{n_p}

The yawing moment produced by the rolling motion is one of the so called *cross derivatives*. It is the existence of these cross derivatives that causes the rolling and yawing motions to be so closely coupled. The wing and tail both contribute to C_{n_p}.

The wing contribution is in two parts. The first comes from the change in

profile drag associated with the change in wing angle of attack. The wing α is increased on the right-hand side and decreased on the left-hand side. These changes will normally be accompanied by an increase in profile drag on the right side, and a decrease on the left side, combining to produce a *positive* (nose-right) yawing moment. The second wing effect is associated with the fore-and-aft inclination of the lift vector which is caused by the rolling in subsonic flight and in supersonic flight when the leading edge is subsonic. Its existence depends on the leading edge suction. The physical situation is illustrated in Fig. 8.15. The directions of motion of two typical

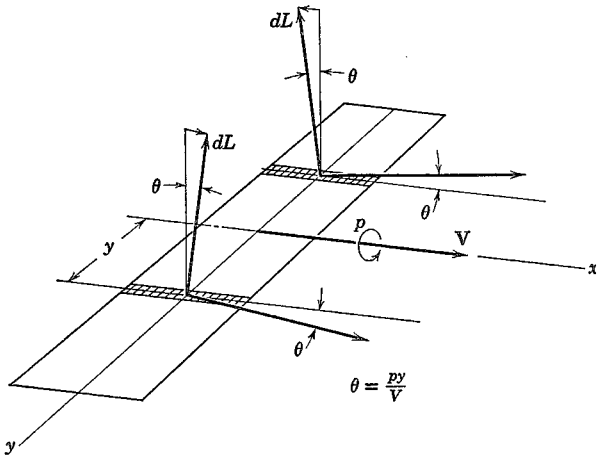

FIG. 8.15 Inclination of C_L vector due to rolling.

wing elements are shown inclined by the angles $\pm\theta = py/V$ from the direction of the vector V. Since the local lift is perpendicular to the local relative wind, then the lift vector on the right half of the wing is inclined forward, and that on the left half backward. The result is a *negative* yawing couple, proportional to the product $C_L\hat{p}$. If the wing leading edges are supersonic, then the leading-edge suction is not present, and the local force remains normal to the surface. The increased angle of attack on the right side causes an increase in this normal force there, while the opposite happens on the left side. The result is a positive yawing couple proportional to $\hat{p}$.

The tail contribution to C_{n_p} is easily found from the tail side force given previously (8.6,2). The incremental C_n is given by

$$(\Delta C_n)_{\text{tail}} = -\Delta C_{y_F} \frac{S_F}{S} \frac{l_F}{b}$$

where l_F is the distance shown in Fig. 8.2. Therefore

$$(\Delta C_n)_{\text{tail}} = a_F \hat{p} \frac{S_F}{S} \frac{l_F}{b} \left(2 \frac{z_F}{b} - \frac{\partial \sigma}{\partial \hat{p}} \right)$$

and

$$(C_{n_p})_{\text{tail}} = a_F V_V \left(2 \frac{z_F}{b} - \frac{\partial \sigma}{\partial p} \right) \tag{8.6,4}$$

where V_V is the vertical-tail volume ratio.

THE DERIVATIVE C_{ha_p}

This derivative gives the change of aileron hinge moment due to rolling. It occurs because of the change in wing angle of attack at the ailerons, and because C_{h_α} of the ailerons is usually nonzero. Let y_a be the spanwise coordinate of the right hand mid-aileron section. Then the approximate change in angle of attack at the right hand aileron is

$$\Delta \alpha = \frac{p y_a}{V}$$

and

$$\Delta C_{ha} = C_{ha_\alpha} \frac{p y_a}{V}$$

Therefore

$$C_{ha_p} = \frac{2 y_a}{b} C_{ha_\alpha} \tag{8.6,5}$$

THE DERIVATIVE C_{hr_p}

The change in vertical-tail angle of attack brought about by p produces a change in the rudder hinge moment. This is given by

$$\Delta C_{hr} = -C_{hr_{\alpha_F}} \hat{p} \left(2 \frac{z_F}{b} - \frac{\partial \sigma}{\partial \hat{p}} \right)$$

Therefore

$$C_{hr_p} = -C_{hr_{\alpha_F}} \left(2 \frac{z_F}{b} - \frac{\partial \sigma}{\partial \hat{p}} \right) \tag{8.6,6}$$

When $C_{hr_{\alpha_F}}$ is negative, as for a simple flap control, then a positive roll produces a positive rudder hinge moment.

8.7 THE r DERIVATIVES (C_{y_r}, C_{l_r}, C_{n_r}, C_{ha_r}, C_{hr_r})

When an airplane has a rate of yaw r superimposed on the forward motion V, its velocity field is altered significantly. This is illustrated for the wing

and vertical tail in Fig. 8.16. The situation on the wing is clearly very complicated when it has much sweepback. The main feature however, is that the velocity of the $\frac{1}{4}$ chord line normal to itself is increased by the yawing on the left-hand side, and decreased on the right side. The aerodynamic forces at each section (lift, drag, moment) are therefore increased on the left-hand side, and decreased on the right-hand side. As in the case

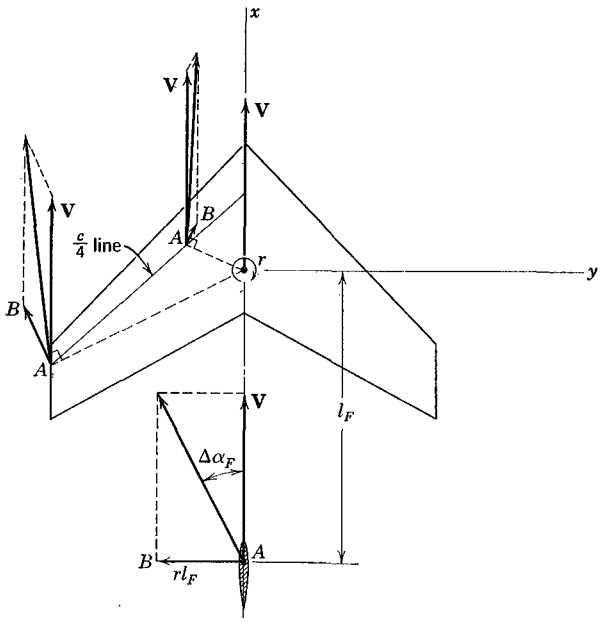

FIG. 8.16 Velocity field due to yawing. $\vec{AB}$ = velocity vector due to rate of yaw r.

of the rolling wing, the unsymmetrical lift distribution leads to an unsymmetrical trailing vortex sheet, and hence a sidewash at the tail. The incremental tail angle of attack is then

$$\Delta\alpha_F = \frac{rl_F}{V} + r\frac{\partial\sigma}{\partial r}$$

or

$$\Delta\alpha_F = \hat{r}\left(2\frac{l_F}{b} + \frac{\partial\sigma}{\partial\hat{r}}\right) \qquad (8.7,1)$$

THE DERIVATIVE C_{y_r}

The only contribution to C_{y_r} that is normally important is that of the tail. From the angle-of-attack change we find the incremental C_y to be

$$(\Delta C_y)_{\text{tail}} = a_F \hat{r} \frac{S_F}{S}\left(2\frac{l_F}{b} + \frac{\partial\sigma}{\partial\hat{r}}\right)$$

Whence

$$(C_{y_r})_{\text{tail}} = a_F \frac{S_F}{S}\left(2\frac{l_F}{b} + \frac{\partial\sigma}{\partial\hat{r}}\right) \tag{8.7,2}$$

THE DERIVATIVE C_{l_r}

This is another important cross derivative; the rolling moment due to yawing. The increase in lift on the left wing, and the decrease on the right wing combine to produce a positive rolling moment proportional to the original lift coefficient C_L. Hence this derivative is largest at low speed. Aspect ratio, taper ratio, and sweepback are all important parameters.

When the vertical tail is large, its contribution may be significant. A formula for it can be derived in the same way as for the previous tail contributions, with the result

$$(C_{l_r})_{\text{tail}} = a_F \frac{S_F}{S}\frac{z_F}{b}\left(2\frac{l_F}{b} + \frac{\partial\sigma}{\partial\hat{r}}\right) \tag{8.7,3}$$

THE DERIVATIVE C_{n_r}

C_{n_r} is the *damping-in-yaw* derivative, and is always negative. The body adds a negligible amount to C_{n_r} except when it is very large. The important contributions for airplanes are those of the wing and tail. The increases in both the profile and induced drag on the left wing and the decreases on the right wing give a negative yawing moment and hence a resistance to the motion. The magnitude of the effect depends on the aspect ratio, taper ratio, and sweepback. For extremely large sweepback, of the order of 60°, the yawing moment associated with the induced drag may be positive: i.e. produce a reduction in the damping.

The side force on the tail also provides a negative yawing moment. The calculation is similar to that for the preceding tail contributions, with the result

$$(C_{n_r})_{\text{tail}} = -a_F V_V \left(2\frac{l_F}{b} + \frac{\partial\sigma}{\partial\hat{r}}\right) \tag{8.7,4}$$

Just as with C_{m_q}, there is a damping-in-yaw provided by the propulsive jet on jet and rocket vehicles. The calculation of ΔC_{m_q} applies exactly to this case as well if M be replaced by N, and q by r. The result is the same as (7.9,20 and 22), i.e.

$$\Delta N_r = -2m'l\bar{\xi}$$

and

$$\Delta C_{n_r} = -4C_T \frac{V}{V_j}\frac{l\bar{\xi}}{\bar{c}^2} \tag{8.7,5}$$

THE DERIVATIVE C_{ha_r}

The change in aileron hinge moment due to yawing velocity is a consequence of the velocity differential between the right and left ailerons. Let the hinge-moment coefficient of the right-hand aileron, at zero aileron angle, be C_{ha_0}. Then the corresponding hinge moment, with no yawing, is $C_{ha_0}(\rho/2)V^2S_ac_a$. This hinge moment is normally balanced by that on the left aileron, so that no load is carried to the pilot's control. Now, when yawing is added, the mean forward velocity at the right-hand aileron is changed from V to $(V - ry_a)$, so that the hinge moment is approximately $C_{ha_0}(\rho/2)(V - ry_a)^2S_ac_a$. To the first order in r, the incremental hinge moment is

$$\Delta H_a = -C_{ha_0}\rho r y_a V S_a c_a$$

On the left-hand side, the increment in H is equal to the above but opposite in sign, so that the two are additive with respect to the stick force, just as though the ailerons were deflected through a small positive angle. The coefficient of ΔH_a is

$$\Delta C_{ha} = -2C_{ha_0}\frac{ry_a}{V} = -4\hat{r}\frac{y_a}{b}C_{ha_0}$$

Since C_{ha} is defined as the hinge moment on *one* aileron then

$$C_{ha_r} = -4\frac{y_a}{b}C_{ha_0} \tag{8.7,6}$$

Table 8.1

Summary—Lateral Derivatives

	C_y	C_l	C_n	C_{ha}	C_{hr}
β	$-\left(C_D + \frac{\partial C_C}{\partial \beta}\right)$ $\left(\frac{\partial C_C}{\partial \beta}\right)_{\text{tail}} = a_F \frac{S_F}{S}\left(1 - \frac{\partial \sigma}{\partial \beta}\right)$	*[a] $-a_F \frac{S_F}{S}\frac{z_F}{b}\left(1 - \frac{\partial \sigma}{\partial \beta}\right)$	* $a_F V_V \left(1 - \frac{\partial \sigma}{\partial \beta}\right)$	Neg.	$-C_{hr_{\alpha_F}}\left(1 - \frac{\partial \sigma}{\partial \beta}\right)$
p	* $-a_F \frac{S_F}{S}\left(2\frac{z_F}{b} - \frac{\partial \sigma}{\partial \hat{p}}\right)$	N.A.[b]	* $a_F V_V \left(2\frac{z_F}{b} - \frac{\partial \sigma}{\partial \hat{p}}\right)$	$2\frac{y_a}{b} C_{ha_\alpha}$	$-C_{hr_{\alpha_F}}\left(2\frac{z_F}{b} - \frac{\partial \sigma}{\partial \hat{p}}\right)$
r	* $a_F \frac{S_F}{S}\left(2\frac{l_F}{b} + \frac{\partial \sigma}{\partial \hat{r}}\right)$	* $a_F \frac{S_F}{S}\frac{z_F}{b}\left(2\frac{l_F}{b} + \frac{\partial \sigma}{\partial \hat{r}}\right)$	$-a_F V_V \left(2\frac{l_F}{b} + \frac{\sigma \partial}{\partial \hat{r}}\right)$ (tail) $-2C_T \frac{V}{V_j}\frac{\xi^2}{\bar{c}^2}$ (jet)	$-4\frac{y_a}{b} C_{ha_0}$	$C_{hr_{\alpha_F}}\left(2\frac{l_F}{b} + \frac{\partial \sigma}{\partial \hat{r}}\right)$
δ_a	Neg.[c]	N.A.	N.A.	C_{ha_δ}	Neg.
δ_r	$a_r \frac{S_F}{S}$	$a_r \frac{S_F}{S}\frac{z_F}{b}$	$-a_r V_V$	Neg.	C_{hr_δ}

[a] * denotes a contribution from the tail only.

[b] N.A. means no convenient formula available.

[c] Neg. means usually negligible.

THE DERIVATIVE C_{hr_r}

The change in the vertical-tail angle of attack (8.7,1) induces a change in the rudder hinge moment. This is given by

$$\Delta C_{hr} = C_{hr_{\alpha_F}} \Delta\alpha_F = C_{hr_{\alpha_F}} \hat{r}\left(2\frac{l_F}{b} + \frac{\partial\sigma}{\partial\hat{r}}\right)$$

where $C_{hr_{\alpha_F}}$ is the derivative, with respect to the vertical-tail angle of attack of the rudder hinge-moment coefficient. Hence

$$C_{hr_r} = C_{hr_{\alpha_F}}\left(2\frac{l_F}{b} + \frac{\partial\sigma}{\partial\hat{r}}\right) \tag{8.7,7}$$

8.8 SUMMARY OF THE FORMULAE

Table 8.1 contains a summary of useful formulae used for estimation purposes.

Stability of steady flight

CHAPTER 9

The preceding chapters have provided the analytical and aerodynamic tools needed to analyze the dynamic behavior of flight vehicles. We now apply them to a consideration of the stability of small disturbances from steady flight. This is an extremely important property of aircraft—first, because steady flight conditions make up most of the flight time of airplanes, and second, because the disturbances in this condition *must be small* for a satisfactory vehicle. If they were not it would be unacceptable for either commercial or military use. The required dynamic behavior is ensured by design—by making the small-disturbance properties of concern (the natural modes, Fig. 3.6) such that either human or automatic control can keep the disturbances that ensue from atmospheric motion, movement of passengers, etc., to an acceptably small level. Finally, as pointed out in Sec. 5.10, the small-disturbance model is actually valid for disturbance magnitudes that seem quite violent to human occupants.

To study the stability of the linear/invariant systems that result from the small-disturbance approximation, we need only the eigenvalues of the system. If the real parts are negative, the system is stable. More complete information about the characteristic modes is usually wanted, however, and is supplied by the eigenvectors. The complete solution for arbitrary initial conditions in the autonomous case follows directly from the eigenvalues and eigenvectors—it is given by any of (3.3,9), (3.3,13), or (3.3,49).

For the most part, the equations of motion are too complicated, even when linearized and simplified as far as is reasonable, to arrive at analytical results of general validity. Hence the technique we use is to demonstrate representative behavior by numerical examples. From these, certain useful analytical approximations can be inferred.

9.1 LONGITUDINAL MODES; FLAT-EARTH APPROXIMATION

Many useful results and insights can be obtained using the flat-Earth approximation. As we showed in Chapter 5, this approximation is valid for a wide range of flight conditions. We begin with the longitudinal modes, for which the relevant small-disturbance equations in nondimensional form are (5.13,18 and 19). We shall consider first a subsonic transport airplane in a reference steady state of horizontal flight, ($\gamma_e = 0$) and initially neglect the z derivatives as well. This is an approximation that is almost universally made in dealing with the flight of airplanes at subsonic speeds. Its significance is explored in Sec. 9.4. Thus the relevant equations are (5.13,19) with $\gamma_e = 0$.

For this class of vehicle there is little error entailed by assuming that the inclination of the thrust vector, α_T, is zero, and we make this assumption.

Since we are concerned with stability of a steady state, i.e. with autonomous behavior, all the elements of the control vector—the last column on the r.h.s. of (5.13,19)—are zero as well. We are left then with an autonomous linear/invariant system with the matrix shown on the facing page.

The general theory for such systems has been given in Sec. 3.3, where it was pointed out that the central elements of the solutions for free motion are the eigenvalues and eigenvectors. To obtain the natural modes of a vehicle, subject to the approximations and restrictions implicit in (9.1,1), it then remains to assign numerical values to the elements of A and to calculate its eigenvalues and eigenvectors.

Numerical Example. The following data pertain to a hypothetical jet transport airplane flying at high altitude.

$W = 100{,}000$ lb $\qquad S = 1667$ ft^2 $\qquad W/S = 60$ psf

$A = 7$ $\qquad \bar{c} = 15.40$ ft $\qquad \rho_e = .000889$ (approx. 30,000 ft altitude)

$V = 500$ mph $= 733$ fps $\qquad \mu = 272$ $\qquad \hat{I}_y = 7\mu$

$C_{L_e} = C_{W_e} = .25$ $\qquad C_{D_e} = .0188$ $\qquad t^* = .0105$ sec

$$C_D = .016 + \frac{C_L^2}{7\pi}$$

$$\mathbf{A} = \begin{bmatrix} \dfrac{C_{T_V} - C_{D_V}}{2\mu} & \dfrac{C_{L_e} - C_{D_\alpha}}{2\mu} & 0 & -\dfrac{C_{W_e}}{2\mu} \\ -\dfrac{C_{L_V} + 2C_{W_e}}{2\mu + C_{L_{\dot\alpha}}} & -\dfrac{C_{L_\alpha} + C_{D_e}}{2\mu + C_{L_{\dot\alpha}}} & \dfrac{2\mu - C_{L_q}}{2\mu + C_{L_{\dot\alpha}}} & 0 \\ \dfrac{1}{\hat{I}_y}\left[C_{m_V} - \dfrac{C_{m_{\dot\alpha}}(C_{L_V} + 2C_{W_e})}{2\mu + C_{L_{\dot\alpha}}}\right] & \dfrac{1}{\hat{I}_y}\left[C_{m_\alpha} - \dfrac{C_{m_{\dot\alpha}}(C_{L_\alpha} + C_{D_e})}{2\mu + C_{L_{\dot\alpha}}}\right] & \dfrac{1}{\hat{I}_y}\left[C_{m_q} + \dfrac{C_{m_{\dot\alpha}}(2\mu - C_{L_q})}{2\mu + C_{L_{\dot\alpha}}}\right] & 0 \\ 0 & 0 & 1 & 0 \end{bmatrix}$$

The state vector is, of course, $[\Delta\hat{V}, \Delta\alpha, \hat{q}, \Delta\theta]$. (9.1,1)

It is assumed that the thrust of the jet engines does not vary with speed, i.e. $\partial T/\partial V = 0$, and that there are no speed effects on the aerodynamic derivatives. The remaining data needed for (9.1,1) are given for this particular vehicle as (see Table 7.1)

$$C_{L_\alpha} = 4.88; \quad C_{m_\alpha} = -4.88(h_n - h); \quad (h_n - h) = .15$$

$$C_{D_\alpha} = \frac{2C_{L_e}}{7\pi} C_{L_\alpha}; \quad C_{L_{\dot\alpha}} = 0; \quad C_{m_{\dot\alpha}} = -4.20$$

$$C_{L_q} = 0; \quad C_{m_q} = -22.9; \quad C_{T_V} = -2C_{T_e} = -2C_{D_e}$$

$$C_{L_V} = C_{D_V} = C_{m_V} = 0.$$

Using the above data, the coefficients of **A** were calculated, and the eigenvalues and eigenvectors found by library subroutines† available for the UTIAS IBM 1130 computer. Let the eigenvalues be $\hat\lambda = \hat n \pm i\hat\omega$ where the $\hat{}$ denotes nondimensional values (note that the independent variable of the differential equations is $\hat t = t/t^*$). The properties of interest are then, in real time:

$$\text{Period, } T = t^* \frac{2\pi}{\hat\omega}$$

$$t_{\text{half}} = -t^* \frac{.69315}{\hat n}$$

$$N_{\text{half}} = t_{\text{half}}/T$$

The results obtained are as follows:

EIGENVALUES

Mode 1: $\hat\lambda = -.3065 \times 10^{-4} \pm .573 \times 10^{-3}\, i$
Mode 2: $\hat\lambda = -.1161 \times 10^{-1} \pm .1891 \times 10^{-1}\, i$

The corresponding periods and damping times are given in Table 9.1. We note that the phugoid mode is of long period (about 2 min) and lightly damped, whereas the short-period mode is quite rapid and very heavily damped. The characteristic transients of these two modes are shown in Fig. 9.1.

† Prepared by Dr. P. C. Hughes. It is perhaps indicative of the times that most of the digital computation needed for this and the following examples was performed, using these subroutines, by a high-school student, David Alexander Etkin.

Table 9.1

Mode	Name	Period (sec)	t_{half} (sec)	N_{half} (cycles)
1	Phugoid[a]	115	237	2.06
2	Short-period	3.48	.626	.18

[a] The phugoid mode was first described by Lanchester (ref. 1.1), who also named it. The name comes from the Greek root for *flee* as in *fugitive*. Actually Lanchester wanted the root for *fly*. Appropriate or not, the word phugoid has become established in aeronautical jargon.

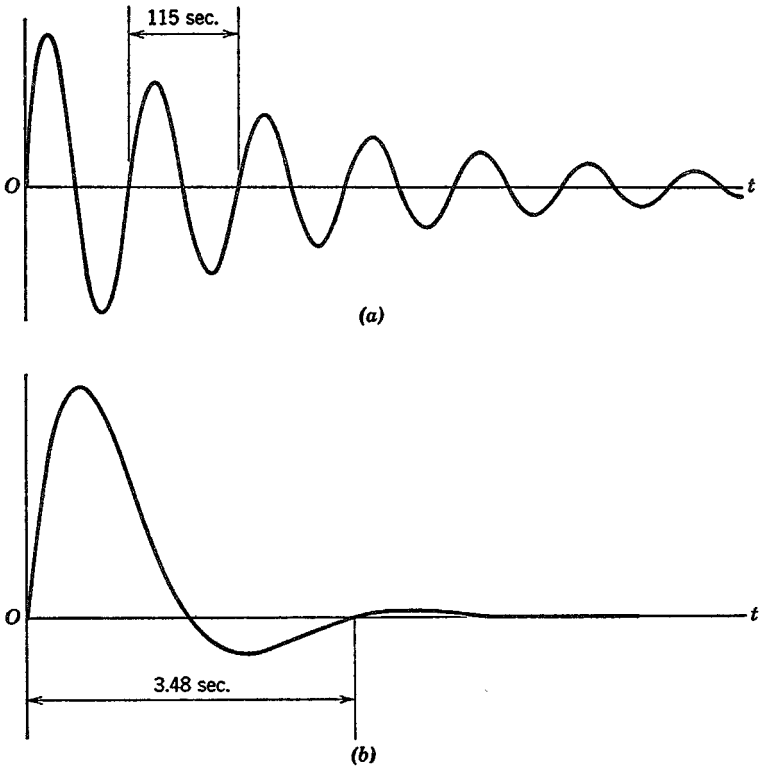

FIG. 9.1 Characteristic transients. (*a*) Phugoid mode. (*b*) Short-period (pitching) mode.

EIGENVECTORS

The eigenvectors corresponding to the above modes are given in the Table 9.2. They are not normalized, being to an arbitrary scale. The first and third columns correspond to $\hat{\omega} > 0$, the second and fourth to $\hat{\omega} < 0$.

Table 9.2

Eigenmatrix $[u_{ij}]$

	Phugoid		**Short-Period**	
$\Delta\hat{V}$	$-.227 \times 10^{-1}$ $+.281\ i$	$-.227 \times 10^{-1}$ $-.281\ i$	$.279 \times 10^{-2}$ $+.180 \times 10^{-2}\ i$	$.279 \times 10^{-2}$ $-.180 \times 10^{-2}\ i$
$\Delta\alpha$	$.639 \times 10^{-3}$ $-.629 \times 10^{-2}\ i$	$.639 \times 10^{-3}$ $+.629 \times 10^{-2}\ i$	$.333$ $+.195\ i$	$.333$ $-.195\ i$
$\hat{q}$	$-.115 \times 10^{-4}$ $+.202 \times 10^{-3}\ i$	$-.115 \times 10^{-4}$ $-.202 \times 10^{-3}\ i$	$-.455 \times 10^{-2}$ $+.578 \times 10^{-2}\ i$	$-.455 \times 10^{-2}$ $-.578 \times 10^{-2}\ i$
$\Delta\theta$	$.353$ $+.116 \times 10^{-2}\ i$	$.353$ $-.116 \times 10^{-2}\ i$	$.329$ $+.383 \times 10^{-1}\ i$	$.329$ $-.383 \times 10^{-1}\ i$

Figure 9.2 is the Argand diagram of the vectors in columns 1 and 3. This is a very effective form of displaying modal characteristics. Since the actual magnitudes of eigenvectors are arbitrary, only the relative lengths of the vectors are shown, taking that of $\Delta\theta = 1.0$. The vectors shown can be imagined as rotating and shrinking (just as in Fig. 3.6*e* except that here we only have those with ω positive); and their projections on the Re axis can be thought of as the real values of the indicated variables.

The phugoid is seen to be a motion in which the speed and pitch angle θ are the main variables, the former leading the latter by roughly 90° in phase, while the angle of attack and the pitch rate remain virtually constant at their reference values. The flight-path angle $\Delta\gamma$ is related to $\Delta\theta$ and $\Delta\alpha$ by (5.10,22), $\Delta\gamma = \Delta\theta - \Delta\alpha$, so that in the phugoid $\Delta\gamma \doteq \Delta\theta$, and the oscillatory flight-path angle lags the speed by about 90°.

In the short-period mode, by contrast, there is negligible speed variation, while the angle of attack oscillates with an amplitude and phase not much different from that of $\Delta\theta$. The difference vector $\Delta\gamma$ is also shown in the figure. This mode as well is one that proceeds essentially in two degrees of freedom, $\Delta\alpha$ and $\Delta\theta$.

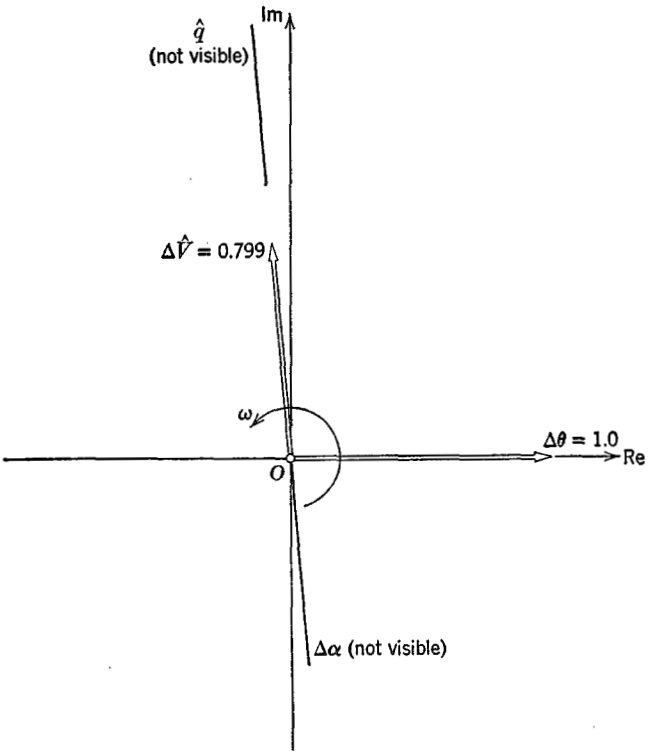

(a)

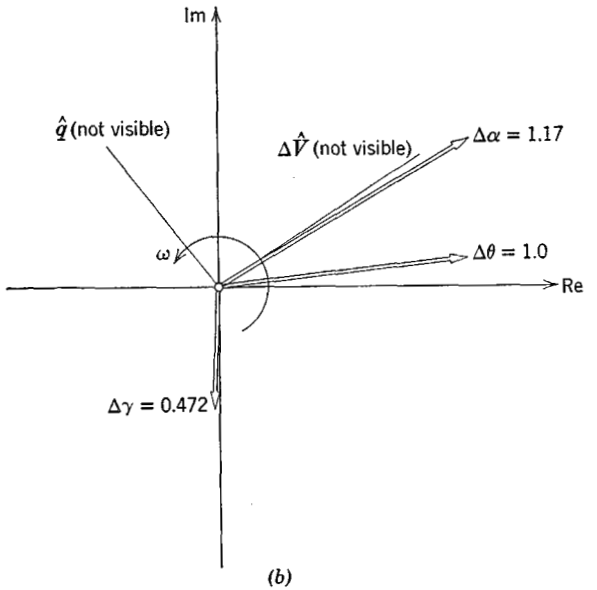

(b)

FIG. 9.2 (*a*) Vector diagram of phugoid mode. (*b*) Vector diagram of short-period mode.

FLIGHT PATHS IN THE CHARACTERISTIC MODES

Additional insight into the modes is gained by studying the flight path. With the atmosphere at rest, the differential equations for the position of the C.G. in F_E are given by (5.13,19), with $\gamma_e = 0$, i.e.

$$\begin{aligned} D\hat{x}_E &= 1 + \Delta\hat{V} \\ D\hat{z}_E &= -(\Delta\theta - \Delta\alpha) \end{aligned} \tag{9.1,2}$$

In a characteristic oscillatory mode with eigenvalues λ, λ^* the variations of $\Delta\hat{V}$, $\Delta\hat{\theta}$, and $\Delta\alpha$ are [cf. (3.3,30)]

$$\begin{aligned} \Delta\hat{V} &= u_{1j}e^{\hat{\lambda}\hat{t}} + u_{1j}^*e^{\hat{\lambda}^*\hat{t}} \\ \Delta\alpha &= u_{2j}e^{\hat{\lambda}\hat{t}} + u_{2j}^*e^{\hat{\lambda}^*\hat{t}} \\ \Delta\theta &= u_{4j}e^{\hat{\lambda}\hat{t}} + u_{4j}^*e^{\hat{\lambda}^*\hat{t}} \end{aligned} \tag{9.1,3}$$

where the constants u_{ij} are the components of the eigenvector corresponding to $\hat{\lambda}$. For the previous numerical example, they are the complex numbers given in Table 9.2 with $j = 1$ for the phugoid and $j = 3$ for the short-period mode. After substituting (9.1,3) in (9.1,2) and integrating we get

$$\begin{aligned} \hat{x}_E &= \hat{t} + \frac{u_{1j}}{\hat{\lambda}}e^{\hat{\lambda}\hat{t}} + \frac{u_{1j}^*}{\hat{\lambda}^*}e^{\hat{\lambda}^*\hat{t}} + \text{const} \\ &= \hat{t} + 2e^{\hat{n}\hat{t}}\,\mathrm{Re}\left[\frac{u_{1j}}{\hat{\lambda}}e^{i\hat{\omega}\hat{t}}\right] + \text{const} \\ \hat{z}_E &= 2e^{\hat{n}\hat{t}}\,\mathrm{Re}\left[\frac{u_{2j} - u_{4j}}{\hat{\lambda}}e^{i\hat{\omega}\hat{t}}\right] + \text{const} \end{aligned} \tag{9.1,4}$$

where Re denotes the real part of the complex number in the square brackets. The dimensional coordinates are obtained by using the additional relations

$$x_E = \frac{\bar{c}}{2}\hat{x}_E, \qquad z_E = \frac{\bar{c}}{2}\hat{z}_E, \qquad t = t^*\hat{t} \tag{9.1,5}$$

For the numerical data of the above example (9.1,4) and (9.1,5) have been used to calculate the flight paths in the two modes, plotted in Fig. 9.3. The magnitudes of the eigenvectors were chosen so that $\theta_{\max}$ is approximately 4° in the phugoid mode, and 10° in the short-period mode. $t = 0$ corresponds to the configuration of variables in Fig. 9.2, and the arbitrary constants of (9.1,4) are zero. The latter choice makes the initial point of the flight paths differ from the origin, but they both approach the x_E axis as $t \to \infty$. Figure 9.3*a* shows that the phugoid is an undulating flight of very long wavelength.

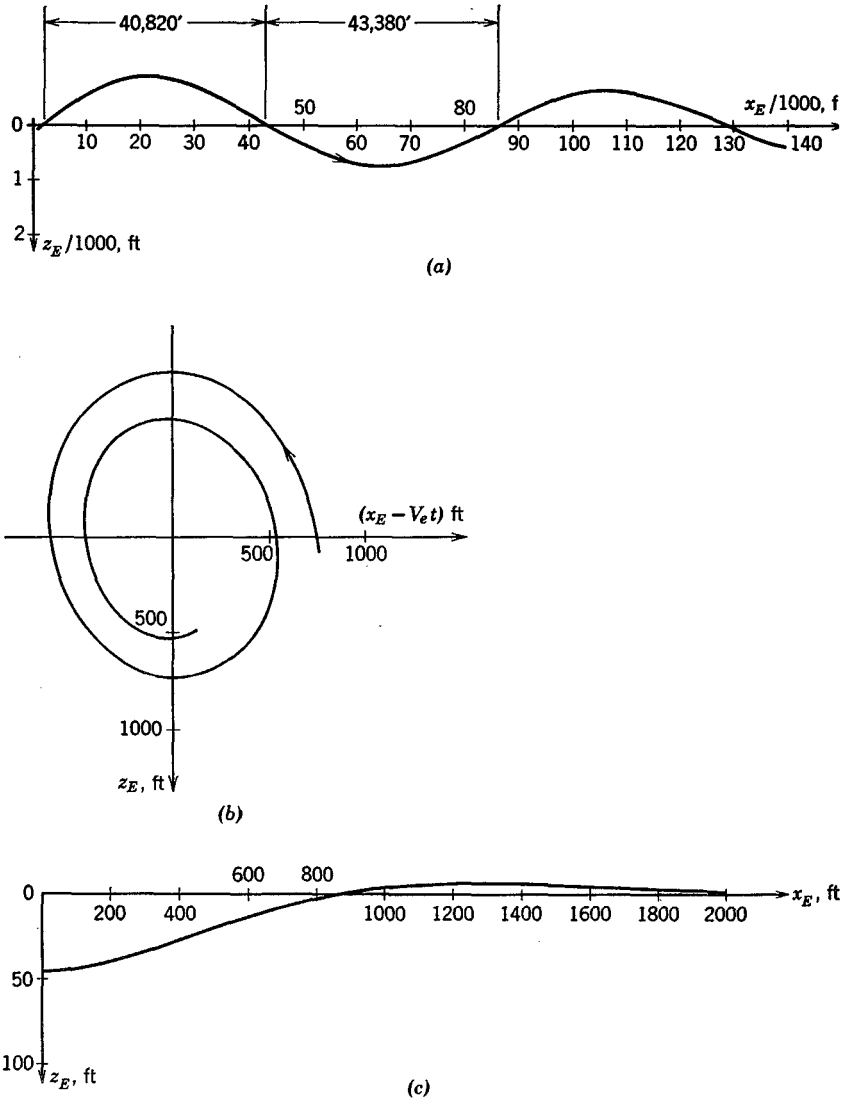

FIG. 9.3 (*a*) Phugoid flight path (fixed reference frame). (*b*) Phugoid flight path (moving reference frame). (*c*) Short-period flight path.

Since $\Delta\alpha \doteq 0$, the vehicle "flies like an arrow," i.e. has its x axis approximately tangent to the trajectory. The mode diagram, Fig. 9.2*a* shows that the speed leads the pitch angle by about 90°, from which we can infer that V is largest at the bottom of the wave and least at the top. This variation in speed results in different distances being traversed during the upper and lower halves of the cycle, as shown in Fig. 9.3*a*. For larger amplitude oscillations, this lack of symmetry in the oscillation becomes much more pronounced (although the linear theory then fails to describe it accurately) until ultimately the upper part becomes first a cusp and then a loop (see Miele, ref. 1.7, p. 273). The motion (see Sec. 9.2) is approximately one of constant total energy, the rising and falling corresponding to an exchange between kinetic and potential energy. Figure 9.3*b* shows the phugoid motion relative to axes moving at the reference speed V_e. This is the relative path that would be seen by an observer flying alongside at speed V_e.

Figure 9.3*c* shows the path for the short-period mode. The disturbance is so rapidly damped that the transient has virtually disappeared within 1000 ft of flight, even though the initial $\Delta\alpha$ and $\Delta\theta$ were very large. The deviation of the path from a straight line is small, the principal feature of the motion being the rapid rotation in pitch.

9.2 APPROXIMATE EQUATIONS FOR THE LONGITUDINAL MODES

It is frequently useful and desirable to have approximate analytical expressions for the periods and dampings of the characteristic modes. These are convenient for assessing the influence of the main flight and vehicle parameters that affect the modes, and are especially useful when conventional methods of servomechanism analysis are applied to automatic control systems (ref. 9.4). There are two approaches generally used to arrive at these approximations. One is to write out a literal expression for the characteristic equation and, by studying the order of magnitude of the terms in it, to arrive at approximate linear or quadratic factors. For example, if the characteristic equation

$$s^4 + c_3 s^3 + c_2 s^2 + c_1 s + c_0 = 0$$

is known to have a "small" real root, an approximation to it may be obtained by neglecting all the higher powers of s, i.e.

$$c_1 s + c_0 \doteq 0$$

Or if there is a "large" complex root, it may be approximated by keeping

only the first three terms, i.e.

$$s^2 + c_3 s + c_2 \doteq 0$$

This method is frequently useful, and sometimes the only reasonable way to get an approximation.

The second method, which has the advantage of providing more physical insight, proceeds from a foreknowledge of the modal characteristics to arrive at approximate system equations of lower order than the exact ones. For the longitudinal modes we use the second method (see below), and for the lateral modes (see Sec. 9.6,1) both methods are needed.

It should be noted that no simple analytical approximations can be relied on to give accurate results under all circumstances. Machine solutions of the exact matrix is the only certain way. The value of the approximations is indicated by examples in the following.

To proceed now to the phugoid and short-period modes, we saw in Fig. 9.2 that some state variables are negligibly small in each of the two modes. This fact suggests certain approximations to them based on reduced sets of equations of motion. These approximations, which are quite useful, are developed below.

PHUGOID MODE

Lanchester's (ref. 1.1) original solution for the phugoid used the assumptions that $\Delta\alpha \equiv 0$ and $T - D \equiv 0$. It follows that there is no net aerodynamic force tangent to the flight path, and hence no work done on the vehicle except by gravity. The motion is then one of constant total energy, as suggested previously. This simplification makes it possible to treat the most general case with large disturbances in speed and flight-path angle (see Miele, ref. 1.7, p. 271 et seq.). Here we content ourselves with a treatment of only the corresponding small-disturbance case, for comparison with the exact numerical result given earlier. The energy condition is

$$E = \tfrac{1}{2}mV^2 - mgz_E = \text{const}$$

or

$$V^2 = V_e^2 + 2gz_E \tag{9.2,1}$$

where the origin of F_E is so chosen that $V = V_e$ when $z_E = 0$. With α constant, and in addition neglecting the effect of q on C_L, then C_L is constant at the value for steady horizontal flight, i.e. $C_L = C_{L_e} = C_{W_e}$, and $L = C_{W_e}\tfrac{1}{2}\rho V^2 S$ or, in view of (9.2,1),

$$L = C_{W_e}\tfrac{1}{2}\rho V_e^2 S + (C_{W_e}\rho g S)z_E = W + kz_E \tag{9.2,2}$$

Thus the lift is seen to vary linearly with the height in such a manner as

always to drive the vehicle back to its reference height, the "spring constant" being

$$k = C_{W_e}\rho g S \tag{9.2,3}$$

The equation of motion in the vertical direction is clearly, when $T - D = 0$,

$$W - L\cos\theta = m\ddot{z}_E$$

or for small θ,

$$W - L = m\ddot{z}_E \tag{9.2,4}$$

On combining (9.2,2) and (9.2,4) we get

$$m\ddot{z}_E + kz_E = 0$$

which identifies a simple harmonic motion of period

$$T = 2\pi\sqrt{\frac{m}{k}} = 2\pi\sqrt{\frac{m}{C_{W_e}\rho g S}}$$

Since $C_{W_e} = mg/\frac{1}{2}\rho V_e^2 S$, this becomes

$$T = \pi\sqrt{2}\,\frac{V_e}{g} \tag{9.2,5}$$

a beautifully simple result, suggesting that the phugoid period depends only on the *speed* of flight, and not at all on the airplane or the altitude! For the above example, $V_e = 733$ fps, and (9.2,5) gives $T = 101$ sec, a value 12.2% different from the correct result, 115 sec.

Although (9.2,5) is a very useful result for the period, the above theory cannot give any information at all about the damping, since thrust and drag were eliminated from consideration and it is precisely these that cause the amplitude of the oscillation to change. For a better approximation, we return to the equations of motion and incorporate a simplification suggested by Fig. 9.2*a*, i.e. $\Delta\alpha \doteq 0$. Note that this is one of Lanchester's two assumptions. If we drop one variable, we must also drop one equation of motion. Now the zero $\Delta\alpha$ may be considered to imply zero pitching moment of inertia, so that pitch equilibrium is always maintained throughout the motion, and this suggests that it is the pitching moment equation that should be dropped. With $\Delta\alpha$ and the C_m equation missing, (9.1,1) reduces to

$$\begin{bmatrix} D\hat{V} \\ \hline 0 \\ \hline D\theta \end{bmatrix} = \left[\begin{array}{c|c|c} \dfrac{C_{T_V} - C_{D_V}}{2\mu} & 0 & -\dfrac{C_{W_e}}{2\mu} \\ \hline -\dfrac{C_{L_V} + 2C_{W_e}}{2\mu + C_{L_{\dot{\alpha}}}} & \dfrac{2\mu - C_{L_q}}{2\mu + C_{L_{\dot{\alpha}}}} & 0 \\ \hline 0 & 1 & 0 \end{array}\right] \begin{bmatrix} \Delta\hat{V} \\ \hline \hat{q} \\ \hline \Delta\theta \end{bmatrix} \tag{9.2,6}$$

For consistency with the previous numerical example, we neglect as well the derivatives C_{L_V}, C_{D_V}, C_{L_q}, $C_{L_{\dot{\alpha}}}$. Now the second of the three equations is an *algebraic* relation, i.e. with the preceding approximations

$$-\frac{C_{W_e}}{\mu}\Delta\hat{V} + \hat{q} = 0 \tag{9.2,7}$$

After using (9.2,7) to eliminate $\hat{q}$ from (9.2,6) we get the second-order system

$$\begin{bmatrix} D\hat{V} \\ D\theta \end{bmatrix} = \begin{bmatrix} \dfrac{C_{T_V}}{2\mu} & -\dfrac{C_{W_e}}{2\mu} \\ \dfrac{C_{W_e}}{\mu} & 0 \end{bmatrix} \begin{bmatrix} \Delta\hat{V} \\ \Delta\theta \end{bmatrix} \tag{9.2,8}$$

The characteristic equation is therefore

$$\begin{vmatrix} \left(\dfrac{C_{T_V}}{2\mu} - s\right) & -\dfrac{C_{W_e}}{2\mu} \\ \dfrac{C_{W_e}}{\mu} & -s \end{vmatrix} = 0$$

The expansion gives the quadratic

$$s^2 - \frac{C_{T_V}}{2\mu}s + \frac{{C_{W_e}}^2}{2\mu^2} = 0 \tag{9.2,9}$$

or

$$s^2 + 2\zeta\hat{\omega}_n s + {\hat{\omega}_n}^2 = 0$$

which has the roots

$$\hat{\lambda} = \hat{n} \pm i\hat{\omega}$$

where

$$\hat{n} = -\zeta\hat{\omega}_n = \frac{C_{T_V}}{4\mu}$$

$$\hat{\omega} = ({\hat{\omega}_n}^2 - \hat{n}^2)^{1/2}$$

$$\hat{\omega}_n = \frac{1}{\sqrt{2}}\frac{C_{W_e}}{\mu}$$

and the damping ratio is

$$\zeta = -\frac{1}{2\sqrt{2}}\frac{C_{T_V}}{C_{W_e}} \tag{9.2,10}$$

The "undamped" period is seen to be

$$T_n = \frac{2\pi}{\hat{\omega}_n} t^*$$

$$= \frac{2\sqrt{2}\,\pi}{C_{W_e}} \cdot \frac{m}{\rho S(\bar{c}/2)} \cdot \frac{\bar{c}}{2V_e}$$

After eliminating C_{W_e} this reduces exactly to (9.2,5) so that the Lanchester result is recovered from (9.2,9) when $C_{T_V} = 0$.

For the case of horizontal flight under consideration here, C_{T_V} depends only on the reference drag coefficient and the type of propulsion system (see Sec. 7.8). For the example airplane in horizontal flight $C_{T_V} = -2C_{D_e}$, and in that case the damping coefficient is

$$\zeta = \frac{1}{\sqrt{2}} \frac{C_{D_e}}{C_{W_e}} = \frac{1}{\sqrt{2}} \left(\frac{D}{L}\right)_e$$

To this approximation, ζ will always vary inversely as the (L/D) ratio, but for constant-power propulsion (instead of constant thrust) the constant is $3/2\sqrt{2}$ (instead of $1/\sqrt{2}$).

The accuracy of the approximation given by (9.2,9) is illustrated on Figs. 9.4*a*, 9.8, and 9.16.

Another approximation that gives better results for the period, but not necessarily for the damping, is one originally due to Bairstow (ref. 1.4) [the derivation is given by Ashkenas and McRuer (ref. 9.5)]. When converted to the notation of this work, it gives

$$\hat{\omega} \doteq \left[\frac{C_{W_e}[C_{m_\alpha}(C_{W_e} + \tfrac{1}{2}C_{L_V}) - \tfrac{1}{2}C_{m_V}(C_{L_\alpha} + C_{D_e})]}{\mu[2\mu C_{m_\alpha} + C_{m_q}(C_{L_\alpha} + C_{D_e})]}\right]^{1/2}$$

$$\hat{n} \doteq \frac{C_{D_e} + \tfrac{1}{2}C_{D_V}}{2\mu} - \frac{\tfrac{1}{2}C_{D_\alpha}C_{m_V}}{2\mu C_{m_\alpha} + C_{m_q}(C_{L_\alpha} + C_{D_e})} \qquad (9.2,11)$$

This also is compared with exact results in the figures that follow.

SHORT-PERIOD MODE

Figure 9.2*b* shows that the speed remains substantially constant in the short-period mode, and this suggests an approximation to the equations in which $\Delta\hat{V} \equiv 0$. Again, one equation must be dropped from the set, and the correct choice is the speed equation of motion. The reduced equations are

then, after neglecting the same derivatives as before,

$$\begin{bmatrix} D\alpha \\ \hline D\hat{q} \\ \hline D\theta \end{bmatrix} = \left[\begin{array}{c|c|c} -\dfrac{(C_{L_\alpha}+C_{D_e})}{2\mu} & 1 & 0 \\ \hline \dfrac{1}{\hat{I}_y}\left(C_{m_\alpha}-\dfrac{C_{m_{\dot\alpha}}(C_{L_\alpha}+C_{D_e})}{2\mu}\right) & \dfrac{1}{\hat{I}_y}(C_{m_q}+C_{m_{\dot\alpha}}) & 0 \\ \hline 0 & 1 & 0 \end{array}\right] \begin{bmatrix} \Delta\alpha \\ \hline \hat{q} \\ \hline \Delta\theta \end{bmatrix} \tag{9.2,12}$$

The characteristic equation is then

$$-s\left|\begin{array}{c|c} -\dfrac{(C_{L_\alpha}+C_{D_e})}{2\mu}-s & 1 \\ \hline \dfrac{1}{\hat{I}_y}\left(C_{m_\alpha}-\dfrac{C_{m_{\dot\alpha}}(C_{L_\alpha}+C_{D_e})}{2\mu}\right) & \dfrac{1}{\hat{I}_y}(C_{m_q}+C_{m_{\dot\alpha}})-s \end{array}\right| = 0 \tag{9.2,13}$$

This expands to give the cubic equation

$$s(s^2 + c_1 s + c_0) = 0$$

where

$$\begin{aligned} c_0 &= -\frac{2\mu C_{m_\alpha} + C_{m_q}(C_{L_\alpha}+C_{D_e})}{2\mu\hat{I}_y} \\ c_1 &= \frac{\hat{I}_y(C_{L_\alpha}+C_{D_e}) - 2\mu(C_{m_q}+C_{m_{\dot\alpha}})}{2\mu\hat{I}_y} \end{aligned} \tag{9.2,14}$$

of which the second-degree factor is the approximation for the short-period roots. The zero root is of no interest. With the numerical values of the preceding example, the roots obtained from (9.2,14) are

$$\hat{\lambda} = -.1162 \times 10^{-1} \pm .1892 \times 10^{-1}\, i$$

which are to be compared to the exact values

$$-.1161 \times 10^{-1} \pm .1891 \times 10^{-1}\, i$$

The errors are seen to be very small, less than $\frac{1}{10}\%$ in both the damping and the period. Equations (9.2,14) give a good approximation to the important short-period oscillation over a wide range of flight and vehicle parameters.

Because of the large influence of C.G. position on C_{m_α}, a critical C.G. position is indicated by (9.2,14) when

$$2\mu C_{m_\alpha} + C_{m_q}(C_{L_\alpha}+C_{D_e}) = 0 \tag{9.2,15}$$

At this condition, c_0 vanishes, and the characteristic equation becomes

$$s(s + c_1) = 0$$

with roots $\hat{\lambda} = 0, -c_1$. The latter corresponds to a damped exponential mode, and the zero root identifies one that is a constant state in the two variables $\Delta\alpha$ and $\hat{q}$. This state, a longitudinal motion at constant speed, α and $\hat{q}$ is none other than the steady pull-up treated in Sec. 6.10. The critical C.G. position is found from (9.2,15) thus

$$2\mu C_{L_\alpha}(h_{\text{crit}} - h_n) + C_{m_q}(C_{L_\alpha} + C_{D_e}) = 0$$

or

$$h_{\text{crit}} = h_n - \frac{C_{m_q}(C_{L_\alpha} + C_{D_e})}{2\mu C_{L_\alpha}} \tag{9.2,16}$$

Comparison of (9.2,16) and (6.10,8) shows that h_{crit} above would be exactly h_m (the control-fixed maneuver point) if C_{D_e} were zero in the former and C_{L_q} zero in the latter. In fact these equations both describe the same flight condition, and the differences between them are entirely due to differences in the detailed assumptions made in their derivations. Specifically, C_{L_q} was neglected in (9.2,12) and no component of the thrust normal to $\bar{V}$ was included in the derivation of (6.10,8). Had the assumptions been strictly compatible, the results would have been identical.

The above analysis shows that the steady pull-up at constant speed can occur without motion of the controls at this C.G. position, and hence it is indeed the condition of zero control motion per g. We can further deduce that movement of the C.G. farther aft causes a reversal of sign of c_0 and hence corresponds to a "static instability" as in a mass-spring-damper with a "negative" spring. In this light the control-fixed maneuver point is seen as a criterion for the divergence of the short-period mode.

9.3 GENERAL THEORY OF STATIC LONGITUDINAL STABILITY

The concept of static stability was introduced in Chapter 3, where it was identified with the nature of the exponential characteristic modes (Figs. 3.6*a* and *b*). In Sec. 3.3 (p. 70) it was pointed out that the vanishing of the constant term in the characteristic equation of a linear/invariant system provides a boundary between asymptotic stability and static instability. This is the criterion that we discuss in this section, and relate to the stability criteria presented earlier in Chapter 6.

The characteristic equation [see (3.3,7)] is

$$|s\mathbf{I} - \mathbf{A}| = 0$$

and clearly the constant term is found by setting $s = 0$, i.e.

$$c_0 = |-\mathbf{A}|$$

The criterion for static stability is then

$$|-\mathbf{A}| > 0 \tag{9.3,1}$$

The application of this criterion is in principle straightforward for any of the linear/invariant systems (5.13,18 to 20) that describe the longitudinal and lateral motions. In the interests of deriving a simple usable analytical result, however, we shall treat the special case represented by (9.1,1), in which the equilibrium flight path is horizontal, and z derivatives are neglected. When $|-\mathbf{A}|$ is expanded we get

$$c_0 = \frac{C_{W_e}}{2\mu\hat{I}_y(2\mu + C_{L_{\hat{\alpha}}})}[(C_{L_\alpha} + C_{D_e})C_{m_V} - C_{m_\alpha}(C_{L_V} + 2C_{W_e})] \tag{9.3,2}$$

Since the factor outside the square brackets is always positive ($C_{L_{\hat{\alpha}}}$ could not be $< -2\mu$ for any reasonable heavier-than-air vehicle) the stability criterion becomes

$$(C_{L_\alpha} + C_{D_e})C_{m_V} - C_{m_\alpha}(C_{L_V} + 2C_{W_e}) > 0 \tag{9.3,3}$$

When comparing (9.3,3) with the static stability criteria discussed in Chapter 6, a minor difference in basic assumptions must be noted. In the preceding development, it was specifically assumed that the thrust vector rotates with the vehicle when α is changed. In the development leading to (6.4,24) by contrast, there is an implicit assumption that the thrust provides *no* component of force perpendicular to $\mathbf{V}$ [see (6.4,18)]. It is this difference that leads to the presence of C_{D_e} in (9.3,3) whereas there is no corresponding term in the numerator of (6.4,24). Had the assumptions been the same, the expressions would be strictly compatible. In any case, C_{D_e} is usually small compared to C_{L_α}, so that the difference is not important. We see that the justification for the statement made in Sec. 6.4, that the slope of the elevator trim curve $(d\delta_{e\text{trim}}/d\hat{V})_\pi$ is a criterion of static stability, is provided by (9.3,3). [Note that $C_{W_e} = C_{L_e}$ in (9.3,3).]

Another stability criterion referred to in Chapter 6 is the derivative dC_m/dC_L (6.3,21). It was pointed out there that this derivative can only be said to exist if enough constraints are imposed on the independent variables α, $\hat{V}$, δ_e, q, etc., on which C_m and C_L separately depend. Such a situation results if we postulate that the vehicle is in rectilinear motion ($q \equiv 0$) at constant elevator angle and throttle setting, with $L = W$, but with varying speed and angle of attack. Such a condition cannot, of course, actually occur in flight because the pitching moment could be zero at only one speed, but it can readily be simulated in a wind tunnel where the model is restrained by a balance. [The argument that follows is quite similar to that of (6.4,18) et seq.] With the above stipulations, C_m and C_L reduce to functions of the

two variables $\hat{V}$ and α, and incremental changes from a reference state $(\ )_e$ are given by

$$\begin{aligned} dC_L &= C_{L_\alpha}\, d\alpha + C_{L_V}\, d\hat{V} \\ dC_m &= C_{m_\alpha}\, d\alpha + C_{m_V}\, d\hat{V} \end{aligned} \tag{9.3,4}$$

The required derivative is then

$$\frac{dC_m}{dC_L} = \frac{C_{m_\alpha} + C_{m_V}\dfrac{d\hat{V}}{d\alpha}}{C_{L_\alpha} + C_{L_V}\dfrac{d\hat{V}}{d\alpha}} \tag{9.3,5}$$

provided $d\hat{V}/d\alpha$ exists. This is guaranteed by the remaining condition imposed, i.e. $L = W$ (implying $\alpha_T \equiv 0$). For then we have

$$W = C_L(\alpha,\ \hat{V})\tfrac{1}{2}\rho V^2 S = \text{const}$$

from which we readily derive

$$(C_{L_\alpha}\, d\alpha + C_{L_V}\, d\hat{V})\tfrac{1}{2}\rho V_e{}^2 S + C_{L_e}\rho V_e S\, dV = 0 \tag{9.3,6}$$

From (9.3,6)

$$(C_{L_V} + 2C_{L_e})\, d\hat{V} + C_{L_\alpha}\, d\alpha = 0$$

or

$$\frac{d\hat{V}}{d\alpha} = -\frac{C_{L_\alpha}}{C_{L_V} + 2C_{L_e}} \tag{9.3,7}$$

After substituting (9.3,7) into (9.3,5) and simplifying we get

$$\left.\frac{dC_m}{dC_L}\right|_{L=W} = \frac{1}{2C_{L_e}C_{L_\alpha}}[C_{m_\alpha}(C_{L_V} + 2C_{L_e}) - C_{L_\alpha}C_{m_V}] \tag{9.3,8}$$

On comparing (9.3,8) with (9.3,3), again neglecting C_{D_e} therein for compatibility of assumptions, and noting that $C_{W_e} = C_{L_e}$, we see that the static stability criterion is

$$\left.\frac{dC_m}{dC_L}\right|_{L=W} < 0 \tag{9.3,9}$$

provided that dC_m/dC_L is calculated with the constraints $\Delta\delta_e = \Delta\pi = q = 0$ and $L \equiv W$. [The quantity on the left side of (9.3,8) and (9.3,9) is sometimes referred to as *speed stability* in the USA, by contrast with "angle of attack" stability. In Great Britain, this term usually has a different meaning, as in Sec. 11.5.]

On using the definition of h_s given in (6.4,26) we find from (9.3,8) that

$$\left.\frac{dC_m}{dC_L}\right|_{L=W} = \left(1 + \frac{C_{L_V}}{2C_{L_e}}\right)(h - h_s) \tag{9.3,10}$$

i.e. that it is proportional to the "stability margin," and when $C_{L_V} \ll 2C_{L_e}$, is equal to it.

Finally, we must check on the significance of the "pitch stiffness" parameter C_{m_α}, to which great importance was attached in Chapter 6. We see from 9.3,3 that when C_{L_V} and C_{m_V} are zero, $C_{m_\alpha} < 0$ does indeed provide an exact criterion for static stability. Even when C_{L_V} and C_{m_V} are not zero, we shall see from the examples to follow that $C_{m_\alpha} < 0$ is still a useful and significant criterion.

9.4 EFFECT OF FLIGHT CONDITION ON THE LONGITUDINAL MODES OF A SUBSONIC JET TRANSPORT

In Sec. 9.1 we gave the representative characteristic modes of a hypothetical subsonic jet airplane for a single set of parameters. It is of considerable interest to enquire into how these characteristics are affected by changes in the major flight variables—speed, altitude, angle of climb, and stability margin. It is also of interest to establish the nature of the approximation $d\hat{\rho}/d\hat{z} \doteq 0$. In this section we present numerical results that illustrate the above features.

9.4.1 EFFECT OF SPEED

When the speed is changed in horizontal flight, the matrix (9.1,1) previously used is still applicable. All the assumptions made in Sec. 9.1 are retained—in particular, no Mach number effects are included—and hence the only quantities that vary are C_{L_e}, C_{D_e}, C_{T_V}, C_{D_α}, and t^*. The eigenvalues and eigenvectors of (9.1,1) have been calculated for a range of speeds, and the variations of the period and damping of the two modes are given in Fig. 9.4. The Lanchester approximation to the phugoid period (9.2,5) is shown for comparison, as well as approximations (9.2,9), (9.2,11), and (9.2,14) to the phugoid and short-period modes, respectively.

The speed domain shown corresponds to a range of C_{W_e} from .2 to 1.8. This is somewhat larger than that over which one might expect the theory to be accurate. The highest speed corresponds to $\mathbf{M} = .82$ at which compressibility effects would be expected to be present in C_{L_α}, C_{D_α}, and C_{T_V}, and possibility in C_{L_V} and C_{m_V}. On the other hand, at the large C_L corresponding to the lowest speed, flow separation effects might be expected to occur on the cruise configuration in the absence of boundary layer control, affecting several of the derivatives.

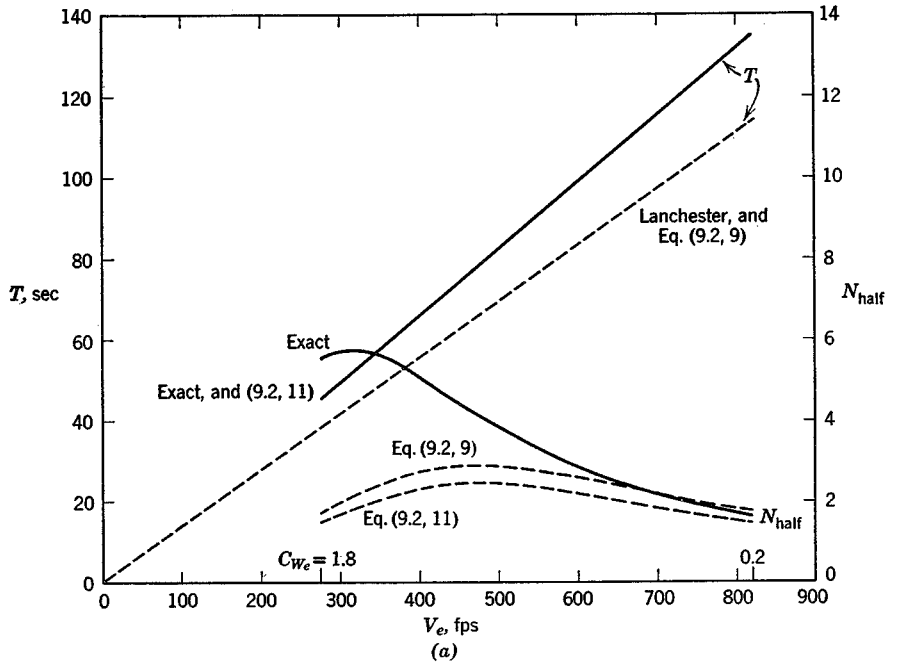

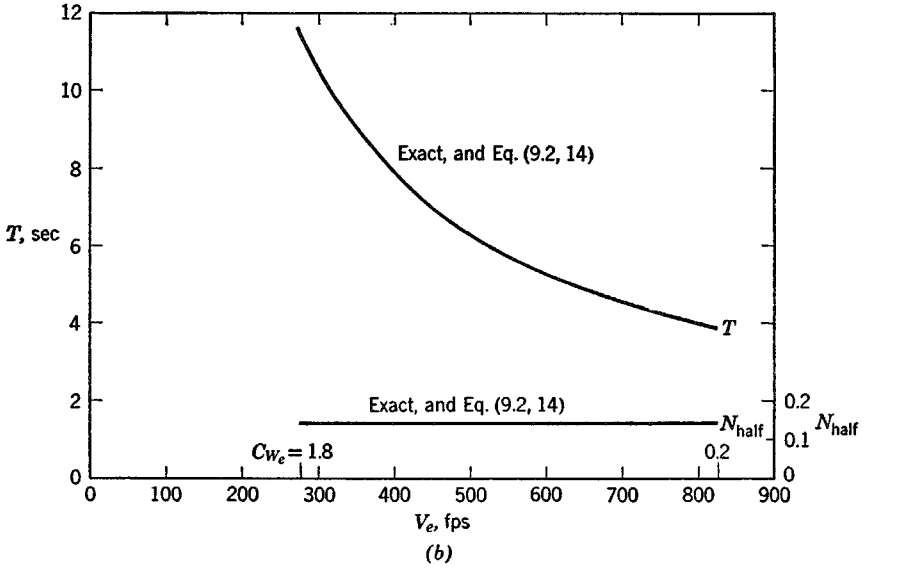

FIG. 9.4 (*a*) Variation of phugoid properties with flight speed, $K_n = .10$. (*b*) Variation of short-period properties with flight speed, $K_n = .10$.

The phugoid period is seen to behave qualitatively as predicted by Lanchester's theory, and the usefulness of the approximate theories for predicting it is evident. Not so for the damping of the phugoid however, for which the approximate theories fail to predict the severe loss of damping at low speeds, where the number of cycles to half amplitude increases to nearly six.

The short-period mode has essentially constant nondimensional eigenvalues [note that C_{W_e} does not appear in (9.2,14)]. The variation shown in T comes almost entirely from that of $t^* = \bar{c}/2V_e$. The approximation given by (9.2,14) is to the accuracy of the graph indistinguishable from the exact solution.

At the lowest speed the separation of the periods of the two modes is much less than at high speeds, their ratio at 274 fps being only 3.9 by contrast with 34.8 at 821 fps.

Figure 9.5 shows the root-locus of the phugoid mode. That for the short-period mode is virtually a pair of conjugate points and is not shown.

Figure 9.6 shows how the modal characteristics (the eigenvectors) have changed at the lowest speed. The most significant feature is that appreciable $\Delta\alpha$ has appeared in the phugoid and $\Delta\hat{V}$ in the short-period mode. This can be traced to the fact that the periods of the two modes are much closer to one another at this speed, and hence that the coupling between the previously

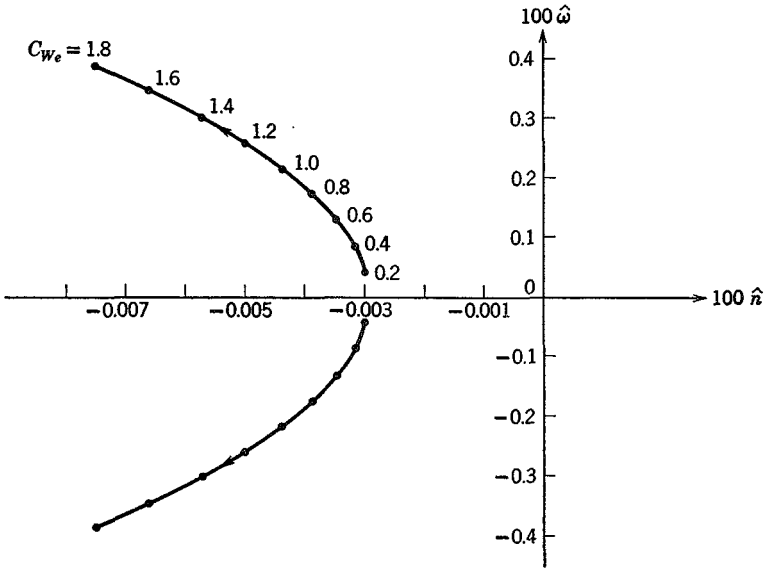

FIG. 9.5 Root locus—phugoid mode, variable C_{w_e}.

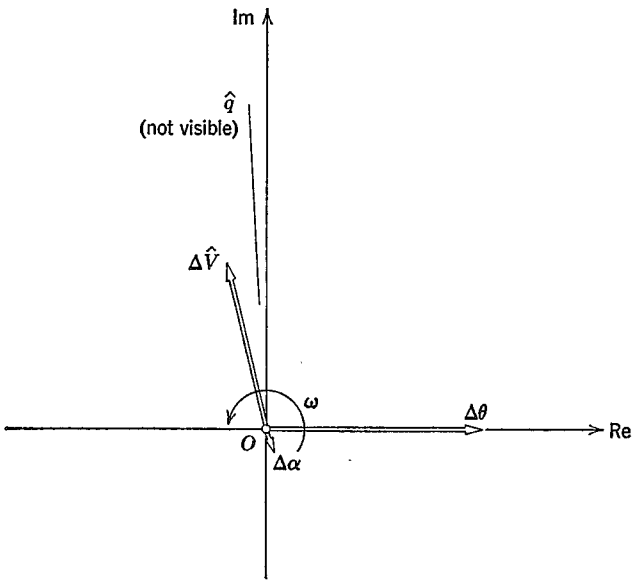

(a)

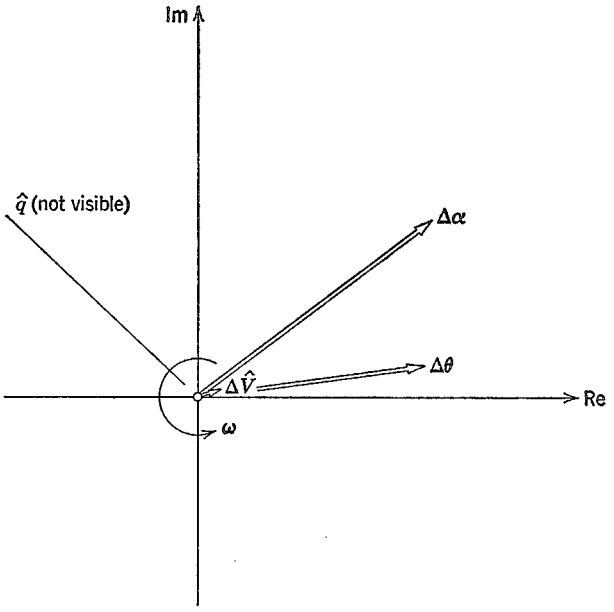

(b)

FIG. 9.6 (*a*) Vector diagram of phugoid mode—$C_{w_e} = 1.8$. (*b*) Short-period mode—$C_{w_e} = 1.8$.

lightly-coupled degrees of freedom is stronger. That is to say, a variation of α at the short-period frequency can induce an appreciable speed change under these conditions and the pitching moment variation during the phugoid (associated mainly with $C_{m_q}\hat{q}$) can induce appreciable changes in α. Now we arrived at the approximations (9.2,9) and (9.2,14) by ignoring $\Delta\alpha$ in one mode and $\Delta\hat{V}$ in the other. It therefore follows that the approximations might be poorer at low speed than at high speed. This is clearly shown for the phugoid damping in Fig. 9.4*a*, but the approximations to the phugoid period, and to the short-period mode, are not appreciably worse at low speed than at high speed.

9.4.2 EFFECT OF ALTITUDE

When the altitude is varied at constant C_{W_e} and constant static margin the density change has two separate effects. The first is on μ and $\hat{I}_y$ which are both smaller at lower altitude, and the second is on the true speed V_e, which also decreases with decrease of altitude. The matrix (9.1,1) is still applicable, and with the same assumptions as used before the only quantities in it that change are μ and $\hat{I}_y$. Computations were carried out for the altitude range 0 to 40,000 ft for $C_{W_e} = .25$ and $K_n = .10$. The results are shown on Figs. 9.7 to 9.11. As with the speed variation previously discussed, the results would not be expected to be accurate at the highest altitude, where the speed is about 900 fps, i.e. $\mathbf{M} \doteq .93$, since compressibility effects were not included in the aerodynamic derivatives. The speed is seen in Fig. 9.7 to vary over a range of 2:1 as the height changes, and this has a large effect on the phugoid periods. This is evident in Fig. 9.8, where the period is seen to vary with height in the same way as does the speed, qualitatively as predicted by the Lanchester formula. From (9.2,14) it follows that $\hat{\omega}_n$ for the short-period varies approximately as $\sqrt{\rho}$, and hence that T varies

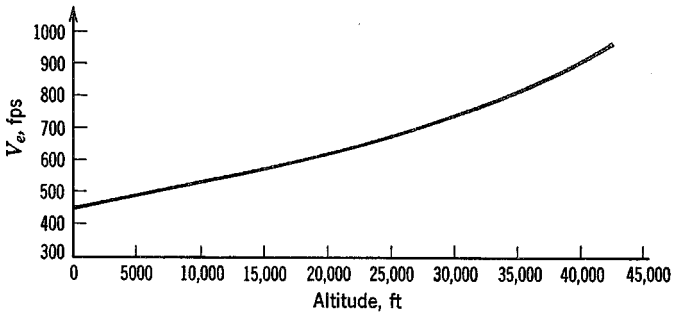

FIG. 9.7 Variation of V_e with altitude–horizontal flight. $C_{w_e} = C_{L_e} = .25$.

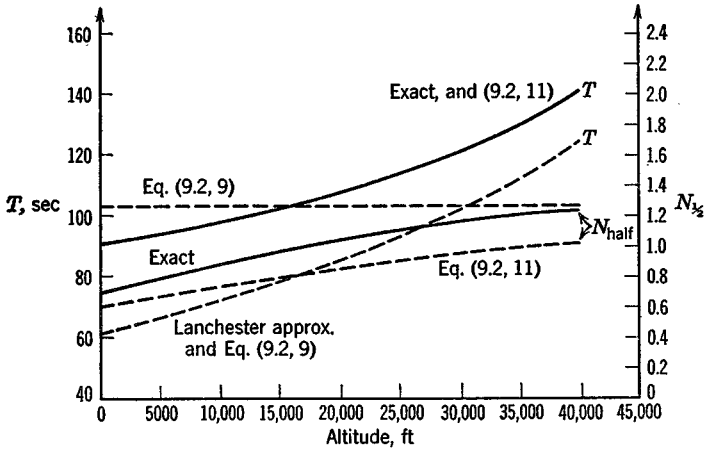

FIG. 9.8 Variation of period and damping of phugoid mode with altitude. $C_{w_e} = .25$.

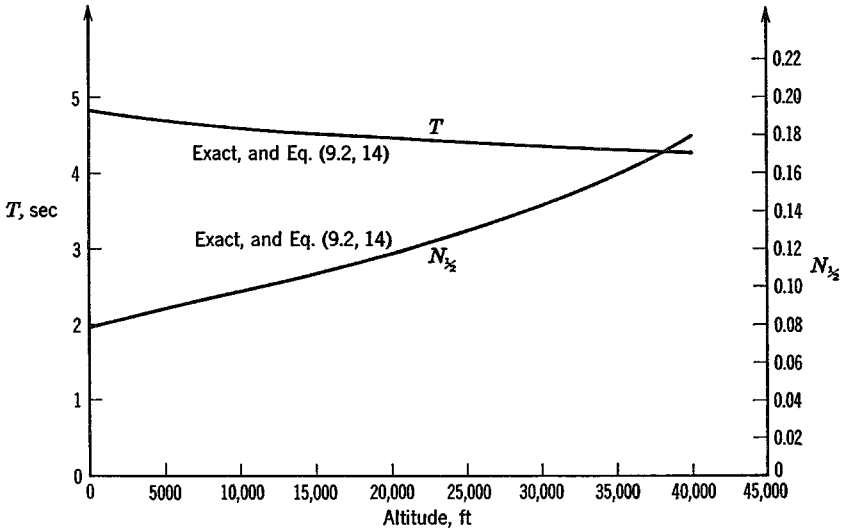

FIG. 9.9 Variation of period and damping of short-period mode with altitude. $C_{w_e} = .25$. $K_n = .10$.

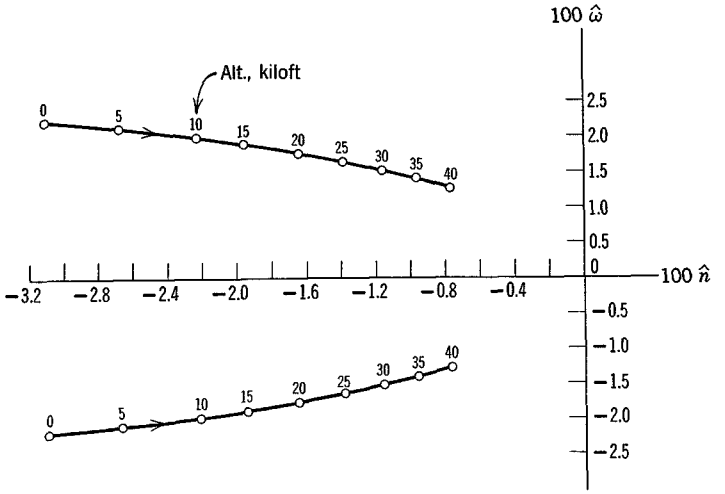

FIG. 9.10 Root locus—short-period mode, variable altitude.

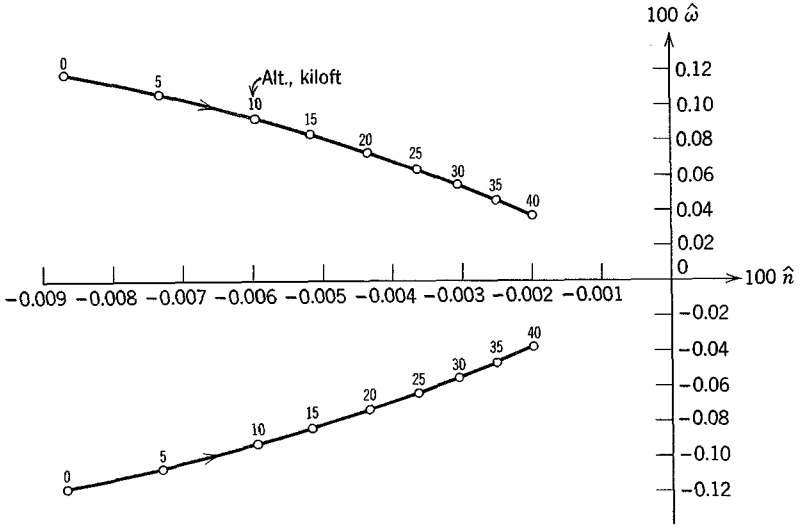

FIG. 9.11 Root locus—phugoid mode, variable altitude.

approximately as $(\sqrt{\rho_e} V_e)^{-1}$. Since $\rho_e V_e^2$ is a constant at constant C_{W_e} the short-period is expected to vary only slightly with height, and this is evident in Fig. 9.9. The damping of both modes is higher in the denser lower atmosphere. This is predicted for the short-period mode by (9.2,14), but not for the phugoid by (9.2,9). The nondimensional roots show large and qualitatively similar variations for both modes in Figs. 9.10 and 11.

9.4.3 EFFECT OF FLIGHT-PATH ANGLE

To calculate the stability characteristics for nonhorizontal flight it is necessary to neglect all the z derivatives, and use the system matrix of (5.13,19). The basic aerodynamic assumptions made in the following calculations are the same as those used in Sec. 9.1 but the following important difference should be noted—the thrust and lift are no longer equal to the drag and the weight, respectively. Instead at angle of climb γ_e we have, when $\alpha_T = 0$,

$$\begin{aligned} C_{T_e} &= C_{D_e} + C_{W_e} \sin \gamma_e \\ C_{L_e} &= C_{W_e} \cos \gamma_e \end{aligned} \tag{9.4,1}$$

Since with the assumptions of the model used, $C_{T_V} = -2C_{T_e}$, this derivative, and hence the coefficient a_{11} of the matrix, vary strongly with γ_e. It is also

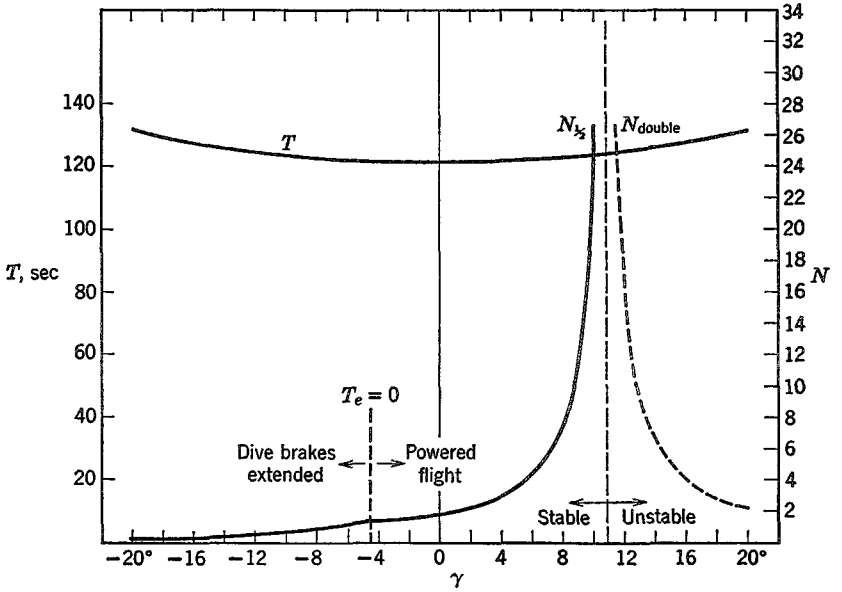

FIG. 9.12 Variation of phugoid mode parameters with γ. $C_{w_e} = .25$, altitude = 30,000 ft.

necessary to note that for negative flight-path angles (diving flight) greater than a few degrees (9.4,1) would require negative thrust. For this range of γ_e we have assumed for the purposes of the example that T_e is zero and that dive brakes are extended to provide the necessary drag, i.e. that

$$C_{D_e} = -C_{W_e} \sin \gamma_e \tag{9.4,2}$$

Thus for γ_e less than the power-off glide angle, $a_{11} = (C_{W_e}/\mu) \sin \gamma_e$. The main results of calculations of the eigenvalues are shown on Figs. 9.12 and 9.13 for the constant values $C_{W_e} = .25$, $\rho_e = .000889$, $K_n = .10$. The short-

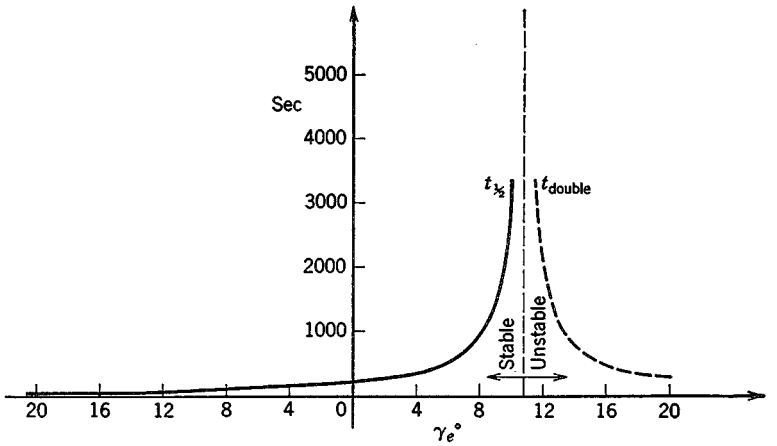

FIG. 9.13 Variation of the time to half amplitude of the phugoid mode with γ.

period mode is not significantly affected by γ_e, but the phugoid is very much. Figure 9.12 shows the variation of its period and damping over the range $-20 \leq \gamma_e \leq 20°$. Although the period varies only slightly, the damping deteriorates rapidly with increasing climb angle until the mode becomes unstable above 10.8°. At 20° climb angle the number of cycles to double amplitude has decreased to about 2.2, but because of the long period the time to double, as shown on Fig. 9.13, is still very long—289 sec.

This behavior of the phugoid damping is approximately predicted by the two-degree-of-freedom analysis. If γ_e be retained from the beginning, with $C_{T_V} = -2C_{T_e}$ for constant-thrust powered flight, the same method that was used to obtain (9.2,9) yields for this case the characteristic equation

$$s^2 + \frac{1}{2\mu}(2C_{D_e} - C_{W_e} \sin \gamma_e)s + \frac{C_{W_e}}{2\mu^2}(C_{W_e} \cos^2 \gamma_e - C_{D_e} \sin \gamma_e) = 0 \tag{9.4,3}$$

The coefficient of s, which gives the damping, decreases as γ_e increases, and

vanishes at the critical angle

$$\gamma_{e_{\text{crit}}} = \sin^{-1} \frac{2C_{D_e}}{C_{W_e}} \tag{9.4,4}$$

For the example, this is 8.6°, somewhat less than the correct value of 10.8° obtained from the complete system of equations.

The unstable phugoid can be shown to be entirely a consequence of the thrust law assumed. If the propulsion system were one of constant power TV instead of constant thrust T, the value of C_{T_V} would be $-3C_{T_e}$ instead of $-2C_{T_e}$ [see (7.8,5)]. In that case the coefficient of s in (9.4,3) turns out to be $3C_{D_e}/2\mu$, a positive number almost independent of climb angle, and the approximate theory indicates no important change of phugoid characteristics with angle of climb. Values of C_{T_V} intermediate between the two values used above would give less reduction in the damping than shown in Fig. 9.12.

9.4.4 EFFECT OF VERTICAL DENSITY-GRADIENT

The effect of the vertical gradient in atmospheric density on the characteristic modes of horizontal flight was first discussed by Scheubel (ref. 9.1), and later in more detail by Neumark (ref. 9.2) and Walkowicz (ref. 9.3). Their principal conclusions were that the short-period motion is unchanged by the density gradient, but that the phugoid period is appreciably shortened by an amount that increases with speed. Neumark also pointed out that the characteristic equation for this case is of the fifth degree and that the extra root is a small one corresponding to the tendency of the vehicle to seek or depart from its equilibrium altitude, depending on whether or not the root is negative. Neumark concluded, based on examples in which the thrust was independent of height, that the damping of the phugoid was unaffected by $d\rho/dz$. In fact, the phugoid damping is very sensitive to the thrust law, and as shown in the example that follows, in which $T \propto \rho$ so that $C_{T_z} = 0$ (a reasonable approximation for jet engines), the damping can be very much reduced at all speeds by the density gradient. Before proceeding to the numerical solutions of the complete equations however, it is instructive to present Scheubel's extension of the simple Lanchester analysis of the phugoid period. In Sec. 9.2 we saw that with Lanchester's approximations there is a vertical "spring stiffness" k given by (9.2,3) that governs the period. When the density varies there is a second "stiffness" k' resulting from the fact that the increased density when the vehicle is below its reference altitude increases the lift, and vice versa. This incremental lift associated with a density change is

$$\Delta L = C_L \tfrac{1}{2} V^2 S \, \Delta\rho$$

so that

$$k' = \frac{\partial \Delta L}{\partial z} = C_{L_e} \tfrac{1}{2} V_e^2 S \frac{d\rho}{dz}$$

From the definitions of $\hat{\rho}$, $\hat{z}$ and noting that $C_{L_e} = C_{W_e}$ we get

$$k' = \frac{2W}{\bar{c}} \frac{d\hat{\rho}}{d\hat{z}} \tag{9.4,5}$$

The density variation in the atmosphere is closely exponential over appreciable altitude ranges, so $d\hat{\rho}/d\hat{z} = (1/\rho_e)(d\rho/d\hat{z})$ is roughly constant. Thus we find that k' is approximately constant, whereas k from (9.2,3) depends on $C_{W_e}\rho$, which varies as V^{-2} for constant weight. The density gradient therefore has its greatest relative effect at high speed. The correction factor for the period, which varies inversely as the square root of the stiffness, is

$$K = \left(\frac{k}{k + k'}\right)^{1/2} = \frac{1}{(1 + k'/k)^{1/2}} \tag{9.4,6}$$

so that the period with density gradient is $T' = KT$. With the given values of k and k' this becomes

$$K = \frac{1}{\left(1 + \dfrac{V_e^2}{g\bar{c}} \dfrac{d\hat{\rho}}{d\hat{z}}\right)^{1/2}} \tag{9.4,7}$$

in which the principal variable is seen to be the speed, occurring in the form of the Froude's number $(V_e^2/g\bar{c})$. The reduction in phugoid period predicted by (9.4,7) for the example airplane is 14% at 500 mph, which is very close to the exact result of 13% (Fig. 9.14).

In order to provide a complete comparison with the approximation based on constant density, we use the fifth-order system (5.13,18) to make numerical calculation for the same conditions as hold in Figs. 9.4 and 9.5. All the z derivatives C_{T_z}, C_{D_z}, C_{L_z}, C_{m_z} have been assumed to be zero, and the only density-gradient effects are embodied in the $d\rho/dz$ terms. Note that $C_{T_z} = 0$ implies a propulsion system in which the thrust is proportional to ρ. With all the assumptions that pertain to this example explicitly incorporated, the system matrix is

$$\begin{bmatrix}
-\dfrac{C_{D_e}}{\mu} & \dfrac{C_{L_e} - C_{D_\alpha}}{2\mu} & 0 & -\dfrac{C_{W_e}}{2\mu} & 0 \\
-\dfrac{C_{W_e}}{\mu} & -\dfrac{C_{L_\alpha} + C_{D_e}}{2\mu} & 1 & 0 & -\dfrac{C_{L_e}}{2\mu} \dfrac{d\hat{\rho}}{d\hat{z}} \\
-\dfrac{C_{W_e} C_{m_{\dot{\alpha}}}}{\mu \hat{I}_y} & \dfrac{1}{\hat{I}_y}\left(C_{m_\alpha} - \dfrac{C_{m_{\dot{\alpha}}}(C_{L_\alpha} + C_{D_e})}{2\mu}\right) & \dfrac{1}{\hat{I}_y}(C_{m_q} + C_{m_{\dot{\alpha}}}) & 0 & -\dfrac{C_{L_e}}{2\mu \hat{I}_y} C_{m_{\dot{\alpha}}} \dfrac{d\hat{\rho}}{d\hat{z}} \\
0 & 0 & 1 & 0 & 0 \\
0 & 1 & 0 & -1 & 0
\end{bmatrix} \tag{9.4,8}$$

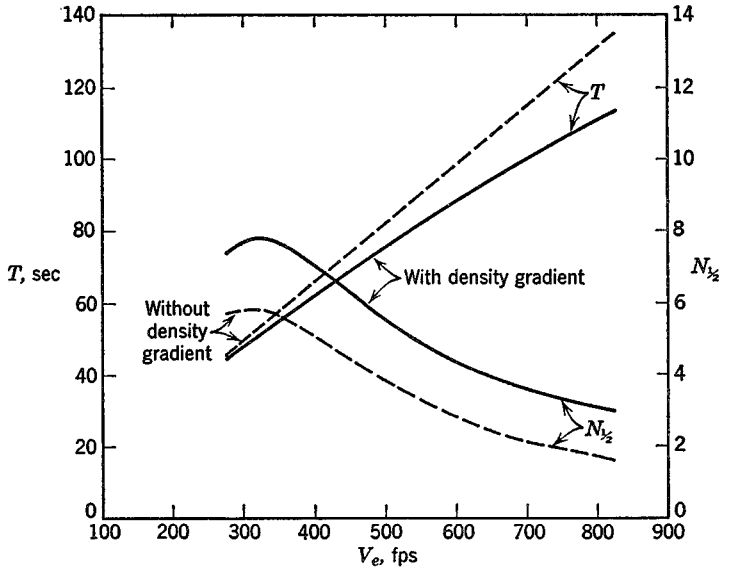

FIG. 9.14 Effect of density gradient on phugoid characteristics. Altitude 30,000 ft.

The value of $d\hat{\rho}/d\hat{z}$ was obtained from the tables for the U.S. Standard Atmosphere (ref. 9.14) as follows:

$$\frac{d\hat{\rho}}{d\hat{z}} = \frac{1}{\rho_e}\frac{\bar{c}}{2}\frac{d\rho}{dz} = -\frac{\bar{c}}{2}\frac{d\log\rho}{dh} \tag{9.4,9}$$

where h is the altitude. From the tabulated data, $d\log\rho/dh$ at about 30,000 ft altitude is found to be -4.16×10^{-5} and hence $d\hat{\rho}/d\hat{z} = \frac{1}{2}(15.40)(4.16)10^{-5} = .000320$. With this value, the eigenvalues of (9.4,8) have been calculated for the same range of speeds as used in Figs. 9.4 and 9.5. The short-period mode is found to be unchanged to three significant digits, in agreement with Neumark, the phugoid damping and period are both altered, and a new stable nonoscillatory mode of long time constant appears. Figure 9.14 shows the quite substantial effects on the phugoid. It is clear from these graphs that neglect of atmospheric density gradient can lead to considerable error. This is especially significant with respect to the damping since the constant-density approximation gives unconservative results.

The fifth root of the characteristic equation is negative, corresponding to a stable subsidence. Its characteristic time, plotted on Fig. 9.15, is seen to be very long. This mode is related to the weak tendency of the vehicle to fly at its equilibrium altitude (note that there is no preferred altitude in the constant-density case). The eigenvector of this mode for $V_e = 561$ mph

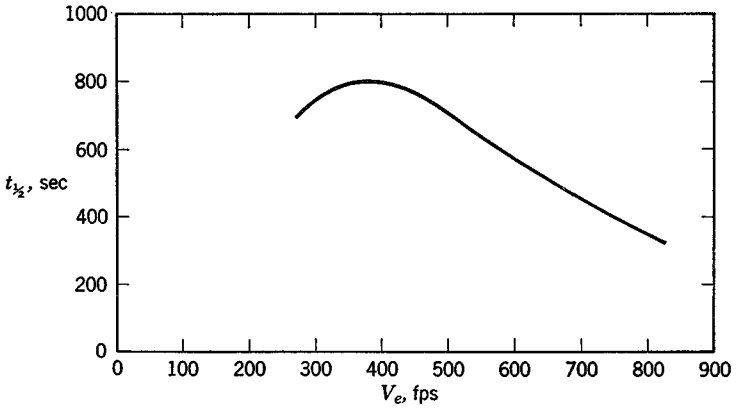

FIG. 9.15 Time to damp of altitude-convergence mode.

is found to be $\Delta\hat{V}:\Delta\alpha:\hat{q}:\Delta\theta:\hat{z}_E = -.161 \times 10^{-3}:.187 \times 10^{-7}:-.398 \times 10^{-9}:.199 \times 10^{-4}:1$ which shows that, like the phugoid, it is a mode with negligible $\Delta\alpha$ and $\hat{q}$. That is, it is an "arrow" mode, in which the vehicle axis is closely aligned with the velocity vector while it drifts slowly back to its equilibrium altitude. The principal degree of freedom is clearly z_E. The relative magnitudes are a little deceptive however because of the small length $(\bar{c}/2)$ used to make z_E nondimensional. For this vehicle, a decrease in altitude of 1000 ft in this mode would correspond to $\Delta\hat{z}_E = 130$ and a ΔV of -2%.

It is instructive to examine the approximation obtained by neglecting $\Delta\alpha$ and the C_m equation, just as was done previously with the fourth-order system. For additional generality, to allow for other than jet engines, we retain the term C_{T_z} in the first equation. When the same procedure is followed as led to (9.2,9) the result is the cubic characteristic equation

$$s^3 - s^2\frac{C_{T_V}}{2\mu} + s\left(\frac{C_{W_e}^{\,2}}{2\mu^2} + \frac{C_{W_e}}{2\mu}\frac{d\hat{\rho}}{d\hat{z}}\right) + \left(C_{T_z} - \frac{C_{T_V}}{2}\frac{d\hat{\rho}}{d\hat{z}}\right)\frac{C_{W_e}}{2\mu^2} = 0 \quad (9.4,10)$$

When the thrust is independent of height and speed, as for a rocket engine, C_{T_z} is given by (7.12,1) as $C_{T_z} = -C_{T_e}\, d\hat{\rho}/d\hat{z}$ and $C_{T_V} = -2C_{T_e}$. The last term of (9.4,10) then disappears, one root is zero, and the remaining two are given by

$$s^2 - s\frac{C_{T_V}}{2\mu} + \left(\frac{C_{W_e}^{\,2}}{2\mu^2} + \frac{C_{W_e}}{2\mu}\frac{d\hat{\rho}}{d\hat{z}}\right) = 0$$

Without the $d\hat{\rho}/d\hat{z}$ term, this is exactly the phugoid approximation (9.2,9),

and the constant term can be identified exactly as the augmented "spring-constant" that led to (9.4,7)—note that the ratio of the last two terms is

$$\frac{C_{W_e}}{2\mu}\frac{d\hat{\rho}}{d\hat{z}} \div \frac{C_{W_e}^{\,2}}{2\mu^2} = \frac{V_e^{\,2}}{g\bar{c}}\frac{d\hat{\rho}}{d}$$

It is clear that the approximation to the fifth root in this case is $\hat{\lambda} = 0$, and that the phugoid is changed only to the extent of the reduced period. The damping term $C_{T_V}/2\mu$ is unaffected by the presence of the density gradient. This is consistent with Neumark's finding for examples in which T is constant.

When the propulsion system is comprised of jet engines, a reasonable approximation is $T \propto \rho$ and independent of V, in which case $C_{T_V} = 2C_{T_e} = -2C_{D_e}$ and $C_{T_z} = 0$. The last term of (9.4,10) is then $(C_{D_e}C_{W_e}/2\mu^2)(d\hat{\rho}/d\hat{z})$, a small positive constant. An approximation to the fifth root is obtained by neglecting the s^2 and s^3 terms of (9.4,10) with the result

$$\hat{\lambda}_5 \doteq -\frac{C_{D_e}\,\partial\hat{\rho}/\partial\hat{z}}{C_{W_e} + \mu\dfrac{\partial\hat{\rho}}{\partial\hat{z}}} \tag{9.4,11}$$

This actually gives a very good approximation to this root for the example treated. It is seen to correspond to a stable convergence. The effect on the remaining phugoid roots can now be inferred. The coefficient of the next-to-the-highest order term in any characteristic equation is equal to the negative of the sum of the roots.† Since the imaginary parts cancel the result is the "sum of the dampings." In this case this yields

$$2\hat{n}_{ph} + \hat{\lambda}_5 = +\frac{C_{T_V}}{2\mu} = -\frac{C_{D_e}}{\mu}$$

where the phugoid roots are $\hat{n}_{ph} \pm i\hat{\omega}_{ph}$. It follows that the "sum of the dampings" is a constant, and hence that the presence of the stable fifth root must be accompanied by a reduction in the damping of the phugoid. Specifically

$$\hat{n}_{ph} = \frac{1}{2}\left(-\frac{C_{D_e}}{\mu} - \hat{\lambda}_5\right) \tag{9.4,12}$$

For the example case at $C_{W_e} = .20$, this gives the reduction in phugoid damping from the constant-density case, $\Delta\hat{n}_{ph}/\hat{n}_{ph}$, within about 1%.

In summary, it is clear that even at subsonic speeds the classical "stability quartic" derived from a uniform-atmosphere model can be significantly in

† Verify by comparing l.h.s. and r.h.s. of $(s - \lambda_1)(s - \lambda_2)\cdots(s - \lambda_n) = s^n + c_{n-1}s^{n-1} + \cdots c_0$. $-c_{n-1}$ is equal to the *trace* of the system matrix **A**, i.e. to the sum of its diagonal elements.

error with respect to the phugoid roots, and the design of autopilot systems to maintain speed and/or altitude may require the use of the more accurate model. At supersonic speeds the effect of density gradient is larger still. However it should be noted that the flat-Earth model itself becomes inadequate at high supersonic speeds (see Sec. 9.10).

9.4.5 EFFECT OF STATIC MARGIN

It was indicated in Chapter 6 that the single most important aerodynamic characteristic for longitudinal stability is the pitch stiffness C_{m_α}, and that it varies strongly with the C.G. position, i.e.

$$C_{m_\alpha} = C_{L_\alpha}(h - h_n)$$

where the *static margin* is $K_n = h_n - h$. The effect of this parameter is demonstrated by using (9.1,1) with variable K_n. The results for all other data the same as in Sec. 9.1 are shown on Figs. 9.16 to 9.19. Figure 9.16 shows that the phugoid period and damping vary rapidly at low static margin, and that the approximation (9.2,9), which does not include the effect of the pitch stiffness, is useful only at large K_n. Approximation (9.2,11), however, gives the trends with K_n quite well. The period goes to infinity, and $N_{½}$ to zero at a value of K_n slightly greater than zero. Figure 9.17 shows the variation of the short-period roots. These too vary strongly with pitch stiffness, the mode becoming nonoscillatory at K_n slightly less than .01.

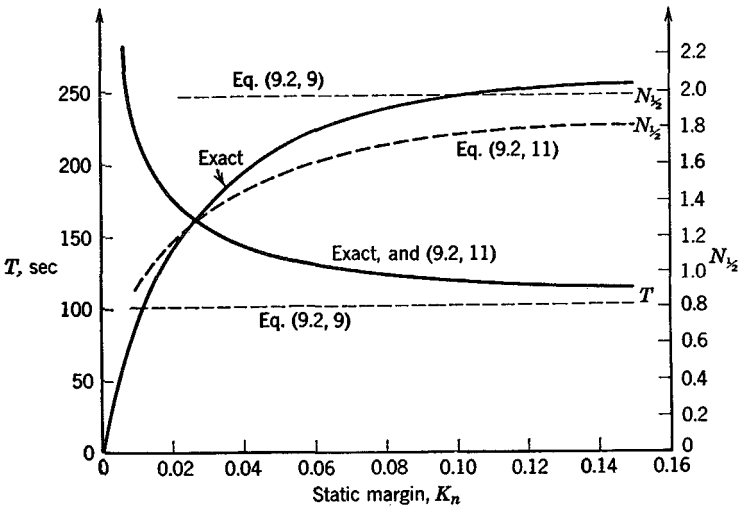

FIG. 9.16 Variation of period and damping of phugoid mode with static margin.

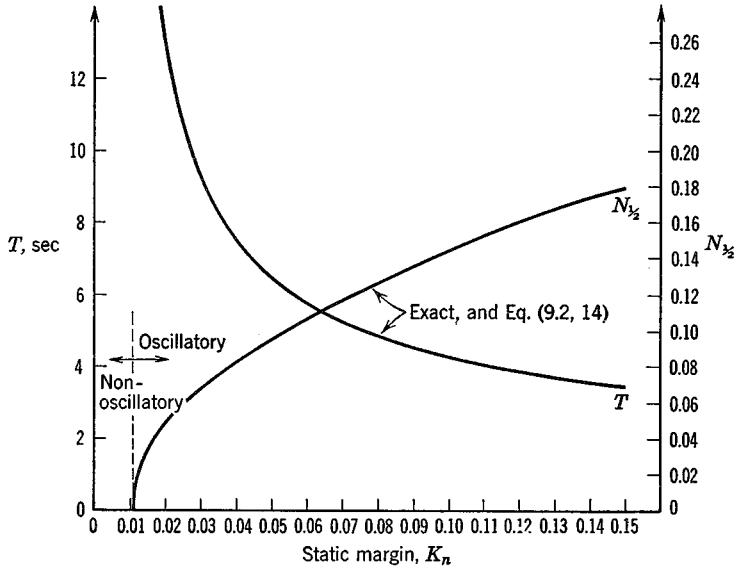

FIG. 9.17 Variation of period and damping of short-period mode with static margin.

The approximation of (9.2,14) is seen to be excellent over the whole oscillatory range.

Additional insight into the behavior of the modes is obtained from the root-locus plots of Fig. 9.18. Figure 9.18*a* shows that the damping $\hat{n}$ of the short-period mode remains essentially constant as K_n decreases, while the frequency $\hat{\omega}$ decreases to zero at K_n between .01 and .02 (point A). The root locus then splits into a pair of real roots, branches AB and AC of the locus. These represent damped aperiodic modes, or subsidences. Figure 9.18*b* shows that the phugoid mode behaves similarly as the C.G. is moved backwards towards the neutral point. At point D, when the C.G. is just forward of the N.P., the oscillatory phugoid also degenerates into a pair of aperiodic modes, the branches DF and DE of the locus. DF is a subsidence and that portion of DE to the right of the origin represents a divergence—i.e. the airplane is statically unstable when K_n is negative.

The behavior of the roots is quite interesting for $h > h_n + .02$. The branch AB of the short-period mode and the branch DF of the phugoid "collide" at F when the C.G. is between 2 and $2\frac{1}{2}\%$ of $\bar{c}$ behind the N.P. A new oscillatory mode then appears corresponding to the branches FG of the locus. This is a stable oscillation whose damping and period are intermediate between those of the two parent modes. The eigenvector for this mode shows that all three degrees of freedom ΔV, $\Delta\alpha$, $\Delta\theta$ are significantly excited, and

hence there is no simple approximation to it. Since the range of C.G. positions in which this mode occurs is that for which there is already one unstable root (DE), it is of academic interest only.

It was shown in Sec. 9.3 that the criterion for static stability is (9.3,3). The calculations presented in Fig. 9.18*b* verify this conclusion, since in the example $C_{m_V} = 0$ and the criterion reduces to $K_n > 0$. When the C.G. is aft of the N.P. the rate of divergence of the unstable mode is as shown in Fig. 9.19 (curve for $C_{m_V} = 0$). The time to double rapidly decreases with decreasing K_n to values too short to be manageable by a human pilot.

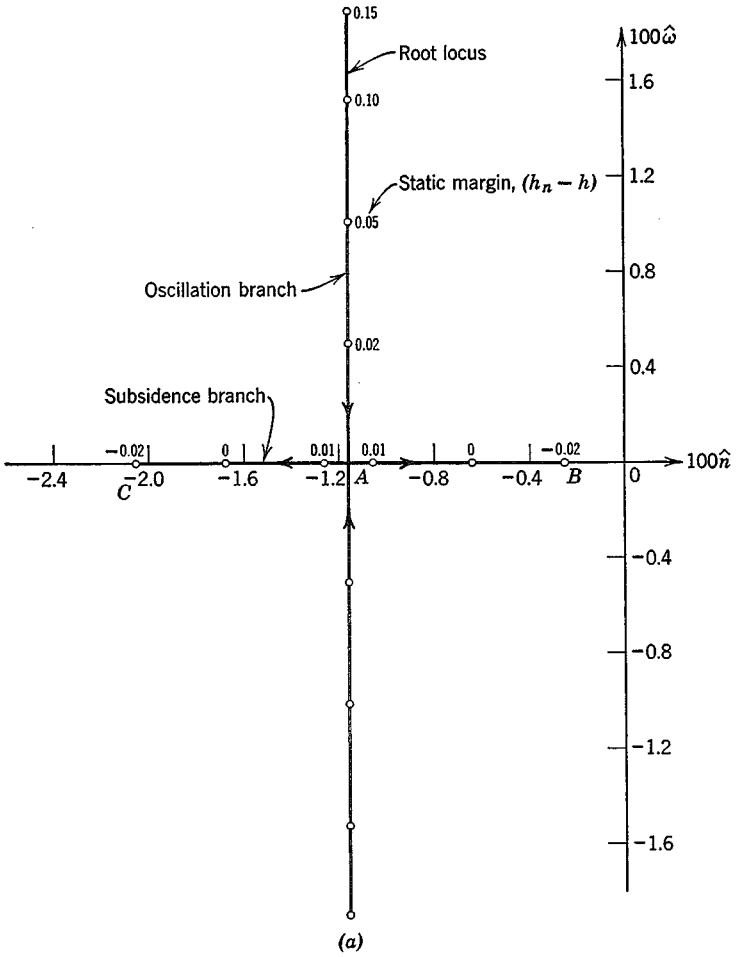

FIG. 9.18 (*a*) Locus of short-period roots, varying C.G. position. $C_{m_V} = 0$. (*b*) Locus of phugoid roots, varying C.G. position. $C_{m_V} = 0$.

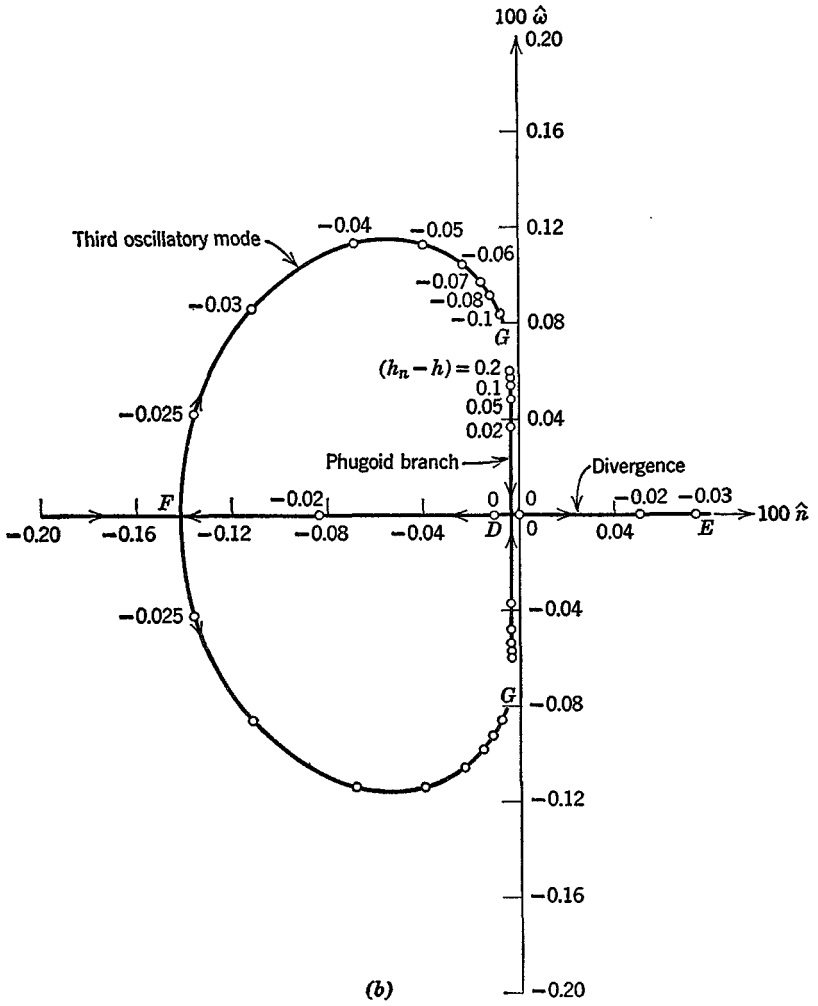

FIG. 9.18. (*Contd.*)

9.4.6 EFFECT OF SPEED DERIVATIVES

In the preceding examples, all the speed derivatives except C_{T_V} were assumed to be zero. Now speed effects are highly dependent on the configuration, and for subsonic airplanes result from both aeroelastic and compressibility effects. They vary widely from one vehicle to another, and can change rapidly with Mach number (implying that the small-disturbance theory is very restricted in that case). It is not therefore feasible to give

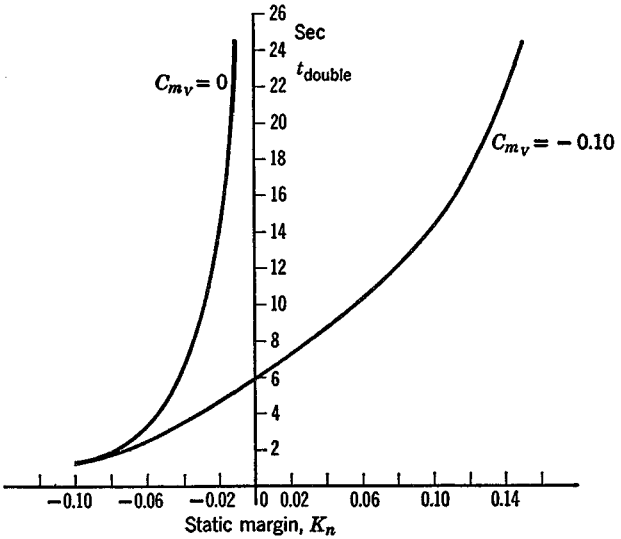

FIG. 9.19 Time to double of the divergent mode.

any generally useful results for speed effects. There is one point, however, which is worth exploring, and that is the effect of C_{m_V} on the roots. Equation (9.3,3) shows that this derivative can affect the static stability, negative values producing a reduction in the stability boundary h_s [see (6.4,26)]. To illustrate this, the value of C_{m_V} has been set equal to $-.10$ in (9.1,1) and the eigenvalues found for the same range of K_n as used in the previous example. This value of C_{m_V} is quite representative of what may occur at high subsonic Mach number. The root loci obtained look much like those presented in Fig. 9.18. The short-period mode is changed only slightly, but the phugoid has an important difference; namely, the divergent branch DE crosses the axis at $K_n = .20$ instead of at zero. Thus there is an unstable divergence over the whole of the C.G. range used in the example. The nature of this divergence is seen in Fig. 9.19, which shows the time to double amplitude. The divergence associated with this value of C_{m_V} is not very rapid for reasonable design values of K_n, i.e. $K_n > .03$, for then $t_{\text{double}} > 8$ sec and the airplane would not be unmanageable. The unstable mode is one involving primarily the speed and flight-path angle (of opposite sign) so that it represents either a climb at increasing climb angle and decreasing speed, or a dive of increasing speed and dive angle. The latter is what was called a "compressibility dive" at the end of World War II. The nonlinear features rapidly take over control of these motions as ΔV increases. For the climb divergence, the reduction of speed and Mach number take the vehicle

back toward the incompressible regime and a reduction in $|C_{m_T}|$ whereas the dive case leads to increasing **M** and possibly an aggravation of the divergence.

9.5 LONGITUDINAL CHARACTERISTICS OF A STOL AIRPLANE

The curves of Figs. 9.4 and 9.5 show that the characteristic modes of an airplane vary markedly with speed, i.e. with the equilibrium weight coefficient C_{W_e}. In particular, the two characteristic periods begin to approach one another as C_{W_e} becomes large. It is of interest to explore this range more fully by considering an STOL airplane, operating in the "powered-lift" region for which C_{W_e} may be much larger. To this end the data given in ref. 7.11, part of which is shown in Fig. 7.6, has been used to obtain a representative set of coefficients for $2.0 \leq C_{W_e} \leq 5.0$. The flight condition assumed is horizontal steady flight, so that $C_D^* = 0$ (see Fig. 7.6*b*). (The particular data used from the reference was that for the aircraft with a large tail in the high position, $i_t = 0$, and $\delta_f = 45°$.) From the given curves, and from cross-plots of the coefficients C_L, C_D, and C_m vs. C_T at constant α, the data in Table 9.3 was derived for the equilibrium condition. Smooth curves were used for interpolation. Since this is not a tilt-wing airplane, α_T is not large in the cases considered, and has been assumed to be zero.

Table 9.3

Basic Data for STOL Airplane

C_{W_e}	C_{T_e}	C_{L_α}	C_{D_α}†	h_n‡	$\frac{\partial C_L}{\partial C_T}$	$\frac{\partial C_D}{\partial C_T}$	$\frac{\partial C_m}{\partial C_T}$
2.0	0.53	5.75	1.19	.500	.705	.285	−.090
2.5	0.72	6.20	1.80	.475	.790	.328	−.070
3.0	0.90	6.65	2.41	.450	.875	.370	−.050
3.5	1.09	7.10	3.02	.424	.955	.411	−.030
4.0	1.28	7.55	3.63	.398	1.025	.450	−.010
4.5	1.46	8.00	4.24	.371	1.097	.488	+.010
5.0	1.65	8.45	4.85	.346	1.165	.525	+.030

† $C_{D_\alpha} = \dfrac{\partial C_D}{\partial C_L} C_{L_\alpha}$

‡ $h_n = .30 - C_{m_\alpha}/C_{L_\alpha}$

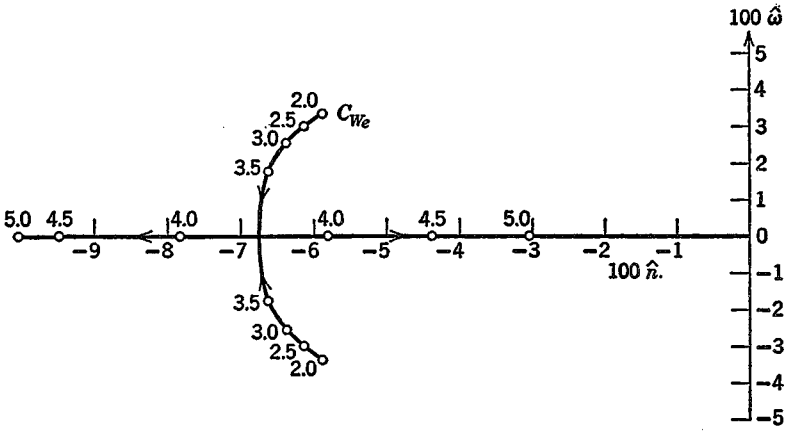

FIG. 9.20 Root locus—short-period mode, STOL airplane.

Since aeroelastic and compressibility effects are negligible at the low speeds of STOL flight the required speed derivatives are given by (see Table 7.1)

$$C_{D_V} = C_{T_V}\frac{\partial C_D}{\partial C_T}; \qquad C_{L_V} = C_{T_V}\frac{\partial C_L}{\partial C_T}; \qquad C_{m_V} = C_{T_V}\frac{\partial C_m}{\partial C_T}$$

For a propeller-driven airplane, the value of C_{T_V} is given by (7.8,5), and an examination of the data on η for a typical constant-speed propeller at low speed† showed that $(V_e/\eta_e)(\partial\eta/\partial V)_e$ is close to unity. Hence we have used $C_{T_V} = -2C_{T_e}$ in this example.

Using the formulae of Table 7.1, the following estimates were made of the q and $\dot{\alpha}$ derivatives:

$$C_{L_q} = 14, \qquad C_{m_q} = -17.9, \qquad C_{L_{\dot{\alpha}}} = 5.5, \qquad C_{m_{\dot{\alpha}}} = -13$$

Finally the following inertial and geometric characteristics were assumed:

$$W = 40{,}000 \text{ lb}, \qquad S = 1000 \text{ ft}^2, \qquad A = 5.42, \qquad \bar{c} = 13.60 \text{ ft}$$

$$\mu = 76.8, \qquad \hat{I}_y = 385, \qquad h = .30$$

With the above data, the coefficients of the system matrix (9.1,1) were evaluated, and its eigenvalues and eigenvectors calculated. The main results are shown on Figs. 9.20 to 9.24. Figures 9.20 and 9.21 show the loci of the roots as C_{W_e} varies between 2 and 5. The effect of C_{W_e} is seen to be large on both modes, the short-period mode becoming nonoscillatory at a value of C_{W_e} somewhat greater than 3.5, and the damping of the phugoid increasing

† The De Havilland Buffalo airplane.

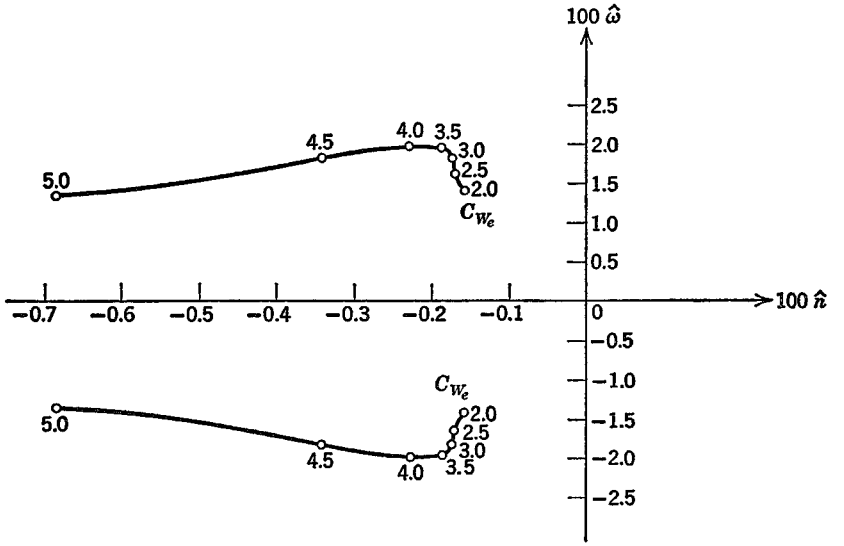

FIG. 9.21 Root locus—phugoid mode, STOL airplane.

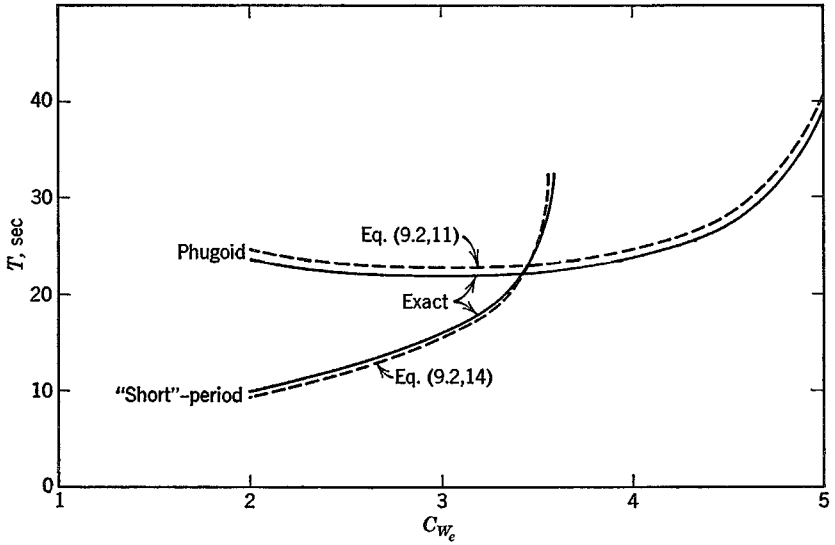

FIG. 9.22 Periods of oscillatory modes, STOL airplane.

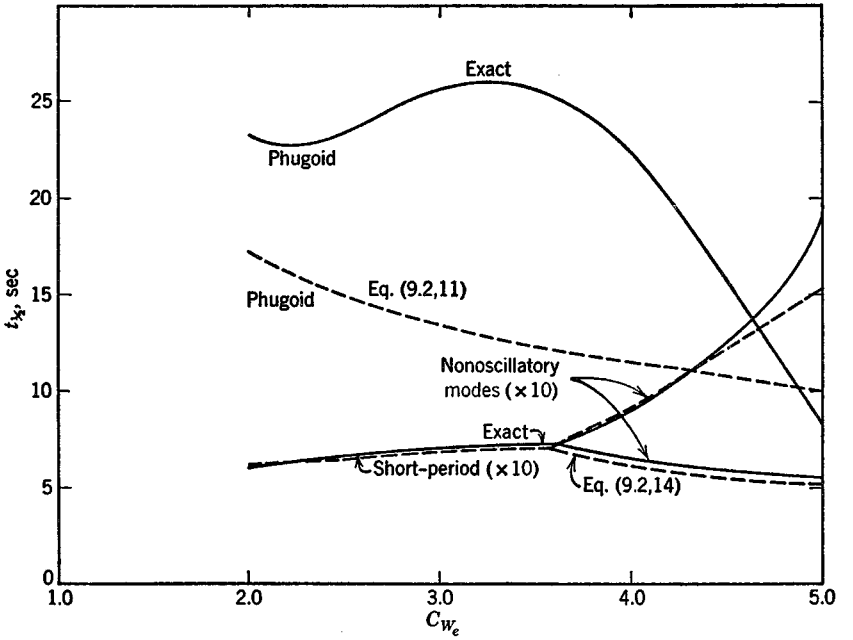

FIG. 9.23 Time to damp of modes, STOL airplane.

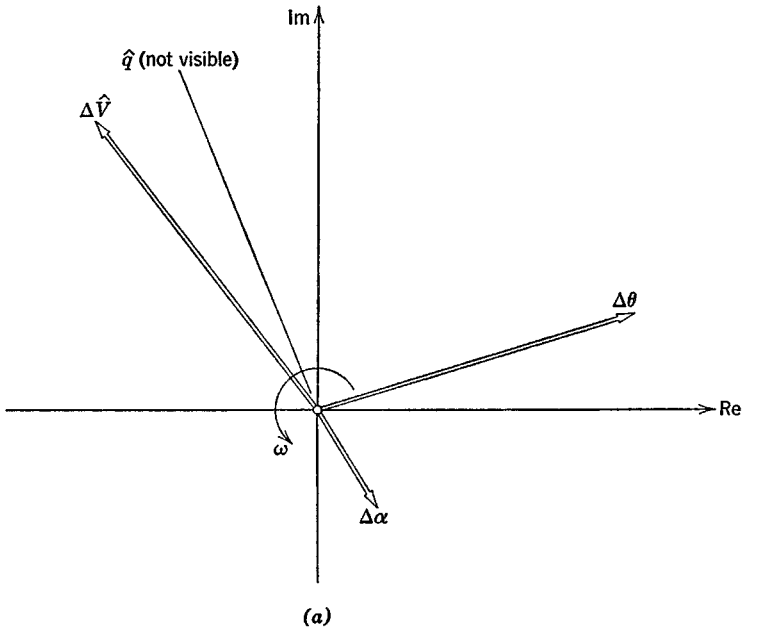

(a)

FIG. 9.24 (*a*) STOL airplane, vector diagram of phugoid mode. $C_{w_e} = 3.5$. (*b*) Short-period mode. $C_{w_e} = 3.5$.

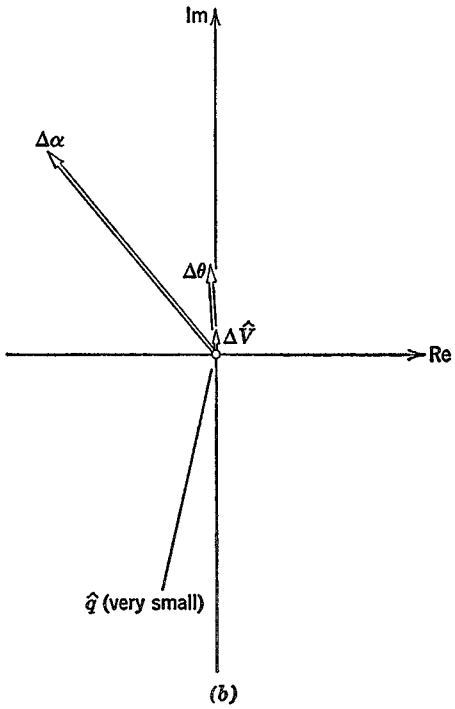

FIG. 9.24 (*Contd.*)

rapidly at the same time. Figure 9.22 shows the two periods, and that they actually cross over at $C_{W_e} \doteq 3.4$. The concept of the phugoid as a "long" period oscillation is evidently not applicable in this situation! The approximations (9.2,11) to the phugoid, and (9.2,14) to the pitching mode are also shown for comparison. It is seen that they give the two periods quite well, and that (9.2,14) also depicts quite accurately the damping of the pitching oscillation and of the two nonperiodic modes into which it degenerates at high C_{W_e}. The phugoid damping, however, is not at all well predicted by the approximate solution, and (9.2,9) gives even larger discrepancies for both period and damping. Figure 9.23 shows the damping times for the modes, and they are all seen to be heavily damped over the whole range.

The eigenvectors for the two modes are shown on Fig. 9.24 for $C_{W_e} = 3.5$, the condition of nearly equal periods. The relative configurations of the vectors are seen to be quite similar to those for the jet transport at $C_{W_e} = 1.8$ (Fig. 9.6), but the magnitudes of $\Delta\alpha$ in the phugoid, and $\Delta\hat{V}$ in the short-period mode are appreciably larger.

Response to actuation of the controls (open loop)

CHAPTER 10

10.1 INTRODUCTION

From the system theory presented in Chapter 3 we see that it is convenient to classify vehicle motion according to whether it is *free* or *forced*. Chapter 9 was devoted to a discussion of a number of examples of the former, and in this chapter we give some illustrations of the latter. The particular cases studied here are those in which the motion results from nonautonomous actuation of the controls. That is, we exclude those in which the controls are moved *in response to* the vehicle motion in accordance with a prescribed law, as by an autopilot. Such motions are the subject matter of Chapter 11. We should recall as well that for linear/invariant systems (Sec. 3.4) there is really only one *fundamental* response problem The impulse response, the step response, and the frequency response are all explicitly related, and the convolution theorem (3.4,41) and (3.4,43) enables the response to any arbitrary control variation to be calculated from a knowledge of either the impulse response or the step response.

In the examples that follow, we consider the response of an airplane to actuation of its principal controls, the throttle and the three aerodynamic control surfaces. The examples include both step and frequency response, and both linear and nonlinear cases.

As shown in Chapter 3, the basic item needed for computing frequency

response, and for formulating response problems analytically is the transfer function that relates the relevant responses and inputs. In the present context the input is the control vector. The required transfer functions can be found either from the standard first-order form of the differential equations of motion, in which case they are given by (3.2,23), or from the Laplace transforms of the equations (5.11,8 to 10) or (5.14,1 to 3). There is an essential theoretical difference between the two methods, since the former implies the representation of the aerodynamic forces by means of aerodynamic derivatives, and the latter allows (but does not require) the use of exact linear aerodynamics (see Sec. 5.11). Practically, there is only a difference between the responses calculated by the two approaches when the aerodynamic control surfaces are moved very rapidly.

LONGITUDINAL CONTROL

The two principal quantities that need to be controlled in symmetric flight are the speed and the flight-path angle, that is to say, the vehicle's velocity vector. To achieve this obviously entails the ability to apply control forces both parallel and perpendicular to the flight path. The former is provided by thrust or drag control, and the latter by lift control via elevator deflection or wing flaps. It is evident from simple physical reasoning (or from the equations of motion) that the main *initial* response to opening the throttle (increasing the thrust) is a forward acceleration, i.e. control of speed. The main *initial* response to elevator deflection is a rotation in pitch, with subsequent change in angle of attack and lift, and hence the development of $\dot{\gamma}$, a rate of change of flight-path angle. When the transients that follow such control actions have ultimately died away, the new steady state that results can be found in the conventional way used in performance analysis. Fig. 10.1 shows the basic relations. The steady speed V at which the airplane flies is governed by the lift coefficient, which is in turn fixed by the elevator angle—see (6.4,13). Hence a constant δ_e implies a fixed V. The flight-path angle γ at any given speed is determined, as shown in Fig. 10.1, by the thrust. Thus the *ultimate* result of moving the throttle at fixed elevator angle (when the thrust line passes through the C.G.) is a change in γ without change in speed. But we saw above that the initial response to throttle is a change in speed—hence the short-term and long-term effects of this control are quite contrary. Likewise we saw that the main initial effect of moving the elevator is to rotate the vehicle and influence γ, whereas the ultimate effect at fixed throttle is to change both speed and γ. The short-term and long-term effects of elevator motion are therefore also quite different. The total picture of longitudinal control is clearly far from simple, and the transients that connect the initial and final responses require investigation. We shall see in the

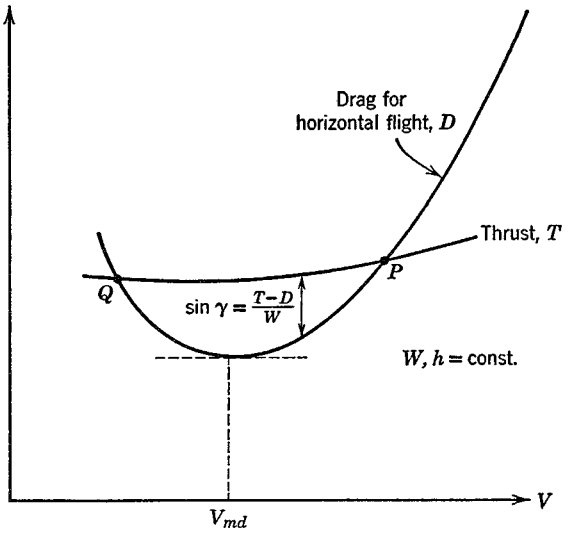

FIG. 10.1 Basic performance graph.

following that these are dominated by the long-period, lightly damped phugoid oscillation, and that the final steady state with step inputs is reached only after a long time. These matters are explored more fully in the following sections.

LATERAL CONTROL

The lateral controls (the aileron and rudder) on a conventional airplane have three principal functions.

1. To provide trim in the presence of asymmetric thrust associated with power plant failure.
2. To provide corrections for unwanted motions associated with atmospheric turbulence or other random events.
3. To provide for turning maneuvers—i.e. rotation of the velocity vector in a horizontal plane.

The first two of these purposes are served by having the controls generate aerodynamic moments about the x and z axes—rolling and yawing moments. For the third a force must be provided that has a component normal to **V** and in the horizontal plane. This is, of course, the component $L \sin \phi$ of the lift when the airplane is banked at angle ϕ. In the equation of motion this appears as the sin ϕ term in (5.9,6). Thus the lateral controls (principally the aileron) produce turns as a secondary result of controlling ϕ.

Ordinarily, the long-term responses to deflection of the aileron and rudder are very complicated, with all the lateral degrees of freedom being excited by each. Solution of the complete equations of motion is the only way to appreciate these fully. Certain useful approximations of lower order are however available.

10.2 RESPONSE TO ELEVATOR INPUT

For the conventional case of cruising flight of airplanes, (5.14,2) can be used for the response to elevator by setting $\overline{\Delta C}_{T_e} = 0$. We shall first make some simplifying assumptions, i.e. that $\alpha_T = 0$, that the reference flight path is horizontal, so $\gamma_e = 0$, and that all of $\hat{G}_{DV}, \hat{G}_{LV}, \hat{G}_{mV}, \hat{G}_{Lq}$ are negligible. It is assumed further that deflecting the elevator can change the lift and moment, but not the drag, so that $\overline{\Delta C}_{D_c} = 0$, $\overline{\Delta C}_{L_c} = G_{L\delta}\,\overline{\Delta\delta}_e$ and $\overline{\Delta C}_{m_c} = G_{m\delta}\,\overline{\Delta\delta}_e$. Then (5.14,2) reduces to

$$\begin{bmatrix} (\hat{G}_{TV} - 2\mu s) & (C_{L_e} - \hat{G}_{D\alpha}) & 0 & -C_{W_e} \\ -2C_{W_e} & -(\hat{G}_{L\alpha} + C_{D_e} + 2\mu s) & 2\mu & 0 \\ 0 & -\hat{G}_{m\alpha} & (\hat{I}_y s - \hat{G}_{mq}) & 0 \\ 0 & 0 & 1 & -s \end{bmatrix} \begin{bmatrix} \Delta\bar{V} \\ \Delta\bar{\alpha} \\ \bar{q} \\ \Delta\bar{\theta} \end{bmatrix} = \begin{bmatrix} 0 \\ \hat{G}_{L\delta} \\ \hat{G}_{m\delta} \\ 0 \end{bmatrix} \Delta\bar{\delta}_e \tag{10.2,1}$$

The aerodynamic transfer functions on the r.h.s. can usually be represented well enough by (see Sec. 5.14)

$$\begin{aligned} \hat{G}_{L\delta} &= C_{L_\delta} \\ \hat{G}_{m\delta} &= C_{m_\delta} + sC_{m_{\dot{\delta}}} \end{aligned} \tag{10.2,2}$$

and $C_{m_{\dot{\delta}}}$ is furthermore frequently neglected.

Let the 4×4 matrix on the l.h.s. of (10.2,1) be denoted $\mathbf{P}$. Then (10.2,1) may be compactly written

$$\mathbf{P} \begin{bmatrix} \Delta\bar{V} \\ \Delta\bar{\alpha} \\ \bar{q} \\ \Delta\bar{\theta} \end{bmatrix} = \begin{bmatrix} 0 \\ \hat{G}_{L\delta} \\ \hat{G}_{m\delta} \\ 0 \end{bmatrix} \Delta\bar{\delta}_e \tag{10.2,3}$$

We premultiply dy $\mathbf{P}^{-1}$ to get

$$\begin{bmatrix} \Delta\bar{V} \\ \Delta\bar{\alpha} \\ \bar{q} \\ \Delta\bar{\theta} \end{bmatrix} = \mathbf{P}^{-1} \begin{bmatrix} 0 \\ \hat{G}_{L\delta} \\ \hat{G}_{m\delta} \\ 0 \end{bmatrix} \Delta\bar{\delta}_e \tag{10.2,4}$$

whence the transfer-function vector for elevator input is

$$\hat{\mathbf{G}} = \begin{bmatrix} \hat{G}_{V\delta} \\ \hat{G}_{\alpha\delta} \\ \hat{G}_{q\delta} \\ \hat{G}_{\theta\delta} \end{bmatrix} = \mathbf{P}^{-1} \begin{bmatrix} 0 \\ \hat{G}_{L_\delta} \\ \hat{G}_{m_\delta} \\ 0 \end{bmatrix} \tag{10.2,5}$$

Since $\mathbf{P}$ is the matrix of the nondimensional equations, then the elements of $\hat{\mathbf{G}}$ relate the Laplace transforms of the nondimensional variables, for example

$$\hat{G}_{V\delta} = \frac{\mathscr{L}[\Delta\hat{V}]}{\mathscr{L}[\Delta\delta_e]}, \qquad \hat{G}_{q\delta} = \frac{\mathscr{L}[\hat{q}]}{\mathscr{L}[\Delta\delta_e]} \tag{10.2,6}$$

The above elements of $\hat{\mathbf{G}}$ do not exhaust the transfer functions of interest. Other response quantities may be wanted—for example, the flight-path angle and the normal load factor. The former is given by $\gamma = \theta - \alpha$, so that

$$\hat{G}_{\gamma\delta} = \hat{G}_{\theta\delta} - \hat{G}_{\alpha\delta} \tag{10.2,7}$$

The latter (see Sec. 6.10) is

$$n = \frac{L}{W}$$

and is unity in the reference condition. The perturbation in n is

$$\Delta n = \frac{\Delta L}{W} = \frac{1}{C_{W_e}} (\Delta C_L + 2C_{L_e} \Delta\hat{V}) \tag{10.2,8}$$

to first order. ΔC_L is conveniently expressed in terms of the state variables as

$$\Delta\bar{C}_L = \hat{G}_{LV}\,\overline{\Delta V} + \hat{G}_{L\alpha}\,\overline{\Delta\alpha} + \hat{G}_{L\bar{q}}\bar{q} + \hat{G}_{L\delta}\overline{\Delta\delta}_e$$

After substituting in the Laplace transform of (10.2,8), and dividing by $\overline{\Delta\delta}_e$ we get

$$\hat{G}_{n\delta} = \frac{\overline{\Delta n}}{\overline{\Delta\delta}_e} = \frac{1}{C_{W_e}} [(\hat{G}_{LV} + 2C_{L_e})\hat{G}_{V\delta} + \hat{G}_{L_\alpha}\hat{G}_{\alpha\delta} + \hat{G}_{L_q}\hat{G}_{q\delta} + \hat{G}_{L\delta}] \tag{10.2,9}$$

The preceding equations can be used directly for machine computation of frequency response functions, which basically requires only routine operations on matrices with complex coefficients; an example of this application is given below. However, for analysis one needs the literal expressions for the various transfer functions, and in some applications one must also find their inverse (the impulse response functions). This is not a practical analytical procedure for the complete system, even with the simplified equation (10.2,1). For obtaining exact solutions for the impulse response or step response, the preferred method is to solve the original differential equations on a digital or analog computer. For analytical work associated with control system design, approximate forms of the transfer functions may be quite useful (refs. 9.4 and 9.5).

We can find approximate transfer functions by using the short-period and phugoid approximations given in Sec. 9.2 as a guide. These would be expected to be useful for inputs whose spectral representations are limited to certain frequency bands appropriate to the mode in question.

SHORT-PERIOD APPROXIMATION

We found in Chapter 9 that a very good approximation to the short-period mode is given by (9.2,14). We therefore make the same additional assumptions here as led to that approximation—viz. $\Delta\hat{V} \equiv 0$, and the speed equation of motion is identically satisfied. The reduced system equation is then found from (10.2,1) to be

$$\begin{bmatrix} -(\hat{G}_{L\alpha} + C_{D_e} + 2\mu s) & 2\mu & 0 \\ -\hat{G}_{m\alpha} & (\hat{I}_y s - \hat{G}_{mq}) & 0 \\ 0 & 1 & -s \end{bmatrix} \begin{bmatrix} \Delta\bar{\alpha} \\ \bar{q} \\ \Delta\bar{\theta} \end{bmatrix} = \begin{bmatrix} \hat{G}_{L\delta} \\ \hat{G}_{m\delta} \\ 0 \end{bmatrix} \Delta\bar{\delta}_e \qquad (10.2,10)$$

The system transfer functions are now most simply found from (10.2,10) by solving for the ratios $\Delta\bar{\alpha}/\Delta\bar{\delta}_e$, etc., with the result

$$\hat{G}_{\alpha\delta} = \frac{\Delta\bar{\alpha}}{\Delta\bar{\delta}_e} = \frac{2\mu\hat{G}_{m\delta} - \hat{G}_{L\delta}(\hat{I}_y s - \hat{G}_{mq})}{(\hat{I}_y s - \hat{G}_{mq})(\hat{G}_{L\alpha} + C_{D_e} + 2\mu s) - 2\mu\hat{G}_{m\alpha}} \qquad (a)$$

$$\hat{G}_{\theta\delta} = \frac{\Delta\bar{\theta}}{\Delta\bar{\delta}_e} = \frac{\hat{G}_{m\delta}(2\mu s + \hat{G}_{L\alpha} + C_{D_e}) - \hat{G}_{L\delta}\hat{G}_{m\alpha}}{s\{(\hat{I}_y s - \hat{G}_{mq})(\hat{G}_{L\alpha} + C_{D_e} + 2\mu s) - 2\mu\hat{G}_{m\alpha}\}} \qquad (b) \quad (10.2,11)$$

$$\hat{G}_{q\delta} = s\hat{G}_{\theta\delta} \qquad (c)$$

When the aerodynamic control transfer functions are replaced by their stability derivative representations, i.e. by (10.2,2) and with

$$\hat{G}_{L\alpha} = C_{L_\alpha}; \qquad \hat{G}_{m\alpha} = C_{m_\alpha} + sC_{m_{\dot{\alpha}}}; \qquad \hat{G}_{mq} = C_{mq}$$

the denominators of the above transfer functions are all polynomials in s that have exactly the same roots as (9.2,14). The numerators become

$$\text{Of } \hat{G}_{a\delta}\colon (C_{L_\delta}C_{m_q} + 2\mu C_{m_\delta}) + s(2\mu C_{m_\delta} - \hat{I}_y C_{L_\delta}) \qquad (a)$$

$$\text{Of } \hat{G}_{\theta\delta}\colon [C_{m_\delta}(C_{L_\alpha} + C_{D_e}) - C_{m_\alpha}C_{L_\delta}] + s[(2\mu C_{m_\delta} + C_{m_{\dot\delta}}(C_{L_\alpha} + C_{D_e}) - C_{L_\delta}C_{m_{\dot\alpha}}] + s^2(2\mu C_{m_{\dot\delta}}) \qquad (b) \quad (10.2,12)$$

Both numerators are of degree one less than their respective denominators.

PHUGOID APPROXIMATION

The phugoid approximation in Sec. 9.2 was based on the assumption that $\Delta\alpha$ is negligibly small and the pitching moment equation is identically satisfied. When the elevator angle is varying however, $\Delta\alpha$ can no longer be assumed small. The equivalent assumption for this case is that pitch equilibrium is maintained, i.e. that

$$\hat{G}_{m\alpha}\,\Delta\alpha + \hat{G}_{mq}\hat{q} + \hat{G}_{m\delta}\,\Delta\delta_e = 0$$

Now we expect this approximation to be useful only at low elevator frequencies, when we can replace the above expression by

$$C_{m_\alpha}\,\Delta\alpha + C_{m_q}\hat{q} + C_{m_\delta}\,\Delta\delta_e = 0$$

We now further assume that $C_{m_q}\hat{q}$ is negligible, so that the angle of attack is given by the quasistatic value

$$\Delta\alpha = -\frac{C_{m_\delta}}{C_{m_\alpha}}\Delta\delta_e \qquad (10.2,13)$$

The usefulness of this assumption is checked a posteriori. With the pitch equation eliminated from (10.2,1) and $\Delta\alpha$ eliminated by (10.2,13), we get the reduced system equation

$$\left[\begin{array}{c|c|c} C_{T_V} - 2\mu s & 0 & -C_{W_e} \\ \hline -2C_{W_e} & 2\mu & 0 \\ \hline 0 & 1 & -s \end{array}\right]\left[\begin{array}{c} \Delta\hat{V} \\ \hline \bar{q} \\ \hline \Delta\bar{\theta} \end{array}\right] = \left[\begin{array}{c} \dfrac{C_{m_\delta}}{C_{m_\alpha}}(C_{L_e} - C_{D_\alpha}) \\ \hline C_{L_\delta} - \dfrac{C_{m_\delta}}{C_{m_\alpha}}(C_{L_\alpha} + C_{D_e} + 2\mu s) \\ \hline 0 \end{array}\right]\Delta\bar{\delta}_e \qquad (10.2,14)$$

The required basic transfer functions are obtained from (10.2,14) as

$$\hat{G}_{V\delta} = \frac{-C_{L_\delta}C_{W_e} + \dfrac{C_{m_\delta}}{C_{m_\alpha}}[C_{W_e}(C_{L_\alpha} + C_{D_e}) + 2\mu C_{D_\alpha}s]}{4\mu^2 s^2 - 2\mu C_{T_V}s + 2C_{W_e}^2} \qquad (a)$$

$$\hat{G}_{\theta\delta} = \frac{-C_{L_\delta}(C_{T_V} - 2\mu s) + \dfrac{C_{m_\delta}}{C_{m_\alpha}}[-2C_{W_e}(C_{W_e} - C_{D_\alpha}) + C_{T_V}(C_{L_\alpha} + C_{D_e}) + 2\mu s(C_{T_V} - C_{L_\alpha} - C_{D_e}) - 4\mu^2 s^2]}{4\mu^2 s^2 - 2\mu C_{T_V}s + 2C_{W_e}^2} \qquad (b) \quad (10.2,15)$$

$$\hat{G}_{q\delta} = s\hat{G}_{\theta\delta} \qquad (c)$$

From (10.2,13) we have in addition

$$\hat{G}_{\alpha\delta} = -\frac{C_{m_\delta}}{C_{m_\alpha}} \qquad (d)$$

and finally

$$\hat{G}_{\gamma\delta} = \hat{G}_{\theta\delta} - \hat{G}_{\alpha\delta} \qquad (e)$$

As expected, the denominators of (10.2,15*a* and *b*) give the same characteristic equation as was used for the phugoid previously, i.e. (9.2,9).

The assumptions on which (10.2,15) are based hold exactly in the limit of zero control frequency, and hence the static gains given by them are correct. Taking the limit $s \to 0$ (see (3.2,4)) we get the gains

$$K_{V\delta} = \frac{C_{m_\delta}(C_{L_\alpha} + C_{D_e}) - C_{m_\alpha}C_{L_\delta}}{2C_{W_e}C_{m_\alpha}} \doteq \frac{C_{m_\delta}C_{L_\alpha} - C_{m_\alpha}C_{L_\delta}}{2C_{W_e}C_{m_\alpha}} \qquad (a)$$

$$K_{\theta\delta} = \frac{C_{m_\delta}[C_{T_V}(C_{L_\alpha} + C_{D_e}) - 2C_{W_e}(C_{W_e} - C_{D_\alpha})] - C_{T_V}C_{m_\alpha}C_{L_\delta}}{2C_{W_e}^2 C_{m_\alpha}} \qquad (b) \quad (10.2,16)$$

$$K_{\alpha\delta} = -\frac{C_{m_\delta}}{C_{m_\alpha}} \qquad (c)$$

If we consider a typical jet transport in cruising flight, $C_{D_e} \ll C_{L_\alpha}$, and $C_{T_V} \doteq 2C_{D_e}$. For this case, the gain in flight-path angle becomes, after simplification,

$$K_{\gamma\delta} = K_{\theta\delta} - K_{\alpha\delta} = \frac{C_{L_\delta}C_{D_e}}{C_{W_e}^2} + \frac{C_{m_\delta}}{C_{m_\alpha}}\frac{C_{D_\alpha}}{C_{W_e}}\left(1 - \frac{C_{D_e}C_{L_\alpha}}{C_{L_e}C_{D_\alpha}}\right) \qquad (10.2,17)$$

The interesting thing about (10.2,17) is that it can change sign as C_{W_e} ($= C_{L_e}$)

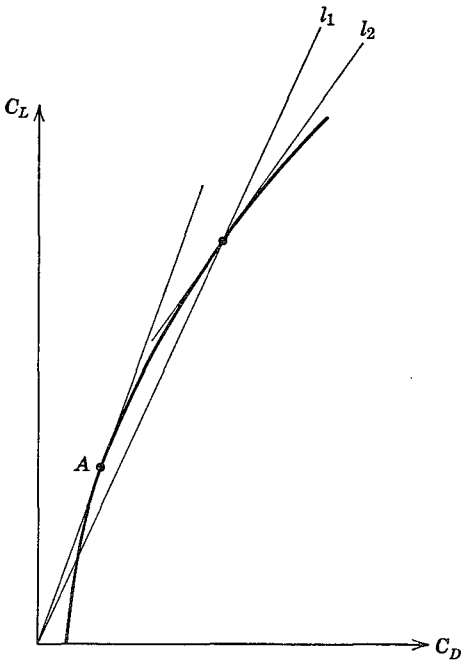

FIG. 10.2 Drag polar, M = const.

varies. With reference to Fig. 10.2 the quantity in parentheses on the r.h.s., for constant Mach number, can be written

$$1 - \frac{C_D}{C_L}\frac{dC_L}{dC_D}$$

where dC_L/dC_D is the slope of the tangent to the drag polar, l_2. Since C_L/C_D is the slope of l_1, it is evident that $(C_D/C_L)(dC_L/dC_D)$ is unity at point A, is <1 for $C_L > C_{L_A}$ and >1 for $C_L < C_{L_A}$. As a result the second term on the r.h.s. of (10.2,17) is negative for $C_L < C_{L_A}$ and positive for $C_L > C_{L_A}$. Because of the first term in (10.2,17) $K_{\gamma\delta}$ does not change sign exactly at A, but at a slightly lower value of C_L. With typical numerical values $K_{\gamma\delta} = 0$ when $(C_D/C_L)(dC_L/dC_D) \doteq 1.05$. The point of all this is that A represents flight at $(L/D)_{\max}$, or at minimum drag, and hence that the ultimate response of flight-path angle to elevator *reverses* when this speed is crossed. At high speed (low C_{L_e})$K_{\gamma\delta}$ is negative, so that up-elevator (stick back) produces a climb, but at low speed the opposite occurs. This result is seen to be entirely compatible with the conclusions reached from performance considerations, see Fig. 10.1. It is seen that the sign of $T - D$ for a speed reduction (associated with a negative $\Delta\delta_e$) is opposite for points P and Q on opposite sides of the minimum-drag speed.

NUMERICAL EXAMPLE—FREQUENCY RESPONSE

For this example we take the same hypothetical jet transport as was used in Sec. 9.1, flying at the same speed and height. For the aerodynamic transfer functions in **P** we use the stability derivative representation, i.e. all but $\hat{G}_{m_\alpha}$ are the same as the corresponding stability derivatives, and $\hat{G}_{m_\alpha} = C_{m_\alpha} + sC_{m_{\dot{\alpha}}}$. In addition, for the control aerodynamics we use

$$\hat{G}_{L_\delta} = C_{L_\delta} = .24/\text{radian}$$
$$\hat{G}_{m_\delta} = C_{m_\delta} = -.72/\text{radian}$$

The exact frequency response was calculated from (10.2,1) and the two approximations from (10.2,11) and (10.2,15) by substituting $s = i\hat{\omega}$ in them. The results are shown on Fig. 10.3 for speed, angle of attack, and flight-path angle.

The exact solutions show that the responses in the "trajectory" variables V and γ are dominated entirely by the large peak at the phugoid frequency. Because of the light damping in this mode, the dynamic gains at resonance are very large. The peak $|\hat{G}_{V_\delta}|$ of about 85 means that a speed amplitude of 10% of V_e would result from an elevator angle amplitude of only $.1 \times 57.3/85 = .068°$. Similarly at resonance an oscillation of 10° in γ would result from about 1/10° elevator amplitude. For both these variables, the response diminishes rapidly with increasing frequency, becoming negligibly small above the short-period frequency. The phase angle for V, Fig. 10.3*b*, is zero at low frequency, diminishes rapidly to −180° at the phugoid frequency (very much like the lightly damped, second-order systems of Fig. 3.17*b*) and subsequently at the short-period frequency undergoes a further drop characteristic of a heavily damped, second-order system. The "chain" concept of high-order systems (Sec. 3.4) is well exemplified by this graph.

By contrast, the attitude variables α and q show important effects at both the phugoid and short-period frequencies. The complicated behavior of α near the phugoid frequency indicates the sort of thing that can occur with high-order systems. It is associated with a pole and a zero of $G_{\alpha\delta}$ occurring close together in the exact transfer function. Again, above the short-period frequency, the amplitude of α and q both fall off rapidly.

As to the approximate solutions shown, one general statement can be made. The short-period approximation is exact as $\omega \to \infty$, and the phugoid approximation is exact as $\omega \to 0$. With a single exception, all the phenomena shown are represented reasonably well by one or other of the approximations. The exception is the α response at the phugoid frequency, which is revealed only by the exact solution. The principal error in the approximations is the displaced peak at the phugoid. This corresponds to the error in the phugoid

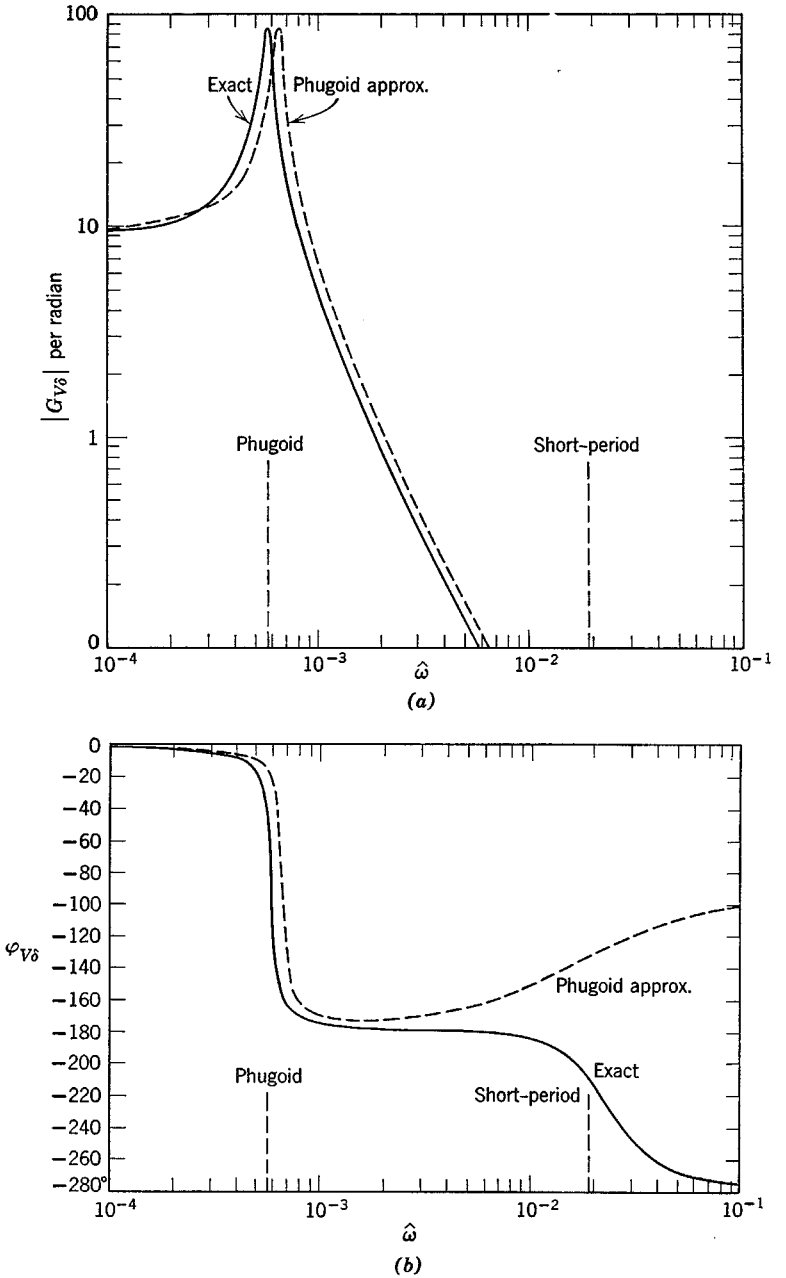

FIG. 10.3 Frequency-response functions, elevator angle input. Jet transport cruising at high altitude. (*a*) Speed amplitude. (*b*) Speed phase angle. (*c*) Angle of attack amplitude. (*d*) Angle of attack phase angle. (*e*) Pitch-rate amplitude. (*f*) Pitch-rate phase angle. (*g*) Flight-path angle amplitude. (*h*) Flight-path angle phase angle.

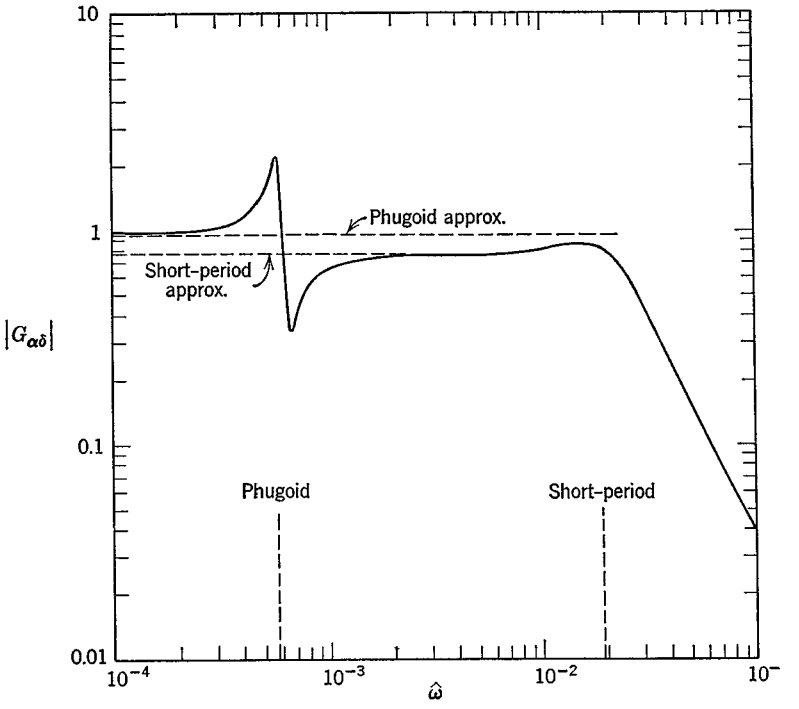

FIG. 10.3. (*Contd.*)

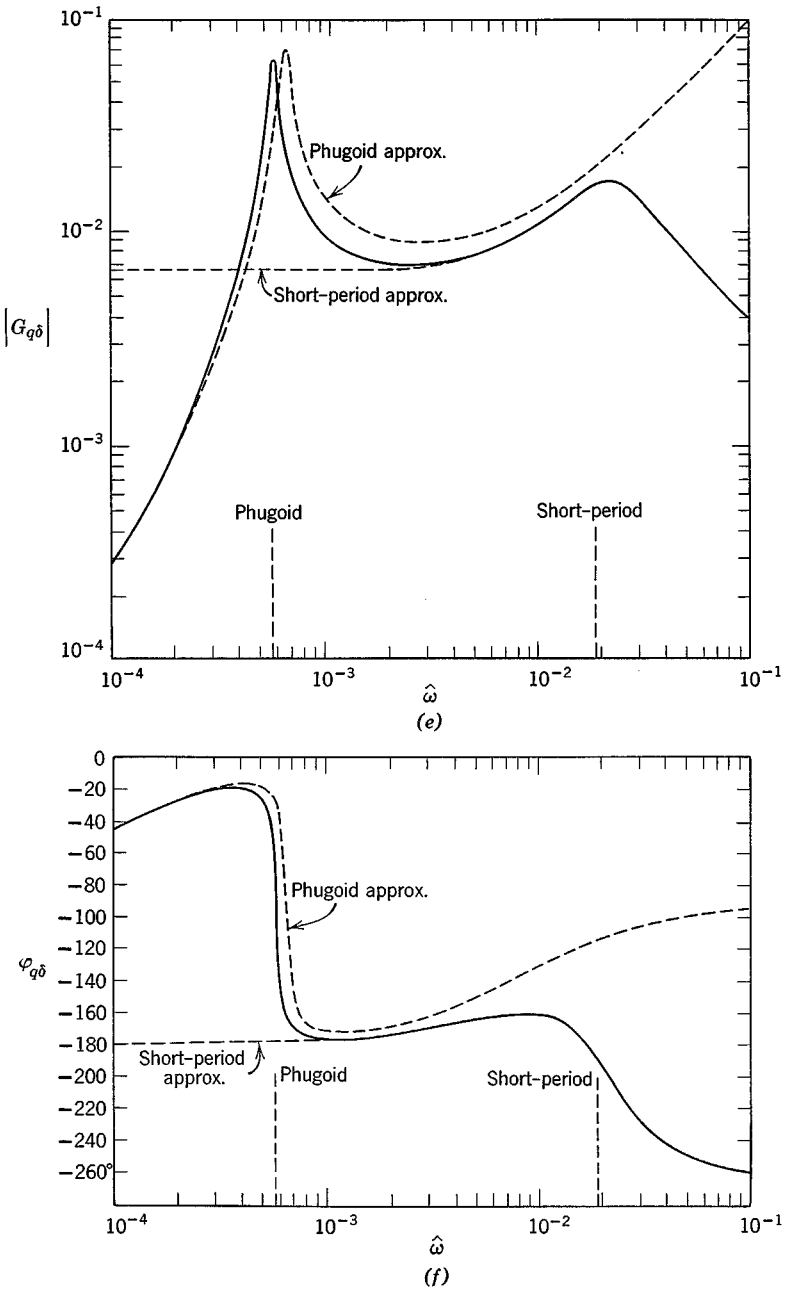

FIG. 10.3. (*Contd.*)

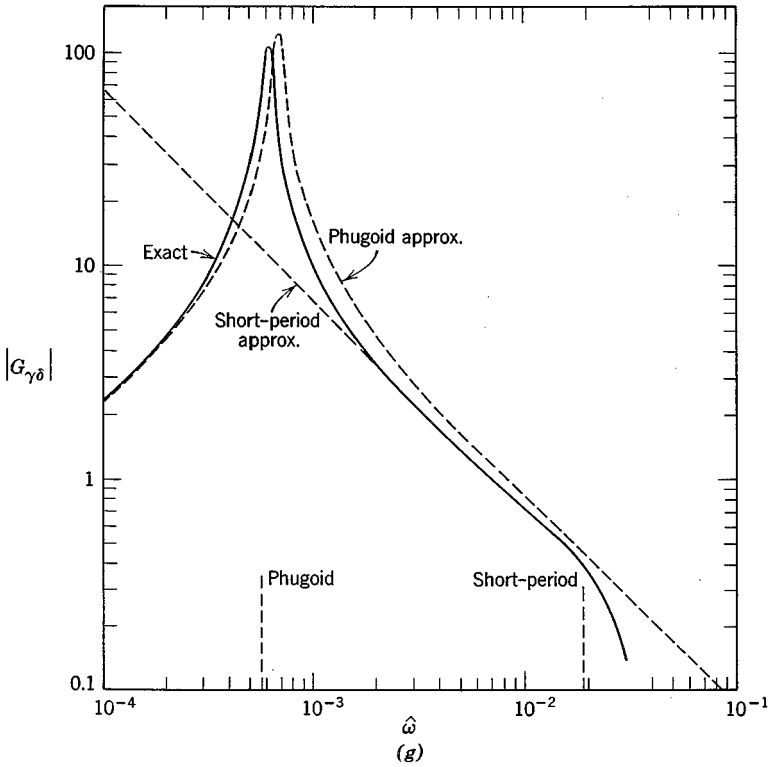

FIG. 10.3. *(Contd.)*

period shown for approximation (9.2,9) on Fig. 9.4*a*. Had the characteristic equation corresponding to (9.2,11) been used instead, the approximation would have been better.

NUMERICAL EXAMPLE—STEP RESPONSE

For the same airplane and flight conditions as in the previous example, the response to a step-function input in the elevator angle was computed, using (5.13,19) mechanized for a 10-volt analog computer. As an aid to readers unfamiliar with analog computation, the details of this one example are set out rather fully. The other examples that follow later were computed in essentially the same way, but the details of scaling and circuits are omitted. With the same assumptions as made previously the differential equations with numerical coefficients are:

$$
\begin{aligned}
D\hat{V} &= -6.92 \times 10^{-5}\,\Delta\hat{V} + 2.55 \times 10^{-4}\,\Delta\alpha - 4.60 \times 10^{-4}\,\Delta\theta \\
D\alpha &= -9.20 \times 10^{-4}\,\Delta\hat{V} - 9.00 \times 10^{-3}\,\Delta\alpha + \hat{q} - 4.42 \times 10^{-4}\,\Delta\delta_e \\
D\hat{q} &= 2.03 \times 10^{-6}\,\Delta\hat{V} - 3.62 \times 10^{-4}\,\Delta\alpha - 1.43 \times 10^{-2}\hat{q} - 3.77 \times 10^{-4}\,\Delta\delta_e \\
D\theta &= \hat{q}
\end{aligned}
\qquad (10.2,18)
$$

To mechanize them for analog computation we make the following transformation of variables:

$$
[V] = s_V\,\Delta\hat{V}; \qquad [\alpha] = s_\alpha\,\Delta\alpha; \qquad [q] = s_q\hat{q}; \qquad [\theta] = s_\theta\,\Delta\theta \qquad (10.2,19)
$$

where the quantities in square brackets, $[V]$ etc., denote machine voltages, and s_V etc. are scale factors. Time scaling is by the law

$$
\tau = s_t\hat{t}
$$

where τ is laboratory clock time, or *macsecs* (for computing machine seconds), and $\hat{t}$ is the nondimensional time variable of the differential equations. To relate the computer results to real flight time t we use

$$
\tau = s_t\frac{t}{t^*}, \qquad t^* = .0105 \text{ sec} \qquad (10.2,20)
$$

On recalling that D in (10.2,18) represents $d/d\hat{t}$, and defining $[\ ]' = (d/d\tau)[\ ]$, the transformation of the equations into differential equations for the

voltages yields

$$
\begin{aligned}
[V]' &= \frac{s_V}{s_t}\left\{-\frac{6.92\times10^{-5}}{s_V}[V]+\frac{2.55\times10^{-4}}{s_\alpha}[\alpha]-\frac{4.60\times10^{-4}}{s_\theta}[\theta]\right\}\\
[\alpha]' &= \frac{s_\alpha}{s_t}\left\{-\frac{9.20\times10^{-4}}{s_V}[V]-\frac{9.00\times10^{-3}}{s_\alpha}[\alpha]\right.\\
&\qquad\left.+\frac{1}{s_q}[q]-4.42\times10^{-4}\Delta\delta_e\right\}\\
[q]' &= \frac{s_q}{s_t}\left\{\frac{2.03\times10^{-6}}{s_V}[V]-\frac{3.62\times10^{-4}}{s_\alpha}[\alpha]\right.\\
&\qquad\left.-\frac{1.43\times10^{-2}}{s_q}[q]-3.77\times10^{-4}\Delta\delta_e\right\}\\
[\theta]' &= \frac{s_\theta}{s_t s_q}[q]
\end{aligned}
\tag{10.2,21}
$$

Note that we have chosen for convenience to give the control angles as $\Delta\delta_e$, rather than $[\delta]/s_\delta$, since $\Delta\delta_e$ not $[\delta]$ is to be specified. The scale factors used were as follows:

$$s_V = 10 \text{ v/unit}$$

$$s_\alpha = 10 \text{ v/radian}$$

$$s_q = 1000 \text{ v/unit}$$

$$s_\theta = 10 \text{ v/radian}$$

Since the response shortly after $t = 0$ is governed mainly by the short-period mode, and the long-term response by the phugoid mode, a single time scale is not appropriate for both. Hence two time scales were used:

To show long-term response: $s_t = 10^{-3}$

To show initial response: $s_t = 10^{-2}$

The analog circuit for $s_t = 10^{-3}$ and $\Delta\delta_e = -.03$ rad is shown in Fig. 10.4, using conventional symbols for integrators, summers, etc.

When $s_t = 10^{-3}$, the time relation, from (10.2,20) is

$$t = \frac{t^*}{s_t}\tau = 10.5\tau$$

and hence the process proceeds about 10 times faster on the computer than in flight. When $s_t = 10^{-2}$, the process proceeds at nearly real flight time.

The results for $\hat{V}$, α, and γ are shown for both time scales on Figs. 10.5 and

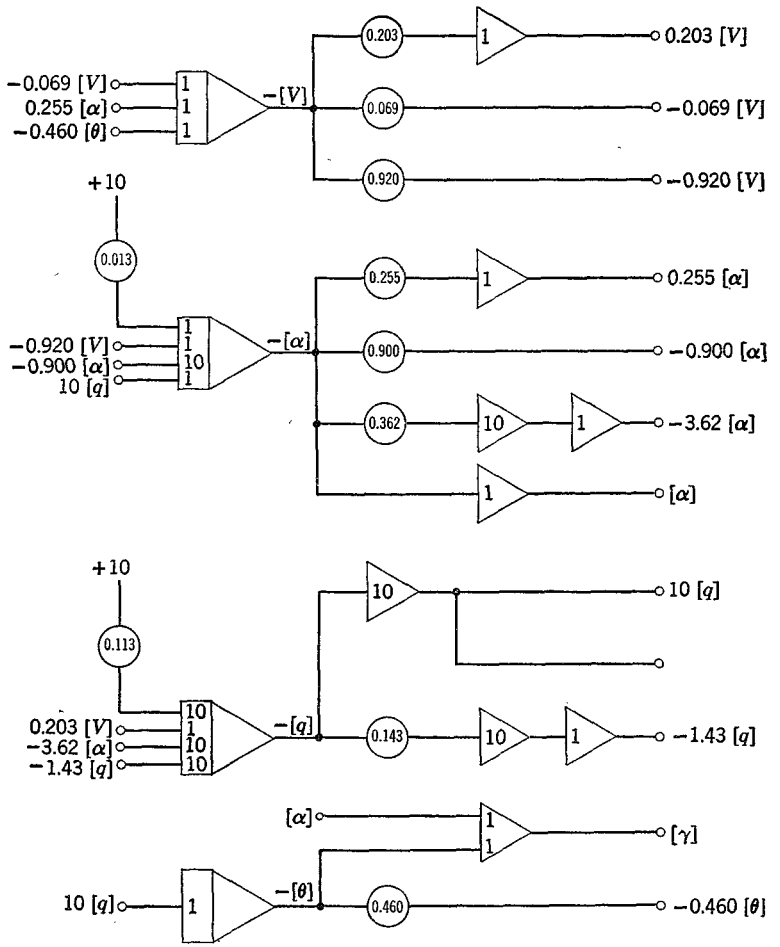

FIG. 10.4 Analog circuit diagram for response to elevator step. $\Delta\delta_e = -.03$ rad, $s_t = 10^{-3}$.

10.6. These curves were recorded by a conventional $x - y$ plotter; the time base was generated on the computer by integrating a constant.

Figure 10.5 shows that α increases rapidly and quickly damps out to its asymptotic value. V and γ, however, make a slow, weakly damped approach to their final values, the initial overshoot being very large for both. If the reason for moving the elevator were to change to a new steady state, the maneuver has not been a very effective one! After 500 sec the oscillations in V and γ have still not disappeared. The behavior near $t = 0$ is shown more clearly on Fig. 10.6; the rapid rise in α is dominated by the short-period mode. It is only after α has changed that the associated increase in lift can

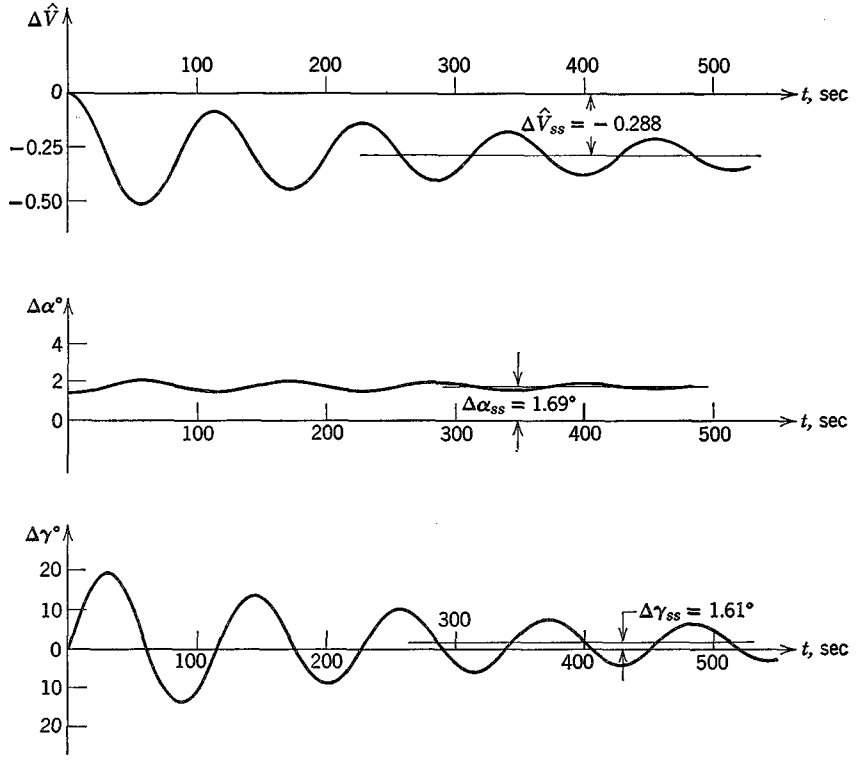

FIG. 10.5 Response to elevator ($\Delta\delta_e = -.03$ rad). Jet transport cruising at high altitude.

act to curve the flight path (via $\Delta L \doteq mV\dot{\gamma}$); thus the increase in γ lags that in α. At the same time the increased drag due to $\Delta\alpha$, and the "downhill" component of the weight combine to produce a reduction in speed, which lags still farther behind. The response in γ is not in fact very rapid. It takes about 10 sec to increase γ by about 10° with this elevator deflection. In this time the vehicle has traveled 7330 ft.

10.3 RESPONSE TO THE THROTTLE

The initial response of an airplane to movement of the throttle is actually quite dependent on the details of the engine control system and on the type of propulsion system. For jet engines it takes an appreciable time for the rpm and thrust to increase after opening the throttle, and this can be an

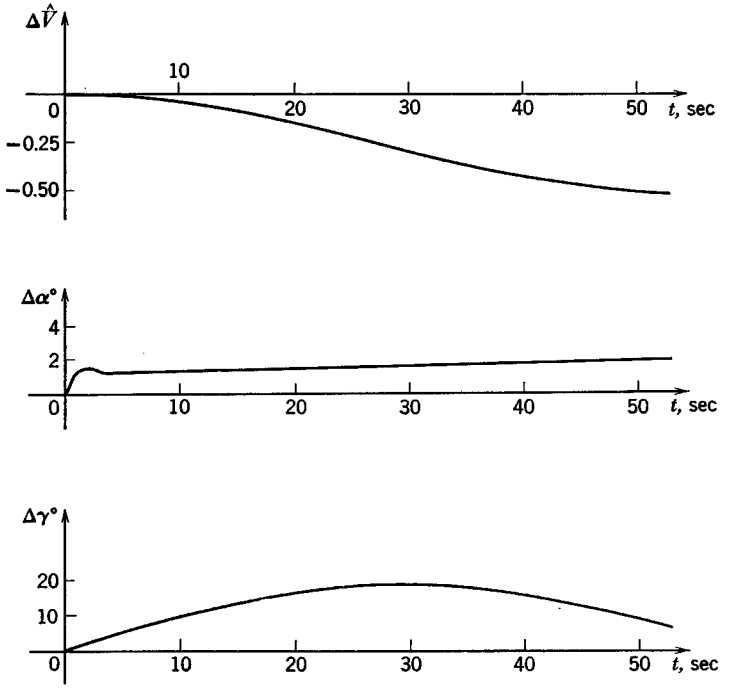

FIG. 10.6 Response to elevator ($\Delta\delta_e = -.03$ rad). Jet transport cruising at high altitude.

important factor in emergency conditions. The response of a propeller, which increases thrust by a change of blade angle, is more rapid. We make the simple assumption here that opening the throttle produces a step change in C_T of amount ΔC_{T_c}. If the thrust line does not pass through the C.G. there is an associated pitching moment (7.3,4) $\Delta C_{m_c} = \Delta C_{T_c} z/\bar{c}$. The l.h.s. of the system equation is then exactly the same as (10.2,1) and the r.h.s. is

$$\begin{bmatrix} -1 \\ 0 \\ z/\bar{c} \\ 0 \end{bmatrix} \Delta\bar{C}_T \qquad (10.3,1)$$

APPROXIMATE TRANSFER FUNCTIONS

Since the main effects of the throttle are the long-term changes in speed and flight-path angle, the phugoid approximation to the equations is an

appropriate one. The same procedure that led to (10.2,14) for this case gives the approximate equations

$$\hat{G}_{VT} = \frac{\Delta \bar{V}}{\Delta \bar{C}_{T_c}} = \frac{\frac{z}{\bar{c}}\frac{C_{W_e}}{C_{m_\alpha}}(C_{L_\alpha} + C_{D_e}) + 2\mu s\left(1 + \frac{z}{\bar{c}}\frac{C_{D_\alpha}}{C_{m_\alpha}}\right)}{f(s)} \qquad (a)$$

$$\hat{G}_{\theta T} = \frac{\Delta\bar{\theta}}{\Delta \bar{C}_{T_c}} = \frac{\begin{array}{l} 2C_{W_e} + \frac{z}{\bar{c}C_{m_\alpha}}[C_{T_V}(C_{L_\alpha} + C_{D_e}) - 2C_{W_e}(C_{L_e} - C_{D_\alpha})] \\ \qquad - 2\mu s\frac{z}{\bar{c}C_{m_\alpha}}(C_{L_\alpha} + C_{D_e}) - 4\mu^2 s^2 \frac{z}{\bar{c}C_{m_\alpha}} \end{array}}{f(s)} \qquad (b)$$

$$\hat{G}_{qT} = \frac{\bar{q}}{\Delta \bar{C}_{T_c}} = s\hat{G}_{\theta T} \qquad (c) \quad (10.3,2)$$

$$\hat{G}_{\alpha T} = \frac{\Delta\bar{\alpha}}{\Delta \bar{C}_{T_c}} = -\frac{z}{\bar{c}C_{m_\alpha}} \qquad (d)$$

$$\hat{G}_{\gamma T} = \frac{\Delta\bar{\gamma}}{\Delta \bar{C}_{T_c}} = \hat{G}_{\theta T} - \hat{G}_{\alpha T} \qquad (e)$$

where $f(s)$ is the denominator of (10 2,15a).

Just as in the case of the elevator response the static gains obtained from (10.3,2) are exact, since the assumptions leading to them are valid in the steady state They are

$$\begin{aligned} K_{VT} &= \frac{\frac{z}{\bar{c}}(C_{L_\alpha} + C_{D_e})}{2C_{m_\alpha}C_{W_e}} \\ K_{\theta T} &= \frac{2C_{W_e}C_{m_\alpha} + \frac{z}{\bar{c}}[C_{T_V}(C_{L_\alpha} + C_{D_e}) - 2C_{W_e}(C_{L_e} - C_{D_\alpha})]}{2C_{m_\alpha}C_{W_e}^2} \\ K_{\alpha T} &= -\frac{z}{\bar{c}C_{m_\alpha}} \end{aligned} \qquad (10.3,3)$$

When $z = 0$, the simplest result is obtained, i.e.

$$\begin{aligned} K_{VT} &= 0 \\ K_{\theta T} &= K_{\gamma T} = \frac{1}{C_{W_e}} \\ K_{\alpha T} &= 0 \end{aligned} \qquad (10.3,4)$$

These show that increasing the thrust (without change of pitching moment)

simply leads to a new steady-state flight condition at increased climb angle and no change of speed. By contrast the other principal longitudinal control, the elevator, ultimately influences both speed and flight-path angle [(10.2,16*a*) and (10.2,17)], albeit the change in the latter may be of either sign depending on flight speed. The simple rule "throttle controls climb and elevator controls speed" is not what it seems. It is true that the throttle is an uncoupled climb control (when $z = 0$) but the elevator is not an uncoupled speed control (except at $\gamma_{\max}$) and the rule only applies to steady states, not to initial transients.

NUMERICAL EXAMPLE—STEP RESPONSE

Analog computations were made for the airplane and flight condition of the previous example, with $\Delta C_{T_c} = .0125$ and with $z/\bar{c} = 0$ and .3 The results for V, α, and γ are shown on Figs 10.7 and 10.8. The motion at this time scale is clearly dominated by the lightly damped phugoid. Consider Fig. 10.7

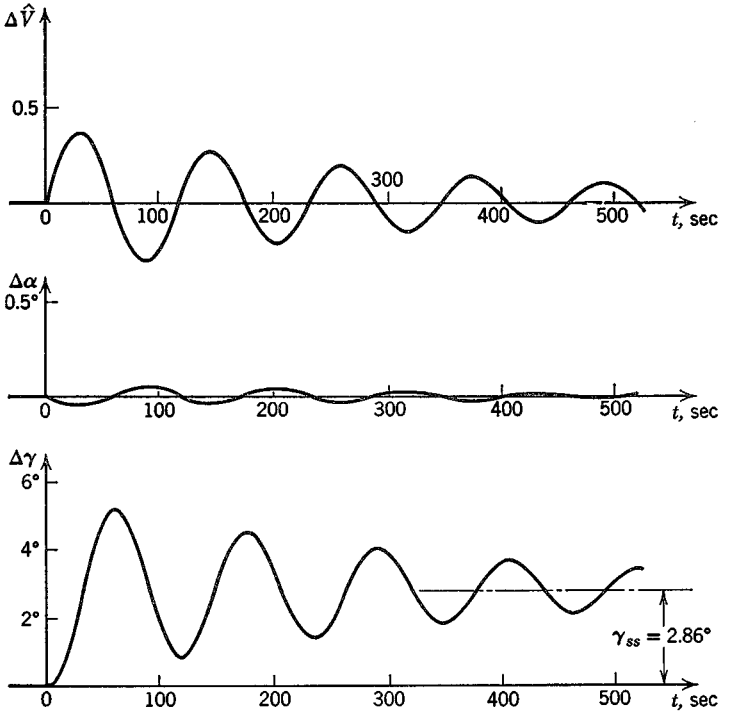

FIG. 10.7 Response to throttle ($\Delta C_T = .0125$). Jet transport crusing at high altitude. Thrust line passing through C.G.

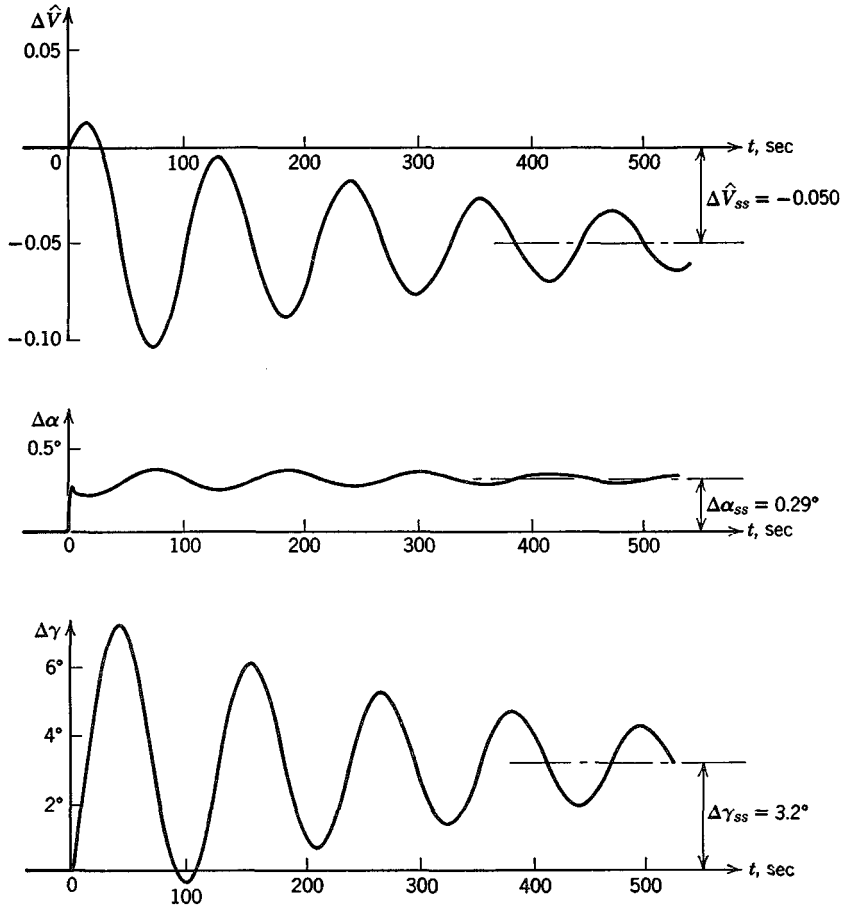

FIG. 10.8 Response to throttle ($\Delta C_T = .0125$). Jet transport cruising at high altitude. Thrust line below C.G., $z/\bar{c} = .30$.

($z/\bar{c} = 0$) first. We see that the speed begins to increase immediately, before the other variables have time to change. It then undergoes a damped oscillation, returning finally to its initial value. The angle of attack varies only slightly, and γ makes an oscillatory approach to its final positive value γ_{ss}. The ultimate steady state is a climb with $\Delta\hat{V} = \Delta\alpha = 0$, the numerical value of γ_{ss} being correctly given by (10.3,4). For the case $z/\bar{c} = .3$, Fig. 10.8, the results differ from the preceding in several significant ways. Although the speed does begin to increase at first, the increase is small and is quickly followed by a reduction of order 10% V_e. The final value is 5% less than V_e, a rather large change. The initial response in α is rapid, being dominated

by the short-period mode, and is not seen in detail at this time scale. Because of the rapid increase in α, and the excess lift that goes with it, there is a much more rapid response in γ than is the case in Fig. 10.7. The amplitude of the γ oscillation is also larger than on Fig. 10.7, and the final state is a climb of appreciably larger inclination. The steady states are again correctly predicted by (10.3,3).

10.4 LATERAL STEADY STATES

The basic flight condition is steady symmetric flight, in which all the lateral variables β, p, r, ϕ are identically zero. Unlike the elevator and the throttle, the lateral controls, the aileron and rudder are not used *individually* to produce changes in the steady state. This is because the steady-state values of β, p, r, ϕ that result from a constant δ_a or δ_r are not generally of interest as a useful flight condition. There are two lateral steady states that are of interest, however, each of which requires the joint application of aileron and rudder. These are the *steady sideslip*, in which the flight path is rectilinear, and the *steady turn*, in which the angular velocity vector is vertical. We look into these below before proceeding to the study of dynamic response to the lateral controls.

THE STEADY SIDESLIP

The steady sideslip is a condition of nonsymmetric rectilinear translation. It is sometimes used, particularly with light airplanes, to correct for cross-wind on landing approaches. Glider pilots also use this maneuver to steepen the glide path, since the L/D ratio decreases due to increased drag at large β. In this flight condition $D = d/d\tau \equiv 0$, and $p = r = y_E = 0$. Thus, with reference to (5.13,17), the only nonzero state variables are β, ϕ, and ψ. For the control terms we use the following, which is a good representation for conventional airplanes:

$$\begin{bmatrix} \Delta C_{y_c} \\ \Delta C_{l_c} \\ \Delta C_{n_c} \end{bmatrix} = \begin{bmatrix} C_{y_{\delta_r}} & 0 \\ C_{l_{\delta_r}} & C_{l_{\delta_a}} \\ C_{n_{\delta_r}} & C_{n_{\delta_a}} \end{bmatrix} \begin{bmatrix} \delta_r \\ \delta_a \end{bmatrix} \tag{10.4,1}$$

With (10.4,1), and the special conditions for steady sideslip, (5.13,17) reduces to

$$\begin{aligned} C_{y_\beta}\beta + C_{W_e}\cos\gamma_e\phi + C_{y_{\delta_r}}\delta_r &= 0 \\ C_{l_\beta}\beta + C_{l_{\delta_r}}\delta_r + C_{l_{\delta_a}}\delta_a &= 0 \\ C_{n_\beta}\beta + C_{n_{\delta_r}}\delta_r + C_{n_{\delta_a}}\delta_a &= 0 \\ \beta + \psi\cos\gamma_e &= 0 \end{aligned} \tag{10.4,2}$$

The fourth equation is the only one containing $\dot{\psi}$, and may be dropped from consideration. The three preceding ones contain the four variables β, ϕ, δ_r, δ_a. Hence an infinite set of solutions exists, in which any one of the four may be selected arbitrarily. If we choose ϕ to be arbitrary the equations can be solved for the corresponding β, δ_r, δ_a (provided of course that its matrix is not singular). Thus

$$\begin{bmatrix} \beta \\ \delta_r \\ \delta_a \end{bmatrix} = \mathbf{A}^{-1} \begin{bmatrix} -C_{W_e} \cos \gamma_e \phi \\ 0 \\ 0 \end{bmatrix}$$

where (10.4,3)

$$\mathbf{A} = \begin{bmatrix} C_{y_\beta} & C_{y_{\delta_r}} & 0 \\ C_{l_\beta} & C_{l_{\delta_r}} & C_{l_{\delta_a}} \\ C_{n_\beta} & C_{n_{\delta_r}} & C_{n_{\delta_a}} \end{bmatrix}$$

As an example, consider the jet transport used previously, at $C_{W_e} = 1.0$, $\gamma_e = 0$, with the β derivatives as in Sec. 9.6. In addition to these we need the control derivatives, for which we use

$$C_{y_{\delta_r}} = .067 \qquad C_{l_{\delta_r}} = .003 \qquad C_{n_{\delta_r}} = -.040$$
$$C_{l_{\delta_a}} = -.065 \qquad C_{n_{\delta_a}} = .005$$

It is evident from (10.4,3) that β, δ_r, and δ_a are all proportional to ϕ, hence the ratios of the angles are constant. The numerical result is:

$$\frac{\phi}{\beta} = .0558; \qquad \frac{\delta_r}{\beta} = 1.675; \qquad \frac{\delta_a}{\beta} = -1.800$$

so that for a sideslip of 10°, the other angles are $\phi = .56°$, $\delta_r = 16.75°$, $\delta_a = -18.00°$. As expected, a slip to the right requires left rudder and right aileron. The control angles are seen to be large; powerful controls are needed to sideslip at large angles. When the matrix **A** is singular, it only indicates that ϕ is zero in the sideslip. In that case the equations can be rearranged to put ϕ on the l.h.s. and β on the r.h.s., in which case the new matrix is very unlikely to be singular.

THE STEADY TURN

We define a "truly banked" turn to be one in which (i) the vehicle velocity vector $\boldsymbol{\omega}$ is constant and vertical (see Fig. 10.9) and (ii) the resultant of gravity and centrifugal force at the mass center lies in the plane of symmetry. This corresponds to flying the turn on the turn-and-bank indicator.† It is quite common for turns to be made at bank angles that are too large for

† Neglecting the fact that the pilot and indicator are not right at the C.G.

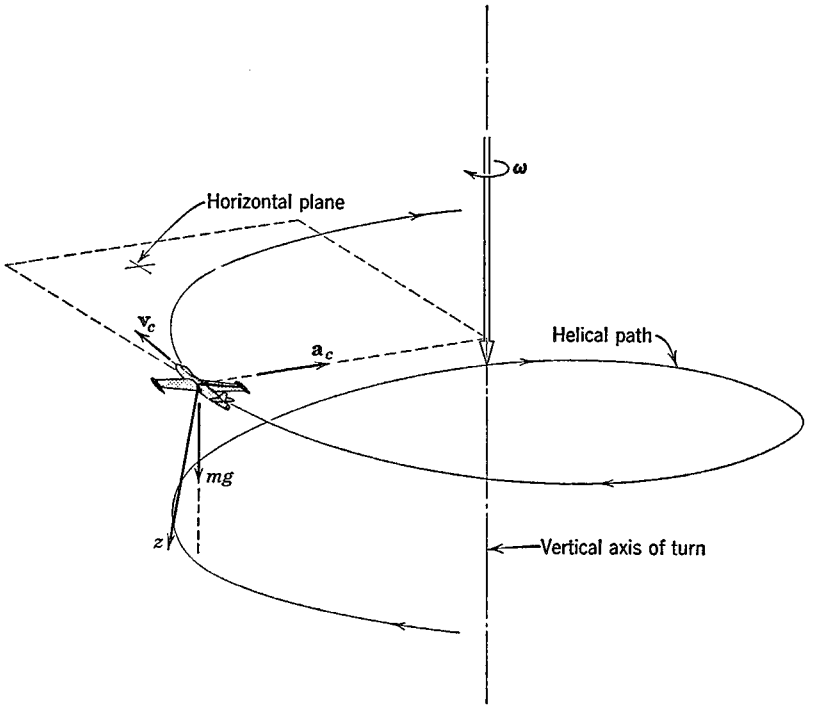

FIG. 10.9 Steady climbing turn.

linearization of $\sin\phi$ and $\cos\phi$ to be acceptable, although all the state variables other than ϕ and V are small. Thus we turn to the basic nonlinear equations in Sec. 5.8 for this analysis. The large bank angle has the consequence that coupling of the lateral and longitudinal equations occurs, since more lift is needed to balance gravity than in level flight. Thus not only the aileron and rudder but the elevator as well must be used for turning at large ϕ.

The body-axis angular rates are given by

$$\begin{bmatrix} p \\ q \\ r \end{bmatrix} = \mathbb{L}_{BV} \begin{bmatrix} 0 \\ 0 \\ \omega \end{bmatrix} \tag{10.4,4}$$

which for small elevation angle θ yields

$$\begin{bmatrix} p \\ q \\ r \end{bmatrix} = \begin{bmatrix} -\theta \\ \sin\phi \\ \cos\phi \end{bmatrix} \omega \tag{10.4,5}$$

We now apply the second condition for a truly banked turn—that the ball shall be centered in the turn-and-bank indicator. This means that the vector $m\mathbf{g} - m\mathbf{a}_c$ shall have no y component. But $m\mathbf{a}_c$ is the resultant external force $\mathbf{f}$, so that from (5.5,3)

$$m\mathbf{g} - m\mathbf{a}_c = m\mathbf{g} - \mathbf{f} = -\mathbf{A}$$

where $\mathbf{A}$ is the resultant aerodynamic force vector. Thus we conclude that the aerodynamic force must lie in the xz plane, and that $Y \equiv 0$. It follows from (5.8,2b), when only ϕ and u are not small, that

$$\begin{aligned} mg \sin \phi &= mru = mrV \\ &= mV\omega \cos \phi \end{aligned} \tag{10.4,6}$$

Hence the bank angle is given by

$$\tan \phi = \frac{\omega V}{g} \tag{10.4,7}$$

We choose the body axes so that $\alpha_x \equiv w \equiv 0$, whence it follows (see Fig. 4.4) that z and z_W coincide, and hence that $L = -Z$. Equation (5.8,2c) then permits the determination of L, i.e.

$$L = -Z = mg \cos \theta \cos \phi - m(pv - qu)$$

which, again to first order, after substituting q from (10.4,5) yields

$$L = mg \cos \phi + mV\omega \sin \phi \tag{10.4,8}$$

When $V\omega$ is eliminated by (10.4,7) we get

$$n = \frac{L}{mg} = \sec \phi \tag{10.4,9}$$

The incremental lift coefficient, as compared with straight flight at the same speed and height, is

$$\Delta C_L = \frac{L - mg}{\frac{1}{2}\rho V^2 S} = (n - 1)C_W \tag{10.4,10}$$

We can now write down the equations governing the control angles. From (5.8,3), to first order, $L = M = N = 0$, so we have the five aerodynamic conditions

$$C_l = C_m = C_n = C_y = 0$$

and

$$\Delta C_L = (n - 1)C_W$$

On expanding these with the usual aerodynamic derivatives, we get

$$\begin{aligned} C_{l_\beta}\beta + C_{l_p}\hat{p} + C_{l_r}\hat{r} + C_{l_{\delta_r}}\delta_r + C_{l_{\delta_a}}\delta_a &= 0 \\ C_{m_\alpha}\Delta\alpha + C_{m_q}\hat{q} + C_{m_{\delta_e}}\Delta\delta_e &= 0 \\ C_{n_\beta}\beta + C_{n_p}\hat{p} + C_{n_r}\hat{r} + C_{n_{\delta_r}}\delta_r + C_{n_{\delta_a}}\delta_a &= 0 \\ C_{y_\beta}\beta + C_{y_p}\hat{p} + C_{y_r}\hat{r} + C_{y_{\delta_r}}\delta_r &= 0 \\ C_{L_\alpha}\Delta\alpha + C_{L_q}\hat{q} + C_{L_{\delta_e}}\Delta\delta_e &= (n-1)C_W \end{aligned} \tag{10.4,11}$$

In these relations $\hat{p}$, $\hat{q}$, $\hat{r}$ are known from (10.4,5), i.e.

$$\begin{bmatrix} \hat{p} \\ \hat{q} \\ \hat{r} \end{bmatrix} = \begin{bmatrix} -\theta\dfrac{b}{2V} \\ \sin\phi\dfrac{\bar{c}}{2V} \\ \cos\phi\dfrac{b}{2V} \end{bmatrix} \omega \tag{10.4,12}$$

The five equations (10.4,11) for the five unknowns $[\beta, \delta_r, \delta_a]$ and $[\Delta\alpha, \Delta\delta_e]$ uncouple into two independent sets:

$$\begin{bmatrix} C_{y_\beta} & C_{y_{\delta_r}} & 0 \\ C_{l_\beta} & C_{l_{\delta_r}} & C_{l_{\delta_a}} \\ C_{n_\beta} & C_{n_{\delta_r}} & C_{n_{\delta_a}} \end{bmatrix} \begin{bmatrix} \beta \\ \delta_r \\ \delta_a \end{bmatrix} = \begin{bmatrix} C_{y_p} & C_{y_r} \\ C_{l_p} & C_{l_r} \\ C_{n_p} & C_{n_r} \end{bmatrix} \begin{bmatrix} \theta \\ -\cos\phi \end{bmatrix} \frac{\omega b}{2V} \tag{10.4,13}$$

and

$$\begin{bmatrix} C_{m_\alpha} & C_{m_{\delta_e}} \\ C_{L_\alpha} & C_{L_{\delta_e}} \end{bmatrix} \begin{bmatrix} \Delta\alpha \\ \Delta\delta_e \end{bmatrix} = -\begin{bmatrix} C_{m_q} \\ C_{L_q} \end{bmatrix} \frac{\omega\bar{c}}{2V}\sin\phi + \begin{bmatrix} 0 \\ (n-1)C_W \end{bmatrix} \tag{10.4,14}$$

Note that the matrix on the l.h.s. of (10.4,13) is the same as that of (10.4,3). When (10.4,9) is used to eliminate ϕ from (10.4,14), and after some routine algebra, the solution for $\Delta\delta_e$ is found to be

$$\Delta\delta_e = (n-1)C_W \frac{C_{m_\alpha} + \dfrac{n+1}{2\mu n}(C_{L_\alpha}C_{m_q} - C_{L_q}C_{m_\alpha})}{C_{L_{\delta_e}}C_{m_\alpha} - C_{L_\alpha}C_{m_{\delta_e}}} \tag{10.4,15}$$

Except for far forward C.G. positions and low speeds, the angles given by (10.4,15) are moderate. The similarity of this expression to that for elevator angle per g in a pull-up (6.10,6*a*) should be noted. They are in fact the same in the limit $n \to \infty$. The elevator angle per g in a turn is therefore not very different from that in a vertical pull-up.

Finally, the lateral control angles are obtained from the solution of (10.4,13)

NUMERICAL EXAMPLE

The values of $[\beta, \delta_r, \delta_a]$ corresponding to low-speed flight at sea level ($C_L = 1$, $\rho = \rho_0$) for the jet transport of the previous examples have been calculated from (10.4,13) and are shown in Fig. 10.10. The numerical data and the aerodynamic coefficients are the same as in Secs. 9.6 and in the steady sideslip above. Both the sideslip angle and the rudder angle are seen to be very much dependent on θ. This may be traced directly to the fact that the roll rate p is proportional to θ and changes sign with it.

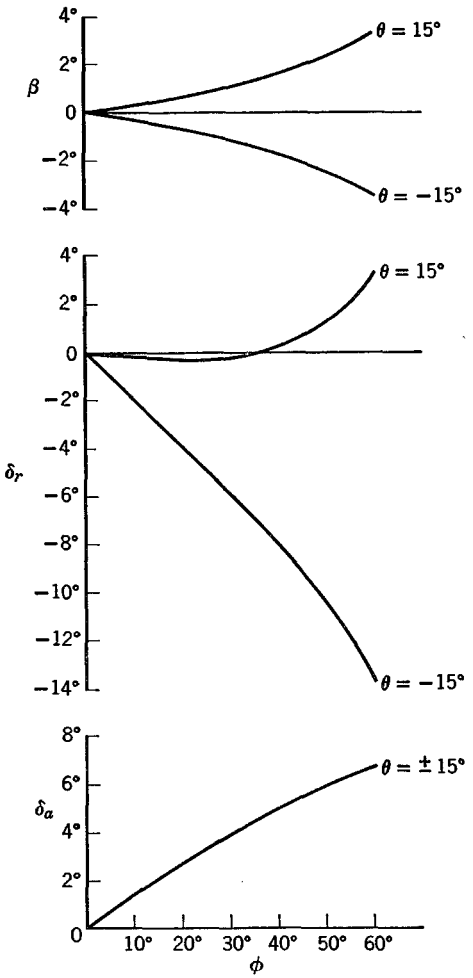

FIG. 10.10 Control angles in a truly banked turn.

Thus the term $C_{n_p}\hat{p}$ in the yawing moment equation is of opposite signs for climb and glide, and affects the rudder angle required to cancel the moment. Since C_y must also be zero, the value of β is in turn affected by that of δ_r. One would expect that the difference in $C_{l_p}\hat{p}$ between climbing and gliding would likewise cause a substantial difference between δ_a for the two cases, whereas no such difference exists. It is fortuitous that in this example the term $C_{l_\beta}\beta$ provides just the difference in the rolling moments needed.

Since $\phi > 0$ represents a right turn, we see that the ailerons are deflected in the "off-bank" sense (stick left), that considerable right rudder is used for gliding turns, but that for climbing turns it may be in either direction.

Finally, it may be remarked that the control angles obtained would have been substantially different had it been stipulated that β, not C_y, should be zero in the turn. It would not then be possible, however, to satisfy the requirement that the ball be centered in the turn-and-bank indicator.

10.5 LATERAL FREQUENCY RESPONSE

The computation of the lateral frequency response is carried out with (5.14,3). The column vector on the r.h.s. is conveniently expressed as

$$-\begin{bmatrix} \overline{\Delta C}_{y_c} \\ \overline{\Delta C}_{l_c} \\ \overline{\Delta C}_{n_c} \\ 0 \end{bmatrix} = \mathbf{Q}\begin{bmatrix} \bar{\delta}_r \\ \bar{\delta}_a \end{bmatrix} \tag{10.5,1}$$

where

$$\mathbf{Q} = \begin{bmatrix} -G_{y_{\delta_r}} & 0 \\ -G_{l_{\delta_r}} & -G_{l_{\delta_a}} \\ -G_{n_{\delta_r}} & -G_{n_{\delta_a}} \\ 0 & 0 \end{bmatrix}$$

Denoting the 4×4 matrix on the l.h.s. of (5.14,3) by $\mathbf{P}$, we get the 4×2 transfer-function matrix

$$\mathbf{G} = \mathbf{P}^{-1}\mathbf{Q} \tag{10.5,2}$$

The elements of $\mathbf{G}$ are specifically

$$\mathbf{G} = \begin{bmatrix} G_{\beta\delta_r} & G_{\beta\delta_a} \\ G_{p\delta_r} & G_{p\delta_a} \\ G_{r\delta_r} & G_{r\delta_a} \\ G_{\phi\delta_r} & G_{\phi\delta_a} \end{bmatrix} \tag{10.5,3}$$

In addition, from the supplementary relations given in (5.14,3) the transfer functions for ψ and y_E are

$$G_{\psi\delta} = \frac{\sec \gamma_e}{As} G_{r\delta}\,; \qquad G_{y\delta} = \frac{1}{s} G_{\beta\delta} + \frac{\cos \gamma_e}{s} G_{\psi\delta} \tag{10.5,4}$$

NUMERICAL EXAMPLE

The frequency-response functions for the jet transport in horizontal flight at 30,000 ft altitude and $C_{L_e} = .25$ were calculated from the above equations. All the aerodynamic transfer functions were replaced by the corresponding derivatives, i.e. $\hat{G}_{y\beta} = C_{y_\beta}$, $\hat{G}_{l\delta_a} = C_{l_{\delta_a}}$ etc. Thus we have neglected terms such as $sC_{l\dot{\delta}_a}$. The numerical values are the same ones used in the previous examples. The results for some of the state variables are shown in Figs. 10.11 and 10.12. Figure 10.11 shows the responses in β, ϕ, and r to rudder input. The principal feature is the peak at the frequency of the Dutch roll, which because of the relatively light damping of this mode, is substantial. For example, a 1° rudder amplitude produces about $4\frac{1}{2}°$ β amplitude and $6\frac{1}{2}°$ roll amplitude. At zero frequency β, p, and r are finite, but ϕ and ψ are infinite. That is, the computed steady state associated with rudder input is a constant rotational motion $\boldsymbol{\omega}_{ss} = \mathbf{i}p_{ss} + \mathbf{k}r_{ss}$. Since the equations were linearized with respect to ϕ and are therefore not valid for large ϕ, this steady state is spurious. The slopes of the high-frequency asymptotes can be predicted from the structure of the general transfer-function matrix. For the given rudder input it yields slopes of -1 for β, r, and -2 for ϕ. These slopes are reached approximately by $\hat{\omega} = .1$ for r and ϕ, but not for β. This is because the coefficient of the cubic term in the numerator of $G_{\beta\delta_r}$ contains the small aerodynamic derivative Cy_{δ_r}.

Figure 10.12 shows similar results for aileron angle input. The absence of the control term $C_{y_{\delta_a}}$ makes the high-frequency asymptote of $|G_{\beta\delta_a}|$ a line of slope -2 instead of -1.

All the amplitude curves on both figures show a rapid reduction of response once the frequency exceeds that of the lateral oscillation mode.

The sharp dip in $|G_{r\delta_r}|$ at $\hat{\omega} \doteq .0025$ is characteristic of a zero in the transfer function lying close to the imaginary axis at this frequency.

APPROXIMATE LATERAL TRANSFER FUNCTIONS

In Sec. 9.7 we presented two approximate second-order systems that simulate the complete fourth-order system insofar as the characteristic modes are concerned. These same approximations can be used to get approximate transfer functions for control response.

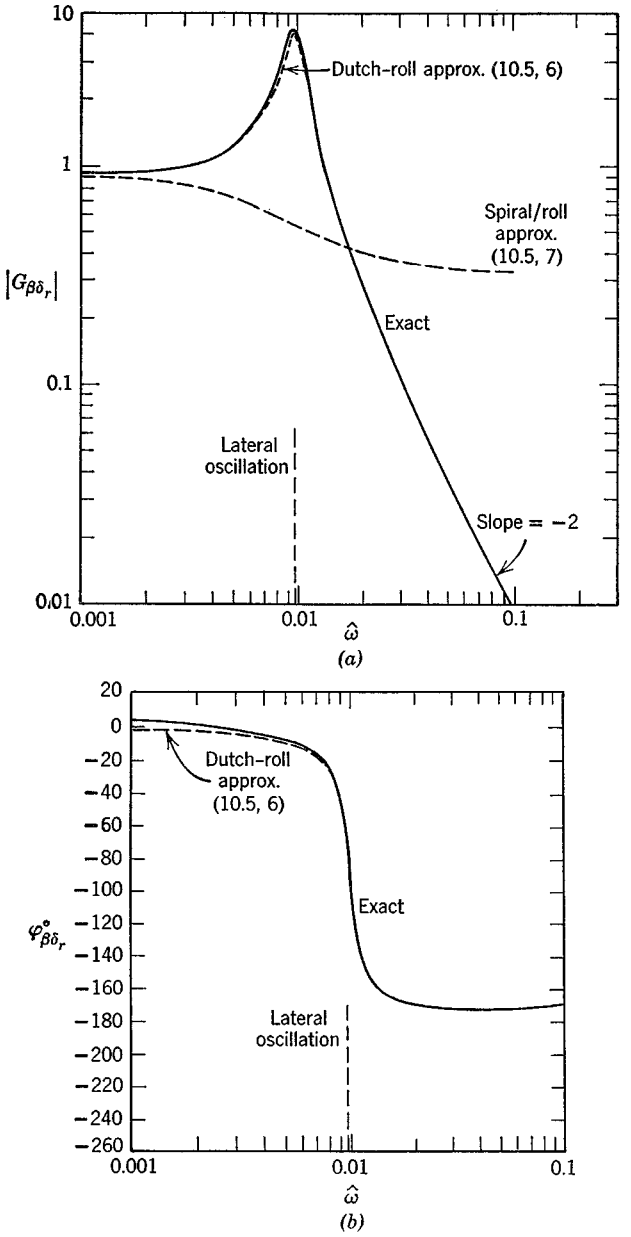

FIG. 10.11 Frequency-Response Functions, rudder angle input. Jet transport cruising at high altitude. (*a*) Sideslip amplitude. (*b*) Sideslip phase. (*c*) Roll amplitude. (*d*) Roll phase. (*e*) Yaw-rate amplitude. (*f*) Yaw-rate phase.

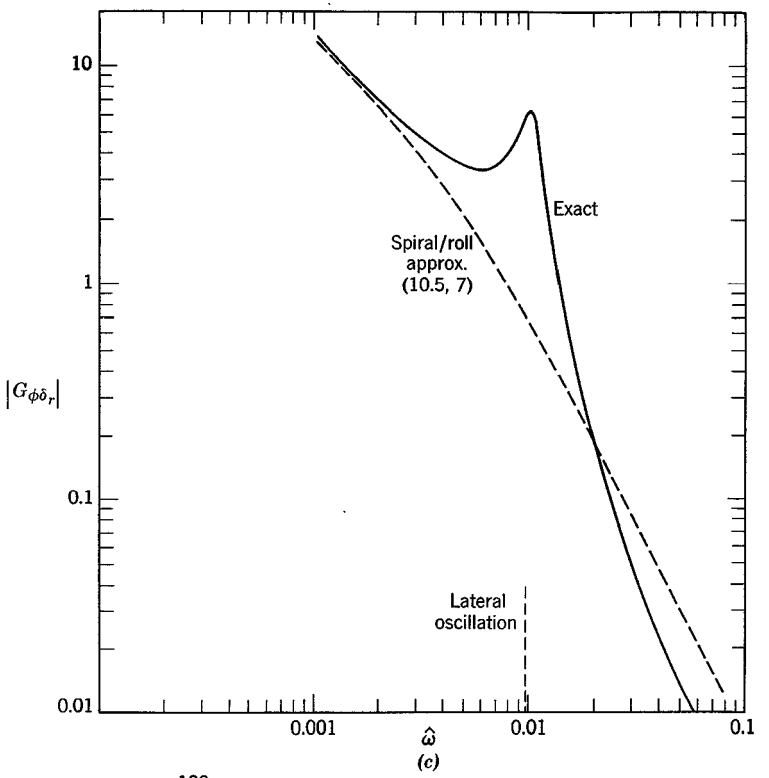

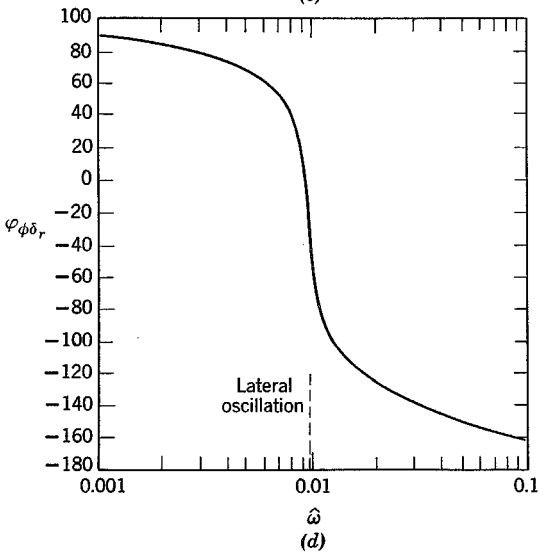

FIG. 10.11. (*Cont.*)

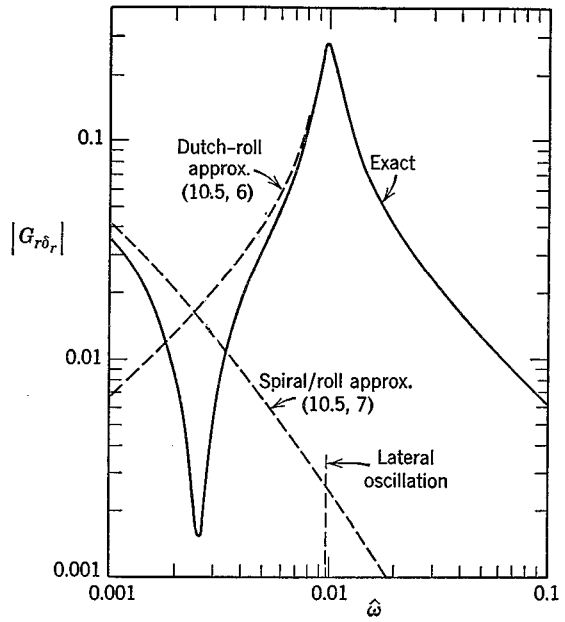

(e)

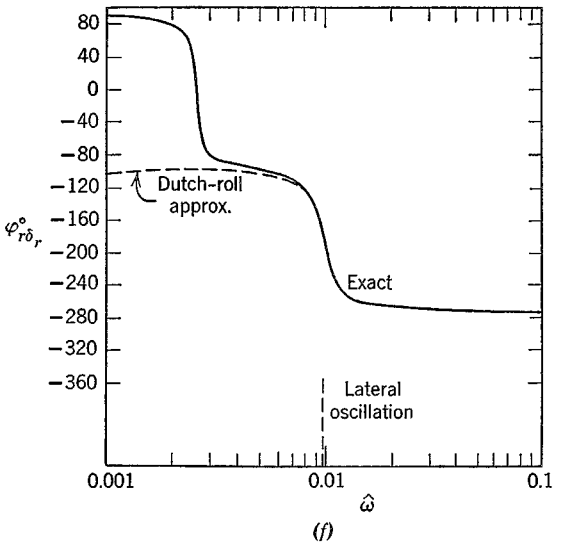

(f)

FIG. 10.11. *(Cont.)*

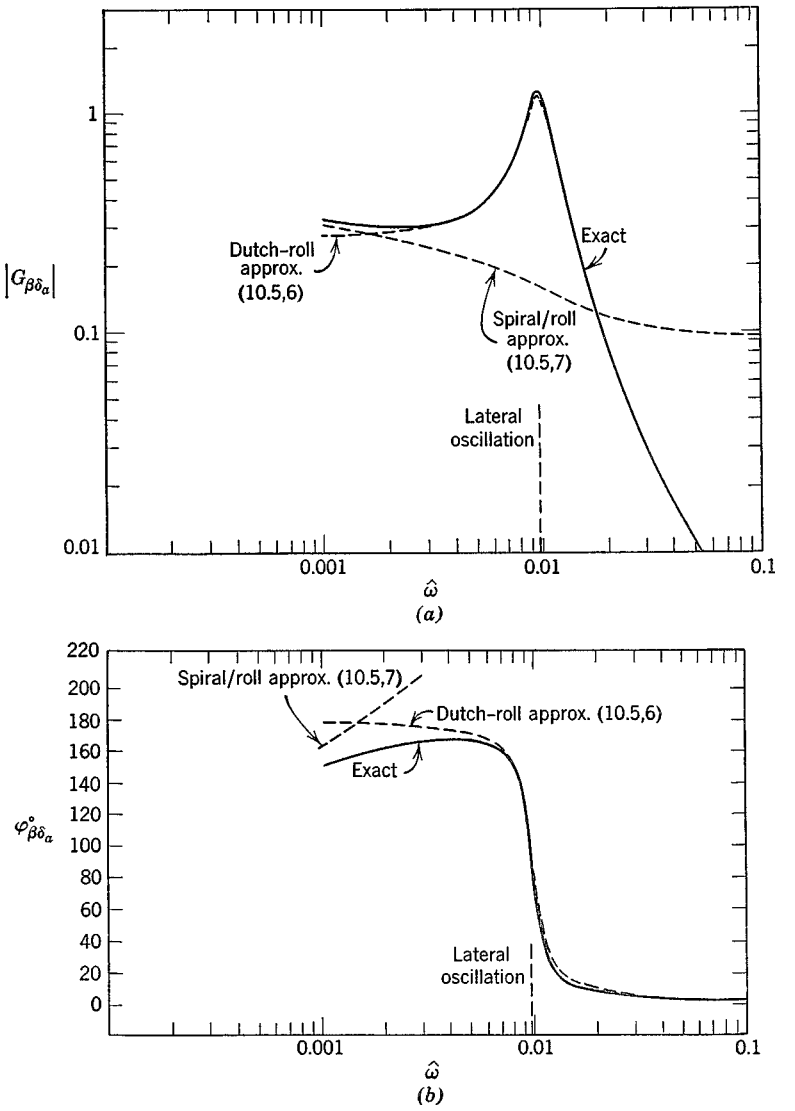

FIG. 10.12 Frequency-Response Functions, aileron angle input. Jet transport cruising at high altitude. (*a*) Sideslip amplitude. (*b*) Sideslip phase. (*c*) Roll amplitude. (*d*) Roll phase. (*e*) Yaw-rate amplitude. (*f*) Yaw-rate phase.

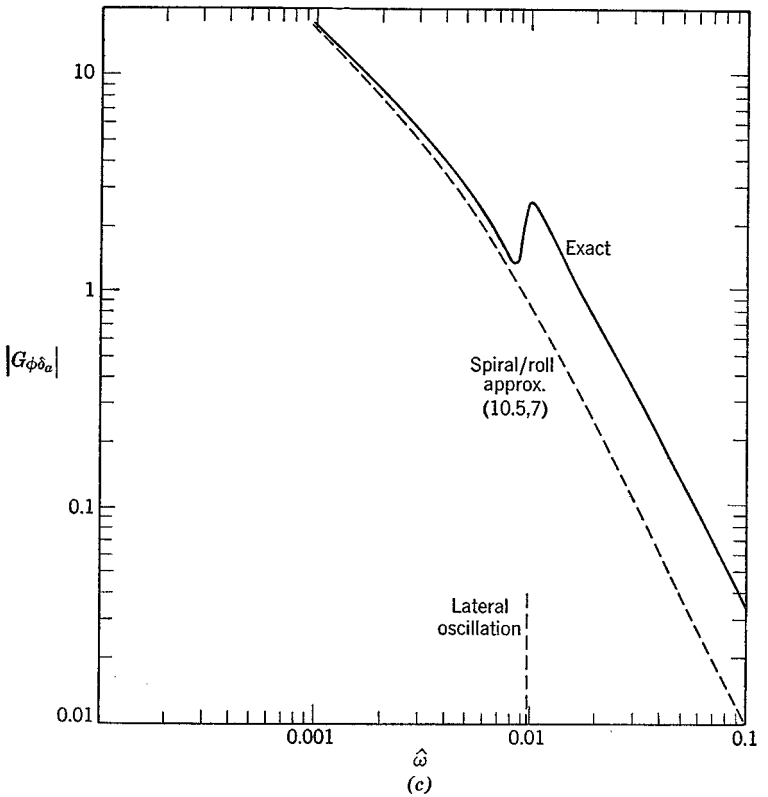

(c)

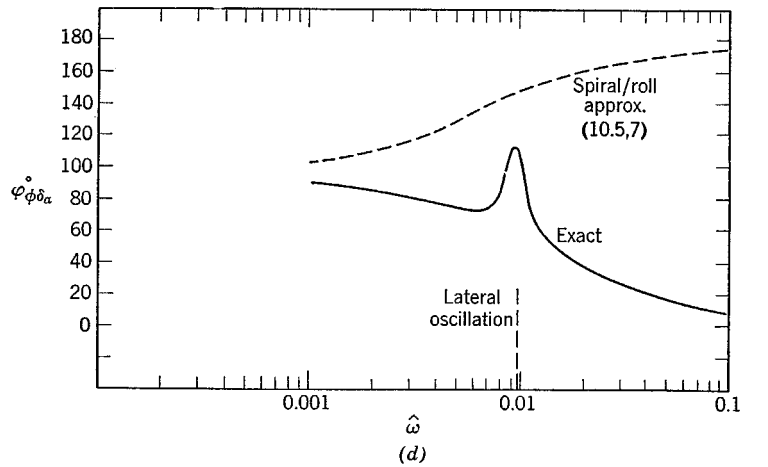

(d)

FIG. 10.12. *(Cont.)*

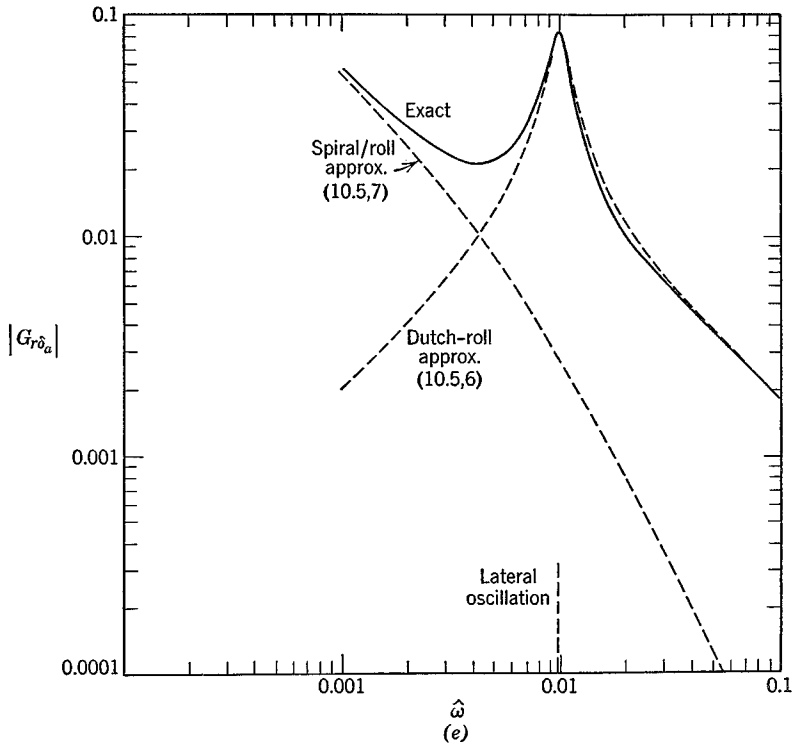

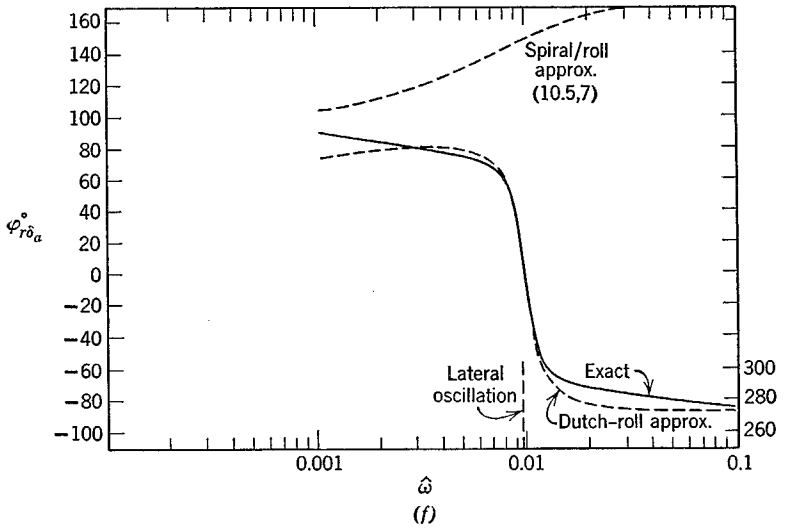

FIG. 10.12. (*Cont.*)

Consider first the Dutch-roll approximation (p.374). Taking the Laplace transform gives

$$\begin{bmatrix} (\mathscr{Y}_\beta - s) & -\dfrac{1}{A} \\ \mathscr{N}_\beta & (\mathscr{N}_r - s) \end{bmatrix} \begin{bmatrix} \bar{\beta} \\ \bar{r} \end{bmatrix} = - \begin{bmatrix} \mathscr{Y}_{\delta_r} & 0 \\ \mathscr{N}_{\delta_r} & \mathscr{N}_{\delta_a} \end{bmatrix} \begin{bmatrix} \bar{\delta}_r \\ \bar{\delta}_a \end{bmatrix} \tag{10.5,5}$$

where

$$\mathscr{Y}_{\delta_r} = \frac{C_{y_{\delta_r}}}{2\mu}$$

$$\mathscr{N}_{\delta_r} = \frac{C_{n_{\delta_r}}}{\hat{I}'_z} + \hat{I}'_{zx} C_{l_{\delta_r}}$$

$$\mathscr{N}_{\delta_a} = \frac{C_{n_{\delta_a}}}{\hat{I}'_z} + \hat{I}'_{zx} C_{l_{\delta_a}}$$

The four transfer functions for β and r responses are readily found from (10.5,5) to be

DUTCH-ROLL APPROXIMATION

$$\begin{aligned} \frac{\bar{\beta}}{\bar{\delta}_r} &= - \frac{(\mathscr{N}_r - s)\mathscr{Y}_{\delta_r} + \dfrac{1}{A}\mathscr{N}_{\delta_r}}{f(s)} \\ \frac{\bar{r}}{\bar{\delta}_r} &= - \frac{(\mathscr{Y}_\beta - s)\mathscr{N}_{\delta_r} - \mathscr{N}_\beta \mathscr{Y}_{\delta_r}}{f(s)} \\ \frac{\bar{\beta}}{\bar{\delta}_a} &= - \frac{\mathscr{N}_{\delta_a}}{A f(s)} \\ \frac{\bar{r}}{\bar{\delta}_a} &= - \frac{(\mathscr{Y}_\beta - s)\mathscr{N}_{\delta_a}}{f(s)} \end{aligned} \tag{10.5,6}$$

where $f(s)$ is the characteristic polynomial (9.7,13).

For the spiral/roll approximations, we proceed similarly with (9.7,10) to solve for the desired ratios. In the following results, the subscripts a and r are omitted from the control derivatives since the same formulas actually apply to both δ_a and δ_r. The only difference is that $\mathscr{Y}_{\delta_a}$ is usually zero [as in (10.5,6)] making the aileron transfer functions simpler than those for the rudder.

SPIRAL/ROLL APPROXIMATION

$$\begin{aligned}
\frac{\bar{\beta}}{\bar{\delta}} &= \frac{a_3 s^3 + a_2 s^2 + a_1 s + a_0}{f(s)} \\
\frac{\bar{\phi}}{\bar{\delta}} &= \frac{b_1 s + b_0}{f(s)} \\
\frac{\bar{r}}{\bar{\delta}} &= \frac{d_2 s^2 + d_1 s + d_0}{f(s)} \\
\frac{\bar{p}}{\bar{\delta}} &= As \frac{\bar{\phi}}{\bar{\delta}}
\end{aligned} \tag{10.5,7}$$

where $f(s)$ is the characteristic polynomial (9.7,11) and

$$a_3 = \mathscr{Y}_\delta; \qquad a_2 = -\mathscr{Y}_\delta(\mathscr{L}_p + \mathscr{N}_r) - \frac{\mathscr{N}_\delta}{A}$$

$$a_1 = \mathscr{Y}_\delta(\mathscr{L}_p\mathscr{N}_r - \mathscr{L}_r\mathscr{N}_p) - \frac{1}{A}(\mathscr{L}_\delta\mathscr{N}_p - \mathscr{L}_p\mathscr{N}_\delta) + \mathscr{L}_\delta\frac{C_{W_e}}{2A\mu}$$

$$a_0 = \frac{C_{W_e}}{2A\mu}(\mathscr{L}_r\mathscr{N}_\delta - \mathscr{L}_\delta\mathscr{N}_r)$$

$$b_1 = \frac{\mathscr{Y}_\delta\mathscr{L}_\beta}{A}; \qquad b_0 = \frac{1}{A^2}(\mathscr{L}_\delta\mathscr{N}_\beta - \mathscr{L}_\beta\mathscr{N}_\delta) + \frac{\mathscr{Y}_\delta}{A}(\mathscr{L}_\beta\mathscr{N}_r - \mathscr{L}_r\mathscr{N}_\beta)$$

$$d_2 = \mathscr{Y}_\delta\mathscr{N}_\beta; \qquad d_1 = \mathscr{Y}_\delta(\mathscr{L}_\beta\mathscr{N}_p - \mathscr{L}_p\mathscr{N}_\beta); \qquad d_0 = \frac{C_{W_e}}{2A\mu}(\mathscr{L}_\delta\mathscr{N}_\beta - \mathscr{L}_\beta\mathscr{N}_\delta)$$

The accuracy of the above approximations is illustrated for the example jet transport on Figs. 10.11 and 10.12. Two general observations can be made: (1) the Dutch-roll approximation gives good results for the higher frequencies, down to a little less than that of this mode, and (2) the spiral/roll approximation is correct in the low frequency limit. In this respect the situation is entirely analogous to the longitudinal case, with the spiral/roll corresponding to the phugoid and the Dutch-roll to the short-period approximation. There are ranges of frequency where neither approximation is satisfactory, as on Figs. 10.11*e* and 10.12*e*. The spiral/roll approximations for the phase angles are not shown on Fig. 10.11, since they are reasonable only at the lowest frequency. For all three variables, β, ϕ, and $\hat{r}$, they increase monotonically to about 180° at the highest frequency, whereas the exact phase angles all decrease in this range.

The reader should note that the agreement shown for the Dutch-roll approximation is not to be expected generally. We saw in Fig. 9.28 that the

damping is not given at all well by this approximation at low speed (high C_{L_e}). Thus the approximate solution at low speed would substantially underestimate the amplitude peaks at the frequency of the lateral oscillation. We repeat that the lateral approximations must be used with caution, and that only the use of the exact equations can guarantee accurate results.

10.6 TRANSIENT RESPONSE TO AILERON AND RUDDER

We have seen previously that useful lateral steady states are produced only by certain definite combinations of the control deflections. It is evident then that our interest in the response to a single lateral control should be focussed primarily on the initial behavior. The equations of motion provide some insight on this question directly. Following a step input of one of the two controls the state variables at $t = 0^+$ are all still zero, and from (5.13,20) we can deduce that their initial rates of change are (using the compact notation)

$$\begin{aligned} D\beta &= \mathscr{Y}_\delta \delta \\ D\hat{p} &= \mathscr{L}_\delta \delta \\ D\hat{r} &= \mathscr{N}_\delta \delta \end{aligned} \tag{10.6,1}$$

The initial sideslip rate $D\beta$ is not of much interest, but the rotational accelerations are. From the last two equations

$$D\hat{\boldsymbol{\omega}} = (\mathbf{i}\mathscr{L}_\delta + \mathbf{k}\mathscr{N}_\delta)\delta$$

and for $t \to 0$, $\hat{\boldsymbol{\omega}} = (\mathbf{i}\mathscr{L}_\delta + \mathbf{k}\mathscr{N}_\delta)\hat{t}\delta$ (10.6,2)

Thus the resultant angular velocity vector, and hence the initial instantaneous axis of rotation, lie in the plane of symmetry as illustrated in Fig. 10.13. Let us investigate the angle ξ that $\boldsymbol{\omega}$ makes with the x axis for the two cases of "pure" controls, i.e. when only one of C_{l_δ} or C_{n_δ} is not zero. For the roll-control case, $C_{n_\delta} = 0$ and

$$\tan \xi_R = \frac{\hat{r}}{\hat{p}} = \frac{\mathscr{N}_\delta}{\mathscr{L}_\delta} = \frac{\hat{I}'_{zx} C_{l_\delta}}{C_{l_\delta} \hat{I}'_x} = \hat{I}'_x \hat{I}'_{zx} \tag{10.6,3}$$

From the definitions given in (5.13,20), (10.6,3) becomes

$$\tan \xi_R = \frac{I_{zx}}{I_z}$$

and is zero if $I_{zx} = 0$, i.e. if Cx is a principal axis. This is just as expected,

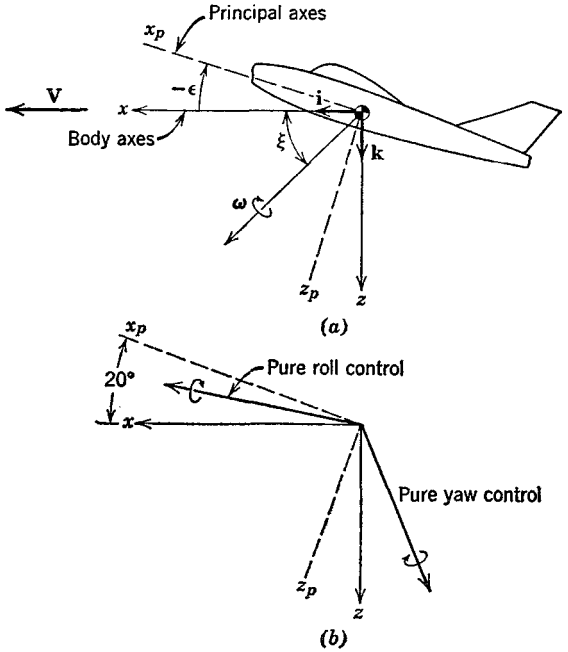

FIG. 10.13 Initial response to lateral control. (*a*) General. (*b*) Example jet transport.

of course, that a moment applied about a principal axis produces rotation about that axis. When I_{zx} is not zero, we get from (5.4,20*b*)

$$\tan \xi_R = \frac{(I_{z_p} - I_{x_p}) \sin \epsilon \cos \epsilon}{I_{z_p} \cos^2 \epsilon + I_{x_p} \sin^2 \epsilon} \tag{10.6,4}$$

Similarly for the pure yaw control, $C_{l_\delta} = 0$ and

$$\tan \xi_Y = \frac{I_{x_p} \cos^2 \epsilon + I_{z_p} \sin^2 \epsilon}{(I_{z_p} - I_{x_p}) \sin \epsilon \cos \epsilon} \tag{10.6,5}$$

These angles are seen to depend on the relative inertias about the principal axes, as well as on ϵ. For example, if $I_{x_p} = .4I_{z_p}$, as is roughly the case for the jet transport we have been considering, then ξ_R and ξ_Y are as on Fig. 10.14. The relations are shown to scale on Fig. 10.13*b* for $\epsilon = -20°$ (high angle-of-attack case). It is observed that there is a tendency for the vehicle to rotate about the principal x axis, rather than about the axis of the aerodynamic moment applied. This comes about because I_{x_p}/I_{z_p} is appreciably less than unity. The jet transport is a relatively high-aspect-ratio machine with wing-mounted engines, and would by no means be considered a "slender"

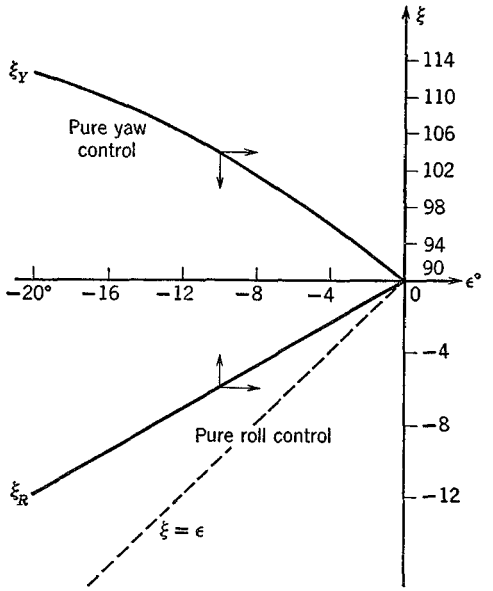

FIG. 10.14 Angle of axis of rotation.

vehicle. For vehicles that are slender, such as the SST or a slender missile, the trend indicated above is very much accentuated. In the limit $I_{x_p} \to 0$, both (10.6,4) and (10.6,5) give the limit

$$\tan \xi = \tan \epsilon$$

which indicates that the vehicle will initially rotate about its principal x axis no matter what the direction of the applied-moment vector. If this rotation were to persist through 90°, then β would be equal to $|\epsilon|$ and α would be reduced to zero. The above analysis tells us how the motion starts, but not how it continues. For that we need solutions of the complete system equations (5.13,20). Solutions for the example jet transport at $C_{L_e} = .25$ at 30,000 ft altitude were obtained by analog simulation of these equations, and the results for β, $\hat{p}$, ϕ, and ψ are shown on Figs. 10.15 and 10.16. Figure 10.15 shows the response to negative aileron angle (corresponding to entry into a right turn). The main feature is the rapid acquisition of roll rate, and its integration to produce bank angle ϕ. The maximum roll rate is achieved in about $1\frac{1}{2}$ sec, and a bank angle of about 25° at the end of 6 sec. Because of the aileron adverse yaw derivative, $C_{n_{\delta_a}} > 0$, the initial yawing moment is negative, causing the nose to swing to the left, with consequent negative ψ and positive β. The positive β, via the dihedral effect $C_{l_\beta} < 0$ produces a

negative increment in C_l, opposing the rolling motion. More than 4 sec elapse before the nose swings into the desired right turn.

Figure 10.16 shows the response to a negative (right) rudder angle of the same magnitude as the aileron angle on Fig. 10.15. This causes the nose to swing rapidly to the right, β being initially roughly equal and opposite to ψ indicating virtually no change in the direction of the velocity vector. The result of $\beta < 0$ (because of $C_{l_\beta}\beta$) is a positive rolling moment and positive ϕ.

Right rudder, like right aileron, is seen to produce a transition into a turn to the right, but neither does so optimally. A correct transition into a truly banked turn requires the coordinated use of both controls, and if there is to be no loss of altitude (see Sec. 10.4) of the elevator as well.

An approximation to the ϕ response to δ_a can be obtained from the single-degree-of-freedom roll analysis corresponding to (9.7,7). With the aileron

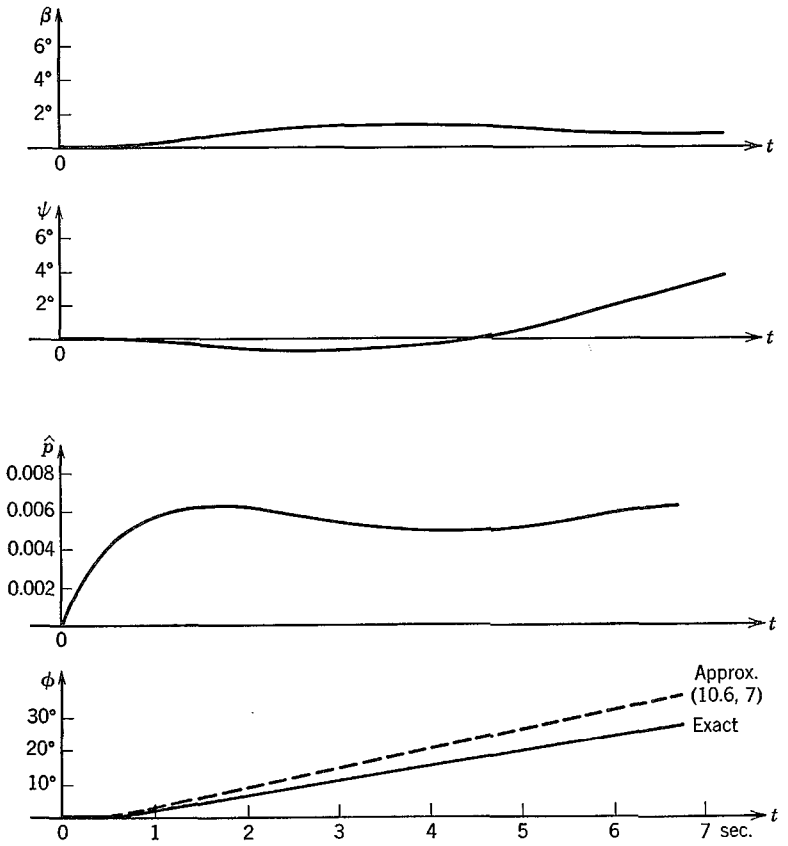

FIG. 10.15 Step response to aileron input. $\delta_a = -2.87°$.

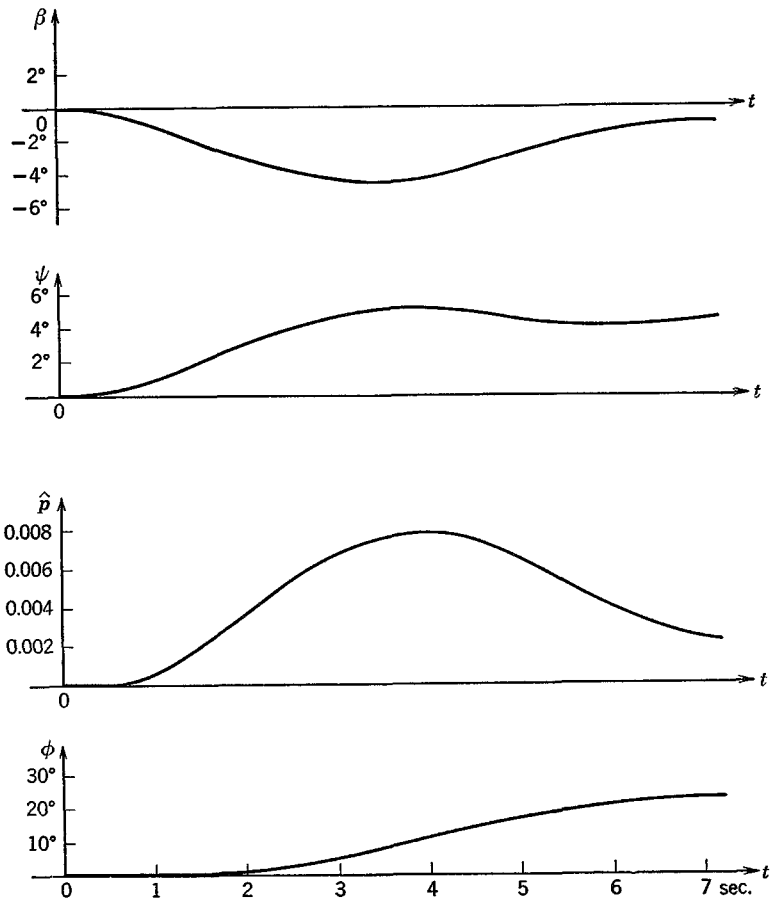

FIG. 10.16 Step response to rudder input. $\delta_r = -2.87°$.

term included this becomes

$$D\hat{p} = \mathscr{L}_p\hat{p} + \mathscr{L}_{\delta_a}\delta_a$$

or

$$AD^2\phi - A\mathscr{L}_p D\phi = \mathscr{L}_{\delta_a}\delta_a \tag{10.6,6}$$

The solution of (10.6,6) for zero initial conditions is

$$\frac{\phi}{\delta_a} = -\frac{\mathscr{L}_{\delta_a}}{A\mathscr{L}_p}\left\{\hat{t} + \frac{1}{\mathscr{L}_p}[1 - \exp(\mathscr{L}_p\hat{t})]\right\} \tag{10.6,7}$$

This result is compared with the exact solution on Fig. 10.15 and is seen to give a good approximation to ϕ over the most important first few seconds. This simple analysis supplies a useful criterion for roll control. It yields as

the steady-state roll rate,

$$\hat{p}_{ss} = -\frac{\mathscr{L}_{\delta_a}}{\mathscr{L}_p}\delta_a$$

or for principal axes,

$$\hat{p}_{ss} = -\frac{C_{l_{\delta_a}}}{C_{l_p}}\delta_a \tag{10.6,8}$$

A requirement on $\hat{p}_{ss}$ for a given vehicle then leads to an aileron design to provide the necessary $C_{l_{\delta_a}}\delta_a$.

10.7 INERTIAL COUPLING IN RAPID MANEUVERS

There is a class of problems, all generically connected, known by names such as *roll resonance*, *spin-yaw coupling*, *inertia coupling*, etc. (refs. 10.1 to 10.9). These have to do with large-angle motions or even violent instabilities that can occur on missiles, launch vehicles, reentry vehicles, and aircraft performing rapid rolling maneuvers. The common feature of all these is that the vehicles tend to be slender, and that rapid rolling is present. In some of the situations that have occurred in practice, complicated nonlinear aerodynamics, and mass and configurational asymmetries have been important factors in determining the motion. This subject as a whole is too large for anything approaching a comprehensive treatment to be given here. However, we present some analysis that reveals some of the underlying principles, and by way of an example show what can happen in rapid rolling maneuvers of aircraft.

Let us begin by examining a very simple hypothetical case. The body in question is axisymmetric with $I_y > I_x$. Its reference flight condition is one of constant $\mathbf{V}$ and $\boldsymbol{\omega}$, both these vectors lying on the axis of symmetry, the x axis. We neglect gravity entirely, and study small perturbations around the reference state. The perturbations are further constrained not to include either $\mathbf{V}$ or the roll rate, which remain constant at $\mathbf{V}_e$ and p_0, respectively. We further assume that the only aerodynamic effects are pitching and yawing moments given by

$$\begin{aligned} C_m &= C_{m_\alpha}\alpha + C_{m_q}\hat{q} \\ C_n &= C_{n_\beta}\beta + C_{n_r}\hat{r} \end{aligned} \tag{10.7,1}$$

Because of the axisymmetry, $C_{n_\beta} = -C_{m_\alpha}$ and $C_{n_r} = C_{m_q}$. Since the essence of this problem is nonlinear inertia coupling between the longitudinal and lateral degrees of freedom, we require the general equations (5.13,8) to (5.13,12) for the formulation. In applying the equations we take both the reference

lengths b and $\bar{c}$ to be equal to a reference diameter d, so that $A = 1$. There are then four variables left in the problem, $[\alpha, \beta, \hat{p}, \hat{r}]$, so we need four equations of motion. These are provided by (5.13,9*b* and *c*) and (5.13,11*a* and *b*). In using the latter two we note that (5.13,8*b* and *c*) show that $\hat{q}_W$ and $\hat{r}_W$ are zero by virtue of the neglect of gravity and aerodynamic forces. (Since the net force is zero, **V** is a constant vector, and the wind axes have motion of translation only.) The pertinent equations are then, on making due allowance for the axisymmetry,

$$\begin{aligned} C_m &= \hat{I}_y D\hat{q} - (\hat{I}_y - \hat{I}_x)\hat{r}\hat{p}_0 \\ C_n &= \hat{I}_y D\hat{r} + (\hat{I}_y - \hat{I}_x)\hat{q}\hat{p}_0 \\ D\alpha &= \hat{q} - \hat{p}_0 \cos\alpha \tan\beta - \hat{r} \sin\alpha \tan\beta \\ D\beta &= \hat{p}_0 \sin\alpha - \hat{r} \cos\alpha \end{aligned} \tag{10.7,2}$$

On combining (10.7,1) with (10.7,2) and performing the usual linearization, the result is (using Laplace transforms of the equations)

$$\begin{bmatrix} C_{m_\alpha} & 0 & (C_{m_q} - \hat{I}_y s) & (\hat{I}_y - \hat{I}_x)\hat{p}_0 \\ 0 & -C_{m_\alpha} & -(\hat{I}_y - \hat{I}_x)\hat{p}_0 & (C_{m_q} - I_y s) \\ s & \hat{p}_0 & -1 & 0 \\ -\hat{p}_0 & s & 0 & 1 \end{bmatrix} \begin{bmatrix} \bar{\alpha} \\ \bar{\beta} \\ \bar{q} \\ \bar{r} \end{bmatrix} = 0 \tag{10.7,3}$$

Now we recognize that we are dealing here with the problem of gyrostability. At very large roll rates, we expect the body to display typical gyroscopic motions that will depend mainly on the signs and magnitudes of C_{m_α} and C_{m_q}. At vanishingly small roll rates, the equations decouple into conventional lateral and longitudinal sets, in which the sign of C_{m_α} (i.e. of the pitch stiffness) is a dominant consideration—for C_{m_α} and C_{m_q} both <0, a stable system is assured. We know that even if $C_{m_\alpha} > 0$, gyroscopic stability (in the sense that motions are bounded) is achieved at large enough spin rates. This is in fact the method of stabilizing rifle bullets and artillery shells. It is therefore intuitively evident that there must be a critical roll rate for the case $C_{m_\alpha} > 0$ above which the vehicle is stable—just like the critical spin rate for a common top. On the other hand there is no such intuitive notion about the case when $C_{m_\alpha} < 0$, i.e. when the system is already stable at zero spin—the common case in aerospace (as opposed to ballistic) applications.

To study the stability we need the characteristic equation of (10.7,3), which is of fourth order

$$c_4 s^4 + c_3 s^3 + c_2 s^2 + c_1 s + c_0 = 0$$

where
$$\begin{aligned} c_4 &= \hat{I}_y^2 \\ c_3 &= -2\hat{I}_y C_{m_q} \\ c_2 &= -2\hat{I}_y C_{m_\alpha} + \hat{p}_0^2 \hat{I}_y^2 + C_{m_q}^2 + (\hat{I}_y - \hat{I}_x)^2 \hat{p}_0^2 \\ c_1 &= 2C_{m_\alpha} C_{m_q} - 2\hat{p}_0^2 C_{m_q} \hat{I}_y \\ c_0 &= [(\hat{I}_y - \hat{I}_x)\hat{p}_0^2 + C_{m_\alpha}]^2 + C_{m_q}^2 \end{aligned} \qquad (10.7,4)$$

Unfortunately, even with all the simplifications already made, this equation is still rather too complicated to permit us to say anything simple about the roots. We therefore make a further simplification, and take $C_{m_q} = 0$. We then have

$$\begin{aligned} c_4 &= \hat{I}_y^2 \\ c_3 &= 0 \\ c_2 &= \hat{p}_0^2[\hat{I}_y^2 + (\hat{I}_y - \hat{I}_x)^2] - 2\hat{I}_y C_{m_\alpha} \\ c_1 &= 0 \\ c_0 &= [(\hat{I}_y - \hat{I}_x)\hat{p}_0^2 + C_{m_\alpha}]^2 \end{aligned}$$

whence
$$\hat{\lambda}^2 = \frac{-c_2 \pm \sqrt{c_2^2 - 4c_0 c_4}}{2c_4} \qquad (10.7,5)$$

WHEN $C_{m_\alpha} > 0$ (AERODYNAMICALLY UNSTABLE CONFIGURATION)

In this case c_4 and c_0 are positive definite whereas c_2 changes sign from negative to positive as p_0 increases. The only possibility for stable roots is $\hat{\lambda}^2 < 0$, in which case $\hat{\lambda}$ is imaginary, corresponding to gyroscopic motion. If $\hat{\lambda}^2$ is real and positive, or complex, there will be at least one root with a positive real part. Thus the conditions to be met are $\hat{\lambda}^2$ real and <0, for which it is necessary and sufficient that $c_2^2 > 4c_0 c_4$. The roll rate required for stability is then given by

$$\hat{p}_0^2 > \frac{4C_{m_\alpha}\hat{I}_y}{\hat{I}_x^2} \qquad (10.7,6)$$

WHEN $C_{m_\alpha} < 0$ (AERODYNAMICALLY STABLE CONFIGURATION)

In this case c_2 and c_4 are positive definite and it is c_0 that can change sign. The condition (10.7,6) still holds, but because C_{m_α} is now negative, it is automatically satisfied. However, the condition that $\hat{\lambda}^2$ be negative now requires that c_0 be positive. So for this case the criterion for $\hat{p}_0$ is obtained from $c_0 > 0$, i.e.

$$[(\hat{p}_0^2 \hat{I}_y - \hat{I}_x) + C_{m_\alpha}] > 0 \qquad (10.7,7)$$

Condition (10.7,7) is met for all values of $\hat{p}_0^2$ except one, at which the l.h.s. = 0. There is thus one roll rate at which the system has "neutral" stability, i.e. for which there is a zero root. The critical value is

$$|\hat{p}_0| = \left[\frac{-C_m}{\hat{I}_y - \hat{I}_x}\right]^{1/2} \tag{10.7,8}$$

To summarize, we have seen that an aerodynamically unstable configuration can be stabilized by spinning it fast enough, and that at a certain critical roll rate an aerodynamically stable configuration becomes neutrally stable. The source of these phenomena is the inertia effects given by the rp and qp terms in the pitching and yawing moment equations. They can be thought of as gyroscopic moments associated with high roll rate. Phillips (ref. 10.1) has analyzed a more general case, in which the vehicle is not axisymmetric, and in which aerodynamic forces as well as moments are retained, i.e. an airplane configuration. In this case he found that there is a band of roll rates within which the vehicle is unstable, the lower critical one being given approximately by the lesser of

$$\left[\frac{-C_{m_\alpha}}{A(\hat{I}_z - \hat{I}_x)}\right]^{1/2} \quad \text{or} \quad \left[\frac{C_{n_\beta}}{\frac{1}{A^3}\hat{I}_y - \hat{I}_x}\right]^{1/2} \tag{10.7,9}$$

[compare with (10.7,8)].

For the jet transport of our examples, with $C_{m_\alpha} = -.488$ the critical rate would be $\hat{p}_{\text{crit}} = .112$, corresponding to the first of the two criteria. From (10.6,8) this vehicle, at $\delta_a = 20°$, achieves $\hat{p}_{ss} = .0528$, a value considerably less than the critical, and hence one would not anticipate any difficulties for this airplane arising from nonlinear inertia coupling.

Since the rolling motion may be thought of in a sense as providing a periodic excitation of the uncoupled longitudinal and lateral oscillations, it proves convenient to look at *stability boundaries* in the plane of the two uncoupled frequencies. This idea was first used by Phillips. The result is typically like that in Fig. 10.17, the exact boundaries depending mainly on the dampings of the two oscillations. A vehicle conventionally stable in nonrolling flight would be represented by a point in the upper right quadrant, the exact position being determined by p_0. As p_0 increases, the point moves radially toward the origin. If it follows a line like A, there will be no instability; but if like B, there is an unstable range of p_0 separating two stable regions as found by Phillips. A vehicle that is statically unstable in both pitch and yaw when nonrolling will correspond to a point in the lower left quadrant, and can be stabilized by a large enough p_0 (line C).

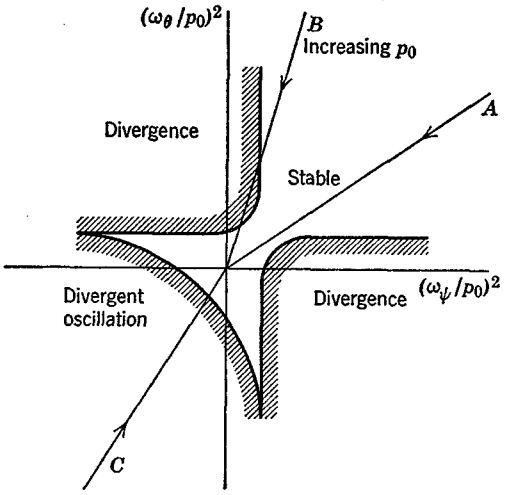

FIG. 10.17 Form of stability boundaries for rolling vehicle. ω_ψ = frequency of yaw oscillation, $\sqrt{N_\beta/I_z}$. ω_θ = frequency of pitch oscillation, $\sqrt{-M_\alpha/I_y}$.

NUMERICAL EXAMPLE—PITCH/ROLL COUPLING OF A SMALL AIRPLANE

To show how the nonlinear inertia terms can affect the motion of an airplane we consider a small maneuverable single-engined jet airplane. Its principal characteristics are

$$W = 6000 \text{ lb}, \quad S = 216 \text{ ft}^2, \quad A = 6.0$$
$$b = 36.0 \text{ ft}, \quad \bar{c} = 6.0 \text{ ft}$$
$$I_x = .170 \times 10^4 \text{ slug ft}^2$$
$$I_y = .120 \times 10^5 \text{ slug ft}^2, \quad I_{zx} = 0$$
$$I_z = .140 \times 10^5 \text{ slug ft}^2$$

Note that I_x/I_z is only .121, as compared with about .4 for the transport airplane. The pertinent aerodynamic data for flight at 500 fps at sea level are given as

$$C_{C_\beta} = -.081, \quad C_{L_\alpha} = 4.35, \quad C_{L_{\dot\alpha}} = C_{L_q} = 0$$
$$C_{m_\alpha} = -.435, \quad C_{m_{\dot\alpha}} = -2.1, \quad C_{m_q} = -9.73$$
$$C_{l_\beta} = -.081, \quad C_{l_p} = -.442, \quad C_{l_r} = .0309$$
$$C_{n_\beta} = .0218, \quad C_{n_p} = 0, \quad C_{n_r} = -.0424$$
$$C_{L_{\delta e}} = 0, \quad C_{m_{\delta e}} = -1.07, \quad C_{l_{\delta a}} = -.24, \quad C_{n_{\delta a}} = 0$$
$$C_{T_{v_W}} = -\beta C_{T_e}, \quad C_{T_{z_W}} = -\Delta\alpha C_{T_e}, \quad C_{T_e} = .017$$

The value of $\hat{p}_{\text{crit}}$ calculated from (10.7,9) is .0796. In applying the general nonlinear equations, we assume that $\Delta\alpha$, β, remain small, that linearization is permissible with respect to them, and that the speed is constant.

With these assumptions, (5.13,8) et seq. yield the following system of equations.

$$-C_{T_e}\beta - C_C + C_W \cos\theta_W \sin\phi_W = 2\mu A\hat{r}_W$$

$$-C_{T_e}\Delta\alpha - C_L + C_W \cos\theta_W \cos\phi_W = -2\mu\hat{q}_W$$

$$C_l = \hat{I}_x A D\hat{p} - \left(\frac{\hat{I}_y}{A^2} - \hat{I}_z A\right)\hat{q}\hat{r}$$

$$C_m = \hat{I}_y D\hat{q} - A(\hat{I}_z - \hat{I}_x)\hat{r}\hat{p}$$

$$C_n = \hat{I}_z D\hat{r} - \left(A\hat{I}_x - \frac{\hat{I}_y}{A^2}\right)\hat{p}\hat{q}$$

$$D\alpha = \hat{q} - \hat{q}_W - \frac{\hat{p}}{A}\beta$$

$$D\beta = \frac{\hat{r}_W}{A} + \frac{\hat{p}}{A}\Delta\alpha - \frac{\hat{r}}{A}$$

$$D\phi_W = \frac{\hat{p}_W}{A} + \hat{q}_W \tan\theta_W \sin\phi_W + \frac{\hat{r}_W}{A}\tan\theta_W \cos\phi_W$$

$$D\theta_W = \hat{q}_W \cos\phi_W - \frac{\hat{r}_W}{A}\sin\phi_W$$

$$\hat{p}_W = \hat{p} + A\beta\hat{q}_W + \Delta\alpha\hat{r}$$

$$C_C = C_{C_\beta}\beta$$

$$C_L = C_{L_\alpha}\alpha$$

$$C_l = C_{l_\beta}\beta + C_{l_p}\hat{p} + C_{l_r}\hat{r} + C_{l_{\delta_a}}\delta_a$$

$$C_m = C_{m_\alpha}\alpha + C_{m_{\dot{\alpha}}}D\alpha + C_{m_q}\hat{q} + C_{m_{\delta_e}}\delta_e$$

$$C_n = C_{n_\beta}\beta + C_{n_p}\hat{p} + C_{n_r}\hat{r}$$

The logical structure of these is essentially as in Fig. 5.6.

The above equations were programmed for solution on a digital computer,

using a Runge-Kutta algorithm for solving differential equations. Solutions were obtained for two different sets of conditions:

(i) Initial condition of rolling at rate p_i, with all other initial values zero, with $|\delta_e|$ at 2°, and with δ_a set at the value required to make $p_{ss} = p_i$ [see (10.6,8)]. Thus the initial value of $\dot{p}$ would be zero, producing a condition somewhat like that of Phillip's analysis.

(ii) All initial values zero, with a pitch maneuver initiated by elevator elevator deflection at $t = 0$ and a subsequent roll maneuver superimposed by a step change in δ_a.

Figure 10.18 shows the angle of attack variation in the first case, (*a*) for pitch-up and (*b*) for pitch-down. A striking result is the difference between positive and negative elevator angle, a difference that results entirely from the nonlinearity of the equations. Even for very large aileron angles, there is no evidence in (*a*) of instability, and only for the case of $|\delta_a| = 14.7°$ does $\Delta\alpha$ become momentarily excessive. On the other hand case (*b*) develop excessive $\Delta\alpha$ quite suddenly when $|\delta_a|$ goes from 4.2 to 6.3°. The difference in behavior in these two cases is largely attributable to the difference in the roll-rate time histories, which in turn results from the fact that $\beta > 0$ in (*a*) and $\beta < 0$ in (*b*). (The roll rate results are not presented on the figures. The following comments are based on the computer output.) In the case $\hat{p}_i = .060$, $\delta_e = 2.0°$, $\hat{p}$ first decreases slightly, then increases with time as a result of rolling moment due to side-slip, crossing over the critical value .0796 at about .8 sec, and remaining larger till the end of the calculation. Very soon after $\hat{p}$ exceeds $\hat{p}_{\text{crit}}$, $\Delta\alpha$ starts to increase rapidly. On the other hand, for $\hat{p}_i = .040$, $\hat{p}$ never reaches the critical value, and $\Delta\alpha$ is "well-behaved." In Fig. 10.18*a*, $\hat{p}_i = .140$, the rolling moment due to sideslip is negative and decreases the roll rate so that it falls below the critical value at $t = 2.6$ sec. This is again compatible with the reduction in $\Delta\alpha$ that occurs at about the same time. It appears that the critical roll rate derived by Phillips is a very useful criterion for a "well-behaved" transient.

Figure 10.19 shows the variation of $\Delta\alpha$ for the second case, which is a realistic maneuver, resulting after 5 sec in a pitch-up (or down) of about 20°, and a roll when $\delta_a = 8°$ of about $1\frac{1}{4}$ revolutions. Again the lack of symmetry between pitch-up and pitch-down is clear, the latter being the unfavorable case for a roll to the left. The difference between $\Delta\alpha$ for $\delta_a = 4°$ and $\delta_a = 8°$ or 10° is striking. In the former case the detailed solution shows $p < p_{\text{crit}}$ for the whole time, whereas the latter two have $p > p_{\text{crit}}$ almost from the onset of the rolling motion. For the pitch-up case as well, p_{crit} is exceeded for $\delta_a = 12°$ and 18°, but not for $\delta_a = 6°$.

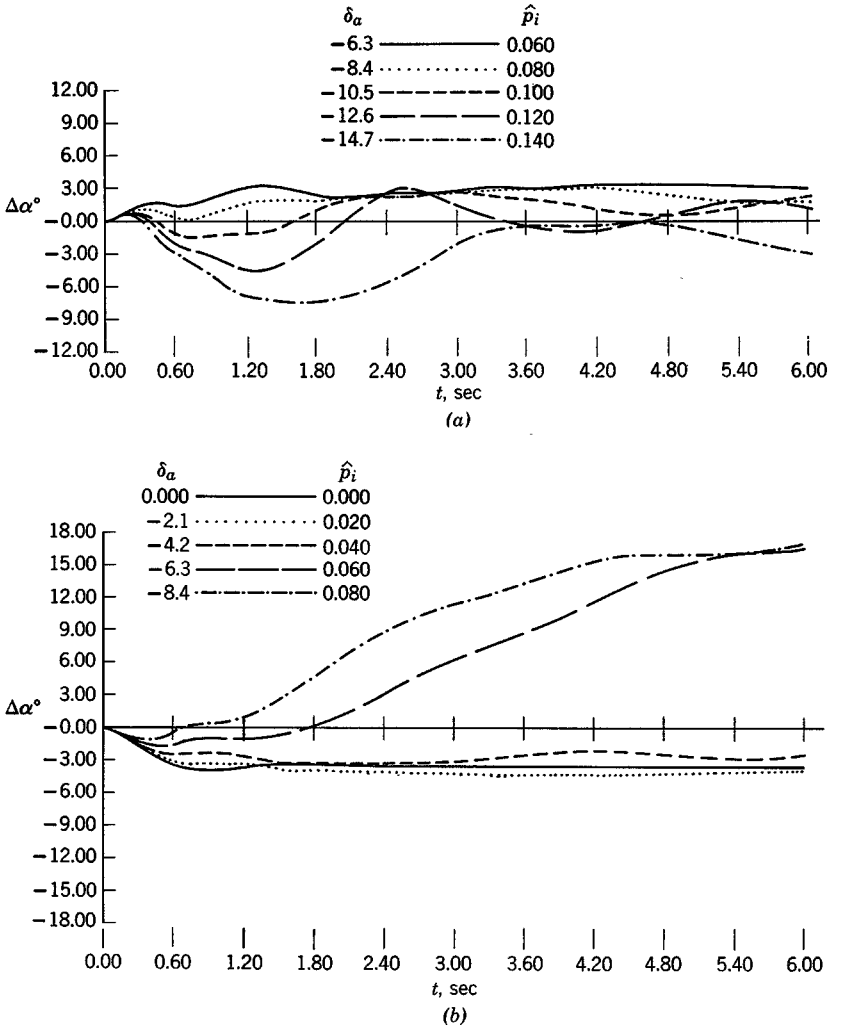

FIG. 10.18 Variation of $\Delta\alpha$ during rapid roll. (*a*) Pitch-up case, $\delta_e = -2.0°$. (*b*) Pitch-down case, $\delta_e = 2.0°$.

In the discussion of these examples we have studiously avoided the use of the word "stability" in describing the solutions, using "well-behaved" instead to denote "acceptable behaviour." We have not in fact discovered anything about the stability of the solution presented, in the strict Lyapunov sense. They may or may not be continuous functions of the initial conditions as $t \to \infty$, (although they certainly appear to be continuous for the range of

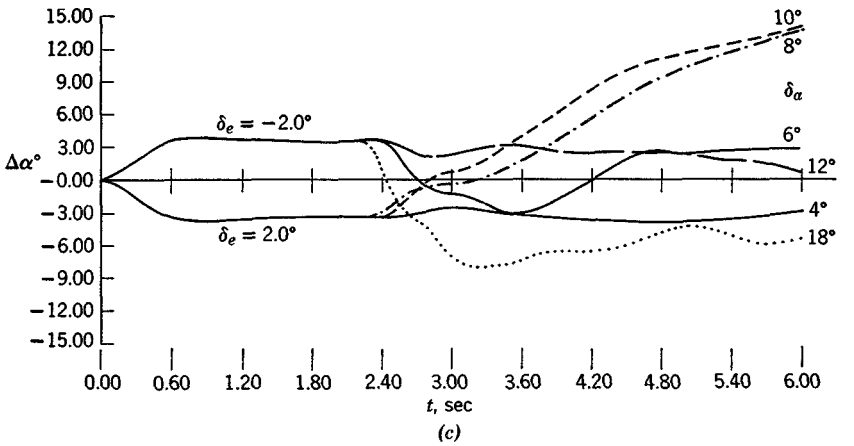

FIG. 10.19 Variation of angle of attack in a combined pitch/roll maneuver.

t considered). Furthermore, the *stability* in that sense is actually *irrelevant* (see closing remarks of Sec. 3.5). Whether or not the maneuver is an acceptable one is governed entirely by the size of the $\Delta\alpha$ and $\Delta\beta$ excursions that can be tolerated without structural failure or loss of control and not by the theoretical stability of the solution.

Closed-loop control

CHAPTER 11

11.1 GENERAL PRINCIPLES

Although open-loop responses of the kind studied in some depth in Chapter 10 are very revealing in bringing out inherent vehicle dynamics, they do not in themselves usually represent real operating conditions. Every phase of the flight of an aerospace vehicle can be regarded as the accomplishment of a set task—i.e. flight on a specified trajectory. That trajectory may simply be a straight horizontal line traversed at constant speed, or it may be a turn, a transition from one symmetric flight path to another, a landing flare, following an ILS or navigation radio beacon, homing on a moving target, etc. All of these situations are characterized by a common feature, namely, the presence of a *desired state*, steady or transient, and of departures from it that are designated as errors. These errors are of course a consequence of the unsteady nature of the real environment and of the imperfect nature of the physical system comprising the vehicle, its instruments, its controls, and its guidance system (whether human or automatic). The correction of errors implies a knowledge of them, i.e. of error-measuring (or state-measuring) devices, and the consequent actuation of the controls in such a manner as to reduce them. This is the case whether control is by human or by automatic pilot. In the former case, the state information sensed is a complicated blend of visual and motion cues, and instrument readings. The logic by which this information is converted into control action is only imperfectly understood,

but our knowledge of the physiological "mechanism" that intervenes between logical output and control actuation is somewhat better (see Chapter 12). In the latter case—the automatic control—the sensed information, the control logic, and the dynamics of the control components are usually well known, so that system performance is in principle quite predictable. The process of using state information to govern the control inputs is known as *closing the loop*, and the resulting system as a *closed-loop control* or *feedback control.* The terms *regulator* and *servomechanism* describe particular applications of the feedback principle. Figure 3.5 shows a general block diagram describing the feedback situation. In the present context we regard $\mathbf{y}$ as the state vector, $H(s)$ as an operator (linear in the figure, but of course not necessarily so) and $\boldsymbol{\epsilon}$ as the control vector. Clearly, since real flight situations virtually always entail closed-loop control, a study of the consequences of closing the loop is in order.

Another factor that cannot be separated from these referred to above is the force amplification or power amplification common in the control systems of large aircraft. As noted in Sec. 6.8, the control forces needed on large high-speed aircraft may exceed the capabilities of human pilots. Thus another dynamic system—powered controls—intervenes between the pilot and the aerodynamic surfaces. Such subsystems are themselves commonly servomechanisms—closed-loop systems that drive the surfaces in response to pilot commands. Thus we are frequently concerned with "loops within loops," a very common situation. For example, the "outermost" loop might be a guidance loop that controls the error in vehicle position relative to an ILS beam. An inner loop might be a *stability augmentation system* (treated later in Sec. 11.4) whose purpose is to improve the inherent lateral dynamics of the vehicle and, finally, within this one there may be still another loop associated with the control-surface servo.

Although flight dynamicists (who usually come from an aerospace engineering background) and control engineers (who frequently have a background in electrical engineering) usually communicate adequately on problems of mutual concern, there is often understandably some difference in their points of view. This is illustrated somewhat facetiously in Fig. 11.1. At one extreme, the control engineer may overemphasize the many elements that comprise the control system, and tend to minimize the role of the dynamics of the vehicle itself—perhaps replacing all its rich and varied detail with oversimplified approximate transfer functions. At the other extreme, the flight dynamicist may substitute some simple algebraic relations for the entire control system. Neither extreme is right for the final solution of real problems, but both may have their merits for certain purposes. We naturally tend here to the flight dynamicist's view of the system in the illustrations that follow. For example, it is sometimes very helpful to consider the loop closure as simply modifying some of the existing aerodynamic derivatives, or

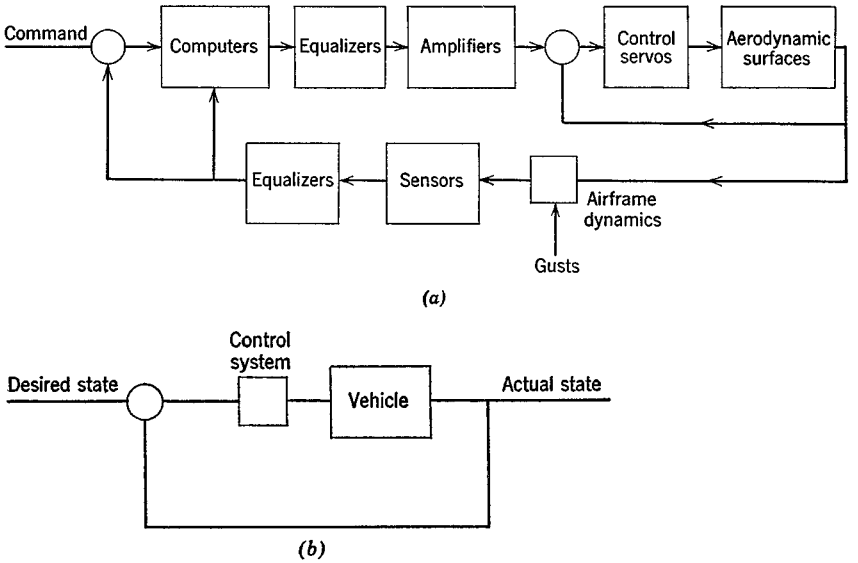

FIG. 11.1 Closed-loop control—two extreme views. (*a*) The control engineer's viewpoint. (*b*) The flight dynamicist's viewpoint.

adding new ones. Specifically let y be any nondimensional state variable, and let a control surface be displaced in response to this variable according to the law

$$\Delta\delta = k\,\Delta y; \qquad k = \text{const}$$

(Here k is a simplified representation of all the sensor and control system dynamics!) Then a typical aerodynamic force or moment coefficient C_a will be incremented by

$$\begin{aligned}\Delta C_a &= C_{a_\delta}\,\Delta\delta \\ &= C_{a_\delta} k\,\Delta y \end{aligned} \tag{11.1,1}$$

This is the same as adding a synthetic increment

$$\Delta C_{a_y} = kC_{a_\delta} \tag{11.1,2}$$

to the aerodynamic derivative C_{a_y}. Thus if y be yaw rate and δ be rudder angle, then the synthetic increment in the yaw-damping derivative is

$$\Delta C_{n_r} = kC_{n_{\delta r}} \tag{11.1,3}$$

which might be the kind of change required to correct a lateral dynamics problem. This example is in fact the basis of the often-applied "yaw damper," a stability-augmentation feature. Again, if y be the roll angle and δ the aileron, we get the *entirely new* derivative

$$C_{l_\phi} = kC_{l_{\delta_a}} \tag{11.1,4}$$

the presence of which can profoundly change the lateral characteristics.

SENSORS

We have already alluded to the general nature of feedback control, and the need to provide *sensors* that ascertain the *state* of the vehicle. When a human pilot is in control, his eyes and kinesthetic senses, aided by the standard flight information displayed by his instruments, provide this information. (In addition, of course, his brain supplies the logical and computational operations needed, and his neuro-muscular system all or part of the actuation.) In the absence of human control, when the vehicle is under the command of an autopilot, the sensors must, of course, be physical devices. As already mentioned, some of the state information needed is measured by the standard flight instruments—air-speed, altitude, rate-of-climb, heading, etc. This information may or may not be of a quality and in a form suitable for incorporation into an automatic control system. In any event it is not generally enough. When both guidance and attitude-stabilization needs are considered, the state information needed may include:

Position and velocity vectors relative to a suitable reference frame.
Vehicle attitude (θ, ϕ).
Rotation rates (p, q, r).
Aerodynamic angles (α, β).
Acceleration components of a reference point in the vehicle.

The above is not an exhaustive list. A wide variety of devices are in use to measure these variables, from Pitot-static tubes to sophisticated inertial-guidance platforms. Gyroscopes, accelerometers, magnetic and gyro compasses, angle-of-attack and sideslip vanes, and other devices all find applications as sensors. The most common form of output is an electrical signal, but fluidic devices (ref. 11.1) are increasingly receiving attention. Although in the following examples we tend to assume that the desired variable can be measured independently, linearly, and without time lag, this is of course an idealization that is only approached but never reached in practice. Every sensing device together with its associated transducer and amplifier is itself a dynamic system, with characteristic frequency response, noise, nonlinearity, and cross-coupling. These attributes cannot finally be ignored in the design of real systems, although one can usefully do so in preliminary work. As an example of cross-coupling effects, consider the sideslip sensor assumed to be available in the stability augmentation system of Sec. 11.4. Assume, as might well be the case, that it consists of a sideslip vane mounted on a boom projecting forward from the nose. Such a device would in general respond not only to $\beta = \sin^{-1}(v/V)$ but also to atmospheric turbulence (side gusts), to roll and yaw rates, and to lateral acceleration a_y at the vane hinge. Thus the output signal would in fact be a complicated mathematical

function of several state variables, representing several feedback loops, rather than being simply proportional to β as assumed in the example. The objective in sensor design is, of course, to minimize all the unwanted extraneous effects, and to provide sufficiently high frequency response and low noise in the sensing system.

This brief discussion serves only to draw attention to the important design and analytical problems related to sensors, and to point out that their real characteristics, as opposed to their idealizations, need finally to be taken into account in design.

11.2 EXAMPLE—SUPPRESSION OF THE PHUGOID

The characteristic lightly damped, low-frequency oscillation in speed, pitch attitude, and altitude that was identified in Chapter 9, was seen in Chapter 10 to lead to large peaks in the frequency-response curves (Fig. 10.3) and long transients (Figs. 10.6 and 10.7). Similarly, in the control-fixed case, there are large undamped responses in this mode to disturbances such as atmospheric turbulence (see Chapter 13). These variations in speed, height, and attitude are in fact not in evidence in actual flight; the pilot (human or automatic) effectively suppresses them, maintaining flight at more or less constant speed and height. The logic by which this process of suppression takes place is not unique. In principle it can be achieved by using feedback signals derived from any one or a combination of pitch attitude θ, altitude z_E, speed V, and their derivatives. In practice, the availability and accuracy of the state information determines what feedback is used. We shall see that a simple negative feedback of pitch attitude suffices effectively to eliminate the phugoid. Pitch attitude is instantly and accurately available from either the real or artificial horizon. We shall also see that operating on speed error can produce pitch maneuvers free of phugoid oscillations.

Consider the system shown in Fig. 11.2, in which θ_C is the pitch command,

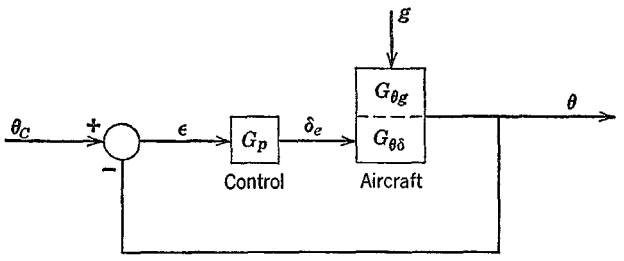

FIG. 11.2 Phugoid suppression system.

$G_p(s)$ is the overall transfer function of the control system, and g is a disturbance (gust) input. The pitch attitude is given by

$$\bar{\theta} = G_{\theta g}\bar{g} + G_{\theta\delta}\,\bar{\delta}_e \tag{11.2,1}$$

and we readily find the overall transfer functions

$$\begin{aligned} \frac{\bar{\theta}}{\bar{\theta}_c} &= \frac{G_p G_{\theta\delta}}{1 + G_p G_{\theta\delta}} \\ \frac{\bar{\theta}}{\bar{g}} &= \frac{G_{\theta g}}{1 + G_p G_{\theta\delta}} \end{aligned} \tag{11.2,2}$$

The stability with respect to θ_c or g inputs is given by the roots of the characteristic equations of these two overall transfer functions. So long as δ_e and g are both inhomogeneous inputs to the linear aircraft system, it can be seen that the denominators of $G_{\theta\delta}$ and $G_{\theta g}$ are the same, each being the characteristic polynomial det $(s\mathbf{I} - \mathbf{A})$ (see Sec. 3.2). Thus we may write

$$G_{\theta\delta} = \frac{N_1}{D} \qquad G_{\theta g} = \frac{N_2}{D} \tag{11.2,3}$$

where N_1, N_2, D are polynomials in s, and the overall transfer functions are

$$\begin{aligned} \frac{\bar{\theta}}{\bar{\theta}_c} &= \frac{G_p N_1}{D + G_p N_1} \\ \frac{\bar{\theta}}{\bar{g}} &= \frac{N_2}{D + G_p N_1} \end{aligned} \tag{11.2,4}$$

The poles of these transfer functions, which are the roots of the characteristic equations, will be the same if $G_p N_1$ and N_2 have no poles (or the same poles), and in that case the stability with respect to gust inputs will be the same as that for pitch command inputs. A reasonably general form for $G_p(s)$ for this application is

$$G_p(s) = \frac{k_1}{s} + k_2 + k_3 s$$

For obvious reasons, the three terms on the r.h.s. are called, respectively, *integral control*, *proportional control*, and *rate control*, because of the way they operate on the error ϵ. The particular form of the controlled system, here $G_{\theta\delta}(s)$, determines which of k_1, k_2, k_3 need to be nonzero, and what their magnitudes should be for good performance. Integral control has the characteristic of a *memory*, and steady-state errors cannot persist when it is present. Rate control has the characteristic of *anticipating* the future values of the error and thus generates *lead* in the control actuation. It turns out

that all we need here is proportional control, so we choose $G_p(s) = K$, a constant, and the characteristic equation is

$$D(s) + KN_1(s) = 0 \tag{11.2,5}$$

To proceed further, we need explicit expressions for N_1 and D. We saw in Sec. 10.2 that the phugoid approximation to $G_{\theta\delta}$ is quite good up to elevator frequencies near that of the short-period mode. Since we may expect that the elevator frequency needed to suppress the phugoid is of the same order as the control-fixed phugoid frequency, we may use (10.2,15*b*) in this analysis (and this is verified a posteriori). We therefore have

$$\begin{aligned} N_1(s) &= n_2 s^2 + n_1 s + n_0 \\ D(s) &= c_2 s^2 + c_1 s + c_0 \end{aligned} \tag{11.2,6}$$

Approximate expressions, good enough for this example, are obtained from (10.2,15*b*) by neglecting C_{L_δ} and assuming $C_{T_V} = -2C_{D_e}$ and $C_{D_e} << C_{L_\alpha}$. We then get

$$\begin{aligned} n_2 &= -4\mu^2 \frac{C_{m_\delta}}{C_{m_\alpha}} \\ n_1 &= -2\mu C_{L_\alpha} \frac{C_{m_\delta}}{C_{m_\alpha}} \\ n_0 &= -2[C_{L_\alpha} C_{D_e} + C_{W_e}(C_{W_e} - C_{D_\alpha})] \frac{C_{m_\delta}}{C_{m_\alpha}} \end{aligned} \tag{11.2,7}$$

$$\begin{aligned} c_2 &= 4\mu^2 \\ c_1 &= 4\mu C_{D_e} \\ c_0 &= 2C_{W_e}^2 \end{aligned} \tag{11.2,8}$$

The characteristic equation is, from (11.2,5) and (11.2,6),

$$(c_2 + Kn_2)s^2 + (c_1 + Kn_1)s + (c_0 + Kn_0) = 0 \tag{11.2,9}$$

and the feedback is seen to affect every term in the equation. We also observe that the numerator of the open-loop transfer function $G_{\theta\delta}$ plays a decisive role in determining the characteristics of the closed-loop system.

The frequency and damping of the system are now obtained from (11.2,9) as

$$\begin{aligned} \omega_n' &= \left(\frac{c_0 + Kn_0}{c_2 + Kn_2}\right)^{1/2} = \omega_n \left(\frac{1 + Kn_0/c_0}{1 + Kn_2/c_2}\right)^{1/2} \\ 2\zeta' &= \frac{c_1 + Kn_1}{\sqrt{(c_2 + Kn_2)(c_0 + Kn_0)}} = 2\zeta \frac{(1 + Kn_1/c_1)}{\sqrt{(1 + Kn_2/c_2)(1 + Kn_0/c_0)}} \end{aligned} \tag{11.2,10}$$

where $\omega_n = (c_0/c_2)^{1/2}$ and $2\zeta = c_1/\sqrt{c_2 c_0}$ are the fixed-control phugoid parameters. Using the data for the jet transport cruising at 30,000 ft altitude given in Sec. 9.1, and $C_{m_\delta} = C_{m_\alpha}$ we get the numerical values

$$\frac{n_0}{c_0} = -2.02, \qquad \frac{n_1}{c_1} = -130, \qquad \frac{n_2}{c_2} = -1.0$$

from which

$$\frac{\omega_n'}{\omega_n} = \left(\frac{1 - 2.02K}{1 - K}\right)^{1/2}$$
$$\frac{\zeta'}{\zeta} = \frac{1 - 130K}{\sqrt{(1 - K)(1 - 2.02K)}} \tag{11.2,11}$$

Even with small gain K the damping of the phugoid is very much increased. The original value was $\zeta = .0535$, so to produce a dead-beat transient for which $\zeta = 1$, we require $\zeta'/\zeta = 18.7$, which is produced by a gain $-K = .17$. Note that the gain is negative, since a positive error ϵ indicates the nose is too low, and up-elevator ($\delta_e < 0$) is required to correct. With the gain needed for $\zeta = 1.0$, we get $\omega_n'/\omega_n = 1.07$, so the frequency has been increased by only 7%, and the phugoid approximation for $G_{\theta\delta}$ is clearly adequate.

This calculation shows how a human or automatic pilot could eliminate the phugoid oscillations quite simply, using readily available state information. The exact control law by which a human pilot actually achieves this result may in fact be somewhat different from that assumed here, but it is probable that θ is the prime variable on which he operates.

CHANGE OF FLIGHT-PATH ANGLE

The phugoid makes its presence known not only in the form of transient perturbations from a steady state, but also in maneuvers, as illustrated in Sec. 10.3. We saw there for example that in changing from level to climbing flight by opening the throttle (Fig. 10.7) there results a protracted, weakly damped approach to the new state that would take some 10 min to complete. Transitions from one value of γ to another are obviously not made in this manner, and the pilot suppresses the oscillation in this case as well. Provided that the correct θ is known for the climb condition, the same technique as discussed above would work, i.e. proportional control operating on pitch-attitude error. We illustrate an alternative concept that does not require any knowledge of the final correct pitch attitude, but that uses speed error alone. Figure 11.3*a* shows the system. In this case it is found that proportional control is not adequate—it serves mainly to shorten the period of the oscillation, but has little effect on the damping. To improve damping needs rate control, so the control law used is

$$G_p(s) = k_1 + k_2 s; \qquad k_1, k_2 > 0 \tag{11.2,12}$$

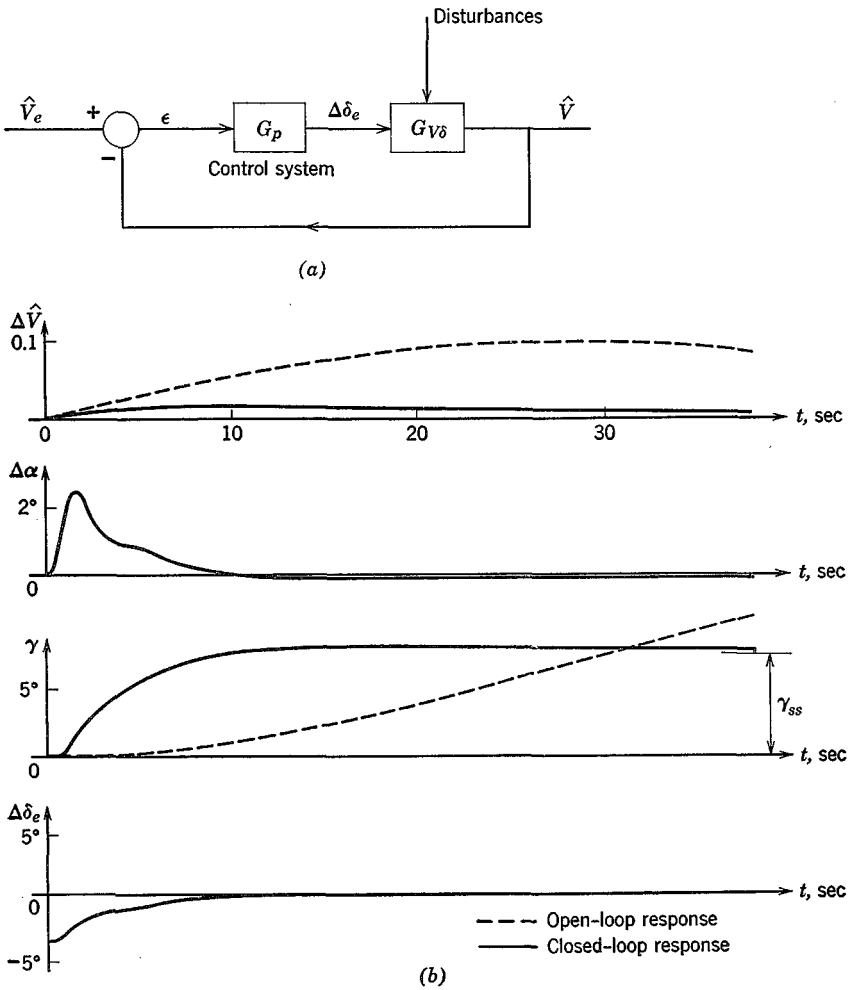

FIG. 11.3 (*a*) System with speed feedback. (*b*) Suppression of phugoid by closed-loop control—response to thrust change.

where the signs of the gains have been chosen to give the required corrections.

Just as in the case of θ feedback above, the characteristic equation can be obtained from the approximate transfer function, in this case $G_{V\delta}$. It is given by (10.2,15*a*), i.e. with the same approximations as used above,

$$G_{V\delta} = \frac{N_3(s)}{D(s)} \qquad (11.2,13)$$

where $D(s)$ is given by (11.2,6) and (11.2,8) and

$$\begin{aligned} N_3(s) &= m_1 s + m_0 \\ m_1 &= 2\mu C_{D_\alpha} C_{m_\delta} / C_{m_\alpha} \\ m_0 &= C_{W_e} C_{L_\alpha} C_{m_\delta} / C_{m_\alpha} \end{aligned} \tag{11.2,14}$$

The characteristic equation [cf. (11.2,5)] is

$$D(s) + (k_1 + k_2 s) N_3(s) = 0$$

which becomes

$$(c_2 + m_1 k_2) s^2 + (c_1 + m_1 k_1 + m_0 k_2) s + (c_0 + k_1 m_0) = 0 \tag{11.2,15}$$

The new characteristic equation is again second order, being the sum of the original one and additional terms. When the signs of the quantities in (11.2,14) are taken into account, the modifications to the three original coffiecients can be summarized thus

c_2: increased by amount proportional to k_2
c_1: increased by amounts proportional to k_1 and k_2
c_0: increased by an amount proportional to k_1

Since there are two free constants, k_1 and k_2, we can analytically satisfy two conditions by means of (11.2,15)—one on the period, and one on the damping of the closed-loop system. This procedure is fairly obvious, and is not elaborated on here. The values of the constants finally chosen have to be constrained of course by practical considerations related to sensor and control hardware limitations. Finally, the approximate analysis has to be verified with the complete system of equations. As an example, Fig. 11.3 shows the response to a step input of thrust obtained using analogue computation of the full system of equations. The constants used were

$$k_1 = .30 \text{ rad/unit}; \qquad k_2 = 1000 \text{ rad/unit}$$

The first corresponds to a deflection of .172° per 1% change in speed, and the second to 25.3° per g of forward acceleration. The airplane and flight condition of the figure are the same as those for Fig. 10.7. The dashed lines show the beginning of the phugoid response that would exist without feedback. This would take about 10 min to decay. The solid lines show the response with feedback, and we see that for all practical purposes the transition is completed smoothly and rapidly—within about 15 sec. There is a small overshoot in γ, and small errors in $\Delta\hat{V}$ and $\Delta\delta$ that die out rather slowly. This feature could be eliminated at the cost of some additional complexity by introducing some integral control. The elevator angle variation required to accomplish the transition is seen to consist of an initial step (up-elevator) followed by a gradual reduction of the deflection. The conditions near $t = 0$ are, of course, somewhat artificial because of the step input used.

A gradual thrust increase would have resulted in a gradual deflection of the elevator. It should be noted that the error in $\Delta\dot{V}$, the primary quantity sensed, is indeed kept quite small. The role of $\Delta\alpha$ is worth commenting on. At the scale of the figure, there is practically no α change in the open-loop case within the time span shown. The "pulse" in α in the closed-loop case clearly has the effect of producing a corresponding pulse in lift that rotates the velocity vector through the required angle.

Finally, it should be observed that in theory a human pilot has all the state information that we have assumed was available. V and $\dot{V}$ could be obtained from an airspeed indicator, and additional information about $\dot{V}$ can be felt as an inertia force (a "seat-of-the-pants" input). An autopilot could readily have ΔV supplied in electronic form by a conventional transducer, but $\dot{V}$ would be somewhat more troublesome. The two principal alternatives would be differentiation of V, or an acceleration signal from an inertial platform.

11.3 EQUATIONS OF MOTION OF THE CONTROL SYSTEMS

Up to this point in our development of the subject we have not found it necessary to consider the dynamics of the vehicle's control systems per se, although the omission of this feature was pointedly noted in the previous section. In fact the dynamics of control systems not only enter into closed-loop behavior but are also implicit in the stability of vehicles with free controls. When the controls are reversible (i.e. when an external force applied at the surface can cause it to move), the stability with free controls may be appreciably different from that with fixed controls. This case can be thought of in a sense as belonging to the feedback class of control problems, since the control angles are then governed by certain inherent aerodynamic and inertial feedbacks.

The wide variety of control system types and configurations in common use, and the variability of the schemes used to provide power or force amplification make it virtually impossible to present a universal analysis of any use. We therefore select one hypothetical model of a control system, and show how its equations of motion are derived. Generally speaking, a similar procedure would apply to other cases. The model is that depicted in Fig. 11.4. It consists of a rigid elevator surface, connected by a rigid frictionless linkage to the pilot's control and to a hydraulic jack. The airframe structure to which the system is attached is also assumed to be rigid. The external forces acting are the pilot control force P, the jack force J, and the aerodynamic hinge moment H_e. Gravity is neglected since it is essentially

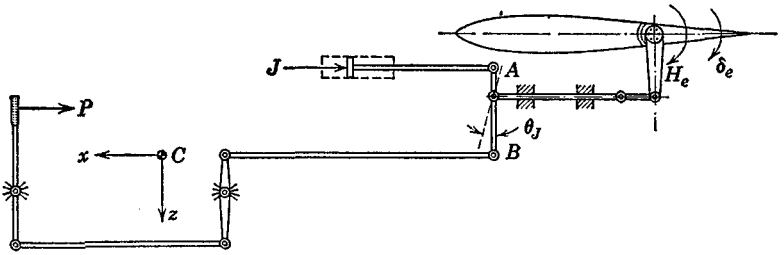

FIG. 11.4 A hypothetical elevator system.

a constant that only affects the equilibrium position slightly. The system has two degrees of freedom relative to the frame F_B, i.e. δ_e and θ_J. The control system shown represents a power assisted elevator, and does not incorporate explicitly any provision for closed-loop positioning of the elevator. This would require a somewhat different physical arrangement, and its governing equation would be different from that derived below.

We obtain the equations of motion by applying Lagrange's equation (5.12,3), the procedure being somewhat analogous to that used in Sec. 5.12. In this application, since rigidity has been assumed, the strain energy U is zero. ϵ_n stands for either δ_e or θ_J, so that there are two equations of motion. As in Sec. 5.12 the generalized force $\mathscr{F}_n$ must include the inertia forces associated with acceleration and rotation of the reference frame F_B.

THE KINETIC ENERGY T

The kinetic energy of the moving masses (elevator, levers, pistons, rods, etc.) can for small displacements always be expressed in the form

$$T = \tfrac{1}{2} I_e \dot{\delta}_e^2 + I_{eJ} \dot{\delta}_e \dot{\theta}_J + \tfrac{1}{2} I_J \dot{\theta}_J^2 \qquad (11.3,1)$$

The coefficients of this equation are *generalized inertias*, and could be computed by integrating the energy associated with $\dot{\delta}_e$ and $\dot{\theta}_J$ over all the moving material system. These inertias are assumed to be constants.

THE GENERALIZED FORCE $\mathscr{F}_n$

The generalized force is given by (5.12,8), where W is the work done by the external aerodynamic and inertia forces during a virtual displacement of the system. Let it be expressed as

$$\Delta W = H_e \Delta\delta_e + P \Delta s_P + J \Delta s_J + \Delta W_i \qquad (11.3,2)$$

where s_P and s_J are the displacements of the forces P and J respectively,

and W_i is the work done by the inertia forces. Thus

$$\frac{\partial W}{\partial \delta_e} = H_e + P\frac{\partial s_P}{\partial \delta_e} + J\frac{\partial s_J}{\partial \delta_e} + \frac{\partial W_i}{\partial \delta_e} \qquad (a)$$

$$\frac{\partial W}{\partial \theta_J} = P\frac{\partial s_P}{\partial \theta_J} + J\frac{\partial s_J}{\partial \theta_J} + \frac{\partial W_i}{\partial \theta_J} \qquad (b) \qquad (11.3,3)$$

The kinematic derivatives $\partial s_P/\partial \delta_e$, etc., are simple constants, readily determined from the geometry of the linkage.

We now require the derivatives of W_i. The inertia force field is given by

$$d\mathbf{f}_i = -(\mathbf{a} - \ddot{\mathbf{r}}')\, dm \qquad (11.3,4)$$

where $\mathbf{a}$ is acceleration of dm relative to F_I given by (5.1,8) and $\mathbf{r}' = [x, y, z]^T$ is its position vector in F_B. The work done in a virtual displacement by this field is

$$\Delta W_i = \int (df_{x_i}\Delta x + df_{y_i}\Delta y + df_{z_i}\Delta z) \qquad (11.3,5)$$

where the integration is taken over the whole control system. To carry out this integration exactly clearly requires complete information about the masses, sizes, and locations of all the moving elements. It is in principle a straightforward albeit tedious process. In the interests of simplicity we neglect all contributions to W_i except those of the elevator surface itself, and that we treat as a lamina lying in the xy plane. The relevant geometry is shown in Fig. 11.5. The displacement of the element dm is in the direction Cz and of magnitude $\xi\,\Delta\delta_e$. Hence only the last term of (11.3,5) is nonzero, so that

$$\Delta W_i = \int df_{z_i}\xi\,\Delta\delta_e$$

On using (11.3,4) and (5.1,8), remembering that $z = \dot{x} = \dot{y} = 0$, we get

$$\Delta W_i = -\Delta\delta_e \int [a_{0_z} + x(pr - \dot{q}) + y(qr + \dot{p})]\xi\, dm \qquad (11.3,6)$$

It follows that

$$\frac{\partial W_i}{\partial \theta_J} = 0$$

$$\frac{\partial W_i}{\partial \delta_e} = -a_{0_z}\int \xi\, dm - (pr - \dot{q})\int x\, dm - (qr + \dot{p})\int y\xi\, dm \qquad (11.3,7)$$

Since elevators are normally symmetric about Cx, the last integral of (11.3,7)

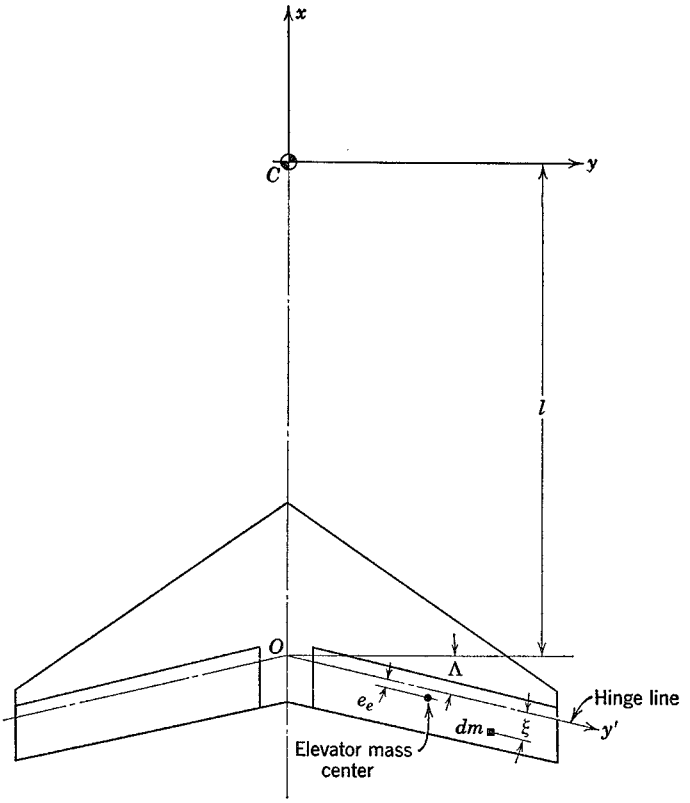

FIG. 11.5 Horizontal tail.

vanishes. The first is, by virtue of the definition of mass center,

$$\int \xi \, dm = m_e e_e \tag{11.3,8}$$

where m_e is the mass of both elevators, and e_e is as shown in Fig. 11.5. The second integral is the product of inertia of the elevator w.r.t. its hinge line and the y axis. It is denoted

$$\int x\xi \, dm = P_{ex} \tag{11.3,9}$$

Equations (11.3,7) now read

$$\frac{\partial W_i}{\partial \theta_J} = 0; \qquad \frac{\partial W_i}{\partial \delta_e} = -m_e e_e a_{0_z} - P_{ex}(pr - \dot{q}) \tag{11.3,10}$$

and finally, on combining (11.3,10) and (11.3,3) we get the generalized forces

$$\mathscr{F}_\delta = \frac{\partial W}{\partial \delta_e} = H_e + k_{11}P + k_{12}J - m_e e_e a_{0_z} - P_{ex}(pr - \dot{q}) \quad (11.3,11)$$

$$\mathscr{F}_\delta = \frac{\partial W}{\partial \theta_J} + k_{21}P + k_{22}J$$

where $[k_{ij}]$ is the matrix of kinematical gearings $\partial s_P/\partial \delta_e$, etc.

EQUATIONS OF MOTION

The equations of motion are obtained by substituting the generalized forces and the kinetic energy in Lagranges equations, i.e

$$I_e \ddot{\delta}_e + I_{eJ}\ddot{\theta}_J = H_e + k_{11}P + k_{12}J - m_e e_e a_{0_z} - P_{ex}(pr - \dot{q}) \qquad (a)$$

$$I_{eJ} \ddot{\delta}_e + I_J \ddot{\theta}_J = k_{21}P + k_{22}J \qquad (b)$$

(11.3,12)

The inertia terms on the r.h.s. of (*a*) are the only nonlinear ones, and in view of the assumptions already made, linearization of these is in order. a_{0_z} is the z component of the acceleration of the vehicle mass center and is given by (5.3,18). Without the Earth rotation terms, and for small disturbances, we get

$$a_{0_z} = \dot{w} - qu$$

From (4.3,4), in the linear case, $w = V\alpha_x$ and $u = V$, so that the linear expression for the acceleration is

$$a_{0_z} = V_e\dot{\alpha} - qV_e$$

and (11.3,12) become

$$I_e \ddot{\delta}_e + I_{eJ}\ddot{\theta}_J = H_e + k_{11}P + k_{12}J - m_e e_e V_e(\dot{\alpha} - q) + P_{ex}\dot{q} \qquad (a)$$

$$I_{eJ} \ddot{\delta}_e + I_J \ddot{\theta}_J = k_{21}P + k_{22}J \qquad (b)$$

(11.3,13)

These equations, when combined with the vehicle equations of motion, convert δ_e from a nonautonomous to an autonomous variable, add θ_J to the autonomous set, and introduce P and J as nonautonomous variables. The aerodynamic force H_e is a function of the state variables, i.e. [cf. (6.5,2)]

$$H_e = H_{e0} + H_V \Delta V + H_\alpha \Delta\alpha + H_{\dot{\alpha}}\dot{\alpha} + H_q q + H_\delta \Delta\delta_e + H_{\dot{\delta}} \dot{\delta}_e \qquad (c)$$

(11.3,13)

and provides aerodynamic coupling (feedback) between the vehicle motion and the control force. Similarly the terms containing α and q in (11.3,13*a*) provide inertial coupling between vehicle and control dynamics.

INERTIAL COUPLING

Although little can be done to influence the aerodynamic coupling, the inertial coupling is amenable to control by design. If the elevator mass center is on the hinge line, $e_e = 0$ and one coupling term vanishes—i.e. acceleration in the z direction will then not tend to induce motion of the control. With reference to Fig. 11.5, we can calculate P_{ex} as follows

$$\begin{aligned} P_{ex} &= \int \xi x \, dm \\ &= -lm_e e_e - \sin \Lambda \int \xi \, |y'| \, dm - \cos \Lambda \int \xi^2 \, dm \end{aligned} \tag{11.3,14}$$

For P_{ex} and e_e both to be zero, we would require

$$\sin \Lambda \int \xi \, |y'| \, dm + \cos \Lambda \int \xi^2 \, dm = 0 \tag{11.3,15}$$

This condition cannot be met if $\Lambda = 0$, but in principle can be if $\Lambda \neq 0$ by the addition of suitable balance weights. When both P_{ex} and e_e are zero we have complete *dynamic balance* of the elevator, and rigid body motion of the vehicle does not induce motion of the control.

The problem of reducing inertia coupling when aeroelastic flutter is the issue is similar to, but not the same as, that discussed here. The relevant product of inertia would in general be a different one [see (11.3,24)].

THE SERVO EQUATION

The pair of equations (11.3,13) do not normally give the whole picture. The control system illustrated in 11.4 is *intended* to operate with θ_J as near to zero as possible. Typically a hydraulic system for this application would sense θ_J as an error, and control the flow of high-pressure fluid to the piston so as to reduce it. A solenoid-controlled servo that could perform this function is illustrated in Fig. 11.6. The ports are such that the actuator is forced to follow the valve spool. In this case the error signal might be generated by a displacement transducer attached to the link AB of Fig 11.4 and used via an intervening electronic system to position the value spool. Alternatively, an entirely mechanical linkage could connect the valve spool to the pilot's control. Servos like this one have the characteristic that the volume rate of flow of oil is very nearly proportional to the valve error, regardless of load.

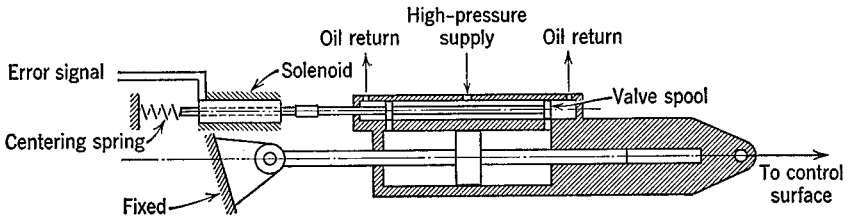

FIG. 11.6 Schematic of solenoid-controlled hydraulic servo.

Since the flow rate is proportional to the velocity of point A, which is a linear combination of $\dot{\delta}_e$ and $\dot{\theta}_J$, and since the valve error is proportional to θ_J, the servo equation in this case would be

$$a\dot{\delta}_e + \dot{\theta}_J = b\theta_J \tag{11.3,16}$$

Adding this equation to (11.3,13) completes the system, and has the effect of transferring J to the autonomous set of state variables, leaving only P as a nonautonomous input. The functioning of the servo itself in the neighborhood of an equilibrium point, as an uncoupled system, is described by putting ΔV, α, and $q = 0$, leading to the control system equations (in Laplace transforms)

$$\begin{bmatrix} (I_e s^2 - H_{\dot{\delta}} s - H_\delta) & I_{eJ} s^2 & -k_{12} \\ I_{eJ} s^2 & I_J s^2 & -k_{22} \\ as & s - b & 0 \end{bmatrix} \begin{bmatrix} \Delta\bar{\delta}_e \\ \bar{\theta}_J \\ \bar{J} \end{bmatrix} = \begin{bmatrix} k_{11} \\ k_{21} \\ 0 \end{bmatrix} \bar{P} \tag{11.3,17}$$

From this equation the $\Delta\bar{\delta}_e/\bar{P}$ transfer function can readily be found. The characteristic equation is found by expanding the determinant of the 3×3 matrix, and is a cubic.

If the servo is powerful enough that θ_J may be assumed to be identically zero, then a substantial simplification results. In that case (11.3,16) is superfluous and J can be eliminated via (11.3,12), i.e.

$$J = \frac{1}{k_{22}} (I_{eJ} \ddot{\delta}_e - k_{21} P) \tag{11.3,18}$$

If furthermore the inertial coupling I_{eJ} is negligibly small, which can be ensured by design, we get the desirable simple result

$$J = -\frac{k_{21}}{k_{22}} P = kP \tag{11.3,19}$$

Assuming both the above conditions to hold, the first system equation reduces to

$$(I_e s^2 - H_{\dot{\delta}} s - H_\delta) \Delta\bar{\delta}_e = \left(k_{11} - \frac{k_{12} k_{21}}{k_{22}}\right) \bar{P} \tag{11.3,20}$$

and gives a second-order transfer function connecting P and $\Delta\delta_e$. The corresponding equation with the α and q terms present is obtained from (11.3,13*a*) as

$$-H_V \Delta\bar{V} + [(m_e e_e V_e - H_{\dot{\alpha}})s - H_\alpha]\ \Delta\bar{\alpha} - (P_{ex}s + m_e e_e V_e + H_q)\bar{q} + (I_e s^2 - H_{\dot{\delta}}s - H_\delta)\,\Delta\bar{\delta}_e = K\bar{P} \quad (11.3,21)$$

where $$K = k_{11}\left(1 - \frac{k_{12}k_{21}}{k_{11}k_{22}}\right)$$

Although perfect dynamic balance of the elevator surface may not always be achieved, the inertia coupling terms are often small. If they can be neglected, we get the simplest equation that still contains the essential ingredients of the control dynamics—i.e. the inertia of the control elements and the aerodynamic feedbacks:

$$-H_V \Delta\bar{V} - (H_{\dot{\alpha}}s + H_\alpha)\,\Delta\bar{\alpha} - H_q\bar{q} + (I_e s^2 - H_{\dot{\delta}}s - H_\delta)\,\Delta\bar{\delta}_e = K\bar{P} \quad (a) \quad (11.3,22)$$

With similar assumptions, the equations for the other two control systems are

Rudder system:

$$-H_\beta\beta - H_p\bar{p} - H_r\bar{r} + (I_r s^2 - H_{\dot{\delta}}s - H_\delta)\,\bar{\delta}_r = K_r\bar{P}_r \quad (b)$$

Aileron system: (11.3,22)

$$-2H_p\bar{p} - 2H_r\bar{r} + (I_a s^2 - 2H_{\dot{\delta}}s - 2H_\delta)\,\bar{\delta}_a = K_a\bar{P}_a \quad (c)$$

For the aileron system, δ_α is the downward deflection of the right-hand surface, assumed equal to the upward deflection of the left-hand surface. I_a is the generalized inertia of the entire system comprising both surfaces and all connected parts, but H is the aerodynamic hinge moment on *one* surface only.

COUPLING OF CONTROLS WITH ELASTIC DEGREES OF FREEDOM

In Sec. 5.12 we presented equations of motion for elastic modes with controls locked in a fixed position, and in the preceding section we have developed the control equations for a rigid airplane. Thus, coupling between controls and elastic motions has been excluded. In fact, as is clear from the existence of the aileron reversal phenomenon (Sec. 8.4), and the effect of flexibility on elevator effectiveness (Sec. 7.4), there are important couplings between the control degrees of freedom and the elastic degrees of freedom. To include these entails modifications to both the elastic equations (5.12,7) and (5.12,12) and control system equations such as (11.3,12). The details depend on

which control system is being considered—aileron, elevator, or rudder—and on its particular design features. We illustrate the process by considering the elevator surface and its coupling with z deflections of the vehicle. We treat a case of one degree of freedom by stipulating $\theta_J = 0$.

The deflection of the structure from the reference position is now given by [cf. (5.12,1)]

$$z'(t) = \sum_{n=0}^{\infty} h_n(x_0, y_0, z_0)\epsilon_n(t) + h_\delta \Delta\delta_e(t)$$

where h_δ is zero except for points of the elevator, where it is $h_\delta = \xi$ and ξ is the distance from the elevator hinge line, as shown on Fig. 11.5. Now the displacement function represented by the last term is not in general orthogonal to the h_n, and hence the integrals of its products with them that appear in the kinetic energy do not vanish. This leads to the appearance of an additional term on the l.h.s. of (5.12,7), viz. (an exercise for the reader)

$$I_n(\ddot{\epsilon}_n + 2\zeta_n\omega_n\dot{\epsilon}_n + \omega_n{}^2\epsilon) + I_{n\delta}\,\ddot{\delta}_e = \mathscr{F}_n \qquad (11.3,23)$$

where

$$I_{n\delta} = \int h_n \xi \, dm$$

the integral being taken over the elevator.

Similarly, the l.h.s. of (11.3,13a) (with $\theta_J = 0$) becomes

$$I_e\,\ddot{\delta}_e + \sum_{n=0}^{\infty} I_{n\delta}\ddot{\epsilon}_n = \cdots \qquad (11.3,24)$$

The terms containing $I_{n\delta}$ in these equations represent inertial couplings between the elevator and elastic degrees of freedom. That in (11.3,23) corresponds to "tail wags dog," i.e. acceleration $\ddot{\delta}_e$ of the elevator generates motion in the nth elastic mode. This may be expected to be a small effect in most cases. That in (11.3,24) represents the converse, "dog wags tail," i.e. elastic mode accelerations $\ddot{\epsilon}_n$ generate motion of the elevator. This contribution is very significant in relation to control-surface flutter, and is minimized by proper mass balancing of the control surface to reduce $I_{n\delta}$ for the critical elastic mode.

The remaining modifications to the equations of motion occur on the r.h.s. For the elastic modes the only addition is one aerodynamic term to $\mathscr{F}_n$, i.e. $A_{n\delta}\,\Delta\delta_e$ to (5.12,12) or $G_{n\delta}\,\Delta\delta_e$ to (5.12,13). These aerodynamic contributions to elastic motion are usually important. The addition to the control equation is also an aerodynamic coupling. There H_e in (11.3,13c) becomes

$$H_e = \cdots + \sum_{n=0}^{\infty} H_{n\delta}\epsilon_n \qquad (11.3,25)$$

In summary, the elastic and control equations are both modified by additional simple inertial terms on the l.h.s and by aerodynamic terms on the r.h.s.

11.4 EXAMPLE—STABILITY AUGMENTATION SYSTEM FOR STOL AIRPLANE

In Sec. 9.8, where we considered an example STOL airplane, we found that the spiral mode was unstable, with an uncomfortably short time to double. We remarked there that a feedback stability augmentation system might be useful. How should we proceed to synthethize such a system? We can choose any of (β, p, r) as variables to sense, and feedback functions of them [cf. (11.2,1)] to produce command signals for the aileron and/or rudder. But which variables shall we choose and what functions of them shall we use? Here the "flight dynamicist's approach" of looking at the feedback control system as a way of modifying the aerodynamic derivatives (Sec. 11.1) is helpful. The full set of synthetic changes that can be made in the six lateral moment derivatives is described by the relations

$$\Delta\begin{bmatrix} L_\beta & N_\beta \\ L_p & N_p \\ L_r & N_r \end{bmatrix} = [k_{ij}]^T \begin{bmatrix} L_{\delta_a} & N_{\delta_a} \\ L_{\delta_r} & N_{\delta_r} \end{bmatrix} \tag{11.4,1}$$

where $[k_{ij}]$ is the 2×3 matrix of feedback gains, i.e.

$$\begin{bmatrix} \Delta\delta_a \\ \Delta\delta_r \end{bmatrix} = [k_{ij}] \begin{bmatrix} \beta \\ p \\ r \end{bmatrix} \tag{11.4,2}$$

Thus for example,

$$\Delta\delta_a = k_{11}\beta + k_{12}p + k_{13}r$$

and

$$\Delta N_p = k_{12}N_{\delta_a} + k_{22}N_{\delta_r} \tag{11.4,3}$$

Equations (11.4,2) are written in dimensional rather than nondimensional form, since the sensing devices used to generate the feedback signals would ordinarily operate on the dimensional physical variables.

These relations must now be applied with good engineering judgment. Stumbling about blindly in the six-dimensional parameter space of the k_{ij} is not a satisfactory way to find the solution. First, the number of nonzero k_{ij} must be kept to a minimum, since each one entails extra hardware or circuitry, adding to weight, cost, complexity, and failure probability. Second, the engineer must take advantage of his understanding of the system and of the

fault to be corrected. Here the fault is that the spiral mode is unstable, the other two modes being stable. We know that the criterion for spiral stability in horizontal flight is (9.7,6)

$$(C_{l_\beta}C_{n_r} - C_{l_r}C_{n_\beta}) > 0 \tag{11.4,4}$$

and that it must be the violation of this criterion that is the cause of the instability. On examining Table 9.9—for example at $C_{W_e} = 4.0$—we find the left hand side of (11.4,3) to be

$$(.010)(-.25) - (.67)(.120) < 0$$

We also observe that there is no hope of correcting the situation without changing the sign of one of the four derivatives. In fact the one to which our attention is naturally directed is C_{l_β}, which is here positive, but is ordinarily negative for "well-behaved" airplanes. A "synthetic" C_{l_β} of the required sign can be introduced by aileron feedback of the form

$$\Delta\delta_a = k_{11}\beta, \qquad k_{11} > 0$$

In fact, an attempt at a solution based on this sideslip feedback for $C_{W_e} = 4.0$ was unsuccessful. When k_{11} was made large enough to stabilize the spiral mode, the lateral oscillation was driven unstable. Now we observe from (9.7,13) that C_{n_r} is the main factor available to control the damping of the lateral oscillation and hence an increase in $|C_{n_r}|$ is indicated. This is also beneficial in meeting (11.4,4) when combined with a change of sign of C_{l_β}. We therefore choose a second nonzero gain, k_{23}, so that the control deflections are given by

$$\begin{aligned} \Delta\delta_a &= k_{11}\beta \qquad k_{11} > 0 \\ \Delta\delta_r &= k_{23}r \qquad k_{23} > 0 \end{aligned} \tag{11.4,5}$$

The control derivatives assumed for this example, representative of those that pertain to a deflected slipstream configuration, are

$$\begin{aligned} C_{l_{\delta_a}} &= -.13/\text{rad} \qquad C_{n_{\delta_r}} = -.30/\text{rad} \\ C_{n_{\delta_a}} &= +.04/\text{rad} \qquad C_{l_{\delta_r}} = +.04/\text{rad} \end{aligned}$$

With these derivatives, and a control law given by (11.4,5), values of k_{11} and k_{23} can readily be found that eliminate the instability in the spiral mode while maintaining a stable lateral oscillation. In point of fact it is only a little more difficult in this case to incorporate a more realistic feedback law than the simple gains of (11.4,5). Consequently the example has not been computed with (11.4,5) but rather by assuming that each control actuator

is a first-order dynamic system of fast response time. The corresponding control equations used were

$$\begin{bmatrix} \dot{\delta}_a \\ \dot{\delta}_r \end{bmatrix} = -\begin{bmatrix} 10\,\Delta\delta_a \\ 12\,\Delta\delta_r \end{bmatrix} + \begin{bmatrix} K_{11} & 0 \\ 0 & K_{23} \end{bmatrix} \begin{bmatrix} \beta \\ r \end{bmatrix} \tag{11.4,6}$$

which implies that the time constants of the aileron and rudder position servos are, respectively, $\frac{1}{10}$ and $\frac{1}{12}$ sec, that there are zero time lags in the β and r sensors, and that the steady-state gains are

Aileron: $k_{11} = K_{11}/10$ deg/deg

Rudder: $k_{23} = K_{23}/12$ deg/(deg/sec)

Equations (11.4,6) are now incorporated into the basic lateral equations of motion to yield the final mathematical system. After converting (11.4,6) to nondimensional form, we get the result (11.4,7). The eigenvalues of (11.4,7)

$$\begin{bmatrix} D\beta \\ D\hat{p} \\ D\hat{r} \\ D\phi \\ D\delta_a \\ D\delta_r \end{bmatrix} = \begin{bmatrix} \frac{Cy_\beta}{2\mu} & \frac{Cy_p}{2\mu} & \frac{Cy_r}{2\mu} - \frac{1}{A} & \frac{Cw_e}{2\mu} & 0 & 0 \\ \frac{Cl_\beta}{\hat{I}'_x} & \frac{Cl_p}{\hat{I}'_x} & \frac{Cl_r}{\hat{I}'_x} & 0 & \frac{Cl_{\delta_a}}{\hat{I}'_x} & \frac{Cl_{\delta_r}}{\hat{I}'_x} \\ \frac{Cn_\beta}{\hat{I}'_z} & \frac{Cn_p}{\hat{I}'_z} & \frac{Cn_\beta}{\hat{I}'_z} & 0 & \frac{Cn_{\delta_a}}{\hat{I}'_z} & \frac{Cn_{\delta_r}}{\hat{I}'_z} \\ 0 & \frac{1}{A} & 0 & 0 & 0 & 0 \\ K_{11}t^* & 0 & 0 & 0 & -10t^* & 0 \\ 0 & 0 & \frac{K_{23}}{A} & 0 & 0 & -12t^* \end{bmatrix} \begin{bmatrix} \beta \\ \hat{p} \\ \hat{r} \\ \phi \\ \Delta\delta_a \\ \Delta\delta_r \end{bmatrix} \tag{11.4,7}$$

were calculated for ranges of K_{11} and K_{23}, and a typical root locus is shown on Fig. 11.7. There is a substantial range of practical gains for which stability is achieved. For example for $K_{11} = 10$, $K_{23} = 20$, the spiral and Dutch-roll characteristics are

Spiral: $t_{1/2} = 7.4$ sec

Oscillation: $T = 12.4$ sec, $N_{1/2} = .21$ cycles

The corresponding control gains are, respectively, 1 deg/deg for the aileron, and 1.67 deg/(deg/sec) for the rudder. These are both quite modest, and would not likely present any exceptional problems of control design.

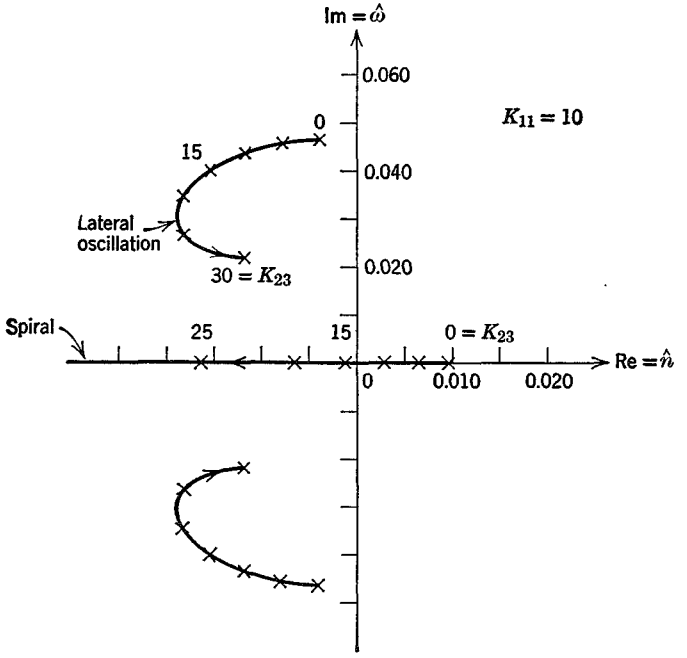

FIG. 11.7 Root loci for stability augmentation system.

ELIMINATION OF STEADY-STATE RUDDER ANGLE

The solution presented above contains a feature which could possibly be undesirable—i.e. there is a steady-state rudder angle associated with constant yaw rate r. This means that the autopilot would generate a rudder deflection during steady turns, with $\delta_r > 0$ for right turns and vice versa. This is opposite to the rudder deflection wanted in the turn (see Sec. 10.4), and hence we have the autopilot opposing the human pilot. If this situation occurred with any frequency, the pilot rating of the aircraft would be adversely affected. On the other hand, $C_{W_e} = 4.0$ represents a very low speed, presumably associated only with landing and take-off, and not ordinarily with turning flight. Thus it would depend on factors somewhat outside the scope of this example whether this steady-state behavior of the autopilot presented a problem or not.

In cruising flight this problem would be more serious, and it would be desired to eliminate it. We illustrate here how it could be done.

The steady-state response of the rudder system can be eliminated by incorporating what amounts to a high-pass filter with zero static gain† in the rudder loop, as shown in Fig. 11.8. The feedback element $K_{23}\tau s/(1 + \tau s)$

† A "washout" circuit.

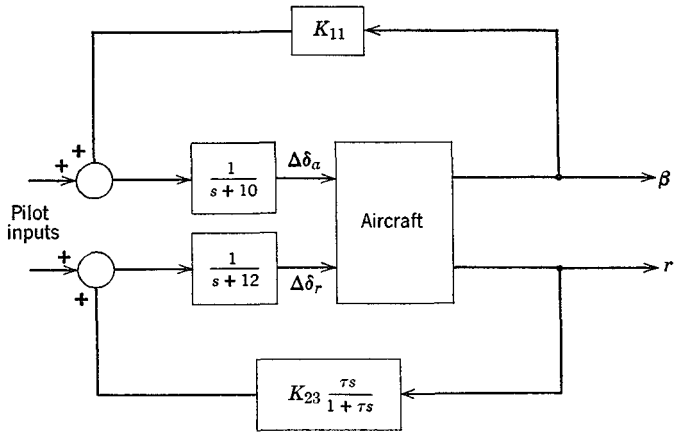

FIG. 11.8 Stability augmentation system for STOL airplane.

has zero static gain (see Sec. 3.2), so that δ_r is zero when $r = \text{const}$. The frequency response of this element is

$$G(i\omega) = \frac{K_{23} i\omega t}{1 + i\omega t} \tag{11.4,8}$$

so that for $\omega\tau \to \infty$, $G(i\omega) \to K_{23}$. Thus by proper choice of τ, the filter can be made to behave like a simple gain of K_{23} above a chosen frequency ω_1. To analyze the system with the filter incorporated, we could find the overall transfer function of the closed-loop system and calculate the roots of the characteristic equation, or alternatively we can modify (11.4,7) to correspond to Fig. 11.8. The latter procedure is by far the simpler in the present instance. The only respect in which (11.4,7) does not apply is in the last of the equations, which now must correspond to

$$\frac{K_{23}\tau s}{1 + \tau s} \cdot \frac{1}{s + 12} \cdot \bar{r} = \Delta\bar{\delta}_r \tag{11.4,9}$$

or

$$[12 + (1 + 12\tau)s + \tau s^2]\,\Delta\bar{\delta}_r = K_{23}\tau s\bar{r}$$

The corresponding differential equation is

$$12\,\Delta\delta_r + (1 + 12\tau)\,\dot{\delta}_r + \tau\ddot{\delta}_r = K_{23}\tau\dot{r} \tag{11.4,10}$$

After conversion to nondimensional form, this becomes

$$D^2\delta_r + (1 + 12\tau)\frac{t^*}{\tau} D\delta_r + \frac{12t^{*2}}{\tau}\Delta\delta_r = \frac{K_{23}}{A} D\hat{r} \tag{11.4,11}$$

On defining a new variable ζ, we can replace this second-order equation by a pair of first-order ones, i.e.

$$\begin{aligned} D\delta_r &= \zeta \\ D\zeta &= \frac{K_{23}}{A} D\hat{r} - 12\frac{t^{*2}}{\tau}\Delta\delta_r - (1 + 12\tau)\frac{t^*}{\tau}\zeta \end{aligned} \tag{11.4,12}$$

The last of (11.4,7) has now to be replaced by the pair (11.4,12). In doing so we eliminate $D\hat{r}$ from (11.4,12) by using the third equation of (11.4,7). The result is shown as (11.4,13).

Computations made with (11.4,13) show that the effect of the autopilot in correcting the spiral instability is very much reduced by the filter unless τ is very large (Fig. 11.9), in which case the effectiveness of the washout circuit is impaired. As has been pointed out previously, however, a slow divergence of the spiral mode is not unacceptable, so a compromise solution is possible without excessive values of τ. For example, with $K_{11} = 15$, $K_{23} = 20$ and $\tau = 10$ sec the modal characteristics are

Spiral: $t_{\text{double}} = 18.1$ sec

Oscillation: $T = 11.4$ sec, $N_{1/2} = .56$ cycles

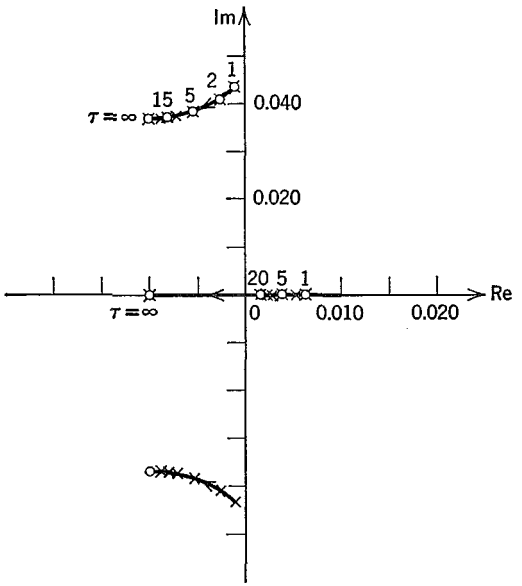

FIG. 11.9 Effect of washout circuit on lateral roots. $K_{11} = 15$, $K_{23} = 20$.

$$
\begin{bmatrix} D\beta \\ D\hat{p} \\ D\hat{r} \\ D\phi \\ D\delta_a \\ D\delta_r \\ D\zeta \end{bmatrix} =
\left[\begin{array}{c|c|c|c|c|c|c}
\frac{C_{y_\beta}}{2\mu} & \frac{C_{y_p}}{2\mu} & \frac{C_{y_r}}{2\mu} - \frac{1}{A} & \frac{C_{W_e}}{2\mu} & 0 & 0 & 0 \\
\hline
\frac{C_{l_\beta}}{\hat{I}'_x} & \frac{C_{l_p}}{\hat{I}'_x} & \frac{C_{l_r}}{\hat{I}'_x} & 0 & \frac{C_{l_{\delta_a}}}{\hat{I}'_x} & \frac{C_{l_{\delta_r}}}{\hat{I}'_x} & 0 \\
\hline
\frac{C_{n_\beta}}{\hat{I}'_z} & \frac{C_{n_p}}{\hat{I}'_z} & \frac{C_{n_r}}{\hat{I}'_z} & 0 & \frac{C_{n_{\delta_a}}}{\hat{I}'_z} & \frac{C_{n_{\delta_r}}}{\hat{I}'_z} & 0 \\
\hline
0 & \frac{1}{A} & 0 & 0 & 0 & 0 & 0 \\
\hline
K_{11}t^* & 0 & 0 & 0 & -10t^* & 0 & 0 \\
\hline
0 & 0 & 0 & 0 & 0 & 0 & 1 \\
\hline
\frac{K_{23}}{A}\frac{C_{n_\beta}}{\hat{I}'_z} & \frac{K_{23}}{A}\frac{C_{n_p}}{\hat{I}'_z} & \frac{K_{23}}{A}\frac{C_{n_r}}{\hat{I}'_z} & 0 & \frac{K_{23}}{A}\frac{C_{n_{\delta_a}}}{\hat{I}'_z} & \frac{K_{23}}{A}\frac{C_{n_{\delta_r}}}{\hat{I}'_z} - 12t^{*2}/\tau & -(1 + 12\tau)\frac{t^*}{\tau}
\end{array}\right]
\begin{bmatrix} \beta \\ \hat{p} \\ \hat{r} \\ \phi \\ \Delta\delta_a \\ \Delta\delta_r \\ \zeta \end{bmatrix}
$$

(11.4,13)

11.5 EXAMPLE—ALTITUDE AND GLIDE-PATH CONTROL

One of the most important problems in the control of flight path is that of following a prescribed line in space, as defined for example by a radio beacon. This is crucial in the landing situation under poor visibility when the airplane flies down the ILS glide slope. We shall discuss this case by considering first a simple approximate model that reveals the main features, and then examining a more realistic, and hence more complicated case.

FLIGHT AT EXACTLY CONSTANT HEIGHT—SPEED STABILITY

The first mathematical model we consider can be regarded as that corresponding to horizontal flight when a "perfect" autopilot controls the angle of attack in such a way as to keep the height error exactly zero. The result will show that the speed variation is stable at high speeds, but unstable at speeds below a critical value near the minimum drag speed. Neumark (11.2) recounts that this criterion was first discovered *in 1910* by Painlevé, and that it was at first accepted by aeronautical engineers and scientists, but later, on the basis of the theory of the phugoid which showed no such effect, was rejected as false. In fact, to the extent that a pilot can control height error by elevator control alone, i.e. to the extent that he approximates the ideal autopilot we have postulated, the instability at low speed will be experienced in manual flight. Since speed variation is the most noticeable feature of this phenomenon, it is commonly referred to as *speed stability.*

The analysis that follows is essentially that of Neumark, but adapted to the notation and methods of this book. The basic assumption that the flight path is *exactly* horizontal implies $\gamma = 0$, or $\theta = \alpha_x$ (see Fig. 4.4.), whence $\Delta\theta = \Delta\alpha$. An exactly horizontal flight path also implies $L \equiv W$. The pitching moment equation is specified to be identically satisfied by means of an appropriate but unspecified control device that supplies the needed pitching moment as required. The system equations are then (5.13,19) with $\Delta\alpha = \Delta\theta$, $\gamma_e = 0$ and the third equation missing. We further specify that $\alpha_T = 0$. The equations are then

$$\left[\begin{array}{c} D\hat{V} \\ \hline D\alpha \\ \hline D\alpha \end{array}\right] = \left[\begin{array}{c|c|c|c} \frac{1}{2\mu}(C_{T_V} - C_{D_V}) & \frac{1}{2\mu}(C_{L_e} - C_{D_\alpha}) & 0 & -\frac{C_{W_e}}{2\mu} \\ \hline -\frac{C_{L_V} + 2C_{W_e}}{2\mu + C_{L_\alpha}} & -\frac{C_{L_\alpha} + C_{D_e}}{2\mu + C_{L_\alpha}} & \frac{2\mu - C_{L_q}}{2\mu + C_{L_\alpha}} & 0 \\ \hline 0 & 0 & 1 & 0 \end{array}\right] \left[\begin{array}{c} \Delta\hat{V} \\ \hline \Delta\alpha \\ \hline \hat{q} \\ \hline \Delta\alpha \end{array}\right] \tag{11.5,1}$$

We now make some simplifying approximations, i.e. that the speed derivatives C_{D_V} and C_{L_V} are negligible and that $2\mu \gg C_{L_{\dot{\alpha}}}$, C_{L_q}. Actually these are very weak approximations for a conventional airplane in cruise configuration. On combining the $\Delta\alpha$ terms of the first two equations, eliminating $\hat{q}$ by means of the third, and observing that $C_{L_e} = C_{W_e}$, we get

$$\begin{aligned} 2\mu D\hat{V} &= C_{T_V}\,\Delta\hat{V} - C_{D_\alpha}\Delta\alpha \\ 0 &= 2C_{L_e}\,\Delta\hat{V} + C_{L_\alpha}\Delta\alpha \end{aligned} \tag{11.5,2}$$

Elimination of $\Delta\alpha$ yields the first-order speed equation

$$2\mu D\hat{V} = \left(C_{T_V} + 2C_{D_\alpha}\frac{C_{L_e}}{C_{L_\alpha}}\right)\Delta\hat{V} \tag{11.5,3}$$

The speed variation following an initial speed error $\Delta\hat{V}_0$ is clearly exponential,

$$\Delta\hat{V} = \Delta\hat{V}_0 e^{t/\hat{T}}$$

with time constant given by

$$\hat{T}^{-1} = \frac{1}{2\mu}\left(C_{T_V} + 2C_{L_e}\frac{C_{D_\alpha}}{C_{L_\alpha}}\right)$$

and time to half by

$$t_{1/2} = -.693t^*\hat{T}\ \text{sec} \tag{11.5,4}$$

We must now specify a propulsion system in order that C_{T_V} may be determined. The result finally obtained depends on this choice, but only in the actual value of the critical speed, not its existence. We arbitrarily choose a constant-thrust engine, for which (see Table 7.1)

$$C_{T_V} = 2C_{T_e} = -2C_{D_e}$$

Equations (11.5,4) then yield

$$t_{1/2} = -.693t^*\left[\frac{C_{L_e}}{\mu}\left(\frac{C_{D_\alpha}}{C_{L_\alpha}} - \frac{C_{D_e}}{C_{L_e}}\right)\right]^{-1} \tag{11.5,5}$$

The factor in the inner parentheses can be rewritten as

$$\left(\frac{dC_D}{dC_L} - \frac{C_D}{C_L}\right)$$

where dC_L/dC_D is the slope of the tangent to the drag polar, and C_L/C_D is the slope of the secant, see Fig. 10.2. Just as in Sec. 10.2, Eq. (10.2,17), this factor passes through zero at the point C'_L, C'_D where L/D is a maximum. It is positive for $C_L > C'_L$ and negative for $C_L < C'_L$. If V' be the speed

corresponding to $(L/D)_{\max}$, then the speed variation is seen to be stable for $V > V'$, but unstable for $V < V'$. That is, speed errors will die out at high speeds, but grow at low speeds. This phenomenon is seen to be related to the change of sign of $K_{y\delta}$ that occurs at the same critical speed (Sec. 10.2).

NUMERICAL EXAMPLE

The jet transport of Sec. 9.1 is used for the example, in horizontal flight at sea level. The data needed for the calculation is as follows:

$$C_{D_e} = .016 + \frac{C_{L_e}^2}{7\pi}; \qquad C_{L_\alpha} = 4.88; \qquad \frac{dC_D}{dC_L} = \frac{2}{7\pi} C_L$$

$$W/S = 60 \text{ psf}; \qquad \mu = 101.8; \qquad \rho = .002378$$

$$V_e = [2(W/S)/\rho C_{L_e}]^{1/2}; \qquad t^* = 7.70/V_e$$

With this data, the values of C_{L_e} and V_e at $(L/D)_{\max}$ are, respectively, $C_L' = .595$ and $V' = 290$ fps. The result of the calculation with (11.5,5) is shown in Fig. 11.10. There is positive "speed stability" above 290 fps, but the characteristic time to half is large, in excess of 75 sec. In the low-speed range (sometimes referred to as "the backside of the polar," with reference to the $C_L - C_D$ "polar" diagram), the motion is unstable, with time to double falling as low as 30.5 sec at $C_{L_e} = 1.6$. A low-speed landing approach with this speed characteristic is undesirable from a handling-qualities standpoint (see Sec. 12.8). On the other hand, the example corresponds to cruising flight, not landing, since wheels and flaps are retracted.

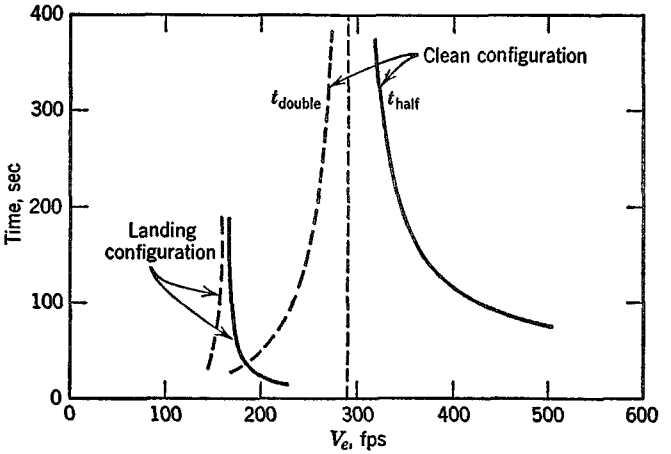

FIG. 11.10 Speed stability of jet transport at sea level.

The speed stability is in fact quite sensitive to the drag characteristics of the airplane. Thus, suppose that undercarriage and flaps have been lowered on the jet transport, with large increases in parasite and included drag reflected in the polar equation

$$C_D = 0.20 + \frac{1.2 C_L^2}{7\pi} \tag{11.5,6}$$

The results for this case, also shown on Fig. 11.10, are very different. The divergence time to double is now greater than 30 sec for all speeds above about 99 mph.

FLIGHT ON ILS GLIDE SLOPE

In the above analysis, we assumed that the airplane was under the control of an ideal autopilot that kept the height error exactly zero. A more realistic model incorporates a feedback control that senses height error and actuates the elevator† in response (see Fig. 11.11). The time lag associated with response of height to elevator input may be expected to lead to stability characteristics significantly different from those of the simple model.

Let us assume then that the airplane is making an automatically controlled approach on ILS. That is, a radio beam defines the glide path, and the pitch autopilot is coupled to the radio signal in such a way that height error is sensed and actuates the elevator. The autopilot and control system are

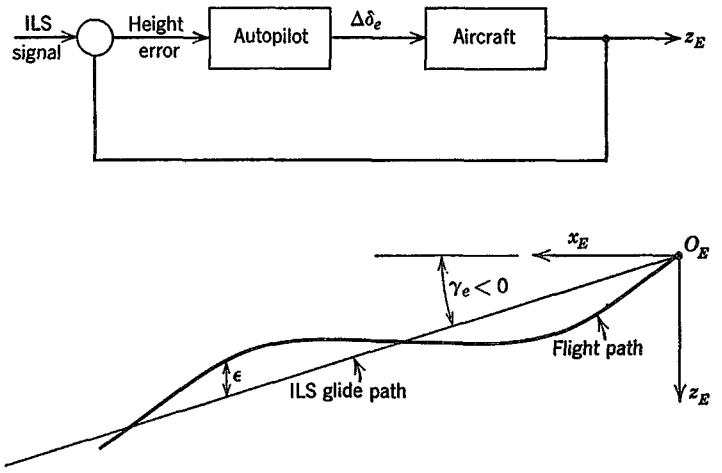

FIG. 11.11 Automatic control of glide path.

† A still more sophisticated system uses control of thrust as well as of elevator. This is capable of producing better system performance provided that thrust responds quickly enough to the control command.

relatively fast-acting compared to the pitch response of the vehicle, so we may reasonably assume a simple gain for the transfer function of these elements. Thus the mathematical model is obtained from (5.13,19) with the additional control law

$$\Delta\delta_e = K_1\epsilon + K_2\dot{\epsilon} \tag{11.5,7}$$

where ϵ is the height error and we have included both proportional and rate terms.

For the class of airplane considered, the standard glide slope is about $2\frac{1}{2}$ to 3°, so little error is introduced by using the equations for $\gamma_e = 0$, and this we do. The height error is defined as

$$\epsilon \doteq z_{E_i} - z_E \tag{11.5,8}$$

where z_{E_i} is the commanded altitude. Thus combining (11.5,7 and 8) we get

$$\Delta\delta_e = -K_1 z_E - K_2\dot{z}_E + K_1 z_{E_i} + K_2\dot{z}_{E_i}$$

which in nondimensional form is

$$\Delta\delta_e = -K_1\frac{\bar{c}}{2}\hat{z}_E - K_2 V_e D\hat{z}_E + K_1\frac{\bar{c}}{2}\hat{z}_{E_i} + K_2 V_e D\hat{z}_{E_i} \tag{11.5,9}$$

From the last of (5.13,19), for $\gamma_e = 0$, we have

$$D\hat{z}_E = -\Delta\gamma = \Delta\alpha - \Delta\theta$$

from which we get

$$\Delta\delta_e = -K_1\frac{\bar{c}}{2}\hat{z}_E - K_2 V_e(\Delta\alpha - \Delta\theta) + K_1\frac{\bar{c}}{2}\hat{z}_{E_i} + K_2 V_e D\hat{z}_{E_i} \tag{11.5,10}$$

For the control inputs in (5.13,19) we take

$$\Delta C_{T_c} = \Delta C_{D_c} = \Delta C_{L_c} = 0$$

and

$$\Delta C_{m_c} = C_{m_\delta}\Delta\delta_e \tag{11.5,11}$$

We assume additionally that a number of derivatives are zero (as in Sec. 9.1), i.e.

$$C_{D_V} = C_{L_V} = C_{m_V} = C_{L_q} = C_{L_{\dot{\alpha}}} = 0$$

The basic system derived from (5.13,19) is then 5×5, with variables $\Delta\hat{V}$, $\Delta\alpha$, $\hat{q}$, $\Delta\theta$, $\hat{z}_E$, with ΔC_{m_c} eliminated via (11.5,10 and 11). The result is given

as (11.5,12).

$$
\begin{bmatrix} D\hat{V} \\ D\alpha \\ D\hat{q} \\ D\theta \\ D\hat{z}_E \end{bmatrix} = \left[\begin{array}{c|c|c} \frac{C_{T_V}}{2\mu} & \frac{C_{L_e} - C_{D_\alpha}}{2\mu} & 0 \\ \hline \frac{-C_{W_e}}{\mu} & -\frac{C_{L_\alpha} + C_D}{2\mu} & 1 \\ \hline -\frac{C_{m_{\dot\alpha}} C_{W_e}}{\hat{I}_y \mu} & \frac{1}{\hat{I}_y}\left[C_{m_\alpha} - \frac{C_{m_{\dot\alpha}}(C_{L_\alpha} + C_{D_e})}{2\mu} - C_{m_\delta} K_2 V_e\right] & \frac{C_{m_q} + C_{m_{\dot\alpha}}}{\hat{I}_y} \\ \hline 0 & 0 & 1 \\ \hline 0 & 1 & 0 \end{array}\right]
$$

$$
\left[\begin{array}{c|c} \frac{-C_{W_e}}{2\mu} & 0 \\ \hline 0 & 0 \\ \hline \frac{K_2 V_e C_{m_\delta}}{\hat{I}_y} & \frac{C_{m_\delta} K_1 \bar{c}}{2\hat{I}_y} \\ \hline 0 & 0 \\ \hline -1 & 0 \end{array}\right] \left[\begin{array}{c} \Delta\hat{V} \\ \hline \Delta\alpha \\ \hline \hat{q} \\ \hline \Delta\theta \\ \hline \hat{z}_E \end{array}\right] + \left[\begin{array}{c} 0 \\ \hline 0 \\ \hline \frac{C_{m_\delta}}{\hat{I}_y}\left(K_1 \frac{\bar{c}}{2} \hat{z}_{E_i} + K_2 V_e D\hat{z}_{E_i}\right) \\ \hline 0 \\ \hline 0 \end{array}\right] \qquad (11.5,12)
$$

NUMERICAL EXAMPLE

Computations of the stability and performance were carried out with (11.5,12) for the same jet transport airplane used in preceding examples, flying at sea level. The drag polar is (11.5,6) corresponding to the landing configuration. The data that differ from those of Sec. 9.1 are as follows:

$$
\begin{aligned} C_{D_\alpha} &= .959, \qquad t^* = .0460 \text{ sec}, \qquad \mu = 101.8, \\ V_e &= 167.4 \text{ fps}, \qquad C_{W_e} = 1.8, \qquad C_{D_e} = .377 \end{aligned}
$$

The eigenvalues corresponding to a range of K_1 and K_2 are shown on Fig. 11.12 in the form of root loci. Point A corresponds to the uncontrolled phugoid, and increasing proportional gain K_1 with zero rate gain produces the branch AB of the locus. The system rapidly goes unstable without error-rate control, but is easily stabilized with a modest value of K_2. For example, at point C on Fig. 11.12, with $K_1 = .002$ (about 12° elevator per 100 ft of height error) and $K_2 = .010$ (about 12° elevator per 20 ft/sec height error-rate), the eigenvalue characteristics are:

Phugoid: period = 10.4 sec
$N_{1/2} = .54$
Three real roots: $t_{\text{halt}} = 94.0, 1.68, 0.86$ sec

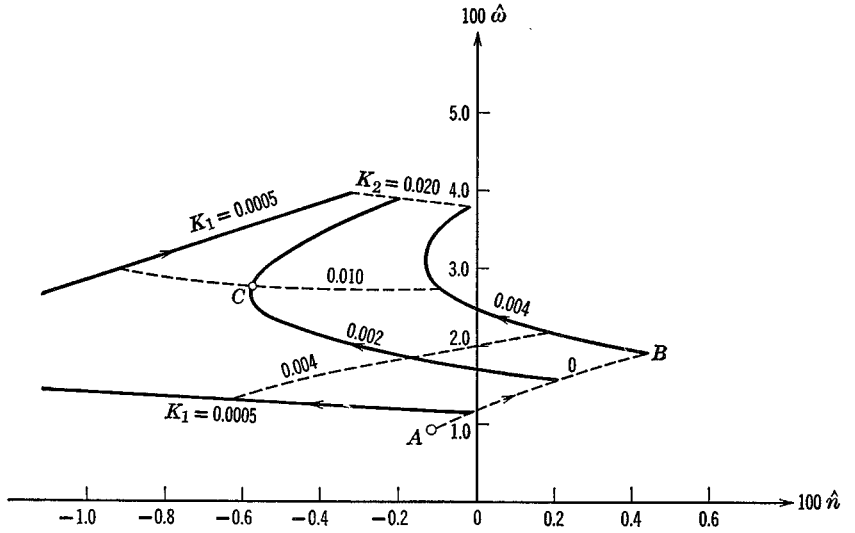

FIG. 11.12 Root locus of glide-path controller.

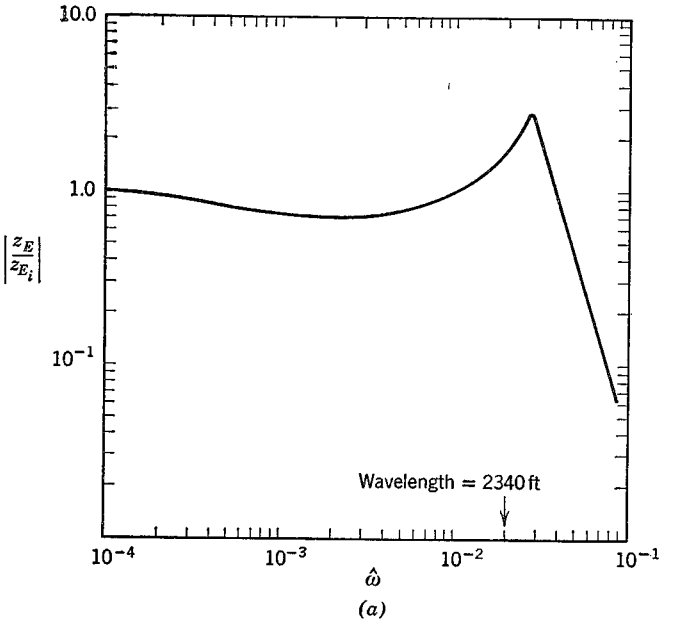

FIG. 11.13 Response of automatic glide-path controller. (*a*) Amplitude. (*b*) Phase angle.

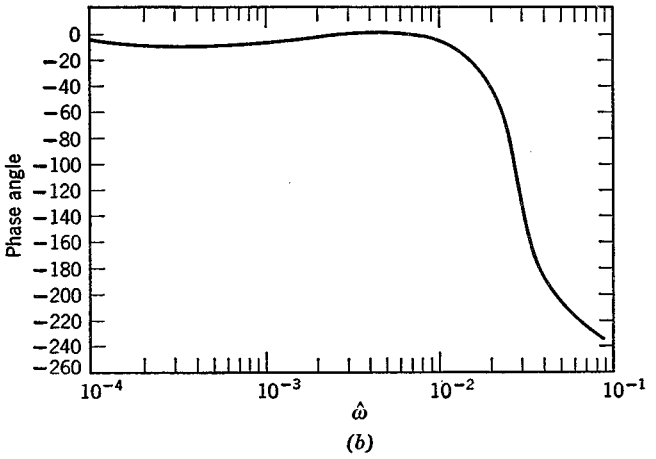

(b)

FIG. 11.13 *(Contd.)*

The short-period mode has disappeared, being replaced by a pair of real roots, and the third real root is associated with the extra degree of freedom.

The performance of the system, i.e. its ability to track the glide slope, can be in part inferred from the frequency response associated with z_{E_i} input and z_E output. This is computed by taking the Laplace transform of (11.5,12) (which simply changes D to s wherever it occurs), replacing s by $i\hat{\omega}$, and solving the resulting complex algebraic equations for the ratio z_E/z_{E_i} as a function of $\hat{\omega}$. The result is shown on Fig. 11.13. The system is seen to be able to follow waves in the ILS beam fairly closely down to wavelengths of the order of $\frac{1}{2}$ mile ($\hat{\omega} = 2 \times 10^{-2}$) at which point a phase lag of 40° has developed. This calculation is not, of course, sufficient to decide on the acceptability of the chosen gains. For that purpose one should calculate actual flight paths in the presence of wind shear and turbulence, and relate the dispersions to what is acceptable for a given mission.

11.6 STABILITY OF CLOSED-LOOP SYSTEMS

We have seen in previous examples how "closing the loop" can modify the basic stability of an airplane. In Sec. 11.4 feedback was used to stabilize an unstable vehicle, and in Sec. 11.5 the addition of a feedback loop to lock on to an altitude or glide reference made a stable vehicle go unstable. We have also seen in the examples how the stability of a linear feedback system can be calculated by formulating the appropriate system matrix and treating it as we would any other linear system.

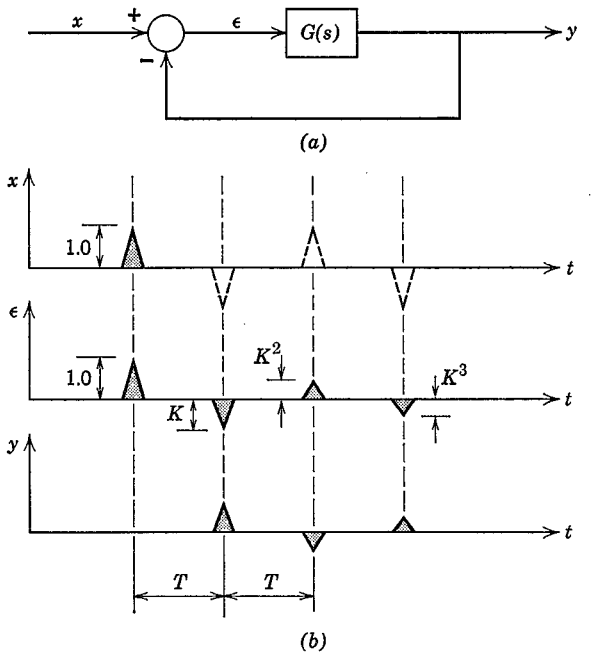

FIG. 11.14 (*a*) Simple feedback system. (*b*) Single-pulse input: $G = Ke^{-Ts}$.

For complicated multiloop systems there is relatively little that can usefully be said in a general way about closed-loop stability. For simple systems, however, as in Fig. 11.14 we can arrive at some general conclusions about the effect of loop gain and phase lag on stability.

CHARACTERISTIC EQUATION

As has been seen in the examples treated, the addition of a feedback loop modifies the characteristic equation, and hence the stability of a system. If the transfer function of Fig. 11.14 is a ratio of two polynomials

$$G(s) = \frac{N(s)}{D(s)}$$

then the overall system transfer function is

$$G'(s) = \frac{\bar{y}}{\bar{x}} = \frac{G}{1+G} = \frac{N/D}{1+N/D} = \frac{N}{N+D}$$

The characteristic equation is then

$$f(s) = N(s) + D(s) = 0$$

which is to be constrasted with the open-loop equation $D(s) = 0$. Thus the change in the characteristic equation is produced by the numerator $N(s)$, and the least possible change is the addition of a constant.

EFFECT OF GAIN

The effect of gain is well illustrated by the familiar public-address acoustic system, in which "whistling" or oscillation occurs when the volume control is set too high. As a model for this case, consider the transfer function Ke^{-Ts}, a simple gain with time delay.

If the system input were a single short pulse (of duration $< < T$) as in Fig. 11.14*b*, the signals in the ϵ and y channels would be as shown, a sequence of alternating pulses at time interval T, all of the same width, but with magnitudes 1, K, K^2 . . . . It is clear that if $K < 1$ the pulses form a diminishing sequence that ultimately dies out, and that if $K > 1$, there is an increasing series which is a divergent, or unstable situation. This would correspond in the case of the P.A. system to an acoustic pulse travelling from the loudspeaker to the microphone and arriving there stronger than the one originally fed in.

EFFECT OF PHASE LAG

Suppose now that the input is a series of pulses, equally spaced but alternating in sign. If the time lag T is such that the feedback pulses fall in the "empty spaces" between the input pulses there is no interference of the pulses, each input can be considered individually, and the criterion for divergence is the same as above, i.e. $K > 1$. If, however, the time lag is such that each return pulse coincides exactly with the next input, as illustrated by the dotted pulses in Fig. 11.14*b*, then the error signal and the ouput form the sequences

$$\begin{array}{lccccc} \epsilon\colon & 1 & -(1+K) & (1+K+K^2) & -(1+K+K^2+K^3)\cdots & \\ y\colon & K & -K(1+K) & K(1+K+K^2) & \cdots & K(1+K+K^2+\cdots) \end{array}$$

The output is seen to contain the sum of a geometric progression of factor K, which is divergent if $K > 1$ and converges to the limit $(1 - K)^{-1}$ if $K < 1$. Thus in the case of the alternating input we find again that the stability criterion is $K < 1$. This is clearly the "worst" phase lag for a pulse train since each return pulse arrives at such a time that it provides the maximum reinforcement to the next input.

SINUSOIDAL INPUT—NYQUIST CRITERION

The above consideration of pulse trains (which can be so easily analyzed) has shown the important effects of loop gain and phase lag on system stability.

These concepts are brought into a somewhat more useful perspective when we consider a sinusoidal input, for all inputs to linear systems can be Fourier-analyzed into separate sinusoids, the individual responses to which can be linearly superposed to construct the output. Suppose then that there is a steady sinusoidal input represented by

$$x = X_0 e^{i\omega t}$$

and a steady sinusoidal output

$$y = Y_0 e^{i\omega t}$$

(This implies of course that the system is stable.) The error is $\epsilon = x - y = \epsilon_0 e^{i\omega t}$, where $\epsilon_0 = X_0 - Y_0$. Now we recognize that the critical phase lag is 180°, since this generates the maximum error signal, just as in the case of the pulse train. So let

$$Y_0 = K\epsilon_0 e^{-i\pi} = -K\epsilon_0$$

Then we get

$$X_0 = \epsilon_0 + Y_0 = Y_0 - Y_0/K = -Y_0 \frac{1 - K}{K}$$

The input required to maintain a steady oscillation of given amplitude is seen to diminish as K increases until it vanishes altogether at $K = 1$, i.e.

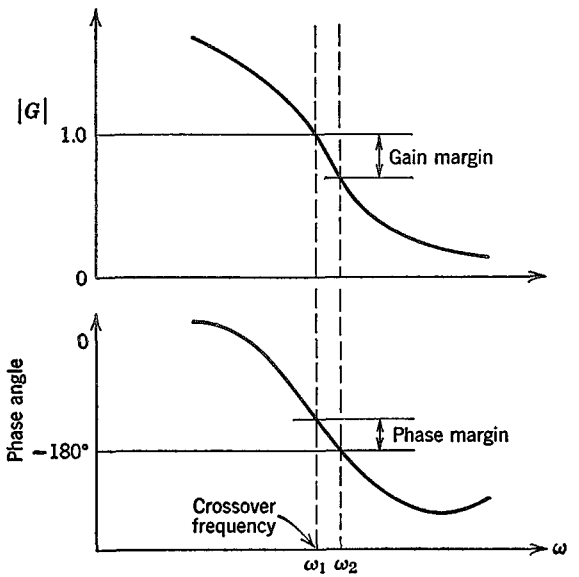

FIG. 11.15 Stability margins.

at $K = 1$ and phase lag of 180°, the system oscillates steadily with no input. This situation clearly represents a stability boundary; further increase in gain corresponds to instability.

The Nyquist criterion (11.4) rigorously derived from a theorem of Cauchy contains the conclusion derived somewhat heuristically above. It uses the frequency response curve for the open-loop system, i.e. $G(i\omega)$, and its relation to the point $(-1, 0)$ of the complex plane, to assess stability. The amount by which the frequency response curve "misses" the critical point $(-1, 0)$ leads to the concepts "gain margin" and "phase margin" illustrated in Fig. 11.15.

Human pilots and handling qualities

CHAPTER 12

By L. D. Reid and B. Etkin

12.1 THE HUMAN PILOT

Although the analysis and understanding of the dynamics of the airplane as an isolated unit (which has been the burden of the preceding chapters) is extremely important, one must be careful not to forget that for many flight situations it is the response of the total system, made up of the human pilot and the aircraft, that must be considered. It is for this reason that the designers of aircraft should apply the findings of studies into the human factors involved in order to ensure that the completed system is well suited to the men who must fly it.

Some of the areas of consideration include:

1. Cockpit environment; the occupants of the vehicle must be provided with oxygen, warmth, light, etc., to sustain them comfortably.
2. Instrument displays; instruments must be designed and positioned to provide a useful and unambiguous flow of information to the pilot.
3. Controls and switches; the control forces and control system dynamics must be acceptable to the pilot, and switches must be so positioned and designed as to prevent accidental operation. Tables 12.1 to 12.3 present typical pilot data concerning control forces.

Table 12.1

Estimates of the Maximum Rudder Forces that can be Exerted for Various Positions of the Rudder Pedal (Ref. 12.1)

Rudder Pedal Position	Distance from Back of Seat, in	Pedal Force, lb
Back	31	246
Neutral	$34\frac{3}{4}$	424
Forward	$38\frac{1}{2}$	334

Table 12.2

Typical Rates of Stick Movement in Flight Test Pull-ups Under Various Loads for 6 in. to 8 in. Deflection (Ref. 12.1)

Case	Maximum Stick load, lb	Average Rate of Stick Motion, in/sec	Time for Full Deflection, sec
1	35	51.85	0.162
2	74	15.58	0.475
3	77	11.00	0.600
4	97	10.27	0.750

4. Pilot workload; the workload of the pilot can often be reduced through proper planning and the introduction of automatic equipment.

The care exercised in considering the human element in the closed-loop system made up of pilot and aircraft can determine the success or failure of a given aircraft design to complete its mission in a safe and efficient manner.

12.2 MATHEMATICAL MODEL OF HUMAN PILOTS—COMPENSATORY DISPLAY

Many critical tasks performed by pilots involve them in activities that resemble those of a servo control system. For example, the execution of a landing approach through turbulent air requires the pilot to monitor the aircraft's altitude, position, attitude, and airspeed and to maintain these variables near their desired values through the actuation of the control system. It has been found in this type of control situation that the pilot

Table 12.3

Hand-Operated Control Forces (From Flight Safety Foundation Human Engineering Bulletin 56-5H) (see figure on page 495)

Direction of Movement		180°	150°	120°	90°	60°	
Pull	Rt. hand	52	56	42	37	24	
	Lft. hand	50	42	34	32	26	
Push	Rt. hand	50	42	36	36	34	
	Lft. hand	42	30	26	22	22	Values given represent maximum exertable force in pounds by the 5 percentile man
Up	Rt. hand	14	18	24	20	20	
	Lft. hand	9	15	17	17	15	
Down	Rt. hand	17	20	26	26	20	
	Lft. hand	13	18	21	21	18	
Outboard	Rt. hand	14	15	15	16	17	
	Lft. hand	8	8	10	10	12	
Inboard	Rt. hand	20	20	22	18	20	
	Lft. hand	13	15	20	16	17	

Note: The above results are those obtained from unrestricted movement of the subject. Any force required to overcome garment restriction would reduce the effective forces by the same amount.

can be modeled by a set of constant-coefficient linear differential equations (termed "human-pilot describing functions"). Much of the original research in the field of human-pilot describing functions has concentrated on the pilot's performance in a single degree of freedom compensatory tracking task with random-appearing system inputs. In a single-degree-of-freedom task the pilot controls a single state variable through the actuation of a single control. A compensatory display is one in which the tracking error is presented, regardless of the source of the error. Fig. 12.1 shows the block diagram for such a task. Here a pilot is concentrating on controlling the pitch attitude

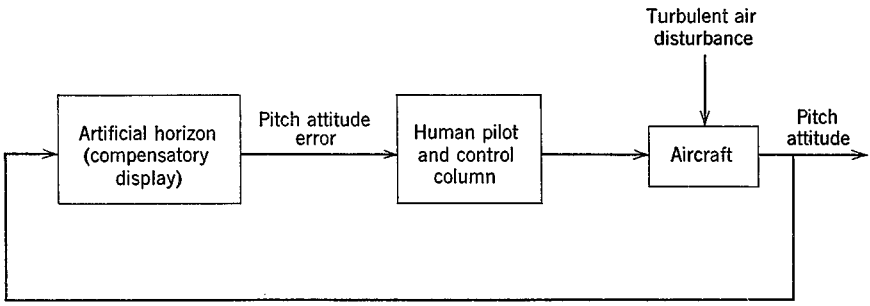

FIG. 12.1 Typical compensatory task.

of the aircraft through the use of the artificial horizon display. The system input in this case is turbulent air which produces random pitching motion of the vehicle.

The pilot model used in compensatory tasks consists of the describing function and the remnant as shown in Fig. 12.2. (See also Sec. 3.5.) Here the task is the same one presented in Fig. 12.1, but the human pilot has been replaced by a mathematical model. The model consists of two parts, as shown: $Y(s)$, the *linear describing function* (written in Laplace transform notation), and $n(t)$ the *remnant*. Since a linear model is never able to describe the pilot completely, $Y(s)$ is insufficient by itself, and it is necessary to include the remnant $n(t)$, which is that signal that must be added in order to have all the time signals circulating in the system of Fig. 12.2 correspond exactly to those of Fig. 12.1 when the identical input is present. The $Y(s)$ selected to describe the pilot in any particular task is chosen so as to minimize that part of the input signal to the aircraft which arises from $n(t)$. Thus the linear pilot model that results is that which accounts for as much pilot input to the aircraft as possible, and a measure of its adequacy is the fraction of the pilot input to the aircraft accounted for by $Y(s)$.

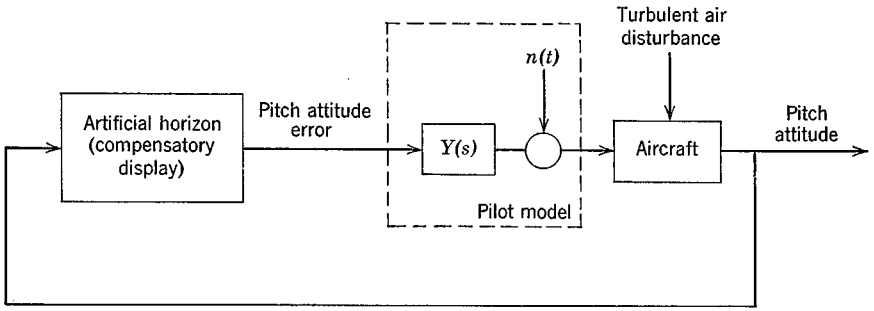

FIG. 12.2 Compensatory task with pilot model.

The human-pilot describing function is useful in studying two classes of problems. In the first the describing functions derived from previous research are utilized to aid the systems designer. With a mathematical description of the pilot at hand he can close the loop around the mathematical description of the proposed vehicle in order to predict the overall system response. The second type of study involves the measurement of actual human-pilot describing functions as the pilot flies a particular vehicle in order to obtain an objective measure of how the task affects the pilot.

Due to the complex nature of the situation it is possible to model the pilot in many ways and to measure the model by employing a variety of techniques. One of the most successful approaches to the measurement problem utilizes power-spectral-density measurements of signals circulating in the control loop. The general case of a tracking task of one degree of freedom with a compensatory display is illustrated in Fig. 12.3*a*. In this task the pilot must control the aircraft response $m(t)$ in such a fashion that it matches as closely as possible the desired aircraft response $i(t)$. The pilot does this by viewing the instantaneous error $e(t)$ and altering his input $o(t)$ to the aircraft. It is found that the pilot's control technique is primarily influenced by the type of input $i(t)$, the dynamics of the control system, the type of display and the dynamics of the aircraft. Any useful pilot model must reflect these influences.

Past research in this field has concentrated on tasks with random appearing input signals $i(t)$ because so many real-world situations involve this type of disturbance. Thus the pilot models that have been developed apply strictly only to tasks with the above type of input. The system of Fig. 12.3*a* is modeled by that of Fig. 12.3*b*. Note that the model includes the dynamics of the control system and that the signal $o(t)$ corresponds to the position of the control column. It has been found that in the frequency band of primary interest and for the type of controls normally found in aircraft, such a model is fairly insensitive to the exact control system used and that pilot models developed on this basis are quite general. Now the linear system of Fig. 12.3*b* can be redrawn as the point by point sum of the two linear systems of Fig. 12.4 (if the aircraft is assumed to be a linear system). It follows that

$$\begin{aligned} e(t) &= e_1(t) + e_2(t) \\ o(t) &= o_1(t) + o_2(t) \\ m(t) &= m_1(t) + m_2(t) \end{aligned}$$

The describing function $Y(s)$ is chosen to minimize the r.m.s. value of $o_2(t)$. Note that this is not the same criterion as used in defining the open-loop describing function in Sec. 3.5, where the mean-square-remnant was minimized in the presence of a *fixed input*. The difference of course is that we are dealing here with a closed-loop system, in which signals derived from the

remnant circulate the loop and appear at the input to the pilot. The process of minimizing $\overline{o_2^2(t)}$ can be carried out in a manner basically similar to that used in Sec. 3.5 with the result (ref. 12.2)

$$Y(i\omega) = \Phi_{io}(\omega)/\Phi_{ie}(\omega) \tag{12.2,1}$$

where $\Phi_{io}(\omega)$ is the cross-spectral density of $i(t)$ and $o(t)$ etc. (See Sec. 2.6). We also find that $\Phi_{in}(\omega) = 0$,—i.e. the remnant is uncorrelated with the input signal $i(t)$. This linear model, $Y(s)$, is a best fit in the root-mean-square

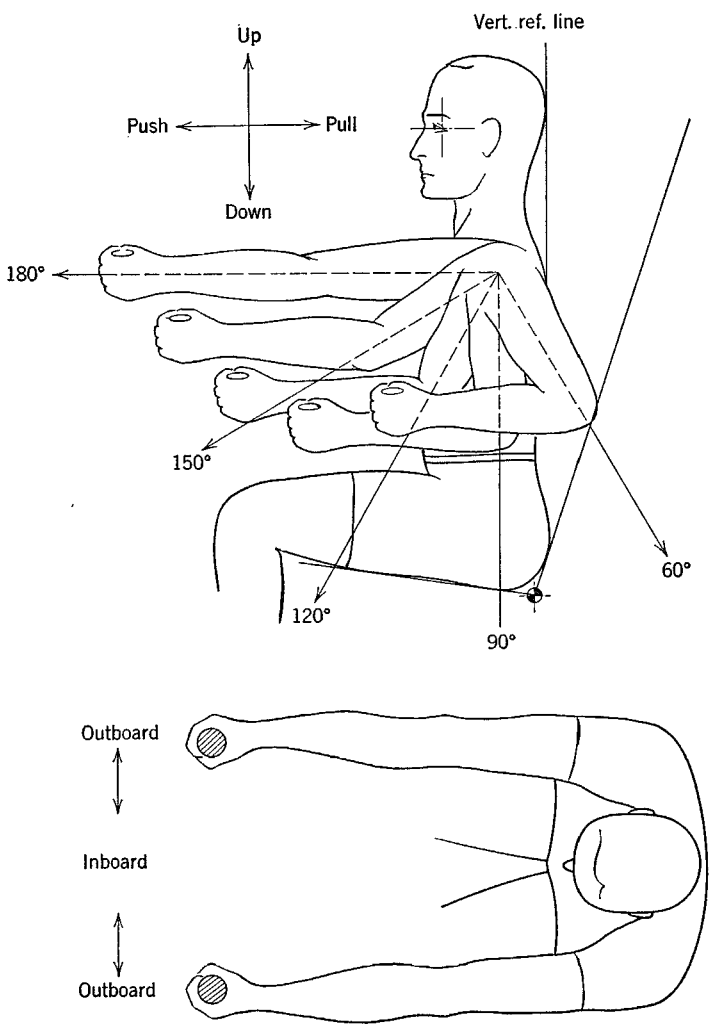

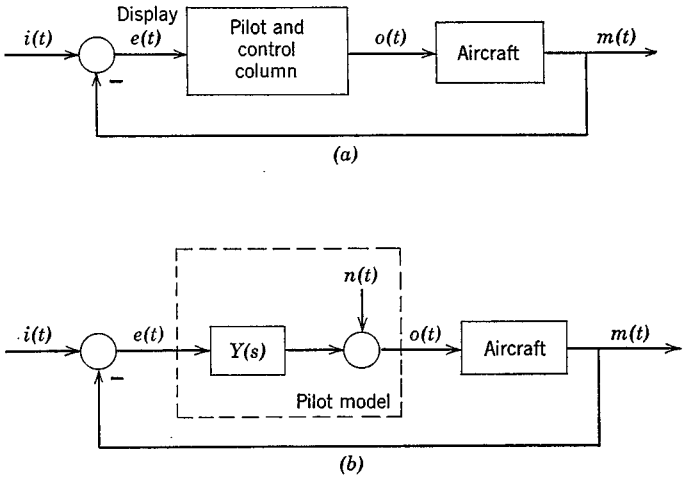

FIG. 12.3 (*a*) General compensatory task. (*b*) Model.

sense. It will not describe the pilot's output exactly. The remnant $n(t)$ is the difference between the actual pilot output and the linear approximation to it. In order to obtain a measure of the adequacy of the linear model, $Y(s)$, a parameter ρ^2 has been defined as

$$\rho^2(\omega) = 1 - \frac{\Phi_{o_2 o_2}(\omega)}{\Phi_{oo}(\omega)}$$

When ρ^2 is near unity, i.e. when $o_2(t) \approx 0$, the model $Y(s)$ is a good approximation of the pilot. Another useful form for ρ^2 can be found by using the

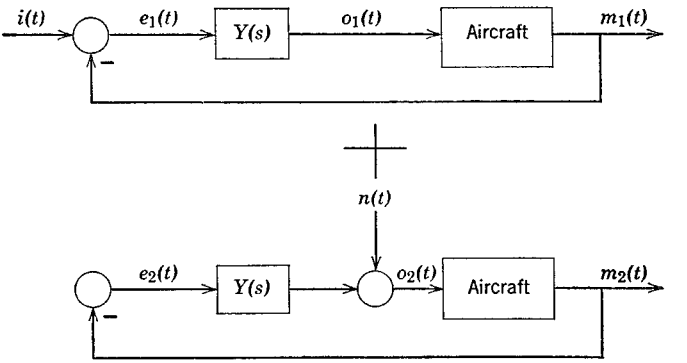

FIG. 12.4 Two-part linear model of the compensatory task.

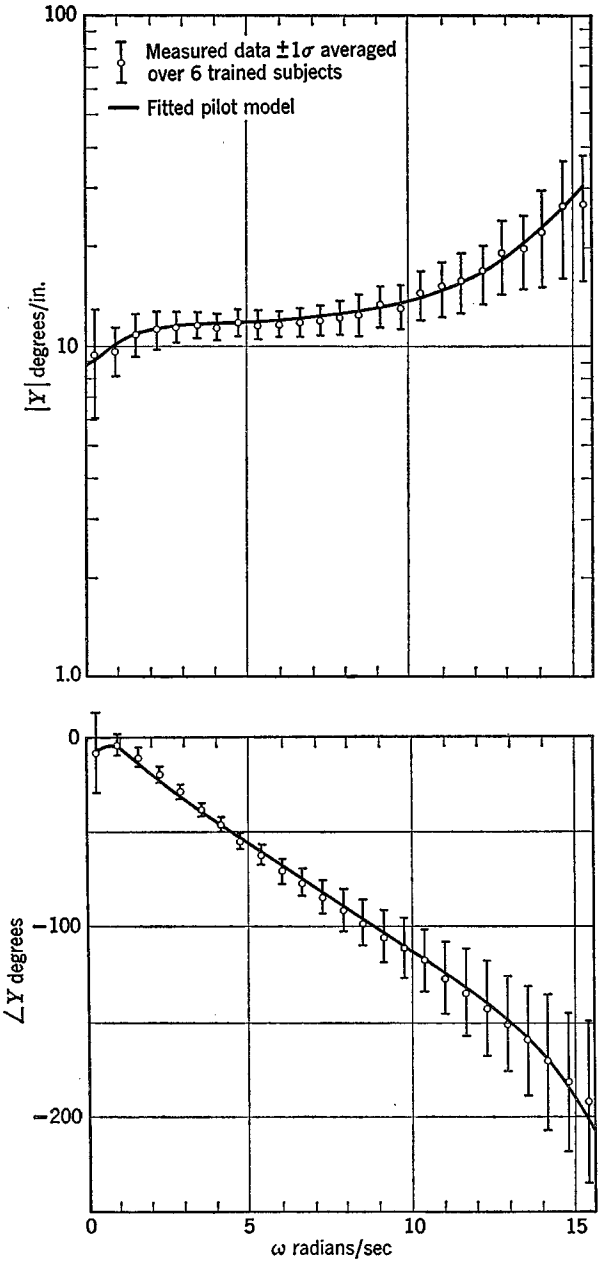

FIG. 12.5 Experimentally measured pilot model, compensatory display. (from ref. 12.5)

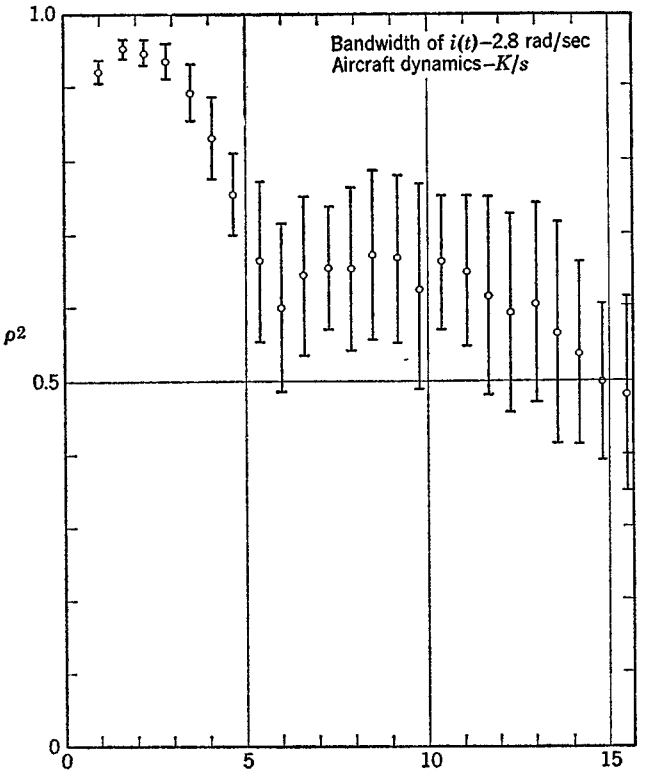

FIG. 12.5 (Contd.)

relationships among the variables in Fig. 12.4 to derive

$$\rho^2(\omega) = \frac{|\Phi_{io}(\omega)|^2}{\Phi_{ii}(\omega)\Phi_{oo}(\omega)}$$

This form is preferred for measurement because it is not possible to measure $o_2(t)$ directly. The remnant $n(t)$ exists because in actuality the human pilot is not operating exactly as a linear/invariant mathematical system. The signal $n(t)$ is a random-appearing variable and hence is not predictable. However, some measurements have been made of its statistical properties (ref. 12.6) over a range of task variables. Figure 12.5 shows a typical experimentally measured pilot describing function together with ρ^2. In this task the input to the pilot was the deflection of the artificial horizon display (in inches) and his output was control column deflection (in degrees). It is seen from the plot of ρ^2 that the describing function models the low-frequency performance of the pilots quite well, but is less satisfactory for $\omega > 5$ rad/sec.

The following form for the describing function has been developed to cover the single-degree-of-freedom compensatory tracking task with a random-appearing input (ref. 12.3):

$$Y(s) = K_p e^{-\tau s} \frac{(T_L s + 1)}{(T_I s + 1)} \left\{ \frac{(T_K s + 1)}{(T'_K s + 1)(T_{N_1} s + 1)\left[\left(\frac{s}{\omega_N}\right)^2 + 2\frac{\zeta_N}{\omega_N} s + 1\right]} \right\} \tag{12.2,2}$$

In this formulation $e^{-\tau s}$ represents the pure transmission time delay within the pilot associated with nerve conduction and stimulation. τ is estimated to range from .06 to .10 sec. The factor in curly brackets is a reasonable representation of the dynamics of the neuromuscular system of the arm with typical values: $1/T_{N_1} = 10\ \text{sec}^{-1}$, $\omega_N = 16.5$ rad/sec, and $\zeta_N = .12$. $(T_K s + 1)/(T'_K s + 1)$ represents a very low frequency lag-lead component. The remaining terms $K_p[(T_L s + 1)/(T_I s + 1)]$ are the adaptive portions of the model; the values of K_p, T_L, and T_I are altered by the pilot to suit the particular system being controlled. It is found that for most engineering applications, in which an exact pilot model is not required at very low and very high frequencies, an adequate approximation is

$$Y(s) = K_p e^{-\tau_e s} \frac{(T_L s + 1)}{(T_I s + 1)(T_N s + 1)} \tag{12.2,3}$$

The following set of adjustment rules for the pilot model have been developed by McRuer et al. (ref. 12.3).

1. Stability: The human adopts a model form to achieve stable control—i.e. one that produces a stable closed-loop system.
2. Form selection—Low frequency: The human adopts a model form to achieve good low-frequency closed-loop system response to the input signal. A low-frequency lag, T_I, is generated when both of the following conditions apply:
   (a) The lag would improve the low-frequency characteristics of the system.
   (b) The aircraft dynamics are such that the introduction of the low-frequency lag will not result in destabilizing effects at higher frequencies that cannot be overcome by a single first-order lead, T_L, of somewhat indefinite but modest size.
3. Form selection—Lead: After good low-frequency characteristics are assured, within the above conditions, lead is generated when the aircraft dynamics together with the pilot time delay are such that a lead term would be essential to retain or improve high-frequency system performance.

4. Parameter adjustment: After adoption of the model *form*, the describing function *parameters* are adjusted so that:
   (a) Closed-loop low-frequency performance in operating on the input signal is optimum in some sense analogous to that of minimum mean-squared tracking error.
   (b) System phase margin, ϕ_M (see Sec. 11.6), is directly proportional to ω_i, the input signal bandwidth (loosely defined as the frequency above which the input spectrum decreases rapidly), for values of ω_i less than about 2.0 rad/sec. The strong effect of forcing-function bandwidth on the phase margin is associated with the variation of T_N with ω_i.
   (c) Equalization time constants T_L or T_I: when form selection requires $1/T_L$ or $1/T_I << \omega_c$, the system crossover frequency (the frequency at which $|G(i\omega)|\,|H(i\omega)|$ equals unity—see Fig. 11.15), it will be adjusted such that low-frequency response will be essentially insensitive to slight changes in T_L or T_I (for $\omega_i << \omega_c$).

5. ω_c Invariance properties:
   (a) Independence of ω_c w.r.t. K_c: Let the aircraft static gain be K_c, and that of the pilot be K_p [see (3.2,4) and (3.4,26)]. After initial adjustment, changes in K_c are offset by changes in the pilot gain, K_p; i.e. system crossover frequency, ω_c, is invariant with K_c.
   (b) Independence of ω_c w.r.t. ω_i: System crossover frequency depends only slightly on the input bandwidth for $\omega_i < 0.8\omega_{co}$. ($\omega_{co}$ is that value of ω_c adopted for $\omega_i << \omega_c$.)
   (c) ω_c Regression: When ω_i nears or becomes greater than $0.8\omega_{co}$, the crossover frequency reduces to values much lower than ω_{co}.

Although the above pilot model was developed to describe the single-degree-of-freedom compensatory tracking task, it is finding more and more use in the general situation of the multiple-loop tracking task. In such a task the pilot controls a number of vehicle variables simultaneously. It has been found that the same basic form of pilot model can be applied in many cases with slight modification to the values of some of the parameters (such as the time delay τ) to account for the additional complexities of the task (such as visually sampling the outputs of several instruments). In this application a single describing function is used to close each control loop actually closed by the pilot. For example, if the task is to control both the pitch and roll attitudes (assuming the pitch and roll modes to be uncoupled), one describing function would close the roll loop while a second would close the pitch loop.

12.3 MATHEMATICAL MODEL OF HUMAN PILOTS—PURSUIT DISPLAY

Pilot models are being developed to describe the control situation when displays other than the compensatory type are utilized. An example of this is the pursuit display. The single-degree-of-freedom tracking task with a pursuit display is identical to the compensatory task of Fig. 12.3*a* except that the displayed variables are different—i.e. the pilot has different information. In the compensatory task only $e(t)$ is displayed (Fig. 12.3) whereas in the pursuit task both $i(t)$ and $m(t)$ are separately displayed. Figure 12.6 illustrates the difference between the two displays for the same system state. It can be seen that additional information is presented to the pilot on the pursuit display. Although $e(t)$ is available in both cases, only the pursuit display separates the error into its components and conveys this information to the pilot. For example, a pursuit display tells the pilot whether his tracking error is due to a difficult input signal, $i(t)$, or due to erratic pilot control of the aircraft, $m(t)$, which in turn can affect his strategy in bringing the tracking

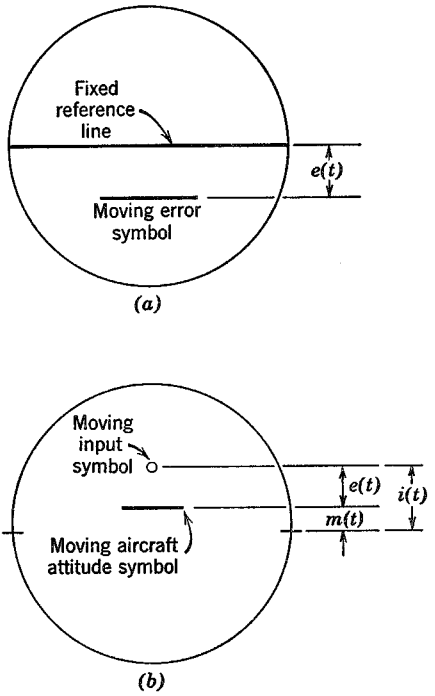

FIG. 12.6 Displays. (*a*) Compensatory. (*b*) Pursuit.

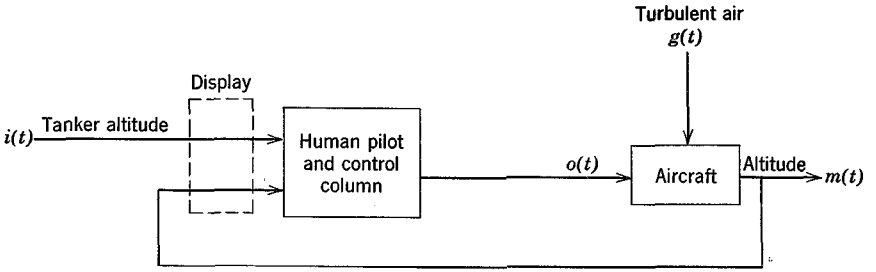

FIG. 12.7 Typical pursuit task.

error under control. Whether the one display or the other is best for the mission at hand is a complex function of the task performed.

A technique for measuring human-pilot describing functions has been developed for the single-degree-of-freedom tracking task with a pursuit display for situations where a secondary disturbance signal is present. This task is shown in Fig. 12.7. It might for example represent a mid-air refueling task where $i(t)$ represents the tanker's altitude and the secondary disturbance $g(t)$ represents turbulence acting on the controlled aircraft. The model of this task can be formulated in several ways. Figure 12.8 shows two useful forms of the model. The pilot is represented by a pair of describing functions ($Y_1(s)$, $Y_2(s)$) or ($Y_3(s)$, $Y_4(s)$) since the pilot is considered to have

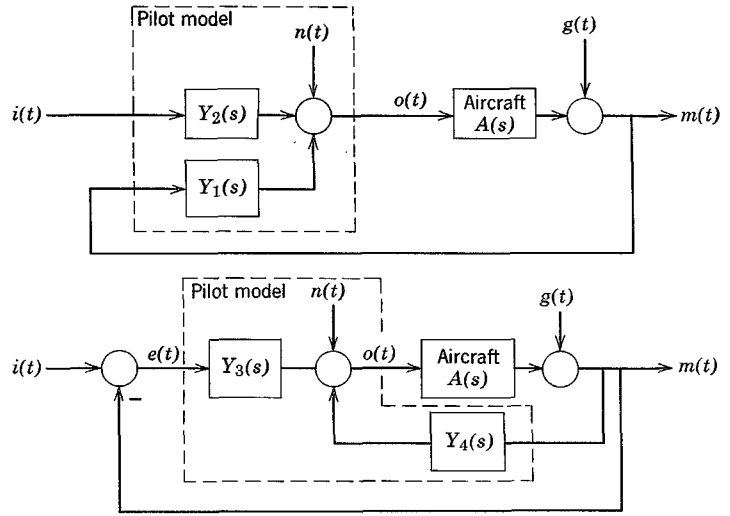

FIG. 12.8 Two models of the pursuit task.

two inputs and one output. [Since $e(t) = i(t) - m(t)$ it is redundant to consider a case with three inputs.] Again $n(t)$ represents the remnant. The describing function pairs are chosen to minimize the root mean square of that part of the vehicle input signal $o(t)$ which is accounted for by $n(t)$ (as was done for the compensatory display). The describing functions that result are [where the aircraft transfer function is $A(s)$]:

$$Y_1(i\omega) = \left(\frac{1}{\phi_1(\omega)} + A(i\omega)\right)^{-1}$$

$$Y_2(i\omega) = (1 - Y_1(i\omega)A(i\omega)) \cdot \phi_2(\omega)$$

$$Y_3(i\omega) = Y_2(i\omega)$$

$$Y_4(i\omega) = Y_1(i\omega) + Y_2(i\omega)$$

where

$$\phi_1(\omega) = \frac{\Phi_{go}(\omega)\Phi_{ii}(\omega) - \Phi_{io}(\omega)\Phi_{gi}(\omega)}{\Phi_{ii}(\omega)\Phi_{gg}(\omega) - \Phi_{ig}(\omega)\Phi_{gi}(\omega)} \qquad (12.3,1)$$

$$\phi_2(\omega) = \frac{\Phi_{io}(\omega)\Phi_{gg}(\omega) - \Phi_{go}(\omega)\Phi_{ig}(\omega)}{\Phi_{ii}(\omega)\Phi_{gg}(\omega) - \Phi_{ig}(\omega)\Phi_{gi}(\omega)}$$

The denominators of (12.3,1) both vanish if either (i) $g(t) = 0$ or (ii) $g(t) = \text{const} \times i(t)$. In either of these cases the measurement of ϕ_1 and ϕ_2, and hence of the describing function pairs, would not be possible. In addition the following are found to hold:

$$\Phi_{in}(\omega) = \Phi_{gn}(\omega) = 0 \qquad (12.3,2)$$

$$\rho^2(\omega) = \left|\frac{1}{1 - Y_1(i\omega)A(i\omega)}\right|^2 \frac{1}{\Phi_{oo}(\omega)} \times \{|Y_2(i\omega)|^2\Phi_{ii}(\omega) + |Y_1(i\omega)|^2\Phi_{gg}(\omega) + 2\,\mathrm{Re}\,[Y_2^*(i\omega) \times Y_1(i\omega)\Phi_{ig}(\omega)]\} \qquad (12.3,3)$$

As yet no general set of rules comparable to those for the compensatory task has been developed to cover this model. A typical measured pursuit model is shown in Fig. 12.9. It was found that the measured data could be fitted quite well by describing functions of the form (12.2,2). The task in this example was the same as the one used for Fig. 12.5, except that a pursuit display was used and a secondary disturbance added. If $g(t)$ is made very small it is assumed that such models will also approximate pursuit tasks with no secondary disturbances.

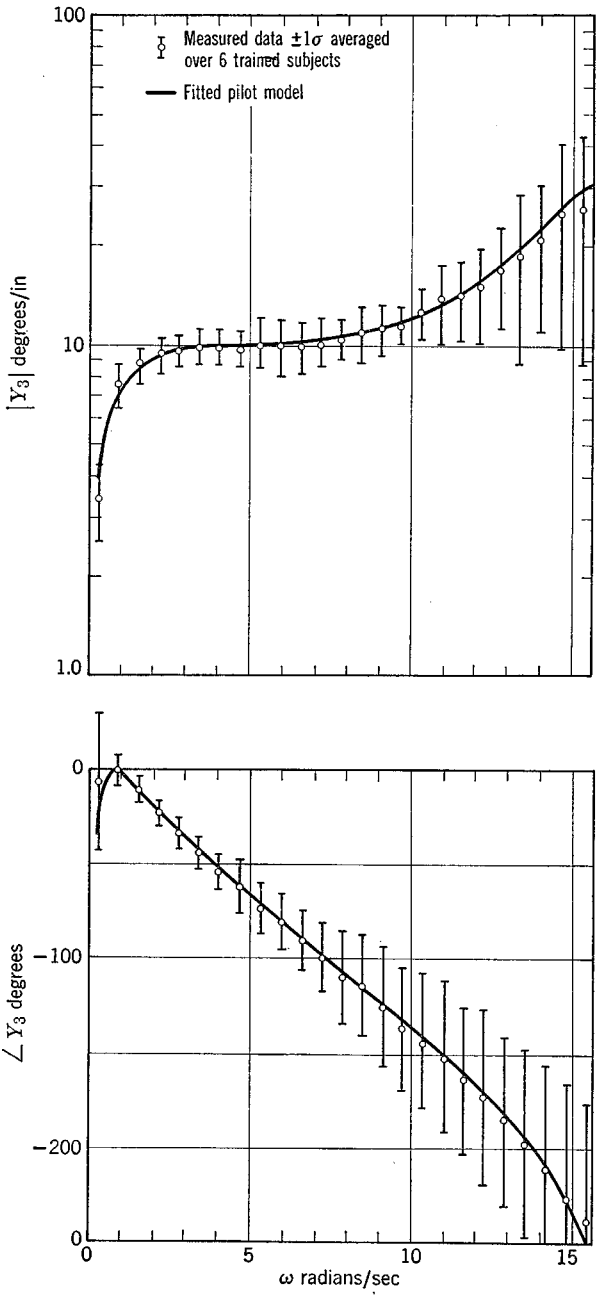

FIG. 12.9 Experimentally measured pilot model; pursuit display. (from ref. 12.5)

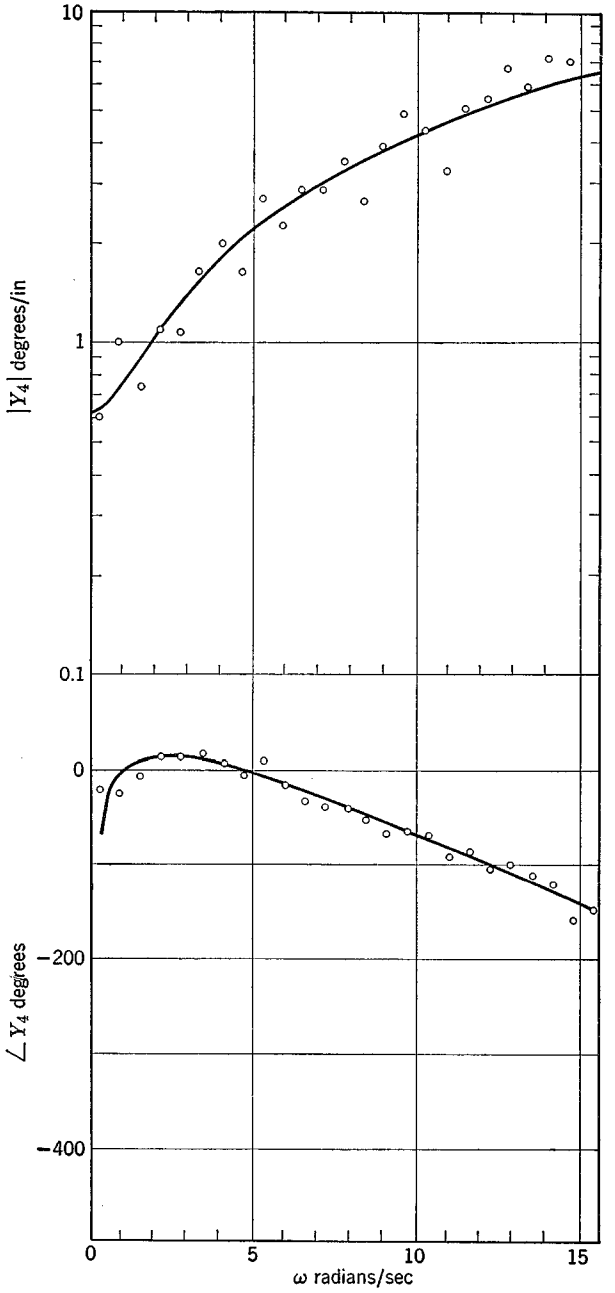

FIG. 12.9 *(Contd.)*

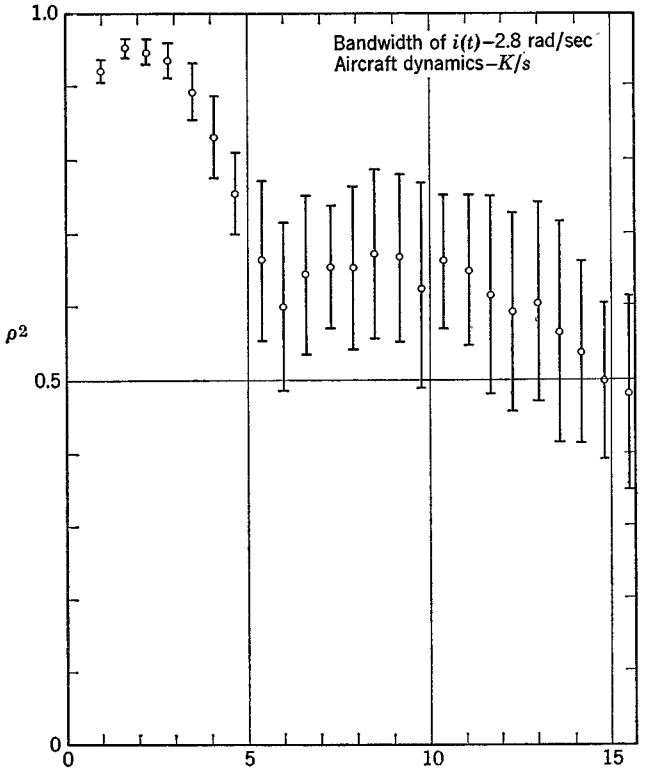

FIG. 12.9 (*Contd.*)

12.4 THE FUTURE ROLE OF THE HUMAN PILOT

In an age where more and more of the aircraft control task is being devolved to automatic equipment (e.g. autopilots, blind landing systems, stability augmentation systems) the role of the human pilot will perhaps slowly change from that of an active element in the man/machine system to that of a manager overseeing the operation of the automatic controls. In this situation the pilot must monitor the performance of the equipment and be prepared to take over in the event of a failure. This philosophy quite rightly predicates that the human pilot should make the final decisions that determine the fate of the craft under his command. Moreover, human pilots are uniquely capable of assessing the meaning of complex data patterns which indicate the state of the vehicle under conditions that the automatic equipment has not been designed to handle (witness Apollo 13!). On the other hand, this *modus operandi* poses a serious problem for the pilot, for he is then expected to assume manual control of a vehicle at a critical time, following a system

failure. If he is unable to make the transition from passive to active control with sufficient speed and precision, disaster could well be the result.

Thus it appears that if the pilot is expected to assume manual control at any time, the system should be so structured that he is either kept actively in the control loop at all times or is constantly made aware of the feel of the present aircraft configuration through some auxiliary task which he can practice on during critical phases of the flight. Research on the ability of pilots to control vehicles following stability augmentation system (SAS) failures has indicated that the resulting step change in vehicle dynamics can lead to an unstable man-machine system and loss of control (ref. 12.29). The mechanism behind this problem is as follows. With the SAS operating properly the vehicle dynamics are satisfactory and the pilot adopts a control technique to suit. The sudden SAS failure results in less satisfactory vehicle dynamics, which demands a much more concentrated effort on the part of the pilot in order to maintain control. Immediately following SAS failure, however, the pilot attempts to continue to employ the control technique he has been using previously with the SAS operative. This combination of man-machine dynamics can lead to an unstable system. If the system is to be fail-safe the pilot must be able to detect the change quickly and alter his control technique in time to recover from the upset. Consequently the advent of more automatic equipment does not diminish the need to study the role of man in the vehicle control loop. On the contrary, it generates new and more difficult problems requiring an even better understanding of the human pilot.

12.5 AIRCRAFT HANDLING QUALITIES

The assessment of handling or flying qualities of airplanes depends in the final analysis on pilot opinion. The earliest requirement (ref. 12.30) simply stated, "During this trial flight of one hour it (the airplane) must be steered in all directions without difficulty and at all times be under perfect control and equilibrium." From this simple but hard-to-interpret statement has evolved a much more quantitative and sophisticated set of criteria. These are still far from perfect, and the introduction of each new class of vehicle, STOL (ref. 12.30), rotorcraft, SST, etc., requires a reassessment of the existing criteria for application in the new situation.

When a pilot flies an aircraft he forms subjective opinions concerning the suitability of the man-machine system for performing the assigned task. In arriving at an assessment he is influenced by many parameters. These

range over a wide spectrum and include:

1. *Aircraft stability*; response to external disturbances such as turbulence.
2. *Aircraft controllability*; the response of the aircraft to actuation of the controls.
3. *Cockpit design*; the ease with which instruments can be read; the comfort of the seat.
4. *View* from the cockpit; on landing approach is a sufficiently clear view of the ground provided?
5. *Mission*; e.g. high-altitude cruise, landing approach in a crosswind.
6. *Pilot's background and emotional and physical state*; the familiarity of the pilot with the present aircraft and mission; impaired functioning arising from emotional and physiological factors.
7. *External environment*; visibility and weather conditions.

The term handling qualities is used to refer to those characteristics *of the aircraft* which the pilot considers to influence the ease of performing the mission. Much of the work in the area of handling qualities has centered on the determination of the influence of aircraft stability and control. It is the aim of this research to establish general specifications, to ensure that future vehicles can complete their intended missions safely, efficiently, and with a minimum of pilot fatigue.

THE RATING OF HANDLING QUALITIES

To be able to assess aircraft handling qualities one must have a measuring technique with which any given vehicle's characteristics can be rated. In the early days of aviation this was done by soliciting the comments of pilots after they had flown the aircraft. However, it was soon found that a communications problem existed with pilots using different adjectives to describe the same flight characteristics. These ambiguities have been alleviated considerably by the introduction of a uniform set of descriptive phrases by workers in the field. The most recent set (ref. 12.12) is referred to as the "Cooper-Harper Scale" where a numerical rating scale is utilized in conjunction with a set of descriptive phrases. This scale is presented in Table 12.4 and is similar but not identical to previous scales developed separately by Cooper and Harper. Care must be taken in interpreting past research, to determine which scale the results are based on. To apply this rating technique it is necessary to describe accurately the conditions under which the results were obtained. In addition it should be realized that the numerical pilot rating (1 to 10) is merely a shorthand notation for the descriptive phrases and as such no mathematical operations can be carried out on them in a rigorous sense. For example a vehicle configuration rated as 6 is not necessarily

Table 12.4

Cooper-Harper Rating Scale (Ref. 12.12)

Aircraft Characteristics	Demands on the Pilot in Selected Task or Required Operation	Pilot Rating
Excellent; highly desirable	Pilot compensation not a factor for desired performance	1
Good; negligible deficiencies	Pilot compensation not a factor for desired performance	2
Fair; some mildly unpleasant deficiencies	Minimal pilot compensation required for desired performance	3
Minor but annoying deficiencies	Desired performance requires moderate pilot compensation	4
Moderately objectionable deficiencies	Adequate performance requires considerable pilot compensation	5
Very objectionable but tolerable deficiencies	Adequate performance requires extensive pilot compensation	6
Major deficiencies	Adequate performance not attainable with maximum tolerable pilot compensation. Controllability not in question.	7
Major deficiencies	Considerable pilot compensation is required for control	8
Major deficiencies	Intense pilot compensation is required to retain control	9
Major deficiencies	Control will be lost during some portion of required operation	10

twice as bad as one rated at 3. The comments from evaluation pilots are extremely useful and this information will provide the detailed reasons for the choice of a rating.

Other techniques have been applied to the rating of handling qualities. For example, attempts have been made to use the overall system performance as a rating parameter. However, due to the pilot's adaptive capability, quite often he can cause the overall system response of a bad vehicle to approach that of a good vehicle, leading to the same performance but vastly differing pilot ratings. Consequently system performance has not proved to be a good rating parameter. A more promising approach involves the measurement of the pilot's physiological and psychological state. Such methods lead to objective assessments of how the system is influencing the human controller. The measurement of human pilot describing functions is part of this technique.

12.6 FLIGHT SIMULATORS

Research in the field of aircraft handling qualities is undertaken for two primary reasons. These are (i) to formulate a set of design criteria which if met will ensure that a new flight vehicle will have adequate handling qualities and (ii) to better understand how the various vehicle and mission parameters affect the human pilot. These problems are tackled by means of experimental programs involving trained pilots and actual aircraft or flight simulators, or through theoretical analyses involving human-pilot describing functions. Most of the recent research has been experimental work carried out with flight simulators.

The flight simulator is a device that creates the illusion of flight to a certain extent for a pilot seated in its cockpit. This is achieved partly by constructing the cockpit to appear like that of the real aircraft. The simulator is then programmed to respond to the actuation of the controls in a fashion which resembles the response of the actual vehicle. This is accomplished by programming the vehicle's equations of motion on an analog or digital computer, using the pilot's control movements as the inputs to the computer system and driving the response system of the simulator with the computer output. The realism achieved with a given simulator depends to a great extent upon the visual and motion cues provided by the response system. The motion response of the simulator can range from none at all for fixed-base simulators, through limited motion in some degrees of freedom, to complete six-degree-of-freedom motion with a variable stability aircraft, which is in fact a flying simulator. The visual cues provided can include instrument displays, closed-circuit television representations of the outside world, or the full visual and instrument display provided by a variable stability aircraft. Figure 12.10 depicts a typical simulator system.

The advantages offered by the flight simulator to researchers in the field of handling qualities are many. With the simulator it is possible to isolate a single system parameter for study, allowing it to vary while holding all other parameters fixed. Situations that would involve an element of danger if a real aircraft were utilized can be simulated with no risk to life or equipment. The lower cost of operating the simulator and the control over environmental factors such as turbulence also favor the simulator. However, care must be exercised in interpreting the results of simulator studies. Since the simulator is usually only an engineering approximation to the actual flight system, the pilot must extrapolate his experience in the simulator in order to relate it to an actual flight situation. The ability of a pilot to do this and hence achieve meaningful handling qualities ratings depends upon his previous flight and simulator experience. In addition, care must be taken to

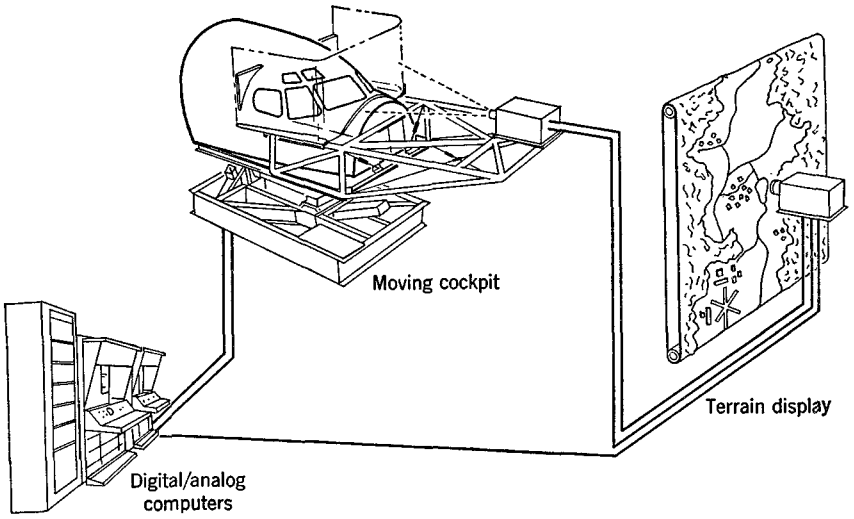

FIG. 12.10 Integrated simulator complex (from ref. 12.25).

provide the pilot with the pertinent stimuli. For example, it would not make sense to use a fixed-base simulator to rate a vehicle in the performance of a mission which normally requires the pilot to sense vehicle motions.

12.7 RESULTS OF HANDLING QUALITIES RESEARCH

Research into aircraft handling qualities is aimed in part at ascertaining which vehicle parameters influence pilot acceptance. It is obvious that the number of possible combinations of parameters is staggering, and consequently attempts are made to study one particular aspect of the vehicle while maintaining all others in a "satisfactory" configuration. Thus the task is formulated in a fashion which is amenable to study. The risk involved in this technique is that important interaction effects can be overlooked. For example, it is found that the degree of difficulty a pilot finds in controlling an aircraft's lateral-directional mode influences his rating of the longitudinal dynamics. Such facts must be taken into account when interpreting test results. Another possible bias exists in handling qualities results obtained in the past because most of the work has been done in conjunction with fighter aircraft.

12.8 LONGITUDINAL HANDLING QUALITIES

In investigating the handling qualities related to longitudinal dynamics, many workers in the field separate the problem into two parts, associated

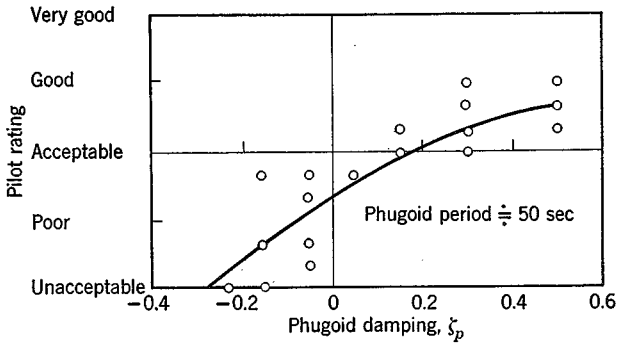

FIG. 12.11 Effect of phugoid damping, ζ_p, on pilot rating (from ref. 12.15).

with the short-period response and phugoid response. Attempts are then made to correlate pilot opinion with the various parameters or with the characteristics of these two modes.

First consider the phugoid response. This mode was discussed at length in Chapter 9, and approximations to the period and damping were given in Sec. 9.2. For conventional fixed-wing airplanes the period is very long and not a significant factor in pilot rating. The damping is important however, and some experimental results (ref. 12.15) are shown on Fig. 12.11. These were obtained in flight under instrument conditions. As the damping of the phugoid mode decreases more attention must be devoted to controlling the associated low-frequency motion, which can be excited by movement of the aircraft controls or by gusts. It is seen that, generally speaking, a divergent phugoid mode (a negative ζ_p) must be avoided. The same study that produced these results found that under *visual* flight conditions, a reduction in the damping from .32 to −.12 had little influence on pilot ratings.

Studies of the effect of the short-period response on pilot ratings have been made using variable stability aircraft (ref. 12.15). Although a range of results have been noted for various tasks and aircraft, the general pattern is as illustrated on Fig. 12.12. It shows a typical plot of pilot "iso-opinion" curves from such an experiment. The solid lines represent curves of constant pilot rating as the values of ω_n and ζ are altered. The regions of satisfactory, acceptable, poor, and unacceptable handling qualities are indicated along with the pilot comments for the various areas in the unacceptable region.

OTHER LONGITUDINAL HANDLING QUALITIES PARAMETERS

Substantial disagreement among results based on correlating pilot ratings with short-period damping and natural frequency (ref. 12.16) has resulted

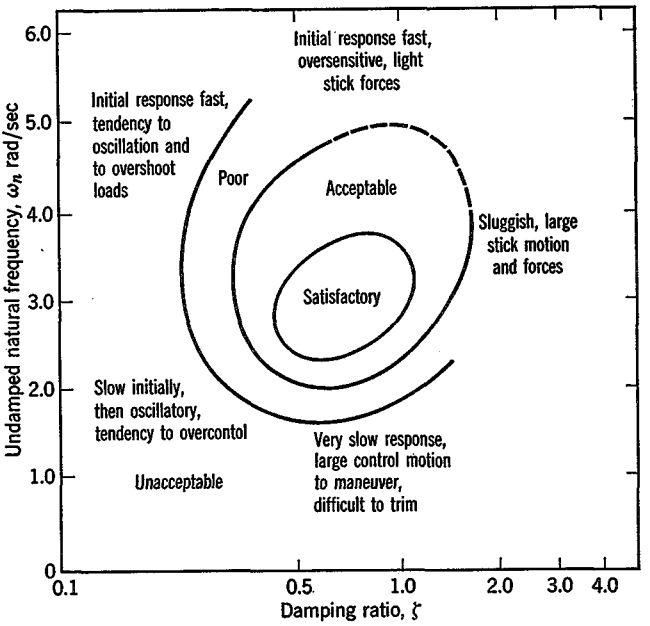

FIG. 12.12 Longitudinal short-period oscillation—pilot opinion contours (from ref. 12.15).

in a search for more meaningful parameters. One such was derived by noting that the pilot's opinion of an aircraft's longitudinal dynamics is very much influenced by the response of the vehicle to control inputs. This in turn depends on terms in *both* the numerator and denominator of the longitudinal transfer functions, whereas the short-period characteristics appear in the denominator only [see (10.2,11)]. An important transfer function is the approximate one relating pitch rate response to elevator angle input, given by (10.2,11*c* and *b*). (See also Figs. 10.6, 10.3.) If we neglect C_{L_δ}, $C_{L_{\dot\alpha}}$, and $C_{m_{\dot\delta}}$ in (10.2,12*b*) and convert to dimensional form, we get the approximation

$$\frac{\bar{q}}{\Delta\bar{\delta}_e} = \frac{M_\delta L_\alpha}{mI_yV}\frac{1 + mVs/L_\alpha}{(s^2 + 2\zeta\omega_n s + \omega_n{}^2)} \tag{12.8,1}$$

where q is in rad/sec, and s corresponds to d/dt, not $d/d\hat{t}$. ω_n (in rad/sec) and ζ are, of course, the approximate short-period frequency and damping, respectively. The quantity (L_α/mV) in the numerator is the lead time constant in this response and has been identified as an important parameter for longitudinal handling qualities (ref. 12.31). In ref. 12.16 it is argued that the appropriate correlation of pilot ratings is with the parameters shown in Fig. 12.13. It is stated that when the aircraft load factor response to angle of

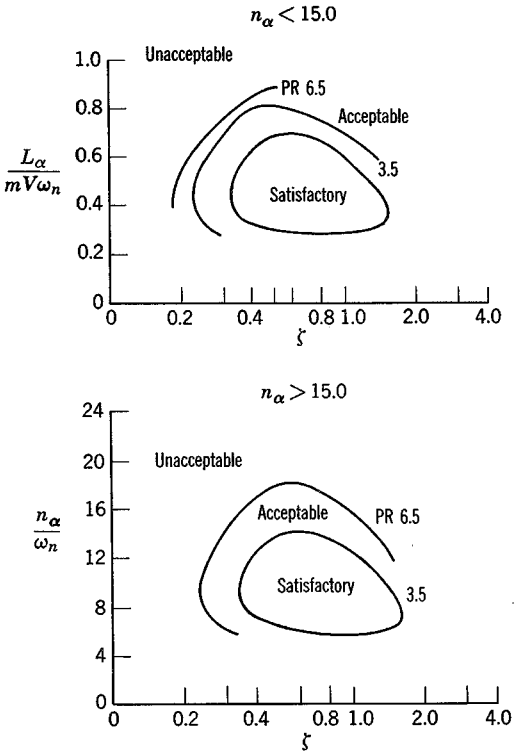

FIG. 12.13 Pilot ratings based on $L_\alpha/mV\omega_n$ and n_α/ω_n (from ref. 12.16).

attack ($n_\alpha = (\partial L/W)/\partial\alpha = L_\alpha/W$) is less than 15 g/rad, pilot opinion correlates well with

$$\frac{L_\alpha}{mV\omega_n} \quad \text{and} \quad \zeta$$

The importance of L_α/mV can easily be inferred. Figure 10.6 shows that the early part of the response to elevator separates clearly into two phases—an initial pitch-up to a nearly steady $\Delta\alpha$, and a subsequent flight-path curvature associated with the lift increment $\Delta L = L_\alpha \Delta\alpha$. The magnitude of the curvature is approximately $\Delta L/mV = (L_\alpha/mV)\,\Delta\alpha$. The changeover in correlating parameter at about n_α of 15 appears to be due to the pilot's concern to control load factor at large n_α, whereas he concentrates on flight path at low n_α. Figure 12.13 shows iso-opinion curves based on the use of these parameters.

An additional parameter has been developed based on the consideration of pilot comments and the physiology of the pilot (ref. 12.17). It is called the

"Control Anticipation Parameter" or *CAP*. The *CAP* is defined to be the ratio of the instantaneous angular acceleration in pitch to the steady-state change in load factor when the pilot applies a step input to the longitudinal control. Thus

$$CAP = \frac{\dot{q}_0}{\Delta n_{ss}} \tag{12.8,2}$$

This theory is based on the fact that in order to make precise adjustments to the flight path, the pilot must infer from the initial attitude response of the vehicle, the ultimate response of the flight path. It is found that the best cue for sensing attitude response is the initial angular acceleration in pitch ($\dot{q}_0$) which the pilot senses through his inner ear. For precision control tasks the pertinent steady-state parameter is taken to be the change in steady-state load factor (Δn_{ss}), which is related to flight-path curvature (see Sec. 6.10).

It is found that if an aircraft has a *CAP* which is too small, the pilot tends to overcontrol and rates the pitch response as sluggish. This comes about as follows.

When the flight path requires adjustment the pilot moves the controls and monitors the effect of this action by noting the size of the $\dot{q}_0$ generated. If the *CAP* is too small no $\dot{q}_0$ will be detected because it is below the threshold of the pilot's inner ear. Consequently he will apply more control input until a $\dot{q}$ is finally sensed. The result is an extremely large Δn_{ss} and the desired response is exceeded.

On the other hand, if the *CAP* is too large, the pilot tends to undershoot his desired flight-path corrections, and rates the response as fast, abrupt, and too sensitive. This occurs because any slight pitch control inputs from the pilot generate a large $\dot{q}_0$ which is interpreted as the prelude to a gross change in vehicle state and not the small desired change. As a result the pilot tends to reduce or reverse his pitch control input to avoid this, resulting in a steady-state response that is too small.

The *CAP* can easily be derived from relations previously given. $\dot{q}_0$ is simply the initial pitching moment divided by I_y, i.e.

$$\dot{q}_0 = \frac{M_\delta \Delta\delta_e}{I_y} \tag{12.8,3}$$

The steady-state load factor is obtained from (10.2,9), in conjunction with the short-period approximation (10.2,11) (note that $G_{V\delta} = 0$ in this approximation). The aerodynamic transfer functions are replaced by stability derivatives, we let $s = 0$, and neglect C_{L_q} and C_{L_δ} to get the approximate

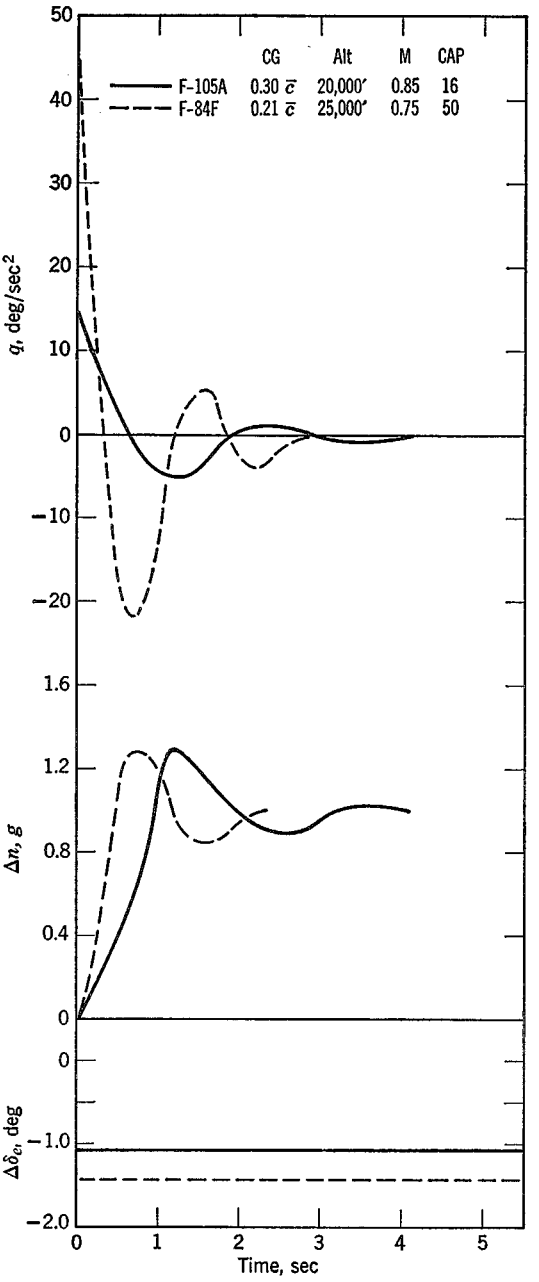

FIG. 12.14 A comparison of the response of two aircraft (from ref. 12.17).

result for the static gains:

$$K_{n\delta} = \frac{C_{L\alpha}}{C_{W_e}} K_{\alpha\delta}$$

$$K_{\alpha\delta} = \frac{2\mu C_{m\delta}}{2\mu \hat{I}_y \hat{\omega}_n^2}$$

$$\frac{\Delta n_{ss}}{\Delta \delta_e} = K_{n\delta} = \frac{C_{L\alpha}}{C_{W_e}} \cdot \frac{C_{m\delta}}{\hat{I}_y \hat{\omega}_n^2} \tag{12.8,4}$$

After conversion to dimensional form we get

$$\frac{\Delta n_{ss}}{\Delta \delta_e} = \frac{L_\alpha M_\delta}{W I_y \omega_n^2}$$

and

$$CAP = \frac{\dot{q}_0}{\Delta n_{ss}} = \frac{L_\alpha}{W \omega_n^2} = \frac{n_\alpha}{\omega_n^2} \tag{12.8,5}$$

The acceptable range in CAP extends upward from about 15 deg/sec^2/g. The upper limit has not been determined, with good pilot ratings obtained from 25–50 deg/sec^2/g. Figure 12.14 compares the pitch response of two different jet fighters. Under the conditions which prevailed for this test, the F-105A with a CAP of 16 deg/sec^2/g received an adverse rating while the F-84F was rated as "good" with respect to formation flying.

SPEED STABILITY

In addition to the vehicle's attitude response, the pilot also considers the speed stability of the aircraft when rating its handling qualities. This is especially true when performing such rectilinear maneuvers as the landing approach. In Sec. 11.5 it was shown that the aircraft response to a disturbance ΔV_0 in forward speed could be written as $\Delta V_0 e^{t/T}$. The response is convergent for T negative. Although no clear criterion for speed stability exists it appears that if in all other respects the aircraft is rated as satisfactory, then the pilot will rate the speed response as satisfactory if it is convergent with a time to half amplitude less than 35 sec. However, it is found that under certain conditions a vehicle can be rated as acceptable even if the speed response is divergent, provided that the time to double amplitude is greater than 17 sec.

LONGITUDINAL CONTROL SYSTEM CHARACTERISTICS ("FEEL")

The pilot commands longitudinal vehicle response mainly through control column inputs. Hence it is found that the characteristics of the control system

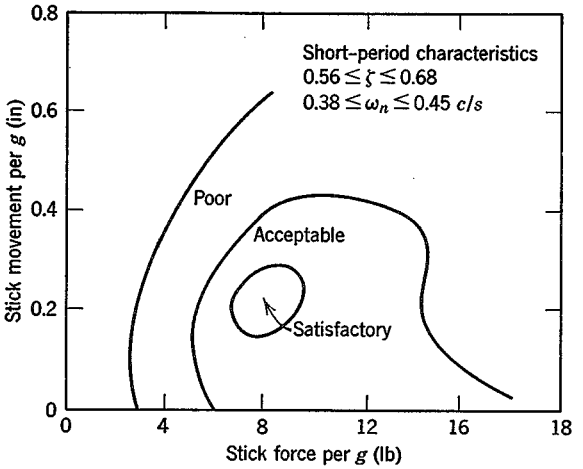

FIG. 12.15 Effect of stick force and stick movement per g on pilot opinion (from ref. 12.15).

influence the handling qualities of the vehicle. An otherwise satisfactory vehicle can be rated as poor due to a control system that does not "feel" right to the pilot. Figure 12.15 shows the manner in which pilot rating varied with stick movement per g and stick force per g in an aircraft with an irreversible control system. It is seen that there is only a relatively small region where a satisfactory rating is achieved, indicating the importance of the proper selection of control system characteristics. The studies which produced these results also determined that pilots do not object to break-out or frictional forces if they are not large when compared to the stick force per g.

12.9 LATERAL-DIRECTIONAL HANDLING QUALITIES

Generally speaking, lateral-directional control is more complex than longitudinal control. This, of course, is due to the fact that two axes of rotation are involved, leading to cross-coupling effects and the use of two primary control surfaces. As a result many groups of parameters are presently being studied to determine their correlation with pilot ratings. The following is intended to introduce the reader to some of these handling qualities parameters and to indicate the trends of research.

The primary lateral-directional control task facing the pilot is the control of bank angle through the aileron control system. The transfer function relating bank angle response to aileron input can be derived from (5.11,10) by putting $\Delta \bar{L}_c = L_\delta \Delta\delta_a$, $\Delta \bar{N}_c = N_\delta \Delta\delta_a$ and solving for the ratio $\bar{\phi}/\Delta\bar{\delta}_a$. The

result is

$$\frac{\bar{\phi}}{\Delta\bar{\delta}_a} = \frac{A_\phi(s^2 + 2\zeta_\phi\omega_\phi s + \omega_\phi{}^2)}{\left(s + \frac{1}{T_s}\right)\left(s + \frac{1}{T_R}\right)(s^2 + 2\zeta_d\omega_d s + \omega_d{}^2)} \qquad (12.9,1)$$

Here the factors in the denominator represent the spiral mode (time constant T_s), the roll mode (time constant T_R), and the lateral oscillation of radian frequency (ω_d) and damping (ζ_d). The values of these four constants come from the solution of the eigenvalue problem, discussed at some length in Chapter 9, where approximate solutions for them are also given. The user of the approximations should note their restricted range of validity. The numerator constants are given below with the aerodynamic transfer functions replaced by the corresponding stability derivatives, and with $Y_p \equiv Y_r \equiv \gamma_e \equiv 0$.

$$A_\phi = L'_\delta \qquad (a)$$

$$2\zeta_\phi\omega_\phi = -\left(N'_r + \frac{Y_v}{m}\right) + N'_\delta L'_r/L'_\delta \qquad (b) \quad (12.9,2)$$

$$\omega_\phi{}^2 = \left(\frac{Y_v}{m}N'_r + N'_\beta\right) - \frac{N'_\delta}{L'_\delta}\left(L'_\beta + \frac{Y_v}{m}L'_r\right) \qquad (c)$$

where

$$L'_i = \frac{L_i + \frac{I_{xz}}{I_z}N_i}{I_x - \frac{I_{xz}{}^2}{I_z}} \qquad (d)$$

$$N'_i = \frac{N_i + \frac{I_{xz}}{I_x}L_i}{I_z - \frac{I_{xz}{}^2}{I_x}} \qquad (e)$$

A partial list of parameter groups used in handling qualities studies includes ω_ϕ/ω_d, $\zeta_d\omega_d$, T_R, T_s, $|\phi/\beta|$, $|\phi/v_E|$, and $\dot{p}$ where $(v_E = v\sqrt{\rho/\rho_0})$.

SPIRAL MODE

The spiral mode time constant, T_s, determines the aircraft's tendency to maintain a given course when cruising. It is generally found that in the case of a divergent spiral mode, pilots will rate the aircraft as satisfactory provided that $|T_s| > 20$ sec.

ROLL CONTROL

If $\omega_\phi = \omega_d$ and $\zeta_\phi = \zeta_d$ so that the two quadratic terms in (12.9,1) cancel, or if only the initial vehicle roll response is considered, then for cases where $1/T_s$ is negligible the roll-to-aileron transfer function reduces to

$$\frac{\bar{\phi}}{\Delta\bar{\delta}_a} \doteq \frac{A_\phi}{s\left(s + \dfrac{1}{T_R}\right)} \tag{12.9,3}$$

which corresponds to the single-degree-of-freedom approximation (9.7,7). It has been found that this transfer function affects pilot ratings significantly. When considering this response it is convenient to look at closed-loop and open-loop control situations separately. Closed-loop control tasks involve the continuous monitoring of system error by the pilot and his responses to this stimulus. Examples of this type of control include formation flying, instrument flight, and landing. Open-loop control differs in that a previously-learned pattern is utilized to respond to a particular flight situation. No continuous monitoring of system error as such is involved and often the maneuver is of very short duration. Examples of this form of control are obstacle avoidance, rapid turn entry, and recovery from sudden upsets.

CLOSED-LOOP ROLL CONTROL

The pilot model of Sec. 12.2 has been used by Ashkenas (ref. 12.21) to study the handling qualities associated with the closed-loop control of bank angle. This application demonstrates the use of pilot models in analyzing the pilot/aircraft system. Figure 12.16 presents the closed-loop situation. It is assumed that the pilot is functioning in a compensatory fashion to

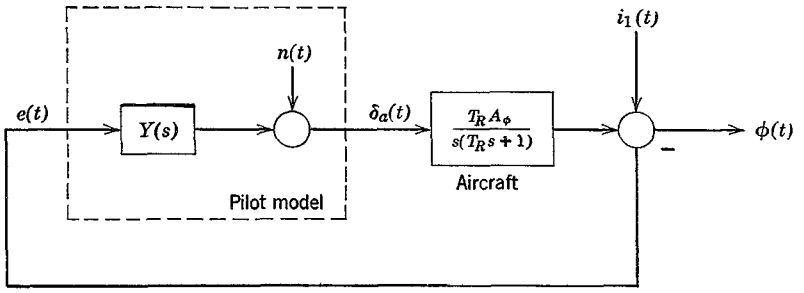

FIG. 12.16 Compensatory closed-loop roll control.

control external disturbances [represented by $i_1(t)$] to the vehicle's bank angle. [Note that this control situation is similar to that of Fig. 12.3b with $i_1(t) = -i(t)$.] In an attempt to achieve the equalization outlined in Sec. 12.2 the pilot adopts a form of describing function that reduces the combined transfer function of the pilot and aircraft as nearly as possible to K/s. This results in an attempt by the pilot to generate a lead equalization term to cancel the $1/(T_R s + 1)$ lag present in the aircraft. In addition, if the analysis is restricted to frequencies near the system crossover frequency, it is found that to a reasonable approximation all the dynamics associated with the pilot's neuromuscular system can be lumped in with the effective time delay as τ_E. This is found to be sufficient for the present application. The forward-loop transfer function is thus of the form

$$Y(s) \cdot \frac{\phi}{\Delta\delta_a} = \frac{K_p e^{-\tau_E s}(T_L s + 1) \cdot A_\phi T_R}{s(T_R s + 1)} \tag{12.9,4}$$

which reduces to

$$\frac{K_p e^{-\tau_E s} \cdot A_\phi T_R}{s} \tag{12.9,5}$$

if the pilot can generate $T_L = T_R$. It is found that human pilots are generally limited to $T_L \leq 5$ sec because of physiological factors. In addition, as T_R is reduced to zero it is found that pilots do not attempt to keep T_L equal to T_R. It appears that as soon as the phase lag contributed by T_R becomes acceptably small the pilot no longer feels the need to compensate for it. Figure 12.17 shows the T_L adopted by pilots for a range of T_R's.

In this isolated control situation, it would appear that the pilot rating could depend upon closed-loop system performance, the gain generated by the pilot, K_p, and T_L. Since the forward-loop transfer function always appears

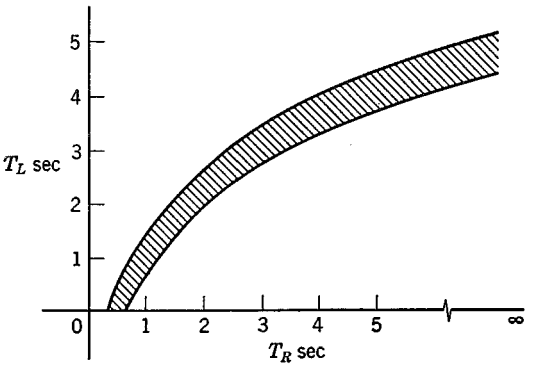

FIG. 12.17 Approximate T_L vs. T_R relationship (from ref. 12.21).

to be approximately K/s, all systems studied will tend to have similar response characteristics. If an experiment is performed wherein T_R is varied and the pilot is allowed to select the system gain A_ϕ at each step so as to be optimum in his opinion, then the rating assigned to each configuration should be mainly influenced by the T_L required of the pilot. The results of such an experiment (ref. 12.21) are given in Fig. 12.18. Here ΔR is the increase in pilot rating associated with T_L above the basic rating for the complete vehicle. The rating becomes less favorable as the pilot is required to generate

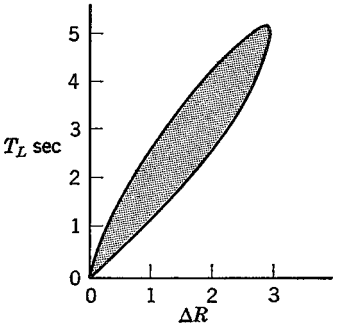

FIG. 12.18 Effect of T_L on pilot rating (from ref. 12.21).

lead (the generation of lead can be thought of as an attempt to anticipate the future input signal).

The optimum gain A_ϕ selected by the pilot for a particular value of T_R is assumed to be uniquely related to the pilot gain generated at the crossover frequency, ω_c. At crossover $|Y(i\omega_c)| \cdot |\bar{\phi}/\Delta\bar{\delta}_a(i\omega_c)| = 1$, and for a particular value of T_R, the optimum value of pilot gain, $|Y(i\omega_c)|_{\text{opt}}$, is assumed to be unique. Based on these assumptions the gain A_ϕ selected by the pilot can be found from (12.9,4) to be

$$A_\phi = \frac{\omega_c\sqrt{\omega_c^2 T_R^2 + 1}}{T_R\,|Y(i\omega_c)|_{\text{opt}}} \tag{12.9,6}$$

OPEN-LOOP ROLL CONTROL

When investigating open-loop roll control it is appropriate to consider the ratio of the roll time constant T_R to some typical maneuver time t_m, and/or the maximum roll acceleration following a unit step aileron input. The Laplace transform of the roll acceleration following a unit step aileron input ($\Delta\bar{\delta}_a = 1/s$) can be found from (12.9,3)

$$\bar{\ddot{\phi}} = \frac{T_R A_\phi}{T_R s + 1}$$

The maximum roll acceleration occurs at $t = 0$, and from the initial value theorem is

$$\ddot{\phi}(0) = \lim_{s \to \infty} s \frac{T_R A_\phi}{T_R s + 1}$$

$$= A_\phi$$

Figure 12.19 gives the pilot rating boundaries obtained from roll response studies of fighter-type aircraft (ref. 12.15). The lower boundary on these iso-opinion curves is blamed on oversensitivity of the controls and probably

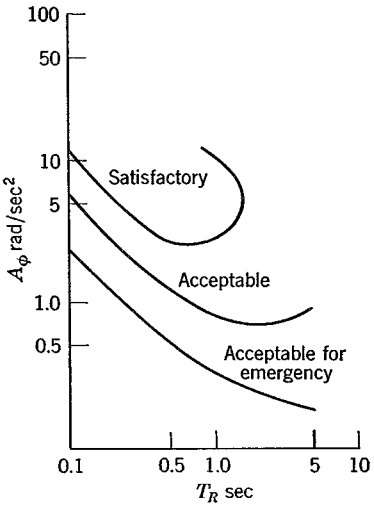

FIG. 12.19 Pilot rating of open-loop roll response (from ref. 12.15).

has the same basis as the poor ratings achieved with overly large values of the CAP discussed in the section on longitudinal handling qualities.

DUTCH-ROLL CHARACTERISTICS

The Dutch-roll oscillation may from a piloting standpoint be termed a nuisance factor. Its oscillatory nature is not purposely induced to perform any maneuver, and its presence may hinder the maintenance of precise flight-path control. Originally attempts were made to correlate pilot opinion with the ratio ϕ/β of the eigenvector and the damping of the oscillation. However, when it was found that pilots desired more damping for a given ϕ/β at lower flight speeds, the parameter $\phi/(u_0\beta)$ or ϕ/v was introduced to replace ϕ/β. Additional studies indicated that the altitude was also important with more damping being desired at higher altitude. This lead to the us-

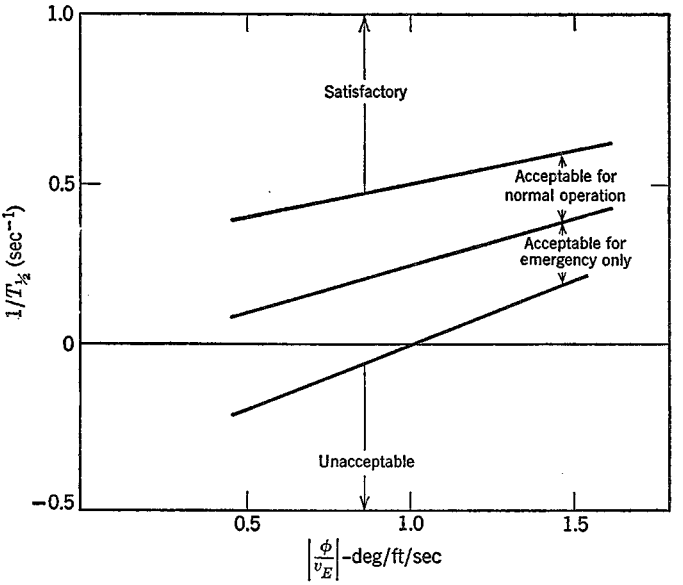

FIG. 12.20 Pilot opinion boundaries for Dutch-roll characteristics (from ref. 12.15).

of $\phi/v\sqrt{\rho/\rho_0}$ or ϕ/v_E. Further refinement then replaced cycles to half amplitude by the inverse of the time-to-half-amplitude, $1/T_{½}$. Figure 12.20 illustrates the pilot rating boundaries plotted on a $1/T_{½}$ vs. ϕ/v_E diagram. This is typical for fighter-type aircraft.

As is often the case in the field of handling qualities, this is not the final answer. In fact some results can be shown to correlate better with bank angle response to rudder input and root-mean-square bank angle response to random gust inputs.

ω_ϕ/ω_d AS A HANDLING QUALITIES PARAMETER

The ratio ω_ϕ/ω_d is a significant parameter when studying lateral-directional handling qualities. If $[\omega_\phi, \zeta_\phi] = [\omega_d, \zeta_d]$ then the quadratic factors in the numerator and denominator of (12.9,1) cancel. Or, to put it another way, the associated poles and zeros exactly cancel. The major consequence of such an occurrence is that the ϕ response to aileron becomes non-oscillatory, a very desirable circumstance. Another consequence would be the disappearance of the valley-peak sequence in the frequency response for ϕ/δ_a, as illustrated in Fig. 10.12*c*. When this special circumstance is not the case, then aileron inputs produce oscillatory responses. The cancellation of the quadratic

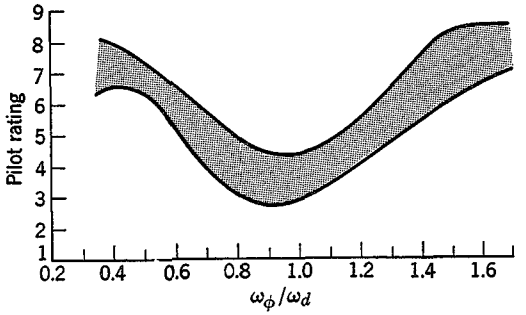

FIG. 12.21 Pilot ratings for a range of ω_ϕ/ω_d (from ref. 12.21).

factors depends mainly on the values of ω_ϕ and ω_d and less on ζ_ϕ and ζ_d. Hence the importance of ω_ϕ/ω_d as a parameter.

Detailed analysis shows that for $\omega_\phi/\omega_d > 1$ favorable yaw is generated, the opposite being true for $\omega_\phi/\omega_d < 1$. The yaw that occurs determines the amount and direction of rudder deflection needed to execute a coordinated turn. In addition, closed-loop bank angle control is difficult when $\omega_\phi/\omega_d > 1$. The general trend of pilot rating with ω_ϕ/ω_d is shown in Fig. 12.21. The general and marked preference for $\omega_\phi/\omega_d = 1$ is apparent. Figure 12.22 gives typical pilot iso-opinion curves for a range of $(\omega_\phi/\omega_d)^2$ and ζ_d. These curves indicate that, depending upon the value of ζ_d, the optimum value of ω_ϕ/ω_d may differ from unity.

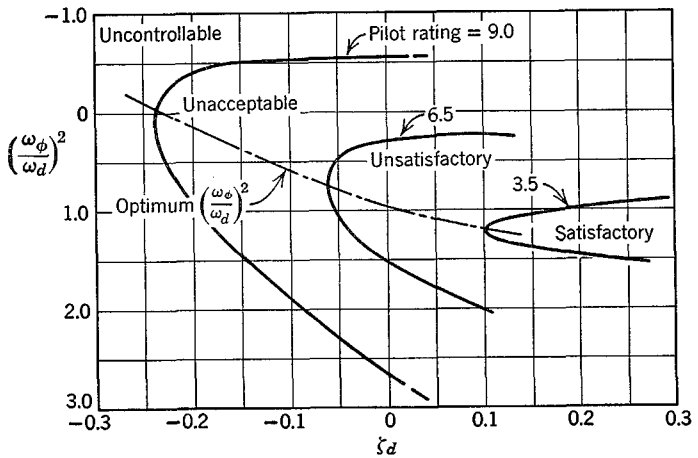

FIG. 12.22 Pilot iso-opinion curves for lateral-directional control (from ref. 12.21).

ROLL CONTROL SYSTEM CHARACTERISTICS ("FEEL")

The roll control system dynamics are important in establishing the handling qualities of an aircraft. From the small amount of research performed in this area the following general remarks apply:

1. Full aileron deflection with a wheel-type control should not require a rotation exceeding 90°.
2. Control sensitivities as high as 0.5 deg/sec rate of roll per degree of wheel displacement can be satisfactory.
3. The force required to apply full control should be about 40 lb.

12.10 HANDLING QUALITIES REQUIREMENTS

As a result of inability to carry out completely rational design of the man-machine combination, it is customary for the government agencies that are responsible for the procurement of military airplanes, or for licensing civil airplanes, to specify compliance with certain handling qualities requirements (e.g. refs. 12.26 to 12.28).

These requirements have been developed from extensive and continuing flight research. In the final analysis they are based on the opinions of research test pilots, substantiated by careful instrumentation. They vary from country to country and from agency to agency, and, of course, are different for different types of aircraft. They are subject to continuous study and modification in order to keep them abreast of the latest research and design information.

The purpose of these regulations is to ensure the safety of operation of new aircraft. If the rules are too lenient or incomplete the result can be degraded performance, poor flight safety, and perhaps an inability to complete the intended mission. On the other hand, if the rules are too stringent the penalties can be degraded performance, added complexity, and reduced economic efficiency. When a new aircraft is designed with novel features and performance characteristics, the old regulations are not always sufficient to cover the situation, and subsequent prolonged vehicle flight testing is then required before it can be certified. In the past, regulations have merely specified minima for the various aspects of handling qualities. It is anticipated that ongoing research in this field will lead to the specification of *optimum* values for the various handling qualities parameters and the definition of acceptable ranges for these parameters.

The following is intended to show the nature, not the detail, of typical handling qualities requirements. Most of the specific requirements can be classified under one of the following headings.

CONTROL POWER

The term control power is used to describe the efficacy of a control in producing a range of steady equilibrium or maneuvering states. For example, an elevator control which by taking positions between full up and full down can hold the airplane in equilibrium at all speeds in its speed range, for all configurations and C.G. positions, is a powerful control. On the other hand a rudder that is not capable at full deflection of maintaining equilibrium of yawing moments in a condition of one engine out and negligible sideslip is not powerful enough. The flying qualities requirements normally specify the specific speed ranges that must be achievable with full elevator deflection in the various important configurations, and the asymmetric power condition that the rudder must balance. They may also contain references to the elevator angles required to achieve positive load factors, as in steady turns and pull-up maneuvers ("elevator angle per g," Sec. 6.10).

CONTROL FORCES

The requirements invariably specify limits on the control forces that must be exerted by the pilot in order to effect specific changes from a given trimmed condition, or to maintain the trim speed following a sudden change in configuration or throttle setting. They frequently also include requirements on the control forces in pull-up maneuvers ("stick force per g," Sec. 6.10).

STATIC STABILITY

The requirement for static longitudinal stability (see Chapter 6) is usually stated in terms of the *neutral point* (defined in Sec. 6.3). It is usually required that the relevant neutral point (stick-free or stick-fixed) shall lie some distance (e.g. 5% of the mean aerodynamic chord) behind the most aft position of the C.G. This ensures that the airplane will tend to fly at a constant speed and angle of attack as long as the controls are not moved.

The requirement on static lateral stability is usually mild. It is simply that the spiral mode (see Chapter 9) if divergent shall have a time to double greater than some stated minimum (e.g. 4 sec).

DYNAMIC STABILITY

Generally the requirement on dynamic stability takes the form of a specification on the time to damp to half amplitude. The damping required for good flying qualities varies with the period.

STALLING AND SPINNING

Finally, most requirements specify that the airplane's behavior following a stall or in a spin shall not include any dangerous characteristics, and that the controls must retain enough effectiveness to ensure a safe recovery to normal flight.

Flight in a turbulent atmosphere

CHAPTER 13

13.1 INTRODUCTION

Of those obstacles with which nature confronts man in his use of the air as a medium of transportation, two are transcendent in importance—poor visibility that prevents him from seeing where he is going, and turbulent movement of the surrounding air that disturbs his vehicle and its flight path. To overcome these obstacles has always been and continues to be a major challenge to aviation. Poor visibility is associated with both darkness and weather, turbulence with weather alone. The former of these obstacles has to a great extent been overcome—modern navigation techniques permit blind flying with adequate safety for all but the critical phases of landing and take-off, and there is hope that the safety margins for these too will ultimately be acceptable.

The subject of this chapter is the second obstacle, turbulence. The motion of an aircraft in turbulence is akin to that of a ship on a rough sea, or an automobile on a rough road. It is subjected to buffeting by random external forces and as a result the attitude angles and trajectory experience random variations with time. The time scale and intensity of these responses are governed by the scale and intensity of the turbulence, as well as the speed and characteristics of the vehicle. Their effect is to produce fatigue in both the pilot and the structure, to endanger the structural integrity of the aircraft, to produce an uncomfortable, possibly even unacceptable, ride for

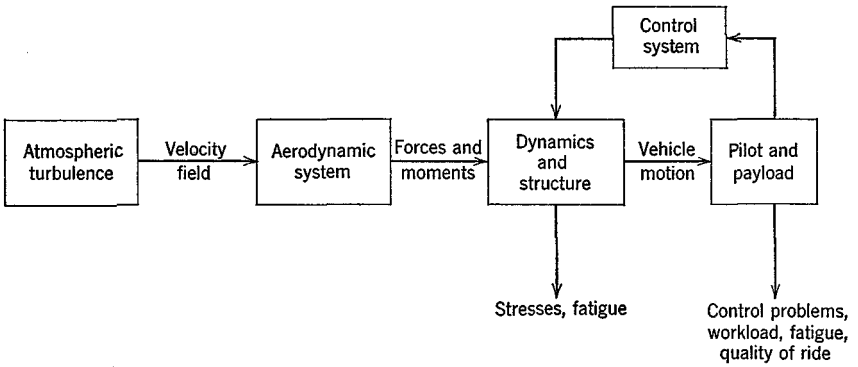

FIG. 13.1 Breakdown of the turbulence problem.

the passengers and cargo, and to impair the precise control of flight path needed for collision avoidance and safe landing.

To understand and analyze these responses, which is to provide the basis for ameliorating them, we dissect the total phenomenon into several parts, as illustrated in Fig. 13.1. The first is to describe the turbulence itself, the "output" of this description being the velocity field in which the airplane is immersed. Next, it is necessary to determine how these velocities result in aerodynamic forces and moments; these in turn become inputs to the mechanical/structural system whose mathematical modelling was the subject of Chapter 5. Finally, the motions and stresses that result serve to define the problems faced by the structure and the pilot. The diagram indicates that the pilot feeds back into the dynamic system via the controls—a feature that cannot be overlooked for realistic analysis. A study of all the problems embraced by the figure clearly spans the disciplines of meterology, aerodynamics, vehicle and structural dynamics, metal fatigue, and human factors. We make no attempt here to go in depth into all of these! The aim of the following is to extend the mathematical models previously given to embrace a description of the turbulence and the inputs provided by it. This model then provides the tool for calculating the responses of interest for any design or operational problem.

Since turbulence is a random process that cannot be described by explicit functions of time, only a statistical, probabilistic approach can be taken. The basic random-process theory needed was presented in Secs. 2.6 and 3.4, and the following relies heavily on that material. In particular the role of input spectra in computing output spectra should be recalled at this point [see (3.4, 48 to 51)], and the role of output spectra in calculating response probabilities (Sec. 2.6).

13.2 DESCRIPTION OF ATMOSPHERIC TURBULENCE

The total velocity field of the atmosphere is variable in both space and time, composed of a "mean" value and variations from it. The mean wind is a problem primarily for navigation and guidance and is not of interest here. We eliminate it by choosing as our reference frame the atmosphere-fixed frame F_A (see Sec. 4.2.4) relative to which the mean motion is zero. Let the velocity of the air relative to F_A at position $\mathbf{r} = [x_1 x_2 x_3]^T$ and time t be

$$\mathbf{u}(\mathbf{r}, t) = [u_1 u_2 u_3]^T \tag{13.2,1}$$

Then $u_i(\mathbf{r}, t)$ are random functions of space and time, i.e. we have to deal with the statistics of a random vector function of four variables (x_1, x_2, x_3, t).

Associated with any given point $\mathbf{r}$ and time t there is a 3×3 *correlation matrix* (second-order tensor)

$$R_{ij}(\boldsymbol{\xi}, \tau) = \langle u_i(\mathbf{r}, t) u_j(\mathbf{r} + \boldsymbol{\xi}, t + \tau) \rangle \tag{13.2,2}\dagger$$

As indicated, it is the ensemble average of the product of u_i at $\mathbf{r}$ and t with u_j at the different point $\mathbf{r} + \boldsymbol{\xi}$ and the later time $t + \tau$. The associated four-dimensional Fourier integral is the 3×3 matrix of four-dimensional *spectrum functions*

$$\theta_{ij}(\Omega, \omega) = \frac{1}{(2\pi)^4} \int_{-\infty}^{\infty} \int \int \int \int R_{ij}(\boldsymbol{\xi}, \tau) e^{-i(\Omega \cdot \xi + \omega\tau)} \, d\xi_1 \, d\xi_2 \, d\xi_3 \, d\tau \tag{13.2,3}$$

The inverse relation for Fourier integrals gives

$$R_{ij}(\boldsymbol{\xi}, \tau) = \int_{-\infty}^{\infty} \int \int \int \int \theta_{ij}(\boldsymbol{\Omega}, \omega) e^{i(\Omega \cdot \xi + \omega\tau)} \, d\Omega_1 \, d\Omega_2 \, d\Omega_3 \, d\omega \tag{13.2,4}$$

The functions R_{ij} and θ_{ij} serve (together with the assumption of normality) to describe the needed statistics of the turbulence. From them all the pertinent results can be derived (see Sec. 2.6); a principle objective of research into atmospheric turbulence is to ascertain their forms, and how their parameters depend on meteorological conditions, terrain, etc.

† $R_{ij}(\mathbf{0}, \tau)$ should not be confused with the time-delayed correlation measured by a fixed instrument in a flow passing it at a mean speed U.

SIMPLIFYING ASSUMPTIONS

Although there is some evidence that atmospheric turbulence is not necessarily normal, or Gaussian (ref. 13.1), many researchers have concluded that it is for practical purposes in many situations. There are great gains in simplicity in calculating the probabilities of exceeding given stress or motion levels if the process is Gaussian (see Sec. 2.6), for then one needs only the information given by the spectral distribution of the variables in question. We therefore assume that the random functions we have to deal with have normal distributions. (This assumption only enters when probabilities are being calculated, not correlations and spectra.)

The most general case, covered by (13.2,2 to 4) allows the turbulence statistics to vary from point to point and time to time—i.e. R_{ij} and θ_{ij} are functions of the base point $\mathbf{r}$ and base time t. One assumption made almost universally is that there is no dependence on t, i.e. that the turbulence is a *stationary process*. A second widely employed assumption is that the turbulence is effectively *homogeneous* i.e. that R_{ij} and θ_{ij} are independent of $\mathbf{r}$ at least along the path flown by the vehicle. At high altitudes, turbulence appears to occur in large patches, each of which can reasonably be taken to be homogeneous—but with differences from patch to patch. At low altitudes, near the ground, there are fairly rapid changes in the turbulence with altitude. However, for airplanes in nearly horizontal flight, homogeneity along the flight path is a reasonable approximation.

In general, the functions R_{ij} and θ_{ij} depend on the directions of the axes of F_A. This is especially so in the ground boundary layer. When this dependence is absent, and the evidence is that this is the case at high altitudes, then the turbulence is *isotropic*, i.e. all the statistical properties at a point are independent of the orientation of the axes. In this case it follows that the three mean-square velocity components are equal, i.e. the *intensity* is

$$\sigma^2 = <u_1^2> = <u_2^2> = <u_3^2> \tag{13.2,5}$$

When the turbulence is stationary and homogeneous it is also *ergodic*, so that time averages can replace ensemble averages—a matter of no small importance for experimental work.

Finally, the last simplifying assumption relates not so much to the turbulence itself but to the nature of the present problem. Airplanes fly for the most part at speeds large compared to the turbulent velocities and to their rates of change. Thus the vehicle can traverse a relatively large patch of turbulence in a time so short that the turbulent velocities have not had time to change very much. This amounts to neglecting t in the argument of $\mathbf{u}(\mathbf{r}, t)$, i.e. to treating the turbulenceas a *frozen* pattern in space. This

assumption is known as "Taylor's hypothesis." Its consequence is that

$$R_{ij}(\boldsymbol{\xi}, \tau) \to R_{ij}(\boldsymbol{\xi}) \qquad \text{and} \qquad \theta_{ij}(\boldsymbol{\Omega}, \omega) \to \theta_{ij}(\boldsymbol{\Omega})$$

and the Fourier integrals of (13.2,3) are triple rather than quadruple. The problem of computing aerodynamic forces and vehicle responses is correspondingly simplified.

Finally, then, the simplest model we can obtain is of homogeneous, isotropic, Gaussian, frozen turbulence. This is the model most commonly used for analysis of flight outside the ground boundary layer. Unfortunately, the strong anisotropy of boundary layer turbulence makes it unsuitable for landing and take-off; and for hovering flight the assumption of frozen turbulence is clearly also invalid.

Batchelor (13.2) has shown that in isotropic turbulence $R_{ij}(\boldsymbol{\xi})$ can be expressed in terms of two fundamental correlations, $f(\xi)$ and $g(\xi)$, viz.

$$\frac{R_{ij}(\boldsymbol{\xi})}{\sigma^2} = [f(\xi) - g(\xi)]\frac{\xi_i \xi_j}{\xi^2} + g(\xi)\delta_{ij} \tag{13.2,6}$$

where $\xi = |\boldsymbol{\xi}|$, δ_{ij} is the Kronecker delta, and σ^2 is given by (13.2,5). It should be observed that R_{ij} is zero whenever $i \neq j$ *and* either ξ_i or ξ_j vanishes, so that $R_{ij}(0) = 0$ for $i \neq j$. Other situations are illustrated in Fig. 13.2, a wing-fin system; the correlation of u_1 at A with either u_2 or u_3 at B vanishes because ξ_1 and ξ_3 are both zero, but that of u_1 at A with u_2 at C is not zero because ξ_1' and ξ_2' are both nonzero. Furthermore, the equation of continuity for an incompressible fluid imposes the condition

$$g = f + \tfrac{1}{2}\xi f' \tag{13.2,7}$$

$f(\xi)$ is known as the *longitudinal* correlation, typified by $R_{11}(\xi_1, 0, 0)$ and is associated with the condition illustrated in Fig. 13.3*a*. $g(\xi)$ is the *lateral*

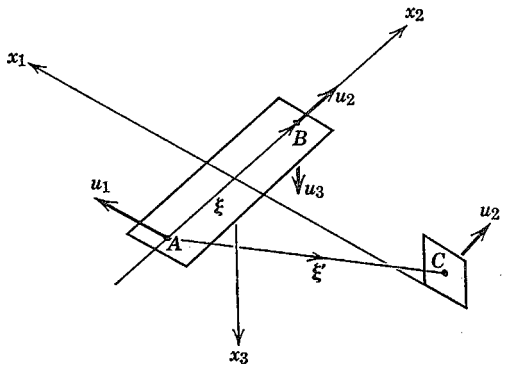

FIG. 13.2 Illustrating vanishing and nonvanishing correlations.

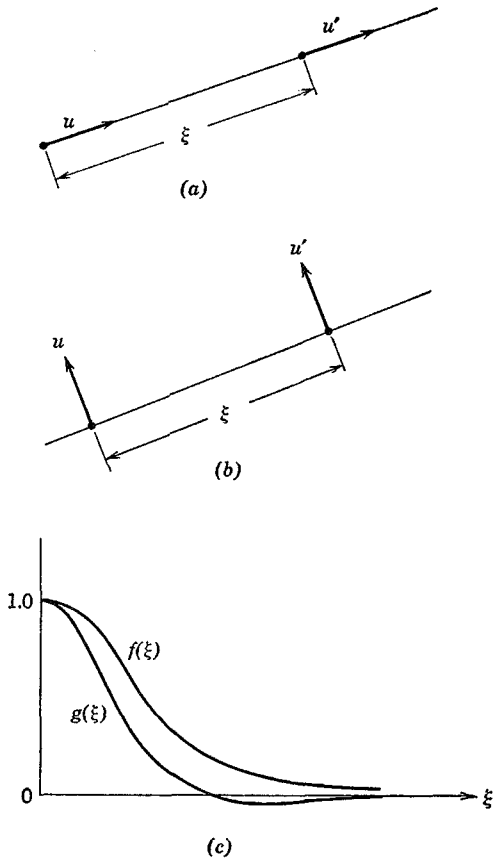

FIG. 13.3 Correlations in isotropic turbulence. (*a*) Longitudinal correlation, $f(\xi) = \langle uu' \rangle$. (*b*) Lateral correlation, $g(\xi) = \langle uu' \rangle$. (*c*) Typical forms of f and g.

correlation, typified by $R_{11}(0, \xi_2, 0)$ and is associated with the condition illustrated in Fig. 13.3*b*. The typical forms of these correlations are shown in Fig. 13.3*c*, when normalized to unity at $\xi = 0$.

The spectrum function in isotropic turbulence is expressible in terms of the basic energy spectrum function $E(\Omega)$, i.e.

$$\theta_{ij}(\boldsymbol{\Omega}) = \frac{E(\Omega)}{4\pi\Omega^4}(\Omega^2\delta_{ij} - \Omega_i\Omega_j) \tag{13.2,8}$$

$E(\Omega)$ is a scalar function that describes the turbulent energy density as a function of wave number magnitude, $\Omega = |\boldsymbol{\Omega}|$ such that

$$\tfrac{1}{2}(\overline{u_1^2} + \overline{u_2^2} + \overline{u_3^2}) = \int_0^\infty E(\Omega)\, d\Omega.$$

As with R_{ij}, the spectral density θ_{ij} is zero whenever $i \neq j$ and Ω_i or Ω_j vanishes. Thus $\theta_{ij}(0) = 0$ for $i \neq j$, and for many special values of the wave number vector.

The mean product of two velocity components at one point in frozen turbulence is $R_{ij}(0)$, which is from (13.2,4) (for frozen turbulence, ω and τ do not appear, and it is a triple integral)

$$\overline{u_i u_j} = \iiint_{-\infty}^{\infty} \theta_{ij}(\Omega_1, \Omega_2, \Omega_3)\, d\Omega_1\, d\Omega_2\, d\Omega_3 \tag{13.2,9}$$

Integration successively w.r.t. Ω_3 and Ω_2 yields the *two-dimensional* (Ψ) and *one-dimensional* (Φ) spectrum functions, i.e.

$$\overline{u_i u_j} = \iint_{-\infty}^{\infty} \Psi_{ij}(\Omega_1, \Omega_2)\, d\Omega_1\, d\Omega_2 = \int_{-\infty}^{\infty} \Phi_{ij}(\Omega_1)\, d\Omega_1 \tag{13.2,10}$$

where

$$\Psi_{ij}(\Omega_1 \Omega_2) = \int_{-\infty}^{\infty} \theta_{ij}(\Omega_1, \Omega_2, \Omega_3)\, d\Omega_3$$

$$\Phi_{ij}(\Omega_1) = \int_{-\infty}^{\infty} \Psi_{ij}(\Omega_1, \Omega_2)\, d\Omega_2 \tag{13.2,11}$$

Note that the mean-square value of any velocity component is [cf. (2.6,11)]

$$\overline{u_i^2} = \int_{-\infty}^{\infty} \Phi_{ii}\, d\Omega_1 \tag{13.2,12}$$

There is a more direct physical interpretation of the one-dimensional spectrum functions than the formal one given above. In homogeneous frozen turbulence consider the measurement of u_i and u_j along the x_1 axis (corresponding to measurement in flight along a straight line, or at a fixed point on a tower when the frozen field sweeps by it with the speed of the mean wind). The corresponding correlation is $R_{ij}(\xi_1, 0, 0)$ and its one-dimensional transform is $\Phi_{ij}(\Omega_1)$ i.e.

$$\Phi_{ij}(\Omega_1) = \frac{1}{2\pi} \int_{-\infty}^{\infty} R_{ij}(\xi_1, 0, 0) e^{-\Omega_1 \xi_1}\, d\xi_1 \tag{13.2,13}$$

Furthermore, if the x_1 axis is traversed at speed U (or the wind past the tower has speed U), then $\xi_1 = U\tau$, where τ is the time interval associated with the separation ξ_1.

Corresponding to the two basic correlations $f(\xi)$ and $g(\xi)$ for isotropic turbulence, are their two Fourier integrals, the *longitudinal* and *lateral one-dimensional spectra*, i.e. $\Phi_{11}(\Omega_1)$ and $\Phi_{33}(\Omega_1)$, respectively. By virtue of the

relation between f and g, Batchelor shows that

$$\Phi_{33}(\Omega_1) = \tfrac{1}{2}\Phi_{11}(\Omega_1) - \tfrac{1}{2}\Omega_1 \frac{d\Phi_{11}(\Omega_1)}{d\Omega_1} \tag{13.2,14}$$

The isotropy, of course, requires the symmetry relations

$$\begin{aligned} \Phi_{ii}(\Omega_j) &= \Phi_{33}(\Omega_1) \qquad \text{if } i \neq j \\ &= \Phi_{11}(\Omega_1) \qquad \text{if } i = j \end{aligned} \tag{13.2,15}$$

Most of the experimental information collected about atmospheric turbulence, on towers and by aircraft, is in the form of the above two one-dimensional spectra.

SPECTRAL COMPONENT OF TURBULENCE

We showed in Sec. 2.6 that a one-dimensional random function could be represented as a superposition of sinusoids (2.6,4). The analogous relation for three-dimensional turbulence is

$$\mathbf{u}(\mathbf{r}) = \iiint_{-\infty}^{\infty} e^{i(\boldsymbol{\Omega}\cdot\mathbf{r})}\, d\mathbf{C}(\boldsymbol{\Omega}) \tag{13.2,14}$$

which indicates that the individual spectral component is a velocity field of the form $\exp i(\Omega_1 x_1 + \Omega_2 x_2 + \Omega_3 x_3)$ and amplitude $d\mathbf{C}$. The triple integral signifies that integration is over $-\infty$ to $+\infty$ in each of the wave number components; or to put it another way, individual sinusoidal waves of all possible wave numbers are superimposed to make up the turbulent field. The individual spectral component has been shown by Ribner (ref. 13.3) to be an

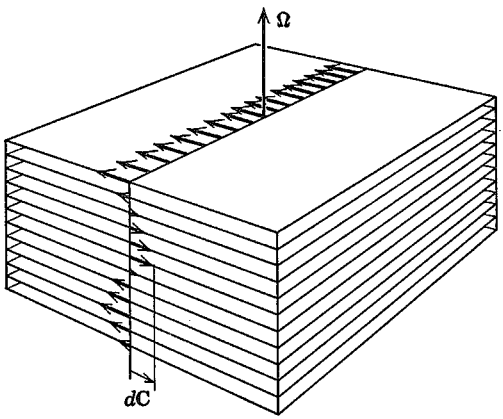

FIG. 13.4 Sinusoidal wave of shearing motion. (After H. S. Ribner, ref. 13.3.)

inclined shear wave as illustrated in Fig. 13.4. The velocity vector is perpendicular to the wave number vector, and is constant in planes normal to it. It is no more surprising that a superposition of waves like that shown can represent turbulence than that an infinite Fourier series can represent an arbitrary random function of time.

The spectral component in two dimensions, say Ω_1 and Ω_2, has the form $\exp i(\Omega_1 x_1 + \Omega_2 x_2)$; and is the sum (more properly integral) of all the three-dimensional waves having the given values Ω_1, Ω_2, but differing Ω_3. It can be pictured as in Fig. 13.5, which shows the node lines and the distribution

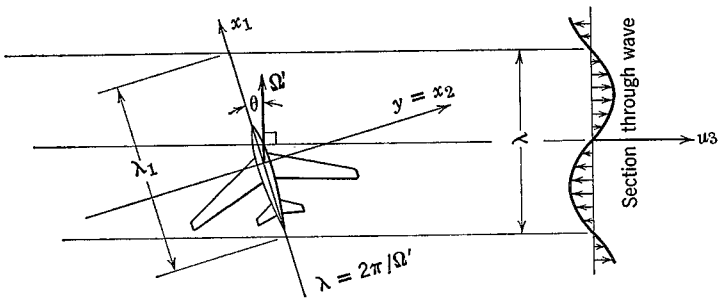

FIG. 13.5 Elementary spectral component in two dimensions. (After H. S. Ribner, ref. 13.4.)

of u_3 through a section of the wave. The two-dimensional wave number vector is $\boldsymbol{\Omega}' = [\Omega_1, \Omega_2]^T$, and is seen to lie at an angle θ to the x_1 axis. The wavelength is $\lambda = 2\pi/\Omega'$ and associated with the components of $\boldsymbol{\Omega}'$ are the wavelengths along the coordinate axes, $\lambda_1 = 2\pi/\Omega_1$ and $\lambda_2 = 2\pi/\Omega_2$.

Finally, the one-dimensional spectral component is a sinusoid on one axis, e.g. $e^{i\Omega_1 x_1}$, and is the sum of all two-dimensional components having the same Ω_1 or λ_1. This is the familiar spectral component of one-dimensional Fourier analysis.

INTEGRAL SCALE

There is an intuitive notion of the *scale* of turbulence. Clearly there are significant differences of "size" between the turbulence in the wing boundary layer, in the wake of the airplane, and in the atmosphere itself. These differences are quantified by a definition of integral scale derived from the correlation function. Thus let

$$L_{ij} = \frac{1}{u_i^2} \int_0^\infty R_{ii}(\boldsymbol{\xi})\, d\xi_j \qquad (13.2,15)$$

be a line integral on the ξ_j axis. It might be called "the j scale of the i velocity component." There are in general nine such scales, e.g. for u_1 measured along the x_1 axis, or u_3 measured along the x_2 axis, etc.

A second notion of scale derives from the spectral representation of turbulence. The wavelength at which the energy density peaks (see Fig. 13.6) is also a scale parameter, and for any given spectrum shape is uniquely related to L (defined below).

In isotropic turbulence, only two different scales are found, associated with the basic correlations f and g, and these are of course simply the areas

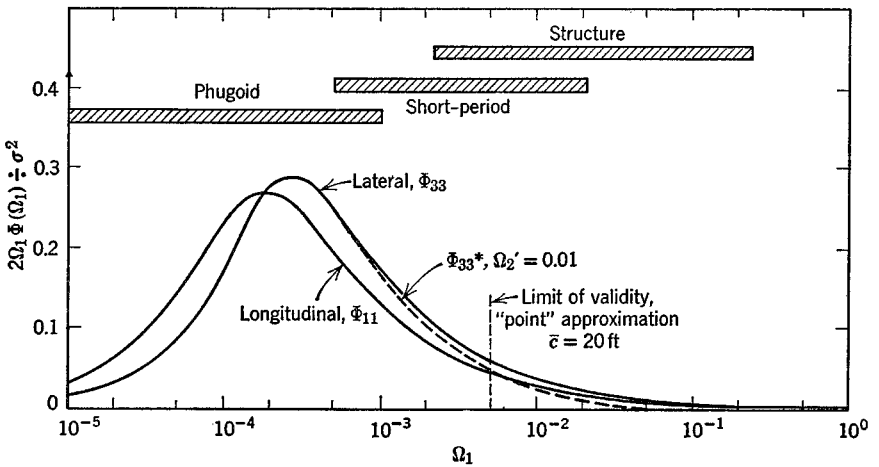

FIG. 13.6 One-dimensional spectra. Isotropic turbulence. Scale $L = 5000$ ft.

under the f and g curves. Because the maximum ordinate is unity, L_{ij} is equal to the width of a rectangle that contains the same area as the correlation curve—i.e. it is a measure of the spatial extent of significant correlation. The two scales are

$$L = L_{ij},\ i = j = \text{area under } f(\xi) = \textit{longitudinal} \text{ scale}$$
$$L' = L_{ij},\ i \neq j = \text{area under } g(\xi) = \textit{lateral} \text{ scale}$$

The continuity condition (13.2,7) yields $L = 2L'$.

The situation with respect to scale is unfortunately more complicated in the ground boundary layer where isotropy does not hold.

MODEL OF HIGH-ALTITUDE TURBULENCE

The experimental data on turbulence in clear air and in thunderstorms, and from altitudes below 5000 to 40,000 ft have been reviewed by Houbolt

et al. (ref. 13.5). They have examined it from the standpoint of scale, intensity, shape of one-dimensional spectra, homogeneity, isotropy, and normality. Their general conclusion is that an adequate model for analysis purposes is the simplest one described above—isotropic, homogeneous, Gaussian, and frozen. The intensity σ varies from very small to as much as 16 fps, and the scale is large, typically of order $L = 5000$ ft. The one-dimensional spectrum function that best fits the data for the vertical component of turbulence is the von Kármán spectrum

$$\Phi_{33}(\Omega_1) = \frac{\sigma^2 L}{2\pi} \frac{1 + \frac{8}{3}(aL\Omega_1)^2}{[1 + (aL\Omega_1)^2]^{11/6}} \tag{13.2,16}$$

$$a = 1.339$$

This spectrum function yields $\Phi \sim \Omega_1^{-5/3}$ as $\Omega_1 \to \infty$, a condition required to satisfy the Kolmogorov law in the so called inertial subrange (ref. 13.6). The energy spectrum function and some useful two- and one-dimensional spectra† of the von Kármán model are

$$E(\Omega) = \frac{55}{9\pi} \sigma^2 L \frac{(aL\Omega)^4}{[1 + (aL\Omega)^2]^{17/6}} \qquad (a)$$

$$\Psi_{11}(\Omega_1, \Omega_2) = \frac{\sigma^2}{6\pi} (aL)^2 \frac{1 + (aL\Omega_1)^2 + \frac{1}{3}(aL\Omega_2)^2}{[1 + a^2L^2(\Omega_1^2 + \Omega_2^2)]^{7/3}} \qquad (b)$$

$$\Psi_{22}(\Omega_1, \Omega_2) = \frac{\sigma^2}{6\pi} (aL)^2 \frac{1 + \frac{1}{3}(aL\Omega_1)^2 + (aL\Omega_2)^2}{[1 + a^2L^2(\Omega_1^2 + \Omega_2^2)]^{7/3}} \qquad (c) \tag{13.2,17}$$

$$\Psi_{33}(\Omega_1, \Omega_2) = \frac{4\sigma^2(aL)^4}{9\pi} \frac{(\Omega_1^2 + \Omega_2^2)}{[1 + a^2L^2(\Omega_1^2 + \Omega_2^2)]^{7/3}} \qquad (d)$$

$$\Phi_{11}(\Omega_1) = \frac{\sigma^2 L}{\pi} \frac{1}{[1 + (aL\Omega_1)^2]^{5/6}} \qquad (e)$$

$$\Phi_{22}(\Omega_1) = \Phi_{33}(\Omega_1) \qquad (f)$$

The inverse Fourier integrals of Φ_{11} and Φ_{33} provide the associated correlation functions (ref. 13.5).

$$f(\xi) = \frac{2^{2/3}}{\Gamma(\frac{1}{3})} \zeta^{1/3} K_{1/3}(\zeta) \qquad (a)$$

$$g(\xi) = \frac{2^{2/3}}{\Gamma(\frac{1}{3})} \zeta^{1/3} [K_{1/3}(\zeta) - \tfrac{1}{2}\zeta K_{2/3}(\zeta)] \qquad (b) \tag{13.2,18}$$

† Note that the spectra used herein are *two-sided*, such that for example $\sigma^2 = \int_{-\infty}^{\infty} \Phi(\Omega_1)\, d\Omega_1$. In ref. 13.5 and in many others, one-sided spectra are used that are double those herein, and the integration is from zero to infinity.

where $\zeta = \xi/(aL)$, and Γ, K denote gamma and Bessel functions, respectively.

With the typical value $L = 5000$ ft, the longitudinal and lateral one-dimensional spectra are as shown in Fig. 13.6. With this form of plotting, $\Omega\Phi$ vs. $\log_{10}\Omega$, the area under an element of the curve is $dA = \text{const} \times \Omega\Phi(1/\Omega)\, d\Omega = \text{const} \times \Phi(\Omega)\, d\Omega$ which is proportional to the contribution of the bandwidth $d\Omega$ to σ^2. Hence the shape of the curve truly shows the turbulent energy distribution.

The peak of $\Omega_1\Phi_{33}$ occurs at $L\Omega_1 = 1.33$, which shows directly how scale affects the spectrum. It also yields the "dominant wavelength," i.e.

$$\lambda_{1_{\text{peak}}} = \frac{2\pi}{\Omega_{1_{\text{peak}}}} = \frac{2\pi}{1.33} L = 4.7L$$

Thus for turbulence of 5000 ft scale, the dominant wavelength is about $4\frac{1}{2}$ miles, and the energy level is down by a factor of 25 at a wave length of 100 ft, the order of the size of an airplane.

For comparison, the ranges of Ω associated with typical rigid-body and structural-mode frequencies are indicated on Fig. 13.6. These show what relative excitation levels of these modes are to be expected from turbulence of this scale. The spectrum shifts without change of shape to the right for smaller L and to the left for larger. For example at a scale $L = 500$ ft, the spectra move to the right by one decade in Ω, and by two decades for $L = 50$ ft. This drastically alters the relative intensity of excitation of the various rigid-body and elastic modes. We shall see later that the difficulty of computing the response in any mode is very much affected by the wavelength λ associated with it. If very large compared to the dimensions of the airplane, the simplest analysis results. On the other hand, for structural modes of relatively short wavelength this condition is not met, and more sophisticated analysis is needed.

MODEL OF LOW-ALTITUDE TURBULENCE

Turbulence near the ground is of the boundary-layer variety (see Fig. 9.36), being variable with height and anisotropic. A model for this case should ideally give the following:

(i) Variation of mean wind with height as function of ground roughness.
(ii) Variation with height of $\overline{u_1^2}$, $\overline{u_2^2}$, $\overline{u_3^2}$.
(iii) Variation with height of all significant scales.
(iv) The form of the spectrum function θ_{ij}, or the correlation function R_{ij}.

Since the scales are much smaller than at high altitude, it becomes more important to have the two-dimensional spectrum functions $\Psi_{ij}(\Omega_1, \Omega_2)$, which enable both streamwise and spanwise variations of turbulent velocity to be

taken into account. The anisotropy also leads to the nonvanishing of the correlation $R_{13} = \langle u_1 u_3 \rangle$ (where x_1 is in the wind direction and x_3 vertical), which is simply related to the turbulent shear stress (Reynolds stress) in the boundary layer.

An interesting fact about low-altitude turbulence is the existence of a gap in the spectrum at a rather useful location. There is considerable evidence to show that the spectrum of wind speed measured by van der Hoven is representative, Fig. 13.7. This is a spectral density of horizontal wind speed taken as a function of time at a fixed point. The gap occurs for periods

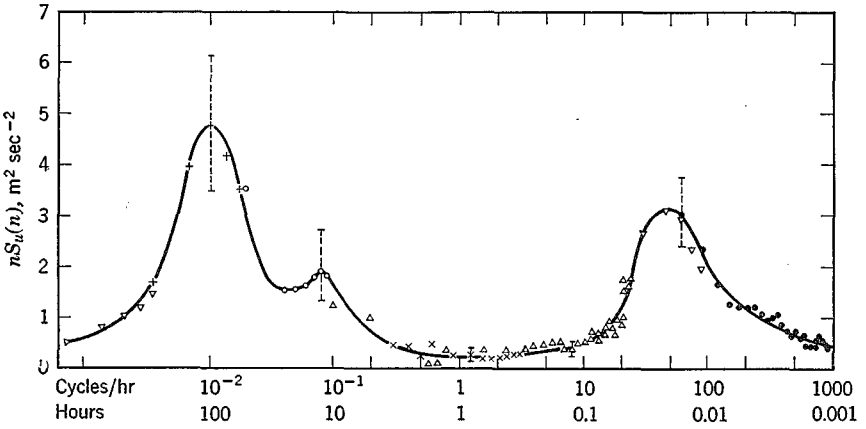

FIG. 13.7 Schematic spectrum of wind speed near the ground estimated from a study of van der Hoven (1957) (from ref. 13.6, p. 43).

greater than 6 min, or frequencies less than 10 cycles per hr. The lobe on the right corresponds to the turbulent energy of interest for flight (cf. Fig. 13.6).

The extensive information available on the wind-induced turbulence near the ground—much of it inconclusive and even contradictory—has recently been reviewed in refs. 13.7, 13.8. From these we adopt the following model as a reasonable representation of presently-available information: the turbulence is Gaussian, stationary, and homogeneous w.r.t. horizontal translations; it is anisotropic, but the one-dimensional spectra display isotropic behavior at the highest wave numbers; the turbulence is symmetric w.r.t. vertical planes.

VELOCITY PROFILE, MEAN WIND:

$$\frac{W}{W_G} = \left(\frac{h}{h_G}\right)^{\alpha} \tag{13.2,19}$$

where W = mean wind, h = height above ground, W_G and h_G are the speed and height outside the friction layer, and α and h_G depend on surface roughness (see Fig. 9.36).

COMPONENT INTENSITIES:

In the layer below about 300 ft:

$$\sigma_1 : \sigma_2 : \sigma_3 = 1 : 0.8 : 0.5 \tag{13.2,20}$$

where $\sigma_i^2 = \langle u_i^2 \rangle$, x_1 is in the wind direction, and x_3 is vertical. Above this height the σ_i tend toward equality at about 1000 ft.

SPECTRUM SHAPES:

The one-dimensional spectra are given by the von Kármán equations (13.2, 16 and 17*e*), with σ in Φ_{ii} replaced by σ_i. Thus because of (13.2,20) there are three different one-dimensional spectra.

SHEAR AND CROSS SPECTRA:

The turbulent shearing stress in the boundary layer results in nonvanishing $\overline{u_1 u_3}$, but symmetry requires $\overline{u_1 u_2} = \overline{u_2 u_3} = 0$. The data suggests

$$\overline{u_1 u_3} = 0.3 \sigma_1 \sigma_3$$

The one-dimensional cross spectrum $\Phi_{13}(\Omega_1)$ is taken to be real, and given by (ref. 13.8)

$$\Phi_{13}(\Omega_1) = \frac{\sigma_1 \sigma_3 \gamma_0}{\left[1 + \dfrac{L\Omega_1}{10}^2\right]^{1/2}} \left[\frac{\Phi_{11}(\Omega_1)}{\sigma_1^2} \frac{\Phi_{22}(\Omega_1)}{\sigma_2^2}\right]^{1/2}$$

in which a representative value of γ_0 is 0.5.

INTEGRAL SCALES:

For the boundary layer as a whole.

$$L_{11} = 20\sqrt{h}$$

$$L_{21} = L_{31} = 0.4h$$

Above about 200 ft, slightly better values are given by

$$L_{11} = 4.2h^{0.73}$$
$$L_{21} = L_{31} = 2.1h^{0.73}$$

13.3 THE INPUT TO THE AIRPLANE

The input to the airplane is the set of incremental aerodynamic forces and moments that derive from the turbulence—six associated with the rigid-body degrees of freedom and others with the elastic degrees of freedom. All of these inputs are, of course, random functions of a single variable, time, and are described statistically by the methods previously given. Once they are known, the problem of calculating system response is relatively routine. Let us illustrate the structure of the problem with a linear/invariant aerodynamic model. Let $\mathbf{g}$ be a vector (g for "gust") that somehow defines the atmospheric velocity field (specific forms for $\mathbf{g}$ are given below), let $\mathbf{f}$ be the associated aerodynamic force vector, and let $\mathbf{T}$ be a matrix of "gust transfer functions" that relates them:

$$\bar{\mathbf{f}}(s) = \mathbf{T}(s)\bar{\mathbf{g}}(s) \tag{13.3,1}$$

The determination of the input then consists of two parts—defining $\mathbf{g}$ and finding the elements of $\mathbf{T}$. When both of these are known, (13.3,1) yields the force vector, which can then be incorporated into the vehicle system equations in a more or less straightforward manner. The details of the process depend very much on the degree of idealization used and the assumptions made; examples are given below.

One approximation that is almost always made is to ignore the departure of the airplane from rectilinear flight, i.e. to assume it samples a frozen field on a straight line. The input statistics can then be derived quite readily from those of the turbulence given in frame F_A. Thus let F_A have axes parallel to F_W, and zero time be chosen so that the coordinates of the airplane mass center relative to F_A are $(V_e t, 0, 0)$. The connection between (x, y, z), the coordinates of a point in F_W, and (x_1, x_2, x_3) the coordinates of a point in F_A is then

$$x_1 = V_e t + x, \qquad x_2 = y, \qquad x_3 = z \tag{13.3,2}$$

We now change notation for the turbulent velocities, to emphasize that they are parallel to the axes of F_W, denoting them (u_g, v_g, w_g). Being functions of (x_1, x_2, x_3) they become functions of (x, y, z, t) via (13.3,2)—or for a *fixed point* of the airplane, functions of t only. The spectral component (see after

13.2,14) is then a velocity field of the form

$$\exp i[\Omega_1(V_e t + x) + \Omega_2 y + \Omega_3 z] = e^{i\Omega_1 V_e t} e^{i(\Omega_1 x + \Omega_2 y + \Omega_3 z)} \qquad (13.3,3)$$

or for the two-dimensional case, the above with the z term absent. It is seen to consist of a time-periodic velocity at any fixed point (x, y, z) of the vehicle.

Even when the system is linear, it is *not in general true* (as was erroneously stated on p. 321 of *Dynamics of Flight—Stability and Control*) that the response to turbulence can be constructed of a superposition of the three separate responses to u_g, v_g, and w_g. This is the case only when there are no cross-correlations between elements of the input vector associated with different components of the turbulence. Equations (3.4,48 and 49) make it clear that there are contributions to response power and cross spectra that derive from cross spectra of the input components. Such cross spectra exist *even in isotropic turbulence* if variations over the vehicle are allowed for, as illustrated in Fig. 13.2 for the points A and C of a wing-fin combination. In spite of the above theoretical condition, practical calculations of gust response are often made for one input component at a time. There is no assurance, however, that significant errors of omission will not occur when that is done.

THE AIRPLANE AS A POINT

The simplest approximation is that in which the variations of (u_g, v_g, w_g) over the vehicle are neglected. The airplane is in effect treated as a point traversing the x_1 axis, with coordinates $(V_e t, 0, 0)$. The input vector is then clearly

$$\mathbf{g} = \begin{bmatrix} u_g \\ v_g \\ w_g \end{bmatrix} \qquad (13.3,4)$$

Furthermore, the usual aerodynamic assumptions that lead to decoupling of the system equations into lateral and longitudinal sets make it possible to separate the response problem into two parts—the longitudinal response to

$$\mathbf{g}_1 = \begin{bmatrix} u_g \\ w_g \end{bmatrix} \qquad (13.3,5)$$

and the lateral response to

$$\mathbf{g}_2 = [v_g] \qquad (13.3,6)$$

The associated force vectors and gust transfer functions are

$$\bar{\mathbf{f}}_1 = \begin{bmatrix} \Delta\bar{C}_{T_g} \\ \Delta\bar{C}_{D_g} \\ \Delta\bar{C}_{L_g} \\ \Delta\bar{C}_{m_g} \end{bmatrix} = \begin{bmatrix} \hat{G}_{Tu_g} & \hat{G}_{Tw_g} \\ \hat{G}_{Du_g} & \hat{G}_{Dw_g} \\ G_{Lu_g} & \hat{G}_{Lw_g} \\ \hat{G}_{mu_g} & \hat{G}_{mw_g} \end{bmatrix} \begin{bmatrix} \bar{u}_g \\ \bar{w}_g \end{bmatrix} \tag{13.3,7}$$

$$= \mathbf{T}_1 \bar{\mathbf{g}}_1$$

$$\bar{\mathbf{f}}_2 = \begin{bmatrix} \Delta\bar{C}_{y_g} \\ \Delta\bar{C}_{l_g} \\ \Delta\bar{C}_{n_g} \end{bmatrix} = \begin{bmatrix} \hat{G}_{yv_g} \\ \hat{G}_{lv_g} \\ \hat{G}_{nv_g} \end{bmatrix} \bar{v}_g = \mathbf{T}_2 \bar{\mathbf{g}}_2 \tag{13.3,8}$$

where $[\hat{u}_g \hat{v}_g \hat{w}_g] = [u_g v_g w_g] \div V_e$.

The disturbing forces ΔC_{T_g} etc. can be incorporated in (5.13, 18 to 20) or (5.14, 1 to 3) by adding them to the associated control term, i.e. by replacing ΔC_{T_c} by $(\Delta C_{T_c} + \Delta C_{T_g})$, etc. Now in the point approximation there is no difference between aerodynamic forces associated with relative translation of the airplane w.r.t. the air whether it is the air that moves or the airplane, and in linear approximation $\hat{v}_g = \beta_g$, $\hat{w}_g = \alpha_g$. Thus the eleven transfer functions above are recognized as being identical to those previously used to relate airplane motion to aerodynamic forces, as follows (note the minus signs, u_g *reduces* the relative velocity, etc.):

$$\mathbf{T}_1 = -\begin{bmatrix} \hat{G}_{TV} & \hat{G}_{T\alpha} \\ \hat{G}_{DV} & \hat{G}_{D\alpha} \\ \hat{G}_{LV} & \hat{G}_{L\alpha} \\ \hat{G}_{mV} & \hat{G}_{m\alpha} \end{bmatrix}; \qquad \mathbf{T}_2 = -\begin{bmatrix} \hat{G}_{y\beta} \\ \hat{G}_{l\beta} \\ \hat{G}_{n\beta} \end{bmatrix} \tag{13.3,9}$$

The adoption of the point approximation means that the airplane is assumed to be vanishingly small with respect to the wavelengths of all significant spectral components (e.g. $\lambda >>$ span in Fig. 13.3). The non-dimensional frequency parameter used in the Theodorsen and Sears functions for unsteady flow effects is $k = \omega\bar{c}/2V_e$, which we can relate to Ω_1 by (13.3,3). It gives $\omega = \Omega_1 V_e$, whence

$$k = \Omega_1 \frac{\bar{c}}{2} = \pi \frac{\bar{c}}{\lambda_1} \tag{13.3,10}$$

Thus $(\bar{c}/\lambda_1) \to 0$ implies $\Omega_1 \bar{c} \to 0$ and $k \to 0$. Hence it is consistent in this

approximation to use the quasistatic aerodynamic representation by aerodynamic derivatives. Finally then the gust transfer functions are

$$\mathbf{T}_1 = -\begin{bmatrix} C_{T_V} & C_{T_\alpha} \\ C_{D_V} & C_{D_\alpha} \\ C_{L_V} & C_{L_\alpha} \\ C_{m_V} & C_{m_\alpha} + sC_{m_{\dot{\alpha}}} \end{bmatrix}; \qquad \mathbf{T}_2 = -\begin{bmatrix} C_{y_\beta} \\ C_{l_\beta} \\ C_{n_\beta} \end{bmatrix} \tag{13.3,11}$$

RANGE OF VALIDITY OF THE POINT APPROXIMATION

It should be observed at the outset that the only excitation of the lateral modes that can exist in this approximation is that provided by v_g. In fact comparable inputs may arise from the spanwise gradients in w_g and u_g, which are explicitly excluded in this approximation. It must therefore be considered of limited usefulness for calculating lateral response.

In considering the validity for longitudinal response, we must ascertain for what limiting values of (Ω_1, Ω_2) or (λ_1, λ_2) the airplane of Fig. 13.5 can be considered to be vanishingly small. We consider the limits on Ω_1 and Ω_2 separately.

For Ω_1 we use the criterion that the complex amplitude of the lift on a finite wing flying through a sinusoidal inclined wave of upwash shall not depart too far from its value at $k = 0$. This problem has been solved by Filotas (ref. 7.16), and from his results we may take as a reasonable upper limit $k \doteq .05$. It follows that the range of validity is

$$\begin{aligned} \Omega_1 \frac{\bar{c}}{2} &< .05 \\ \frac{\lambda_1}{\bar{c}} &> \frac{\pi}{.05} \doteq 60 \end{aligned} \tag{13.3,12}$$

For an airplane with mean chord of 20 ft, this yields $\Omega_1 < .005$, and as shown on Fig. 13.6 for large-scale turbulence a small part of the turbulent energy is contained in the spectral components of wavelength shorter than this. This fraction increases rapidly, however, with decrease in L or increase in chord.

For the limit on Ω_2 we again use Filotas' result for finite wings. He finds that the effect of spanwise variation is given by the factor

$$\frac{4}{\Omega_2 b} J_1\left(\frac{\Omega_2 b}{2}\right)$$

where J_1 denotes a Bessel function of the first kind and b is the wing span. This factor is unity when $\Omega_2 = 0$, and decreases by roughly 10% at $\Omega_2 b/2 = 1$.

We therefore take this value as the upper limit for Ω_2 in the point approximation, i.e.

$$\frac{\Omega_2 b}{2} < 1$$
$$\frac{\lambda_2}{b} > \pi \tag{13.3,13}$$

For an airplane of span 100 ft, the upper limit on Ω_2 is 2×10^{-2}. Its effect is not immediately apparent, however, as was the case with the Ω_1 limit. To evaluate it, we must calculate the *truncated* one-dimensional spectra

$$\Phi_{ij}^*(\Omega_1) = \int_{-\Omega_2'}^{\Omega_2'} \Psi_{ij}(\Omega_1, \Omega_2)\, d\Omega_2 \tag{13.3,14}$$

in which the integration excludes those wave numbers that exceed the valid limit. These truncated spectra cannot be evaluated explicitly in terms of elementary functions for the von Kármán spectra, but can be for the Dryden spectra. Formulae and graphs of the latter are given in ref. 13.10. To show the effect of truncation, $\Phi_{33}^*(\Omega_1)$ has been evaluated numerically for the von Kármán spectrum, with $L = 5000$ ft, $b = 200$ ft, and $\Omega_2' = 2/b$. The result is shown on Fig. 13.6. It is seen to be quite close to the basic spectrum Φ_{33} for these values of scale and span, the difference being confined to the high wave numbers. The areas under Φ_{33} and Φ_{33}^* differ by only a few percent. For smaller scale of turbulence the difference increases.

In summary we may conclude that for many cases, especially for large-scale turbulence and small airplanes, the point approximation can give useful results of good accuracy for the longitudinal rigid-body responses. It is probably better, and certainly simpler, to use the basic (not truncated) one-dimensional spectra, on the grounds that including the small contribution from the short-wavelength components of the spectrum with an inaccurate theory is better than leaving them out altogether. On the other hand, no such general statement can be made about the responses in the structural or lateral rigid-body modes.

THE FINITE AIRPLANE

The finite extent of the airplane is seen to be important when significant variations of gust velocity can occur between one point and other—e.g. between right and left wing tips, or between wing and tail. An example of these effects for a wing is seen in the experimental results of Nettleton (ref. 13.14), a sample of which is shown in Fig. 13.8. This is a rather extreme case in that the scale of the turbulence L is about equal to the wing chord. The aspect ratio is effectively infinite. Here w is the upwash measured a short

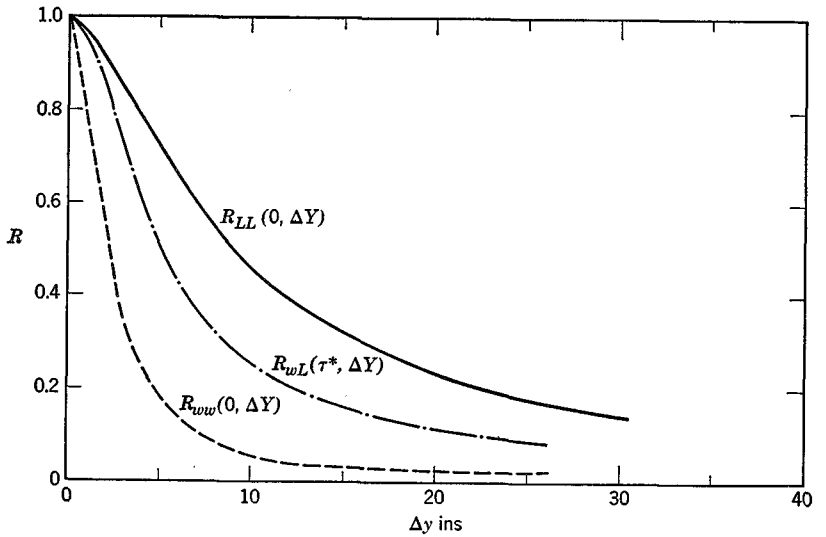

FIG. 13.8 Spanwise cross-correlations of a wing in small-scale turbulence.

distance in front of the wing, L is the lift measured on a small strip of wing, Δy is the spanwise separation of two lift strips, or of one strip and the upwash probe, and τ^* is the time delay for which $R_{wL}(\Delta y, \tau)$ is a maximum. A relatively small correlation length for w is seen to lead to a larger correlation length for (w, L) and a still larger one for (L, L).

To allow for such effects, i.e. to remove altogether or in part the limitations we found above on wave number, naturally entails some cost in additional complexity of analysis or experiment. We outline below the principles of five methods of doing this that seem adequately to span the spectrum of possible approaches, although they are not all-inclusive. In all the analysis methods the approximation is made that the airplane has no significant z dimension, i.e. that variations of the gust field with z are negligible. The turbulence is then characterized by a two-dimensional spectrum function $\Psi(\Omega_1, \Omega_2)$ or its associated correlation function. Each of the methods has advantages and limitations, and the choice for any particular study will reflect the problem itself, the kind and extent of aerodynamic information and computing machinery available, and the tastes of the analyst.

THE "PANEL" METHOD (ref. 13.5)

In this method the principle aerodynamic surfaces are divided into N panels, as illustrated in Fig. 13.9. At a reference point of the nth panel the

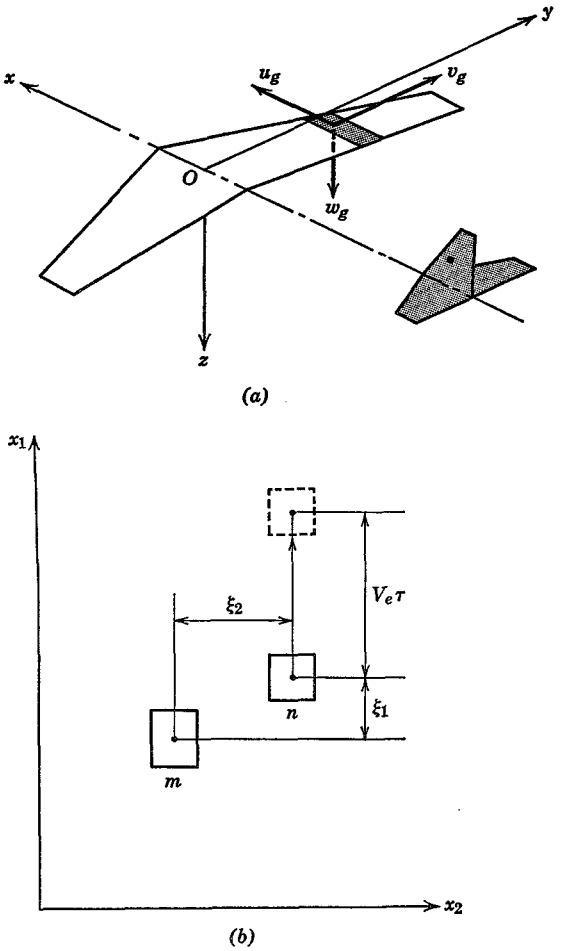

FIG. 13.9 The panel method.

turbulent velocities are $[u_{g_n}(t), v_{g_n}(t), w_{g_n}(t)]$, and the gust vector $\mathbf{g}$ is the $3N$ column of all these components. The force vector is then

$$\bar{\mathbf{f}} = \mathbf{T}\bar{\mathbf{g}} \tag{13.3,15}$$

where $\mathbf{f}$ is an $(M \times 1)$ vector, M being dependent on the problem, and $\mathbf{T} = [t_{ij}]$ is an $(M \times 3N)$ matrix of aerodynamic coefficients. To carry out the analysis of $\mathbf{f}$ and subsequently of the spectra of vehicle response one must first evaluate all the $3MN$ transfer functions $t_{ij}(s)$ and then apply the

input/output theorem (3.4,48). The latter includes all the cross-spectral densities of the components of **g**, which do not all vanish.

When the method is applied for one velocity component only, say w_g, and for a relatively small number of panels, the matrix **T** is not excessive in size. The time functions for the input elements are obtained by using (13.3,2), and the relevant cross spectra are derived from them (note that in this formulation each input and output quantity is a function of time only). Consider for example the w_g components at the mth and nth panels, $w_{g_m}(t)$ and $w_{g_n}(t)$. The cross-correlation is

$$R'_{mn}(\tau) = \overline{w_{g_m}(t) \cdot w_{g_n}(t + \tau)}$$

which by using Fig. 13.9*b* we can identify as

$$R'_{mn}(\tau) = R_{33}(\xi_1 + V_e\tau, \xi_2, 0)$$

where ξ_1 and ξ_2 are as shown, and R_{33} is obtained from (13.2,6) as

$$R_{33} = \sigma^2 g\{(\xi_1 + V_e\tau)^2 + \xi_2^2\}.$$

$g(\xi)$ for the von Kármán model is given by (13.2,18). The Fourier integral of $R'_{mn}(\tau)$ is then the required one-dimensional input spectrum

$$\phi'_{mn}(\omega) = \frac{1}{2\pi}\int_{-\infty}^{\infty} R'_{mn} e^{-i\omega\tau}\, d\tau.$$

For further details of the panel method the reader is referred to ref. 13.5 and the literature cited therein.

SKELTON'S METHOD

A method proposed by Skelton (ref. 13.11) for a study of a VTOL airplane is in some respects similar to both the preceding and following methods, yet different from each. In it three points on the vehicle, for example two wing tips and the tail, are used to identify nine inputs—three gust components at each of these three control points, thus

$$\mathbf{g} = [u_{g_1}, v_{g_1}, \ldots, w_{g_3}]^T,$$

a (9×1) vector. The method is therefore similar to the panel method in that the gust vector is defined by the turbulent velocities at a discrete set of points. To compute the aerodynamic transfer functions Skelton assumes

that the disturbance velocity field is linear in both x and y, so that a change in w_{g_1} for example implies a change in w_g over the whole vehicle of an amount proportional to the perpendicular distance from the line passing through points 2 and 3. In making an assumption about the whole velocity field associated with each input it resembles the following method. The complete gust matrix **T** in this formulation of the analysis, for six degrees of freedom would be a (6×9) matrix. However it would with the usual assumptions separate into two smaller matrices for lateral and longitudinal subsystems.

For further details the reader is referred to ref. 13.11.

THE POWERS SERIES METHOD

A method proposed by the author (refs. 13.9, 13.10) is a "natural" extension of the point approximation to higher order. In it the velocity field of the airplane is expanded in a Taylor series around the C.G. Thus a typical component such as w_g would be described by

$$w_g(x, y, t) = w_g(t) + w_{g_x}(t)x + w_{g_y}(t)y + \tfrac{1}{2}w_{g_{xx}}(t)x^2 + \cdots \quad (13.3,16)$$

in which $w_g(t)$, $w_{g_x}(t) \cdots$ denote values of w_g, $\partial w_g/\partial x \cdots$ at the C.G. Since the velocity field is now completely fixed by the coefficients of series like (13.3,16), the vector describing the gust field is the column of all these coefficients. In ref. 13.10 the elements of the vector are separated into those that produce longitudinal and lateral forces, i.e.

$$\mathbf{g}_1 = \begin{bmatrix} u_g \\ w_g \\ u_{g_x} \\ w_{g_x} \\ v_{g_y} \\ \cdot \\ \cdot \\ \cdot \end{bmatrix} \quad ; \quad \mathbf{g}_2 = \begin{bmatrix} v_g \\ v_{g_x} \\ u_{g_y} \\ w_{g_y} \\ \cdot \\ \cdot \\ \cdot \end{bmatrix} \quad (13.3,17)$$

where only the coefficients of the linear terms in the Taylor series expansions have been listed. The number of terms retained fixes both the domain of validity in wave number space and the complexity of the analysis.

We consider now the limits of validity of the first-order Taylor expansion corresponding to (13.3,17). The method of ref. 13.9 [Eqs. (9.1) et seq.] when applied to the linear part only of the velocity field yields values of C_L and C_m in good agreement with the exact Sears function for $k < .5$. Thus the

limit on Ω_1 is given by [cf. (13.3,12)]

$$\text{or} \qquad \Omega_1 \frac{\bar{c}}{2} < .5 \qquad \frac{\lambda_1}{\bar{c}} > 6 \tag{13.3,18}$$

A large gain in the valid range of Ω_1 (one decade) is obtained relative to the point approximation, but only at the cost of using transfer functions for unsteady oscillatory motion to represent the aerodynamics. If quasi-steady aerodynamics is used (e.g. $G_{L_\alpha} = C_{L_\alpha}$ etc.) then (3.3,12) still holds. It may well be questioned why the power-series method should be used at all with unsteady aerodynamics—why not preferably go directly to the exact two-dimensional transfer functions for gust penetration (see Ribner's method below)? The advantage, if any, of this method rests in the availability, or ease of obtaining, results for oscillatory translation and rotation of the vehicle.† The theoretical and experimental problems posed by the oscillatory boundary condition have proved more tractable in the past than that of the "running wave" characteristic of gust penetration; solutions for oscillatory motions have been vigorously pursued in connection with flutter analyses, and measurements of oscillatory transfer functions, although by no means easy, are much simpler than those for gust penetration.

The limit on Ω_2 is assessed from a consideration of the rolling moment acting on the wing. An argument based on symmetry considerations (only antisymmetric distributions of velocity produce rolling moments) shows that an expansion in wave number would be of the form

$$C_l = ae^{ikt}\Omega_2 \frac{b}{2} - k\left(\Omega_2 \frac{b}{2}\right)^2 + \cdots \tag{13.3,19}$$

Filotas' approximate solution for rolling moment can in fact be expressed in this form, with $k = \frac{1}{12}$. Now the linear power series approximation, as we show below, is equivalent to retaining only the first term in (13.3,19). Hence the error can be assessed from the $\Omega_2{}^3$ term, leading to the limit for about 10% error, $\Omega_2 b < 2$ which is the same as (13.3,13) for the lift in the point approximation.

In summary then, the first-order power series method, with quasi-steady aerodynamics, has the effect of extending the point approximation to embrace lateral responses, with the limitations

$$\lambda_1/\bar{c} > 60 \qquad \lambda_2/b > \pi$$

If unsteady oscillatory aerodynamics are used, the λ_1 limitation is relaxed to $\lambda_1/\bar{c} > 6$.

† The method was presented at a time when no "two-dimensional Sears function" was available.

We turn now to the gust transfer function for the power series method. As an example let us consider the equations for rigid-body response, and use the first-order series. Then from (13.3,17) we get [cf. (13.3,7)—for simplicity of notation, the subscript g has been omitted here]

$$\mathbf{T}_1 = \begin{bmatrix} \hat{G}_{Tu} & \hat{G}_{Tw} & \hat{G}_{Tu_x} & \hat{G}_{Tw_x} & \hat{G}_{Tv_y} \\ \hat{G}_{Du} & \hat{G}_{Dw} & \hat{G}_{Du_x} & \hat{G}_{Dw_x} & \hat{G}_{Dv_y} \\ \hat{G}_{Lu} & \hat{G}_{Lw} & \hat{G}_{Lu_x} & \hat{G}_{Lw_x} & \hat{G}_{Lv_y} \\ \hat{G}_{mu} & \hat{G}_{mw} & \hat{G}_{mu_x} & \hat{G}_{mw_x} & \hat{G}_{mv_y} \end{bmatrix} \tag{13.3,20}$$

with an obviously similar matrix for $\mathbf{T}_2$. In the quasi-steady approximation, some of these matrix elements would be neglected, and the remaining ones would be expressed as aerodynamic derivatives. We have already discussed the aerodynamic forces associated with (u_g, v_g, w_g), i.e. the elements of the first two columns above, which are identical with (13.3,7). The remaining elements describe the effect of "gust-gradients" on the airplane. The gradient terms w_x, w_y correspond to linearly varying downwash over the airplane surface, which provides boundary conditions on relative motion precisely equivalent to rigid-body pitch and roll rotations of the vehicle—see Fig. 7.13, which illustrates the w_x case. The equivalent rates of pitch and roll are readily found for an upwash wave of unit amplitude given by [see (13.3,3)]

$$w_g(x, y, t) = e^{i\Omega_1 V_e t} e^{i(\Omega_1 x + \Omega_2 y)} \tag{a}$$

i.e.

$$p_g = -\left.\frac{\partial w_g}{\partial y}\right|_0 = -w_{g_y} = -i\Omega_2 w_g \tag{b}$$

$$\hat{p}_g = -w_{g_y} t^* \tag{13.3,21}$$

and

$$q_g = \left.\frac{\partial w_g}{\partial x}\right|_0 = i\Omega_1 w_g \tag{c}$$

$$\hat{q}_g = q_g t^*$$

note that

$$\Omega_1 V_e t = \Omega_1 \frac{\bar{c}}{2} \hat{t} = k\hat{t}$$

Associated with these velocity-gradient terms are aerodynamic forces and moments exemplified by

$$\Delta C_l = C_{l_p} \hat{p}_g = -C_{l_p} t^* w_{g_y}$$

$$\Delta C_m = C_{m_q} t^* w_{g_x}$$

etc.

The x and y gradients of u_g and v_g that appear in (13.3,17) do not have correspondingly elegant general interpretations. For example, the influence

of u_{g_y} on unswept wings of large aspect ratio is clearly like that of yaw rate, with equivalent value

$$r_g = \left.\frac{\partial u_g}{\partial y}\right|_0 = u_{g_y} = i\Omega_2 u_g \tag{13.3,22}$$

However, for small aspect ratio or swept wings the situation is not so simple. For a further discussion of the gradient terms, see ref. 13.10.

Finally, the matrix of input spectra is needed to complete the analysis. For the vector g_1 of (13.3,17) and for isotropic turbulence this would be the 5×5 Hermitian matrix:

$$\mathbf{\Phi} = \begin{bmatrix} \Phi_{uu} & 0 & 0 & 0 & \Phi_{uv_y} \\ \cdot & \Phi_{ww} & 0 & \Phi_{ww_x} & 0 \\ \cdot & \cdot & \Phi_{u_x u_x} & 0 & \Phi_{u_x v_y} \\ \cdot & \cdot & \cdot & \Phi_{w_x w_x} & 0 \\ \cdot & \cdot & \cdot & \cdot & \Phi_{v_y v_y} \end{bmatrix} \tag{13.3,23}$$

The zero elements arise from isotropy (ref. 13.10).

Formulae and graphs of the above spectrum functions associated with the Dryden model of the turbulence are given in ref. 13.10. (No corresponding information is available for the von Kármán spectrum, although it can readily be derived.)

RIBNER'S METHOD

The method proposed by Ribner (ref. 13.4) does not fit the pattern of the foregoing ones in that no function equivalent to $\mathbf{g}(t)$ is explicitly defined. Instead the response is found as a superposition of responses to individual spectral components like that pictured in Fig. 13.5. Thus let the w_g component of a single wave be described by [cf. (13.3,21*a*)]

$$dW e^{ikt} e^{i(\Omega_1 x + \Omega_2 y)}$$

This time-periodic velocity field induces periodic incremental pressure distributions that integrate to periodic incremental forces and moments, of which for example the lift is described by

$$dL e^{ikt}$$

The relationship between the lift and the velocity is given by an aerodynamic transfer function, $\Gamma(\Omega_1, \Omega_2)$, i.e.

$$dL = \Gamma(\Omega_1, \Omega_2)\, dW$$

(note that $k = \Omega_1 \bar{c}/2$). The mean-square incremental lift produced by the whole turbulent field is then given by the basic response theorem [(3.4,51)

extended to two dimensions]

$$L^2 = \int_{-\infty}^{\infty}\int |\Gamma(\Omega_1, \Omega_2)|^2 \Psi_{33}(\Omega_1, \Omega_2)\, d\Omega_1\, d\Omega_2$$

and the one-dimensional spectrum for lift is

$$\Phi_{LL}(\Omega_1) = \int_{-\infty}^{\infty} |\Gamma(\Omega_1, \Omega_2)|^2 \Psi_{33}(\Omega_1, \Omega_2)\, d\Omega_2$$

Any vehicle response variable such as angle of attack or load factor is treated like the lift above, but the transfer function is of course different.

The heart of this approach is the availability of aerodynamic transfer functions like Γ, of which a whole matrix is in general required for all the generalized forces and moments associated with rigid and elastic degrees of freedom, and with u_g, v_g, and w_g inputs. There are methods available for calculating some of these transfer functions for some wing shapes (refs. 7.16, 13.12), and for propellers (ref. 13.13).

In view of the fact pointed out previously, that the spectra of vehicle responses to u_g, v_g, w_g cannot in general be simply superposed (owing to the nonvanishing of certain cross-correlations or cross spectra), the three velocity components should, strictly speaking, be considered simultaneously. Ribner's method has not yet been explicitly extended to cover this case.

THE SIMULATION METHOD

When the system equations are nonlinear or the input is nonstationary the foregoing methods of analysis all fail. In such situations one approach is to construct an appropriate mathematical model of the system—analog or digital—and feed in random inputs representing the turbulence. The statistical properties of the output can then be determined by analogue or digital analysis techniques.

In this connection mention should be made of a possible experimental technique that does not appear to have been applied yet. It would consist of exposing a rigid model of the vehicle to a wind-tunnel flow simulating the real turbulence. Force transducers could then produce time records of the actual input forces, thus bypassing the whole problem represented by the second box of Fig. 13.1. The measured forces and moments provide directly the required inputs to the mathematical model, which could be connected on line. In transient situations an ensemble of records could supply the appropriate statistics.

13.4 AN EXAMPLE

We shall calculate the longitudinal response of the jet transport used in previous examples, cruising at 30,000 ft through turbulence of 5000 ft scale. In this situation the point approximation is valid, and (13.3,7 and 11) give the needed input function. For the aerodynamic derivatives we use the same numerical values as in Sec. 9.1. The system equations are used in Laplace transfrom form, i.e. (5.14,2) with α_T and γ_e both zero.

We noted in Sec. 11.2 that the phugoid oscillation could be suppressed by the pilot by a simple feedback of pitch-attitude to the elevator deflection. We provide for this in the following equations by including the control equation $\Delta\delta_e = -K\theta$. On combining the equations we get:

$$\mathbf{A}(s)\bar{\mathbf{y}}(s) = \mathbf{B}(s)\begin{bmatrix}\bar{u}_g\\ \bar{w}_g\end{bmatrix} \tag{13.5,1}$$

where $(\bar{u}_g, \bar{w}_g)$ are Laplace transforms of the nondimensional gust velocities $(\hat{u}_g, \hat{w}_g)$, and

$$\mathbf{A} = \left[\begin{array}{c|c|c|c|c} (C_{T_V} - C_{D_V} - 2\mu s) & C_{L_e} - C_{D_\alpha} & 0 & -C_{W_e} & 0 \\ \hline -(C_{L_V} + 2C_{W_e}) & -(C_{L_\alpha} + C_{D_e} + 2\mu s) & 2\mu - C_{L_q} & 0 & -C_{L_\delta} \\ \hline -C_{m_V} & -(C_{m_\alpha} + sC_{m_{\dot\alpha}}) & -(C_{m_q} - \hat{I}_y s) & 0 & -C_{m_\delta} \\ \hline 0 & 0 & 1 & -s & 0 \\ \hline 0 & 0 & 0 & K & 1 \end{array}\right] \tag{13.5,2}$$

$$\bar{\mathbf{y}} = [\overline{\Delta V} \quad \overline{\Delta\alpha} \quad \bar{q} \quad \overline{\Delta\theta} \quad \overline{\Delta\delta_e}]^T \tag{13.5,3}$$

$$\mathbf{B} = \left[\begin{array}{c|c} C_{T_V} - C_{D_V} & -C_{D_\alpha} \\ \hline -C_{L_V} & -C_{L_\alpha} \\ \hline -C_{m_V} & -C_{m_\alpha} \\ \hline 0 & 0 \\ \hline 0 & 0 \end{array}\right] \tag{13.5,4}$$

The required frequency-response functions are found by substituting $s = ik(= i\Omega_1 V_e t^*)$ and solving the resulting complex algebraic equation for the ratios $\bar{y}_i(ik)/\bar{u}_g$ and $\bar{y}_i(ik)/\bar{w}_g$.

A response variable of interest not directly included in the above is the load factor. It is defined by $\Delta n = \Delta L/W$. The lift increment ΔL is taken

as the sum of two parts, that due to aircraft motion ($\Delta\alpha$, ΔV) and that due to atmospheric motion (u_g, w_g). The result obtained is

$$\begin{aligned} \frac{\overline{\Delta n}}{\bar{w}_g} &= \frac{C_{L_\alpha}}{C_{W_e}}\left(\frac{\overline{\Delta\alpha}}{\bar{w}_g} - 1\right) + 2\frac{\overline{\Delta V}}{\bar{w}_g} && (a) \\ \frac{\overline{\Delta n}}{\bar{u}_g} &= \frac{C_{L_\alpha}}{C_{W_e}}\frac{\overline{\Delta\alpha}}{\bar{u}_g} + 2\left(\frac{\overline{\Delta V}}{\bar{u}_g} - 1\right) && (b) \end{aligned} \qquad (13.5,5)$$

Some of the more interesting transfer functions and output spectra are plotted in Figs. 13.10 and 13.11. In Fig. 13.10 we show the squares of the moduli of the transfer functions for speed, angle of attack, pitch attitude, and load factor for vertical gust input. Both stick-fixed and controlled motion are shown. All the motion responses fall off rapidly at high wave number (or high frequency), but the load factor response tends to the constant value associated with flight on a rectilinear path at constant speed (i.e. no *motion* response). At wave numbers above 10^{-2} the load factors are progressively more approximate because of the neglect of unsteady aerodynamics. Much more accurate values could be obtained by the simple expedient of multiplying these by a reduction factor for finite wings in sinusoidal gusts—obtained from the generalized Sears function as given by Filotas (ref. 7.16). [The appropriate factor is actually Filotas' $|S(k_1, A)|^2$.]

The effect of the simple elevator-control law (the simple gain is not, of course, the optimum control law for reducing gust response) is seen, as expected, to eliminate the phugoid peaks and substantially to reduce the pitch response for all frequencies lower than that of the short-period mode. With respect to α response, the airplane is seen to act like a low-pass filter, with cut-off frequency at the short-period mode.

On combining these transfer functions with the input spectrum, we get the output spectra, e.g. for speed response

$$\Phi_{VV}(\Omega_1) = \left|\frac{\overline{\Delta V}}{\bar{w}_g}\right|^2 \Phi_{33}(\Omega_1) \qquad (13.5,6)$$

etc. These are shown on Fig. 13.11. (Note that these are two-sided spectra—twice the area gives the mean square.) It is seen that the point approximation is quite adequate in this example for giving the responses in the motion variables (ΔV, $\Delta\alpha$, θ) but is less satisfactory for the load factor, for which a substantial fraction of the mean-square value is contributed by frequencies above the limit of validity of this approximation. The use of a corrected transfer function as noted above would improve the accuracy of this result appreciably.

If the gust input vector were extended to include the gust-gradient term

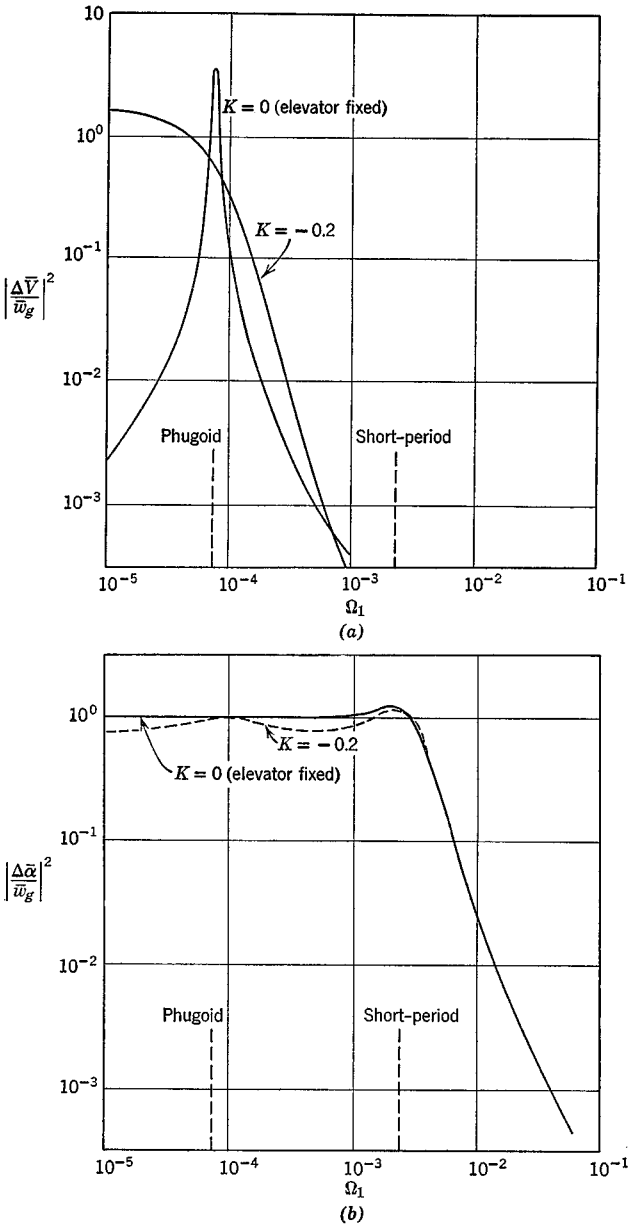

FIG. 13.10 Transfer functions for response to w_g input. Jet transport cruising at 30,000 ft and 500 mph with pitch feedback.

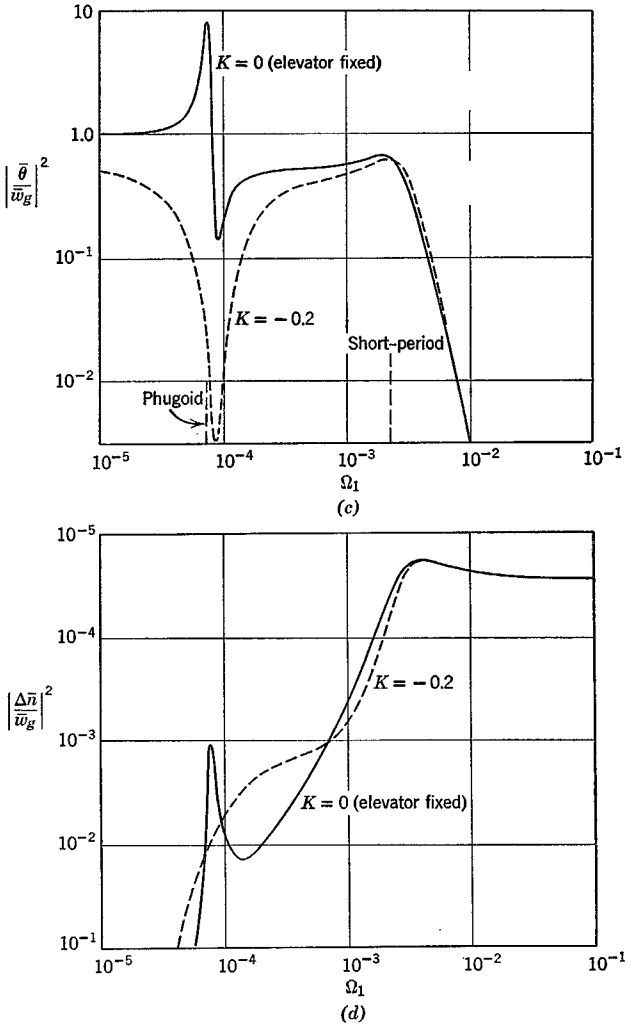

FIG. 13.10. (*Cont.*)

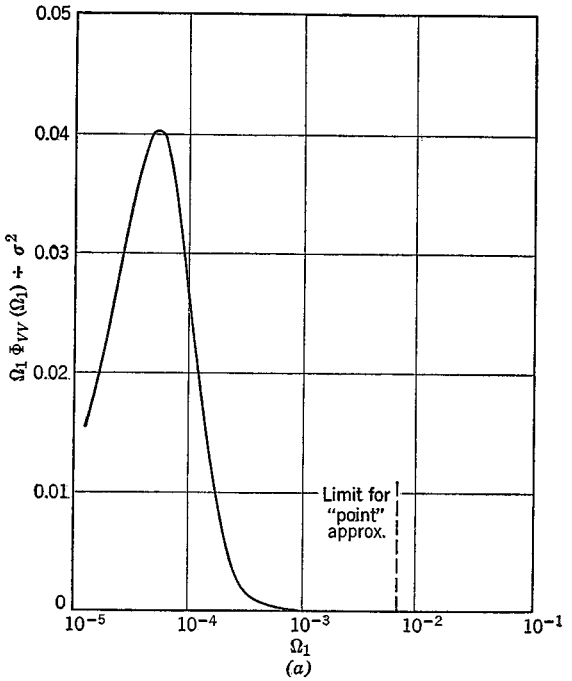

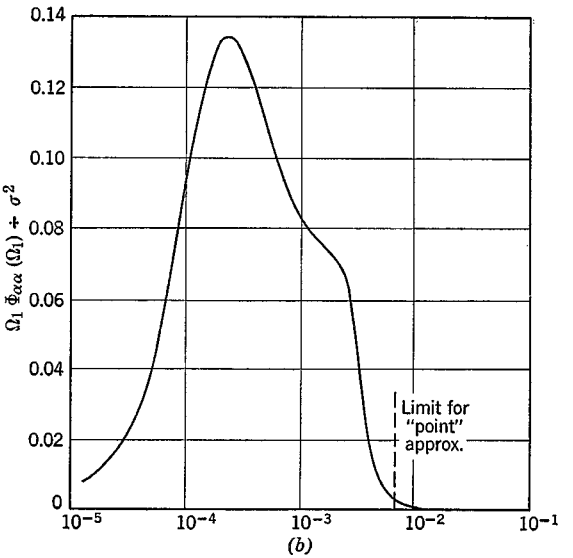

FIG. 13.11 Power spectra of response to w_g input. Jet transport cruising at 30,000 ft and 500 mph with pitch feedback.

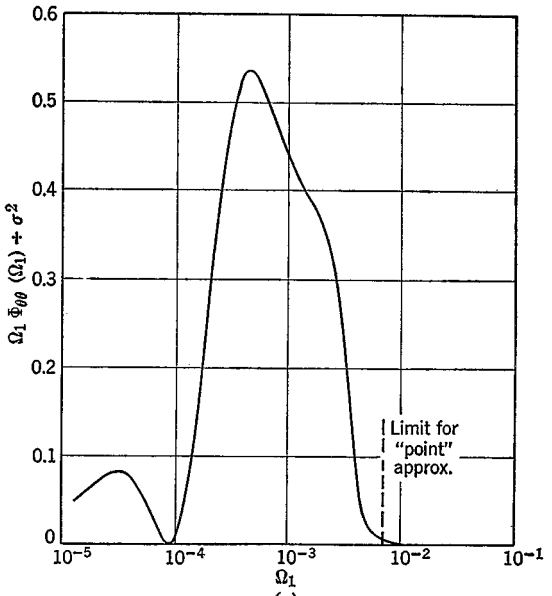

(c)

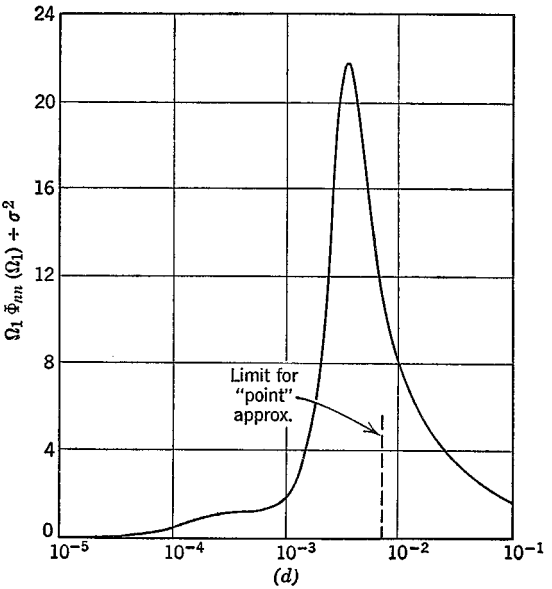

(d)

FIG. 13.11. (*Cont.*)

$\partial w_g/\partial x = q_g$, then the right-hand side of (13.5,1) would read

$$\cdots = \mathbf{B}'(s)\begin{bmatrix}\bar{u}_g\\ \bar{w}_g\\ \bar{q}_g\end{bmatrix} \tag{13.5,7}$$

where $\bar{q}_g$ is the Laplace transform of $\hat{q}_g = q_g t^*$, and $\mathbf{B}'(s)$ would be like $\mathbf{B}(s)$ but with the additional column $[0 \quad -C_{L_q} - C_{M_q} \quad 0 \quad 0]^T$. In this case the general response theorem (3.4,49) would have to be used to calculate outputs, since the cross spectra of both u_g and w_g with q_g are not zero (ref. 13.10). This would entail the calculation not only of the moduli of the transfer functions, but of their real and imaginary parts. [An alternative but equivalent method for this case was given in *Dynamics of Flight—Stability and Control* (Sec. 10.6), that does not use the input cross spectra.]

13.5 GUST ALLEVIATION

The term gust alleviation interpreted in its broadest sense can mean the reduction of any response variable associated with the turbulence. If in these responses we include structural stresses and vehicle accelerations as well as attitude and trajectory variables it may well be that reducing one response increases another. For example, if pitch attitude is controlled to try to keep the lift constant, then a reduction in $\overline{\Delta L^2}$ would be associated with increases in $\overline{\Delta\theta^2}$ and $\overline{q^2}$. The term gust alleviation is sometimes used in a more restricted sense, applied to the load factor only.

When one tries to control load factor by a feedback control to the elevator, the inherent time lag associated with pitching motion is usually such as to make this approach not highly effective (ref. 13.15). When a wing flap control is simultaneously used, however, to control the wing lift almost instantaneously in response to aircraft normal acceleration, pitch rate, and pitch attitude, reductions of an order of magnitude in $\overline{\Delta n^2}$ can be achieved (ref. 13.16).

This illustrates the direction in which we must go in striving for *ideal* gust alleviation (no doubt unachievable in practice). That is, the perturbations in all forces and moments produced by the gust field should be just cancelled by automatic fast-acting aerodynamic devices, such as flaps and spoilers, circulation control, etc. The ideal result would be a vehicle that would have the same motion and structural stresses in rough air as in smooth—i.e. rectilinear translation and unity load factor, but with its various automatic gust alleviation devices being very active indeed. To be successful

such a system would probably need gust field sensors (perhaps angle of attack and sideslip vanes much like those used in the measurement of turbulence by aircraft) located at strategic points such as wing tips and tail. With suitable input-rate terms incorporated, sufficient lead time for actuating the aerodynamic devices might be obtained. There does not appear to be any *fundamental* technological impediment to achieving very substantial reductions in gust response by this approach. Considerations of weight, cost, and reliability, however, may present serious economic and operational impediments.

BIBLIOGRAPHY

Chapter 1

1.1 F. W. Lanchester. *Aerodonetics*. A. Constable & Co. Ltd., London, 1908.

1.2 G. H. Bryan and W. E. Williams. The Longitudinal Stability of Aerial Gliders. *Proc. Roy. Soc. London*, ser. A, vol. 73, pp. 100–116, 1904.

1.3 G. H. Bryan. *Stability in Aviation*. Macmillan Co., London, 1911.

1.4 L. Bairstow. *Applied Aerodynamics*, 2nd ed. Longmans, Green and Co., 1939.

1.5 B. Etkin and P. C. Hughes. Explanation of the Anomalous Spin Decay of Satellites with Long Flexible Antennae. *J. Spacecraft*, vol. 4, no. 9, Sept. 1967.

1.6 B. M. Jones. *Aerodynamic Theory* (ed. by W. F. Durand), vol. 5. Springer, Berlin, 1935.

1.7 A. Miele. *Flight Mechanics—1. Theory of Flight Paths*. Addison-Wesley Pub. Co., Reading Mass., 1962.

1.8 A. W. Babister. *Aircraft Stability and Control*. Pergamon Press, Oxford, 1961.

1.9 R. L. Bisplinghoff and H. Ashley. *Principles of Aeroelasticity*. John Wiley & Sons, Inc., New York, 1962.

1.10 E. Seckel. *Stability and Control of Airplanes and Helicopters*. Academic Press, New York, 1964.

1.11 T. Hacker. *Flight Stability and Control*. Elsevier Pub. Co., New York, 1970.

1.12 R. C. Duncan. *Dynamics of Atmospheric Entry*. McGraw-Hill Book Co., Inc., New York, 1962.

1.13 C. D. Perkins. Development of Airplane Stability and Control Technology. *J. Aircraft* vol. 7, no. 4, 1970.

Chapter 2

2.1 J. Heading. *Matrix Theory for Physicists*. Longmans, Green and Co., London, 1958.

such a system would probably need gust field sensors (perhaps angle of attack and sideslip vanes much like those used in the measurement of turbulence by aircraft) located at strategic points such as wing tips and tail. With suitable input-rate terms incorporated, sufficient lead time for actuating the aerodynamic devices might be obtained. There does not appear to be any *fundamental* technological impediment to achieving very substantial reductions in gust response by this approach. Considerations of weight, cost, and reliability, however, may present serious economic and operational impediments.

BIBLIOGRAPHY

Chapter 1

1.1 F. W. Lanchester. *Aerodonetics*. A. Constable & Co. Ltd., London, 1908.

1.2 G. H. Bryan and W. E. Williams. The Longitudinal Stability of Aerial Gliders. *Proc. Roy. Soc. London*, ser. A, vol. 73, pp. 100–116, 1904.

1.3 G. H. Bryan. *Stability in Aviation*. Macmillan Co., London, 1911.

1.4 L. Bairstow. *Applied Aerodynamics*, 2nd ed. Longmans, Green and Co., 1939.

1.5 B. Etkin and P. C. Hughes. Explanation of the Anomalous Spin Decay of Satellites with Long Flexible Antennae. *J. Spacecraft*, vol. 4, no. 9, Sept. 1967.

1.6 B. M. Jones. *Aerodynamic Theory* (ed. by W. F. Durand), vol. 5. Springer, Berlin, 1935.

1.7 A. Miele. *Flight Mechanics—1. Theory of Flight Paths*. Addison-Wesley Pub. Co., Reading Mass., 1962.

1.8 A. W. Babister. *Aircraft Stability and Control*. Pergamon Press, Oxford, 1961.

1.9 R. L. Bisplinghoff and H. Ashley. *Principles of Aeroelasticity*. John Wiley & Sons, Inc., New York, 1962.

1.10 E. Seckel. *Stability and Control of Airplanes and Helicopters*. Academic Press, New York, 1964.

1.11 T. Hacker. *Flight Stability and Control*. Elsevier Pub. Co., New York, 1970.

1.12 R. C. Duncan. *Dynamics of Atmospheric Entry*. McGraw-Hill Book Co., Inc., New York, 1962.

1.13 C. D. Perkins. Development of Airplane Stability and Control Technology. *J. Aircraft* vol. 7, no. 4, 1970.

Chapter 2

2.1 J. Heading. *Matrix Theory for Physicists*. Longmans, Green and Co., London, 1958.

2.2 R. A. Frazer, W. J. Duncan, and A. R. Collar. *Elementary Matrices.* Cambridge University Press, 1938.

2.3 G. F. D. Duff and D. Naylor. *Differential Equations of Applied Mathematics.* John Wiley & Sons, Inc., New York, 1966.

2.4 H. S. Carslaw and J. C. Jaeger. *Operational Methods in Applied Mathematics*, 2nd ed. Oxford University Press, London, 1947.

2.5 S. O. Rice. *Mathematical Analysis of Random Noise.* Pts. I and II. *Bell Syst. Tech. Jour.*, vol. XXIII, no. 3, July 1944; Pts. III and IV, vol. XXIV, no. 1, Jan. 1945.

2.6 C. L. Johnson. *Analog Computer Techniques.* McGraw-Hill Book Co., Inc., New York, 1956.

2.7 T. D. Truitt and A. E. Rogers. *Basics of Analogue Computers.* John F. Rider Pub. Inc., New York, 1960.

2.8 J. R. Rice and F. P. Beer. First-Occurrence Time of High-Level Crossings in a Continuous Random Process. *J. Acoust. Soc.*, vol. 39, no. 2, Feb. 1966.

2.9 F. P. Beer and W. C. Lennox. Determination of the Survival Probability of a Launch Vehicle Rising through a Random Wind Field. *J. of Spacecraft and Rockets*, vol. 3, no. 4, April 1966.

2.10 J. S. Bendat and A. G. Piersol. *Measurement and Analysis of Random Data.* John Wiley & Sons, Inc., New York, 1966.

2.11 B. Noble. *Applied Linear Algebra.* Prentice-Hall, Inc., N.J., 1969.

2.12 G. A. Korn and T. M. Korn. *Electronic Analog and Hybrid Computers.* McGraw-Hill Book Co., Inc., New York, 1964.

Chapter 3

3.1 L. A. Zadeh and C. A. Desoer. *Linear System Theory.* McGraw-Hill Book Co., Inc. 1963.

3.2 J. LaSalle and S. Lefschetz. *Stability by Lyapunov's Direct Method with Applications.* Academic Press, New York, 1961.

3.3 *Selected Papers from AGARD Structures and Materials Panel. AGARD Rept. 511*, Oct. 1964.

3.4 A. Ralston and H. S. Wilf. *Mathematical Methods for Digital Computers*, vol. 2, John Wiley & Sons, Inc., New York, 1967.

3.5 E. J. Routh. *Dynamics of a System of Rigid Bodies*, 6th ed. Macmillan & Co., London, 1905.

3.6 W. J. Duncan. *Control and Stability of Aircraft.* Cambridge University Press, Cambridge, 1952.

3.7 J. Morris. The Routh and Routh-Hurwitz Stability Criteria. *Aircraft Engineering*, vol. 34, no. 395, Jan. 1962.

3.8 J. E. Gibson. *Nonlinear Automatic Control.* McGraw-Hill Book Co. Inc., New York, 1963.

3.9 D. Graham and D. McRuer. *Analysis of Nonlinear Control Systems.* John Wiley & Sons, Inc., New York, 1961.

3.10 T. E. Stern. *Theory of Nonlinear Networks and Systems.* Addison-Wesley Pub. Co., Reading, Mass., 1965.

3.11 R. Pringle, Jr. On the Capture, Stability, and Passive Damping of Artificial Satellites. *NASA Rept. CR-139,* Dec. 1964.

3.12 B. Etkin. A Simple Method for the Analogue Computation of the Mean-Square Response of Airplanes to Atmospheric Turbulence, *J. Aero. Sci.,* vol. 28, no. 10, 1961.

3.13 B. Etkin. Dynamics of Aerospace Vehicles—A Quarter Century of Change and Two Current Problems. *CASI Journal,* vol. 11, no. 8, Oct. 1965.

3.14 R. G. Brown and J. W. Nilsson. *Introduction to Linear Systems Analysis.* John Wiley & Sons, Inc., New York, 1962.

Chapter 5

5.1 R. L. Halfman. *Dynamics,* vols. 1 and 2. Addison-Wesley Pub. Co., Reading, Mass., 1962.

5.2 R. D. Milne. Dynamics of the Deformable Airplane. *ARC R & M 3345,* 1964.

5.3 M. J. Abzug. Effects of Certain Steady Motions on Small-Disturbance Airplane Dynamics. *J. Aero. Sci.,* vol. 21, no. 11, 1954.

5.4 B. Etkin. Longitudinal Dynamics of a Lifting Vehicle in Orbital Flight. *J. Aero. Sci.,* vol. 28, no. 10, 1961.

5.5 G. H. Bryan. *Stability in Aviation.* Macmillan Co., London, 1911.

5.6 M. Tobak. On the Use of the Indicial Function Concept in the Analysis of Unsteady Motions of Wings and Wing-Tail Combinations. *NACA Rept. 1188,* 1954.

5.7 B. Etkin. Aerodynamic Transfer Functions: An Improvement on Stability Derivatives for Unsteady Flight. *Univ. of Toronto UTIA Rept. 42,* 1956.

5.8 W. P. Rodden. An Aeroelastic Parameter for Estimation of the Effect of Flexibility on the Lateral Stability and Control of Aircraft. *J. Aero. Sci.* vol. 23, no. 7, 1956.

5.9 M. D. McLaughlin. A Theoretical Investigation of the Short-Period Dynamic Longitudinal Stability of Airplanes Having Elastic Wings of 0° to 60° Sweepback. *NACA TN 3251,* 1954.

5.10 Aeroelastic Effects from a Flight Mechanics Standpoint. *AGARD Conference Proceedings,* no. 46, March 1970.

5.11 Y. C. Fung. *The Theory of Aeroelasticity.* John Wiley & Sons, Inc., New York, 1955.

5.12 R. L. Bisplinghoff, H. Ashley, and R. L. Halfman. *Aeroelasticity.* Addison-Wesley Pub. Co., Reading, Mass., 1955.

5.13 W. C. Hurty and M. F. Rubinstein. *Dynamics of Structures*. Prentice-Hall Inc., N.J., 1964.

5.14 J. A. Thelander. Aircraft Motion Analysis. *USAF Rept. FDL-TDR-64-70*, 1965.

5.15 J. L. Synge and B. A. Griffith. *Principles of Mechanics*. McGraw-Hill Pub. Co., Inc., New York, 1942.

5.16 M. Tobak and W. E. Pearson. On Nonlinear Longitudinal Dynamic Stability. *NASA Rept. TR R-209*, 1964.

5.17 H. R. Hopkin. A Scheme of Notation and Nomenclature for Aircraft Dynamics and Associated Aerodynamics. *R.A.E. Tech. Rept. 66200* (5 parts), 1966.

5.18 R. S. Rangi. Nonlinear Effects in the Longitudinal Dynamics of a Lifting Vehicle in a Circular Orbit. *Univ. of Toronto UTIAS Tech. Note 40*, 1960.

5.19 A. M. Drummond. Performance and Stability of Hypervelocity Aircraft Flying on a Minor Circle. *Univ. of Toronto UTIAS Rept. 135*, 1968.

5.20 H. Glauert. A Nondimensional Form of the Stability Equations of an Aeroplane. *ARC R & M 1093*, 1927.

5.21 G. S. Byushgens and R. V. Studnev. Dynamics of the Spatial Motion of an Aircraft (translated from Russian). *NASA TT F-555*, 1969.

5.22 H. H. B. M. Thomas. Estimation of Stability Derivatives (State of the Art). *RAE Tech. Note Aero 2776*, 1961; also *AGARD Rept. 339*.

Chapter 6

6.1 J. Shapiro. *Principles of Helicopter Engineering*. McGraw-Hill Book Co. Inc., New York, 1955.

6.2 J. P. Campbell. *Vertical Take Off and Landing Aircraft*. MacMillan, New York, 1962.

6.3 E. L. Houghton and A. E. Brock. *Aerodynamics for Engineering Students*. Edward Arnold Ltd., London, 1960.

6.4 J. N. Nielsen. *Missile Aerodynamics*. McGraw-Hill Book Co., Inc., New York, 1960.

6.5 H. Ashley and M. Landahl. *Aerodynamics of Wings and Bodies*. Addison-Wesley Pub. Co., Reading, Mass., 1965.

6.6 E. A. Bonney. *Engineering Supersonic Aerodynamics* McGraw-Hill, New York, 1950.

6.7 A. H. Flax and H. R. Lawrence. The Aerodynamics of Low-Aspect Ratio Wing-Body Combinations. *Cornell Aero Lab. Rept. CAL-37*, 1951.

6.8 R. W. Truitt. *Hypersonic Aerodynamics*. Ronald Press, New York, 1959.

6.9 D. E. Ellison and L. V. Malthan. *USAF Stability and Control Methods*. Handbook issued by U.S.A.F. Flight Control Division, Flight Dynamics Laboratory, W.P.A.F.B., Ohio, July 1963.

6.10 A. Miele. *Flight Mechanics 1: Theory of Flight Paths.* Addison-Wesley, Reading, Mass., 1962.

6.11 W. R. Kolk. *Modern Flight Dynamics.* Prentice-Hall, Inc., N.J., 1961.

6.12 S. B. Gates. Proposal for an Elevator Manoeuvreability Criterion. *ARC R & M 2677*, 1942.

6.13 K. J. Orlik-Rückemann. Methods of Measurement of Aircraft Dynamic Stability Derivatives. *CAI Jour.* vol. 6, no. 10, 1960.

6.14 G. J. Hancock. Problems of Aircraft Behaviour at High Angles of Attack. *AGARD Rept. 136*, Dec. 1969.

6.15 R. H. Neely and R. F. Griner. Summary and Analysis of Horizontal-Tail Contribution to Longitudinal Stability of Swept-Wing Airplanes at Low Speeds. *NASA TR R-49*, 1959.

6.16 D. E. Ellison and D. E. Hoak. Stability Derivative Estimation at Subsonic Speeds. Douglas Aircraft Co., Long Beach, Calif., Paper 4164, 1967.

Chapter 7

7.1 R. O. Schade. Free-Flight Tunnel Investigation of Dynamic Longitudinal Stability as Influenced by the Static Stability Measured in Wind Tunnel Force Tests Under Conditions of Constant Thrust and Constant Power. *NACA TN 2075*, 1950.

7.2 H. S. Ribner. Field of Flow About a Jet and Effect of Jets on Stability of Jet-Propelled Airplanes. *NACA Wartime Rept. L213*, 1946.

7.3 H. S. Ribner. Notes on the Propellor and Slip-Stream in Relation to Stability. *NACA Wartime Rept. L25*, 1944.

7.4 H. S. Ribner. Formulas for Propellors in Yaw and Charts of the Side-Force Derivative. *NACA Rept. 819*, 1945.

7.5 E. Priestley. A General Treatment of Static Longitudinal Stability with Propellors, with Application to Single Engine Aircraft. *ARC R & M 2732*, 1953.

7.6 R. E. Kuhn. Semiempirical Procedure for Estimating Lift and Drag Characteristics of Propeller-Wing-Flap Configurations for V/STOL Airplanes. *NASA Memo 1-16-59L*, Feb. 1959.

7.7 N. D. Ellis. Aerodynamics of Wing-Slipstream Interaction. *Univ. of Toronto UTIAS Rept. 169*, 1971.

7.8 J. Weil and W. C. Sleeman, Jr. Prediction of the Effects of Propellor Operation on the Static Longitudinal Stability of Single-Engine Tractor Monoplanes with Flaps Retracted. *NACA Rept. 941*, 1949.

7.9 R. Smelt and H. Davies. Estimation of Increase in Lift Due to Slipstream. *ARC R & M 1788*, 1937.

7.10 C. B. Millikan. The Influence of Running Propellors on Airplane Characteristics. *J. Aero Sci.*, vol. 7, no. 3, 1940.

7.11 R. J. Margason, A. D. Hammond, and G. L. Gentry. Longitudinal Stability and Control Characteristics of a Powered Model of a Twin-Propeller Deflected-Slipstream STOL Airplane Configuration. *NASA TN D-3438*, 1966.

7.12 M. Tobak. On the Use of the Indicial Function Concept in the Analysis of Unsteady Motions of Wings and Wing-Tail Combinations. *NACA Rept. 1188*, 1954.

7.13 J. W. Miles. Unsteady Flow Theory in Dynamic Stability. *J. Aero. Sci.*, vol. 17, no. 1, 1950.

7.14 J. W. Miles. On the Compressibility Correction for Subsonic Unsteady Flow. *J. Aero. Sci.* vol. 17, no. 3, 1950.

7.15 W. P. Rodden and J. P. Giesing. Application of Oscillatory Aerodynamic Theory to Estimation of Dynamic Stability Derivatives. *J. Aircraft*, vol. 7, no. 3, 1970.

7.16 L. T. Filotas. Approximate Transfer Functions for Large Aspect Ratio Wings in Turbulent Flow. *J. Aircraft* vol. 8, no. 6, June 1971.

7.17 H. C. Garner and R. D. Milne. Asymptotic Expansion for Transient Forces from Quasi-Steady Subsonic Wing Theory. *The Aeronautical Quarterly*, vol. 17, Nov. 1966.

7.18 G. W. Brune. Low-Frequency Approximation in Unsteady Aerodynamics. *J. Aircraft*, vol. 6, no. 5, 1969.

7.19 B. W. McCormick, Jr. *Aerodynamics of V/STOL Flight*. Academic Press, New York, 1967.

Chapter 8

8.1 W. H. Michael, Jr. Analysis of the Effects of Wing Interference on the Tail Contributions to the Rolling Derivatives. *NACA Rept. 1086*, 1952.

8.2 J. J. Donegan, S. W. Robinson, Jr., and O. B. Gates, Jr. Determination of Lateral-Stability Derivatives and Transfer-Function Coefficients from Frequency-Response Data for Lateral Motions. *NACA Rept. 1225*, 1955.

8.3 B. H. Beam. A Wind-Tunnel Test Technique for Measuring the Dynamic Rotary Stability Derivatives at Subsonic and Supersonic Speeds. *NACA Rept. 1258*, 1956.

8.4 J. P. Campbell and M. O. McKinney. Summary of Methods for Calculating Dynamic Lateral Stability and Response and for Estimating Lateral Stability Derivatives. *NACA Rept. 1098*, 1952.

8.5 H. S. Ribner. The Stability Derivatives of Low-Aspect-Ratio Wings at Subsonic and Supersonic Speeds. *NACA TN 1423*, 1947.

Chapter 9

9.1 F. N. Scheubel. The Effect of Density Gradient on the Longitudinal Motion of an Aircraft. *Luftfahrtforschung*, vol. 19, no. 4, 1942.

9.2 S. Neumark. Longitudinal Stability, Speed and Height. *RAE Rept. Aero 2265*, 1948; also *Aircraft Engineering*, Nov. 1950.

9.3 T. F. Walkowicz. Dynamic Longitudinal Response of an Airplane at High Subsonic Mach Numbers. MIT Dept. Aero. Eng., Ph.D. thesis, 1948.

9.4 I. L. Ashkenas and D. T. McRuer. Optimization of the Flight-Control, Airframe System. *J. Aerospace Sci.*, vol. 27, no. 3, March 1960.

9.5 I. L. Ashkenas and D. T. McRuer. Approximate Airframe Transfer Functions and Application to Single-Sensor Control Systems. *USAF WADC Rept. 58-82*, 1958.

9.6 A. G. Davenport. Rationale for Determining Design Wind Velocities. *J. Struct. Div. ASCE*, vol. 86, 1960.

9.7 B. Etkin. Effect of Wind Gradient on Glide and Climb. *J. Aero. Sci.*, vol. 14, no. 6, 1947.

9.8 B. Etkin. Longitudinal Dynamics of a Lifting Vehicle in Orbital Flight. *J. Aerospace Sci.*, vol. 28, no. 10, Oct. 1961.

9.9 A. M. Drummond. Performance and Stability of Hypervelocity Aircraft Flying on a Minor Circle. *Univ. of Toronto UTIAS Rept. 135*, 1968.

9.10 R. E. Roberson. Gravitational Torques on a Satellite Vehicle. *J. Franklin Inst.*, vol. 265, no. 1, Jan. 1958.

9.11 E. V. Laitone and Y. S. Chou. Phugoid Oscillations at Hypersonic Speeds. *AIAA paper 64-474*, June 1964.

9.12 N. X. Vinh and A. Dobrzelecki. Nonlinear Longitudinal Dynamics of an Orbital Lifting Vehicle. *NASA CR-1449*, Oct. 1969.

9.13 M. Tobak and H. J. Allan. Dynamic Stability of Vehicles Traversing Ascending or Descending Paths Through the Atmosphere. *NACA TN 4275*, 1958.

9.14 U.S. Committee on Extension to Standard Atmosphere. *U.S. Standard Atmosphere, 1962*. U.S. Government Printing Office, Superintendent of Documents, Washington, D.C.

Chapter 10

10.1 W. H. Phillips. Effect of Steady Rolling on Longitudinal and Directional Stability. *NACA TN. 1627*, 1948.

10.2 R. R. Heppe and L. Celinker. Airplane Design Implications of the Inertia Coupling Problem. *IAS Preprint 723*, 1957.

10.3 H. J. Curfman. Theoretical and Analog Studies of the Effects of Nonlinear Stability Derivatives on the Longitudinal Motions of an Aircraft in Response to Step Control Deflections and to the Influence of Proportional Automatic Control. *NACA Rept. 1241*, 1955.

10.4 D. W. Rhoads and J. M. Schuler. A Theoretical and Experimental Study of Airplane Dynamics in Large-Disturbance Maneuvers. *J. Aero. Sci.*, vol. 24, no. 7, 1957.

10.5 G. W. Stone. The Magnus Instability of a Sounding Rocket. *AIAA Paper 66-62*, 1966.

10.6 H. R. Vaughn. Boundary Conditions for Persistent Roll Resonance on Re-Entry Vehicles. *Sandia Corp., Rept. SC-RR-287*, 1967.

10.7 J. J. Pettus. Equilibrium Roll Rate Theory for a Re-Entry Vehicle. *General Electric Co., Missile & Space Div., Rept. 67SD234*, 1967.

10.8 W. J. G. Pinsker. Charts of Peak Amplitudes in Incidence and Sideslip in Rolling Manoeuvres Due to Inertia Cross Coupling. *RAE Rept. No. Aero 2604*, April 1958.

10.9 W. J. G. Pinsker. Critical Flight Conditions and Loads Resulting from Inertia Cross-Coupling and Aerodynamic Stability Deficiencies. *RAE Tech. Note Aero. 2502*, March 1957.

Chapter 11

11.1 J. W. Tanney. Fluidics. *Progress in Aeronautical Sciences*, vol. 10, Pergamon Press, Oxford, 1970.

11.2 S. Neumark. Longitudinal Stability Below Minimum Drag Speed, and Theory of Stability under Constraint. *ARC R & M 2983*, 1957.

11.3 P. Painlevé. Étude sur le Régime Normal d'un Aeroplane. *La Technique Aeronautique* vol. 1, pp. 3–11, Paris, 1910.

11.4 W. R. Evans. *Control System Dynamics*. McGraw-Hill Pub. Co., New York, 1954.

11.5 D. Graham and D. McRuer. *Analysis of Nonlinear Control Systems*. John Wiley & Sons, Inc., New York, 1961.

11.6 J. H. Blakelock. *Automatic Control of Aircraft and Missiles*. John Wiley & Sons, Inc., New York, 1965.

11.7 J. H. Laning, Jr., and R. H. Battin. *Random Processes in Automatic Control*. McGraw-Hill Pub. Co., New York, 1956.

11.8 S. B. Anderson, H. C. Quigley, and R. C. Innis. Stability and Control Considerations for STOL Aircraft. *CASI Jour.*, vol. 12, no. 5, May 1966.

11.9 A. C. Robinson. Survey of Dynamic Analysis Methods for Flight Control Design. *J. Aircraft*, vol. 6, no. 2, 1969.

11.10 J. D. Welch and R. E. Wilson. Cross-Coupling Dynamics and the Problems of Automatic Control in Rapid Rolls. *IAS Preprint 691*, 1957.

Chapter 12

12.1 The Human Pilot. Vol. III of *Bur. Aero. Rept. AF-6-4*, 1954.

12.2 D. T. McRuer and E. S. Krendel. Dynamic Response of Human Operators. *USAF, WADC TR56-524*, 1957.

12.3 D. T. McRuer, D. Graham, E. Krendel, and W. Reisiner, Jr. Human Pilot Dynamics in Compensatory Systems. *USAF, AFFDL-TR-65-15*, 1965.

12.4 E. P. Todosiev, R. E. Rose, G. A. Bekey, and H. L. Williams. Human Tracking Performance in Uncoupled and Coupled Two-Axis Systems. *TRW Systems Rept. 4380-6003-R0000*, 1965.

12.5 L. D. Reid. The Measurement of Human Pilot Dynamics in a Pursuit-Plus-Disturbance Task. *Univ. of Toronto, UTIAS Rept. 138*, 1969.

12.6 M. Gordon-Smith. An Investigation into Certain Aspects of the Describing Function of a Human Operator Controlling a System of One Degree of Freedom. *Univ. of Toronto, UTIAS Rept. 149*, 1970.

12.7 J. I. Elkind. Characteristics of Simple Manual Control Systems. *MIT Tech. Rept. No. 111*, 1956.

12.8 R. W. Allen and H. R. Jex. An Experimental Investigation of Compensatory and Pursuit Tracking Displays with Rate and Acceleration Control Dynamics and a Disturbance Input. *NASA CR 1082*, 1968.

12.9 R. J. Wasicko, D. T. McRuer, and R. E. Magdaleno. Human Pilot Dynamic Response in Single-Loop Systems with Compensatory and Pursuit Displays. *USAF, AFFDL-TR-66-137*, 1966.

12.10 D. T. McRuer, H. R. Jex, W. F. Clement, and D. Graham. A Systems Analysis Theory for Displays in Manual Control. *Systems Technology Inc., Hawthorne, Calif., Rept. 163-1*, 1968.

12.11 J. D. McDonnell. Pilot Rating Techniques for the Estimation and Evaluation of Handling Qualities. *USAF, AFFDL-TR-68-76*, 1968.

12.12 G. E. Cooper and R. P. Harper, Jr. The Use of Pilot Rating in the Evaluation of Aircraft Handling Qualities. *NASA TN D-5153*, 1969.

12.13 F. O'Hara. Prediction of Aircraft Flying Qualities by Flight Simulators and Other Methods, with Flight Comparisons. *AIAA Paper No. 64-555*, 1964.

12.14 D. H. Perry. Flight Simulation—Some Aspects of Its Use for Studies of Aircraft Handling Qualities. *RAE Tech. Memo Aero 952*, 1966.

12.15 F. O'Hara. Handling Criteria. *J. Roy Aero. Soc.*, vol. 71, no. 676, pp. 271–291, 1967.

12.16 H. A. Shomber and W. M. Gertsen. Longitudinal Handling Qualities Criteria: An Evaluation. *J. Aircraft*, vol. 4, no. 4, pp. 371–376, 1967.

12.17 W. Bihrle, Jr. A Handling Qualities Theory For Precise Flight Path Control. *USAF, AFFDL-TR-65-198*, 1966.

12.18 J. W. Carlson and R. K. Wilson. Flying Qualities Criteria Problems and Some Proposed Solutions. AGARD Specialists Meeting on Stability and Control, Cambridge, England, Sept. 1966.

12.19 P. L. Bisgood. A Review of Recent Research on Handling Qualities and Its Application to the Handling Problems of Large Aircraft. *ARC R & M No. 3458*, 1964, and *RAE Tech. Rept. 68022*, Jan. 1968.

12.20 I. L. Ashkenas and D. T. McRuer. The Determination of Lateral Handling Quality Requirements From Airframe—Human Pilot System Studies. *USAF, WADC TR-59-135*, 1959.

12.21 I. L. Ashkenas. Some Open- and Closed-Loop Aspects of Airplane Lateral-Directional Handling Qualities. *AGARD Rept. 533*, 1966.

12.22 D. A. DiFranco. Flight Investigation of Longitudinal Short Period Frequency Requirements and PIO Tendencies. *USAF, AFFDL-TR-66-163*, 1967.

12.23 J. I. Meeker and G. W. Hall. In-Flight Evaluation of Lateral-Directional Handling Qualities For The Fighter Mission. *USAF, AFFDL-TR-67-98*, 1967.

12.24 W. E. McNeill. Calculated and Flight Measured Handling Qualities Factors of Three Subsonic Jet Transports. *NASA TN D-4832*, 1968.

12.25 R. H. Klein, R. B. Archer, and D. W. Lew. S.S.T. Handling Characteristics During Approach and Landing Flight Regimes. *USAF, AFFDL-TR-65-227*, 1965.

12.26 C. R. Chalk and R. K. Wilson. Airplane Flying Qualities Specification Revision. *J. Aircraft*, vol. 6, no. 3, pp. 232–239, 1969.

12.27 Airworthiness Standards: Transport Category Airplanes. *FAA Part 25*, 1969.

12.28 Flying Qualities of Piloted Airplanes. Military Specification. *USAF, MIL-F-8785*, 1959.

12.29 D. H. Weir and A. V. Phatak, Model of Human Operator Response to Step Transitions in Controlled-Element Dynamics. *NASA CR-671*, Jan. 1967.

12.30 C. B. Westbrook. The Status and Future of Flying Qualities Requirements. *AIAA Paper 65-313*, July 1965.

12.31 C. R. Chalk. Fixed-base Simulator Investigation of the Effects of L_α and True Speed on Pilot Opinion of Longitudinal Flying Qualities. *USAF ASD-TDR-63-399*, Nov. 1963.

12.32 K. H. Doetsch, Jr., D. G. Gould, and D. M. McGregor. A Flight Investigation of Lateral-Directional Handling Qualities for V/STOL Aircraft in Low Speed Manoeuvering Flight. *USAF, AFFDL-TR-69-41*, Aug. 1969.

12.33 R. O. Anderson. A New Approach to the Specification and Evaluation of Flying Qualities. *USAF, AFFDL Rept. TR-69-120*, 1970.

12.34 C. T. Morgan, J. S. Cook, A. Chapanis, and M. W. Lund. *Human Engineering Guide to Equipment Design*. McGraw-Hill Book Co. N.Y. 1963.

Chapter 13

13.1 J. A. Dutton. Present Challenges in Prediction of the Effects of Atmospheric Turbulence on Aeronautical Systems. *Progress in Aeronautical Sciences*, vol. 11, Pergamon Press, Oxford, 1971.

13.2 G. K. Batchelor. *Theory of Homogeneous Turbulence*. Cambridge Univ. Press, Cambridge, 1953.

13.3 H. S. Ribner. Shock-Turbulence Interaction and the Generation of Noise. *NACA TN 3255*, 1954.

13.4 H. S. Ribner. Spectral Theory of Buffeting and Gust Response: Unification and Extension. *J. Aero. Sci.*, vol. 23, no. 12, 1956.

13.5 J. C. Houbolt, R. Steiner, and K. G. Pratt. Dynamic Response of Airplanes to Atmospheric Turbulence Including Flight Data on Input and Response. *NASA TR-R-199*, 1964.

13.6 J. L. Lumley and H. A. Panofsky. *The Structure of Atmospheric Turbulence.* Interscience, New York, 1964.

13.7 H. W. Teunissen. Characteristics of the Mean Wind and Turbulence in the Planetary Boundary Layer. *Univ. of Toronto UTIAS Rev. 32*, 1970.

13.8 E. R. Case, P. A. Maritan, and M. Gorjup. Development of a Low-Altitude Gust Model and its Application to STOL Aircraft Response Studies (2 vols.). *DeHavilland Aircraft Co., Repts. DIR-68-15, 16*, 1969.

13.9 B. Etkin. A Theory of the Response of Airplanes to Random Atmospheric Turbulence. *J. Aero. Sci.*, vol. 26, no. 7, 1959.

13.10 B. Etkin. Theory of the Flight of Airplanes in Isotropic Turbulence—Review and Extension. *AGARD Rept. 372*, 1961.

13.11 G. B. Skelton. Investigation of the Effects of Gusts on V/STOL Craft in Transition and Hover. *USAF Rept. AFFDL-TR-68-85*, 1968.

13.12 F. W. Diederich. The Response of an Airplane to Random Atmospheric Disturbances. *NACA TN 3910*, 1957.

13.13 J. B. Barlow. Theory of Propeller Forces in a Turbulent Atmosphere. *Univ. of Toronto UTIAS Rept. 155*, 1970.

13.14 T. R. Nettleton. Experimental Investigation of the Lift on a Wing in Turbulence. *Univ. of Toronto UTIAS Rept.* (to be published).

13.15 R. McClean. The Optimization of an Autopilot for an Airplane Subjected to Random Atmospheric Turbulence. *Univ. of Toronto UTIA Tech. Note 45*, 1960.

13.16 K. Nakagawa. An Analysis of Gust-Alleviation System for Transport Airplanes. *Japan Soc. for Aero. & Space Sci. Trans.*, vol. 7, no. 10, 1964.

13.17 F. W. Diederich. The Dynamic Response of a Large Airplane to Continuous Random Atmospheric Disturbances. *J. Aero. Sci.*, vol. 23, no. 10, 1956.

13.18 J. M. Eggleston. A Theory for the Lateral Response of Airplanes to Random Atmospheric Turbulence. *NACA TN 3954*, 1957.

13.19 J. K. Zbrozek. A Study of the Longitudinal Response of Aircraft to Turbulent Air. *RAE Rept. Aero 2530*, 1955.

13.20 W. R. Sears. Some Aspects of Nonstationary Airfoil Theory and Its Practical Application. *J. Aero. Sci.*, vol. 8, pp. 104–108, 1941.

13.21 J. Taylor. *Manual on Aircraft Loads.* AGARDograph 83, Pergamon Press, Oxford, 1965.

13.22 J. P. Giesing, W. P. Rodden, and B. Stahl. Sears Function and Lifting Surface Theory for Harmonic Gust Fields. *J. Aircraft.*, vol. 7, no. 3, 1970.

13.23 F. P. Beer and G. Trevino. An Approximate Method for the Determination of the Response of a Large Aircraft to Atmospheric Turbulence. *AIAA Paper No. 70-544*, 1970.

13.24 P. M. Reeves. A Non-Gaussian Turbulence Simulation. *USAF Rept. AFFDL-TR-69-67*, 1969.

13.25 C. G. B. Mitchell. Assessment of the Accuracy of Gust Response Calculations by Comparison with Experiments. *J. Aircraft*, vol. 7, no. 2, 1970.

13.26 W. H. Austin, Jr. Development of Improved Gust Load Criteria for USAF Aircraft. *USAF Rept. SEG-TR-67-28*, 1967.

13.27 J. Burnham. Atmospheric Turbulence at the Cruise Altitudes of Supersonic Transport Aircraft. *Progress in Aeronautical Sciences*, vol. 11, Pergamon Press, Oxford, 1971.

13.28 E. D. Geisler. Wind Effects on Launch Vehicles. *AGARDograph 115*, 1970.

13.29 J. G. Jones. The Speed Response of an Aircraft Constrained to Fly Along a Straight Path in the Presence of Turbulence at Low Altitude. *RAE Tech. Rept. 67242*, Sept. 1967.

INDEX

B

C

D

E

F

G

H

I

M

Errata

- Some of these errata are simple typos, while others are more technically important.
- The symbol → means "should be replaced by."
- Line $n\uparrow$ means "line n from the bottom."
- The collaboration of Prof. P.C.Hughes in the preparation of these Errata is gratefully acknowledged.

— — —

Page 74, line 3 $\uparrow$:

$$\frac{1}{(s^2-n^2)+\omega^2} \rightarrow \frac{1}{(s-n)^2+\omega^2}$$

Page 74, line 2 $\uparrow$:

Table 3.3 → Table 2.3

Page 88, line 10:

$$\zeta = 7 \rightarrow \zeta = 0.7$$

Page 94, Eqs. (3.4,47) and (3.4,48):

$$4T \rightarrow 4\pi T$$

in five places.

Page 99, Eq. (3.5,8):

$$4T \rightarrow 4\pi T$$

in two places.

Page 118, parag following Eq. (4.6,2), line 1:

$$L_{ab} \rightarrow \dot{L}_{ab}$$

Page 123, first line of Eq. (5.1,6):

$$pz \rightarrow qz$$

Page 148, Fig. 5.4, Block 4, Input 1:

$$p_W\ ,\ r_W \rightarrow q_W\ ,\ r_W$$

Page 150, Fig. 5.6, Block 4:

$$p_W\ ,\ r_W \rightarrow q_W\ ,\ r_W$$

Page 151, Fig. 5.7, Block 2:

$$b \rightarrow p$$

Page 181, line 2 after Eq. (5.13,14):

dimensional → nondimensional

Page 192, Eq. (5.15,7), eighth equation:

Should read

$$(Z_q)' = Z_q \cos\varepsilon + X_q \sin\varepsilon$$

Page 227:

Eq. (6.5,6) should be labeled Eq. (6.6,5)

Page 241, Eq. (6.10,11):

$$C_{h_q}\hat{q} \rightarrow C_{he_q}\hat{q}$$

Page 241, Eq. (6.10,12):

$$C_{h_q}C_{L_\alpha} \rightarrow C_{he_q}C_{L_\alpha}$$

Page 246, Eqs. (7.1,2) and (7.1,3):

$$C_{h\alpha}\alpha \rightarrow C_{he\alpha}\alpha$$

Page 250, Fig. 7.4, caption:

". . . (b) Constant thrust and power, and $z_p = 0$."

Page 251, Eqs. (7.3,4) and (7.3,5):

$$\sin\gamma \rightarrow \tan\gamma$$

Page 252, Eq. (7.3,6c), RHS:

$$= \frac{P}{W}\sqrt{\frac{\rho}{2w}}\frac{z_p}{\bar{c}}C_L^{3/2}$$

Page 252, Eq. (7.3,6d), RHS:

$$= \frac{3}{2}\frac{P}{W}\sqrt{\frac{\rho}{2w}}\frac{z_p}{\bar{c}}C_L^{1/2}$$

Page 269, Eq. (7.3,6d), RHS:

Insert equation label (7.9,3) to the right of the equation for C_{he_q} .

Page 284, Eq. (7.10,11), RHS:

Delete minus sign, i.e.,

$$= 2a_t V_H \frac{\partial \varepsilon}{\partial \alpha}$$

Page 316, Eq. (8.7,5):

Should read

$$\Delta N_r = -m'\xi^2$$

$$\Delta C_{n_r} = -2C_T \frac{V}{V_j}\left(\frac{\xi}{b}\right)^2$$

Page 317, Table 8.1:

Regarding the expression for ΔC_{n_r} :

$$-a_F V_V \left(2\frac{l_F}{b} + \frac{\sigma\partial}{\partial\hat{r}}\right) \rightarrow -a_F V_V \left(2\frac{l_F}{b} + \frac{\partial\sigma}{\partial\hat{r}}\right)$$

and

$$-2C_T \frac{V}{V_j}\left(\frac{\xi}{\bar{c}}\right)^2 \rightarrow -2C_T \frac{V}{V_j}\left(\frac{\xi}{b}\right)^2$$

Page 346, line 8:

[see (7.8,5)] → [see (7.8,2)]

Page 350, Eq. in line 3:

$$\frac{V_e^2}{g\bar{c}}\frac{d\hat{p}}{d} \rightarrow \frac{V_e^2}{g\bar{c}}\frac{d\hat{p}}{d\hat{z}}$$

Page 351, line 4 above Fig 9.16:

Remove the comma in "The period goes to infinity, and $N_{1/2}$ to zero at . . ."

Page 364, line 6↑:

Should read

$$\beta : \hat{p} : \hat{r} = -0.0136 : 1.0 : -0.0291$$

Page 374, Eq. preceding Eq. (9.7,13):

$$N_r r \rightarrow N_r \hat{r}$$

Page 429, line 13↑:

Should read:

". . . matrix. For the given rudder input it yields asymptotic slopes of -2 for β and ϕ, and -1 for r. These slopes are reached approximately by $\hat{\omega} = 0.1$ for r and β, but not for ϕ."

Pages 436 & 437:

The heading "**DUTCH ROLL APPROXIMATION**" should be the first line on p. 436, and the heading "**SPIRAL/ROLL APPROXIMATION**" should directly precede the last paragraph on p. 436.

Page 444, Eq. (10.7,3), 2nd row of square matrix, last element:

$$I_y \rightarrow \hat{I}_y$$

Page 445, line 6↑:

". . . can change sign." → ". . . can change from positive to zero."

Page 445, Eq. (10.7,7):

Should read

$$[(\hat{p}_0^2 \hat{I}_y - \hat{I}_x) + C_{m_\alpha}]^2 > 0$$

Page 446, Eq. (10.7,8), numerator:

$$C_m \rightarrow C_{m_\alpha}$$

Page 464, Eq. (11.3,7), second integral on RHS:

$$\int x dm \rightarrow \int x\xi dm$$

Page 466, second line of Eq. (11.3,11):

Should read

$$F_\theta = \frac{\partial W}{\partial \theta_j} = k_{21}P + k_{22}J$$

Page 472, just below Eq. (11.4,4):

Table 9.9 → Table 9.6

[Eq.] (11.4,3) → [Eq.] (11.4,4)

Page 473, Eq. (11.4,7), the 3-3 element of the square matrix:

$$\frac{C_{n_\beta}}{\hat{I}'_z} \rightarrow \frac{C_{n_r}}{\hat{I}'_z}$$

Page 481, just below Eq. (11.5,6):

Should read

$$C_D = 0.2 + \frac{1.2C_L^2}{7\pi}$$

Page 517, Eq. (12.8,5):

Should read

$$CAP = \cdots = \left(\frac{L_\alpha}{W\omega_n^2}\right)^{-1} = \left(\frac{n_\alpha}{\omega_n^2}\right)^{-1}$$

Pages 556 & 557, and page 562:

Eqs. (13.5,1)–(13.5,7) should be labeled (13.4,1)–(13.4,7).